UNIVERSITA' DEGLI STUDI DI VERONA

DIPARTIMENTO DI BIOTECNOLOGIE

Scuola di dottorato in Scienze Naturali e Ingegneristiche

DOTTORATO DI RICERCA IN BIOTECNOLOGIE

Ciclo XXXII

Con il contributo di ERC (European Research Council) Starting Grant SOLENALGAE

Study of Molecular Mechanisms to Increase Carbon Use Efficiency in Microalgae

S.S.D. BIO/04 FISIOLOGIA VEGETALE

Coordinatore: Prof. Matteo Ballottari

Tutor: Prof. Matteo Ballottari

Dottoranda:

Michela Cecchin

Table of contents

Summary **5**

Introduction **10**

1.1 The microalgae world 11
1.2 The oxygenic photosynthesis 14
1.3 Aerobic cellular respiration 29
1.4 Energy reserve in green algae 36
1.5 Strategies to improve microalgae strain 41
1.6 References 45

Chapter 1 : *Chlamydomonas reinhardtii* **50**

Section A:

LPA2 protein is involved in the PSII assembly in *Chlamydomonas reinhardtii* 52

Section B:

Impaired mitochondrial transcription termination disrupts the stromal redox poise in *Chlamydomonas* 78

Chapter 2 : *Chlorella* genus **123**

Section A:

Molecular basis of autotrophic vs mixotrophic growth in *Chlorella sorokiniana* 125

Section B:

Chlorella vulgaris genome assembly and annotation reveals the molecular basis for metabolic acclimation to high light conditions 157

Section C:

Effect of CO_2 concentration on photosynthetic and respiratory pathways in two green algal species of the *Chlorella* genus 198

Chapter 3 : Marine algae **219**

Section A:

Improved lipid productivity in *Nannochloropsis gaditana* in nitrogen replete conditions by selection of pale green mutants 221

Section B:

Incorporating a molecular antenna in diatom microalgae cells enhances photosynthesis 255

Conclusion **276**

Future perspective **282**

Summary

The primary process for biomass and oxygen production on our planet is the photosynthetic conversion of light into chemical energy for CO_2 fixation. Half of the oxygen and of the carbon present worldwide is produced by microalgae. Compared to plants, microalgae take advantages to have a short life cycle, can be cultivated in none-arable land employing waste products and wastewater-derived effluent as nutrient and do not participate to the food or fuel competition. Nowadays, with the increasing of world population these limitations of the traditional crops become more and more significant. For these reasons microalgae are emerging as renewable sources of food/feed, biofuel and high value products as nutraceutical and pharmacological products.

Microalgae comprise a heterogenous group of organisms living in almost all the habitat on our planet, making them a huge source of peculiar characteristics and properties only partially known and exploited. *Chlamydomonas reinhardtii* is the model species of green algae, the class of microalgae evolutionary closest to plant, the most studied and characterized and the only one where nuclear genome and both organelles genomes can be genetically modified. Other green microalgae of exceptional interest are several species of *Chlorella* genus. They have been used commercially over the past 40 years as food and feed supplement for their fast growth rate and their high resistance to biotic and abiotic stresses. Differently from green algae that contain chloroplasts of endosymbiotic origin, heterokont algae contain secondary plastids derived from endosymbiotic red algae. Diatoms and *Nannochloropsis spp.* are heterokont marine algae that had attracted attention due to their large amount of lipid accumulation interesting for biofuels production.

Nevertheless, the potential of microalgae for photosynthetic production of biomass has not been fully exploited, due to their relatively low photosynthetic efficiency in photobioreactor reaching 1-3% of yield instead of the potential 9-10%. A biotechnological approach is required in order to domesticate microalgae for mass cultivation, as it was already done for plants.

Chloroplast is the site of the photosynthetic process: in the thylakoid membrane light is collected by antennae systems of the supercomplexes, PSII and PSI, that works in series in order to remove electrons from water and transfer them to $NADP^+$ producing NADPH. During the electron transport protons are transfer across the membrane generating an electrochemical gradient that is used by ATPase to make ATP. ATP and NADPH produced by this light phase are used by Calvin-Benson cycle to fix CO_2 into sugars. In parallel in the mitochondrion another electron transport chain take place, consuming oxygen and NADH and releasing NAD^+ and ATP. Sugars oxidized thought the cellular respiration provided substrate for this mitochondrial electron transport chain. A constantly balance

between chloroplast and mitochondrion activity is fundamental for the survival of the cells and to overcome the ever-changing environmental conditions.

In order to better understand the alga's biology and allow to design biotechnological approaches to improve biomass yield, in this PhD thesis we investigated the molecular mechanism involved in the microalgae carbon use efficiency.

In the **Chapter 1** we studied the model algae *C. reinhardtii*, the most thoroughly characterized unicellular algae.

In the **section A** the molecular mechanism at the base of Photosystem II assembly were investigated. PSII core complex of *C. reinhardtii* contains at least 20 subunits with various cofactors, including electron donors and acceptors, however no detailed studies of the assembly factors have been performed. In this work we focus our attention of a putative assembly factor of PSII, in particular of the CP43 subunit, called LPA2 (low PSII accumulation 2), previously identified in *A. thaliana*, which functions are however still unclear. A candidate *LPA2* gene in *C. reinhardtii* was identified by homology with *A. thaliana* and its role was studied *in vivo* thank to a CRISPR-cas9 mutant. *lpa2* mutant showed an impaired PSII assembly and an enhanced electron transport around PSI to supplement photosynthetic energy production, but this increase was insufficient to support photoautotrophic growth. Moreover, the mutant showed a slower PSII repair. These data demonstrated that LPA2 protein is involved in both *de novo* biogenesis and repair of PSII.

In the **section B** the relationship between chloroplast and mitochondrion metabolisms was explored studying a mutant of *C. reinhardtii* knockout for a mitochondrial transcription factor. *stm6* is a knockout mutant for a gene encoding for MOC1 protein, a mitochondrial mTERF protein that act as transcription terminator preventing the read-through transcription at specific site in the mitochondrial genome. Previous studies demonstrated that the loss of MOC1 decreased the amount of transcripts encoding the oxidative phosphorylation complex I subunit *nd1* and resulted in a light-sensitive phenotype. In this work we investigated how a mutation affecting the mitochondrial respiration perturbed light acclimation of the strain. We found a stimulated mitochondrial reducing equivalent uptake with a significant increase of the alternative pathway by AOX. This is responsible for decreasing reducing power available in the stroma misleading the feedback photoprotective mechanisms used to handle exposure to high light as chlororespiration.

Chapter 2 regards algae of the Trebouxiophyceae family, in particular two species of *Chlorella* genus were analysed. Despite the importance of this genus for industrial application, biotechnologically

intervention to substantially increase biomass and metabolite productivity are slowed down by limited availability of high-quality genomes and transcriptome.

In the **section A** we elucidated the molecular basis of the improved growth and biomass yield in mixotrophic condition, where the cross-talk between chloroplast and mitochondria metabolism is essential for efficient biomass production. Some microalgae species, as *C. sorokiniana*, are able to combine an autotrophic metabolism with the utilization of reduced carbon source available in the medium, in a so called mixotrophic condition. Acetate is an industrial waste product that can be exploited for this aim, fostering the revenues of industrial cultivation. The *de novo* assembly transcriptome allowed to identify the regulation of several genes involved in control of carbon flux. Despite a reduction of the chlorophylls content per cell, photosynthetic properties were not significantly affected in mixotrophy compared to autotrophy. Interestingly, in presence of acetate the upregulation of the phosphoenolpyruvate carboxylase enzyme was reported suggesting a switch toward a C4-like carbon fixation in order to recover CO_2 releases by acetyl-CoA oxidation.

In the **section B** genetic basis of the highly productive phenotype of *C. vulgaris* was examined. We investigated the low light *vs.* high light adaptation of *C. vulgaris* cells starting from the *de novo* genome assembly, functional annotation and gene expression analysis to correlate the physiological observation. Nuclear and organelle genomes were obtained combining accurate short-reads Illumina, long PacBio reads and Bionano optical mapping, allowing to assembly a near-chromosome scale genome of 14 scaffolds and the two complete circular organelle genomes. The high-light growth condition induced a strong decreased of chlorophylls level and a strong induction of lipid accumulation. The existence of a cytosolic fatty acid biosynthetic pathway was suggested and its upregulation upon high-light exposure was observed. All the genes encoding for photosynthetic subunit and genes involved in the key metabolic pathway were identified. Finally, was reported an evidence of a horizontal gene transfer from the chloroplast to the mitochondria.

In the **section C** the two *Chlorella* species previously analysed were investigated for their physiologic and metabolic responses to different CO_2 availability highlighting different metabolic response among green algae. Indeed, rearrangements of mitochondrial and chloroplast metabolisms in 3% CO_2 compared to atmospheric level of CO_2 were evaluated. Increased photosynthates production in both *C. vulgaris* and *C. sorokiniana* is at the base of the observed increased biomass yield in CO_2 condition: sugars produced in the chloroplast are indeed redirected to the biosynthesis mainly of lipids (TAG) in *C. vulgaris*, and proteins in *C. sorokiniana*, indicating a general enhanced metabolism. In *C. sorokiniana* in 3% CO_2 were observed several reorganizations of the photosynthetic machinery, while the total dark respiration was essentially unaffected. The opposite condition was observed in *C. vulgaris* where the

3% CO_2 induced an improved uptake of reducing power by chloroplast leading to a reduced mitochondrial respiration.

The last chapter (**Chapter 3**) is focused on the marine algae *Nannochloropsis gaditana* and the diatom *Thalassiosira weissflogii.* These species differ in the pigment composition compared to green algae that typically contain chlorophyll *a* and *b*. *N. gaditana* contains only the chlorophyll *a* instead *T. weissflogii* contains chlorophylls *a* and *c*. In order to improve the carbon use efficiency in these species we focused our efforts in the manipulation light harvesting mechanisms with a no GMO approach.

In the **section A** a chemical mutant of *N. gaditana* with a reduction chlorophyll content per cell combined with increased lipids productivity was isolated and characterized. *e8* mutant showed a general reorganization of plastid assembly leading to a similar functioning of the photosynthetic apparatus on a chlorophyll basis. The mutant did not show an increased biomass accumulation but induced an increased lipid content, a class of macromolecules with a higher energy content per gram. This is in any case an indication of improved light energy conversion in line with an improved light penetration in the photobioreactor and more homogenous light availability due to the reduced chlorophyll content per cell in the mutant. Moreover, thank to Illumina sequencing, we found putative genes responsible of the observed phenotype, as the mutation in the *dgd1* gene, a possible candidate being involved in the biosynthesis of one of the major lipids found in the thylakoid membrane. A reduced chlorophyll content per cell coupled with a better light distribution in photobioreactor is likely at the base of the increased lipid productivity.

In the **section B** was reported a proof-of-concept that is possible increased the biomass yield introducing an artificial antenna dyes that improve the light capture without resorting to genetic modification. The *T. weissflogii* cells were grown together with an artificial cyanine molecular antenna (Cy5) that extends the absorbance range of the photosynthetic apparatus exploiting light energy in the orange spectral region. The dye was incorporate in the algae increasing light dependent growth, oxygen and biomass production. Time-resolved spectroscopy data indicates that a Cy5-chlorophyll *a* energy transfer mechanism happen, compatible with a FRET process.

Introduction

1.1 The microalgae world

It has been was estimated that there are 72,500 species of algae in the biosphere but an accurate count of the total number has not yet been performed. Algae are a large, diverse, polyphyletic group of photosynthetic organisms that include from unicellular microalgae to algae that can reach 45m in length. Algae can growth in unusual environment as hot springs, salt lakes, snow and ice, but growth mainly in water, both fresh and saltwater. The higher diversity among algae is not only respect to size and shape, but also with respect to the formation of various chemical compounds through different biosynthetic pathways. Thanks to the photosynthetic process, they provide core ecosystem functions such as supplying half the oxygen present in the atmosphere and contributing to half of the total carbon fixation worldwide (Li-Beisson et al. 2019; Salomé and Merchant 2019).

The fascinating and diverse biochemistry of algae can have a global impact indeed microalgae have different area of application from food/feed to pharmaceuticals. Microalgae offer several advantages compared to plants: they have a relatively simple cell division with a short cell cycle and are fully photosynthetically active; they can growth in saline or waste water and do not require arable land, avoiding the competition for food/feed production, unlike most plant crops. Moreover, they can be used in food or aquaculture industries and for environmental applications such as bioremediation: can be used to remove pollutants, including phytoremediation of domestic waste-water or to reduce the CO_2 content in industrial emissions. Microalga are rich in protein, lipid and carbohydrates, some species are also rich in pigments, for example carotenoids as astaxanthin and β-carotene useful as food supplement, trace elements and mineral that can be useful for the human healthy.

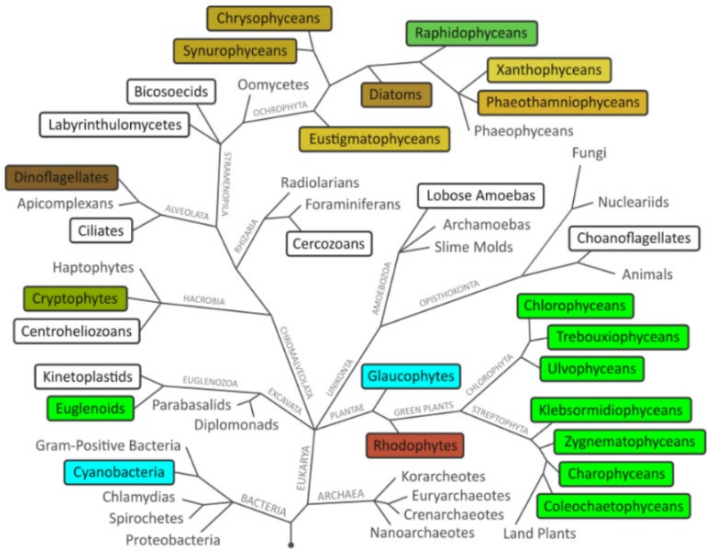

Figure 1. Phylogenetic tree highlighting the diversity and distribution of algae, colours indicate the diversity of pigmentation (www.keweenawalgae.mtu.edu/index.htm).

As mentioned at the beginning, microalgae comprise a large group of organisms that can be classified in the phylogenetic tree show in figure 1. The green lineage or Viridiplantae includes green algae and land plants and is one of the major groups of oxygenic photosynthetic eukaryotes. Inside that we found the Chlorophyta phylum, that includes most of the described species of green algae. It can be divided in three classes: the freshwater or terrestrial Trebouxiophyceae and Chlorophyceae and the coastal Ulvophyceae.

The model species of green algae, *Chlamydomonas reinhardtii* (Figure 2) belong to Chlorophyceae class, especially it is a unicellular, oval-shaped, algae that measures about 5 x 10 µm. This alga is the most thoroughly characterized unicellular algae, is a model for cell biology, microscopy and cell metabolism, moreover it is the only algae where nuclear genome and both organelles genomes can be genetically modified (Salomé and Merchant 2019). The cell of *C. reinhardtii* is surrounded by a cell wall of glycoproteins and carbohydrates that embedded a contractile vacuole, that control the intracellular tonicity, a single cup-shaped chloroplast, that occupies over half of the cell volume, and the other eukaryotic organelles. Starch granules are present between thylakoids membrane stacks and surrounding the pyrenoid, that is the site of CO_2 fixation. Moreover, chloroplast includes a specialized domain called eyespot that contain carotenoid granules and it is important for the detection of the quality, quantity and direction of the light. Finally, a pair of cilia is localized at one pole of the cell. Usually *C. reinhardtii* cells have an asexual cell cycle that required about 8-10 h in constant growth light. Under adverse conditions, as nutrient scarcity, a sexual cycle could occur (Salomé and Merchant 2019).

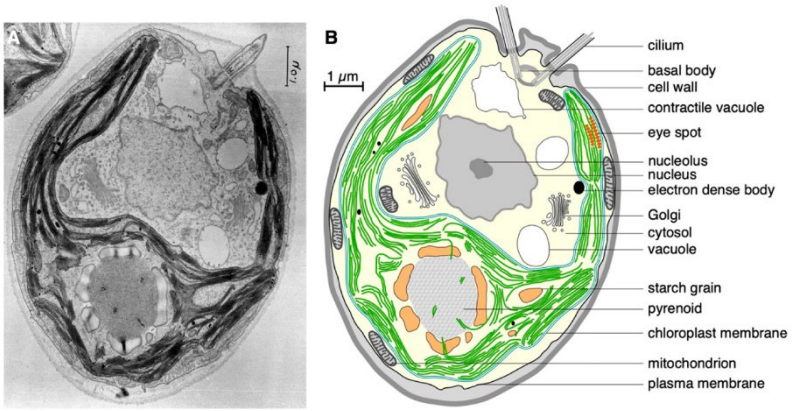

Figure 2. (A)Transmission electron micrograph (TEM) of a *Chlamydomonas* cell. (B) Drawing of a *C. reinhardtii* cell based on the TEM image in (A) (Salomé and Merchant 2019).

The class of Trebouxiophyceae includes an important microalgae genus, the *Chlorella* genus. It comprises unicellular microalgae spherical-shaped with a size ranging from 2 to 10 µm. They are interesting for their rapid growth rate, easily cultivation and scale up and broad industrial application

from biofuel to food additives. Moreover, they contain a high protein, carotenoids and vitamins content. However, the lack of genetic resources and the low efficacy of transformation methods has prevented the development of genetic engineering in these species. Two *Chlorella* species, *C. vulgaris* (GRAS Notice No. GRN000396) and *A. protothecoides* (*C. protothecoides*) (GRAS Notice No. GRN000519), have been categorized as "generally recognized as safe" (GRAS), so are safe for human consumption (Yang et al. 2016). Another *Chlorella* species, *C. sorokiniana*, is interesting for its strong adaptability to the environment, such as high tolerance to temperature (up to 42°C) and CO_2 concentration (up to 40%).

Differently from green algae that contain chloroplasts of endosymbiotic origin, heterokont algae contain secondary plastids derived from endosymbiotic red algae. Among heterokont algae there are diatoms and the *Nannochloropsis spp.*, both are marine unicellular algae that had attracted attention due to their large amount of lipid accumulation interesting for biofuels production. Indeed, triacylglycerol accumulation of *Nannochloropsis spp.* can reach 38% of its total biomass on dry weight basis under nitrogen depletion (Lin et al. 2019). Moreover, the species *Nannochloropsis gaditana* is rich in high-value polyunsaturated fatty acids (FA) (e.g., EPA and DHA), that are important elements for human diet, for example DHA plays a crucial role as anti-inflammation molecule in allergic diseases. Diatoms are responsible for ~40% of total organic carbon produced annually in marine ecosystems. Moreover, they have a wide range of applications, from biofuels, due to their high lipids content, to photonics, due to their silica cell walls. *Thalassiosira weissflogii* is a particularly interesting species due to its carbon acquisition mechanism, based on a C4-like pathway (Zeng et al. 2019, 2020), for this reason it's a well-study algae together with the model diatoms *Phaeodactylum tricornutum*.

1.2 The oxygenic photosynthesis

Green algae, plants and cyanobacteria produce oxygen starting from CO_2, water and light in a process called photosynthesis, it allows the fixation of the carbon into organic molecules and it is therefore the primary source of biomass present on the earth. In particular the photosynthetic process is a redox reaction that uses water as electron donor and leads to the carbon dioxide (CO_2) fixation and to the formation of molecular oxygen (O_2) as by-product, which is essential for the survival of aerobic organisms. The equation of the photosynthetic reaction is the following:

$$nH_2O + nCO_2 + light \rightarrow (CH_2O)n + nO_2$$

Especially the photosynthetic process could be subdivided into a light phase, for which the light is necessary, and a metabolic light-independent phase (Figure 3).

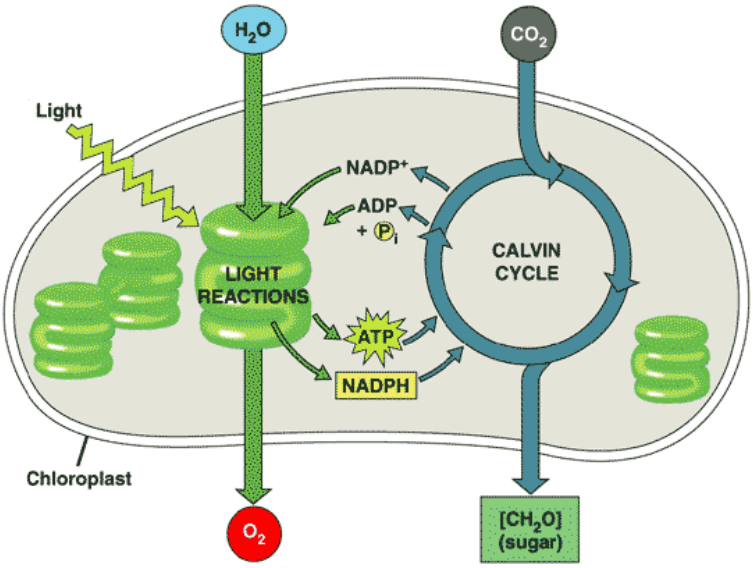

Figure 3. Schematic representation of light-dependent and metabolic phases of photosynthetic process.

During the light-dependent phase the energy from sunlight is captured, as photons, and used to make high-energy molecules (ATP) and reducing power (NADPH), according to the equations:

$$ADP + Pi + energy \rightarrow ATP$$

$$2\ NADP^+ + 2\ H_2O + light \rightarrow 2\ NADPH + O_2 + 2H^+$$

Instead in the light-independent phase ATP and NADPH are used to reduce CO_2 into carbohydrate through the Calvin-Benson-Bassham cycle (Benson and Calvin 1950).

1.2.1 Chloroplast

The reactions of all the photosynthetic process occur in specific organelles called chloroplasts (Figure 4). These special types of plastids are embedded to a double membrane, the external one is permeable to water and different ions and metabolite, instead the internal one is permeable only to small molecule uncharged like O_2. Inside the double membrane there is an extensively folded internal membrane system called thylakoids membrane. These are extensively folded and organized into two distinct domains: the grana domains, which are characterized by ~5–20 layers of cylindrical stacks of thylakoid membrane disks, and the stroma lamellae, which are unstacked thylakoids that connect the grana stacks forming a physically continuous network that separates an internal space, called lumen, from an external space, called stroma (Gao et al. 2018). Grana are tightly packed with photosynthetic complexes, indeed proteins occupy around 70-80% of the area.

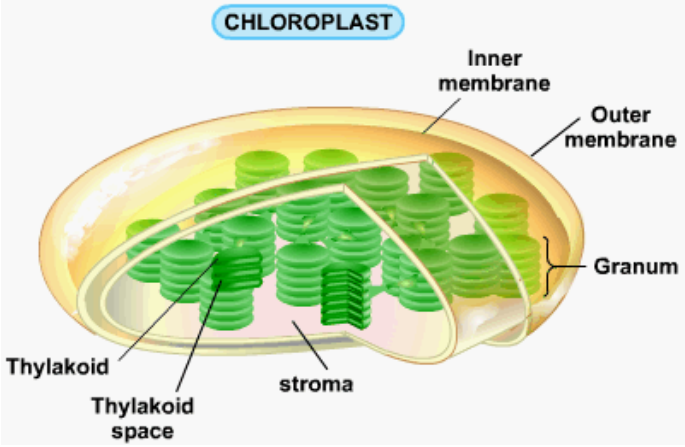

Figure 4. Schematic structure reconstruction of a chloroplast.

The soluble enzymes of light-independent phase reactions of the photosynthesis are in the stroma, instead the light-phase reactions happen in the thylakoid membrane. In particular in the light-phase three multi-protein membrane complexes, called photosystem II (PSII), photosystem I (PSI) and cytochrome b_6f cooperate to generate a proton gradient across the thylakoid membrane while transferring electrons from water to $NADP^+$. Then the chloroplast ATP synthase (ATPase) uses the chemical and electric potential of the proton gradient to generate ATP. These complexes are not evenly distributed throughout thylakoids: PSII resides mainly in grana membranes and it is segregated from PSI, which is almost exclusively localized in the stroma lamellae, Cyt-b_6f is distributed in grana and grana margins and ATPase localizes predominantly in the stroma lamellae.

The cell of the model algae *Chlamydomonas reinhardtii* contains about 80 copies of the chloroplast genome, which is a circular molecule of 205 kb with two inverted repeats and it is organized in large

protein-DNA complexes called nucleoids. These complexes are associated with DNA replication and repair, transcription, RNA processing, and translation. The chloroplast genome contains 99 genes, including a full set of 30 tRNA genes, 5 rRNA genes, 17 ribosomal protein genes, 32 genes involved in photosynthetic pathways (including Rubisco large subunit) and 5 genes for RNA polymerase subunits (Maul et al. 2002). One plastid gene contains introns (*psbA*), while another is present as three distinct loci that are independently transcribed (*psaA*) and post-transcriptionally joined (Salomé and Merchant 2019).

1.2.2 The light-dependent phase

Two types of photosystems, namely photosystem II (PSII, water-plastoquinone oxidoreductase) and photosystem I (PSI, plastocyanin-ferredoxin oxidoreductase), are responsible for the light-driven electron transport. Both of which are multi-subunit membrane protein complexes that bind numerous chlorophylls (Chls), carotenoids (Cars), and other cofactors. In particular, each photosystem is composed of a core complex and a peripheral antenna system, the latter collects light energy and transfers it to the reaction center (RC). Moreover, for the light-dependent phase are needed other two complexes: cytochrome b_6f (plastoquinone-plastocyanin oxidoreductase) and F-ATPase (proton-motive force-driven ATP synthase) (Figure 5).

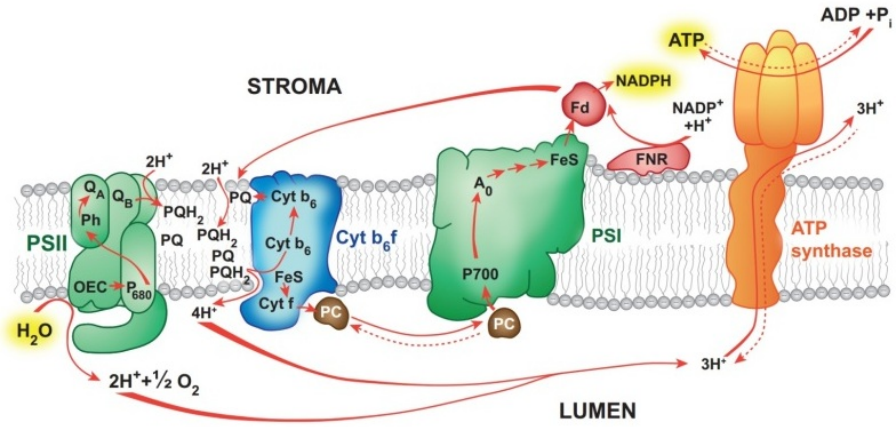

Figure 5. Schematic representation of the light-dependent phase of the photosynthesis.

The first step is the light harvesting. Chlorophylls and other pigments in PSI and PSII antennae systems harvest light and funnel it to the photosynthetic reaction center, further inducing the excitation of chlorophylls known as P680 for PSII and P700 for PSI to initiate the proton translocation across the membrane. In PSII, P680 undergoes charge separation, becoming $P680^+$, then one electron is transferred to a quinone acceptor, called pheophytin (Pheo), and then to a plastoquinone (PQ)

molecule at the Q_A-site. Meanwhile, a water molecule, the authentic electron donor, is oxidized to molecular oxygen and $P680^+$ is eventually reduced. In particular, the missing electron on $P680^+$ is recovered through the oxidation of a tyrosine residue also referred to as Yz. Yz extracts an electron from a cluster of four manganese atoms (OEC, oxygen-evolving complex), which binds two substrate water molecules. Upon four consecutive events of charge separation of P680, the manganese cluster accumulates a total of four oxidizing equivalents, which are used to oxidize two water molecules leading to the formation of O_2, the release of protons in the inner thylakoid space and the return of manganese cluster to the reduced state. The electron on Q_A is then transferred to the PQ at the Q_B-site, which works as a two-electron acceptor and becomes fully reduced and protonated after two photochemical turnovers of the RC. The reduced plastoquinone (plastoquinol, PQH_2) then unbinds from the PSII and are transferred to the thylakoid-embedded cytochrome b_6f, concomitant with the release of two protons to the luminal side of the membrane. The cyt-b_6f oxidizes plastoquinol to plastoquinone and reduces plastocyanin. And then, the plastocyanin is oxidized by PSI. In the PSI, upon photon absorption, a charge separation occurs with the electron transfer through a Chl and a bound quinone (Q_A) to a set of 4Fe-4S clusters. From these clusters, the electron is used to reduce ferredoxin on the stromal side. Two ferredoxin molecules can reduce $NADP^+$ to NADPH, by ferredoxin–$NADP^+$ reductase (FNR) enzyme.

Together, PSII generates the most positive redox potential, while PSI generates the powerful naturally occurring reductant NADPH (Figure 6). The photocatalytic activity of PSII and PSI is linked by the cytochrome b_6f complex, and the proton-motive force generated during the process are utilized by the F-ATPase to generate ATP, which together with NADPH are supplied as energy compounds for sugar synthesis from carbon dioxide by the light-independent reaction (Gao et al. 2018).

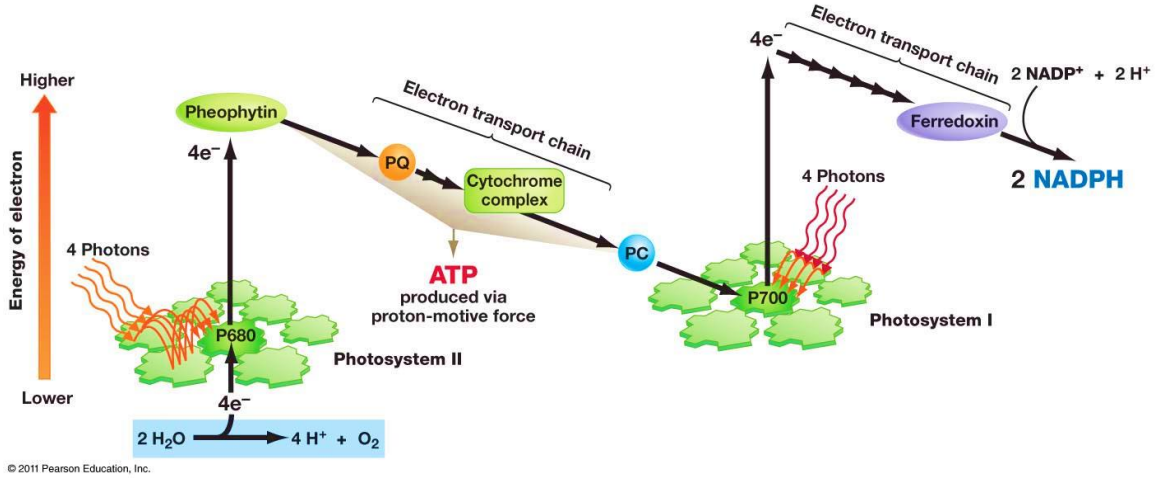

Figure 6. Z-scheme of Bendall and Hill that show as the two photosystems act in series. Cofactors involved in electron translocation between H_2O and $NADP^+$ are indicated.

1.2.3 The light-independent phase

During the light-independent phase of photosynthesis, atmospheric CO_2 is reduced to carbohydrates, using the chemical free energy (ATP and NADPH) produced during the light reactions. The light-independent phase includes a series of reactions (Figure 7), overall indicated as Calvin-Benson-Bassham cycle (Benson and Calvin 1950) that can be summarised with the following reactions:

$$3\ CO_2 + 3\ Ru5P + 3\ H_2O + 6\ ATP + 6\ H^+ + 6\ NADPH \rightarrow 6\ GAP + 6\ ADP + 6\ NADP^+ + 6\ Pi$$

$$5\ GAP + 3\ ATP \rightarrow 3\ Ru5P + 3\ ADP$$

The Calvin cycle allows the synthesis of one glyceraldehyde (GAP) from three CO_2 molecules and the regeneration of Ribulose-5-phosphate (Ru5P) to preserve the cyclic character of the process. In particular starting from three molecules of ribulose 1,5 bisphosphate (Ru5P) are formed 6 molecules of glyceraldehyde (GAP), one of which is the net gain, the other 5 are used to regenerate Ru5P. The triose-phosphates generated by the Calvin-Benson cycle in the chloroplast are subsequently metabolized to build carbohydrates and other cellular constituents.

The key enzyme is the ribulose-1,5-bisphosphate carboxylase/oxygenase, called Rubisco, which allows the incorporation of CO_2 in the cycle. Rubisco is found in the stroma, has an extremely slow catalytic rate and is the most abundant soluble protein in the chloroplast.

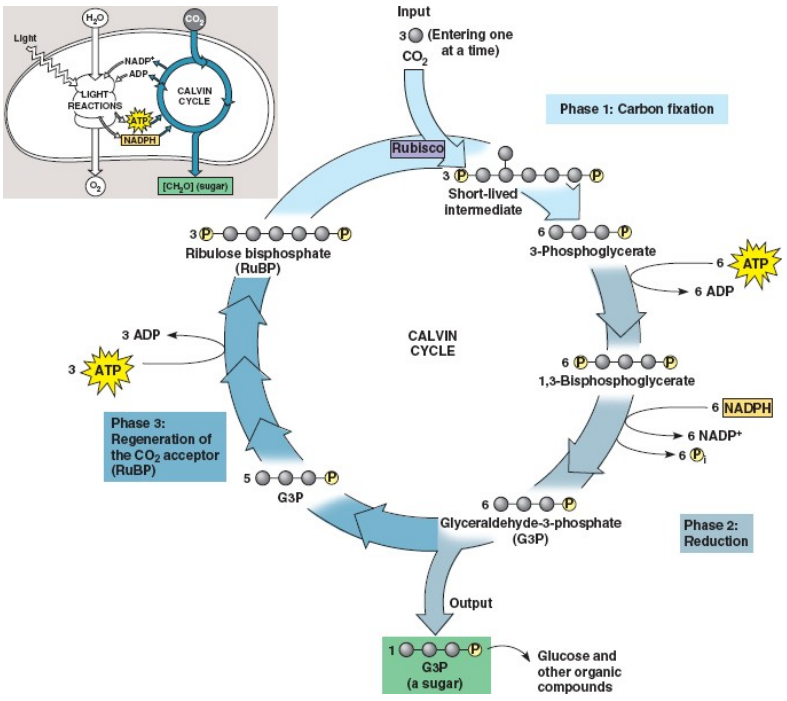

Figure 7. Enzymatic steps involved in the Calvin-Benson-Bassham cycle.

Many enzymes of the Calvin cycle catalyze reversible reactions in common with the glycolytic pathway of carbohydrate degradation, it is therefore essential that there are mechanisms by which,

in light, the synthetic apparatus is "turned on" and the degradation apparatus is "turned off". This also implies that after a period of darkness an induction period is needed to have a perfectly active Calvin cycle. The regulatory mechanisms exploit oxidation-reduction mechanisms, changes in pH and in the concentration of Mg^{2+} ions.

Photorespiration

Rubisco also catalyses the oxygenation of ribulosio-5-biphosphate (Ru5BP) in the presence of oxygen (O_2), generating one molecule of 3-phosphoglycerate (3-PGA) and one of 2-phosphoglycolate (2-PG) at the cost of one ATP and one NAD(P)H.

2-PG is harmful for cellular metabolism; thus, it is rapidly converted to 3-PGA by the photorespiratory pathway (Figure 8). This pathway has nine enzymatic steps which takes place in three organelles (chloroplast, peroxisome, and mitochondria) and in the cytosol. The process generates one molecule each of hydrogen peroxide (H_2O_2) and ammonia (NH_3) that can be toxic if they accumulate to high levels. The ammonia released during the glycine decarboxylation step is reassimilated by plastidic glutamine synthetase (GS) and ferredoxin-dependent glutamate synthase (Fd-GOGAT) systems (Simkin, López-Calcagno, and Raines 2019).

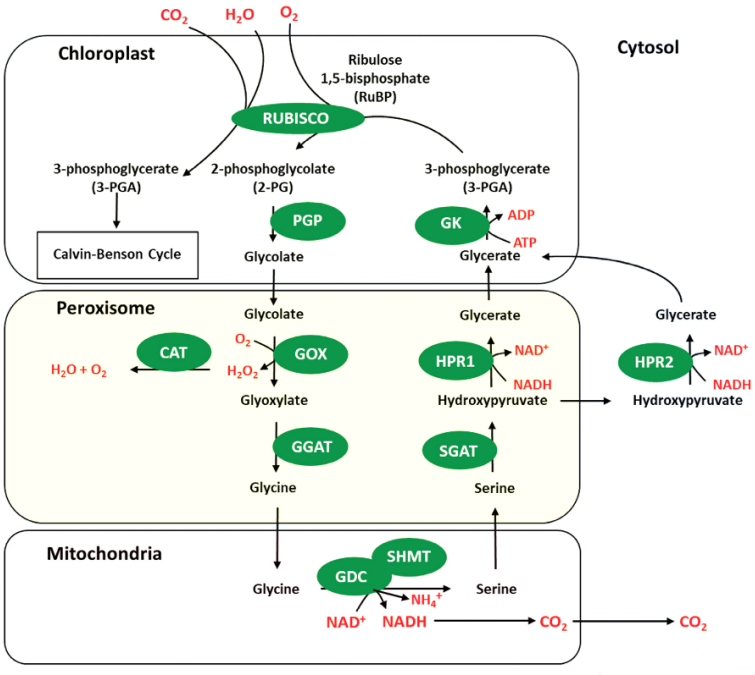

Figure 8. Representation of photorespiration. Glycolate oxidase (GOX), 2-phosphoglycerate phosphatase (PGP), serine-glyoxylate transaminase (SGAT), glycine-2-oxoglutarate aminotransferase (GGAT), glycerate-3-kinase (GK), hydroxypyruvate reductase (HPR), glycine decarboxylase (GDC), catalase (CAT), serine hydroxymethyltransferase (SHMT), Rubisco. Modified from Simkin, López-Calcagno, and Raines 2019.

1.2.4 Photosynthetic pigments

The photosynthetic pigments are responsible for light absorption, charge separation and energy transfer toward the reaction centre in both photosystems. These pigments can be divided in two main classes: chlorophylls and carotenoids.

Chlorophylls

Chlorophylls consist of a central magnesium atom surrounded by a porphyrin ring (a cyclic tetrapyrrole) with attached a side chain of 20 carbon atoms, known as phytol chain, responsible for the hydrophobicity.

In the photosynthetic organisms occurs several types of chlorophylls: chlorophylls *a* and *b* are the major types found in higher plants and green algae; chlorophylls *c* with Chl *a*, is found in diatoms, while Chl *d* and *f* occur cyanobacteria. Different chlorophylls are distinguished from their substitutions, e.g. Chl *a* e *b* differ in a substituent in the second pyrrole ring, being a methyl for the former, an aldehyde for the latter (Figure 9).

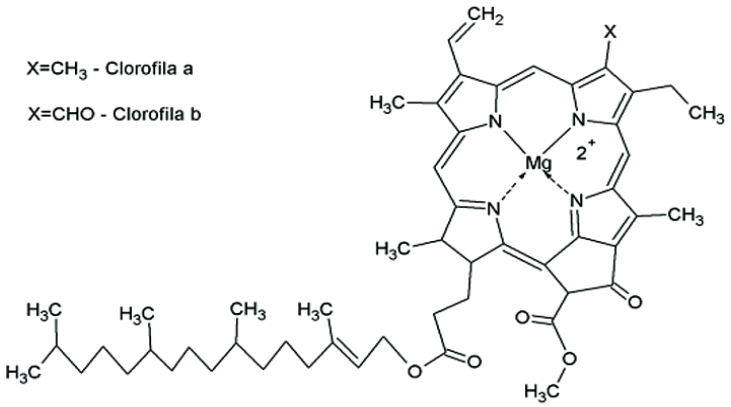

Figure 9. Structure of chlorophyll *a* and *b*.

The characteristic ability of Chls to absorb light in the visible region is due to the high number of conjugated double bonds present in these molecules. Light absorption by chlorophylls lead to a transition of an electron to excited states, in particular the absorption spectra are characterized by two main bands : the Q_y transition in the red region of the spectrum and the Soret transition in the blue region (Figure 10). The transition of an electron from S_0 to S_1 (the first excited state) corresponds to the Q_y transition in the red region of the absorption spectrum (around 640 nm for Chl *b* and 670 nm for the Chl *a*). Another absorption band, called Q_x, is visible in the red region of the spectrum (around 580-640 nm), even if it is partly masked by the Q_y vibronic transitions: it corresponds to the transition of a ground state (S_0) electron to the second excited state (S_2). The transition to higher states corresponds to the Soret band, visible in the blue region of the absorption spectrum (around 430 and 460 nm for Chl *a* and Chl *b*, respectively).

Chlorophyll *a* and *b* absorption properties are well known to be modulated by the protein environment in which they are located. Moreover chlorophylls are indispensable for the proper folding of some photosynthetic proteins, as the LHC proteins (Paulsen, Finkenzeller, and Kühlein 1993) .

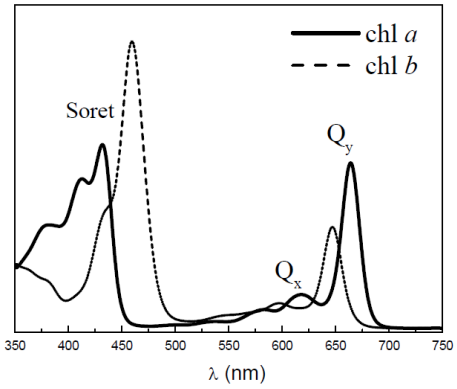

Figure 10. Absorption spectra in acetone 80% of chlorophyll *a* and *b*.

Carotenoids

Carotenoids are tetraterpene molecules (C_{40}) derived from 8 isoprene units, which include carotenes and xanthophylls. Carotenes contain a conjugated system of double bonds consisting of carbon and hydrogen, while xanthophylls include oxygen atoms in their terminal rings.

The double carbon-carbon bonds interact with each other in a process called conjugation, and the π-electrons delocalization in the conjugated double bonds system leads to the light absorption in the visible range 400-500 nm. When carotenoids absorb light, electrons are transferred from the ground state (S_0) to the second excited singlet state (S_2); this strongly dipole-dipole transition is responsible for the characteristic absorption spectrum. The first excited singlet state (S_1) cannot be populated from the ground state by photon absorption, due to symmetry reasons. Carotenoids are indispensable in light harvesting and energy transfer during photosynthesis and in the protection of the photosynthetic apparatus against photooxidative damage. Most carotenoids are bound to integral membrane proteins, associated with light-harvesting complexes (LHCs), where they absorb light across a broader range of the spectral region and transfer the energy to chlorophyll, initiating the photochemical events of photosynthesis. There are also carotenoids located in the core complexes of both photosystems, and in the cytochrome b_6f complex, where they promote the stability and functionality of the photosynthetic apparatus (Varela et al. 2015). Carotenoids, such as chlorophylls, are linked to a protein matrix that influences their spectral characteristics. The polypeptides involved bind carotenoids in a non-covalent way thanks to hydrophobic interactions and hydrogen bridges with the oxygen atoms present in xanthophylls.

More than 700 types of carotenoids were identified in nature, the most abundant carotenoids associated with thylakoid membranes are the α- and β-Carotene (α-Car, β-Car) and the xanthophylls Lutein (Lut), Violaxanthin (Vio), Neoxanthin (Neo) and Zeaxanthin (Zea). The composition of carotenoids in the thylakoids is not constant, rather it rapidly changes according to the intensity of incident light, or during the acclimation to long-term stress.

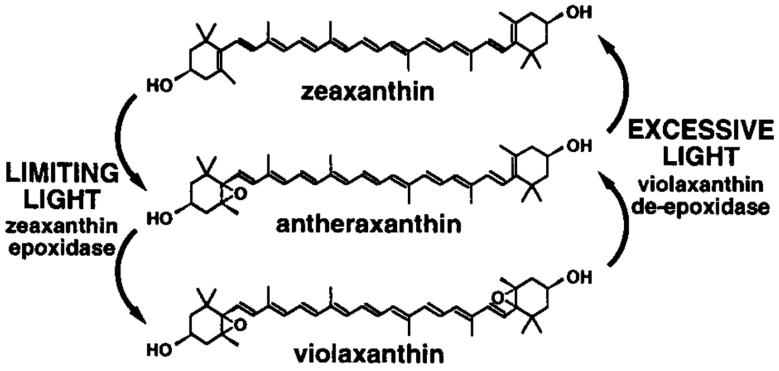

Figure 11. Schematic representation of the xanthophylls cycle.

Three xanthophylls, violaxanthin, antheraxanthin and zeaxanthin, take part to the so-called cycle of xanthophylls, which consists in a light-dependent, reversible de-epoxidation of violaxanthin to zeaxanthin via the intermediate antheraxanthin (Figure 11). Zeaxanthin decrease light absorption during excess light condition, thus, the regulation of the xanthophyll cycle has an important physiological influence in the response to high light. The de-epoxidation reactions converting violaxanthin to zeaxanthin are catalysed by violaxanthin de-epoxidase (VDE) enzyme (Yamamoto and Kamite 1972), a lumenal enzyme activated by acidification of the lumenal compartment (Gilmore and Yamamoto 1992), which occur when there is an excess of light: that condition saturates the electron transport capacity increasing the transmembrane proton gradient. The enzyme zeaxanthin epoxidase (ZE), located in stromal side of the thylakoid membranes and constitutively activated (Bouvier et al. 1996), catalyses the epoxidation reaction which completes the cycle. The xanthophylls cycle is a key component in the activation of several photo-protection mechanisms as thermal energy dissipation of excess excitation energy (NPQ), this point will be discussed later in the thesis.

1.2.5 Photosystems organization in green algae

Each photosystem is multi-protein supercomplexes composed by a core complex, involved in the light harvesting, charge separation and electron transport, and by a peripheral antenna system, involved in the light harvesting and that transfer the excitation energy to the reaction centre in the core complexes. The core complexes of both PSII and PSI have been well conserved from

cyanobacteria to higher plants, whereas their antenna systems are considerably diverse among different species (Pan et al. 2019).

PSII structure

Photosystem II (PSII) is water-plastoquinone oxidoreductase capable of absorbing light and splitting water. In particular, in *C. reinhardtii*, it is organized as a dimer that consists of 2 PSII core complexes (C_2), 2 strongly bound LHCII trimers (S-LHCIIs), 2 moderately bound LHCII trimers (M-LHCIIs), and 2 naked LHCII trimers (N-LHCIIs) also called L-LHCIIs (loosely bound), forming the $C_2S_2M_2N_2$ supercomplex. The antennae system comprises other two subunit: CP26 and CP29 that are associated with each PSII core (Figure 12, Shen et al. 2019). In addition, the PSII supercomplex contained Chl *a*, Chl *b*, neoxanthin, loroxanthin, violaxanthin, lutein, and β-carotene.

The structure of one monomeric core comprises 4 intrinsic transmembrane subunits (D1/PsaA, D2/PsbD, CP43/PsbC, and CP47/PsbB), 13 low-molecular-mass intrinsic transmembrane subunits (PsbE, PsbF, PsbH, PsbI, PsbJ, PsbK, PsbL, PsbM, PsbTc, PsbW, PsbX, PsbZ, and Psb30), and 1 extrinsic subunit (PsbO) attached at the luminal surface (Shen et al. 2019). The monomeric complex acts as intermediate form in the normal assembly pathway or in the damage-repair cycle.

The core subunits are encoded by *psb* genes, most of which are plastidial encoded (Pagliano, Saracco, and Barber 2013), instead the LHCII proteins are all encoded in the nucleus by 9 *lhcbm* genes (Lhcbm1-6, Lhcbm8, Lhcbm9 and Lhcbm11). The LHCII complexes help regulate energy flow to the reaction centers by participating in both light harvesting and energy dissipation (Neilson and Durnford 2010).

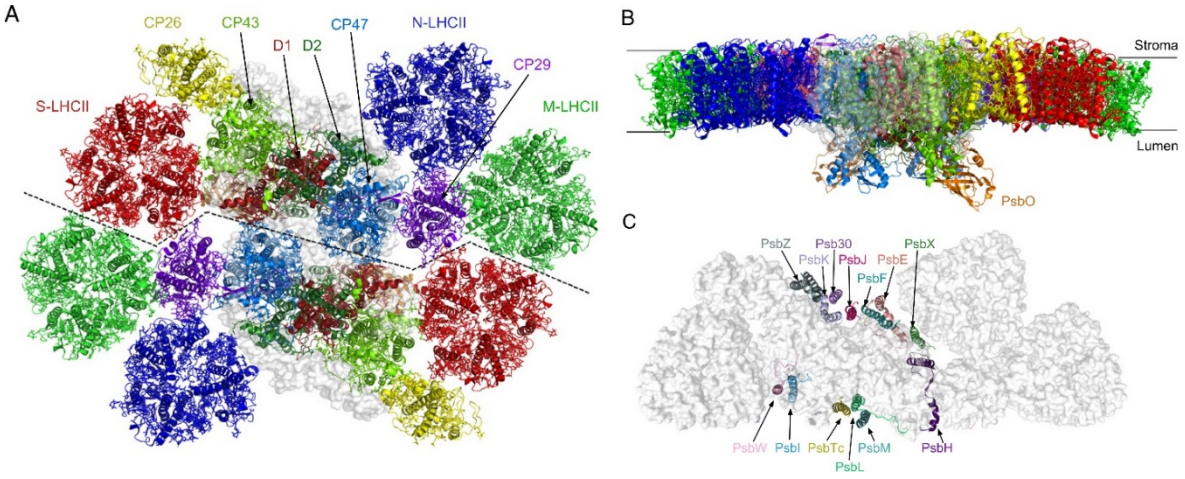

Figure 12. Architecture of the $C_2S_2M_2N_2$-PSII–LHCII supercomplex from *C. reinhardtii.* (A) Representation of the overall structure with a top view from the stromal side. (B) Side view along the membrane plane. (C) The arrangement of 13 small membrane-intrinsic proteins in each monomer viewed from the stromal side (Shen et al. 2019).

PSI structure

Photosystem I (PSI) is a plastocyanin:ferredoxin oxidoreductase responsible for light-driven charge separation and electron transfer from plastocyanin on the lumenal side of the thylakoid membrane to ferredoxin on the stromal side.

In *C. reinhardtii* the core complex is composed by 14 subunit (PsaA-L and PsaN-PsaO) similar to that of plants, instead the antenna system is larger than that of plants with a double belt of light harvesting protein (LHC) (Su et al. 2019). In particular the central part of the core complex is composed of two large proteins, PsaA and PsaB, which binds almost all of the cofactors of the electron transfer chain. PsaC together with PsaD and PsaE forms the docking site for ferredoxin on the stromal side of the membrane. PsaF and PsaN are important for electron transfer from plastocyanin to P700. PsaJ is a hydrophobic protein located close to PsaF and plays a role in the stabilization of this subunit conformation. PsaH, PsaI, PsaL, and PsaO form a cluster of integral membrane proteins and they are involved in interactions with LHCII during state transitions. Finally PsaG and PsaK are located near PsaA and PsaB, respectively, and have been proposed to be important for the association of the outer antenna with the core (Drop et al. 2011) (Figure 13).

Finally, the PSI supercomplex binds chlorophylls *a* and *b* and the carotenoids loroxanthin, lutein, neoxanthin, violaxanthin and β-carotene (Pan et al. 2019).

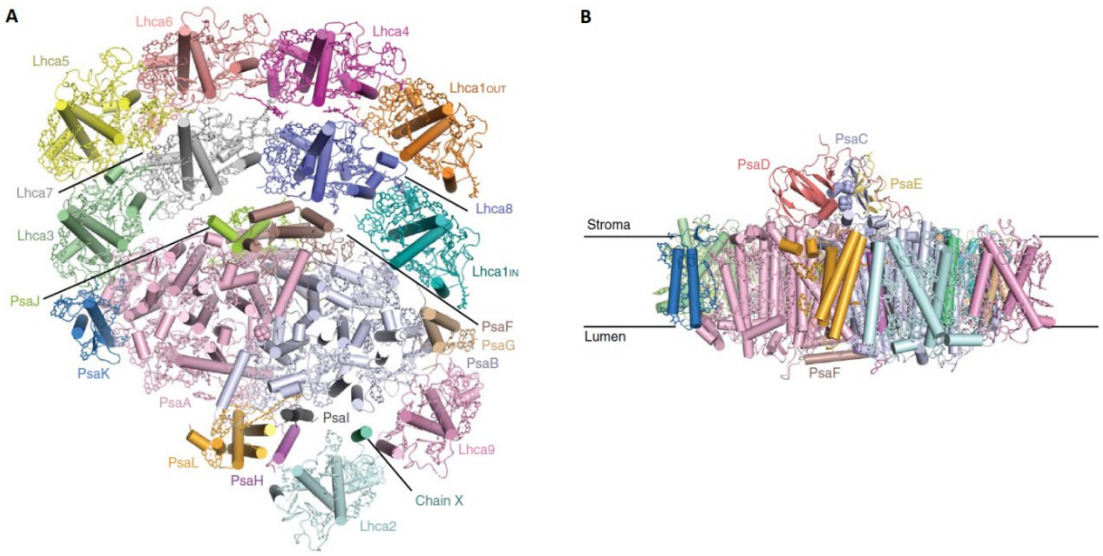

Figure 13. Structure of *C. reinhardtii* PSI supercomplexes. A) PSI-10LHCI structure view from the stromal side. B) Side view of the structure (Su et al. 2019).

The genes encode for the antennae system are called *lhca*. In *C. reinhardtii* among 9-10 *lhca* gene products have been identify, but the exact copy number of Lhca protein and their location within the CrPSI-LHCI supercomplexes are still unclear: 8 or 10 LHCI could bind the PSI core. In the PSI-10LHCI model, 8 LHCI form a double belt at the PsaF side, and two additional Lhca proteins are weakly

associated to the PsaB side. The PSI-8LHCI structure lacks the two protein in the side layer and further lacks two core subunits, PsaG and PsaH, which are stabilized by LHCI side layer in the PSI-10LHCI supercomplexes. The detachment of the side layer may allow the fast regulation of the PSI antenna size, moreover this dissociation has been suggested to be important in the formation of the PSI–LHCI–cyt b_6f supercomplex that is involved in the cyclic electron flow (Su et al. 2019).

1.2.6 Photoprotection mechanism

Algae must face a dynamic environment ever-changing: temperature, CO_2 concentration, quality and quantity of light are some of the changing factors that every organism have to overcome in order to survive. These environmental fluctuations differentially affect the efficiency of electron transfer and metabolic reactions, imbalance the rate of NADPH/ATP utilization and excitation energy available. Any disequilibrium can lead to overreduction of photosynthetic electron acceptors and promote the generation of reactive oxygen species (ROS) and finally to photooxidative stress. Algae evolved several photoprotective mechanisms to fine-tune the supply of energy avoiding ROS formation and preventing photoinhibition.

Non-Photochemical Quenching

Non-photochemical quenching (NPQ) is a process that dissipates excess excitation energy as heat to avoid or decrease photooxidative damage from high light or other stress conditions. This process quenched the excess of ^{1}Chl* and so is measured from the decrease of Chl fluorescence from PSII. NPQ includes short term responses to rapid fluctuations in light, as well as long term responses to acclimation to high light exposure.

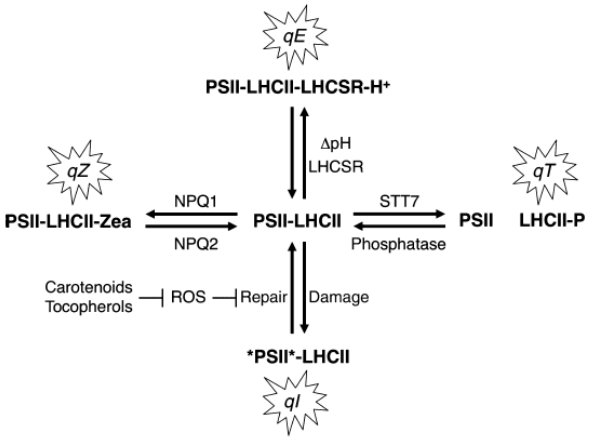

Figure 14. NPQ mechanisms in *C. reinhardtii* (Erickson, Wakao, and Niyogi 2015).

In particular, NPQ can be subdivide in four components (Figure 14): qE, energy-dependent quenching; qT, state transition-dependent quenching; qZ, zeaxanthin-dependent quenching and qI, photoinhibitory quenching (Erickson, Wakao, and Niyogi 2015). qI is the slowest component because

is referred to photoinhibition of PSII, in particular to the oxidative damage to the D1 core protein. This protein is degraded and replaced allowing to control electron flow to PSI, which will become irreversibly damaged if the capacity of the electron acceptors is exceeded. qZ and qT are induced on a time scale of minutes: qZ represents the quenching due to the accumulation of zeaxanthin bound to LHCII, is a ΔpH independent quenching; qT is related to phosphorylation of migratory LHCII antenna complexes (see the following paragraph for details). Finally, qE is the rapidly reversible component of NPQ, the major and most intensively investigated one. qE depends on acidification of the thylakoid lumen upon formation of high ΔpH across the thylakoid membrane under excess light and requires expression of stress-related LHC protein, LHCSR in *C. reinhardtii*. Two types of LHCSR proteins of *C. reinhardtii* have been identified: LHCSR3 and LHCSR1. They are transcriptionally up-regulated in response to the shift from low light to high light, but they are differential expressed in response to CO_2 concentration. Plants rely on another protein PSBS, that like LHCSR, acts as a sensor of lumen pH for activating quenching (Erickson et al. 2015).

State transitions

The antennae systems of PSI and PSII have a different composition and hence a different light absorption spectrum, with PSII being more effective in absorbing blue light and PSI in absorbing far-red light. Algae need to rapidly adjust the relative absorption cross-sections of both photosystems in function of light quality and quantity. This regulation occurs via so-called state transitions, and it involves the relocation of LHCs between PSII and PSI.

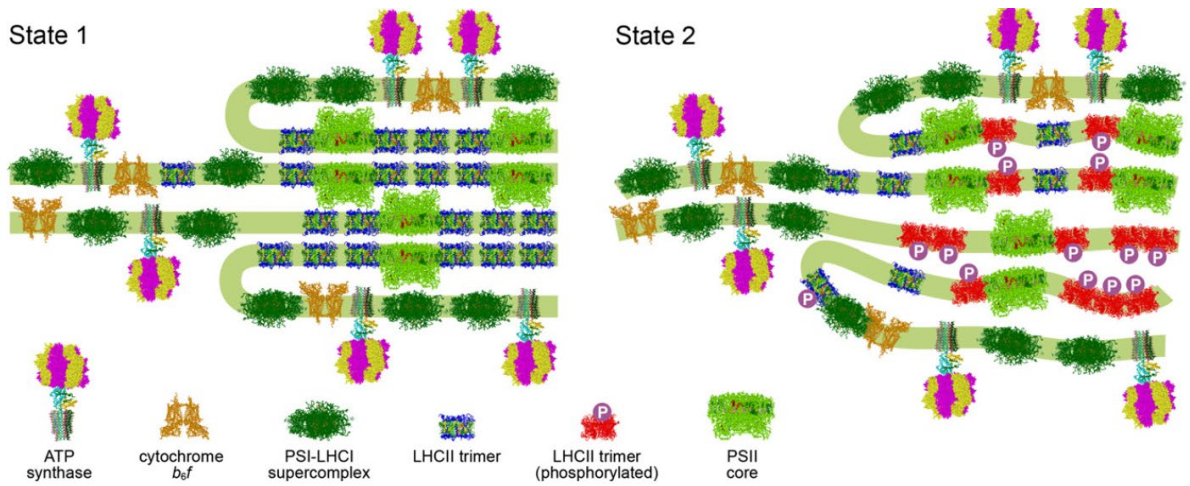

Figure 15. Proposed remodelling of the photosynthetic supercomplexes during state transitions in *C. reinhardtii* by Minagawa and Tokutsu, 2015. Side views of the membrane planes showing alterations in the thylakoid ultrastructure and photosystem supercomplex composition.

State 2 occurs when PSII is too excited, this cause the accumulation of reduced plastoquinone, resulting in the phosphorylation of LHCII protein by a serine-threonine protein kinase and their subsequent dissociation from PSII and association with PSI. Oxidation of the plastoquinone pool induces the opposite effect, regenerating State 1 (Figure 15). The kinase, STT7 in green algae and STN7 in vascular plants, is responsible for the LHCII phosphorylation.

In plant the amount of LHCII that dissociates from PSII is identical to the amount that re-associates with PSI, about 20% of total LHCIIs migrate, instead in *C. reinhardtii*, Ünlü et al. 2014 demonstrate that less than one LHCII trimer attaches per PSI complex on average, and almost 80% of LHCIIs can migrate. Indeed, in *C. reinhardtii* exists two types of state transition: one is the classical LHCII migration, like in plants, that explains a 10–20% reduction of the PSII light-harvesting capacity, the other is a phosphorylation-dependent quenching of aggregated LHCIIs, specific of green algae. This type of state transitions cause only the reduction of the excitation level of PSII and explains 80% change in the light-harvesting capacity observed in *C. reinhardtii* (Minagawa and Tokutsu 2015). Moreover, Nagy et al. 2014 found that state transitions in *C. reinhardtii* deeply affect the organization of chloroplast thylakoid membranes by introducing reorganizations at different levels of the structural complexity, in particular affecting the stacking and periodicity of the photosynthetic membranes (Figure 15).

Seems that in *A. thaliana*, the association of LHCII to PSI plays an important role in long-term acclimation to different light, instead in *C. reinhardtii* state transitions seems more important in the short-term response mechanisms to increase photoprotection (Ünlü et al. 2014).

Alternative electron transport

As mentioned at the beginning of this section, a balance of NADPH/ATP utilization and excitation energy available is fundamental for cells surviving. Different mechanisms have been proposed to be responsible for re-equilibration of the NADPH/ATP balance and avoiding overreduction of the NADPH stromal pool and of photosynthetic electron acceptors.

The most studied alternative pathway is cyclic electron transport (CET, in red in Figure 16), in which electrons are transferred from ferredoxin (Fd) to the plastoquinone (PQ) pool, generating a trans-thylakoid H^+ gradient (ΔpH) without net production of NADPH. Two pathways of PSI cyclic electron transport are known: one is antimycin A sensitive, involves ferredoxin (Fd), proton gradient regulation 5 (PGR5) protein, and proton gradient regulation like 1 (PGRL1) protein, the other is described as antimycin A insensitive, that involves the multiple-subunit NADH dehydrogenase complex (NDH-1) for land plant chloroplasts, instead for microalgae involves a plastidial type II NAD(P)H dehydrogenase (NDA2) (Dang et al. 2014).

Another alternative electron transport is the pseudo-cyclic electron transport (pseudoCET, in blue in Figure 16). This referred to two different pathways: the water–water cycle or Mehler reactions and the flavodiiron (Flv) pathway. The first one depends on O_2 reduction around PSI. Resulting ROS is scavenged by superoxide dismutase (SOD) and ascorbate peroxidase (APX). Flv pathway mediates direct reduction of O_2 to H_2O using likely NADPH or Fd as electron donor (Shikanai and Yamamoto 2017).

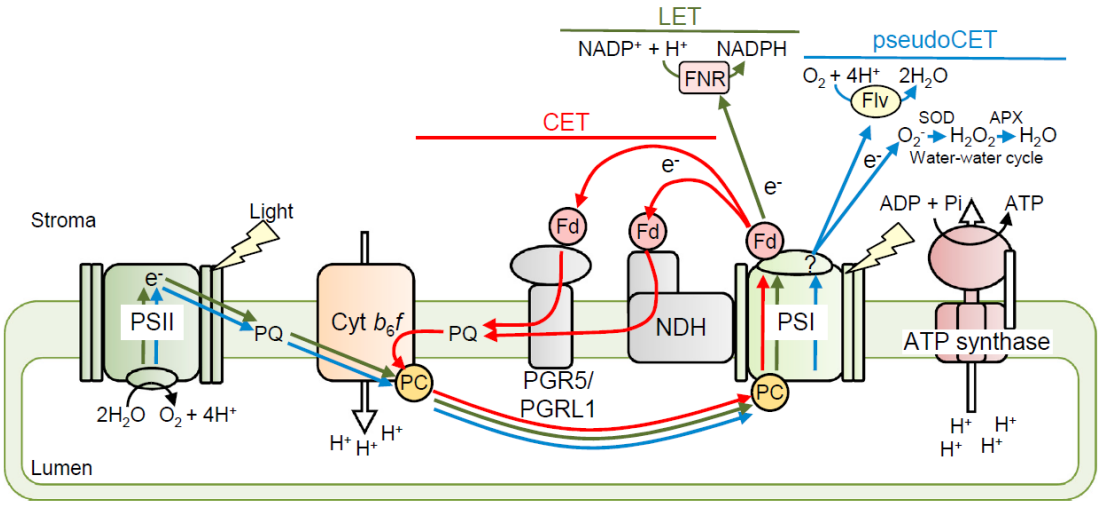

Figure 16. Representation of photosynthetic electron transport and alternative electron transport (Shikanai and Yamamoto 2017)

Chloroplasts also contain an alternate oxidase (PTOX) that oxidizes PQH_2 and reduces O_2 to H_2O. Electron flow from PSII through PTOX could generate ATP from proton accumulation at PSII, however, only one proton is transferred into the lumen per electron transferred from PSII through PTOX. PTOX is involved also in the chlororespiration, a light-independent electron transport pathway (Bennoun 1982) that involves the non-photochemical reduction of PQ by a chloroplast NADPH dehydrogenase and the oxidation of PQH_2 by a terminal oxidase (PTOX). In *Chlamydomonas* the protein involved are the chloroplastic type II NADPH dehydrogenase (NDA2) and two plastid terminal oxidases (PTOX1 and PTOX2) (Jans et al. 2008). Chlororespiration provides a mechanism to prevent the complete oxidation of the plastoquinone pool in the dark, as well as, to prevent its complete reduction in excess light. Moreover, it modulates the activity of cyclic electron flow around photosystem I and facilitate NADPH oxidation to dissipate photosynthetic reducing equivalents reducing photoinhibition and the production of ROS species (Erickson et al. 2015).

1.3 Aerobic cellular respiration

In photosynthetic cells coexists two main bioenergetic processes: photosynthesis and mitochondrial respiration. Indeed, both involve an electron transport chain coupled to ATP synthesis. In particular, photosynthesis converts light energy into chemical energy (NADPH and ATP) and allows the net fixation of carbon, then respiration converts reducing power contained in carbohydrates into phosphorylating power releasing CO_2 (Figure 17).

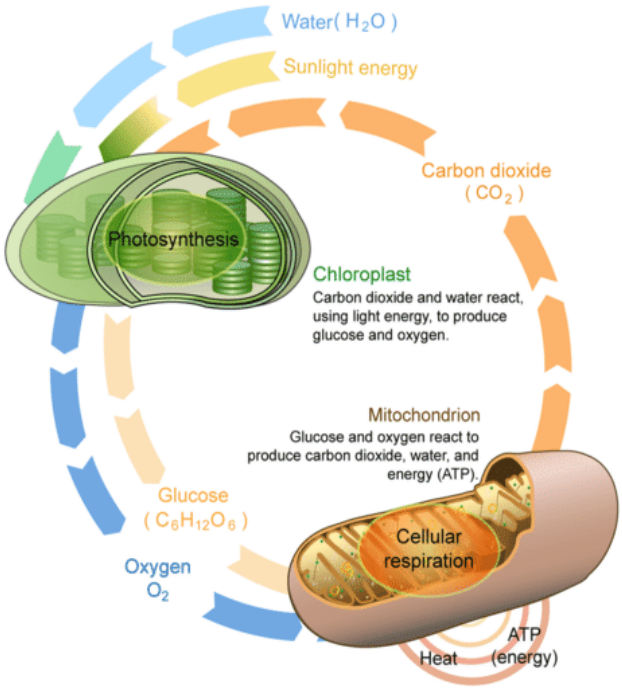

Figure 17. Schematic view of the relationship between chloroplast and mitochondrion metabolism.

Cellular respiration involves many chemical reactions, that can be summed up in this equation:

$$(CH_2O)n + nO_2 \rightarrow nCO_2 + nH_2O + ATP$$

The reactions of cellular respiration can be grouped into three stages: glycolysis, that oxidized glucose in pyruvate; Krebs cycle, that completely oxidized pyruvate producing CO_2 and reducing power (NADH and $FADH_2$); electron transport chain, that together with the oxidative phosphorylation make the major quantity of ATP (Figure 18). The last two process happen in the mitochondrion, in the matrix and in the cristae respectively, the first one in the cytosol.

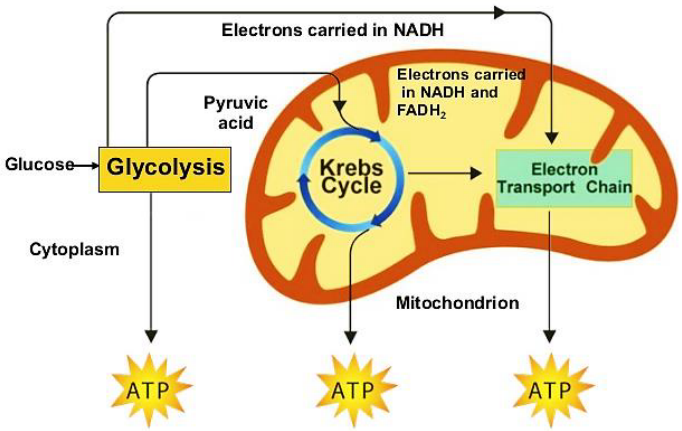

Figure 18. Overview of the cellular respiration steps.

1.3.1 Mitochondrion

Mitochondria are the main organelles of the cellular respiration. Mitochondrion is a double-membrane bound organelle that generates most of the chemical energy (ATP) in the cell, for this reason it is also defines as the 'powerhouse' of the cell. It is composed by an outer membrane, that is permeable to small molecule, thanks to some integral membrane protein called porins, and an inner membrane, that folds over many times forming layered structures called cristae, that increased considerably the surface area (Figure 19). The inner membrane hosts the multi-protein complexes of the respiratory chain and the ATPase complex. The internal space is referred as matrix, instead the space between the two membrane is referred as intermembrane space. The last one has a composition similar to the cytosol, being the outer membrane permeable to small molecule, instead the matrix includes soluble enzyme, the mitochondrial DNA and the ribosomes.

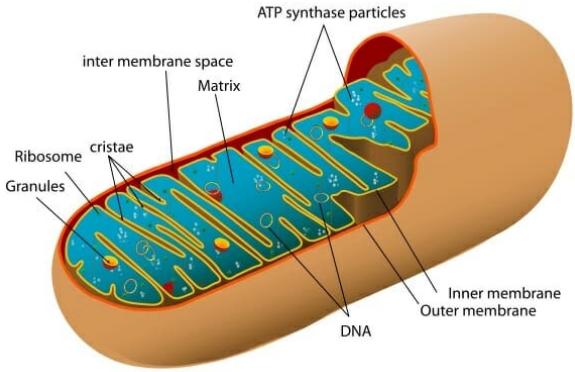

Figure 19. Schematic structure reconstruction of a mitochondrion.

Chlamydomonas reinhardtii mitochondrial proteome includes approximately 350 proteins, while the mitochondrial genome, a sequence of 15.8 kb, contains only 12 genes, seven encode for respiratory chain proteins, three for transfer RNAs (tRNAs), and the other are small and large subunit ribosomal

RNAs (Popescu and Lee 2007; Yang et al. 2015). Therefore, the majority of proteins contributing to mitochondrial function, including respiratory activity, are nucleus-encoded and imported into the organelle by the Transporter Inner Membrane and Transporter Outer Membrane (TIM-TOM) systems (Yang et al. 2015).

Each cell contains about 130 copies of the mitochondrial genome (Salomé and Merchant 2019) .

1.3.2 Glycolysis

Glycolysis is a cytoplasmic pathway which breaks down glucose into three-carbon compounds called pyruvate and generates NADH and ATP. Glycolysis takes place in 10 steps as describe in Figure 20.

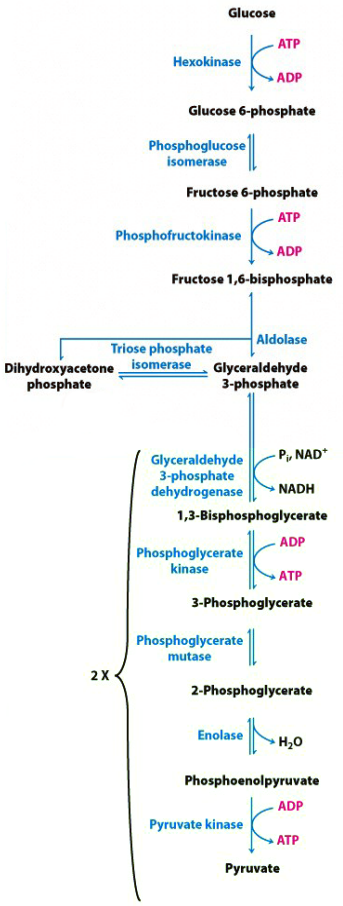

Figure 20. Enzymatic steps of the glycolysis pathway.

The whole pathway can be summarized in the following equation:

$$1 \text{ glucose} + 2 \text{ NAD}^+ + 2 \text{ ADP} \rightarrow 2 \text{ pyruvate} + 2 \text{ NADH} + 2 \text{ ATP} + 2 \text{ H}_20$$

Only three steps of the glycolysis are irreversible: hexokinase (HK), phosphofructokinase (PFK) and pyruvate kinase (PK) enzyme reactions. The other enzyme catalysed reversible reaction that take part

also to the gluconeogenesis process, the metabolic pathway that results in the generation of glucose from non-carbohydrate carbon substrates. In particular the PFK is the rate-limiting enzyme and it is inhibited by high ATP concentration and high citrate concentration (Chaudhry et al., 2019).

Glycolysis makes ATP (2 ATP are used but 4 ATP are produced) without the use of oxygen but can occurs in the presence of oxygen as well. In the aerobic respiration, the pyruvate formed from the pathway can be used in the Krebs cycle and go through oxidative phosphorylation to be oxidized into carbon dioxide and water.

Pentose phosphate pathway

Parallel to glycolysis there is an alternative pathway called oxidative pentose phosphate pathway (OPPP, Figure 21). It could be distinct in two phases: in first one, called the oxidative phase, NADPH is generated by irreversible reaction, in the second one 5-carbon sugars are synthetized by reversible reactions. For first glucose-6-phosphate (G6P) is oxidized to 6-phosphoglucolactone (6-PGL) by G6P-dehydrogenase (GDH), then it is further converted to 6-phosphogluconate (6-PG) and then to ribulose-5-phosphate (Ru5P), this is the oxidative phase that gives 2 NADPH molecules and 1 CO2 molecule per C6. The nonoxidative phase regenerates fructose-6-phosphate (Fru-6-P) and triose-phosphate (C3) from Ru5P (C5) (Johnson and Alric 2013).

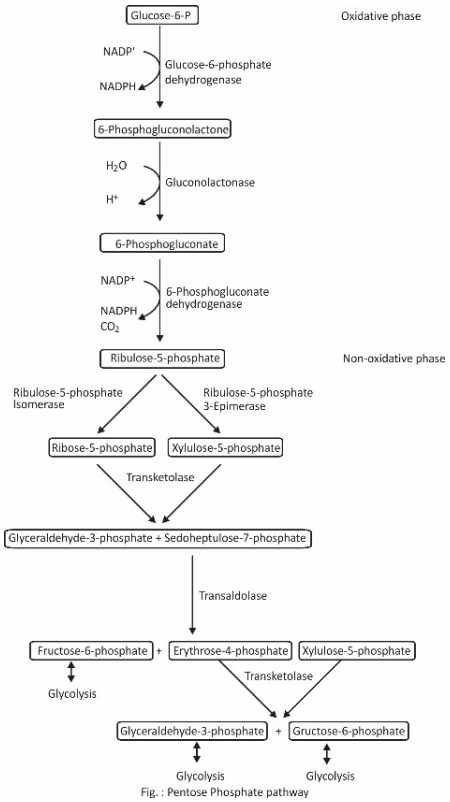

Figure 21. Enzymatic steps of the oxidative pentose phosphate pathway.

The main purpose of this pathway is the generation of reducing equivalents, in the form of NADPH, used in reductive biosynthesis, such as fatty acid synthesis. Moreover, it regulates the 5-carbon sugars pool that includes important molecules as ribose-5-phosphate used in the synthesis of nucleotides and erythrose-4-phosphate used in the synthesis of aromatic amino acids.

1.3.3 Krebs Cycle

The Krebs cycle (Krebs and Johnson 1980), also known as tricarboxylic acid (TCA) cycle or citric acid cycle, includes a series of reactions that lead to the complete oxidation of glucose derivatives to carbon dioxide. The Krebs cycle is the final common pathway for the oxidation of amino acids, fatty acids, and carbohydrates that enter is the cycle as acetyl-CoA. Moreover, the Krebs cycle produced building blocks for many important processes, including the synthesis of fatty acids, steroids, amino acids for building proteins, and the purines and pyrimidines. Thus, acetyl-CoA is a key metabolite of both catabolic and anabolic metabolism.

Under aerobic conditions, the pyruvate generated from glucose by glycolysis is oxidatively decarboxylated to form acetyl-CoA by the irreversible reaction of the pyruvate dehydrogenase complex (PDH, Figure 22). This multi-enzymatic complex is composed of three enzymes involving five cofactors and it controls the entrance of the cycle, for this reason it is under complex regulation by allosteric and covalent modification.

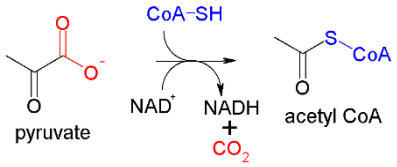

Figure 22. Reaction of the pyruvate dehydrogenase complex.

Acetyl-CoA enter in the Krebs cycle reacting with oxaloacetate to form citrate. The cycle includes eight major steps and the formation of oxaloacetate, the molecule used in the first step to preserve the cyclic character of the process, as show in Figure 23.

Summarizing the total reaction of the Krebs cycle is the following:

$$1 \text{ pyruvate} + 2H_2O + 3NAD^+ + 1FAD^{++} \rightarrow 3CO_2 + 4NADH + 1\ FADH_2$$

NADH and $FADH_2$ are then used during the oxidative phosphorylation to make ATP.

The crucial point during the cycle is the citrate synthetase enzyme that is mainly regulator. It is controlled by a lot of factor including the quantity of acetyl-CoA, oxalacetate, succinyl-CoA, ATP, NADH and citrate.

Glyoxylate cycle

Many bacteria, algae and plants are able to exploit acetate or other compounds that yield acetyl-CoA. They make use of a metabolic pathway that converts two-carbon acetyl units into four-carbon units (succinate). These reactions sequence, called the glyoxylate cycle (Figure 23), bypasses the two decarboxylation steps of the Krebs cycle. In particular, one key enzyme, isocitrate lyase, converts isocitrate to form succinate and glyoxylate. A second key enzyme, malate synthase, condenses glyoxylate and a second molecule of acetyl-CoA to form malate. The subsequent oxidation of malate regenerates the oxaloacetate. Thus, the succinate that was formed by isocitrate lyase can be withdrawn from the cycle and used for cell carbon biosynthesis. A key difference from the Krebs cycle is that two molecules of acetyl-CoA enter per turn of the glyoxylate cycle, compared with one in the Krebs cycle. The glyoxylate cycle allows to grow on acetate because the cycle bypasses the decarboxylation steps of the Krebs cycle.

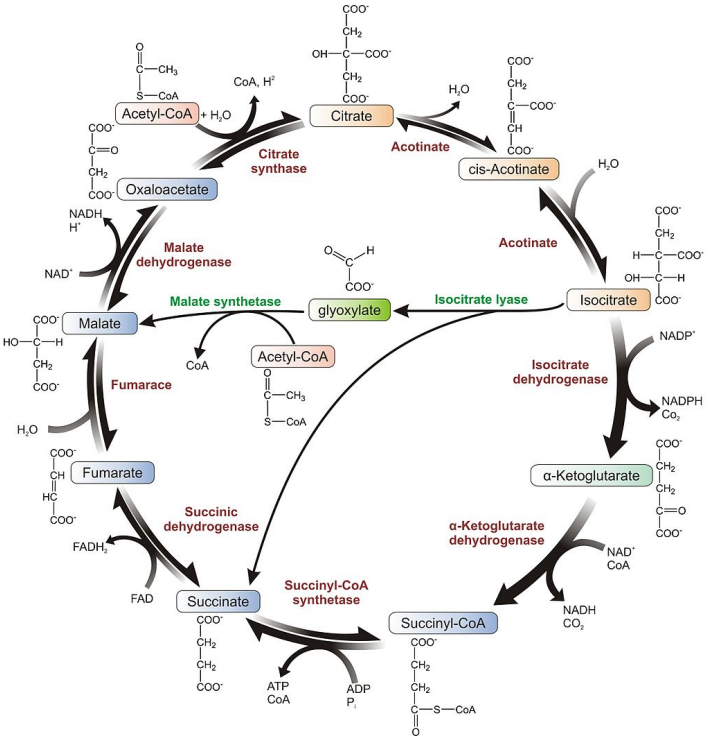

Figure 23. Krebs cycle and by-pass steps of the glyoxylate cycle.

1.3.4 Oxidative phosphorylation

The mitochondrial electron transport chain (mETC, Figure 24) is the site of oxidative phosphorylation. It uses reducing power generated from glycolysis, pyruvate dehydrogenase complex and Krebs cycle to establish an electrochemical transmembrane gradient that leads ATP synthesis.

The electron transport chain is composed of the ATP synthase complex (called also complex V) and four oxidoreductase complexes: the NADH dehydrogenase (complex I), the succinate dehydrogenase

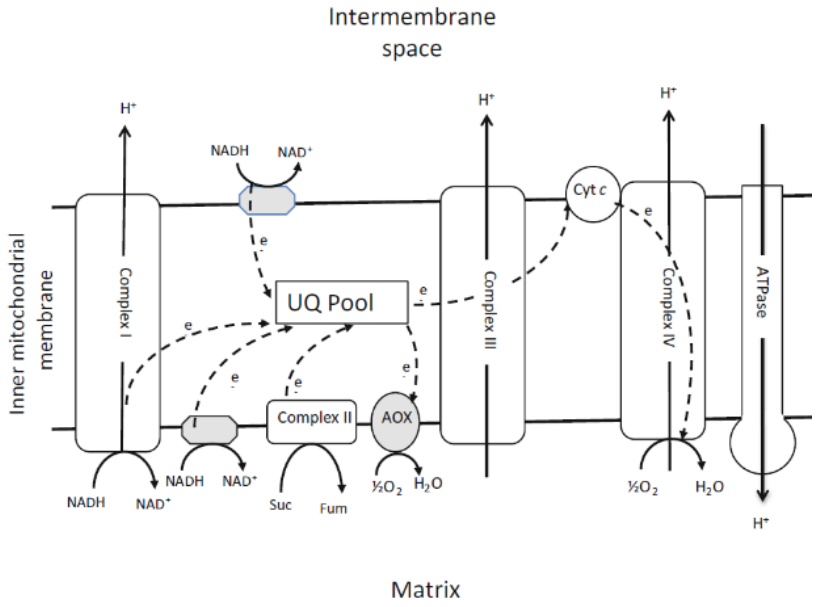

Figure 24. Schematic representation of the electron transport chain in the mitochondrion (Raven and Beardall, 2016).

(complex II), the cytochrome c reductase (complex III), and the cytochrome c oxidase (complex IV). All these complexes reside within the inner mitochondrial membrane.

Complexes I and II transfer electrons from NADH or $FADH_2$ onto ubiquinone, which freely diffuse within the inner mitochondrial membrane until the complex III. Indeed, it transfers electrons from ubiquinol to cytochrome c. This small protein is localized in the space between the outer and inner mitochondrial membrane. Finally, complex IV transfers electrons from cytochrome c onto molecular oxygen. Three of the four oxidoreductase complexes couple electron transport with translocation of protons from the mitochondrial matrix to the intermembrane space generating a proton gradient that is used by complex V to catalyse the formation of ATP by the phosphorylation of ADP (Boekema and Braun 2007).

In addition, could be present an alternative oxidase (AOX) that directly couples the oxidation of ubiquinol with the reduction of O_2 to H_2O. AOX introduces a branch in the mETC such that electrons in ubiquinol are partitioned between the cytochrome pathway (complex III, cyt c, complex IV) and AOX. AOX dramatically reduces the energy (ATP) yield of respiration since it is not proton pumping and since electrons flowing to AOX bypass the proton pumping complexes III and IV. These enzymes are considered to form the basis of an overflow protection mechanism for the respiratory chain under certain physiological conditions, *e.g.* high light conditions (Vanlerberghe 2013).

1.4 Energy reserve in green algae

Algae have two main types of energy reserves: starch (or other polyglucans) and lipids. Green algae utilized starch, however in diatoms there is chrysolaminarin, in red algae floridean starch and glycogen and in euglenophytes paramylon.
Starch, in general, and lipids serve as energy source and as a supply of carbon allowing the cells to become completely independent of a direct supply of energy and carbon from photosynthetic activity.

1.4.1 Lipid metabolism

Lipids constitute an important part of the algae biomass, reaching until the 90% of the dry weight (Chen and Jiang 2017). Moreover, microalgae lipids are interesting as a source of valuable nutritional ingredients, such as long-chain polyunsaturated fatty acids (LC-PUFA, *e.g.* EPA and DHA) and as precursors for biodiesel production. However, given the huge diversity of microalgae and their distinct evolutionary history, lipids metabolism and composition vary substantially among microalgae world.

The major lipid classes are membrane lipids and storage lipids, in the form of triacylglycerol (TAG); other lipid classes, present in small amount, comprise terpenoids, sphingolipids, hydrocarbons and sterols. Among the membrane lipids we found glycosylglycerides, mainly monogalactosyldiacylglycerol (MGDG), digalactosyldiacylglycerol (DGDG) and sulphoquinovosyldiacylglycerol (SQDG); betaine lipids, as diacylglyceryl-O-(N,N,N-trimethyl)-homoserine (DGTS), 1,2-diacylglyceryl-3-O-2'(hydroxymethyl)-(N,N,N-trimethyl)-beta-alanine (DGTA) and diacylglycerylcarboxylhydroxymethylcholine (DGCC); and phosphoglycerides, principally phosphatidylcholine (PtdCho), phosphatidylethanolamine (PtdEtn) and phosphatidylglycerol (PtdGro). MGDG, DGDG, SQDG together with phospholipid phosphatidylglycerol (PG) are the main chloroplast lipids.

De novo fatty acid biosynthesis

De novo fatty acid biosynthesis occurs in the stroma of the chloroplast and requires carbon in the form of acetyl-CoA, energy (ATP) and reducing power (NADPH). In algae grown photoautotrophically acetyl-CoA is mostly produced by the oxidative decarboxylation of pyruvate through the PDH enzyme (Figure 22), other sources are the direct conversion of acetate through acetyl-CoA synthetase (ACS) or the cleavage of citrate by ATP-citrate lyase (ACL).

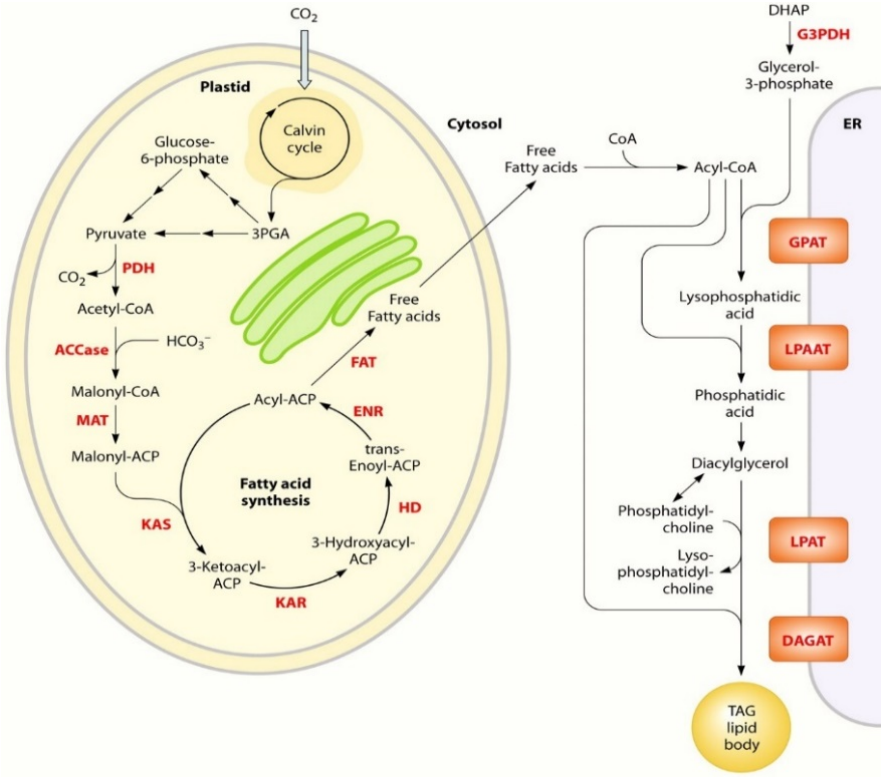

Figure 25. Representative pathways in microalgal lipid biosynthesis shown in black and enzymes shown in red. ACCase, acetyl-CoA carboxylase; ACP, acyl carrier protein; CoA, coenzyme A; DAGAT, diacylglycerol acyltransferase; DHAP, dihydroxyacetone phosphate; ENR, enoyl-ACP reductase; FAT, fatty acyl-ACP thioesterase; G3PDH, gycerol-3-phosphate dehydrogenase; GPAT, glycerol-3-phosphate acyltransferase; HD, 3-hydroxyacyl-ACP dehydratase; KAR, 3-ketoacyl-ACP reductase; KAS, 3-ketoacyl-ACP synthase; LPAAT, lyso-phosphatidic acid acyltransferase; LPAT, lyso-phosphatidylcholine acyltransferase; MAT, malonyl-CoA:ACP transacylase; PDH, pyruvate dehydrogenase complex; TAG, triacylglycerols (Radakovits et al. 2010).

The first step of the fatty acid biosynthesis (Figure 25) is the carboxylation of acetyl-CoA to produce malonyl-CoA by the acetyl-CoA carboxylase (ACCase). The malonyl-CoA is then converted to malonyl-acyl carrier protein (ACP) that is then ligated to an acetyl-CoA to form a 3-ketoacyl-ACP. This enter in a cycle in which is reduced, dehydrated and reduced again until 6-carbon-ACP is formed. The enzymes involved in this cycle (KAS, KAR, HD, ENR) collectively form the fatty acid synthase (FAS). Termination of the chain elongations is carried out by an acyl-ACP thioesterase (FAT or TE) which hydrolyses acyl-ACP to form free fatty acids and ACP (Li-Beisson et al. 2019). The neo-synthesized FAs are usually further elongated in the endoplasmic reticulum (ER), instead a fraction of the acyl-ACPs are used in plastids for the generation of phosphatidic acid (PA) by the acylation of glycerol-3-phospate (G3P). PA is a key intermediate for the formation of PG, moreover PA can be dephosphorylated to generate diacylglycerol (DAG). DAGs are used for the formation of thylakoid glycolipids including galactolipids, MGDG, DGDG and SQDG in the plastid envelope membranes. The free fatty acid exported from the plastid enter into glycerolipid biosynthetic pathways in the ER, leading to the formation of DAGs. These are used to synthesize extraplastidic membrane lipids

including phosphatidylcholine (PC), phosphatidylethanolamine (PE) and DGTS. Some phospholipids can return to the plastid, for the synthesis of thylakoid glycolipids. DAGs are also used for the TAG synthesis that are packaged in oil droplets in the cytosol. In particular TAG synthesis is catalysed by diacylglycerol:acyl-CoA acyltransferases (DAGATs) using acyl-CoA and DAG or by phospholipid:diacylglycerol acyltransferase (PDAT), which use phospholipids as acyl donor and DAG as acyl acceptor (Xu et al., 2016).

Lipid catabolism

Lipid catabolism plays an important role in microalgae indeed cells rapidly remodel or degrade storage lipids to face changes in temperature, light and/or nutrient conditions, ensuring cells survival and growth. Nitrogen starvation is one of the stronger stress related to lipid metabolism, indeed N depletion trigger accumulation of TAG in the lipid droplet, partly synthesising *de novo* FA and partly recycling membrane lipids, by contrast, N resupply causes massive degradation of the TAGs and resynthesise of membrane lipids.

Fatty acid degradation is an oxidative process that produce acetyl-CoA. It requires highly specialized enzyme called lipases and involves trafficking of FA released from all organelles to peroxisomes. FA has to be activated to its CoA ester then, in the form of acyl-CoA, are ready for the oxidative attack at the β-carbon position, starting the fatty acid β-oxidation. The location of FA β-oxidation varies extensively in microalgae occurring either in the peroxisome, the mitochondrion or both. The core reactions of FA β-oxidation require a cyclic reaction of four enzymatic steps: oxidation, hydration, dehydrogenation and thiolytic cleavage of an acyl-CoA. An acetyl-CoA is cleaved off the acyl-CoA each round of the β-oxidation. The end product is acetyl-CoA, H_2O_2 and NADH. Acetyl units are usually utilized through the glyoxylate cycle after the synthesis of 4-carbon compounds as succinate. That can enters the Krebs cycle in mitochondria, releasing malate which can be converted to hexose and sucrose in the cytosol via gluconeogenesis (Kong et al. 2018; Li-Beisson et al. 2019).

1.4.2 Starch metabolism

Starch is a polysaccharide that constitute the storage form of carbohydrate in plastids. It is composed of amylopectin, a branched chain of glucose units, that is the major component of starch, and amylose, which can be helical or linear.

The substrate for starch synthesis (Figure 26, A) is the activated glucosyl donor, ADP-Glucose (ADPGlc). In particular, fructose-6-phosphate (Fru6P), an intermediate of the Calvin Cycle, is converted to glucose-6-phosphate (Glc6P) and then into glucose-1-phosphate (Glc1P) that is, finally,

converts into ADPGlc and inorganic pyrophosphate by an ADP-glucose pyrophosphorylase (AGPase). Then starch synthases (SSs) enzymes catalyze the elongation of glucans transferring the glucosyl moiety from the sugar nucleotide to the non-reducing end of the growing polyglucan chain. Soluble SSs forms are involved in amylopectin synthesis, whereas the granule-bound starch synthase (GBSS) forms participate in amylose synthesis. Branching enzymes (BEs) and isoamylase (ISA) enzymes cleave linear glucose chain and transfer the cleaved portion to a glucose residue to form branches allowing the granule crystallization.

Starch is degraded (Figure 26, B) by hydrolysis of the constituent glucans to maltose and glucose. For first, glucan water dikinase (GWD) and phosphoglucan water dikinase (PWD) phosphorylate the surface of the starch granule, making it accessible for β-amylase action that hydrolyse the linear chains. Then is required a debranching enzyme (DBE) enzyme that release malto-oligosaccharides. Starch is also metabolized to branched glucans by α-amylase and to linear glucans by α-amylase, ISA3, and pullulanase. These linear glucans are further metabolized through β-amylase to maltose, through a debranching enzyme (DPE) to glucose or through starch phosphorylase to glucose-1-phosphate. Maltose and glucose are then transported from chloroplast to cytosol (Busi et al. 2014; Zeeman, Kossmann, and Smith 2010).

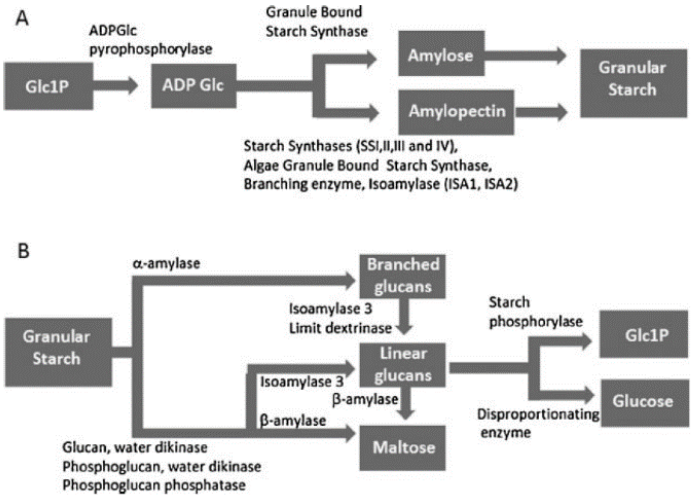

Figure 26. Starch synthesis (A) and degradation (B) pathways in chloroplasts (Busi et al. 2014).

1.4.3. Regulation of the carbon flux into the cell: organelle communication

The photosynthetic process produces NADPH and ATP that are subsequently used to drive CO_2 assimilation via the Calvin-Benson cycle. Thus, global outputs of photosynthesis are triose phosphate, *i.e.* glyceraldehyde 3-phosphate (GA3P), reducing equivalents (NADPH) and phosphorylating power (ATP). These three compounds support all activities in a cell. The efficient production, management and partition of the three major photosynthetic products (C, ATP and NADPH) are essential. Cell membranes are not permeable to these molecules, therefore coordinating NAD(P)H and ATP levels

between various subcellular compartments requires specific trafficking mechanisms. Communication between organelles is critical for survival of photosynthetic organisms (Burlacot, Peltier, and Li-beisson 2019).

Into details, a shared metabolite pool between chloroplast and mitochondrion can maintains a sink for excess reducing equivalents and a source for additional ATP. These are needed to sustain carbon fixation and protect the photosynthetic electron transport chain from damage by over-reduction of the chloroplast (Erickson et al. 2015). In addition to chloroplasts and mitochondria, peroxisomes are a third subcellular compartment involved in energetic metabolism. Indeed, NADH is produced by β-oxidation of fatty acids.

Communication among chloroplast, mitochondrion and peroxisome is summarized in Figure 27.

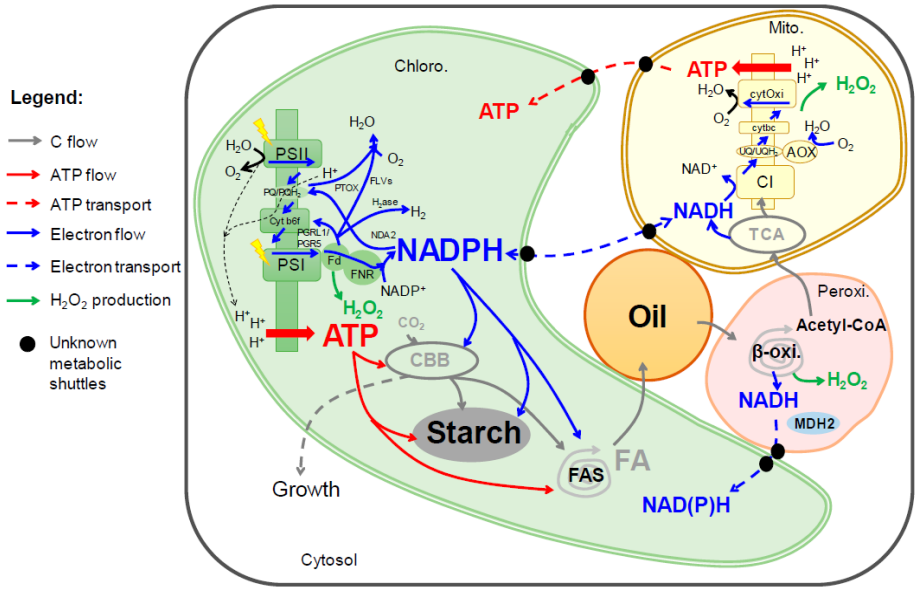

Figure 27. Schematic view of the regulation of the ATP/NADPH pool in *Chlamydomonas reinhardtii* (Burlacot, Peltier, and Li-beisson 2019).

For *Chlamydomonas reinhardtii* several shuttles have been proposed include: the ADP/ATP translocator, malate/oxaloacetate or malate/aspartate shuttle or triose phosphate translocator. In particular, malate dehydrogenase (MDH) catalyses the reversible oxidation of NAD(P)H to $NAD(P)^+$, oxidizing malate to oxaloacetate (OAA) in the meantime. Malate or OAA can be shuttled across subcellular membranes by metabolite transporters. MDH transporter are involved both in the chloroplast-mitochondrion communication that in the chloroplast-peroxisomal communication. Another shuttle is the dihydroxyacetone 3–phosphate (DHAP)/3–phosphoglycerate (3–PGA) shuttle. DHAP export coupled with its oxidation to 3–PGA generates NADH (or NADPH) for respiratory energy production. The rate of shuttling depends on the rate at which chloroplastic 3–PGA is reduced and cytosolic DHAP is oxidized (Hoefnagel, Atkin, and Wiskich 1998).

1.5 Strategies to improve microalgae strain

In the past, in order to improve microalgae applicability, in terms of biomass yield and synthesis of high-value product, the aim was to enhance photo-bioreactor design, reduce energy consumption for microalgae harvesting and enhance the extraction techniques for high-value compounds. In the recent years, the rapid development of molecular biotechnology, from whole genome sequencing to gene editing techniques, expanded the aim to genetic, systematic and synthetic engineering. In particular, the availability of genome and its functional annotation allow the reconstruction of genome-scale metabolic networks. These lead to hypothesis to iteratively guide experiments to further improve knowledge of alga's biology and help the metabolic engineering to enhanced features of interest (Figure 28). Thus, the application of genome scale data, together to the omics technologies, are becoming fundamental on the development of hypothesis-driven research in algae biotechnologies.

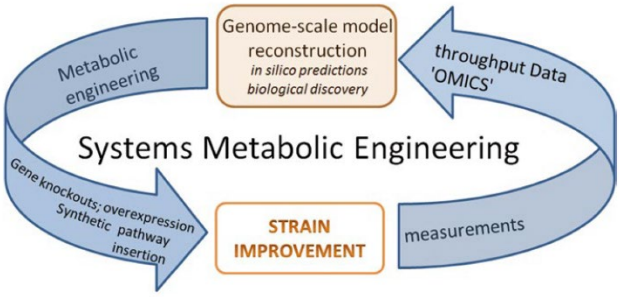

Figure 28. Relationship between -omics and strain improvement (Dal'Molin et al. 2016).

For these reasons, omics data are gathering more and more interest, so much that we talk of 'algomics', defines as the study of microalgal cell metabolism using omics technologies such as genomics, transcriptomics, proteomics, and metabolomics (Salama et al. 2019). The significant advances in the next-generation sequencing technology allow to obtain high throughput data with low cost, facilitating the rapid accumulation of genomic sequences that provide data to apply omics technology. In Nov. 2018 the number of public available algal sequenced genomes was estimated to be 40–60. Most of them belong to the division of Chlorophyta, instead the second most populous group of microalgae with sequenced genomes are diatoms (Fu et al. 2019). Similarly, several organelles, including mitochondria and plastid, have also been sequenced in microalgae. Integration of different 'omics' datasets with the evidence of functional role of genes give insight into biochemical and regulatory networks to understand and control microalgal physiology and metabolic pathways. Moreover, these omics data enable application of gene editing technologies. Indeed, the

CRISPR system allows to perform precise gene manipulation, but genomic information is necessary. Currently, this technique was applied only in few algae species, as *Chlamydomonas reinhardtii* (Baek et al. 2018), *Nannochloropsis* species (Ajjawi et al. 2017; Naduthodi et al. 2019) and *P. tricornutum* (diatom, Nymark et al. 2016). To date, conventional bioengineering approaches relying on random insertion of transgenes, allowing reverse genetics studies of gene function or the expression of gene of interest. The last available approach to generate mutants is the random mutagenesis by physical methods (UV-light, γ- and X-rays) or chemical mutagens, *e.g.* N'-nitro-N nitrosoguanidine (NTG) and ethyl methanesulfonate (EMS). In this case, lots of single nucleotide polymorphisms (SNPs) are accumulates in the same mutant, making difficult to understand what is gene/genes responsible for a phenotype or leading to lethal mutations. The advantages are that transformation protocols as well as genomic information are not necessary, moreover it avoids restrictions to GMO for outdoor production system.

State of art in order to improve carbon use efficiency

Algal biomass basically has three major components: lipids, proteins, and carbohydrates (Figure 29). Proteins are the main component of most algae species (30-71% on a dry basis), carbohydrates concentration ranges from 4% to 58% on a dry basis and lipids concentration range between 2% and 19% in most species, but can reach 80–85% in some cases (Bhujade et al. 2017). The Krebs cycle is a crucial metabolic pathway that links carbohydrate, lipid, and protein metabolism, but how algae control carbon partitioning is not yet fully understood. It's important to consider that improved carbon use efficiency leads to increase not only in the total biomass productivity, but also change the

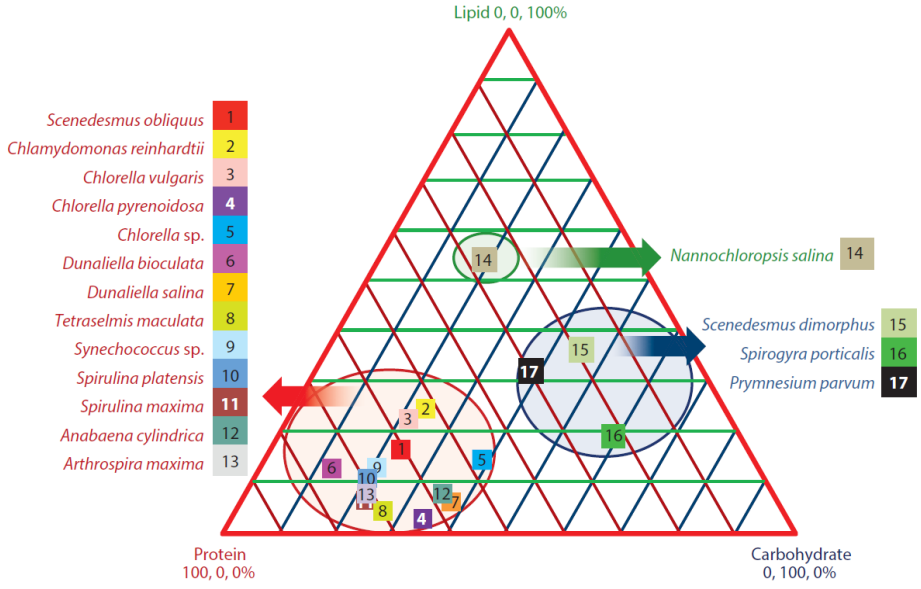

Figure 29. Lipid, protein, and carbohydrate composition of various algae (Bhujade et al. 2017)

algae composition, two aspects that are closely interlinked with the photosynthetic efficiency and that are critical to reach the prefixed goals. For example, starch can be fermented to bioethanol, instead lipids can be transesterificated to produce biodiesel, and finally protein can be useful in feed and food supplements. Increasing of algal biomass can be induced, either by controlling environment conditions or by introducing genetic modifications.

Growth conditions are key factors to increase biomass yield. Each species has specific needs in term of light, nutrients, temperature and pH that must be optimized. The induction of some stress alters biochemical pathways leading to the accumulation of specific products, for example N-starvation is widely used strategy to increase lipid accumulation. Indeed, cells redirect carbon skeleton from proteins into pyruvate, the central carbon metabolism intermediate, which could be used to synthetized lipids. However, N-starvation also leads to growth retardation or even cell death. Another possibility is supplying carbon sources as glucose, glycerol or acetate in a heterotrophic or mixotrophic growth, indeed several microalgae are able to growth using different organic substrate. This overcome the limitations due to light availability increasing the biomass yield but adding extra production costs.

Regarding genetic modification, metabolic pathways inside algal cells can be altered to increase the production of carbohydrates, lipids, and other important compounds of interest. For example, Ajjawi et al. 2017 generates CRISPR-cas9 mutant of *Nannochloropsis gaditana,* which accumulated about double lipid content compared to WT strain by alteration of a transcription factor that redirect the metabolism from proteins to lipid synthesis. In *C. reinhardtii* mutants of phosphoenolpyruvate carboxylase (PEPC) showed an increased total fatty acids production due to the redirection of carbon flux through lipid biosynthesis. Indeed, PEPC catalyses the conversion of PEP in oxalacetate that can enter in Krebs cycle providing substrates for protein biosynthesis. Thus, in the knock-down mutants the blockage of flux towards TCA pathway redirect carbon flux to lipid production. This was confirmed by an over-expression mutants of *CrPEPC1* gene in which was observed an increased carbon flux to the TCA, but not to fatty acid synthesis (Deng et al. 2014; Wang et al. 2017).

Pinto et al. 2013 increased production of a metabolite of interest, hydrogen, engineering *C. reinhardtii* strain with a lower rubisco levels, activity and stability. Rubisco normally plays a key role in the Calvin cycle that is the main competitor for the reducing power required by hydrogenases. On the other hand, rubisco inefficiency is a main limiting step for CO_2 fixation rate and thus for biomass yield. Rubisco has been studied intensively and is a prime target for genetic engineering to improve photosynthetic efficiency. The main strategies adopted were the direct engineering of rubisco by targeted and random mutagenesis, directed evolution and overexpression in cyanobacteria and tobacco (Wei et al. 2017). However, these efforts were limited by the difficulty of simultaneously

elevating catalytic rate and substrate specificity of rubisco. Other strategy was applied by Wei et al. 2017 that overexpressed a rubisco activase gene in *N. oceanica*, enhancing photosynthesis and improving productivity of both biomass (+46%) and lipids (+41%).

Another strategy to increased biomass yield is improve the utilization of the light source: a huge problem in the microalgae cultivation is the cell shading. Indeed, cells in the layers close to the light receive an excess light energy, instead cells in the inner layers receive an insufficient irradiation. This cause photoinhibition in the external layer and photolimitation in the inner layer, reducing the growth rate and the overall productivity. To address this issue, one approach is reducing the light-harvesting complexes of cells. This strategies was applied for *Chlamydomonas* for which several mutants were generated (Jeong et al. 2017; Kirst et al. 2012; Perrine, Negi, and Sayre 2012), but also in the non-model species of the *Chlorella* genus. Both for *C. vulgaris* (Dall'Osto et al. 2019) and *C. sorokiniana* (Cazzaniga et al. 2014) chemical mutants with a reduction in the antenna systems were selected, showing an increased biomass of 68% and 30%, respectively, compared to WT strain. Another strategy is enhancing light utilization by altering the light composition. Fu et al. 2017 expressed an enhanced green fluorescent protein (eGFP) in the model diatom *Phaeodactylum tricornutum*, allowing absorption of excess blue light and its intracellular emission in the green spectral band. The engineered *P. tricornutum* achieved 28% higher efficiency in photosynthesis than the parental strain. Further, its reaches 50% more biomass production rate respect to its WT strain under simulated outdoor sunlight conditions.

Understanding carbon metabolism and energy conversion mechanisms in microalgae is the first step to achieve significant progress in yields to make microalgae competitive in the market for the production of biofuels and bioproducts of interest.

1.6 References

Ajjawi, Imad, John Verruto, Moena Aqui, Leah B. Soriaga, Jennifer Coppersmith, Kathleen Kwok, Luke Peach, Elizabeth Orchard, Ryan Kalb, Weidong Xu, Tom J. Carlson, Kristie Francis, Katie Konigsfeld, Judit Bartalis, Andrew Schultz, William Lambert, Ariel S. Schwartz, Robert Brown, and Eric R. Moellering. 2017. "Lipid Production in *Nannochloropsis gaditana* Is Doubled by Decreasing Expression of a Single Transcriptional Regulator." *Nature Biotechnology*.

Baek, Kwangryul, Jihyeon Yu, Jooyeon Jeong, Sang Jun Sim, Sangsu Bae, and Eon Seon Jin. 2018. "Photoautotrophic Production of Macular Pigment in a *Chlamydomonas Reinhardtii* Strain Generated by Using DNA-Free CRISPR-Cas9 RNP-Mediated Mutagenesis." *Biotechnology and Bioengineering*.

Bennoun, P. 1982. "Evidence for A Respiratory-Chain in the Chloroplast." *Proceedings of the National Academy of Sciences of the United States of America-Biological Sciences* 79(14):4352–56.

Benson, A. A. and M. Calvin. 1950. "Carbon Dioxide Fixation by Green Plants." *Annual Review of Plant Physiology and Plant Molecular Biology* 1:25–42.

Bhujade, Ramesh, Mandan Chidambaram, Avnish Kumar, and Ajit Sapre. 2017. "Algae to Economically Viable Low-Carbon-Footprint Oil." *Annual Review of Chemical and Biomolecular Engineering* 8(1):335–57.

Boekema, Egbert J. and Hans Peter Braun. 2007. "Supramolecular Structure of the Mitochondrial Oxidative Phosphorylation System." *Journal of Biological Chemistry* 282(1):1–4.

Bouvier, F., A. d'Harlingue, P. Hugueney, E. Marin, A. Marion-Poll, and B. Camara. 1996. "Xanthophyll Biosynthesis. Cloning, Expression, Functional Reconstitution, and Regulation of Beta-Cyclohexenyl Carotenoid Epoxidase from Pepper (*Capsicum Annuum*)." *The Journal of Biological Chemistry* 271(46):28861–67.

Burlacot, Adrien, Gilles Peltier, and Yonghua Li-beisson. 2019. "Subcellular Energetics and Carbon Storage in *Chlamydomonas*." (Figure 1):1–15.

Busi, María V., Julieta Barchiesi, Mariana Martín, and Diego F. Gomez-Casati. 2014. "Starch Metabolism in Green Algae." *Starch/Staerke* 66(1–2):28–40.

Cazzaniga, Stefano, Luca Dall'Osto, Joanna Szaub, Luca Scibilia, Matteo Ballottari, Saul Purton, and Roberto Bassi. 2014. "Domestication of the Green Alga *Chlorella Sorokiniana*: Reduction of Antenna Size Improves Light-Use Efficiency in a Photobioreactor." *Biotechnology for Biofuels*.

Chaudhry R, Varacallo M. Biochemistry, Glycolysis. In: StatPearls [Internet]. Treasure Island (FL): StatPearls Publishing; 2019 Jan.

Chen, Hao Hong and Jian Guo Jiang. 2017. "Lipid Accumulation Mechanisms in Auto- and Heterotrophic Microalgae." *Journal of Agricultural and Food Chemistry* 65(37):8099–8110.

Dal'Molin C.G.O., Nielsen L.K. (2016) Algae Genome-Scale Reconstruction, Modelling and Applications. In: Borowitzka M., Beardall J., Raven J. (eds) The Physiology of Microalgae. Developments in Applied Phycology, vol 6. Springer, Cham

Dall'Osto, Luca, Stefano Cazzaniga, Zeno Guardini, Simone Barera, Manuel Benedetti, Giuseppe Mannino, Massimo E. Maffei, and Roberto Bassi. 2019. "Combined Resistance to Oxidative Stress and Reduced Antenna Size Enhance Light-to-Biomass Conversion Efficiency in *Chlorella vulgaris* Cultures." *Biotechnology for Biofuels* 12(1):1–17.

Dang, Kieu-Van, Julie Plet, Dimitri Tolleter, Martina Jokel, Stéphan Cuiné, Patrick Carrier, Pascaline Auroy, Pierre Richaud, Xenie Johnson, Jean Alric, Yagut Allahverdiyeva, and Gilles Peltier. 2014. " Combined Increases in Mitochondrial Cooperation and Oxygen Photoreduction Compensate for Deficiency in Cyclic Electron Flow in *Chlamydomonas Reinhardtii*." *The Plant Cell* 26(7):3036–50.

Deng, Xiaodong, Jiajia Cai, Yajun Li, and Xiaowen Fei. 2014. "Expression and Knockdown of the PEPC1 Gene Affect Carbon Flux in the Biosynthesis of Triacylglycerols by the Green Alga *Chlamydomonas Reinhardtii*." *Biotechnology Letters*.

Drop, Bartlomiej, Mariam Webber-Birungi, Fabrizia Fusetti, Roman Kouřil, Kevin E. Redding, Egbert J. Boekema, and Roberta Croce. 2011. "Photosystem I of *Chlamydomonas reinhardtii* Contains Nine Light-Harvesting Complexes (Lhca) Located on One Side of the Core." *The Journal of Biological Chemistry* 286(52):44878–87.

Erickson, Erika, Setsuko Wakao, and Krishna K. Niyogi. 2015. "Light Stress and Photoprotection in *Chlamydomonas reinhardtii*." *Plant Journal* 82(3):449–65.

Fu, Weiqi, Amphun Chaiboonchoe, Basel Khraiwesh, Mehar Sultana, Ashish Jaiswal, Kenan Jijakli, David R. Nelson, Ala'a Al-

Hrout, Badriya Baig, Amr Amin, and Kourosh Salehi-Ashtiani. 2017. “Intracellular Spectral Recompositioning of Light Enhances Algal Photosynthetic Efficiency.” *Science Advances* 3(9):1–12.

Fu, Weiqi, David R. Nelson, Alexandra Mystikou, Sarah Daakour, and Kourosh Salehi-Ashtiani. 2019. “Advances in Microalgal Research and Engineering Development.” *Current Opinion in Biotechnology* 59:157–64.

Gao, Jinlan, Hao Wang, Qipeng Yuan, and Yue Feng. 2018. “Structure and Function of the Photosystem Supercomplexes.” *Frontiers in Plant Science* 9(March):1–7.

Gilmore, A. M. and H. Y. Yamamoto. 1992. “Dark Induction of Zeaxanthin-Dependent Nonphotochemical Fluorescence Quenching Mediated by ATP.” *Proceedings of the National Academy of Sciences of the United States of America* 89(5):1899–1903.

Hoefnagel, Marcel H. N., Owen K. Atkin, and Joseph T. Wiskich. 1998. “Interdependence between Chloroplasts and Mitochondria in the Light and the Dark.” *Biochimica et Biophysica Acta - Bioenergetics* 1366(3):235–55.

Jans, Frédéric, Emmanuel Mignolet, Pierre Alain Houyoux, Pierre Cardol, Bart Ghysels, Stéphan Cuiné, Laurent Cournac, Gilles Peltier, Claire Remacle, and Fabrice Franck. 2008. “A Type II NAD(P)H Dehydrogenase Mediates Light-Independent Plastoquinone Reduction in the Chloroplast of *Chlamydomonas*.” *Proceedings of the National Academy of Sciences of the United States of America* 105(51):20546–51.

Jeong, Jooyeon, Kwangryul Baek, Henning Kirst, Anastasios Melis, and Eon Seon Jin. 2017. “Loss of CpSRP54 Function Leads to a Truncated Light-Harvesting Antenna Size in *Chlamydomonas reinhardtii*.” *Biochimica et Biophysica Acta - Bioenergetics*.

Johnson, Xenie and Jean Alric. 2013. “Central Carbon Metabolism and Electron Transport in *Chlamydomonas reinhardtii*: Metabolic Constraints for Carbon Partitioning between Oil and Starch.” *Eukaryotic Cell*.

Kirst, Henning, Jose Gines Garcia-Cerdan, Andreas Zurbriggen, Thilo Ruehle, and Anastasios Melis. 2012. “Truncated Photosystem Chlorophyll Antenna Size in the Green Microalga *Chlamydomonas reinhardtii* upon Deletion of the TLA3-CpSRP43 Gene.” *Plant Physiology*.

Kong, Fantao, Ismael Torres Romero, Jaruswan Warakanont, and Yonghua Li-Beisson. 2018. “Lipid Catabolism in Microalgae.” *New Phytologist* 218(4):1340–48.

Krebs, H. A. and W. A. Johnson. 1980. “The Role of Citric Acid in Intermediate Metabolism in Animal Tissues.” *FEBS Letters* 117(August):K2–10.

Li-Beisson, Yonghua, Jay J. Thelen, Eric Fedosejevs, and John L. Harwood. 2019. “The Lipid Biochemistry of Eukaryotic Algae.” *Progress in Lipid Research* 74(January):31–68.

Lin, Way-Rong, Shih-I. Tan, Chuan-Chieh Hsiang, Po-Kuei Sung, and I. Son Ng. 2019. “Challenges and Opportunity of Recent Genome Editing and Multi-Omics in Cyanobacteria and Microalgae for Biorefinery.” *Bioresource Technology* 291(June):121932.

Maul, J. E., J. W. Lilly, L. Cui, C. W. dePamphilis, W. Miller, E. H. Harris, and D. B. Stern. 2002. “The *Chlamydomonas reinhardtii* Plastid Chromosome: Islands of Genes in a Sea of Repeats.” *Plant Cell* 14(1040-4651 (Print)):2659–79.

Minagawa, Jun and Ryutaro Tokutsu. 2015. “Dynamic Regulation of Photosynthesis in *Chlamydomonas reinhardtii*.” *Plant Journal* 82(3):413–28.

Naduthodi, Mihris Ibnu Saleem, Prarthana Mohanraju, Christian Südfeld, Sarah D’Adamo, Maria J. Barbosa, and John Van Der Oost. 2019. “CRISPR-Cas Ribonucleoprotein Mediated Homology-Directed Repair for Efficient Targeted Genome Editing in Microalgae *Nannochloropsis oceanica* IMET1.” *Biotechnology for Biofuels*.

Nagy, Gergely, Renáta Ünnep, Ottó Zsiros, Ryutaro Tokutsu, Kenji Takizawa, Lionel Porcar, Lucas Moyet, Dimitris Petroutsos, Gyozo Garab, Giovanni Finazzi, and Jun Minagawa. 2014. “Chloroplast Remodeling during State Transitions in *Chlamydomonas reinhardtii* as Revealed by Noninvasive Techniques in Vivo.” *Proceedings of the National Academy of Sciences of the United States of America* 111(13):5042–47.

Nakamura Yonghua Li-Beisson Editors, Yuki. n.d. *Subcellular Biochemistry 86 Lipids in Plant and Algae Development*.

Neilson, Jonathan A. D. and Dion G. Durnford. 2010. “Structural and Functional Diversification of the Light-Harvesting Complexes in Photosynthetic Eukaryotes.” *Photosynthesis Research* 106(1–2):57–71.

Nymark, Marianne, Amit Kumar Sharma, Torfinn Sparstad, Atle M. Bones, and Per Winge. 2016. “A CRISPR/Cas9 System Adapted for Gene Editing in Marine Algae.” *Scientific Reports*.

Pagliano, Cristina, Guido Saracco, and James Barber. 2013. “Structural, Functional and Auxiliary Proteins of Photosystem II.”

Photosynthesis Research 116(2–3):167–88.

Pan, Xiaowei, Peng Cao, Xiaodong Su, Zhenfeng Liu, and Mei Li. 2019. "Structural Analysis and Comparison of Light-Harvesting Complexes I and II." *Biochimica et Biophysica Acta (BBA) - Bioenergetics* (June):0–1.

Paulsen, H., B. Finkenzeller, and N. Kühlein. 1993. "Pigments Induce Folding of Light-Harvesting Chlorophyll a/b-Binding Protein." *European Journal of Biochemistry / FEBS* 215(3):809–16.

Perrine, Zoee, Sangeeta Negi, and Richard T. Sayre. 2012. "Optimization of Photosynthetic Light Energy Utilization by Microalgae." *Algal Research*.

Pinto, T. S., F. X. Malcata, J. D. Arrabaça, J. M. Silva, R. J. Spreitzer, and M. G. Esquível. 2013. "Rubisco Mutants of *Chlamydomonas reinhardtii* Enhance Photosynthetic Hydrogen Production." *Applied Microbiology and Biotechnology*.

Popescu, Cristina E. and Robert W. Lee. 2007. "Mitochondrial Genome Sequence Evolution in *Chlamydomonas*." *Genetics* 175(2):819–26.

Radakovits, Randor, Robert E. Jinkerson, Al Darzins, and Matthew C. Posewitz. 2010. "Genetic Engineering of Algae for Enhanced Biofuel Production." *Eukaryotic Cell* 9(4):486–501.

Raven J.A., Beardall J. (2016) Dark Respiration and Organic Carbon Loss. In: Borowitzka M., Beardall J., Raven J. (eds) The Physiology of Microalgae. Developments in Applied Phycology, vol 6. Springer, Cham

Salama, El Sayed, Sanjay P. Govindwar, Rahul V. Khandare, Hyun Seog Roh, Byong Hun Jeon, and Xiangkai Li. 2019. "Can Omics Approaches Improve Microalgal Biofuels under Abiotic Stress?" *Trends in Plant Science* 24(7):611–24.

Salomé, Patrice A. and Sabeeha S. Merchant. 2019. "A Series of Fortunate Events: Introducing *Chlamydomonas* as a Reference Organism." *The Plant Cell* 31(8):1682–1707.

Shen, Liangliang, Zihui Huang, Shenghai Chang, Wenda Wang, Jingfen Wang, Tingyun Kuang, Guangye Han, Jian-Ren Shen, and Xing Zhang. 2019. "Structure of a $C_2S_2M_2N_2$-Type PSII-LHCII Supercomplex from the Green Alga *Chlamydomonas reinhardtii*." *Proceedings of the National Academy of Sciences of the United States of America*.

Shikanai, Toshiharu and Hiroshi Yamamoto. 2017. "Contribution of Cyclic and Pseudo-Cyclic Electron Transport to the Formation of Proton Motive Force in Chloroplasts." *Molecular Plant* 10(1):20–29.

Simkin, Andrew J., Patricia E. López-Calcagno, and Christine A. Raines. 2019. "Feeding the World: Improving Photosynthetic Efficiency for Sustainable Crop Production." *Journal of Experimental Botany* 70(4):1119–40.

Su, Xiaodong, Jun Ma, Xiaowei Pan, Xuelin Zhao, Wenrui Chang, Zhenfeng Liu, Xinzheng Zhang, and Mei Li. 2019. "Antenna Arrangement and Energy Transfer Pathways of a Green Algal Photosystem-I–LHCI Supercomplex." *Nature Plants* 5(3):273–81.

Ünlü, Caner, Bartlomiej Drop, Roberta Croce, and Herbert Van Amerongen. 2014. "State Transitions in *Chlamydomonas reinhardtii* Strongly Modulate the Functional Size of Photosystem II but Not of Photosystem I." *Proceedings of the National Academy of Sciences of the United States of America* 111(9):3460–65.

Vanlerberghe, Greg C. 2013. "Alternative Oxidase: A Mitochondrial Respiratory Pathway to Maintain Metabolic and Signaling Homeostasis during Abiotic and Biotic Stress in Plants." *International Journal of Molecular Sciences* 14(4):6805–47.

Varela, João C., Hugo Pereira, Marta Vila, and Rosa León. 2015. "Production of Carotenoids by Microalgae: Achievements and Challenges." *Photosynthesis Research* 125(3):423–36.

Wang, Chaogang, Xi Chen, Hui Li, Jiangxin Wang, and Zhangli Hu. 2017. "Artificial MiRNA Inhibition of Phosphoenolpyruvate Carboxylase Increases Fatty Acid Production in a Green Microalga *Chlamydomonas reinhardtii*." *Biotechnology for Biofuels*.

Wei, Li, Qintao Wang, Yi Xin, Yandu Lu, and Jian Xu. 2017. "Enhancing Photosynthetic Biomass Productivity of Industrial Oleaginous Microalgae by Overexpression of RuBisCO Activase." *Algal Research*.

Xu C., Andre C., Fan J., Shanklin J. (2016) Cellular Organization of Triacylglycerol Biosynthesis in Microalgae. In: Nakamura Y., Li-Beisson Y. (eds) Lipids in Plant and Algae Development. Subcellular Biochemistry, vol 86. Springer, Cham

Yamamoto, H. Y. and L. Kamite. 1972. "The Effects of Dithiothreitol on Violaxanthin De-Epoxidation and Absorbance Changes in the 500-Nm Region." *Biochimica et Biophysica Acta* 267(3):538–43.

Yang, Bo, Jin Liu, Yue Jiang, and Feng Chen. 2016. "*Chlorella* Species as Hosts for Genetic Engineering and Expression of Heterologous Proteins: Progress, Challenge and Perspective." *Biotechnology Journal* 11(10):1244–61.

Yang, Wenqiang, Claudia Catalanotti, Tyler M. Wittkopp, Matthew C. Posewitz, and Arthur R. Grossman. 2015. “Algae after Dark: Mechanisms to Cope with Anoxic/Hypoxic Conditions.” *Plant Journal* 82(3):481–503.

Zeeman, Samuel C., Jens Kossmann, and Alison M. Smith. 2010. “Starch: Its Metabolism, Evolution, and Biotechnological Modification in Plants.” *Annual Review of Plant Biology* 61(1):209–34.

Zeng, Xiaopeng, Peng Jin, Yingying Jiang, Haimei Yang, Jiahui Zhong, Zhe Liang, Yingyan Guo, Peiyuan Li, Quanting Huang, Jinmei Pan, Hua Lu, Yanyun Wei, Dinghui Zou, and Jianrong Xia. 2020. “Light Alters the Responses of Two Marine Diatoms to Increased Warming.” *Marine Environmental Research*.

Zeng, Xiaopeng, Peng Jin, Dinghui Zou, Yuxian Liu, and Jianrong Xia. 2019. “Responses of Carbonic Anhydrases and Rubisco to Abrupt CO2 Changes of Seawater in Two Marine Diatoms.” *Environmental Science and Pollution Research*.

Chapter 1

Chlamydomonas reinhardtii

Section A:

LPA2 protein is involved in the PSII assembly in *Chlamydomonas reinhardtii*

Section B:

Impaired mitochondrial transcription termination disrupts the stromal redox poise in *Chlamydomonas*

Section A

LPA2 protein is involved in the PSII assembly in *Chlamydomonas reinhardtii*

J. Jeong[1]*, **M. Cecchin**[2]*, W. Son[3]*, S. Park[1], L. Zuliani[2], S. Cazzaniga[2], S. Bae[3], M. Ballottari[2] and E. Jin[1]

*J. Jeong, M. Cecchin, and W. Son contributed equally to this work

[1]Department of Life Science, Hanyang University, Seoul, Korea

[2]Department of Biotechnology, Università degli studi di Verona, 37154 Verona, Italy

[3]Department of Chemistry, Hanyang University, Seoul, Korea

This work was submitted to Plant Physiology.

In this work we studied the role of a protein of *C. reinhardtii* involved in the assembly of the PSII supercomplexes. To drive light-dependent photosynthesis in photosynthetic eukaryotes, the proper assembly of photosystem II (PSII) is essential. In *Arabidopsis*, the CP43/PsbC PSII subunits is assembled into the PSII complex via its interaction with an auxiliary protein called low PSII accumulation 2 (LPA2). However, the function of the LPA2 protein in the green microalga *Chlamydomonas reinhardtii* is unknown. To elucidate the function of LPA2 in *C. reinhardtii in vivo*, we generated a knockout *lpa2* mutant by using the CRISPR-Cas9 target-specific genome-editing system. Biochemical analyses showed a drastic reduction in the level of CP43 in the mutants and accordingly lower levels of F_v/F_m and PSII supercomplex compared with the wild type. Our profile of chloroplast proteins in the *lpa2* mutant showed an increase in the level of a subunit of the cytochrome b_6f complex, which accepts electrons from PSII, and also an increased level of the LHCI and Rubisco subunits, suggesting that the mutant compensated for its PSII deficiency. Accordingly, *lpa2* had increased PSI activity, cyclic electron transport and state transition. A strong reduction in the level of CP43 in *lpa2* led to a reduction in the chlorophyll (Chl) content per cell and destabilized PSII, resulting in an impairment of photoautotrophic growth. Taken together, our data indicate that in *C. reinhardtii*, LPA2 is required for PSII assembly and for its proper function.

INTRODUCTION

Photosystem II (PSII) is the initial complex in the linear electron transport of photosynthesis in chloroplasts (Nelson and Junge 2015). It comprises the light-harvesting antenna complex that absorbs sunlight and the core complex that converts light into photochemical energy (Govindjee et al. 2001; Wobbe et al. 2016). The PSII core complex contains at least 20 subunits with various cofactors, including electron donors and acceptors (Gokhale and Sayre 2009). Due to the structural complexity of PSII, the proper assembly of its subunits is important for its function (Nickelsen and Rengstl 2013; Lu 2016). The biogenesis of PSII is a stepwise assembly process (Nickelsen and Rengstl 2013; Lu 2016). The first step is the formation of the reaction center (RC) complex, which is composed of the D1 and D2 proteins (Nanba and Satoh 1987; Anbudurai et al. 1994). Then, the RC complex sequentially binds to the inner antenna proteins CP47 and CP43 (Boehm et al. 2011). Next, the oxygen-evolving complex assembles on the lumenal side of the PSII pre-complex, which is converted into an active monomeric PSII (Bricker et al. 2012). Finally, the active PSII forms dimers and is surrounded by the peripheral light-harvesting antenna complex, which completes the *de novo* biogenesis of PSII (Wobbe et al. 2016).

Unsurprisingly, many regulatory factors are involved in the properly organization of PSII subunits. Of these, Psb27 in cyanobacteria interacts with CP43 and PSII during both *de novo* biogenesis and repair of PSII (Komenda et al. 2012). Because two Psb27 homologs have been identified in the green lineage, the role of cyanobacterial Psb27 was proposed to be divided between two genes in eukaryotes (Nickelsen and Rengstl 2013). One of them, Psb27-H2 (LPA19), participates in *de novo* PSII assembly by interacting with D1 and CP43 (Wei et al. 2010). In cyanobacteria, CP43 incorporation into PSII requires another assembly factor, Sll0606, whose absence produces a drastic reduction in the level of PSII (Zhang et al. 2010). A homolog of Sll0606 is found in the unicellular algae *Chlamydomonas reinhardtii*, but not in the land plant *Arabidopsis thaliana*, suggesting that Sll0606 might be functionally replaced by other proteins in higher plants (Chi et al. 2012; Nickelsen and Rengstl 2013). One possible replacement is LPA2, which has been suggested to interact with CP43 during PSII assembly in *A. thaliana*, even if based on reports which have been then retracted (Ma et al. 2007; Cai et al. 2010). LPA2 homologs have been found in other higher plants but not in *C. reinhardtii* or cyanobacteria (Chi et al. 2012; Nickelsen and Rengstl 2013). Therefore, CP43 assembly was not expected to require an LPA2 homolog in *C. reinhardtii*, but no detailed study of the assembly factors for CP43 in this microalga had been performed.

In this work, we identified an LPA2 homolog in the *C. reinhardtii* genome and we investigated the function of this interesting protein *in vivo*. We used the ribonucleoprotein (RNP)-mediated CRISPR-Cas9 system to generate a target-specific knockout mutant (*lpa2*) of *C. reinhardtii*. In the absence of

the LPA2 protein, the mutant had a reduced amount of CP43 and dysfunctional PSII supercomplexes. These results indicate that LPA2 is required for efficient CP43 assembly in PSII biogenesis in *C. reinhardtii*. In addition, the *lpa2* mutant had enhanced electron transport around PSI, suggesting that PSI can be used to dissipate excitation energy in PSII-deficient conditions.

RESULTS

LPA2 gene in *C. reinhardtii*

The putative *LPA2* gene (Cre02.g105650) was newly identified in the *C. reinhardtii* genome based on the amino acid sequence similarity between its product and the LPA2 in *A. thaliana* (Fig. 1). Homologs were also identified in the green linage, including chlorophytes, but not in cyanobacteria,

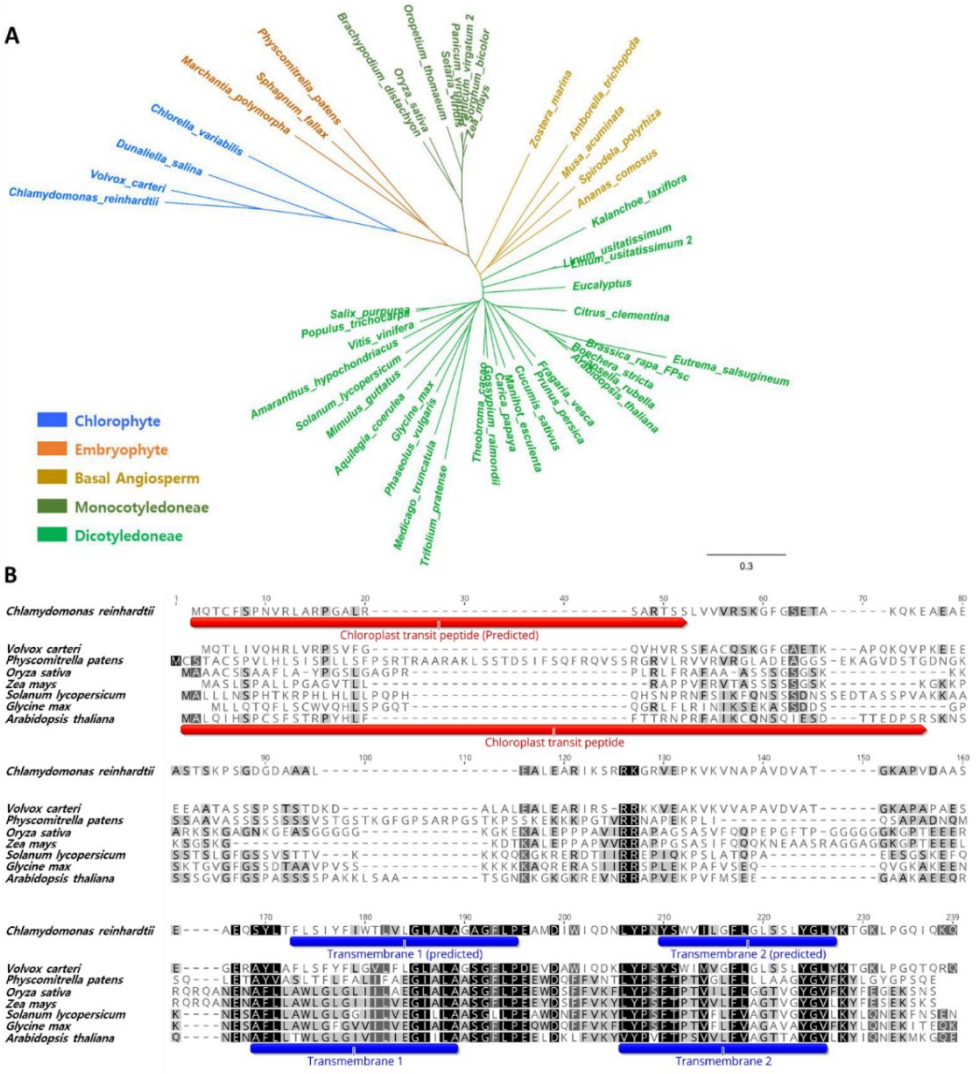

Figure 1. Phylogenetic tree (A) and amino acid sequence alignment (B) of LPA2 homologs in the green lineage. The 48 sequences were aligned using MUSCLE alignment, and selected species representing each clade are shown in B. The phylogenetic tree was obtained using the Neighbor-joining method and all analyses were conducted in Geneious R10 software. Accession numbers of LPA2 homologs used are available in the Supplemental Table S1.

suggesting that the LPA2 protein is of eukaryotic origin (Fig. 1A). The *C. reinhardtii LPA2* gene (*CrLPA2*) encodes a protein of 175 amino acids, including a 24 amino acid-long chloroplast transit peptide predicted by Predalgo software (https://giavap-genomes.ibpc.fr/predalgo/) and two transmembrane domains (amino acids 109–131 and 146–163) determined by TMHMM software (http://www.cbs.dtu.dk/services/TMHMM/). The CrLPA2 protein shares 23.2% identity and 43.2% similarity with its *Arabidopsis* homolog (Fig. 1B).

To validate the function of the *C. reinhardtii* LPA2, we analyzed the light dependent expression of *LPA2*. We exposed *C. reinhardtii* strain CC503 to high light (500 µmol photons $m^{-2}s^{-1}$) for 0, 30, and 60 min and used qRT-PCR to analyze the transcript levels of *ELIP*, *LPA2* ,and *psbC* (Supplemental Fig. S1A). *LPA2* expression increased after exposure to high light, similar to the expression of *ELIP* and *psbC*, indicating light-dependent expression. Western blotting revealed the presence of LPA in the purified chloroplasts, specifically in the thylakoid membranes but not in the stromal fraction (Supplemental Fig. S1B).

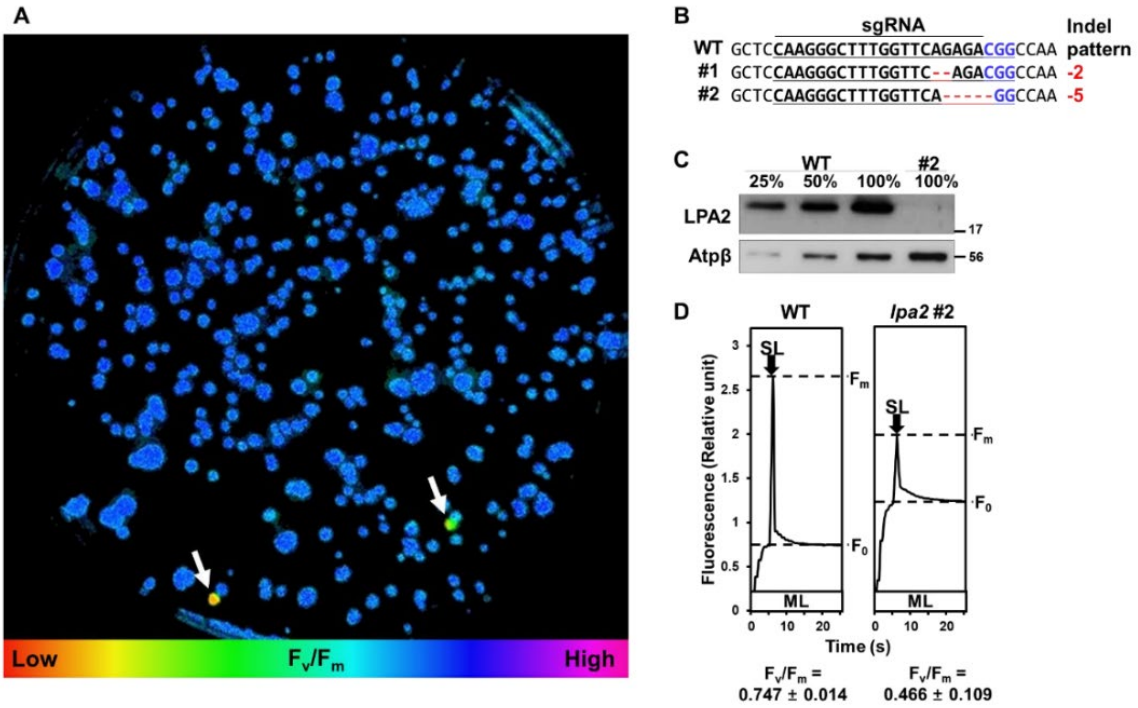

Figure 2. CRISPR-Cas9 mediated *lpa2* mutant generation in *C. reinhardtii*. A. The measurement of F_v/F_m to select putative *LPA2* gene knockout mutants grown on TAP agar medium under 50 µmol photons $m^{-2}s^{-1}$. The cells (marked with white arrows) presenting lower F_v/F_m than the background cells were picked and confirmed by Sanger sequencing. B. DNA sequence alignment of the wild type (WT) and *lpa2* mutants obtained from Figure 2A (#1–2) at the *LPA2* locus. The 20-bp target sequence of sgRNA is underlined, and the PAM sequence is shown in blue. The column on the right indicates the number of inserted (+) or deleted (−) bases. C. Immunoblot with LPA2 and Atpβ (loading control) antibodies in the WT and *lpa2#2* mutant, which was used for all further experiments. Proteins were loaded on the basis of equal cell numbers, and the WT samples were loaded at three different concentrations (25, 50, and 100%). D. The measurement of Chl fluorescence kinetics in the WT and *lpa2#2* mutant grown in liquid TAP medium under 50 µmol photons $m^{-2}s^{-1}$. The measuring light (ML) and saturating light (SL) were 5 and 1250 µmol photons $m^{-2}s^{-1}$, respectively. The F_v/F_m differed significantly between the WT and *lpa2* mutant, as determined by student *t*-test (n=4; the values shown are means ± SD; $p<0.05$).

Generation of knock-out mutants without the *LPA2* gene in *C. reinhardtii*

To further characterize *C. reinhardtii* LPA2, we generated target-specific knockout mutants by using preassembled Cas9 protein–small guide RNA (sgRNA) RNP complex–mediated CRISPR-Cas9. The *lpa2* mutants were generated by sgRNA2 containing the 5′-CAAGGGCTTTGGTTCAGAGACGG-3′ sequence (Table S2). Based on a previous study on an LPA2 homolog (Chi et al. 2012), we screened for mutants showing abnormal Chl fluorescence. Transformants with lower F_v/F_m fluorescence signals than the background cells (Fig. 2A) were selected for Sanger sequencing analysis of the target locus. All such transformants had small indels in the *LPA2* gene (Fig. 2B). The transformation efficiency, calculated as the ratio of the number of mutants to the total colony number, was 0.495%, which was similar to the mutation frequency obtained from the total gDNA of CRISPR-Cas9-transfected cells (0.4%; Table S3). We selected the *lpa2#2* mutant for further investigation because it had a frame-shift mutation that led to the early termination of the LPA2 protein. The absence of the LPA2 protein in the mutant was verified by immunoblotting (Fig. 2C). Analysis of the *lpa2#2* mutant for potential off-target effects by targeted deep sequencing revealed no indels (Table S4).

Decreased chlorophyll content in the *lpa2* mutant

As first revealed during mutant screening, the *lpa2* mutant had an aberrant F_v/F_m fluorescence signal (Fig. 2D). Interestingly, although the F_m/Chl ratio of the mutant was similar to that of the wild type, the F_0/Chl ratio of the mutant was increased, resulting in a low F_v/F_m fluorescence signal. The increased F_0/Chl ratio suggests the partial disconnection of antenna complexes from PSII.

To understand the change in Chl fluorescence caused by the mutation, we analyzed the Chl-binding properties of the *lpa2* mutant (Table 1). In photoautotrophic cultures, the mutant exhibited a 53% reduction in total Chl content per cell in comparison with the wild type, while the Chl *a*/*b* ratio were not significantly affected. The reduction in Chl content per cell was not related to a change in cell size, which was similar in the mutant compared to WT strain (Table 1).

	Chl/cell (pg/cell)	Chl a/b ratio	Chl/car	Cell dimension (diameter, µm)
WT	2.50 ± 0.11	2.61 ± 0.01	3.20 ± 0.03	8.92 ± 0.81
lpa2	1.17 ± 0.05*	2.47 ± 0.07	2.82 ± 0.08*	8.39 ± 0.75

Table 1. Chlorophyll (Chl) content for cells, Chl a/b ratio, Chl/carotenoids ratio and cell dimensions of the wild type (WT) and *lpa2* mutant. Significantly different values in *lpa2* versus WT are indicated by *, as determined by student *t*-test (n=3; the values shown are means ± SD; $p < 0.05$) .

The *lpa2* mutant accumulates a low amount of CP43 and CP47

We investigated the effect of the *LPA2* gene mutation on the organization of photosynthetic complexes in isolated thylakoid membranes (Fig. 3). In the 2D-Deriphat/SDS-PAGE analysis, the intensity of the bands representing the PSII core and PSII supercomplexes was markedly reduced in the *lpa2* mutant, with a particularly strong decrease in the CP43/CP47 band.

These results were then confirmed by western blot analyses of specific photosystem subunits in the *lpa2* mutant (Fig. 4) showing the strongest decrease in CP43 (26.3 ± 12.0% of the wild type; Figure 4B) followed by CP47 (42.5 ± 2.4%). As reported in Supplemental Figure S4, the expression level of *PsbC* gene was not changed in *lpa2* mutant compared to WT, suggesting that the reduced CP43 accumulation was related to impaired PSII assembly. Only a slight decrease in D1, D2 and PsbO was observed in the mutant, while PsbP was essentially unaffected. The accumulation of LHCII complexes in the *lpa2* mutant was similar to that in the wild type, indicating that the LHCII/PSII ratio in the mutant was increased. PSI accumulation was not affected by the *LPA2* mutation (Fig. 4C), with a consequent increase in the PSI/PSII ratio in the *lpa2* mutant in comparison with the wild type.

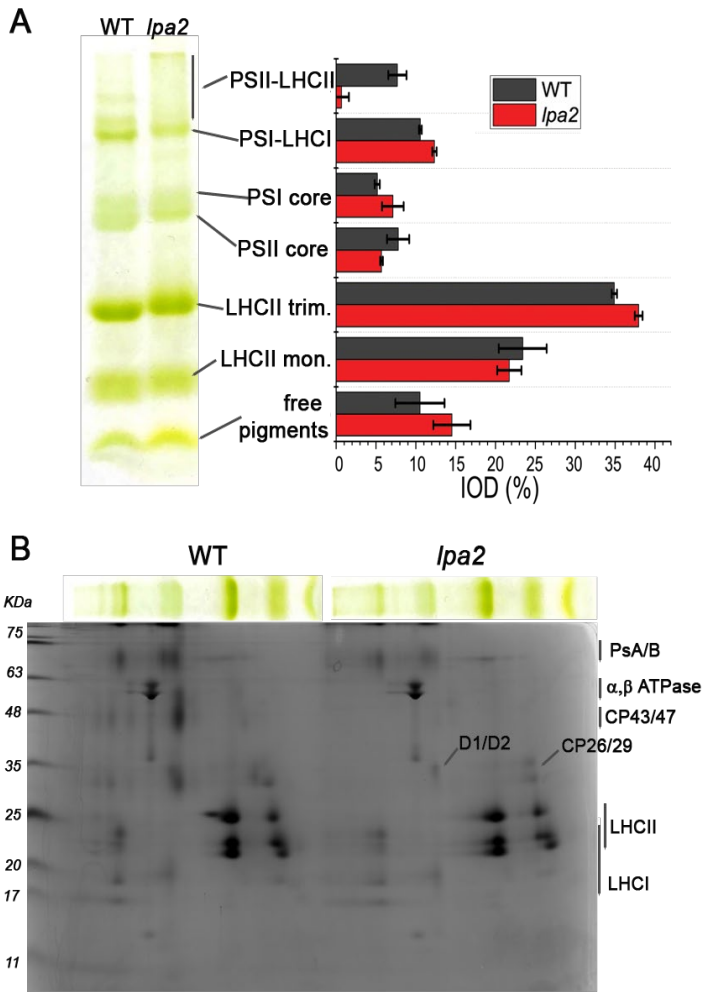

Figure 3. 2D-Deriphat/SDS-PAGE of purified thylakoid membranes. Deriphat-PAGE of WT and *lpa2* mutant, (A) density of each band was quantified by densitometry, PSII-supercomplex (PSII-LHCII) are indicated. Second dimension of 2D-Deriphat/SDS-PAGE were performed running the Deriphat-PAGE lanes in Tris-Tricine poly-acrylamide gel (B).

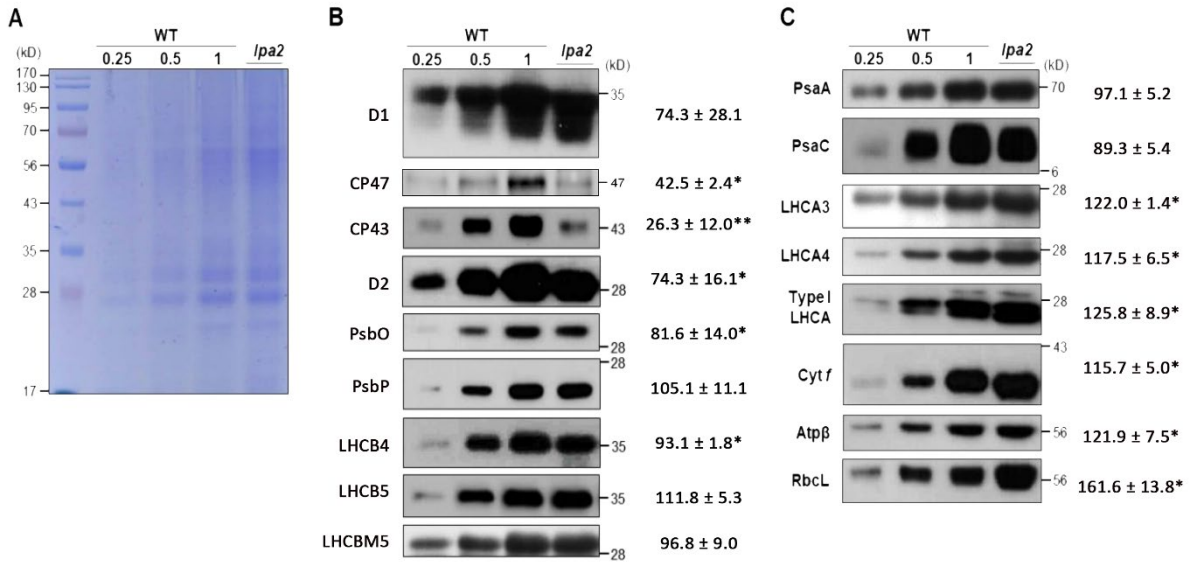

Figure 4. Coomassie blue stained SDS-PAGE gel (A) and immunoblot analysis (B, C) of chloroplast proteins from the wild type (WT) and *lpa2* mutant. Results from immunoblotting with antibodies against PSII-LHCII are presented in B, and results from immunoblotting with antibodies against PSI-LHCI, Cyt *f*, Atpβ, and RbcL are presented in C. Each lane was loaded on a per Chl basis (1 µg), and the WT samples were loaded at three different concentrations (0.25, 0.5, and 1 µg). The amounts of proteins in the *lpa2* mutant compared to the WT are presented next to the protein bands (n ≥ 3; the values shown are means ± SD). The statistical significance of differences between WT and *lpa2* is indicated as * if $p < 0.05$ and ** if $p < 0.01$, as determined by student *t*-test.

Interestingly, the number of LHCI subunits in the mutant increased to an average of 125% of the wild type, suggesting that PSI had increased its light harvesting activity when PSII was partially destabilized.

The accumulation of the cytochrome b_6f complex and ATP synthase was investigated by western blotting with antibodies specific to cytochrome *f* and the ATPase β-subunit, respectively (Fig. 4C). The levels of both subunits were slightly increased in the *lpa2* mutant. The large Rubisco subunit, a representative enzyme of the Calvin-Benson cycle, was clearly increased in the mutant (1.6 times the wild-type level). Thus, the low amounts of CP43 and PSII in the *lpa2* mutant caused an increase in the levels of the cytochrome b_6f complex, Rubisco and ATP synthase, which contribute to reduce the excitation pressure on the photosynthetic apparatus oxidizing plastoquinone pool, and regenerating $NADP^+$ and ADP respectively.

The *lpa2* mutant had impaired photoautotrophic growth and reduced photosynthetic activity

To investigate how the mutation affected the growth, WT and *lpa2* mutant were cultivated under phototrophic, mixotrophic and heterotrophic conditions. Under heterotrophic conditions (with acetate as a source of organic carbon, Fig. 5A), the growth of *lpa2* mutant was similar compared to the WT case, demonstrating that the mutation introduced was not affecting light-independent cell functions. In mixotrophy, *lpa2* mutant was growing slower than that of the wild type (Fig. 5C).

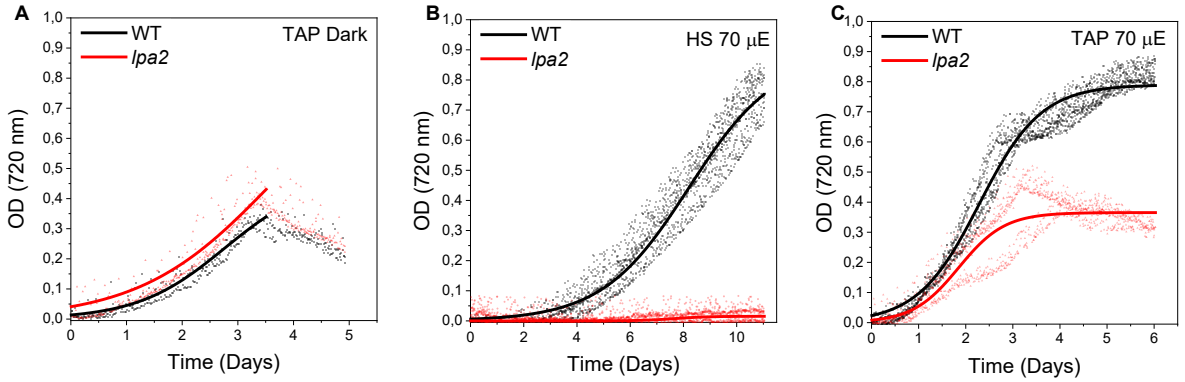

Figure 5. Growth curves of WT and *lpa2* mutant. Heterotrophic (A), phototrophic (B) an mixotrophic (C) growth of the *lpa2* mutant measured in liquid medium and compared to the WT (wild type). Growth curves were fitted by using Hill function (n=4).

Instead, under autotrophic conditions, the growth of *lpa2* was severely impaired (Fig. 5B), presumably because the lower photosynthetic activity of the mutant could not maintain whole-cell metabolism under these conditions.

Photosynthetic activity of *lpa2* mutant was then analyzed by pulse-amplitude-modulated (PAM) fluorescence (Fig. 6). The fraction of the absorbed light used for PSII photochemistry (ΦPSII) was lower in the mutant than in the wild type at light intensities below 400 µmol $m^{-2}s^{-1}$ but similar at higher irradiances (Fig. 6A and B). The controlled thermal dissipation of the absorbed excitation

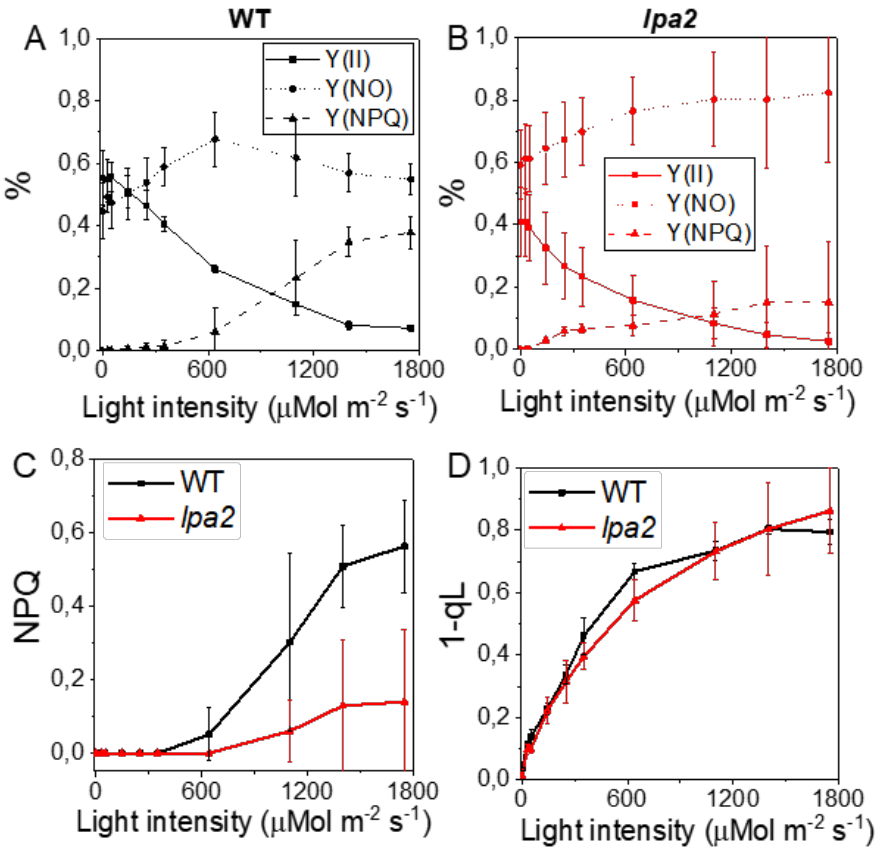

Figure 6. Light intensity response curves of fluorescent photosynthetic parameters. Intensity response curves for ϕPSII, ϕNPQ, and ϕNO in the wild type (WT) and *lpa2* mutant are shown in A and B respectively. (C,D) reported NPQ and 1-q_L respectively. Error bars are indicated as standard deviation (n=3).

energy (ΦNPQ) was also lower in the *lpa2* mutant than in the wild type, whereas the fraction of absorbed energy lost by uncontrolled dissipation (ΦNO) was higher in *lpa2* (Fig. 6A and B).

Accordingly, the NPQ values (calculated as $(F_m-F_m')/F_m'$) were lower in the *lpa2* mutant than in the WT, implying a lower photoprotective capacity in the mutant (Fig. 6C). The fraction of closed PSII centers, calculated from the $1-q_L$ value, was similar in *lpa2* mutant compared to wild type (Fig. 6D). This result indicates that despite the reduced efficiency of PSII, the redox state of Q_A was kept similar to the WT case at the different light intensities due to an adaptation of the overall photosynthetic apparatus. We further investigated PSII activity by measuring the light-dependent oxygen evolution curves and found reduced oxygen evolution on a per-cell basis in the *lpa2* mutant, confirming its reduced photosynthetic activity (Fig. 7A). On a chlorophyll basis, we found that the *lpa2* mutant had similar O_2 evolution compared to WT (Fig. 7B); this result is likely related to adaptation events at the level of the photosynthetic apparatus as a consequence of reduced PSII activity.

Then we investigated the organization of the photosynthetic apparatus on the basis of 77K fluorescence emission spectra. In the *lpa2* mutant, the spectra showed the presence of disconnected LHC proteins with a peak at 680 nm, confirming the partial destabilization of the PSII complexes (Supplemental Fig. S2). Interestingly, the *lpa2* mutant had increased PSI fluorescence at 715 nm, suggesting an increased PSI/PSII ratio.

We reasoned that the altered amounts of LHC in the *lpa2* mutant might affect the state transitions that balance the energy between PSI and PSII using LHCII migration from PSII to PSI. We examined the capacity of WT and *lpa2* mutant to perform state transitions by measuring the 77K fluorescence

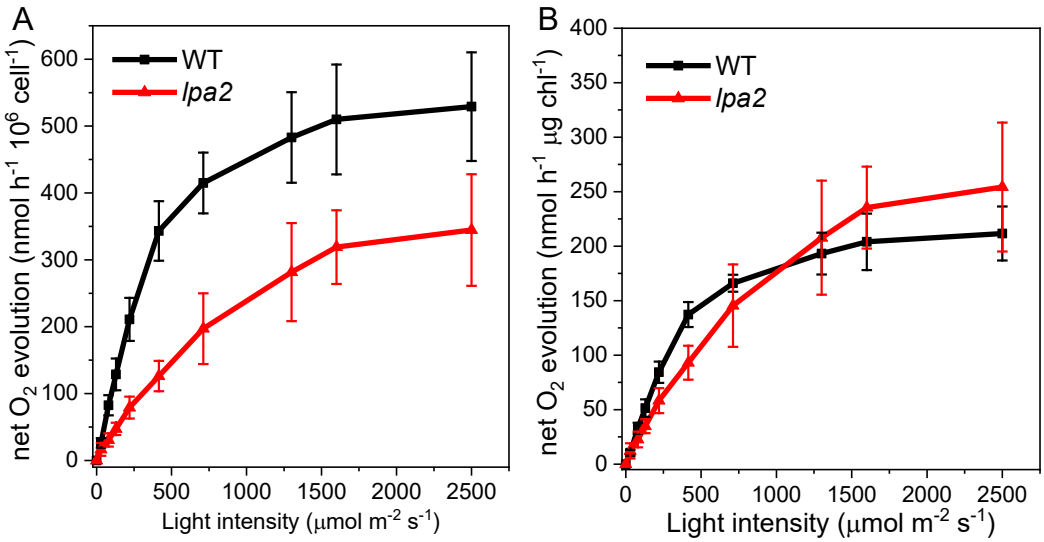

Figure 7. Oxygen evolution rates of WT and *lpa2* mutant in response to different light intensities were measured subtracting the rate of oxygen consumption in the dark. Net oxygen evolution rates were normalized to total cell contents (A), or to Chl content (B). Error bars are indicated as standard deviation (n=3).

emission spectra of cells under state 1 or state 2 conditions (Fig. 8A and B). The *lpa2* mutant showed increased migration of light harvesting antenna proteins to PSI under state 2 conditions, suggesting an increased pool of mobile LHCII subunits, likely as a consequence of the reduced PSII assembly (Fig. 8C).

The *lpa2* mutant has enhanced electron transport flow around PSI

To examine whether the increased amount of PSI affected its activity, we measured PSI activity as maximum P700 oxidation, which was higher on a per Chl basis in the *lpa2* mutant than in the wild type (Fig. 8D) but similar on a per cell basis due to the reduced Chl content per cell in the mutant (Supplemental Fig. S3A). These results are in agreement with the western blotting results (Fig. 4) and suggest that the defect in PSII activity increased PSI activity in the *lpa2* mutant.

We then measured the electrochromic shift (ECS) to estimate the proton-motive force (*pmf*) across the thylakoid membranes generated by the light-driven electron flux. The *pmf* in the *lpa2* was similar

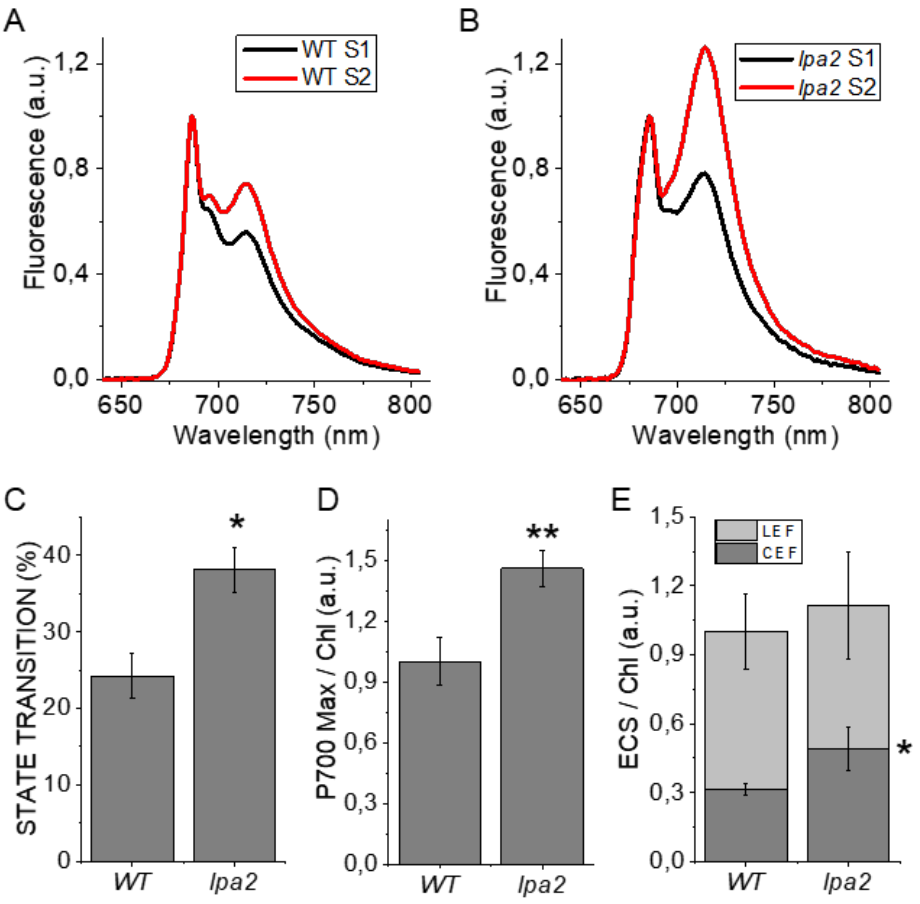

Figure 8 State transitions analysis by 77K fluorescence emission spectra of the wild type (WT; A) and *lpa2* mutant (B) in state 1 (S1) or state 2 (S2) conditions. (C, D) Maximal P700 oxidation on a Chl basis in the WT and *lpa2* mutant. E. Linear electron flow (LEF) and cyclic electron flow (CEF) of the WT and *lpa2* estimated from the electrochromic shift (ECS) on a Chl basis. Errors are reported as standard deviation, the statistical significance of differences between WT and mutant is indicated as * if $p < 0.05$ and ** if $p < 0.01$, as determined by unpaired two sample *t*-test (n=4).

to that in the WT (Fig. 8E; Supplemental Fig. S3B). Considering the reduced PSII activity in the *lpa2* mutant, we investigated the possible influence of cyclic electron flow (CEF) around PSI on *pmf* by measuring the ECS in the presence of DCMU to inhibit linear electron flow. The *lpa2* mutant had an increased fraction of *pmf* related to CEF (Fig. 8E and Supplemental Fig. S3B), causing a similar total *pmf* despite decreased PSII activity.

LPA2 as a possible player in D1 repair in *C. reinhardtii*

High light damages PSII, which increases the need for its *de novo* assembly or repair. Under high light, the expression of the *LPA2* transcript in both the *lpa2* mutant and wild type was increased (Supplemental Fig. S4), suggesting that LPA2 might have a repair function. To explore the potential role of the LPA2 protein in repairing D1 proteins, we performed light shift experiments and monitored the rate of photodamage or recovery from photo-inhibition. We monitored and quantified the level of D1 protein during high light exposure in the presence or absence of lincomycin, a chloroplast protein biosynthesis inhibitor, to quantify D1 decay kinetics in the absence of its synthesis (Fig. 9). In the *lpa2* mutant, the level of D1 protein decreased faster than in the wild type when they were shifted from low light to high light (Fig. 9), indicating that LPA2 might be involved in D1 repair and PSII assembly.

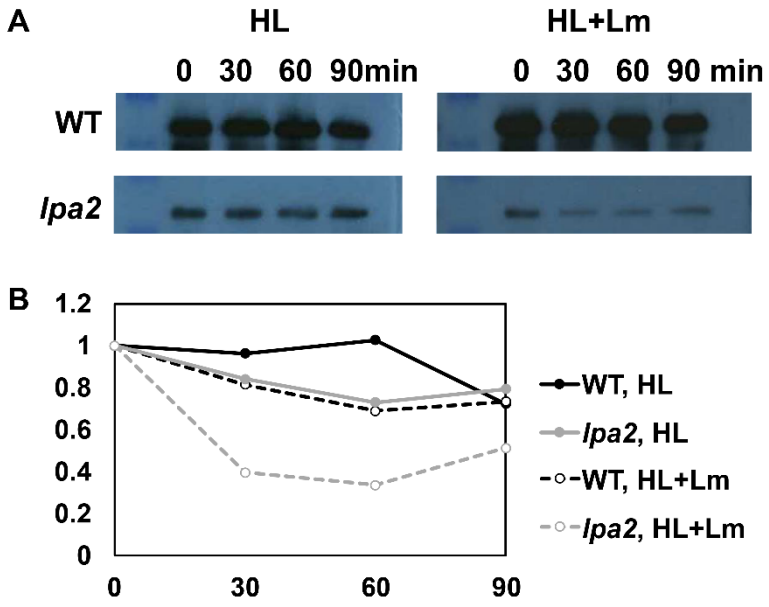

Figure 9. Time course analysis for the loss of the D1 protein after a low light (LL) to high light (HL) shift. The wild type (WT; black circles with solid line) and *lpa2* mutant (gray circles with dashed line) were grown under LL to the late log phase. The cells were incubated in the presence of lincomycin (Lm). Protein blots probed with antibodies against the D1 protein are shown in A; 20µg of total proteins were loaded for each lane. Densitometric quantification of the corresponding protein blots for the WT and *lpa2* mutant are shown in B.

DISCUSSION

Although photosynthetic eukaryotes have, through endosymbiosis, acquired chloroplasts that perform oxygenic photosynthesis, the chloroplast genome does not encode all the proteins necessary for the photosynthetic machinery (Fischer et al. 2016). Numerous nuclear genes not only directly encode the components of the photosynthetic apparatus, but also regulate multiple proteins for the biogenesis and assembly of protein complexes in the chloroplast, e.g., the CpSRP54, CpSRP43, CpFTSY, and LTD proteins from the chloroplast signal recognition particle pathway participate in LHCP assembly (Kirst and Melis 2014; Jeong et al. 2017; Ziehe et al. 2017; Jeong et al. 2018). In the green microalga *C. reinhardtii*, an early study on several mutants that lack PSII subunits revealed that the absence of CP43 did not affect the synthesis of D1, D2, or CP47 under continuous light, and the loss of D1, D2, or CP47 did not alter CP43 synthesis (de Vitry et al. 1989). The fact that the synthesis and accumulation of CP43 are independent of other RC components implies the existence of specific factors for the assembly of CP43. Therefore, to expand our understanding of PSII biogenesis and assembly in *C. reinhardtii*, we used the CRISPR-Cas9 methodology to investigate a nuclear-encoded protein, LPA2, and elucidate its role in PSII biogenesis via a photochemical and biochemical analysis of a *lpa2* mutant.

LPA2 is required for CP43 assembly in the PSII of *C. reinhardtii*

CP43 is a 43kDa chlorophyll-binding protein that contains six transmembrane helices (Bricker 1990). It functions as an inner PSII antenna by transferring excitation energy from the peripheral antenna complexes to the RC (Bricker and Frankel 2002). It is also essential for oxygen evolution in PSII by providing lumenal residues for the ligation of the Mn_4CaO_5 cluster and interactions with oxygen evolving complex proteins (Suorsa and Aro 2007; Umena et al. 2011; Bricker et al. 2012). Because of these important properties, *Synechocystis* PCC 6803 or *C. reinhardtii* mutants that lack the *psbC* gene product cannot grow phototrophically or show detectable oxygen evolution (Roegner et al. 1991; Zerges et al. 2003; Marín-Navarro et al. 2007). Likewise, the lack of the LPA2 protein, which is localized in the thylakoid membranes, resulted in a drastic reduction in CP43 and the inability of the *lpa2* mutant to grow in minimal medium (Fig. 5B). Because the *psbC* transcript remained in the mutant at the wild-type level (Supplemental Fig. S4), these results suggest that the LPA2 protein is involved in the post-translational regulation or integration of CP43 in the thylakoid membranes.

The *lpa2* mutant showed reduced D1 regeneration at high light intensity (Fig. 9). D1 is the PSII component most sensitive to excess light energy (Melis 1999; Nickelsen and Rengstl 2013); photodamaged D1 is rapidly replaced with newly synthesized D1 (Nickelsen and Rengstl 2013; Järvi et al. 2015; Lu 2016). For D1 replacement, PSII is partially disassembled by the detachment and

reassembly of CP43 (Nickelsen and Rengstl 2013; Järvi et al. 2015; Lu 2016). In *A. thaliana*, LPA3 is a major factor required for CP43 detachment during D1 repair; no evidence suggests that LPA2 is involved in PSII repair (Chi et al. 2012; Järvi et al. 2015). However, our D1 regeneration results in the *lpa2* mutant indicate that *C. reinhardtii* LPA2 is likely involved in CP43 cooperation during PSII repair, as well as, in *de novo* biogenesis of PSII.

Lack of LPA2 affects the accumulation of the photosynthetic machinery

The absence of the LPA2 protein increased the F_0/Chl ratio and shifted the peak of the 77K fluorescence emission spectra to 680nm in the *lpa2* mutant, indicating that the efficiency of excitation energy transfer from the antenna complex to the RC is reduced due to the partial disconnection of the PSII-LHCII supercomplex (Fig. 2D, 8B and Supplemental Fig. S2). Likewise, native Deriphat-PAGE showed a lower level of the PSII-LHCII supercomplexes in the mutant, if any (Fig. 3), but the unconnected LHCII remained as a free antenna (Fig. 4). A large decrease in CP43 and CP47 in the mutant implies that *C. reinhardtii* LPA2 participates in their accumulation, being these subunits an important link between the PSII RC and antenna complex. The reduced PSII assembly in *lpa2* caused a reduction of PSII activity on a cell basis (Fig. 7A), which contributed to the strong reduction in growth observed in the *lpa2* mutant (Fig. 5), which became even more severe under autotrophic conditions, which cause the whole-cell metabolism to rely on photosynthesis. The increase in the ΦNO of the mutant also indicates insufficient photoprotective regulation of energy dissipation, which poses a serious problem for mutant survival without a carbon source (Fig. 6B).

It is noteworthy that the reduced PSII level increased the PSI/PSII ratio in the mutant. Unlike PSII, the abundance of PSI core subunits and PSI activity were not reduced by the lack of LPA2 protein (Fig. 4 and 8D). These observations differ from previous reports showing lower PSI activity in mutants defective in PSII biogenesis (Zhang et al. 2011; Wang et al. 2013). These features suggest that the *lpa2* mutant might preferentially operate PSI-mediated electron transport flow to release excitation pressure and generate trans-thylakoid proton transport to compensate for the inactive PSII. Indeed, the fraction of CEF, which is critical in maintaining the *pmf*, was increased in the *lpa2* mutant compared to the WT (Fig. 8E).

The imbalance between PSII and PSI in the *lpa2* mutant resulted in another interesting phenotype: overaccumulation of the cytochrome b_6f complex and Rubisco, which are downstream acceptors of electron flow, possibly to release excess energy. Similarly, ATP synthase content was increased in *lpa2* mutants, suggesting a faster relaxation of lumen acidification (Fig. 4). However, the observed reorganization of photosynthetic apparatus in the *lpa2* mutant is not sufficient to sustain autotrophic growth, likely due to reduced NADPH formation and increased photosensitivity.

In this study, we demonstrated that *C. reinhardtii* LPA2 is essential for the assembly of PSII complexes, being specifically involved in CP43 attachment to PSII core. However, the detailed mechanism by which LPA2 plays that role should be investigated further. The process of PSII protein assembly is complicated, and the functions of various assembly factors are almost certainly coordinated. Some of these factors, such as LPA1/rep27, PAM68, and Alb3, which function in the same step, could form a protein complex (Armbruster et al. 2010), so it is necessary to build a protein interaction network that can provide a comprehensive view of the interplay among different assembly factors, repair complexes, and PSII subunits. PSII assembly factors such as Alb3 and PAM68 emerged early in the evolution of photosynthetic organisms because they are present in all cyanobacterial groups, green algae, and land plants (Chi et al. 2012). LPA2, on the other hand, is present in photosynthetic eukaryotes (Fig. 1), but no homolog of LPA2 has been identified in the cyanobacterium *Synechocystis* PCC6803, suggesting that LPA2 appeared in the green plant lineage (Chi et al., 2012).

In conclusion, the knockout mutation of *LPA2* in *C. reinhardtii* resulted in a drastic reduction in the level of PSII, with a concomitant decrease in its efficiency. Under high irradiance, the decay kinetics of the D1 protein in *lpa2* mutant are much faster than in the wild type, indicating that LPA2 might take part in the D1 repair cycle. More interestingly, the *lpa2* mutant increased the accumulation of the cytochrome b_6f complex, ATP synthase, and PSI proteins to overcome the PSII deficiency caused by the *LPA2* mutation. Therefore, *lpa2* mutant had increased PSI activity and CEF to supplement photosynthetic energy production, but those increases were insufficient to support photoautotrophic growth. Thus, the LPA2 protein is a critical factor for PSII assembly, both *de novo* biogenesis and repair, in *C. reinhardtii*.

MATERIALS AND METHODS

Sequence alignments and phylogenetic analysis. LPA2 homologs in the green lineage were identified by BLAST searches and are summarized in Table S1. The amino acid sequences were aligned using MUSCLE with the default settings (Edgar 2004). A phylogenetic tree was constructed using the Neighbor-joining method with 1000 bootstrap replicates (Saitou and Nei 1987). All analyses were performed using Geneious R10 software.

CRISPR-Cas9-driven mutagenesis. All procedures were performed according to Baek et al. (2016) using 100 μg of Cas9 protein and 70 μg of gRNA. After CRISPR-Cas9 transformation, cells were incubated in TAP liquid medium supplemented with 40 mM sucrose for 12 h and harvested for genotype characterization or immediately diluted (to 2×10^3 cells) and plated on TAP medium containing 1.5% agar to obtain single colonies. The colonies were screened on the basis of the F_v/F_m fluorescence signal using a Walz Imaging PAM System (M-series; Heinz Walz GmbH). To confirm the mutation of the target site, the putative mutants were further analyzed by Sanger sequencing.

Genotype characterization. Genomic DNA was extracted as described in Jeong et al. (2018). For Sanger sequencing, the target regions were PCR-amplified with specific primers (5'-GTAGTGTGCTTACATTTGCTGATT-3' and 5'-CTACTGCTTCTGGATCTGTCC-3' for the *lpa2* gene locus). The PCR products were separated by agarose gel electrophoresis, eluted from the gel, and sequenced (Macrogen). For targeted deep sequencing, genomic DNA segments that encompassed the nuclease target sites were amplified using Phusion polymerase (New England Biolabs). Equal amounts of the PCR amplicons were subjected to paired-end read sequencing using the Illumina MiSeq platform. The obtained next-generation sequencing data were analyzed using Cas-Analyzer (Park et al. 2017). Reads that occurred only once were excluded to remove errors associated with amplification and sequencing. Insertions and deletions (indels) located around the Cas9 cleavage site (3 bp upstream of the protospacer–adjacent motif sequence) were considered to be mutations induced by Cas9. To examine the occurrence of potential off-target mutation sites, we used Cas-OFFinder (Bae et al. 2014), which lists potential off-target sites with a DNA or RNA bulge in length that differ from the on-target sites by up to 4 nucleotides.

Pigment and cell size analysis. Pigment analyses were performed by HPLC as described in Lagarde et al. (2000). Cell size was investigated using Countless®II FLautomated cell counter (Thermo Fisher).

Growth analysis. *C. reinhardtii* strains were grown in minimal (HS) medium or in presence of acetate (TAP medium (Kropat et al 2011)). Growths were evaluated in 80 ml photobioreactors in Multi-cultivator system (Photon Sysrtem Instrumets, Cech republic) growing the different strains at 70 μmol photons m^{-2} s^{-1} in HS or TAP medium, for autotrophic and mixotrophic condition respectively, or in the dark in TAP medium for the heterotrophic condition.

2D-Deriphat/SDS-PAGE electrophoresis. 2D-Deriphat/SDS-PAGE analysis was performed as described in Jeong et al. (2018). Thylakoid membranes isolated according to Ferrante et al. (2012) at a Chl concentration of 0.5 mg/mL were solubilized with *n*-dodecyl-α-D-maltoside (final concentration 0.75% for both wild type and *lpa2*), incubated on ice for 10 min, and centrifuged at 20,000 ×*g* for 10 min to remove unsolubilized material. Thylakoid membrane proteins (25 μg Chl) were loaded in each lane. After separation, one-dimensional native Deriphat–PAGE strips were cut and soaked in SDS-PAGE stacking buffer containing 5 M urea twice for 25 min each. The proteins were then separated by SDS-PAGE (12% gel containing 2 M urea). The acrylamide gels were stained with Coomassie blue. Immunoblot analysis for profiling chloroplast proteins was performed as described by Jeong et al. (2018). Antibodies were purchased from Agrisera, except for LPA2 antibody. Polyclonal antibodies for LPA2 protein were raised against two peptides, CGFGSETAKQKEAEAEASTSKP and EALEARIKSRRKGRVEPKVKVC (Abrfontier).

Photosynthetic activity analysis. PSII activity was analyzed by fluorescence measurements on whole cells using a Dual-PAM 100 instrument (WALZ). Specifically, φPSII, φNO, φNPQ, and NPQ were measured using different actinic lights from 0 to 1700 μmol photons $m^{-2}s^{-1}$. 77K fluorescence emission spectra were acquired with a charge-coupled device spectrophotometer (JBeamBio) as previously described in Allorent et al. 2013. State transitions were measured on whole cells induced to state 1 or state 2 as described in Fleischmann et al. (1999). Maximum P700 activity was measured with the Dual-PAM 101 following the kinetics of transient absorption at 830 nm after a pulse of saturating light. Whole cells were treated with DCMU (3-(3,4-dichlorophenyl)-1,1-dimethylurea), ascorbate, and methyl-viologen, as described in Bonente et al. 2012. Electrochromic shift measurements were performed using a Photosynq that set the actinic light at 500 μmol photons $m^{-2}s^{-1}$. Light dependent O_2 evolution curves were measured using Clark-electrode as reported in Perozeni et al., 2019.

***De novo* biosynthesis of the D1 protein.** To block the translation of the chloroplast-encoded D1 protein, lincomycin, an inhibitor of plastid protein biosynthesis, was added to the cultures as described in Jin et al. (2003), and the cells were incubated under either normal growth light (50 μmol photons $m^{-2}s^{-1}$) or high light (500 μmol photons $m^{-2}s^{-1}$). Cells were harvested 0, 30, 60, and 90 min after the light treatment, and the cell pellets were resuspended in Laemmli sample buffer (Laemmli 1970) without bromophenol blue. After vigorous vortexing, the protein content of the crude extracts was measured using Bradford reagent (Bio-Rad) and 20μg of total proteins were loaded for each lane. SDS-PAGE and immunoblot analyses were performed using an antibody against the D1 protein (Agrisera).

RNA expression analysis. Total RNA was isolated from high light treated cells using a RNeasy Plant Mini Kit (Qiagen). Total RNA (1 μg) was used as a template for cDNA synthesis using SuperScript III reverse transcriptase (ThermoFisher Scientific). Then, the cDNA was used as a template to amplify *PsbC* with real-time PCR using SYBR Premix Ex Taq II (TaKaRa) and a Thermal Cycler Dice Real Time System (TaKaRa). The relative quantities of the transcript were normalized to those of the constitutively expressed *RACK1* gene. The primer sequences used for the amplification were 5'-CAAGAACGTCGTGCTGCTGAA-3' and 5'-CCTGCGTGCCATAAGTGACC-3' for PsbC, 5'-GCTCGCGATGTGTTTGCTTTC-3' and 5'-TGGTGAGGGAGAATAGCAGGA-3' for ELIP, 5'-CAACTACAGCTGGGTGATCCT-3' and 5'-AGTGTCCAGCTCCCTTTCAG-3' for LPA2 , and 5'-GGCTGGGACAAGATGGTCAA-3' and 5'-GAGAAGCACAGGCAGTGGAT-3' for RACK1.

ACKNOWLEDGEMENTS

This research was supported by the Korea CCS R&D Center (NRF-2014M1A8A1049273) funded by the Korean government (Ministry of Science and ICT) to EJ and by the ERC Starting Grant SOLENALGAE (679814) to M.B.

AUTHOR CONTRIBUTION

EJ and MB designed and moderated the research. SB coordinated the generation of the mutant strains. JJ, MC, WS, LZ, SC, SP, and SB performed experiments. JJ, MC, MB, and EJ wrote the paper. All the authors analyzed and contributed to data interpretation.

REFERENCES

Allorent G, Tokutsu R, Roach T, Peers G, Cardol P, Girard-Bascou J, Seigneurin-Berny D, Petroutsos D, Kuntz M, Breyton C, Franck F, Wollman FA, Niyogi KK, Krieger-Liszkay A, Minagawa J, Finazzi G (2013) A dual strategy to cope with high light in *Chlamydomonas reinhardtii*. Plant Cell 25:545-557.

Anbudurai PR, Mor TS, Ohad I, Shestakov SV, Pakrasi HB (1994) The ctpA gene encodes the C-terminal processing protease for the D1 protein of the photosystem II reaction center complex. Proceedings of the National Academy of Sciences 91:8082-8086

Armbruster U, Zuhlke J, Rengstl B, Kreller R, Makarenko E, Ruhle T, Schunemann D, Jahns P, Weisshaar B, Nickelsen J, Leister D (2010) The *Arabidopsis* thylakoid protein PAM68 is required for efficient D1 biogenesis and photosystem II assembly. Plant Cell 22:3439-3460.

Bae S, Park J, Kim J-S (2014) Cas-OFFinder: a fast and versatile algorithm that searches for potential off-target sites of Cas9 RNA-guided endonucleases. Bioinformatics 30:1473-1475.

Baek K, Kim DH, Jeong J, Sim SJ, Melis A, Kim J-S, Jin E, Bae S (2016) DNA-free two-gene knockout in C*hlamydomonas reinhardtii* via CRISPR-Cas9 ribonucleoproteins. Sci Rep-Uk 6:30620.

Boehm M, Romero E, Reisinger V, Yu J, Komenda J, Eichacker LA, Dekker JP, Nixon PJ (2011) Investigating the early stages of Photosystem II assembly in *Synechocystis sp.* PCC 6803: isolation of CP47 and CP43 complexes. Journal of biological chemistry 286:14812-14819.

Bonente G, Pippa S, Castellano S, Bassi R, Ballottari M (2012) Acclimation of *Chlamydomonas reinhardtii* to different growth irradiances. The Journal of biological chemistry 287:5833-5847.

Bricker TM (1990) The structure and function of CPa-1 and CPa-2 in Photosystem II. Photosynth Res 24:1-13.

Bricker TM, Frankel LK (2002) The structure and function of CP47 and CP43 in Photosystem II. Photosynth Res 72:131.

Bricker TM, Roose JL, Fagerlund RD, Frankel LK, Eaton-Rye JJ (2012) The extrinsic proteins of Photosystem II. Biochim Biophys Acta 1817:121-142.

Cai, Wenhe, Jinfang Ma, Wei Chi, Meijuan Zou, Jinkui Guo, Congming Lu, and Lixin Zhang. 2010. “Cooperation of LPA3 and LPA2 Is Essential for Photosystem II Assembly in *Arabidopsis*.” *Plant Physiology*.

Cardol P, Bailleul B, Rappaport F, Derelle E, Beal D, Breyton C, Bailey S, Wollman FA, Grossman A, Moreau H, Finazzi G (2008) An original adaptation of photosynthesis in the marine green alga *Ostreococcus*. Proceedings of the National Academy of Sciences of the United States of America 105:7881-7886.

Chi W, Ma J, Zhang L (2012) Regulatory factors for the assembly of thylakoid membrane protein complexes. Philosophical transactions of the royal society B: biological sciences 367:3420-3429

de Vitry C, Olive J, Drapier D, Recouvreur M, Wollman FA (1989) Posttranslational events leading to the assembly of photosystem II protein complex: a study using photosynthesis mutants from *Chlamydomonas reinhardtii*. J Cell Biol 109:991-1006.

Edgar RC (2004) MUSCLE: multiple sequence alignment with high accuracy and high throughput. Nucleic acids research 32:1792-1797.

Ferrante P, Ballottari M, Bonente G, Giuliano G, Bassi R (2012) LHCBM1 and LHCBM2/7 Polypeptides, Components of Major LHCII Complex, Have Distinct Functional Roles in Photosynthetic Antenna System of *Chlamydomonas reinhardtii*. Journal of Biological Chemistry 287:16276-16288.

Fischer WW, Hemp J, Johnson JE (2016) Evolution of oxygenic photosynthesis. Annual review of earth and planetary sciences 44:647-683.

Fleischmann MM, Ravanel S, Delosme R, Olive J, Zito F, Wollman FA, Rochaix JD (1999) Isolation and characterization of photoautotrophic mutants of *Chlamydomonas reinhardtii* deficient in state transition. The Journal of biological chemistry 274:30987-30994.

Gokhale Z, Sayre RT (2009) Photosystem II, a structural perspective. In: Stern DB, Witman GB (eds) The *Chlamydomonas* Sourcebook (Second Edition). Academic Press, London, pp 573-602.

Govindjee, Kern JF, Messinger J, Whitmarsh J (2001) Photosystem II. In: eLS. John Wiley & Sons, Ltd.

Järvi S, Suorsa M, Aro E-M (2015) Photosystem II repair in plant chloroplasts - Regulation, assisting proteins and shared components with photosystem II biogenesis. Biochimica et Biophysica Acta (BBA) - Bioenergetics 1847:900-909.

Jeong J, Baek K, Kirst H, Melis A, Jin E (2017) Loss of CpSRP54 function leads to a truncated light-harvesting antenna size in *Chlamydomonas reinhardtii*. Biochim Biophys Acta Bioenerg 1858:45-55.

Jeong J, Baek K, Yu J, Kirst H, Betterle N, Shin W, Bae S, Melis A, Jin E (2018) Deletion of the chloroplast LTD protein impedes LHCI import and PSI–LHCI assembly in *Chlamydomonas reinhardtii*. J Exp Bot 69:1147-1158.

Jin E, Yokthongwattana K, Polle JE, Melis A (2003) Role of the reversible xanthophyll cycle in the photosystem II damage and repair cycle in *Dunaliella salina*. Plant Physiol 132:352-364.

Kirst H, Melis A (2014) The chloroplast signal recognition particle (CpSRP) pathway as a tool to minimize chlorophyll antenna size and maximize photosynthetic productivity. Biotechnol Adv 32:66-72.

Komenda J, Knoppová J, Kopečná J, Sobotka R, Halada P, Yu J, Nickelsen J, Boehm M, Nixon PJ (2012) The Psb27 Assembly Factor Binds to the CP43 Complex of Photosystem II in the Cyanobacterium *Synechocystis sp*. PCC 6803. Plant Physiol 158:476-486.

Kropat, Janette, Anne Hong-Hermesdorf, David Casero, Petr Ent, Madeli Castruita, Matteo Pellegrini, Sabeeha S. Merchant, and Davin Malasarn. 2011. "A Revised Mineral Nutrient Supplement Increases Biomass and Growth Rate in *Chlamydomonas reinhardtii*." *Plant Journal*.

Laemmli UK (1970) Cleavage of structural proteins during the assembly of the head of bacteriophage T4. Nature 227:680-685.

Lagarde D, Beuf L, Vermaas W (2000) Increased production of zeaxanthin and other pigments by application of genetic engineering techniques to *Synechocystis sp.* strain PCC 6803. Appl Environ Microbiol 66:64-72

Lu Y (2016) Identification and roles of photosystem II assembly, stability, and repair factors in *Arabidopsis*. Frontiers in plant science 7 (168).

Ma, Jinfang, Lianwei Peng, Jinkui Guo, Qingtao Lu, Congming Lu, and Lixin Zhang. 2007. "LPA2 Is Required for Efficient Assembly of Photosystem II in *Arabidopsis thaliana*." *Plant Cell*.

Marín-Navarro J, Manuell AL, Wu J, P. Mayfield S (2007) Chloroplast translation regulation. Photosynth Res 94:359-374.

Melis A (1999) Photosystem-II damage and repair cycle in chloroplasts: what modulates the rate of photodamage in vivo? Trends in Plant Science 4:130- .

Nanba O, Satoh K (1987) Isolation of a photosystem II reaction center consisting of D-1 and D-2 polypeptides and cytochrome b-559. Proceedings of the national academy of sciences 84:109-112

Nelson N, Junge W (2015) Structure and energy transfer in photosystems of oxygenic photosynthesis. Annual review of biochemistry 84 (1):659-683.

Nickelsen J, Rengstl B (2013) Photosystem II assembly: from cyanobacteria to plants. Annual review of plant biology 64:609-635.

Park J, Lim K, Kim J-S, Bae S (2017) Cas-analyzer: an online tool for assessing genome editing results using NGS data. Bioinformatics 33:286-288.

Perozeni, Federico, Giulio Rocco Stella, and Matteo Ballottari. 2018. "LHCSR Expression under HSP70/RBCS2 Promoter as a Strategy to Increase Productivity in Microalgae." *International Journal of Molecular Sciences*.

Roegner M, Chisholm DA, Diner BA (1991) Site-directed mutagenesis of the psbC gene of photosystem II: isolation and functional characterization of CP43-less photosystem II core complexes. Biochemistry 30:5387-5395.

Saitou N, Nei M (1987) The neighbor-joining method: a new method for reconstructing phylogenetic trees. Molecular Biology and Evolution 4:406-425.

Suorsa M, Aro E-M (2007) Expression, assembly and auxiliary functions of photosystem II oxygen-evolving proteins in higher plants. Photosynth Res 93:89-100.

Umena Y, Kawakami K, Shen J-R, Kamiya N (2011) Crystal structure of oxygen-evolving photosystem II at a resolution of 1.9 Å. Nature 473:55.

Wang P, Liu J, Liu B, Feng D, Da Q, Wang P, Shu S, Su J, Zhang Y, Wang J, Wang H-B (2013) Evidence for a Role of Chloroplastic m-Type Thioredoxins in the Biogenesis of Photosystem II in *Arabidopsis*. Plant Physiol 163:1710-1728.

Wei L, Guo J, Ouyang M, Sun X, Ma J, Chi W, Lu C, Zhang L (2010) LPA19, a Psb27 Homolog in *Arabidopsis thaliana*, Facilitates D1 Protein Precursor Processing during PSII Biogenesis. Journal of Biological Chemistry 285:21391-21398.

Wobbe L, Bassi R, Kruse O (2016) Multi-level light capture control in plants and green algae. Trends in plant science 21:55-68.

Zerges W, Auchincloss AH, Rochaix J-D (2003) Multiple translational control sequences in the 5′ leader of the chloroplast psbC mRNA Interact with nuclear gene products in *Chlamydomonas reinhardtii.* Genetics 163:895-904

Zhang D, Zhou G, Liu B, Kong Y, Chen N, Qiu Q, Yin H, An J, Zhang F, Chen F (2011) HCF243 Encodes a Chloroplast-Localized Protein Involved in the D1 Protein Stability of the *Arabidopsis* Photosystem II Complex. Plant Physiol 157:608-619.

Zhang S, Frankel LK, Bricker TM (2010) The Sll0606 Protein Is Required for Photosystem II Assembly/Stability in the Cyanobacterium *Synechocystis sp.* PCC 6803. Journal of Biological Chemistry 285:32047-32054.

Ziehe D, Dunschede B, Schunemann D (2017) From bacteria to chloroplasts: evolution of the chloroplast SRP system. Biol Chem 398:653-661.

SUPPLEMENTARY INFORMATION

Supplemental tables

Table S1. Accession numbers of LPA2 homologs used in the phylogenetic analysis.

Species	Group	Gene bank/Phytozome accession number
Amaranthus hypochondriacus	Dicotyledoneae	AHYPO_006270-RA
Amborella trichopoda	Basal Angiosperm	evm_27.model.AmTr_v1.0_scaffold00058.17
Ananas comosus	Basal Angiosperm	Aco026752
Aquilegia caerulea	Dicotyledoneae	Aqcoe7G073500
Arabidopsis thaliana	Dicotyledoneae	AT5G51545
Boechera stricta	Dicotyledoneae	Bostr.15774s0292
Brachypodium distachyon	Monocotyledoneae	Bradi3g02420
Brassica rapa FPsc	Dicotyledoneae	Brara.C01471
Capsella rubella	Dicotyledoneae	Carubv10027154m
Carica papaya	Dicotyledoneae	evm.model.supercontig_3.292
Chlamydomonas reinhardtii	Chlorophyte	Cre02.g105650
Chlorella variabilis	Chlorophyte	XP_005849843.1
Citrus clementina	Dicotyledoneae	Ciclev10005924m
Cucumis sativus	Dicotyledoneae	Cucsa.251500.1
Dunaliella salina	Chlorophyte	Dusal.0628s00005.1
Eucalyptus grandis	Dicotyledoneae	Eucgr.A02878
Eutrema salsugineum	Dicotyledoneae	Thhalv10015015m
Fragaria vesca	Dicotyledoneae	mrna21269.1-v1.0-hybrid
Glycine max	Dicotyledoneae	Glyma.09G232600
Gossypium raimondii	Dicotyledoneae	Gorai.001G046100
Kalanchoe laxiflora	Dicotyledoneae	Kalax.0009s0079
Linum usitatissimum	Dicotyledoneae	Lus10031710
Linum usitatissimum 2	Dicotyledoneae	Lus10031131
Manihot esculenta	Dicotyledoneae	Manes.14G034000
Marchantia polymorpha	Embryophyte	Mapoly0002s0242
Medicago truncatula	Dicotyledoneae	Medtr4g035825
Mimulus guttatus	Dicotyledoneae	Migut.F00451

Musa acuminata	Basal Angiosperm	GSMUA_Achr1T08220_001
Oropetium thomaeum	Monocotyledoneae	Oropetium_20150105_14227A
Oryza sativa	Monocotyledoneae	Os02g03250
Panicum virgatum	Dicotyledoneae	Pavir.Ab00158
Panicum virgatum	Monocotyledoneae	Pavir.Aa03429
Panicum virgatum 2	Monocotyledoneae	Pavir.J26988
Phaseolus vulgaris	Dicotyledoneae	Phvul.011G004500
Physcomitrella patens	Embryophyte	Pp3c26_11240V3
Populus trichocarpa	Dicotyledoneae	Potri.015G129600
Prunus persica	Dicotyledoneae	Prupe.2G280700
Salix purpurea	Dicotyledoneae	SapurV1A.0456s0270.1
Setaria viridis	Monocotyledoneae	Sevir.1G102700
Solanum lycopersicum	Dicotyledoneae	Solyc03g083570
Sorghum bicolor	Monocotyledoneae	Sobic.004G023400
Sphagnum fallax	Embryophyte	Sphfalx0027s0201
Spirodela polyrhiza	Basal Angiosperm	Spipo16G0002300
Theobroma cacao	Dicotyledoneae	Thecc1EG014960t1
Trifolium pratense	Dicotyledoneae	Tp57577_TGAC_v2_mRNA15623
Vitis vinifera	Dicotyledoneae	GSVIVT01018558001
Volvox carteri	Chlorophyte	Vocar.0083s0005.1
Zea mays	Monocotyledoneae	GRMZM2G043500_T01

Table S2. Target sequences of sgRNA used to recognize the *lpa2* gene.

	RGEN target (5' to 3')	Position	Cleavage position (%)	Direction	GC content (%, w/o PAM)	Out-of-frame score	Mismatches				
							0	1	2	3	4
gRNA1	GTTGTCCGCTCCAAGGGCTTTGG	79	18.03	+	60	59.4	1	0	0	0	8
gRNA2	CAAGGGCTTTGGTTCAGAGACGG	90	20.11	+	50	74.4	1	0	0	0	5
gRNA3	GCAAGCACCTCCAAGCCGTCGGG	139	29.41	+	65	50.2	1	0	0	2	17
gRNA4	CAAGGGGCGTGTTGAGCCCAAGG	216	44.02	+	65	62.7	1	0	0	0	11

Table S3. Mutation (insertion and deletion; indel) frequency of wild type and RGEN-transfected cells for each sgRNA.

Target sites	Cells	Total counts	Mutation counts	Mutation ratio (%)
lpa2	Wild type	53898	21	0.00%
	gRNA1	52609	71	0.10%
	Wild type	42061	3	0.00%
	gRNA2	41760	172	0.40%
	Wild type	32156	2	0.00%
	gRNA3	34532	492	1.40%
	Wild type	334	0	0.00%
	gRNA4	316	0	0.00%

Table S4. Analysis of off-target effects in the wild type and *lpa2* mutant. Mutation frequencies at potential off-target sites of the *lpa2* gene-specific sgRNA2 were measured by targeted deep sequencing in the wild type and *lpa2#2*. Potential off-target sites that differed from the on-target sites by up to 4 nucleotides were selected. Different nucleotides between the on-target and off-target are highlighted in red.

Target (5' to 3')	Cells	Total counts	Mutation counts	Mutation ratio (%)
CAAGtGCTTTGGcTtcGAGACGG	Wild type	31640	0	0.00%
	lpa2 #2	23022	0	0.00%
gAAGGGCTgTGGgTCAGAGgAGG	Wild type	145319	53	0.00%
	lpa2 #2	129094	63	0.00%
CgAGGGCTTTGGTgCcGgGATGG	Wild type	274203	2190	0.80%
	lpa2 #2	255326	1996	0.80%
CgAGGGCTTTGGTgCcGgGATGG	Wild type	165055	747	0.00%
	lpa2 #2	155692	622	0.00%
CAAGGGCTTcGGTgCAGccAAGG	Wild type	45015	5	0.00%
	lpa2 #2	41168	10	0.00%
CAAGcGCTTTGcaTCAGAGgTGG	Wild type	30798	0	0.00%
	lpa2 #2	29474	2	0.00%

Supplemental figures

Figure S1. ***LPA2* expression in *C. reinhardtii*.** A. RNA expression analysis of *LPA2* with *psbC* and *ELIP* in *Chlamydomonas reinhardtii*. qRT PCR was performed with the RNAs extracted from wild type cells exposed to high light (500 µmol photons m^{-2} s^{-1}) for 0, 30, and 60 minutes (n ≥ 3; values shown are means ± SE). B. Immunoblot analysis of WT *C. reinhardtii* fractions. C, chloroplast fraction; S, stroma fraction; T, thylakoids fraction. Proteins were loaded on an equal protein basis (30 µg).

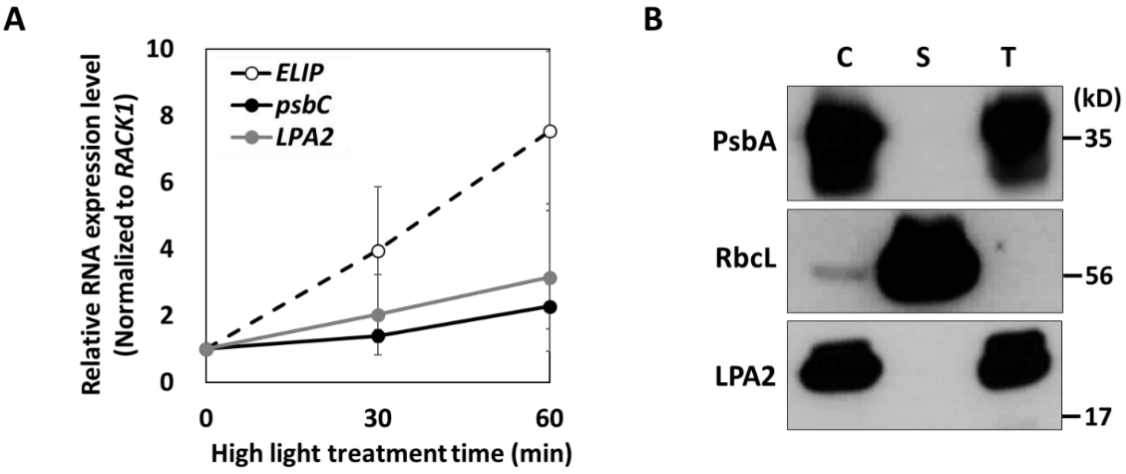

Figure S2. **77K fluorescence emission spectra of wild type (WT) and *lpa2* mutant.**

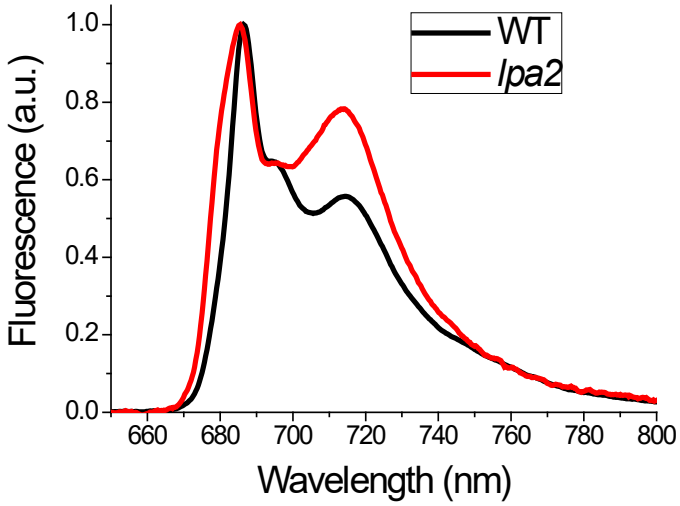

Figure S3. Maximum P700 oxidation (A) and light dependent Electrochromic Shift (ECS; B) normalized on a cell basis.

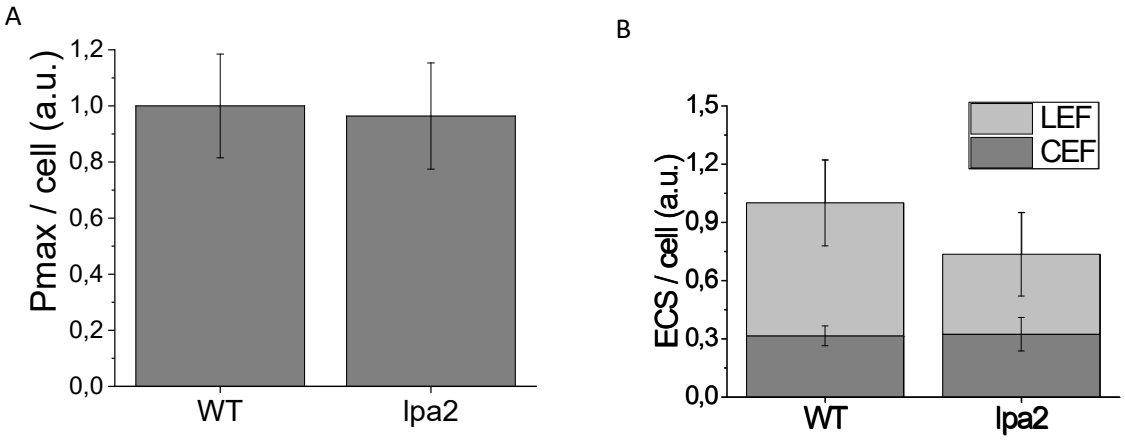

Figure S4. The comparison of transcription level of *PsbC* and *LPA2* in WT and *lpa2* mutant. Time course analysis of relative *psbC* and *LPA2* transcripts in both WT and *lpa2* mutant.

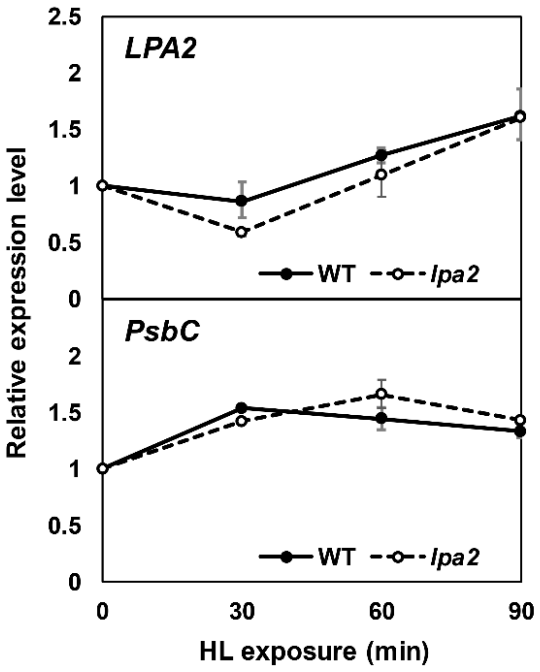

Section B

Impaired mitochondrial transcription termination disrupts the stromal redox poise in *Chlamydomonas*

A. Uhmeyer[1], **M. Cecchin**[2], M. Ballottari[2] and L. Wobbe[1]

[1]Bielefeld University, Faculty of Biology, Center for Biotechnology, 33615 Bielefeld, Germany

[2]Università degli Studi di Verona, Department of Biotechnology, 37134 Verona, Italy

This work was published in Plant physiology in July 2017.

In this section we investigate the relationship between chloroplast and mitochondrial metabolisms. We characterized the *Chlamydomonas reinhardtii* mutant *stm6* that is devoid of the mitochondrial transcription termination factor MOC1, resulting in enhanced photosynthetic hydrogen production and diminished light tolerance. We analysed the modulation of mitochondrial and chlororespiration during the acclimation of *stm6* and the *MOC1*-complemented strain to excess light. Although light stress stimulated mitochondrial respiration via the energy-conserving cytochrome *c* pathway in both strains, the mutant was unable to finetune the expression and activity of oxidative phosphorylation complex I in excess light, which was accompanied by an increased mitochondrial respiration via the alternative oxidase pathway. Furthermore, *stm6* failed to fully activate chlororespiration and cyclic electron flow due to a more oxidized state of the chloroplast stroma, which is caused by an increased mitochondrial electron sink capacity. Increased susceptibility to photoinhibition of PSII in *stm6* demonstrates that the MOC1-dependent modulation of mitochondrial respiration helps control the stromal redox poise as a crucial part of high-light acclimation in *C. reinhardtii*.

INTRODUCTION

Photosynthetic organisms apply multiple strategies to adjust their photosynthetic machineries and the cellular metabolism to changes in light quality and quantity (Noguchi and Yoshida, 2008). So far most of the studies carried out to analyze the mechanisms underlying light acclimation in higher plants and green algae have focused on the adjustment of biochemical processes in the chloroplast, as a response to constantly changing external factors affecting photosynthetic performance such as light availability. However, it is quite evident that unperturbed photosynthetic activity requires functional mitorespiration in the light (Noguchi and Yoshida, 2008), and this dependence was demonstrated by the characterization of mutants (Dutilleul et al., 2003; Sweetlove et al., 2006; Schönfeld et al., 2004) primarily affected in mitochondrial metabolism that display a severe impairment of photosynthetic performance.

Several functions of mitochondrial respiration in the light are discussed, and among the proposed functions is the prevention of a stromal overreduction under excess light conditions, implicating the export of chloroplast reducing equivalents and their consumption by mitochondria (Noguchi and Yoshida, 2008; Zhang et al., 2012). In higher plants, the non-proton pumping, respiratory enzyme alternative oxidase seems to be required for this “electron sink” function of mitochondria (Vishwakarma et al., 2014). In contrast to the components of the cytochrome *c* pathway, which pump protons across the inner mitochondrial membrane, enzymes of the alternative pathway do not contribute to ATP formation and are not inhibited by a large electrochemical proton gradient, which can exist under stress conditions (Rasmusson and Wallström, 2010). Besides dissipating excess reducing power in the chloroplast, a flow of reducing equivalents from the chloroplast to mitochondria can completely replace photophosphorylation as a source of cellular ATP, as was recently shown for the diatom *Phaeodactylum tricornutum* (Bailleul et al., 2015).

For the unicellular green alga *Chlamydomonas reinhardtii*, a large collection of *dum* mutants exists (for review, see Salinas et al., 2014), which lack individual components of the cytochrome pathway. These mutants have been characterized in detail regarding their photosynthetic performance under low-light conditions in the presence acetate (Cardol et al., 2003). The phenotype of *dum* mutants was characterized by a decreased quantum efficiency of linear photosynthetic electron transport and a block in state II with increased rates of cyclic electron transport (Cardol et al., 2003; Cardol et al., 2009). Furthermore, nonphotochemical plastoquinone reduction via chlororespiration is elevated in the mutants (Cardol et al., 2003; Houyoux et al., 2011). Although photosynthetic performance is decreased and light acclimation perturbed in *dum* mutants grown mixotrophically (Cardol et al., 2003), even the most affected *dum* mutants in terms of mitochondrial ATP production do not show a light-sensitive phenotype under photoautotrophic conditions (Dorthu et al., 1992; Cardol et al.,

2009). In contrast to observations made with *dum* mutants lacking complexes of the cytochrome pathway, a knockdown of the alternative oxidase AOX1 does not result in a decreased photosynthetic performance of *C. reinhardtii* cells, as can be concluded from an unaltered photosynthetic light saturation curve (Mathy et al., 2010).

Another *C. reinhardtii* mutant, affected in mitochondrial respiration and designated *stm6*, was identified in a forward genetics screen aiming at the identification of nuclear genes implicated in light acclimation processes (Schönfeld et al., 2004). The gene, knocked-out in this mutant, encodes the mitochondrial mTERF (Kleine and Leister, 2015) factorMOC1, which binds specifically to a sequence within the mitochondrial rRNA-coding module *S3* and prevents read-through transcription at this site by acting as a transcription terminator in vivo (Wobbe and Nixon, 2013). Besides decreasing the amount of unprocessed mitochondrial sense transcripts, a loss of MOC1 leads also to diminished amounts of mature transcripts encoding the oxidative phosphorylation (OXPHOS) complex I subunit *nd1* (Wobbe and Nixon, 2013). An interesting aspect of the phenotype displayed by *stm6* is that processes primarily located in the chloroplast are severely affected by the absence of functional mitochondrial transcription termination: the mutant produces high amounts of hydrogen under anaerobic conditions in the light (Kruse et al., 2005) and shows a reduced nonphotochemical quenching capacity associated with decreased light tolerance (Nguyen et al., 2011).

Enhanced photobiological hydrogen production could be partly explained by an increased respiratory consumption of acetate (Kruse et al., 2005) via cyanide-insensitive pathways (Schönfeld et al., 2004) that results in an earlier onset of hydrogen production by a quicker establishment of anaerobic conditions required for the activation of the hydrogenase pathway (Kruse et al., 2005; Doebbe et al., 2010; Nguyen et al., 2011). Additionally, this faster transition from aerobic to anaerobic conditions in sulfur-depleted *stm6* cultures was recently proposed to reduce the exposure time of PSII to reactive oxygen species formed in sulfur-deprived cells when the PSII repair cycle is impaired. In this study, a higher residual PSII activity was seen for *stm6* within the anaerobic phase and suggested as an explanation for the higher hydrogen production capacity, since both wild type and *stm6* maintained electron flow to the hydrogenase by water-splitting and linear electron transport (Volgusheva et al., 2013). However, several studies demonstrated the competition between cyclic electron flow and hydrogen production in *C. reinhardtii* (Tolleter et al., 2011; Steinbeck et al., 2015), and the inability of *stm6* to switch from linear to cyclic electron flow under anaerobic conditions (Kruse et al., 2005) should largely contribute to its elevated hydrogen production capacity.

Mitochondrial transcription termination mediated by MOC1 is enhanced following exposure of photoautotrophic *C. reinhardtii* cultures to excess light, which is accompanied by a strong accumulation of MOC1 under these conditions (Wobbe and Nixon 2013). At the same time, *stm6*

shows reduced growth under photoautotrophic high-light conditions (Schönfeld et al., 2004; Nguyen et al., 2011) and strong lipid peroxidation already under low-light conditions in acetate-containing medium (Schönfeld et al., 2004). Impaired accumulation of protein LHCSR3, as a key factor required for energy dependent quenching (qE), together with a lowered nonphotochemical quenching capacity were proposed to contribute to the high-light sensitivity of *stm6* (Nguyen et al., 2011), but the connection between perturbed light acclimation and altered mitochondrial respiration remained unclear.

In this study, we analyzed the modulation of mitochondrial respiration/chlororespiration and the impact of mitochondrial reductant uptake on the stromal redox poise following a transfer of photoautotrophic *C. reinhardtii* cultures from low light to high light that either contained or were devoid of MOC1.

RESULTS

A knockout of MOC1 perturbs the modulation of mitochondrial respiration occurring as a long-term response to excess light

As reported previously (Wobbe and Nixon, 2013), a transfer of photoautotrophically grown *C. reinhardtii* cultures from low light (100 µmol photons m^{-2} s^{-1}) to high light (1500 µmol photons m^{-2} s^{-1}) triggers an accumulation of the mitochondrial transcription termination factor MOC1 (Fig. 1A). Under these conditions, MOC1 accumulation enhances transcription termination at its binding site in the mitochondrial genome, resulting in a decline of mitochondrial antisense RNA levels, which originate from read-through transcription at an unoccupied binding site. In the same study (Wobbe and Nixon, 2013), expression of the *nd1* gene, encoding a mtDNA-encoded subunit of OXPHOS complex I, was shown to be most affected by a *MOC1* knockout among the protein-encoding genes present in the mitochondrial genome of *C. reinhardtii*. Under photoheterotrophic cultivation conditions and using moderate light intensities, absence of MOC1 results in a decreased accumulation of *nd1* transcripts (Wobbe and Nixon, 2013).

To analyze whether the high light-induced accumulation of MOC1 is accompanied by changes in the level of *nd1* transcripts (Fig. 1B), RT-qPCR was performed with RNA samples derived from low light- and high light-acclimated cells, which either contained MOC1 or were devoid of it. In the *MOC1*-complemented strain, referred to as *B13* (Schönfeld et al., 2004) in the following, *nd1* levels (Fig. 1B, black bars) remained unaltered after the onset of high light exposure (1.30 ± 0.37 [SE] at t_{3h} with t_0 set to 1). In the *MOC1* knockout mutant *stm6*, *nd1* levels were significantly ($P < 0.05$) lower than respective *B13* levels during high light exposure and at t_0 (Fig. 1B, red bars). While in strain *B13* the prestress levels of transcript *nd1* were maintained during prolonged high light exposure, *stm6*

displayed a different behaviour with lower transcript levels found at higher light intensities (0.72 ± 0.03 at t_0 versus 0.37 ± 0.14 at t_{3h}; $P < 0.1$). In line with earlier findings (Wobbe and Nixon, 2013), the differences seen between *B13* and *stm6* levels of *cox1*, encoding a subunit of OXPHOS complex IV, were insignificant for all time points (Fig. 1B, gray/orange bars; $P > 0.1$). Furthermore, none of the two strains showed significant alterations of the *cox1* transcript level after 3 h of high light exposure ($P > 0.1$). High light-induced changes in the level of *cob* transcript (green/blue bars), which encodes

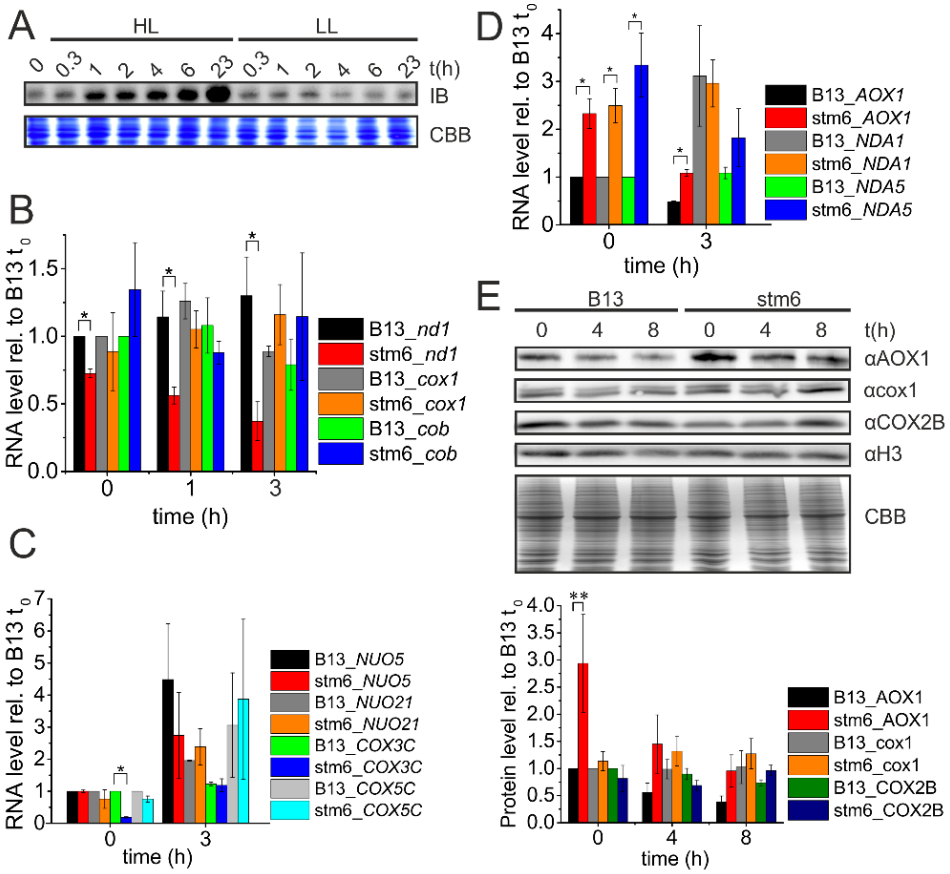

Figure 1. Gene expression modulation of mitorespiratory components in response to excess light is altered in mutant *stm6*. A, Immunodetection of MOC1 (IB) in the MOC1-complemented strain (B13). A photoautotrophic culture was grown at a low light intensity (100 µmol photons m^{-2} s^{-1}) before splitting it into two new cultures at t_{0h}. One of the cultures was cultivated at low light intensity (LL) and the other one under high light conditions (1500 µmol photons m^{-2} s^{-1}). Protein samples were taken at indicated time points. Loading control: Coomassie Brilliant Blue (CBB) stain. B, RT-qPCR analysis of *nd1*, *cox1*, and *cob* transcript levels in *B13* and *stm6* before (0h) and distinct hours after the onset of high light stress. Expression levels were normalized to the mRNA level of *B13* at t_{0h} (set to 1). SEs are derived from three biological replicates, each including at least three technical replicates (n = 3). Asterisks indicate significant differences between *B13* and *stm6* according to a two-tailed Student's t test (*$P < 0.05$; **$P < 0.1$). C, mRNA levels of nucleus-encoded complex I (*NUO5/21*) and complex IV subunits (*COX3C/5C*) before (0 h) and after exposure to high light (3 h). SEs are derived from two biological replicates, each including three technical replicates (n = 2). D, Expression levels of transcripts encoding mitochondrial alternative oxidase (*AOX1*) and two different rotenone-insensitive NAD(P)H dehydrogenases (*NDA1/5*). SEs are derived from three biological replicates, each including three technical replicates (n = 3). E, Immunodetection of proteins AOX1, cox1, COX2B, and histone H3. Top: Representative immunoblot results. Loading control: Immunodetection of histone H3 and Coomassie Brilliant Blue-staining (CBB). Bottom: Relative protein levels (B13 t_0 set to 1) obtained by densitometric scanning of immunoblot signals. Error bars indicate the SE derived from three biological replicates, each including three technical replicates (n = 3).

an OXPHOS complex III subunit, were insignificant, and for none of the time points significant strain-to-strain differences in *cob* levels could be observed (P > 0.1). To analyze the impact of high light stress on the expression of nucleus-encoded components of OXPHOS complex I and IV, two representative subunits were chosen for each respiratory complex (Fig. 1C). Transcript accumulation during high light acclimation could be observed for only *NUO21* in strain *B13* (gray bar; 1 versus 1.96 ± 0.01; P< 0.05), and differences between *stm6* and *B13* were seen for only *COX3C* at t_0 (green/ blue bars; 1 versus 0.19; P < 0.05).

We also analyzed if the application of high light stress alters the expression of genes encoding components of the alternative respiratory pathway in the mitochondrion (Fig. 1D). In *Chlamydomonas*, the gene *AOX1* encodes the major mitochondrial alternative oxidase (Dinant et al., 2001; Baurain et al., 2003), and *AOX1* mRNA levels declined in response to high light in both strains. Transcript levels of *AOX1* were, however, significantly (P < 0.05) higher in *stm6* (red bars) compared to *B13* (black bars) before (t_0; 2.33 ± 0.31 for *stm6* with *B13* set to 1) and during growth in high light (t_{3h}; 1.08 ± 0.07/*stm6* and 0.48 ± 0.01/*B13*). In contrast to *AOX1*, expression of the *NDA1* gene increased during cultivation of *B13* in high light (3.11 ± 1.05 at t_{3h} versus 1 at t_0; gray bars; P > 0.1). This gene encodes a matrix-facing rotenone-insensitive NAD(P)H dehydrogenase located in the inner mitochondrial membrane (Lecler et al., 2012). This strong difference between *NDA1* transcript levels in low and high light cultivated cells could not be seen in *stm6* (2.49 ± 0.36 at t_0 versus 2.96 ± 0.49 at t_{3h}; orange bars), which showed high levels already under low light conditions (2.49 ± 0.36 versus 1; P < 0.05). A higher mRNA level in *stm6* versus *B13* under low light conditions (3.34 ± 0.67 versus 1; P < 0.05) could also be observed for *NDA5* (UniProt KB: A6YT86; green/blue bars; see Supplemental Table S1 for Phytozome locus names), which encodes a putative rotenone-insensitive NAD(P)H dehydrogenase that is targeted to the mitochondrion according to the prediction tool PredAlgo (Tardif et al., 2012). *NDA1* and *NDA5* mRNA levels did not differ significantly between high light-grown *stm6* and *B13* cells (P > 0.1), and changes in the transcript level between low and high light conditions were insignificant for *NDA5* in both cell lines (P > 0.1).

The higher level of *AOX1* mRNA in *stm6* versus *B13* under limited and excess light conditions was also reflected by higher AOX1 protein levels in low light- (t_0; 2.94 ± 0.90 versus 1; P < 0.1) and high light-cultivated (t_8; 0.96 ± 0.30 versus 0.39 ± 0.11; P > 0.1) *stm6* cells in comparison to those of cell line *B13* (Fig. 1E, αAOX1). In both strains the AOX1 level decreased following the exposure to high light (*stm6*/P > 0.1; *B13*/P < 0.05). Protein levels of the complex IV subunit COX2B (Fig. 1E, αCOX2B) declined in *B13* by about 25% (1 at t_0 versus 0.74 ± 0.05; P < 0.05). A similar, steady decline could not be observed for *stm6*, since COX2B protein levels remained almost unaltered after a transfer from low light to high light (0.82 ± 0.24 at t_0 versus 0.96 ± 0.10 at t_{8h}; P > 0.1). The levels of cox1 protein

did not differ significantly between both strains, and high light acclimation was not accompanied by significant changes in the amount of this protein either (P values > 0.1).

Overall, expression analyses revealed that *stm6* fails to maintain the prestress level of mitochondrial transcripts encoding the complex I subunit *nd1*, but expresses genes encoding enzymes required for alternative modes of respiration at higher levels than *B13*. While the protein and transcript levels of *AOX1* are constitutively higher in *stm6* compared to *B13* (Fig. 1, D and E), differences in the transcript levels of *NDA1/5* are more prominent under low light conditions (Fig. 1D). The acclimation to excess light implicates a strong down-regulation of *AOX1* expression, whereas observed transcriptional changes (Fig. 1C; *COX3C/5C*) and the analysis of protein levels (COX2B; cox1; Fig. 1E) do not indicate a similar expression pattern for complex IV components.

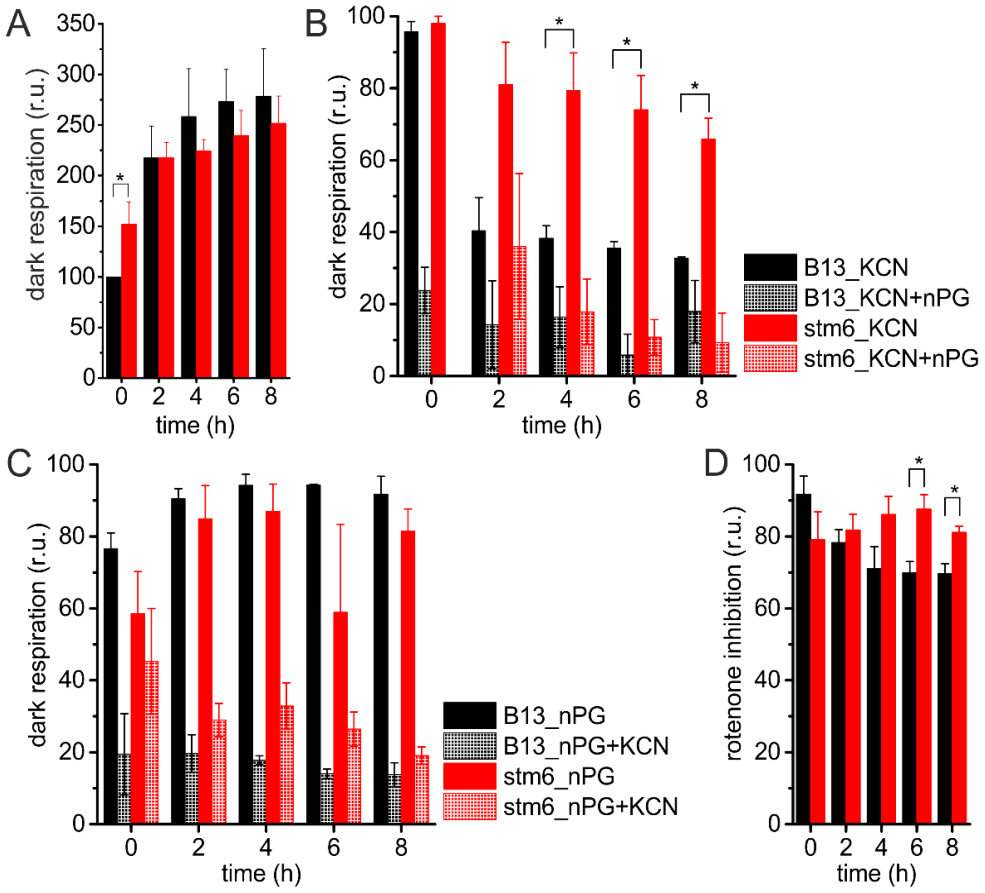

Figure 2. Perturbed acclimation of mitochondrial respiration in response to high light in the absence of MOC1. A, Dark respiration in *stm6* (red bars) and *B13* (black bars) before (t_0) and after the onset of high light stress (t2-8h). Values are normalized to the respiration rate determined for *B13* at t_0 (set to 100%). Error bars represent the SE derived from five biological replicates (n = 5). Asterisks indicate significant differences between *B13* and *stm6* according to a two-tailed Student's t test (P < 0.05). B, The relative contribution of alternative respiration (AOX/PTOX) to dark respiration. Alternative respiration was measured as dark respiration in the presence of 1 mM KCN, which could be inhibited by 1 mM nPG (KCN+nPG). Values are given relative to the dark respiration in the absence of inhibitor (set to 100%). SEs are derived from three biological replicates (n = 3). C, the relative contribution of OXPHOS complex IV to dark respiration was measured as dark respiration in the presence of 1 mM nPG, which could be inhibited by 1 mM KCN (nPG+KCN). D, Inhibition of OXPHOS complex I by the addition of 100 µM rotenone. Error bars indicate the SE derived from six biological replicates (n = 6).

To investigate if the differences between *stm6* and *B13* that were seen in regard to the expression modulation of genes implicated in mitochondrial respiration (Fig. 1) are translated into a distinct respiratory activity, dark respiration rates were determined for mutant *stm6* (red bars) and *B13* (black bars) before and after cultivation in excess light for several hours (Fig. 2A). In photoautotrophic low light conditions, *stm6* showed an increased rate of dark respiration (152 ± 21% [SE] versus 100% for *B13*), which is in accordance with higher respiratory rates previously found for the mutant during cultivation in the presence of acetate (Kruse et al., 2005). In both strains, exposure to excess light for 8 h dramatically increased the rates of dark respiration (∼180% [*B13*] and ∼150% [*stm6*] increase relative to t_0), and similar rates were recorded after prolonged high light cultivation (t_{8h}: 278 ± 47%/*B13* and 252 ± 27%/*stm6*).

A more detailed analysis of mitochondrial respiration in both strains revealed further differences (Fig. 2, B–D). Within mitochondrial respiration, oxygen can be either consumed via the classical cytochrome *c* pathway, implicating the full respiratory chain with OXPHOS complexes I, II, III, and IV, or by action of nonproton-pumping (energy-dissipative) pathways composed of the enzymes AOX (Moore et al., 2013) and rotenone-insensitive (type II) dehydrogenases (Møller et al., 1993). Importantly, the latter pathway, although efficient in consuming reducing power, does not contribute to ATP synthesis, whereas operation of the cytochrome c pathway generates a strong proton motive force enabling ATP production. In addition to respiratory pathways located in mitochondria, chlororespiration (Bennoun, 1982) can contribute to dark respiration. Within this pathway, electrons from NADPH can be transferred to oxygen via the concerted action of the plastid-localized NADPH:plastoquinone oxidoreductase NDA2 (Jans et al., 2008) and a plastid terminal oxidase (PTOX), which transfers electrons from plastoquinol to oxygen (Nawrocki et al., 2015). To determine the relative contribution of cyanide-sensitive complex IV (cytochrome *c* oxidase) and cyanide-insensitive alternative respiration (AOX and PTOX activity) to mitochondrial respiration (Fig. 2B), rates of dark respiration were analyzed in the presence/absence of potassium cyanide (Mathy et al., 2010). Complex IV-based activity was inhibited by adding potassium cyanide (Fig. 2B; *B13*/ *stm6*_KCN) to assess the relative activity of alternative respiration, which was subsequently inhibited (*B13*/ *stm6*_KCN+nPG) by the addition of *n*-propyl gallate (nPG; Møller et al., 1988; Vanlerberghe 2013). In low light-acclimated (t_0) cells of *B13* and *stm6*, the addition of KCN had similar effects (95.7 ± 2.9 [SE] for *B13* and 98.0 ± 2.0 for *stm6*) on the rates of dark oxygen uptake, but in contrast to *B13* cyanide-insensitive respiration could be fully inhibited by the addition of nPG in *stm6* (t_0; *B13*/*stm6*_KCN+nPG), indicating that oxygen consumption in cyanide-treated *B13* cultures was not merely based on alternative respiration (AOX+PTOX). In the course of high light-treatment (t_{2h}–t_{8h}), strong differences in the activity of cyanide-insensitive respiration between *stm6* and *B13* became

evident. Cyanide-insensitive respiration was significantly higher in *stm6* versus *B13* (t_{4h}–t_{8h}; $P < 0.05$) and at the end of the time-course, *stm6* displayed a 2-fold higher relative contribution of cyanide-insensitive respiration (65.8 ± 5.8 versus 32.7 ± 0.4). Except for time points t_0 and t_{2h}, the residual respiration, unrelated to complex IV activity or alternative respiration and observed after adding KCN along with nPG to *B13* and *stm6* cultures, was comparable. The acclimation to high light was accompanied by a significant decrease (t_0 versus t_{8h}; $P < 0.05$ for *B13* and *stm6*) in the relative contribution of alternative respiration, which was more pronounced in *B13* (63% decrease in *B13* versus 32% in *stm6* from t_0 to t_{8h}). A more prominent decrease of alternative respiration following high light acclimation in *B13* versus *stm6* could also be observed, when alternative respiration was calculated by subtracting residual respiration (KCN + nPG) from cyanide-insensitive respiration (KCN) before normalizing to cell counts (Supplemental Fig. S1). While for *B13* an ∼50% reduction (100% at t_0 versus 50 ± 21% at t_{8h}; $P < 0.1$) in alternative respiration rates per cell was notable, such a decrease could not be observed for *stm6* (213 ± 50% at t_0 versus 295 ± 167% at t_{8h}; $P > 0.1$). In addition, cellular rates of alternative respiration were higher in *stm6* compared to *B13* throughout the entire time-course. The higher amounts of AOX1 protein in *stm6* (∼2-fold) compared to *B13* (Fig. 1E; αAOX1), which were observed in low light and excess light conditions, indicate that alternative respiration, highly active in *stm6*, is mainly composed of AOX1-based oxygen consumption. When nPG addition preceded the addition of KCN (Fig. 2C; *B13*/ *stm6*_nPG), the differences between *B13* and *stm6* were statistically insignificant ($P > 0.05$), indicating that complex IV contributes to mitochondrial respiration to a comparable extent in both strains. This is in good agreement with the comparable expression of complex IV subunits in *B13* and *stm6* (Fig. 2; COX3C/5C; COX2B; cox1) observed for light-stressed cells. The increase in the relative contribution of nPG-insensitive (complex IV) respiration seen for both strains after a transfer from low to high light (from 76.6 ± 4.3% to 91.7 ± 5.0% in *B13* and from 58.5 ± 11.6% to 81.5 ± 6.2% in *stm6*) was not statistically significant ($P > 0.05$). Respiration in the presence of nPG could be effectively inhibited by the addition of KCN, demonstrating that nPG-insensitive respiration was mainly composed of complex IV activity (*B13*/*stm6*_nPG+KCN).

The inhibitor rotenone in conjunction with dark respiration measurements can be used to disentangle complex I-based electron transfer from NADH to ubiquinone and the respective transfer catalyzed by rotenone-insensitive type II-dehydrogenases (Møller et al., 1993; Lecler et al., 2012). To assess the relative contribution of complex I activity to mitochondrial electron transport in low light- and high light acclimated cells, the inhibiting effect of rotenone on dark respiration was analyzed in *B13* and *stm6* (Fig. 2D). The effect of rotenone on dark respiration increased during the acclimation to excess light in *B13* (91.8 ± 5.0% at t_0 versus 69.7 ± 2.7% at t_{8h}; $P < 0.05$), indicating that the

acclimation to excess light implicates a modulation of complex I activity. An increased engagement of complex I in mitochondrial electron transport following high light acclimation could not be noted for *stm6* (79.1 ± 7.7% at t_0 versus 81.2 ± 1.7% at t_{8h}). After several hours of high light exposure, rotenone had significantly smaller (~10–15%) effects on dark respiration in *stm6* compared to *B13* (t_{6h} and t_{8h}; $P < 0.05$). A lower contribution of complex I to mitochondrial respiration in light-stressed *stm6* cells corresponds well to the mutants' inability to maintain the prestress level of mitochondrial transcript *nd1*, encoding a key subunit of complex I, after the exposure to excess light (Fig. 1B, nd1). Higher transcript levels of NDA1 and NDA5 (Fig. 1D), encoding rotenone insensitive NAD(P)H dehydrogenases, in low light acclimated *stm6* cells were, however, not reflected by a lower sensitivity of dark respiration toward rotenone (Fig. 2D, t_0).

It should be noted, however, that the effects exerted on dark respiration by KCN were much more prominent than those seen for nPG or rotenone. Especially for inhibitors of the alternative pathway, it is known that their effect on dark respiration is moderate and that the actual contribution of alternative respiration is obscured by compensatory changes in other pathways, if used alone (Møller et al., 1988).

An analysis of the respiratory activity displayed by *stm6* and *B13* under high light stress revealed remarkable differences. Mitochondrial electron transport in the mutant implicates energy-dissipating pathways to a greater extent, which produce less ATP per molecule of oxygen consumed. A higher contribution of respiratory electron flow based on the activity of AOX (Fig. 2B) is in good agreement with the higher mRNA and protein levels found for AOX1 before and during exposure to excess light (Fig. 1, D and E). In both strains, the exposure to light stress stimulated mitochondrial respiration (Fig. 2A) and increased the relative contribution of energy-conserving pathways involving complex IV (Fig. 2, B and C). A diminished contribution of AOX-based respiration under high light conditions in both strains fits well to the decrease in protein levels in response to light stress (Fig. 1E). Although AOX activity decreases in both strains following exposure to high light, the remaining AOX1 activity in *stm6* is higher than that observed in *B13*, which is in accordance with higher AOX1 levels detected in light-stressed *stm6* cells (Fig. 1E). Although transcript analyses suggest that *stm6* accumulates higher amounts of rotenone-insensitive dehydrogenases under low light conditions, a lower sensitivity of dark respiration toward rotenone could not be seen for *stm6* under these conditions. In contrast to *B13*, however, the mutant fails to adjust complex I activity in response to excess light, and the lower relative contribution of complex I (Fig. 2D) corresponds nicely to the decline in *nd1* transcript levels following the onset of light stress (Fig. 1B).

The MOC1-free mutant fails to induce chlororespiration in response to excess light

A knockout (Schönfeld et al., 2004) or knockdown (Nguyen et al., 2011) of MOC1 has been reported to decrease the growth rate of *C. reinhardtii* cells under high light conditions. We wanted to assess whether this reduced light tolerance is caused by an increased susceptibility of *stm6* to photoinhibition. The degree of photoinhibition upon exposure to high light can be estimated by measuring the quantum yield of PSII (F_v/F_m) following a dark incubation (Maxwell and Johnson, 2000).

Within the first 2 h of high light treatment, the MOC1- complemented strain *B13* (black squares) showed a significant decline of the maximum PSII quantum yield (from 0.76 ± 0.02 [SE] to 0.55 ± 0.02; Fig. 3A). From the second hour onwards, however, F_v/F_m values did not decline further, indicating successful acclimation to high light stress in the presence of MOC1 (0.52 ± 0.02 at t_{8h}). In contrast, the maximum quantum yield decreased continuously in *stm6* (red circles) and was significantly lower in the mutant compared to the complemented strain after 8 h of cultivation (0.52 ± 0.02 [*B13*] versus 0.25 ± 0.04 [*stm6*]). Importantly, starting values were almost identical in both

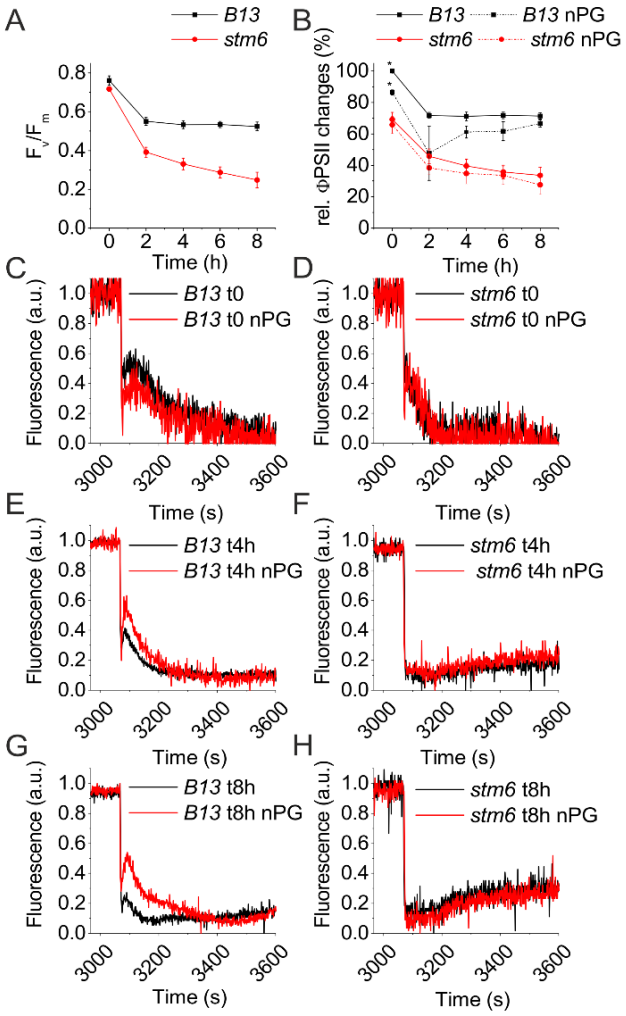

Figure 3. The mutant *stm6* shows stronger photoinhibition and lower chlororespiration than the MOC1-complemented strain under high light conditions. A, F_v/F_m of dark-adapted *B13* (black squares) and *stm6* (red circles) cells determined after photoautotrophic growth in low light (100 µmol photons m^{-2} s^{-1}; t_0) or following exposure to high light (1500 µmol photons m^{-2} s^{-1}; $t_{2\text{-}8h}$) for several hours. Error bars indicate the SE derived from five biological replicates (n = 5). B, ΦPSII determined for *B13* (black squares; t_0 set to 100%) and *stm6* (red circles) during actinic light illumination (800 µmol photons m^{-2} s^{-1}) in the presence (dotted lines) or absence (continuous lines) of nPG. Error bars indicate the SE derived from three biological replicates (n = 3) and asterisks significant nPG effects (P < 0.05). C, Kinetics of chlorophyll fluorescence emission in the dark after 5 min of illumination with 150 µmol photons m^{-2} s^{-1} white actinic light for *B13* (C, E, and G) and *stm6* (D, F, and H). Samples were taken from low light (t_0)- and high light-acclimated (t_{4h}, t_{8h}) cultures and nPG added to inhibit PTOX.

strains (0.76 ± 0.02 [*B13*] versus 0.72 ± 0.01 [*stm6*]), which demonstrates that observed differences are high light induced.

An analysis of the stoichiometric composition of the photosynthetic apparatus in low and high light acclimated cells revealed further differences between *stm6* and *B13* (Table I; Supplemental Fig. S2). Immunodetection of CP43, PSAA, and LHCII was used to quantify changes in the amount of PSII, PSI, and major light harvesting antenna, respectively (Supplemental Fig. S2). In *B13*, the PSI/PSII ratio declined after 8 h of high light exposure, while the opposite trend was observed for *stm6*, which was mainly based on a decrease in CP43 levels (from 0.99 ± 0.16 to 0.43 ± 0.02), which were used as a proxy for PSII. To confirm the different PSI and PSII accumulation in *B13* and *stm6*, the PSI/PSII ratios were evaluated also by electrochromic shift measurements (Bailleul et al., 2010). While at t_0 a similar PSI/ PSII ratio was detected for *stm6* and *B13* (1.39 ± 0.23 and 1.60 ± 0.12, respectively), after 8 h of illumination a decrease of the PSI/PSII ratio was evident for *B13* (PSI/PSII ratio decreased to 0.87 ± 0.16), but not for *stm6*, where rather a significant increase of the PSI/PSII ratio was observed (to 1.80 ± 0.23). This increase in the PSI/PSII ratio and the reduction in CP43 levels observed in *stm6* might be partly attributed to the strong photoinhibition seen for *stm6* cells cultivated in excess light (Fig. 3A). Consistently, LHCII/PSII ratios increased during the high light treatment only in *stm6* (2.71 ± 0.57 at t_{8h} versus 0.63 ± 0.10 at t_0).

Altered mitochondrial respiration has been shown to affect chlororespiration in *C. reinhardtii* (Houyoux et al., 2011), a process that can dissipate excess reducing equivalents formed in high light (Houyoux et al., 2011) or during nitrogen deprivation (Saroussi et al., 2016). To investigate, if an altered PTOX activity in *B13* affects photosynthetic electron transport and the plastoquinone (PQ) pool redox state (Fig. 3B) in the light, we determined the quantum yield of PSII (ΦPSII) in the presence and absence of nPG (Formighieri et al., 2012). In *B13* (black squares), inhibition of PTOX (dotted lines) significantly ($P < 0.05$) reduced ΦPSII in low light grown cells (t_0; 100% versus 86.4 ± 1.6% [SE]), whereas the effects of nPG addition were insignificant ($P > 0.05$) in low light-acclimated

Low Light (t_0)		
	B13	*Stm6*
ARSA	1.00 ± 0.06	0.97 ± 0.02
PSAA	1.00 ± 0.09	0.67 ± 0.10
CP43	1.00 ± 0.03	0.99 ± 0.16
LHCII	1.00 ± 0.07	0.62 ± 0.03
PSI/PSII	1.00 ± 0.11	0.67 ± 0.10
LHCII/PSII	1.00 ± 0.07	0.63 ± 0.10
High light (t_{8h})		
	B13	*Stm6*
ARSA	1.00 ± 0.14	1.08 ± 0.10
PSAA	0.74 ± 0.10	0.53 ± 0.04
CP43	0.97 ± 0.14	0.43 ± 0.02
LHCII	0.93 ± 0.15	1.17 ± 0.24
PSI/PSII	0.77 ± 0.16	1.21 ± 0.26
LHCII/PSII	0.96 ± 0.21	2.71 ± 0.57

Table 1. Stoichiometric changes in components of the photosynthetic apparatus following excess light acclimation. Results from immunoblot analyses (Supplemental Fig. S1) in conjunction with densitometric scanning of blot signals performed with LL- and HL-grown *stm6* and *B13* cultures and antisera raised against psaA, CP43, LHCII, and ARSA. The relative content of PSI (psaA) and PSII (CP43) was determined on a per chlorophyll basis; SDs are derived from five biological replicates.

stm6 cultures (red circles, 69.3 ± 4.4% versus 65.8 ± 5.5%). The reduced photochemical quantum yield (~30% lower) of low light-acclimated *stm6* cells in comparison to those of *B13* could reflect the lowered PSI/PSII ratio (Table I) besides a diminished activity of PTOX. ΦPSII differences caused by nPG addition were insignificant ($P > 0.05$) in high light acclimated cells (t_{2h}-t_{8h}) of both strains.

Chlororespiration was thus investigated in both strains by recording the post illumination F_0 fluorescence rise in the presence of nPG, which can be used to assess the nonphotochemical reduction of the plastoquinone pool via NAD(P)H:plastoquinone oxidoreductases (Fig. 3, C–H). In the case of *B13*, a transient increase of F_0 was evident at t_0 or after 4 and 8 h of high light illumination, which was further increased in the presence of nPG at t_{4h} and t_{8h}. These results demonstrate that high light increases the rate of nonphotochemical plastoquinone reduction in *B13*. Differently, in the case of *stm6*, neither a transient F_0 rise nor an effect of nPG could be detected, indicating very low, if any, activity of nonphotochemical PQ reduction in the mutant. As a control, we performed the same experiment on the *dum20* mutant (Remacle et al., 2001; Salinas et al., 2014), which lacks the nd1 subunit of OXPHOS complex I and is thus characterized by a low mitorespiration. As reported in Supplemental Figure S3, *dum20* displayed a strong post illumination F_0 fluorescence rise upon high

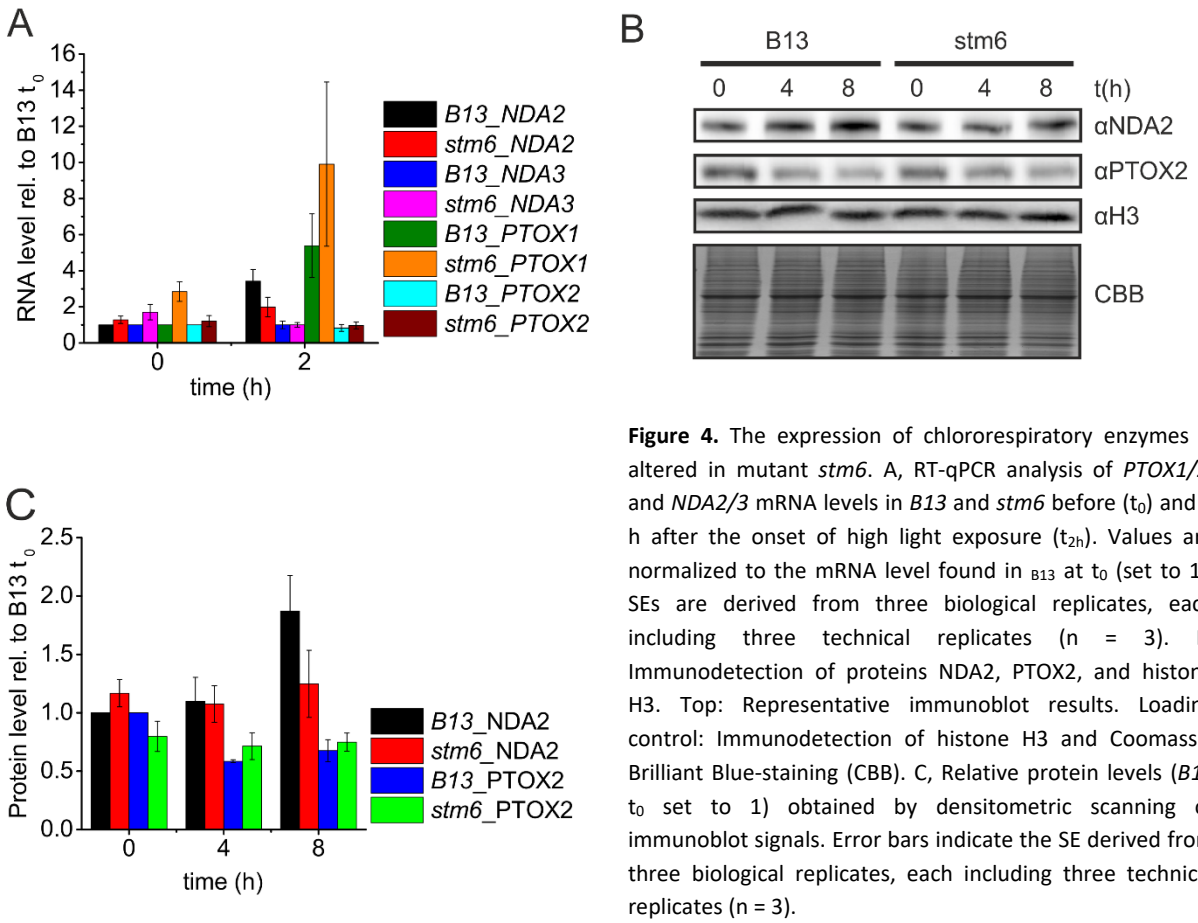

Figure 4. The expression of chlororespiratory enzymes is altered in mutant *stm6*. A, RT-qPCR analysis of *PTOX1/2*, and *NDA2/3* mRNA levels in *B13* and *stm6* before (t_0) and 2 h after the onset of high light exposure (t_{2h}). Values are normalized to the mRNA level found in $_{B13}$ at t_0 (set to 1). SEs are derived from three biological replicates, each including three technical replicates (n = 3). B, Immunodetection of proteins NDA2, PTOX2, and histone H3. Top: Representative immunoblot results. Loading control: Immunodetection of histone H3 and Coomassie Brilliant Blue-staining (CBB). C, Relative protein levels (*B13* t_0 set to 1) obtained by densitometric scanning of immunoblot signals. Error bars indicate the SE derived from three biological replicates, each including three technical replicates (n = 3).

light treatment and nPG addition, which was more pronounced than the one seen for *B13* or *stm6*. This high rate of PQ reduction in the dark is likely a consequence of the stromal overreduction caused by reduced mitorespiration and has been reported for other mitochondrial mutants before (Houyoux et al., 2011). To rule out that effects seen on F_0 fluorescence by the addition of nPG are caused by AOX inhibition, we analyzed the F_0 rise in an AOX1 knockdown mutant (T53; Mathy et al., 2010) and the reference strain (Supplemental Fig. S4). The relative increase in post illumination fluorescence following nPG treatment was comparable in both strains (Supplemental Fig. S4, A and B; ~1.9 [parental] versus ~1.85 [T53]). As reported before (Mathy et al., 2010), AOX1 expression was diminished to undetectable levels in strain T53 (Supplemental Fig. S4C). Therefore, the strong rise in F_0 fluorescence upon nPG addition should mainly reflect an inhibition of PTOX.

In the next step, we analyzed the expression modulation of chlororespiratory enzymes following exposure of *B13* and *stm6* cells to excess light (Fig. 4A). The *C. reinhardtii* nuclear genome encodes two PTOX genes, and PTOX2 was shown to represent the major oxidase controlling the PQ redox poise in the dark (Houille- Vernes et al., 2011). Although PTOX1 activity is comparably low in dark-acclimated *C. reinhardtii* cells (Houille-Vernes et al., 2011), residual chlororespiratory activity in a PTOX2 knockout mutant together with the phenotype caused by heterologous Cr-PTOX1 expression in tobacco (Ahmad et al., 2012; Feilke et al., 2016) indicate that this enzyme functions as a plastoquinol: oxygen oxidoreductase in vivo. For the dissipation of excess reducing equivalents, PTOX enzymes need to work in concert with chloroplast type II-NAD(P)H dehydrogenases. In response to high light treatment (t_{2h}), the mRNA encoding NDA2 accumulated between two and 3-fold, with a higher induction noted for *B13* (3.42 ± 0.64 versus 1.99 ± 0.54 in *stm6*; $P > 0.1$). In contrast, the mRNA level of NDA3, which is chloroplast localized according to a proteomics study (Terashima et al., 2011), but whose function remains unknown, remained unaltered in response to light stress in strains *B13* and *stm6*.

Following high light exposure, the mRNA encoding PTOX1 accumulated in both cell lines (5.39 ± 1.76 versus 1 [*B13*] and 9.90 ± 4.55 versus 2.84 [*stm6*]; $P > 0.1$), with a higher starting level at t_0 detected in *stm6* (2.84 ± 0.55 versus 1 in *B13*; $P > 0.1$). In contrast, in both strains the level of PTOX2 mRNA did not differ between time points t_0 and t_{2h}.

In addition to mRNA levels, the protein levels of NDA2 and PTOX2 were analyzed (Fig. 4B) because a chlororespiratory function of these two enzymes has already been demonstrated (Jans et al., 2008; Desplats et al., 2009; Houille-Vernes et al., 2011). Only in *B13*, NDA2 protein levels increased significantly by about 87% after a transition from low light to excess light (from 1 [t_0] to 1.87 ± 0.30 [t_{8h}]; $P < 0.05$), whereas NDA2 levels remained almost unaltered in *stm6* (1.17 ± 0.12 versus 1.25 ± 0.29). Similarly, PTOX2 levels declined significantly by ~30% only in *B13* (1 versus 0.68 ± 0.09; P <

0.05), but not in *stm6* (0.80 ± 0.13 versus 0.75 ± 0.08). Thus, high light-acclimated cells of *B13* accumulated higher levels of NDA2 than those of *stm6* (1.87 ± 0.30 versus 1.25 ± 0.29; P > 0.1), while the levels of PTOX2 were comparable (0.68 ± 0.09 versus 0.75 ± 0.08).

An absence of MOC1 impairs the acclimation of *C. reinhardtii* to excess light, as can be seen by the higher susceptibility of mutant *stm6* to photoinhibition (Fig. 3A). Besides differences in stoichiometric adjustments leading to an altered composition of the photosynthetic apparatus (Table I), a modulation of chlororespiration as another acclimatory response to excess light is affected in *stm6* (Figs. 3, B–H). At least for high light acclimated cells, the lower activity of chlororespiration in *stm6* versus *B13* can be partly explained by the lower expression level of the NAD(P)H:plastoquinone oxidoreductase NDA2 (Fig. 4B), which accumulates following exposure to light stress in *B13* but not in *stm6*. An accumulation of NDA2 in response to light stress has been reported before (Houyoux et al., 2011) and correlates well with the higher activity of nonphotochemical PQ reduction in high light-treated cells of *B13* (Fig. 3, E and G).

A deregulated mitorespiration in mutant *stm6* perturbs the stromal redox poise

Absence of MOC1 in the mutant *stm6* leads to a different modulation of respiratory activity in the mitochondrion and chloroplast (Figs. 1–4). At least in low light-acclimated cells, consumption of cellular reducing equivalents based on mitorespiration is higher in the mutant (Fig. 2A). The strong reduction of chlororespiratory activity in *stm6* (Fig. 3, C–H) indicates that altered respiratory activity in the mitochondrion, also seen in the modes of mitochondrial electron transport preferred by *stm6* versus *B13* (Figs. 1E and 2, B and D), might affect the chloroplast redox state. Chlororespiration implicates nonphotochemical plastoquinone reduction using NADPH as a reducing equivalent, and its activity is correlated with the stromal redox poise (Houyoux et al., 2011).

To determine the redox state of the chloroplast stroma (NADPH:$NADP^+$ ratio) in *stm6*, *B13*, and a dum mutant (Salinas et al., 2014), P700 oxidation kinetics were recorded for low light- and high light-acclimated cultures (Fig. 5). The *dum20* mutant (Remacle et al., 2001) was included as a reference strain to characterize the effects of a lower activity of mitochondrial respiration on the stromal redox state.

Oxidation of P700 and accumulation of $P700^+$ (the photooxidized primary electron donor of PSI) was followed as a decreased A_{705} during illumination of the sample with orange actinic light of different intensities (from 35 to 940 µmol photons m^{-2} s^{-1}), exciting both PSI and II (Fig. 5). Oxidation kinetics were normalized to the maximum level of $P700^+$ determined at 940 µmol photons m^{-2} s^{-1} upon addition of methyl viologen and ascorbate. Upon illumination with actinic light, a sharp absorbance decrease can be observed at 705 nm due to a fast rate of electron transport from PSI to $NADP^+$ and a

slow rereduction mediated by electron flow from NADPH back to $P700^+$ or from the activity of PSII and linear electron flow (Alric et al., 2010). A steady-state amount of $P700^+$ is reached when both electron transport processes operate at equal rates. In the absence of PSI photoinhibition, the total amount of $P700^+$ that can be obtained is therefore mainly determined by the capacity of electron sinks downstream of PSI ($NADP^+$ availability) and the activity of cyclic and linear electron flow.

In low light-acclimated cultures (Fig. 5A), *stm6* (red curve) accumulated the largest fraction of $P700^+$ when actinic light intensities exceeding 35 µmol photons m^{-2} s^{-1} were used. The lowest steady-state amount of photooxidizable P700 was seen for strain *dum20* (blue curve), which correlates well with the highly reductive cellular redox state and stimulated cyclic electron flow reported for dum mutants (Cardol et al., 2003; Houyoux et al., 2011).

Similarly, *stm6* showed also the largest fraction of $P700^+$ after 8 h of growth under high light conditions (Fig. 5C), even at the lowest actinic light intensity investigated (35 µmol photons m^{-2} s^{-1}). Again, *dum20* mutant showed the lowest fraction of $P700^+$ compared to *B13* and *stm6*, when higher light intensities (560 and 940 µmol photons m^{-2} s^{-1}) were used, while similar P700 oxidation levels were seen for *B13* and *dum20* only at lower actinic light intensities.

To block linear and cyclic electron flow during the P700 oxidation measurement, the photosynthetic electron transport inhibitors 3-(3,4-dichlorophenyl)-1,1-dimethylurea (DCMU) and 2,5-dibromo-6-

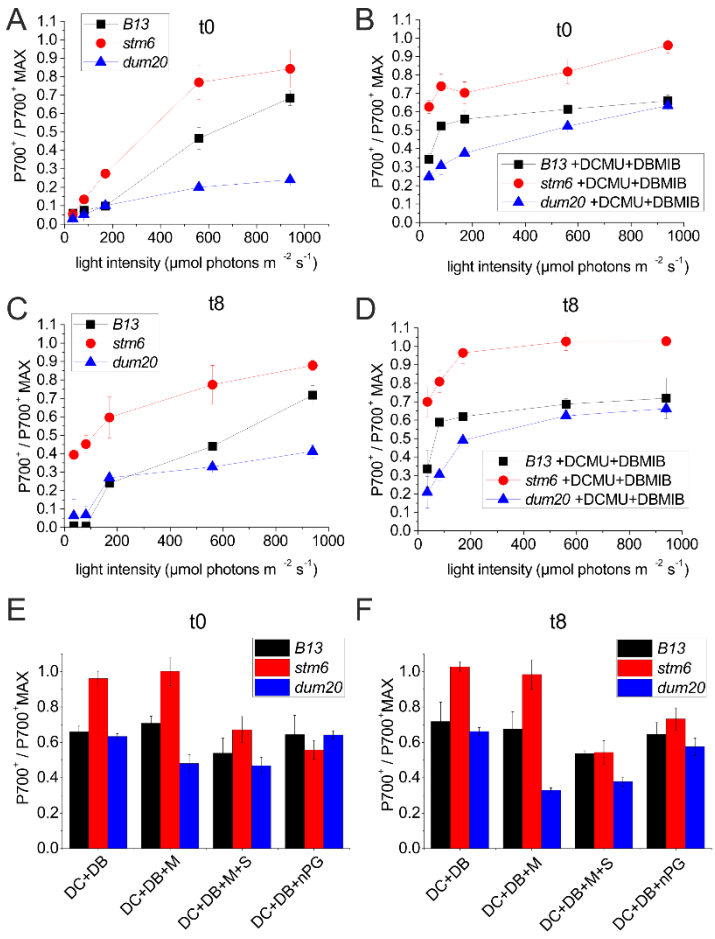

Figure 5. Stromal overoxidation in *stm6* is caused by a higher mitochondrial reductant sink capacity. A to D, $P700^+$ accumulation as assessed by the absorbance change at 705 nm during illumination with orange actinic light at different light intensities (35, 82, 170, 560, and 940 µmol photons m^{-2} s^{-1}). Samples derived from *B13* (black curve), *stm6* (red curves), and *dum20* (blue curves) cultures were analyzed before (A and B) and after acclimation to high light for 8 h (C and D). Measurements were performed in the absence (A and C) or presence (B and D) of DCMU and DBMIB, which inhibits P700 reduction by linear and cyclic electron transport. P700 oxidation kinetics were normalized to the maximum $P700^+$ obtained at 940 µmol photons m^{-2} s^{-1} in presence of 1mM ascorbate and 1mM methyl viologen. E and F, $P700^+$ oxidation level per PSI determined for *B13* (black), *stm6* (red), and *dum20* (blue) cultures grown for 8 h under high light conditions. Prior to the measurement inhibitors of photosynthetic electron transport were either added to the cultures alone (DCMU [DC]+DBMIB [DB], or together with inhibitors of respiratory electron transport (myxothiazol [M], nPG, or myxothiazole along with salicyl hydroxamic acid [S]). Error bars indicate the SD from three biological replicates (n = 3).

isopropyl-3-methyl-1,4-benzoquinone (DBMIB) were added (Fig. 5, B and D). Under this condition, rereduction of $P700^+$ via PSII activity and due to electron recycling from reduced primary acceptors to PSI is abolished. The obtainable $P700^+$ fraction is then only determined by the availability of primary downstream electron acceptors and hence the stromal redox state. Following the inhibition of photosynthetic electron transport with DCMU and DBMIB, samples showed a higher fraction of $P700^+$, especially at lower light intensities. Again, and independent of the light intensity used, the highest $P700^+$ fraction was noted for *stm6*. *B13* and *dum20* were characterized by a much lower $P700^+$ fraction compared to *stm6*, with *dum20* being the strain with the lowest level of $P700^+$, especially at lower actinic light intensities. These analyses confirmed that the higher We next wanted to analyze the impact of mitochondrial electron sink capacity on the stromal redox state in further detail by adding inhibitors of mitochondrial electron transport prior to P700 measurements conducted with high-light acclimated *stm6* (red bars), *B13* (black), and *dum20* (blue) cultures (Fig. 5, E and F). These experiments were performed using an actinic light intensity of 940 µmol photons m^{-2} s^{-1} and by normalizing the observed $P700^+$ to the maximum level of $P700^+$ obtained, as described above. In addition, all experiments were performed in the presence of PET inhibitors (DCMU+DBMIB) to ensure that the differences observed in photooxidizable P700, seen after inhibition of mitochondrial electron transport, indeed reflect a limited availability of $NADP^+$ in the chloroplast stroma and not differences in the $P700^+$ rereduction rate based on PSII activity and cyclic electron flow. As shown in Figure 5, B and D, *stm6* accumulates the largest amounts of $P700^+$, followed by *B13* and *dum20*, when PET is inhibited by adding DCMU and DBMIB. Addition of myxothiazol, which can be used to inhibit the cyt bc1 complex (OXPHOS complex III) of the mitochondrial respiratory chain (von Jagow and Engel, 1981), showed marked effects on $P700^+$ accumulation only in strain *dum20*, while effects in *B13* and *stm6* were not evident (Fig. 5, E and F; DC+DB+M) for both t_0 and t_{8h} samples.

The absence of a myxothiazol effect in *B13* and *stm6* might be explained by a rapid activation of the alternative oxidase pathway in these strains, which bypasses complex III by transferring electrons from reduced ubiquinone directly to oxygen. AOX activity is known to represent a “safety vale” preventing an overreduced state of the cell under conditions when complex III is inhibited (Vishwakarma et al., 2015). Effects seen in *dum20* indicate that the activation of the alternative pathway might be delayed in this mutant, resulting in an overreduced mitochondrial redox state, which eventually translates into a more reduced chloroplast stroma. Inhibitors of AOX were thus applied to investigate the relation between AOX activity and stromal redox poise. P700 measurements performed in the presence of DCMU, DBMIB, and nPG (Fig. 5, DC+DB+nPG) showed a strong reduction in the oxidizable P700 fraction in the case of *stm6*, whereas effects on *dum20* and

B13 were absent (t_0) or less pronounced (t_{8h}). It is worth mentioning that the remarkable nPG effect on P700 oxidation in *stm6* should not be related to PTOX inhibition, since in this mutant chlororespiration was almost not induced (Fig. 3).

A complete inhibition of mitochondrial respiration (Fig. 5, E and F; DC+DB+M+S) can be achieved by the combined use of myxothiazol and salicylhydroxamic acid (SHAM; Schonbaum et al., 1971), which inhibits complex III and AOX at the same time. Addition of these inhibitors strongly diminished the $P700^+$ fraction in *stm6* and *B13* for both types of samples (t_0 and t_{8h}), whereas the effect in *dum20* was negligible compared to the effect caused by adding myxothiazol alone. Full inhibition of mitochondrial respiration or inhibition of AOX prior to the measurement of P700 oxidation kinetics led to almost identical steady-state levels of $P700^+$ in *stm6* and *B13* (Fig. 5), indicating that marked differences in $P700^+$ levels in the presence of PET inhibitors (Fig. 5, B and D) can be explained by a low (*dum20*), high (*stm6*), and wild-type-like (*B13*) reductant sink capacity of the mitochondrion. Importantly, the overoxidized state of the chloroplast stroma in *stm6* can be transformed in a reduced state by blocking AOX activity or mitorespiration completely, demonstrating that the high availability of $NADP^+$ is caused by a stimulated mitorespiration and not by an increased sink capacity of the Calvin cycle for NADPH (Alric et al., 2010). The consequences of the higher P700 activity observed in *stm6* compared to *B13* were then further investigated by measuring the kinetics of plastocyanin (PC) oxidation. As expected, *stm6* showed a higher level of PC oxidation and a faster kinetics compared to *B13*, when normalized to the PSI content (Supplemental Fig. S5). This indicates

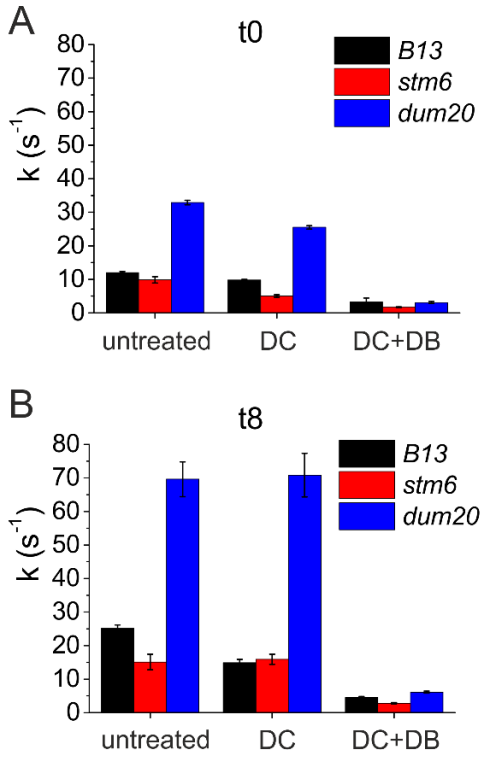

Figure 6. Cyclic electron flow capacity is diminished in *stm6* cells. $P700^+$ dark rereduction rates ($e^- s^{-1}$ per PSI) deduced from first-order dark recovery kinetics of P700 after 20 s of saturating light illumination. Low (t_0; A) and high light (t_{8h}; B) acclimated cells of *B13*, *stm6*, and *dum20* were subjected to P700 measurements without or following addition of PET inhibitors (DCMU [DC] / DMCU+DBMIB [DB]) SDs are derived from five independent biological experiments (n = 5).

that the more oxidized stroma stimulates the oxidation of PSI electron donors. Taken together, these results indicate that the flow of reducing equivalents from the chloroplast to mitochondria is enhanced in *stm6*.

In addition to recording the kinetics of P700 oxidation in the light, $P700^+$ rereduction (Supplemental Fig. S6) was also analyzed after switching off the light, once a steady-state level of photooxidized P700 was reached. The dark rereduction rate of $P700^+$ can be used to estimate the rate of cyclic electron flow, especially when cells are treated with DMCU (Alric et al., 2010). $P700^+$ rereduction rates were determined for *B13*, *stm6*, and *dum20* after growth in either low (t_0) or high (t_8) light intensities (Fig. 6). In low light-and *stm6* (9.8 ± 1.0 s^{-1}). These rates were decreased by ~23% upon addition of DCMU in *B13* and *dum20*, while a stronger decrease was measured in *stm6* (~50% decrease), indicating a substantial contribution of cyclic electron flow in *B13* and *dum20* but not in *stm6*. Addition of DCMU and DBMIB instead strongly slowed down $P700^+$ rereduction, with the lowest rate seen for *stm6*. Growth in high light increased the observed rate in all strains. Cyclic electron flow (CEF) rates obtained from untreated samples were still far lower in *stm6* (15.1 ± 2.3 s^{-1}) compared to *B13* (25.1 ± 1 s^{-1}) and *dum20* (69.6 ± 5.2 s^{-1}). Interestingly, the comparison of P700 rereduction rates observed in samples containing or lacking DCMU demonstrates that only in *B13* a substantial linear electron flow was detected, while for both *stm6* and *dum20* the CEF rates were similar to the rate of P700 rereduction in the absence of DCMU. The higher CEF rate observed for *dum20* compared to *stm6* at t_{8h} suggests that in *dum20* the absence of a DCMU effect is likely related to a strong CEF activation, while in *stm6* reduction of linear electron flow is due to PSII photoinhibition, as witnessed by the strong reduction of F_v/F_m after 8 h of high light treatment (Fig. 3A).

We also analyzed if the lower activity of CEF seen for *stm6* under low light conditions (Fig. 6A, DC) could be caused by an altered expression of genes PGR5 and PGRL1 (Supplemental Fig. S7). The proteins PGR5 and PGRL1 have already been shown to represent crucial components of the ferredoxin-dependent pathway of cyclic electron transport in *C. reinhardtii* (Petroutsos et al., 2009; Johnson et al., 2014). Comparable levels of PGR5/PGRL1 mRNA (Supplemental Fig. S7, A and B) and PGRL1 protein (Supplemental Fig. S7C) could be detected in *stm6* and *B13*, when low light and high light-acclimated cultures were analyzed. At least for PGRL1 it can be stated that the amount of this protein should not limit the overall CEF capacity in mutant *stm6*.

In conclusion, the higher rate of mitochondrial reductant consumption in *stm6* results in a higher availability of PSI electron acceptors and thus a less reduced stroma (Fig. 5), which could provide an explanation for the low rate of cyclic electron flow observed in this mutant (Fig. 6A).

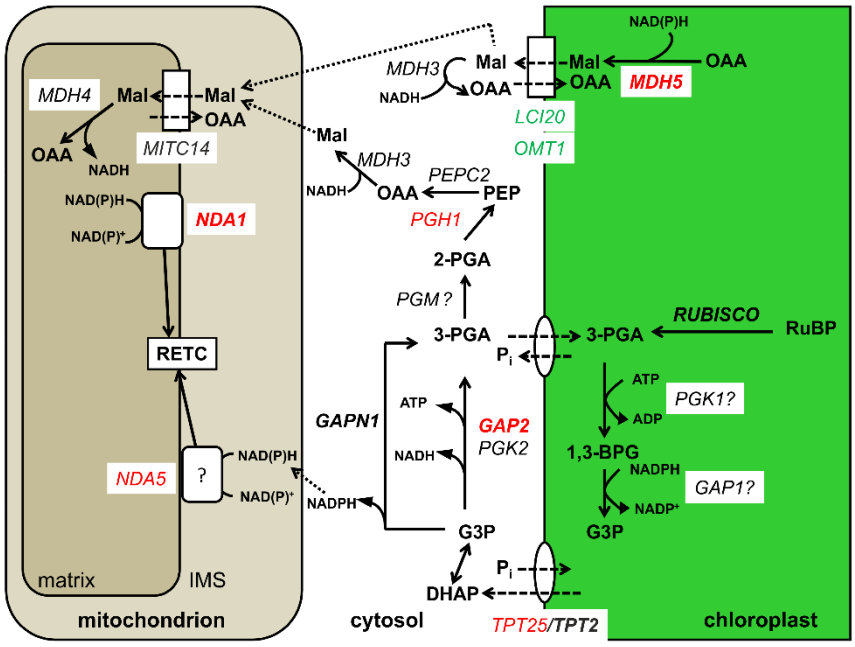

Figure 7. Overview of the putative pathways that contribute to the export of excess reducing equivalents from the chloroplast to mitochondria in *C. reinhardtii*. Genes, up-regulated in *stm6* (Fig. 8) under low-light conditions are highlighted in red and those that are down-regulated in green. Genes up-regulated in response to light stress are written in bold. 1,3-BPG, 1,3-bisphosphoglycerate; RuBP, ribulose-1,5-bisphosphate; 2-PGA, 2-phosphoglycerate; LCI20, low CO2-inducible gene; OMT1, 2-oxoglutarate/malate transporter; MITC14, dicarboxylate-tricarboxylate carrier; MDH3-5, malate dehydrogenase; PGK1/2, phosphoglycerate kinase; GAP1/2, glyceraldehyde-3-phosphate dehydrogenase; GAPN1, nonphosphorylating glyceraldehyde-3- phosphate dehydrogenase; PGM, phosphoglycerate mutase; PGH1, enolase.

Several genes encoding components of chloroplast-mitochondria crosstalk pathways are up-regulated in low light-acclimated *stm6* cells

Different pathways for the export of chloroplast reducing equivalents to mitochondria have been identified by previous studies conducted mainly with higher plants (Noguchi and Yoshida, 2008). The triose phosphate-phosphate transporter (TPT) shuttle exports dihydroxyacetone phosphate (Fig. 7) from the chloroplast to the cytosol, which is then converted into glyceraldehyde-3-phosphate (G3P) that can be consumed by glycolysis following two distinct pathways (Fig. 7; GAPN1 and GAP2/PGK2). The nonphosphorylating NADP-dependent glyceraldehyde-3-phosphate dehydrogenase (GAPN1; UniProt KB: A8IYT1; see Supplemental Table S1 for Phytozome locus numbers) catalyzes the conversion of G3P into 3-phosphoglycerate (3-PGA) and NADPH, while a two-step reaction implicating the phosphorylating, NAD-dependent glyceralaldehyde-3-phosphate dehydrogenase (GAP2; A8JFT3) and phosphoglycerate kinase (PGK2; A8JFT4) leads to additional ATP formation. In higher plants, most of the cytosolic G3P should be consumed by the NADP-specific GAP, since its NAD-specific counterpart has a lower affinity for G3P (Scagliarini et al., 1990; Noguchi and Yoshida,

2008). 3-PGA can be reimported into the chloroplast via exchange with inorganic phosphate. Reducing equivalent formed by these glycolytic reactions can be directly consumed by external (intermembrane space-facing; NDex) type II dehydrogenases, and NDA5 (A6YT86; Fig. 1D) is one of the two rotenone-insensitive NAD(P)H dehydrogenases with predicted mitochondrial targeting sequences. This enzyme might represent the NDex enzyme of *C. reinhardtii*, since NDA1 (Lecler et al., 2012) was shown to be located at the inner mitochondrial membrane (matrix-facing; NDin). A BLAST analysis performed with a bona fide TPT from *Arabidopsis* (*Arabidopsis thaliana*; APE2; Schneider et al., 2002) predicts the existence of four close homologs (e-values in the range of 3.2×10^{-93} to 4.5×10^{-52}), namely TPT3/APE2 UniProt KB: A8HN02), TPT2/PPT2 (Q7XJ66), TPT25/ CGL51 (A8JFB4), and TPT1 (Q84XW3), with chloroplast transit sequences according to Predalgo (Tardif et al., 2012).

Under low light conditions *stm6* displays a significantly ($P < 0.05$) higher mRNA expression of the putative TPT encoded by gene TPT25 (1.97 ± 0.31 [SE] versus 1 in *B13*; Fig. 8A). Expression of the genes TPT2 (~2.2-fold in *B13*; $P < 0.05$; ~1.5-fold in *stm6*; $P > 0.1$) and TPT25 (~1.7-fold in *B13* [$P > 0.1$]; ~1.4-fold in *stm6* [$P > 0.1$]) is induced by high light in both strains, whereas TPT1 is down-regulated (0.35 ± 0.11 versus 1 in *B13*; 0.59 ± 0.18 versus 1.09 ± 0.18 in *stm6*; $P < 0.05$ for *B13*). Accumulation of GAPN1-encoding mRNAs (~2-fold) could also be observed following high light treatment in both strains but was only significant ($P < 0.05$) in the case of *B13*. Induction of GAP2 was only noted for *B13* (~1.6-fold; $P < 0.05$), which was probably due to a higher GAP2 mRNA level in low light acclimated *stm6* cells (1.74 ± 0.32; $P < 0.1$; Fig. 8B). Significant differences in the mRNA level of

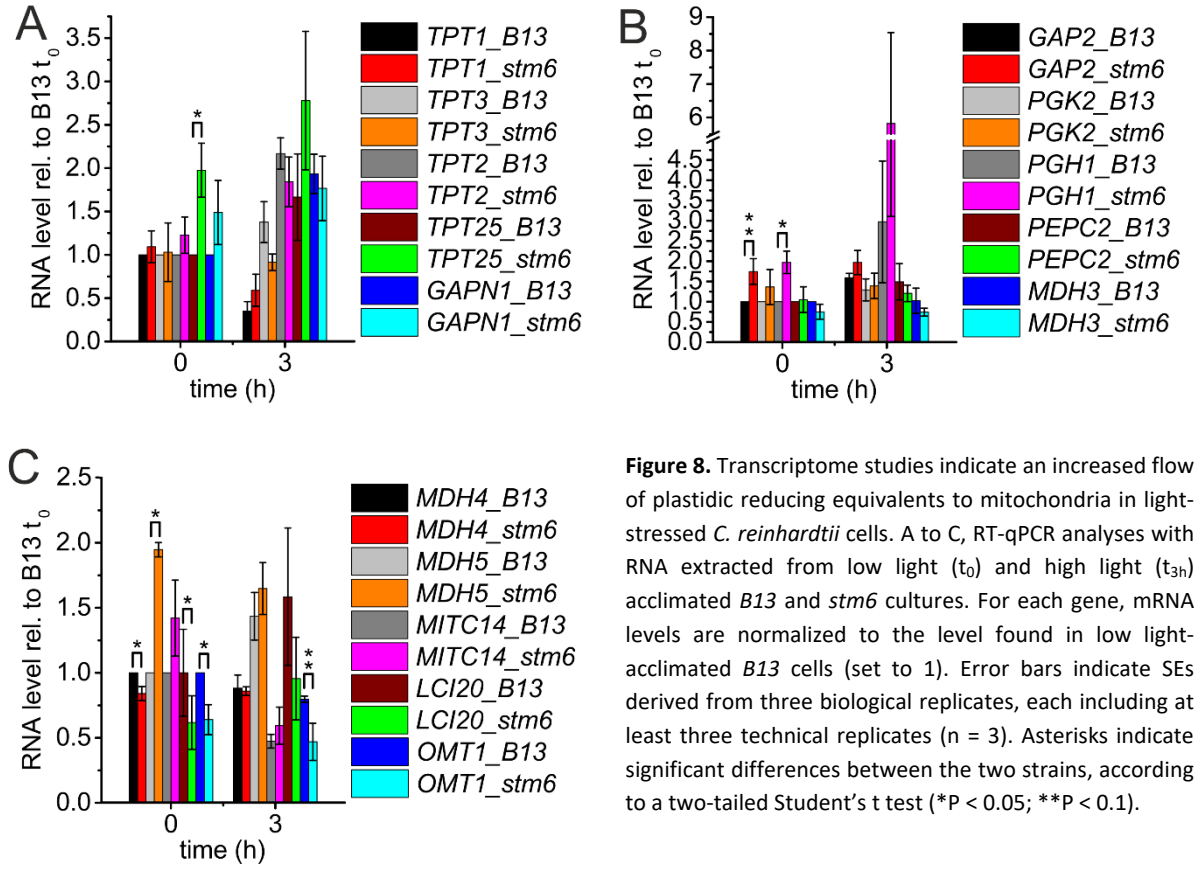

Figure 8. Transcriptome studies indicate an increased flow of plastidic reducing equivalents to mitochondria in light-stressed *C. reinhardtii* cells. A to C, RT-qPCR analyses with RNA extracted from low light (t_0) and high light (t_{3h}) acclimated *B13* and *stm6* cultures. For each gene, mRNA levels are normalized to the level found in low light-acclimated *B13* cells (set to 1). Error bars indicate SEs derived from three biological replicates, each including at least three technical replicates (n = 3). Asterisks indicate significant differences between the two strains, according to a two-tailed Student's t test (*$P < 0.05$; **$P < 0.1$).

PGK2 could not be seen in response to high light exposure, and both strains displayed similar mRNA levels in low and high light (Fig. 8B).

Cytosolic 3-PGA formed by the action of either GAPN1 or GAP2/PGK2 can be further consumed by glycolytic reactions (PGM, PGH1 [A8JH98]; Fig. 7) to yield phosphoenolpyruvate, which is convertible into malate (Mal) via a two-step reaction involving phosphoenolpyruvate carboxylase (PEPC2 [Q6R2V6]) to yield oxaloacetate [OAA]). The conversion of OAA into Mal consumes NADH and is catalyzed by MDH3 (A8J0W9), which likely represents the cytosolic NAD dependent malate dehydrogenase of *C. reinhardtii*.

Dicarboxylate-tricarboxylate carriers have been identified as shuttle systems for the import of cytosolic malate into plant mitochondria (Picault et al., 2004; Noguchi and Yoshida, 2008). The *Arabidopsis* gene At5g19760 encodes a protein with confirmed dicarboxylate-tricarboxylate carriers activity (Picault et al., 2002), and the closest homolog (e-value 4.7 x 10^{-113}) encoded by the nuclear genome of *C. reinhardtii* is MITC14 (A8J3F7; MITC14 in Fig. 7). Subsequent to its import into mitochondria, conversion of Mal into OAA via malate dehydrogenase generates NADH and MDH4 (A8JHU0) likely fulfils this function in mitochondria of *C. reinhardtii*. MITC14 as well as MDH4 can be detected in the mitochondrial proteome (Atteia et al., 2009).

Another export system for excess reducing equivalent formed in the chloroplast is the malate-oxaloacetate shuttle that comprises a plastidic malate dehydrogenase, which transfers reducing equivalents onto OAA to form Mal. Mal is then exported from the chloroplast in exchange with oxaloacetate by transporters located on the chloroplast envelope (Noguchi and Yoshida 2008). In silico analyses suggest that the Mal-OAA shuttle active in *C. reinhardtii* could be constituted by MDH5 (Q9FNS5), which is the only NADP-dependent enzyme (Lemaire et al., 2005) with a predicted chloroplast localization and transporters OMT1 (A8JDE3; Terashima et al., 2011) and LCI20 (A8HXJ4; Johnson and Alric 2013).

Higher levels of transcripts encoding the enolase PGH1 could be detected in *stm6* versus *B13* in low light (Fig. 8B; 1.97 ± 0.28 versus 1 at t_0; $P < 0.05$), and in both strains exposure to light stress was accompanied by the accumulation of PGH1 transcript (2.97 ± 1.50 versus 1 in *B13* and 5.82 ± 2.71 versus 1.97 ± 0.28 in *stm6*; $P > 0.1$). The levels of PEPC2 and MDH3 transcripts remained almost unaltered.

Excess light significantly reduced the level of MITC14 in *stm6* (from 1.42 ± 0.29 at t_0 to 0.59 ± 0.14 at t_{3h}; $P < 0.1$) and in *B13* (from 1 to 0.47 ± 0.05; $P < 0.05$). No differences could be observed for the levels of MDH4 RNA in both strains, but MDH5 mRNA was expressed at higher amounts in low light-acclimated *stm6* cells (1.95 ± 0.05 versus 1; $P < 0.05$). In *B13*, MDH5 levels slightly increased in response to light stress (1.43 ± 0.18 versus 1; $P < 0.1$), whereas levels declined in *stm6* (1.95 ± 0.05

versus 1.65 ± 0.20; P > 0.1). Higher levels of MDH5 mRNA in low light-acclimated *stm6* cells were accompanied by lower levels of OMT1 (0.64 ± 0.11; P < 0.05) and LCI20 (0.62 ± 0.02; P < 0.05) mRNA.
Growth of the complemented strain in excess light caused an increased mRNA expression of triosephosphate-phosphate translocators (TPT2, TPT25) and GAPN1,which is required for the conversion of G3P to 3-PGA in a reaction implicating the formation of NADPH in the cytosol. Working in concert with NDA5, the combined operation of TPTs and GAPN1 could provide a pathway for the transport for chloroplast reducing equivalents to mitochondria in light-stressed *C. reinhardtii* cells. The high light induction of genes GAP2 and PGH1 might indicate an increased conversion of cytosolic 3-PGA into malate. However, mRNA expression of the genes potentially involved in the transport of cytosolic malate into mitochondria (MITC14) and its oxidation to oxaloacetate (MDH4) was not induced by high light. In addition to the triosephosphate shuttle, the malate valve can be a means to export chloroplast reducing equivalents to mitochondria. Exposure to light stress was accompanied by a higher mRNA expression of the putative malate valve component MDH5, but transporters potentially involved in the export of malate from the plastid (OMT1, LCI20) were not expressed at higher levels under high light.
The induction of several genes, likely implicated in the transport of reducing equivalents from chloroplast to mitochondria, fits well to the observed increase in mitochondrial respiration in response to light stress (Fig. 2A). Regarding the increased cooperation between mitochondria and chloroplast in *stm6* (Fig. 5), it is difficult to deduce further supportive evidence from the analysis of mRNA levels, since the number of differentially regulated genes in *stm6* versus *B13* is too small to see a general trend. Furthermore, genes belong to different pathways, making it difficult to depict a pathway preferentially used by *stm6* (Fig. 7).

DISCUSSION

In *C. reinhardtii* the mitochondrial mTERF protein MOC1 was demonstrated to act as a transcription terminator, which is needed to prevent read-through transcription at specific sites in the mitochondrial genome. As has been shown previously, under photoheterotrophic conditions a loss of MOC1 in mutant *stm6* leads to a specific decrease in the levels of transcript nd1, which encodes a subunit of mitochondrial complex I (Wobbe and Nixon 2013). Intriguingly, the perturbed regulation of mitochondrial gene expression in *stm6* results in a light-sensitive phenotype under photoautotrophic conditions (Nguyen et al., 2011). In this study, we analyzed how a deregulated mitochondrial respiration in mutant *stm6* might contribute to a decreased light tolerance in photoautotrophic conditions. The light-sensitive phenotype displayed by *stm6* indicates that MOC1 could play a special role during the acclimation of *C. reinhardtii* cells to excess light, and the transfer

of low light-acclimated cells to higher light intensities indeed resulted in a strong accumulation of the MOC1 protein (Fig. 1A). This strong accumulation correlates well with the reduced level of mitochondrial antisense RNAs, which are formed as a result of improper transcription termination at the MOC1 binding site that has been observed in high light-acclimated wild-type cells in a previous study (Wobbe and Nixon 2013). Increased transcription termination in light-stressed wild-type cells should favour the formation of protein encoding sense transcripts and result in more prominent differences between the nd1 RNA levels present in MOC1-containing cells and those devoid of MOC1. Indeed, transcript levels of nd1 differed more strongly between *B13* and *stm6* under excess light conditions (Fig. 1B). The RNA level of nucleus-encoded complex I and complex IV subunits did not differ significantly between light-stressed *stm6* and *B13* cells, and only for NUO21 an induction by high light could be observed in strain *B13* (Fig. 1C). Immunoblot analyses (Fig. 1E) demonstrated that the amount of the nucleus-encoded complex IV subunit COX2B declined (*B13*) following high light acclimation or remained unchanged (*stm6*). Considered that there is no concomitant increase in the protein level of mitochondrially encoded cox1 (Fig. 1E), a higher availability of nucleus-encoded complex IV subunits should anyway not result in higher amounts of complex IV in light-stressed cells. The decline of nd1 transcript levels in high light-treated *stm6* cells suggests that an enhanced transcription termination, based on a higher availability of MOC1 in light-stressed wild-type cells, is needed to guarantee a sufficient provision of this mRNA in mitochondria during the acclimation to excess light.

Light stress induces a switch from the energy-dissipating to the energy-conserving mode of mitochondrial electron transport

In contrast to the phosphorylating (ATP-generating) cytochrome *c* pathway, composed of OXPHOS complexes I-V, which are assembled from a multitude of nuclear and mitochondrial subunits, the nonphosphorylating pathway (implicating AOX and type II NAD(P)H dehydrogenases) does not rely on multisubunit complexes. This should facilitate activity modulation of the latter pathway based on expression control in response to excess light (Noguchi and Yoshida, 2008), and in *Arabidopsis* mRNA expression of transcripts encoding distinct isoforms of AOX is induced by the application of high light stress (Yoshida et al., 2009, 2011). For *C. reinhardtii* a different response following exposure to light stress could be observed, but more importantly the RNA and protein levels of AOX1 in *stm6* exceeded those of *B13* in low and high light conditions (Fig. 1, D and E). At least under low light conditions, the amount of transcripts encoding the type II-NAD(P)H dehydrogenases NDA1 and NDA5 was also elevated in *stm6* versus *B13* (Fig. 1D). These findings are in good agreement with the higher contribution of cyanide- (Fig. 2B) and rotenone-insensitive respiration (Fig. 2D) to mitochondrial

respiration in *stm6*. In principle, cyanide-insensitive respiration can be composed of mitochondrial AOX activity and chlororespiration. The low activity of chlororespiration (Fig. 3) and the overaccumulation of AOX1 protein (Fig. 1E) suggest that the high activity of cyanide-insensitive respiration in *stm6* is mainly composed of AOX-dependent oxygen consumption. A higher activity of AOX in *stm6* has also been observed under photoheterotrophic conditions before (Schönfeld et al., 2004). Furthermore, the lower contribution of complex I to dark respiration in *stm6* compared to *B13* (Fig. 2D, t_{6h} and t_{8h}) indicates that the diminished availability of nd1 transcripts (Fig. 1B) might represent a limitation for the assembly of complex I in this strain. Overall light stress induced a switch from energy-dissipating mitorespiration based on the AOX pathway to the energy-conserving cytochrome *c* pathway. This modulation of respiratory activity in the mitochondrion was mainly achieved by a strong down-regulation of AOX1 expression (Fig. 1, D and E) in response to light stress, a process that occurs in both strains. Importantly, however, *stm6* still retains a high AOX1 activity (Fig. 2B; Supplemental Fig. S1) and AOX1 protein levels that exceed those of *B13*. The higher relative contribution of complex I activity to respiration in light-stressed *B13* versus *stm6* cells (Fig. 2D) might reflect the inability of mutant *stm6* to maintain the prestress level of transcript nd1 during light stress exposure (Fig. 1B). The modulation of AOX1 activity noted for light-stressed cells of *C. reinhardtii* differs from the high light response observed in *Arabidopsis*, which up-regulates AOX activity following exposure to excess light (Yoshida et al., 2007). It should be noted, however, that a recent study demonstrated that AOX accumulation in high light acclimated *Arabidopsis* plants does not result in an increased activity of alternative respiration, while excess light stimulates the activity of the cytochrome *c* pathway (Florez-Sarasa et al., 2016).

Impaired fine-tuning of complex I activity by a deactivation of MOC1-dependent transcription termination stimulates mitochondrial respiration

Besides a switch in the preferred mode of respiratory electron transport, total rates of dark respiration increased significantly in mutant and wild type when challenged by light stress (Fig. 2A). In line with this observation, several genes encoding components of the crosstalk pathways, connecting chloroplast and mitochondria in *C. reinhardtii*, were induced on the transcript level by excess light (Figs. 7 and 8). This stimulation of dark respiration has already been described as the phenomenon termed light enhanced dark respiration (Padmasree et al., 2002) and is positively correlated with the light intensity and the duration of pre illumination in *C. reinhardtii* (Xue et al., 1996). Enhanced provision of photosynthate as a substrate for mitochondrial respiration is discussed as the mechanism behind the observed light enhanced dark respiration (Padmasree et al., 2002). While low light-acclimated cells of *stm6* displayed a higher dark respiration rate compared to *B13*

(Fig. 2A; t_0), these rates were similar in high light-acclimated *B13* and *stm6* cultures (t_{2h}-t_{8h}). For high light-acclimated *stm6* cells it has, however, to be considered that light stress causes severe PSII photoinhibition in this strain (Figs. 3, A and B, and 6B; Table I). The higher respiratory capacity of *stm6* observed under low light conditions (Fig. 2A, t_0), could therefore be obscured in light-stressed cells by the reduced provision of respiratory substrates as result from the decline in PSII activity (Fig. 3, A and B).

Higher rates of dark respiration in acetate-containing media have been observed before (Kruse et al., 2005) and were proposed to represent one of the main reasons for the rapid induction of photosynthetic hydrogen production in this mutant (Nguyen et al., 2011; Volgusheva et al., 2013). Considering the effect of a MOC1 inactivation on mitochondrial nd1 expression (Wobbe and Nixon, 2013; Fig. 1B) and the lower activity of complex I found in *stm6* (Fig. 2D), the up-regulation of nonphosphorylating pathways in *stm6* seems counterintuitive, since a reduced electron flow through complex I should reduce mitochondrial ATP yields. An increase of total respiration rates in the mitochondrion, however, might represent a compensatory mechanism that helps to maintain sufficient ATP production. A complete deficiency of complex I has different outcomes in higher plants and the green alga *C. reinhardtii* (Sabar et al., 2000; Remacle et al., 2001; Kuhn et al., 2015). While complex I mutants from *C. reinhardtii* show decreased rates of dark respiration (Remacle et al., 2001), corresponding *Arabidopsis* and tobacco (*Nicotiana tabacum*) mutants show an increased dark respiration and a concomitant stimulation of AOX-based respiration (Sabar et al., 2000; Kühn et al., 2015). A stimulation of total mitorespiration and AOX activity was also observed in an *Arabidopsis* mutant, which contains only trace amounts of functional complex I (Kühn et al., 2015). It remains, however, difficult to compare the situation in *stm6* with the one existing in constitutive complex I mutants, since *stm6* still retains a significant complex I activity, although the modulation of complex I activity is perturbed (Fig. 2D).

The enhanced electron sink capacity of mitochondria in *stm6* perturbs the chloroplast redox poise

While mitorespiration in *stm6* is increased under low light conditions, the activation of the chlororespiratory pathway by light stress is perturbed (Figs. 2A and 3, C– H). The diminished activity of chlororespiration in *stm6* is partly caused by an inability to induce the expression of NDA2 as a component of the chlororespiratory pathway (Fig. 4B). On the other hand, it has been proposed that chlororespiration, a pathway that consumes NADPH, could be activated as a response to the stromal overreduction, occurring in *C. reinhardtii* during growth in high light (Houyoux et al., 2011). The reduced activity of this pathway in the mutant should therefore also reflect the more oxidized stroma found in *stm6* (Fig. 5). This could also be noted (Supplemental Fig. S3) for the *dum20* strain

used in this study, whose stromal compartment is overreduced (Fig. 5, *dum20*). These observations indicate a negative correlation between the capacity of mitochondrial reductant uptake and the activity of chlororespiration. Experiments with inhibitors for complex III and AOX (Fig. 5) revealed that the differences seen between *dum20*, *B13*, and *stm6* in terms of their stromal redox state (Fig. 5) are largely attributable to the distinct activity of mitochondrial respiration in these strains. Similar stromal redox states in *B13* and *stm6* following complete inhibition of mitochondrial respiration or specific inhibition of the alternative pathway (Fig. 5) further demonstrate that the more oxidized stroma in chloroplasts of *stm6* is a direct result of an increased mitochondrial reductant sink capacity with a significant contribution of the AOX pathway (Figs. 1, D and E, and 2B). Although evidence for an enhanced flow of plastidic reducing equivalents to mitochondria in *stm6* exists (Figs. 2 and 5), mRNA expression analyses of genes encoding components of the chloroplast-to-mitochondria crosstalk pathways (Figs. 7 and 8) did not provide further insights into the pathways preferentially used by *stm6*. Additional work will be needed to depict the precise mode of redox crosstalk between chloroplast and mitochondria in *stm6*.

Light acclimation mechanisms controlled by the stromal redox state are affected in *stm6*

The question arises how the stimulation of mitochondrial reductant uptake and the resulting perturbation of the stromal redox poise in *stm6* contribute to its light-sensitive phenotype (Figs. 3, A and B, and 6B; Table I). A transfer of *stm6* cells from low light to high light conditions causes strong photoinhibition of PSII as can be seen by a loss of activity (Fig. 3A) and a diminished number of PSII complexes compared to high light-acclimated *B13* cells (Table I).

The enzyme PTOX has been proposed to act as a "safety valve," protecting PSII by preventing the overreduction of the PQ pool (Ort and Baker, 2002). A significant impact of PTOX inhibition on the PQ pool redox state could only be noted for low light-acclimated *B13* cultures (Fig. 3B), indicating that PTOX activity contributes more to PSII protection in *B13* compared to *stm6*. PTOX can be either supplied with electrons from water-splitting at PSII, or from the oxidation of NADPH by NADPH:plastoquinone oxidoreductases. The latter pathway feeds electrons into the PQ pool in a PSII-independent fashion and involves NDA2 in *C. reinhardtii* (Jans et al., 2008; Houyoux et al., 2011). This pathway is severely impaired in low light- and high light-acclimated cells of *stm6*, as demonstrated by the absence of a post illumination F_0 rise in this mutant (Fig. 3, C–H). Besides the limited substrate supply for the nonphotochemical reduction of the PQ pool in the more oxidized stroma of *stm6* (Fig. 5), activity could be additionally restricted by the availability of NDA2 (Fig. 4). Although chlororespiration should be a means to prevent PQ pool overreduction and could dissipate excess

reducing equivalents in the chloroplast, the restricted electron flow capacity of this pathway challenges its prominent role for PSII protection under high light conditions (Nawrocki et al., 2015).

Among the most important mechanisms for PSII protection is the so-called energy-dependent quenching qE, which reduces PSII excitation pressure under excess light conditions and is activated by an acidification of the thylakoid lumen (Wobbe et al., 2016). The strongly diminished qE capacity of mutants lacking components of the ferredoxin-PGRL1/PGR5 pathway of cyclic electron flow indicates that this process is required for the lumen acidification, which triggers qE (Kukuczka et al., 2014; Johnson et al., 2014). A reduced nonphotochemical quenching capacity has also been demonstrated for *stm6*, which could be partly explained by an inability to induce the expression of LHCSR3 (Nguyen et al., 2011). Low light-acclimated cells of *stm6* show a reduced CEF capacity compared to *B13* (Fig. 6A, t_0), which could impede acclimation mechanisms that are triggered by an acidification of the thylakoid lumen, such as qE or chlororespiration. Recently, it was shown that PTOX1 from *C. reinhardtii*, when heterologously expressed in tobacco, only attaches to the thylakoid membrane under alkaline conditions in the stroma (Feilke et al., 2016), which suggests that chlororespiration might be fine-tuned by CEF rates. The reduced CEF capacity of *stm6* cells prior to the onset of light stress might thus restrict the induction of qE and contribute to PSII photoinhibition. High CEF rates are typically seen following the establishment of an overreduced state in *C. reinhardtii* cells, which can be achieved by the inhibition of mitochondrial respiration in anaerobic conditions (Takahashi et al., 2013). Against this background, the low CEF activity of *stm6*, whose stroma is more oxidized (Fig. 5, t_0), fits well to its stimulated mitochondrial respiration in low light conditions (Fig. 2A, t_0). In addition to the CEF pathway, implicating PGR5 and PGRL1, another pathway involving NDA2 exists in *C. reinhardtii* (Jans et al., 2008; Desplats et al., 2009), which can represent the main CEF pathway under certain stress conditions (Saroussi et al., 2016). The activity of NDA2-dependent, nonphotochemical PQ reduction is low in *stm6* (Fig. 3, C–H) and at the same the modulation of NDA2 expression is perturbed in the mutant (Fig. 4B). This altered activity of NDA2 should contribute to the CEF phenotype noted for *stm6*. For low light-acclimated cells of *stm6*, the diminished activity of NDA2 (Fig. 3, C and D) cannot be explained by a limited availability of the enzyme (Fig. 4B, t_0), but should rather reflect a restricted substrate supply in a more oxidized stroma (Fig. 5, t_0), which is in turn caused by a stimulated mitorespiration. Increased mitorespiration observed in *stm6* is thus responsible for decreasing reducing power in the stroma, subtracting the feedback mechanism used by green algae and higher plants to manage exposure to high light. In this context, it should be noted that this study was conducted with cultures grown in CO_2-enriched air (2% [v/v]), which was recently found to be associated with a low contribution of LHCSR3-dependent qE to photoprotection (Correa-Galvis et al., 2016; Polukhina et al., 2016). It is therefore likely that the impairment of other

photoprotective mechanisms, controlled by the stromal redox state, also contributes to the enhanced susceptibility of *stm6* to photoinhibition. In general, the need for a mitochondrial electron sink that helps reduce the excitation pressure in the chloroplast should also depend on NPQ capacity as another mechanism to avoid the accumulation of excess reducing equivalents. The extent of cooperation between mitochondria and chloroplast might therefore differ between distinct metabolic modes of a *C. reinhardtii* cell, as the preference for a certain photoacclimation strategy changes in response to an altered carbon supply (Polukhina et al., 2016). A study, conducted with a PGRL1-deficient cell line from *C. reinhardtii*, which cannot reequilibrate the plastidic ATP/NADPH balance based on CEF activation, revealed that this mutant adapts to the CEF impairment based on higher rates of Mehler reactions and Mehler-like reactions catalyzed by flavodiiron proteins at PSI, besides an increased cooperation between chloroplast and mitochondria (Dang et al., 2014). This indicates that an uptake of excess reducing equivalents by mitochondria is only one of several mechanisms that help prevent overreduced states in a *C. reinhardtii* chloroplast during the acclimation to excess light.

As mentioned above, in *C. reinhardtii*, CEF is stimulated by anaerobic conditions, a physiological situation that is associated with a decreased capacity of the mitochondrion to act as a reductant sink and that ultimately leads to an overreduced state of the chloroplast stroma (Takahashi et al., 2013). Interestingly, *stm6* also shows impaired CEF under anaerobic conditions (Kruse et al., 2005), which resemble the full inhibition of mitorespiration caused by inhibitor treatment (Fig. 5, E and F). Under anaerobic, hydrogen-producing conditions, *stm6* prefers linear photosynthetic electron transport to the hydrogenase to prevent an accumulation of reducing equivalents in the chloroplast (Kruse et al., 2005; Volgusheva et al., 2013). A difference between these two mechanisms that relieve the plastidic redox pressure, caused by a diminished mitochondrial uptake of reducing equivalents, might be the regulation of involved components. So far, a redox regulation of hydrogenase activity has not been described, but several lines of evidence exist for the activity modulation of PGRL1 by the thioredoxin system, whose activity state is itself tightly coupled to the stromal redox poise (Petroutsos et al., 2009; Hertle et al., 2013). Against this background, it might be speculated that the impaired activation of CEF is a consequence of the perturbed redox poise in chloroplasts of *stm6*.

A previous study revealed that *stm6* shows a state transition phenotype by being blocked in state I under aerobic conditions when light, preferentially exciting PSII, is applied, while anaerobiosis induces state II in *stm6* cells (Schönfeld et al., 2004). This phenotype could also be connected to the perturbed stromal redox poise in *stm6*, since the activity of STT7 kinase, which initiates state I–state II transitions by phosphorylating LHCII proteins, was proposed to be regulated by the ferredoxin-thioredoxin system (Rintamäki et al., 2000). Interestingly, *stm6* shows an enhanced mitochondrial

electron sink capacity and is blocked in state I, while *dum* mutants, characterized by lower rates of mitochondrial respiration, are blocked in state II (Cardol et al., 2003). The fact that anaerobiosis, a situation when mitochondrial respiration is inhibited, can be used to drive *stm6* into state II, further supports the view that an altered mitorespiration in *stm6* contributes to the state transition phenotype.

The switch from nonphosphorylating to phosphorylating (energy conserving) modes of mitochondrial respiration, seen during the acclimation to excess light (Fig. 2), could serve two functions. Besides relieving the chloroplast redox pressure caused by excess light, the increased contribution of the cytochrome *c* pathway should generate extra ATP. A metabolic modelling study conducted with *C. reinhardtii* indicated that under photoautotrophic conditions, an export of sugar (G3P/dihydroxyacetone phosphate) from the chloroplast coupled to its consumption via glycolysis, TCA cycle, and oxidative phosphorylation is associated with higher ATP yields than those that can theoretically be obtained by photophosphorylation in the chloroplast (Kliphuis et al., 2011). In diatoms, it was recently shown that carbon dioxide fixation depends on the import of mitochondrial ATP into the chloroplast, which is generated from reducing equivalents that were formed in the chloroplast (Bailleul et al., 2015). The enhancement of mitochondrial transcription termination (Wobbe and Nixon, 2013) caused by elevated levels of MOC1 (Fig. 1A) could be a central part of the regulatory switch observed in mitochondria of light-stressed *C. reinhardtii* cells, and its impairment leads to a perturbed chloroplast redox poise.

CONCLUSION

In *C. reinhardtii*, the acclimation to excess light not only modulates photosynthetic electron transport but also the modes of mitochondrial electron flow by favouring ATP-forming pathways. An increased cooperation between mitochondria and chloroplast in light stress is evidenced by higher rates of mitochondrial respiration and the transcriptional up-regulation of metabolic pathways that connect plastidic and mitochondrial NAD(P)H pools. In addition to mitochondrial respiration, chlororespiration is activated when *C. reinhardtii* is exposed to excess light. A loss of the mTERF protein MOC1, which is needed for proper transcription termination in *C. reinhardtii* mitochondria, disrupts mitochondrial light acclimation and stimulates mitochondrial reducing equivalent uptake in the MOC1-free mutant *stm6* based on a high activity of the AOX pathway. The constitutively enhanced electron sink capacity of mitochondria in *stm6* is detrimental for the activation of photoprotective mechanisms controlled by the stromal redox poise such as chlororespiration and partly explains its high-light sensitive phenotype.

MATERIALS AND METHODS

Chemicals and Enzymes. nPG, potassium cyanide, DCMU, DBMIB, myxothiazol, and SHAM were purchased from Sigma-Aldrich.

Statistical Analysis. Students' two-tailed t test for independent samples was applied to statistically evaluate results, and two significance thresholds were distinguished ($P < 0.05$/$P < 0.1$). Error bars indicate either SE or SD, and the number of replicates used to calculate SE and SD is indicated in the figure legends.

Strains and Culture Conditions. The MOC1 knockout mutant *stm6* was generated via random insertion of plasmid pArg7.8 (Debuchy et al., 1989), carrying the Arg-7 gene, into the nuclear genome of the Arg auxotrophic strain, *CC1618*. The MOC1-complemented strain *B13* (Schönfeld et al., 2004) was generated by cotransforming *stm6* with a 37-kb *Moc1*-containing cosmid isolated from a cosmid library and the *Cry1* gene as a dominant selectable marker conferring resistance to emetine (plasmid p613; Nelson et al., 1994). Mutant *dum20* (Remacle et al., 2001) and the AOX1 knockdown strain (T53; parental strain *cw15 arg7-8 mt*$^+$) along with its reference strain *cw15 mt*$^+$ (strain 83; Mathy et al., 2010) were kindly provided by C. Remacle (University of Liége, Belgium). *dum20* is derived from wild type 137C and lacks OXPHOS complex I activity completely, due to the deletion of one T at codon 243 of the mitochondrial gene *nd1* (Remacle et al., 2001). Liquid cultures of *Chlamydomonas reinhardtii*, bubbled with carbon dioxide-enriched air (2% v/v), were cultivated photoautotrophically in HSM (Harris, 2009) at low/moderate (100 µmol photons m^{-2} s^{-1}) and high light (1500 µmol photons m^{-2} s^{-1}) conditions in FMT 150 photobioreactors (Photon Systems Instruments).

SDS-PAGE and Immunoblotting. For the preparation of SDS-PAGE samples, cell pellets containing 10^7 cells were resuspended in 100 µL lysis buffer (2% [w/v] SDS, 60 mM Tris-HCl, pH 6.8, 100mM dithiothreitol, and 10% [w/v] glycerol) and boiled for 5 min at 95°C. The protein concentration in samples was determined using the amido black assay (Popov et al., 1975). Protein samples (10 µg per lane) were separated on 10% (w/v) or 15% (w/v) denaturing SDS-PAGE gels containing 6 M urea and stained with Coomassie Brilliant Blue R-250 or electroblotted onto nitrocellulose membrane (0.2-mm pore size; GE Healthcare). Immunoblotting analyses were performed using specific primary antibodies and a horseradish peroxidase-conjugated secondary antibody (Agrisera). Signals were visualized using the FUSION-FX7 detection system (Peqlab). The following polyclonal antisera were used as primary antibodies: rabbit anti-MOC1 (Wobbe and Nixon 2013), rabbit anti-AOX1 (kindly provided by SabeehaMerchant), rabbit anti-cox1 (S. Merchant), anti-COXIIb (Agrisera; product AS06151), rabbit anti-histone H3 (Agrisera; product AS10710), rabbit anti-NDA2 (kindly provided by Claire Remacle (University of Liège, Belgium)), rabbit anti-PTOX2 (kindly provided by Xenie Johnson, CEA, Cadarache), and rabbit anti-PGRL1 (kindly provided by M. Hippler, University of Muenster,

Germany). Immunodetection and quantification of proteins PSAA, CP43, LHCII, and ARSA (Formighieri et al., 2013) was performed as described previously (Bonente et al., 2012).

RT-qPCR. Real-time RT-PCR was performed with total RNA samples that were subjected to DNaseI (RQ1 RNase-free DNase; Promega) digest prior to reverse transcription and PCR amplification using the SensiFAST SYBR No-ROX One-Step Kit (BIOLINE). SYBR Green I fluorescence was recorded on a DNA Engine Opticon (Bio-Rad). Per sample 100 ng total RNA was used and *RPL13* (gene ID: 5718254) as well as *RACK1* (gene ID: 5723548) served as housekeeping genes. Primer sequences are given in Supplemental Table S2. Relative mRNA expression levels for transcripts in mutant *stm6* and the complemented strain (*B13*) were calculated according to Pfaffl (2001).

Whole Cell Respiration. Samples derived from low light (t_0)-/high light ($t_{2\text{-}8h}$)-acclimated photoautotrophic *stm6*/*B13* cultures were subjected to respiratory rate measurements in the dark using a Clark-type O_2 electrode (Oxygraph Plus; Hansatech Instruments; Clark, 1956). Respiratory rates (RR), measured at 25°C, were normalized to haemocytometer cell counts (Neubauer Improved) in order to compare total rates of cellular respiration in *B13* and *stm6*. To discriminate between the individual contributions of the alternative, the cytochrome *c* pathway, and complex I versus rotenone-insensitive dehydrogenases, dark respiration measurements were conducted as follows: cell samples (10^7 cells in 2 mL) were directly transferred from photobioreactors to the measurement chamber of the Clark electrode. After 1 min, respiration rates were recorded for 2 min prior to the addition of the first inhibitor. Then respiration rates were recorded for 2 additional min before the second inhibitor (omitted for complex I) was added to the sample and measurements were continued for another 2 min. Alternative respiration (AOX+PTOX) was inhibited by adding 1 mM nPG (Cournac et al., 2000; Møller et al., 1988), while the cytochrome *c* oxidase pathway (complex IV) was inhibited by adding 1 mM potassium cyanide (KCN; Mathy et al., 2010). Rotenone (Møller et al., 1993; Lecler et al., 2012) was used at a concentration of 100 µM to inhibit complex I activity. To assess the relative contribution of the cytochrome *c* oxidase pathway, respiration was first measured in the absence of inhibitors (set to 100%) before alternative respiration was inhibited by adding nPG. Cytochrome c-dependent respiration was then inhibited using KCN and the residual respiration determined in relation to the uninhibited state. The contribution of alternative respiration was determined by reversing the order of inhibitor addition (KCN followed by nPG).

Chlorophyll Fluorescence Analyses. To determine the F_v/F_m and ΦPSII of low light (t_0)- and high light ($t_{2\text{-}8h}$)- acclimated cells grown in photoautotrophic media, 2 mL samples of the culture were incubated in the dark and aerated for 20 min. Chlorophyll fluorescence changes were recorded during a 10 min induction curve with actinic light (800 µmol photons m^{-2} s^{-1}) using a Mini PAM

(Waltz) and fluorescence parameters calculated according to the following equations (Maxwell and Johnson 2000):

$$\Phi PSII = \frac{Fm' - Ft}{Fm'}$$

$$\frac{F_V}{F_m} = \frac{F_m - F_0}{F_m}$$

Chlorophyll rereduction in the dark after illumination with 150 µmol photons m^{-2} s^{-1} was measured in the presence or absence of 1 mM nPG as described by Houille-Vernes et al. (2011).

P700 Oxidation Kinetics. PSI reaction center activity was monitored as a transient decrease of 705 nm absorption as previously described, using a JTS 10-LED pump-probe spectrometer (Bio-Logic SAS; Bonente et al., 2012). In particular, P700 oxidation kinetics were measured applying an actinic orange light at different light intensities, from 35 to 940 µmol photons m^{-2} s^{-1}. DCMU, DBMIB, myxothiazol, SHAM, and nPG were added as reported in "Results" before measurements at concentrations of 10 µM, 2 µM, 5 µM, 1mM, and 1mM, respectively. Maximal $P700^+$ levels were determined at 940 µmol photons $m^{-2}s^{-1}$ in the presence of DCMU, DBMIB, ascorbate (2 mM), and methyl viologen (1 mM). $P700^+$ rereduction kinetics in the dark were investigated after 30 s of illumination with 940 µmol photons m^{-2} s^{-1} and fitted with an exponential function (Alric et al., 2010). Plastocyanin oxidation kinetics were measured using the same set up described for P700 oxidation kinetics but using a probing light at 740 nm.

PSI/PSII Ratio Analysis by Electrochromic Shift . Electrochromic shift was measured to evaluate the PSI/PSII ratio on whole cells untreated or treated with DCMU and hydroxylamine as described by Bailleul et al. (2010).

ACKNOWLEDGMENTS

We acknowledge K. Rojek and L. Meyer zur Verl for technical and experimental assistance. We thank S. Merchant, C. Remacle, X. Johnson, and M. Hippler for the provision of antisera. We also thank C. Remacle for providing the AOX1 knockdown strain. We are grateful to the Center for Biotechnology (CeBiTec) at Bielefeld University for access to the Technology Platforms.

AUTHOR CONTRIBUTION

A.U. and M.C. performed most of the experiments; M.B. and L.W. performed and designed the experiments; L.W. conceived the project and wrote the article with contributions of all the authors.

REFERENCES

Ahmad, N., Michoux, F., and Nixon, P. J. (2012) Investigating the production of foreign membrane proteins in tobacco chloroplasts : Expression of an algal plastid terminal oxidase. PLoS ONE 7 : e41722

Alric, J., Lavergne, J., and Rappaport, F. (2010) Redox and ATP control of photosynthetic cyclic electron flow in *Chlamydomonas reinhardtii* (I) aerobic conditions. Biochim Biophys Acta 1797 : 44-51

Atteia, A., Adrait, A., Brugière, S., Tardif, M., van Lis, R., Deusch, O., Dagan, T., Kuhn, L., Gontero, B., Martin, W., Garin, J., Joyard, J., and Rolland, N. (2009) A proteomic survey of *Chlamydomonas reinhardtii* mitochondria sheds new light on the metabolic plasticity of the organelle and on the nature of the α-proteobacterial mitochondrial ancestor. Mol Biol Evol 26 : 1533-1548

Bailleul, B., Berne, N., Murik, O., Petroutsos, D., Prihoda, J., Tanaka, A., Villanova, V., Bligny, R., Flori, S., Falconet, D., Krieger-Liszkay, A., Santabarbara, S., Rappaport, F., Joliot, P., Tirichine, L., Falkowski, P. G., Cardol, P., Bowler, C., and Finazzi, G. (2015) Energetic coupling between plastids and mitochondria drives CO_2 assimilation in diatoms. Nature 524 : 366-369

Bailleul, B., Cardol, P., Breyton, C., and Finazzi, G. (2010) Electrochromism : a useful probe to study algal photosynthesis. Photosynth Res 106 : 179-189

Baurain, D., Dinant, M., Coosemans, N., and Matagne, R. F. (2003) Regulation of the alternative oxidase Aox1 gene in *Chlamydomonas reinhardtii*. Role of the nitrogen source on the expression of a reporter gene under the control of the Aox1 promoter. Plant Physiol 131 : 1418-1430

Bennoun, P. (1982) Evidence for a respiratory chain in the chloroplast. Proc Natl Acad Sci USA 79 : 4352-4356

Bonente, G., Pippa, S., Castellano, S., Bassi, R., and Ballottari, M. (2012) Acclimation of *Chlamydomonas reinhardtii* to different growth irradiances. J Biol Chem 287 : 5833-5847

Cardol, P., Gloire, G., Havaux, M., Remacle, C., Matagne, R., and Franck, F. (2003) Photosynthesis and state transitions in mitochondrial mutants of *Chlamydomonas reinhardtii* affected in respiration. Plant Physiol 133 : 2010-2020

Cardol, P., Alric, J., Girard-Bascou, J., Franck, F., Wollman, F.-A., and Finazzi, G. (2009) Impaired respiration discloses the physiological significance of state transitions in *Chlamydomonas*. Proc Natl Acad Sci 106 : 15979-15984

Clark, L. C. J. (1956) Monitor and control of blood and tissue oxygen tensions. ASAIO Journal 2 : 41-48

Correa-Galvis, V., Redekop, P., Guan, K., Griess, A., Truong, T. B., Wakao, S., Niyogi, K. K., and Jahns, P. (2016) Photosystem II subunit PsbS is involved in the induction of LHCSR protein-dependent energy dissipation in *Chlamydomonas reinhardtii*. J Biol Chem 291 : 17478-17487

Cournac, L., Josse, E. M., Joet, T., Rumeau, D., Redding, K., Kuntz, M., and Peltier, G. (2000) Flexibility in photosynthetic electron transport : a newly identified chloroplast oxidase involved in chlororespiration. Philos Trans R Soc Lond B Biol Sci 355 : 1447-1454

Dang, K.-V., Plet, J., Tolleter, D., Jokel, M., Cuiné, S., Carrier, P., Auroy, P., Richaud, P., Johnson, X., Alric, J., Allahverdiyeva, Y., and Peltier, G. (2014) Combined increases in mitochondrial cooperation and oxygen photoreduction compensate for deficiency in cyclic electron flow in *Chlamydomonas reinhardtii*. Plant Cell 26 : 3036-3050

Debuchy, R., Purton, S., and Rochaix, J. D. (1989) The argininosuccinate lyase gene of *Chlamydomonas reinhardtii* : an important tool for nuclear transformation and for correlating the genetic and molecular maps of the ARG7 locus. EMBO J 8 : 2803-2809

Desplats, C., Mus, F., Cuine, S., Billon, E., Cournac, L., and Peltier, G. (2009) Characterization of Nda2, a plastoquinone-reducing type II NAD(P)H dehydrogenase in *Chlamydomonas* chloroplasts. J Biol Chem 284 : 4148-4157

Dinant, M., Baurain, D., Coosemans, N., Joris, B., and Matagne, R. F. (2001) Characterization of two genes encoding the mitochondrial alternative oxidase in *Chlamydomonas reinhardtii*. Curr Genet 39 : 101-108

Doebbe, A., Keck, M., La Russa, M., Mussgnug, J. H., Hankamer, B., Tekce, E., Niehaus, K., and Kruse, O. (2010) The interplay of proton, electron, and metabolite supply for photosynthetic H_2 production in *Chlamydomonas reinhardtii*. J Biol Chem 285 : 30247-30260

Dorthu, M. P., Remy, S., Michel-Wolwertz, M. R., Colleaux, L., Breyer, D., Beckers, M. C., Englebert, S., Duyckaerts, C., Sluse, F. E., and Matagne, R. F. (1992) Biochemical, genetic and molecular characterization of new respiratory-deficient mutants in *Chlamydomonas reinhardtii*. Plant Mol Biol 18 : 759-772

Dutilleul, C., Driscoll, S., Cornic, G., De Paepe, R., Foyer, C. H., and Noctor, G. (2003) Functional mitochondrial complex I is required by tobacco leaves for optimal photosynthetic performance in photorespiratory conditions and during transients. Plant Physiol 313 : 264-275

Feilke, K., Streb, P., Cornic, G., Perreau, F., Kruk, J., and Krieger-Liszkay, A. (2016) Effect of *Chlamydomonas* plastid terminal oxidase 1 expressed in tobacco on photosynthetic electron transfer. Plant J 85 : 219-228

Florez-Sarasa, I., Noguchi, K., Araujo, W. L., Garcia-Nogales, A., Fernie, A. R., Flexas, J., and Ribas-Carbo, M. (2016) Impaired cyclic electron flow around photosystem I disturbs high-light respiratory metabolism. Plant Physiol 172 : 2176-2189

Formighieri, C., Cazzaniga, S., Kuras, R., and Bassi, R. (2013) Biogenesis of photosynthetic complexes in the chloroplast of *Chlamydomonas reinhardtii* requires ARSA1, a homolog of prokaryotic arsenite transporter and eukaryotic TRC40 for guided entry of tail-anchored proteins. Plant J 73 : 850-861

Formighieri, C., Ceol, M., Bonente, G., Rochaix, J. D., and Bassi, R. (2012) Retrograde signaling and photoprotection in a gun4 mutant of *Chlamydomonas reinhardtii*. Mol Plant 5 : 1242-1262

Harris, E.H. (1989) The Chlamydomonas Sourcebook : A Comprehensive Guide to Biology and Laboratory Use. Academic Press, San Diego.

Hertle, Alexander P., Blunder, T., Wunder, T., Pesaresi, P., Pribil, M., Armbruster, U., and Leister, D. (2013) PGRL1 is the elusive ferredoxin-plastoquinone reductase in photosynthetic cyclic electron flow. Mol Cell 49 : 511-523

Houille-Vernes, L., Rappaport, F., Wollman, F.-A., Alric, J., and Johnson, X. (2011) Plastid terminal oxidase 2 (PTOX2) is the major oxidase involved in chlororespiration in Chlamydomonas. Proc Natl Acad Sci 108 : 20820-20825

Houyoux, P. A., Ghysels, B., Lecler, R., and Franck, F. (2011) Interplay between non-photochemical plastoquinone reduction and re-oxidation in pre-illuminated *Chlamydomonas reinhardtii* : a chlorophyll fluorescence study. Photosynth Res 110 : 13-24

Jans, F., Mignolet, E., Houyoux, P. A., Cardol, P., Ghysels, B., Cuine, S., Cournac, L., Peltier, G., Remacle, C., and Franck, F. (2008) A type II NAD(P)H dehydrogenase mediates light-independent plastoquinone reduction in the chloroplast of *Chlamydomonas*. Proc Natl Acad Sci USA 105 : 20546-20551

Johnson, X., and Alric, J. (2013) Central carbon metabolism and electron transport in *Chlamydomonas reinhardtii* : metabolic constraints for carbon partitioning between oil and starch. Eukaryot Cell 12 : 776-793

Johnson, X., Steinbeck, J., Dent, R. M., Takahashi, H., Richaud, P., Ozawa, S., Houille-Vernes, L., Petroutsos, D., Rappaport, F., Grossman, A. R., Niyogi, K. K., Hippler, M., and Alric, J. (2014) Proton gradient regulation 5-mediated cyclic electron flow under ATP- or redox-limited conditions : a study of ΔATPase pgr5 and ΔrbcL pgr5 mutants in the green alga *Chlamydomonas reinhardtii*. Plant Physiol 165 : 438-452

Kleine, T., and Leister, D. (2015) Emerging functions of mammalian and plant mTERFs. Biochim Biophys Acta 1847 : 786-797

Kliphuis, A. M., Klok, A. J., Martens, D. E., Lamers, P. P., Janssen, M., and Wijffels, R. H. (2012) Metabolic modeling of *Chlamydomonas reinhardtii* : energy requirements for photoautotrophic growth and maintenance. J Appl Phycol 24 : 253-266

Kruse, O., Rupprecht, J., Bader, K. P., Thomas-Hall, S., Schenk, P. M., Finazzi, G., and Hankamer, B. (2005) Improved photobiological H_2 production in engineered green algal cells. J Biol Chem 280 : 34170-34177

Kuhn, K., Obata, T., Feher, K., Bock, R., Fernie, A. R., and Meyer, E. H. (2015) Complete mitochondrial complex I deficiency induces an up-regulation of respiratory fluxes that is abolished by traces of functional complex I. Plant Physiol 168 : 1537-1549

Kukuczka, B., Magneschi, L., Petroutsos, D., Steinbeck, J., Bald, T., Powikrowska, M., Fufezan, C., Finazzi, G., and Hippler, M. (2014) Proton gradient regulation5-like1-mediated cyclic electron flow is crucial for acclimation to anoxia and complementary to nonphotochemical quenching in stress adaptation. Plant Physiol 165 : 1604-1617

Lecler, R., Vigeolas, H., Emonds-Alt, B., Cardol, P., and Remacle, C. (2012) Characterization of an internal type-II NADH dehydrogenase from *Chlamydomonas reinhardtii* mitochondria. Curr Genet 58 : 205-216

Lemaire, S. D., Quesada, A., Merchan, F., Corral, J. M., Igeno, M. I., Keryer, E., Issakidis-Bourguet, E., Hirasawa, M., Knaff, D. B., and Miginiac-Maslow, M. (2005) NADP-malate dehydrogenase from unicellular green alga *Chlamydomonas reinhardtii*. A first step toward redox regulation? Plant Physiol 137 : 514-521

Mathy, G., Cardol, P., Dinant, M., Blomme, A., Gerin, S., Cloes, M., Ghysels, B., DePauw, E., Leprince, P., Remacle, C., Sluse-Goffart, C., Franck, F., Matagne, R. F., and Sluse, F. E. (2010) Proteomic and functional characterization of a *Chlamydomonas reinhardtii* mutant lacking the mitochondrial alternative oxidase 1. J Proteome Res 9 : 2825-2838

Maxwell, K., and Johnson, G. N. (2000) Chlorophyll fluorescence-a practical guide. J Exp Bot 51 : 659-668

Møller, I. M., Bérczi, A., van der Plas, L. H. W., and Lambers, H. (1988) Measurement of the activity and capacity of the alternative pathway in intact plant tissues : Identification of problems and possible solutions. Physiol Plant 72 : 642-649

Møller, I. M., Rasmusson, A. G., and Fredlund, K. M. (1993) NAD(P)H-ubiquinone oxidoreductases in plant mitochondria. J Bioenerg Biomembr 25 : 377-384

Moore, A. L., Shiba, T., Young, L., Harada, S., Kita, K., and Ito, K. (2013) Unraveling the heater : new insights into the structure of the alternative oxidase. Annu Rev Plant Biol 64 : 637-663

Nawrocki, W. J., Tourasse, N. J., Taly, A., Rappaport, F., and Wollman, F. A. (2015) The plastid terminal oxidase : its elusive function points to multiple contributions to plastid physiology. Annu Rev Plant Biol 66 : 49-74

Nelson, J. A., Savereide, P. B., and Lefebvre, P. A. (1994) The CRY1 gene in *Chlamydomonas reinhardtii* : structure and use as a dominant selectable marker for nuclear transformation. Mol Cell Biol 14 : 4011-4019

Nguyen, A. V., Toepel, J., Burgess, S., Uhmeyer, A., Blifernez, O., Doebbe, A., Hankamer, B., Nixon, P., Wobbe, L., and Kruse, O. (2011) Time-course global expression profiles of *Chlamydomonas reinhardtii* during photo-biological H_2 production. PloS one 6 : e29364

Noguchi, K., and Yoshida, K. (2008) Interaction between photosynthesis and respiration in illuminated leaves. Mitochondrion 8 : 87-99

Ort, D. R., and Baker, N. R. (2002) A photoprotective role for O_2 as an alternative electron sink in photosynthesis? Curr Opin Plant Biol 5 : 193-198

Padmasree, K., Padmavathi, L., and Raghavendra, A. S. (2002) Essentiality of mitochondrial oxidative metabolism for photosynthesis : optimization of carbon assimilation and protection against photoinhibition. Crit Rev Biochem Mol Biol 37 : 71-119

Petroutsos, D., Terauchi, A. M., Busch, A., Hirschmann, I., Merchant, S. S., Finazzi, G., and Hippler, M. (2009) PGRL1 participates in iron-induced remodeling of the photosynthetic apparatus and in energy metabolism in *Chlamydomonas reinhardtii*. J Biol Chem 284 : 32770-32781

Pfaffl, M. W. (2001) A new mathematical model for relative quantification in real-time RT-PCR. Nucleic Acids Res 29 : e45

Picault, N., Palmieri, L., Pisano, I., Hodges, M., and Palmieri, F. (2002) Identification of a novel transporter for dicarboxylates and tricarboxylates in plant mitochondria. Bacterial expression, reconstitution, functional characterization, and tissue distribution. J Biol Chem 277 : 24204-24211

Picault, N., Hodges, M., Palmieri, L., and Palmieri, F. (2004) The growing family of mitochondrial carriers in *Arabidopsis*. Trends Plant Sci 9 : 138-146

Polukhina, I., Fristedt, R., Dinc, E., Cardol, P., and Croce, R. (2016) Carbon supply and photoacclimation cross talk in the green alga *Chlamydomonas reinhardtii*. Plant Physiol 172 : 1494-1505

Popov, N., Schmitt, M., Schulzeck, S., and Matthies, H. (1975) Reliable micromethod for determination of the protein content in tissue homogenates. Acta Biol Med Ger 34 : 1441-1446

Rasmusson, A. G., and Wallström, S. V. (2010) Involvement of mitochondria in the control of plant cell NAD(P)H reduction levels. Biochem Soc Trans 38 : 661-666

Remacle, C., Baurain, D., Cardol, P., and Matagne, R. F. (2001) Mutants of *Chlamydomonas reinhardtii* deficient in mitochondrial complex I : characterization of two mutations affecting the nd1 coding sequence. Genetics 158 : 1051-1060

Rintamäki, E., Martinsuo, P., Pursiheimo, S., and Aro, E. M. (2000) Cooperative regulation of light-harvesting complex II phosphorylation via the plastoquinol and ferredoxin-thioredoxin system in chloroplasts. Proc Natl Acad Sci USA 97 : 11644-11649

Sabar, M., De Paepe, R., and de Kouchkovsky, Y. (2000) Complex I impairment, respiratory compensations, and photosynthetic decrease in nuclear and mitochondrial male sterile mutants of *Nicotiana sylvestris*. Plant Physiol 124 : 1239-1250

Salinas, T., Larosa, V., Cardol, P., Marechal-Drouard, L., and Remacle, C. (2014) Respiratory-deficient mutants of the unicellular green alga *Chlamydomonas* : a review. Biochimie 100 : 207-218

Saroussi, S. I., Wittkopp, T. M., and Grossman, A. R. (2016) The type II NADPH dehydrogenase facilitates cyclic electron flow, energy-dependent quenching, and chlororespiratory metabolism during acclimation of *Chlamydomonas reinhardtii* to nitrogen deprivation. Plant Physiol 170 : 1975-1988

Scagliarini, S., Trost, P., Valenti, V., and Pupillo, P. (1990) Glyceraldehyde 3-phosphate : NADP reductase of spinach leaves : steady state kinetics and effect of inhibitors. Plant Physiol 94 1337-1344

Schneider, A., Hausler, R. E., Kolukisaoglu, U., Kunze, R., van der Graaff, E., Schwacke, R., Catoni, E., Desimone, M., and Flügge, U. I. (2002) An *Arabidopsis thaliana* knock-out mutant of the chloroplast triose phosphate/phosphate translocator is severely compromised only when starch synthesis, but not starch mobilisation is abolished. Plant J 32 : 685-699

Schonbaum, G. R., Bonner, W. D., Jr., Storey, B. T., and Bahr, J. T. (1971) Specific inhibition of the cyanide-insensitive respiratory pathway in plant mitochondria by hydroxamic acids. Plant Physiol 47 : 124-128

Schönfeld, C., Wobbe, L., Borgstadt, R., Kienast, A., Nixon, P. J., and Kruse, O. (2004) The nucleus-encoded protein MOC1 is essential for mitochondrial light acclimation in *Chlamydomonas reinhardtii*. J Biol Chem 279 : 50366-50374

Steinbeck, J., Nikolova, D., Weingarten, R., Johnson, X., Richaud, P., Peltier, G., Hermann, M., Magneschi, L., and Hippler, M. (2015) Deletion of Proton Gradient Regulation 5 (PGR5) and PGR5-Like 1 (PGRL1) proteins promote sustainable light-driven hydrogen production in *Chlamydomonas reinhardtii* due to increased PSII activity under sulfur deprivation. Front Plant Sci 6 : 892

Sweetlove, L. J., Lytovchenko, A., Morgan, M., Nunes-Nesi, A., Taylor, N. L., Baxter, C. J., Eickmeier, I., and Fernie, A. R. (2006) Mitochondrial uncoupling protein is required for efficient photosynthesis. Proc Natl Acad Sci 103 : 19587-19592

Takahashi, H., Clowez, S., Wollman, F. A., Vallon, O., and Rappaport, F. (2013) Cyclic electron flow is redox-controlled but independent of state transition. Nat Commun 4 : 1954

Tardif, M., Atteia, A., Specht, M., Cogne, G., Rolland, N., Brugière, S., Hippler, M., Ferro, M., Bruley, C., Peltier, G., Vallon, O., and Cournac, L. (2012) PredAlgo : A new subcellular localization prediction tool dedicated to green algae. Mol Biol Evol 29 : 3625-3639

Terashima, M., Specht, M., and Hippler, M. (2011) The chloroplast proteome : a survey from the *Chlamydomonas reinhardtii* perspective with a focus on distinctive features. Curr Genet 57 : 151-168

Tolleter, D., Ghysels, B., Alric, J., Petroutsos, D., Tolstygina, I., Krawietz, D., Happe, T., Auroy, P., Adriano, J. M., Beyly, A., Cuine, S., Plet, J., Reiter, I. M., Genty, B., Cournac, L., Hippler, M., and Peltier, G. (2011) Control of hydrogen photoproduction by the proton gradient generated by cyclic electron flow in *Chlamydomonas reinhardtii*. Plant Cell 23 : 2619-2630

Vanlerberghe, G. C. (2013) Alternative oxidase : a mitochondrial respiratory pathway to maintain metabolic and signaling homeostasis during abiotic and biotic stress in plants. Int J Mol Sci 14 : 6805-6847

Vishwakarma, A., Bashyam, L., Senthilkumaran, B., Scheibe, R., and Padmasree, K. (2014) Physiological role of AOX1a in photosynthesis and maintenance of cellular redox homeostasis under high light in *Arabidopsis thaliana*. Plant Physiol Biochem 81 : 44-53

Vishwakarma, A., Tetali, S. D., Selinski, J., Scheibe, R., and Padmasree, K. (2015) Importance of the alternative oxidase (AOX) pathway in regulating cellular redox and ROS homeostasis to optimize photosynthesis during restriction of the cytochrome oxidase pathway in *Arabidopsis thaliana*. Ann Bot 116 : 555-69

Volgusheva, A., Styring, S., and Mamedov, F. (2013) Increased photosystem II stability promotes H_2 production in sulfur-deprived *Chlamydomonas reinhardtii*. Proc Natl Acad Sci USA 110 : 7223-7228

Von Jagow, G., and Engel, W. D. (1981) Complete inhibition of electron transfer from ubiquinol to cytochrome b by the combined action of antimycin and myxothiazol. FEBS Lett 136 : 19-24

Wobbe, L., and Nixon, P. J. (2013) The mTERF protein MOC1 terminates mitochondrial DNA transcription in the unicellular green alga *Chlamydomonas reinhardtii*. Nucleic Acids Res 41 : 6553-6567

Wobbe, L., Bassi, R., and Kruse, O. (2016) Multi-level light capture control in plants and green algae. Trends Plant Sci 21 : 55-68

Xue, X., Gauthier, D. A., Turpin, D. H., and Weger, H. G. (1996) Interactions between photosynthesis and respiration in the green alga *Chlamydomonas reinhardtii* (characterization of light-enhanced dark respiration). Plant Physiol 112 : 1005-1014

Yoshida, K., Terashima, I., and Noguchi, K. (2007) Up-regulation of mitochondrial alternative oxidase concomitant with chloroplast over-reduction by excess light. Plant Cell Physiol 48 : 606-614

Yoshida, K., and Noguchi, K. (2009) Differential gene expression profiles of the mitochondrial respiratory components in illuminated *Arabidopsis* leaves. Plant Cell Physiol 50 : 1449-1462

Yoshida, K., Watanabe, C. K., Hachiya, T., Tholen, D., Shibata, M., Terashima, I., and Noguchi, K. (2011) Distinct responses of the mitochondrial respiratory chain to long- and short-term high-light environments in *Arabidopsis thaliana*. Plant Cell Environ 34 : 618-628

Zhang, L. T., Zhang, Z. S., Gao, H. Y., Meng, X. L., Yang, C., Liu, J. G., and Meng, Q. W. (2012) The mitochondrial alternative oxidase pathway protects the photosynthetic apparatus against photodamage in Rumex K-1 leaves. BMC Plant Biology 12 : 40

SUPPLEMENTARY INFORMATION

Supplemental tables

Table S1. Phytozome locus numbers of genes analysed in the present study.

Name	Description	Phytozome locus name	UniProt KB
NDA5	Type-II NADH dehydrogenase	Cre16.g671000	A6YT86
GAPN1	glyceraldehyde-3-phosphate dehydrogenase (NADP) [EC:1.2.1.9] non-phosphorylating GAPDH	Cre12.g556600	A8IYT1
GAP2	Glyceraldehyde 3-phosphate dehydrogenase	Cre07.g354200	A8JFT3
PGK2	Phosphoglycerate kinase	Cre07.g354250	A8JFT4
TPT3/APE2	Triose phosphate transporter	Cre01.g045550	A8HN02
TPT2	Triose phosphate/phosphate translocator	Cre06.g263850	Q7XJ66
TPT25/CGL51	Triose phosphate transporter	Cre16.g663800	A8JFB4
TPT1	Triose phosphate transporter	Cre08.g379350	Q84XW3
PGH1	Enolase	Cre12.g513200	A8JH98
PEPC2	Phosphoenolpyruvate carboxylase	Cre03.g171950	Q6R2V6
MDH3	NAD-dependent malate dehydrogenase	Cre02.g145800	A8J0W9
MITC14	Mitochondrial substrate carrier protein, possible 2-oxoglutarate/malate carrier	Cre16.g672650	A8J3F7
MDH4	NAD-dependent malate dehydrogenase, mitochondrial	Cre12.g483950	A8JHU0
MDH5	NADP-dependent malate dehydrogenase, chloroplastic	Cre09.g410700	Q9FNS5
OMT1	Oxoglutarate:malate antiporter	Cre17.g713350	A8JDE3
LCI20	2-oxoglutarate/malate translocator	Cre06.g260450	A8HXJ4

Table S2. Sequences of primers used for RTQPCR experiments.

Gene	Sequence 5` to 3` (fw / rev)
cob	gcctacccaactccaatgaa / gtgagcgtaacgcaagatca
cox1	tggtaatgccagccctattc / taagcggtccaaccagtacc
nd1	acgcgacccatttgatctac / agcgaagaacagggcagtaa
NUO5	attgaggaggccatcaccaa / gtactcaaagcccgacacac
NUO21	agaacccgacctttccgatt / aaatggaggtgaacagagcg
COX5C	caagcaaggctgtctatgcg / taccgcttctcgttccagtg
COX3C	ctgcagtcctctgccttcg / ctccttcttgtcgtcaccgt
AOX1	atgcacctcatcaccttcct / atgtcttgacagcctcctcc
NDA5	gttagggaaggggcttggat / caccacaccacaacaatggc
PTOX1	gatgaagagtgcagcgcattt / ttgaagttgtcccagcccag
PTOX2	acctgttcgacgagttccag / gcagcaatgtccttggcaat
NDA2	ttccgtagctgtgggtttcc / tggatgaaaatgcccctccc
NDA3	cctgaagaagaagtacccggc / acccttgagcaacaccttgt
PGR5	gtccacccagtctaccaacg / aagcagcttgcagaagtcct
PGRL1	cttccactcgtgtgggatgt / cgcagtagtcagcagcaaca
MDH5	gcgaagaaggcctatggagt / caccggaagcaagcatgaat
OMT1	tgaatgtggtcgctcaggc / cgtagtgatgatgcccacga
LCI20	cattgcgacgctgttcgtg / ctgtgcgcaagcgacttgat
MDH3	cggctggtcaaattggctatg / taagcgccatccactagctc
MDH4	tacgatattgctggcacccc / cggcgttgatcttgaacagg
DTC	cagaagatgacccccaaccc / tccatgaacacgagcgtgaa
TPT1	caacgtgctgtccaagaagc / ctgagcttccagccctcaaa
TPT3	tcccatcatgttcggtgtgg / gcagtgccatccagagactt
TPT2	aagggcaaggacatgtcagg / agaacaccatcgacaggcag
TPT25	cgagccttgtcagccagatt / ggctgtcacaggaagacgag
GAP2	caaggtctccaccgactacg / ggtcacgacaacgtcatcca
GAPN1	tggtgcagtgcttccatgc / cttcttggcgatggagatgcc
PGK2	cagagcgccaggtttcattt / gagcatgcaggcaccaaaag
PGH1	gggcaaacgtctggcaaata / cgaagaggacaccagttggg
PEPC2	gcgtggtctttgagagctga / ctctgggctaggtctctggt
NDA1	tccagttccgtgttcattg / gggaataccaaaggtgctg

Supplemental figures

Figure S1. Alternative respiration in *B13* and *stm6* normalized to the cell number. Alternative respiration per cell was calculated by subtracting residual respiration rates in the presence of both inhibitors (KCN+nPG) from cyanide-insensitive respiration (only KCN) before normalizing to cell counts. Values are given relative to alternative respiration rates found in low light-acclimated *B13* cells (set to 100%). Error bars indicate the standard error derived from three biological replicates (n=3). Asterisks (*:p<0.05; **:p<0.1) indicate significant differences between *B13* and *stm6* according to a two-tailed Student`s t-test.

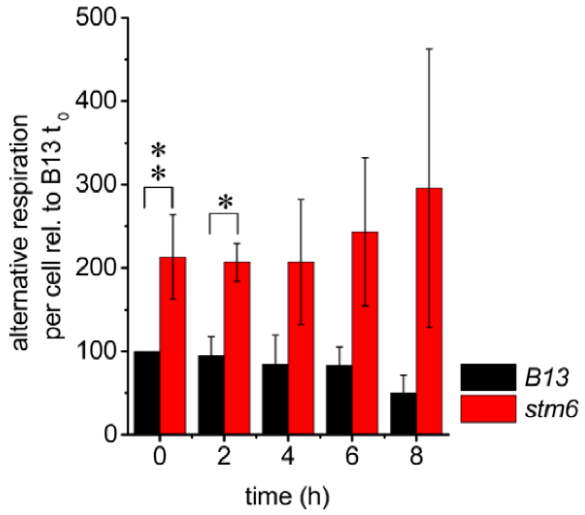

Figure S2. Representative immunoblots. See table 1.

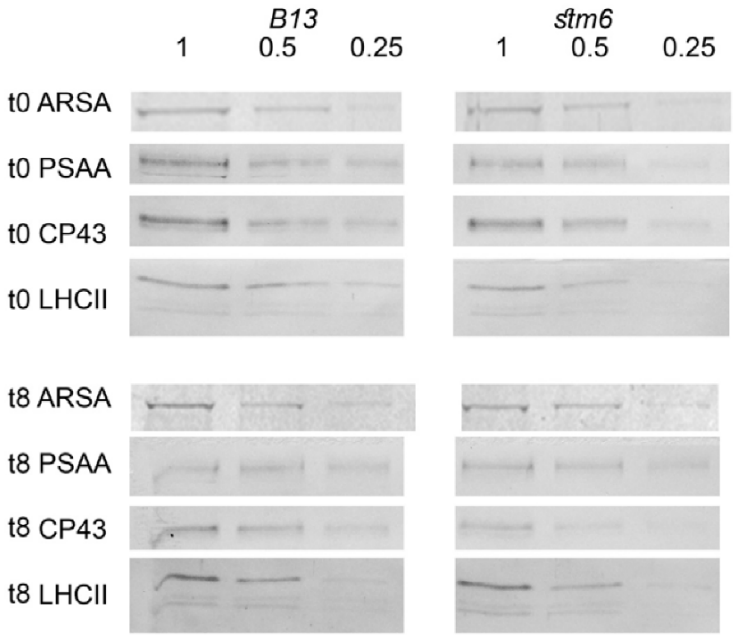

Figure S3. Post-illumination F_0 fluorescence rise in low light- and high light acclimated cultures of the mitochondrial *dum20* mutant. Kinetics of chlorophyll fluorescence emission in the dark after five minutes of illumination with 150 µmol photons m^{-2} s^{-1} white actinic light. Measurements were conducted before (t_0) and after the exposure to excess light (t_{4h}/t_{8h}). n-propyl gallate (nPG) was added to inhibit PTOX.

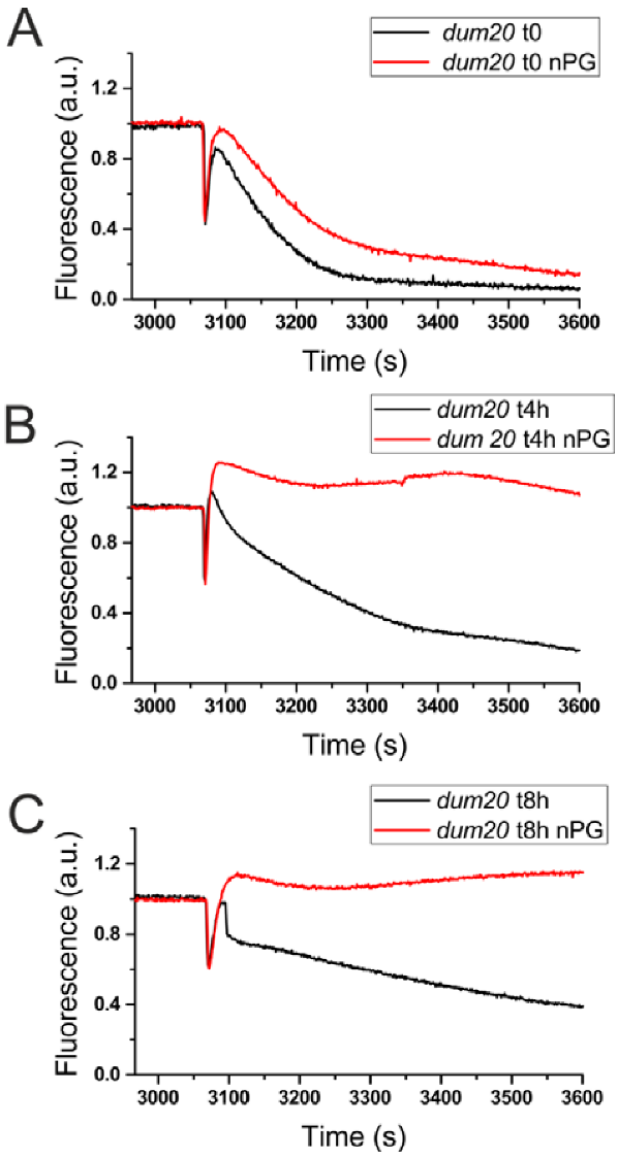

Figure S4. Post-illumination F_0 fluorescence rise in high light-acclimated cultures of an *AOX1* knock-down strain. (A and B): Kinetics of chlorophyll fluorescence emission in the dark after five minutes of illumination with 150 µmol photons m^{-2} s^{-1} white actinic light. Measurements were conducted after the exposure to excess light for eight hours. N-propyl gallate (nPG) was added to inhibit PTOX. An AOX1 knock-down strain (T53) was used along with its reference strain.

(C): Immunodetection of AOX1 (upper panel) in the reference strain and T53. A Coomassie brilliant blue stain (CBB) served as a loading control.

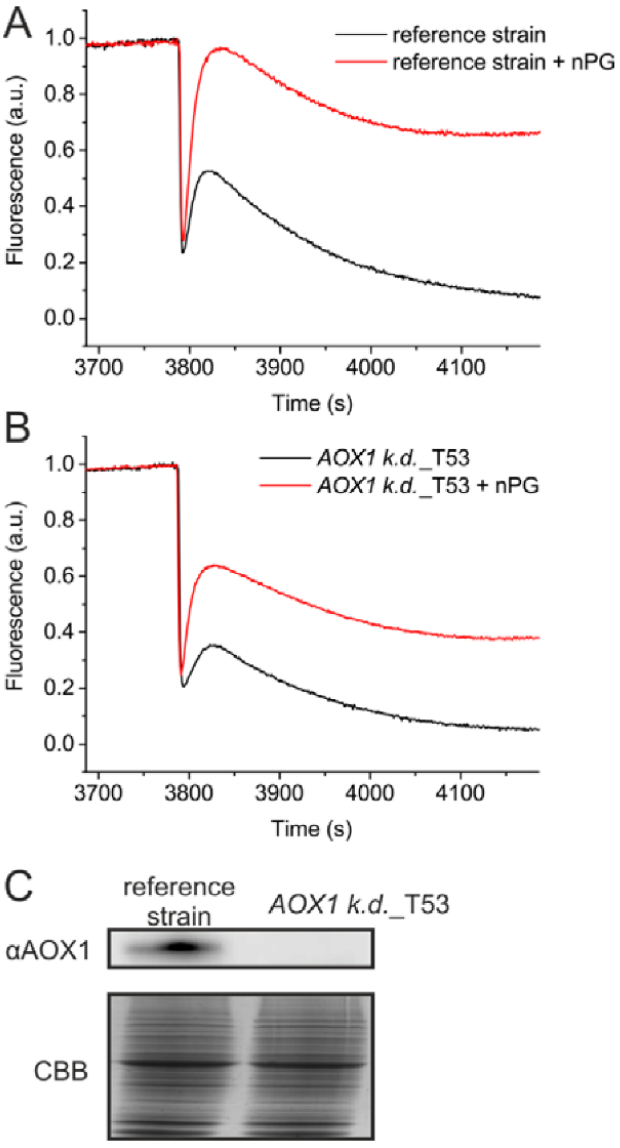

Figure S5. Plastocyanin oxidation. Plastocyanin oxidation was measured as transition absorption at 740 nm. Oxidation kinetics were normalized to PSI content.

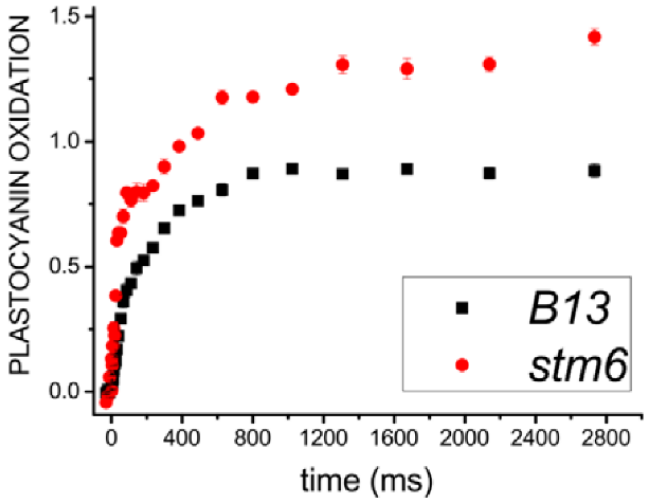

Figure S6. P700⁺ dark re-reduction curves.

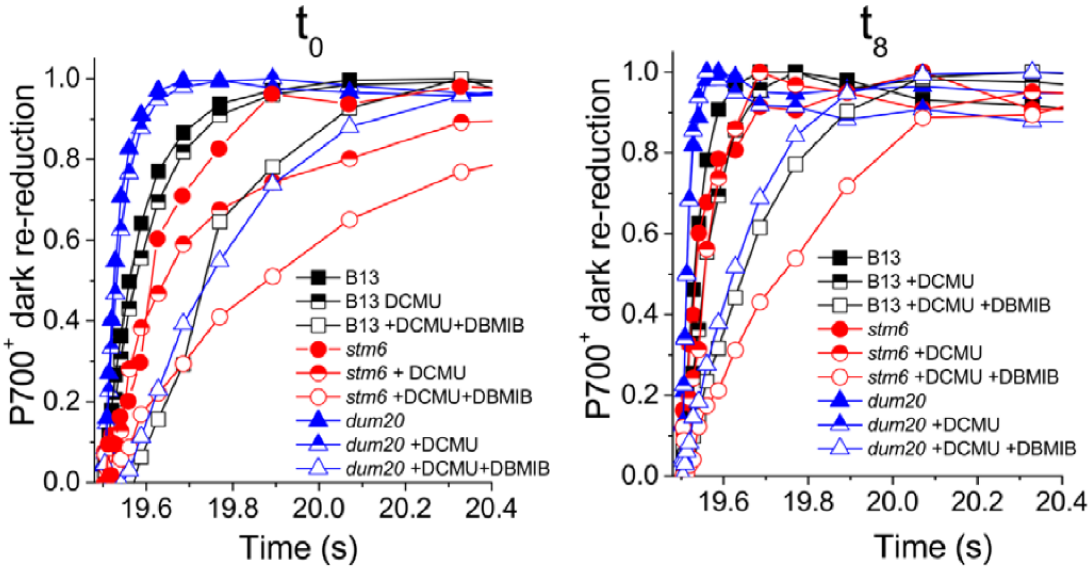

Figure S7. Expression of PGRL1 and PGR5. (A and B): RTqPCR analysis of PGR5/PGRL1 transcript levels in *B13* (black bars) and *stm6* (red bars) following exposure to excess light. Standard errors are derived from three biological replicates, each including at least two technical replicates (n=3). (C): Immunodetection of protein PGRL1. Left part: Representative immunoblot results.Loading control: Immunodetection of histone H3 and Coomassie brilliant blue staining (CBB). Right part: Relative protein levels (*B13* t_0 set to 1) obtained by densitometric scanning of immunoblot signals. Error bars indicate the standard error derived from two biological replicates, each including two technical replicates (n=2).

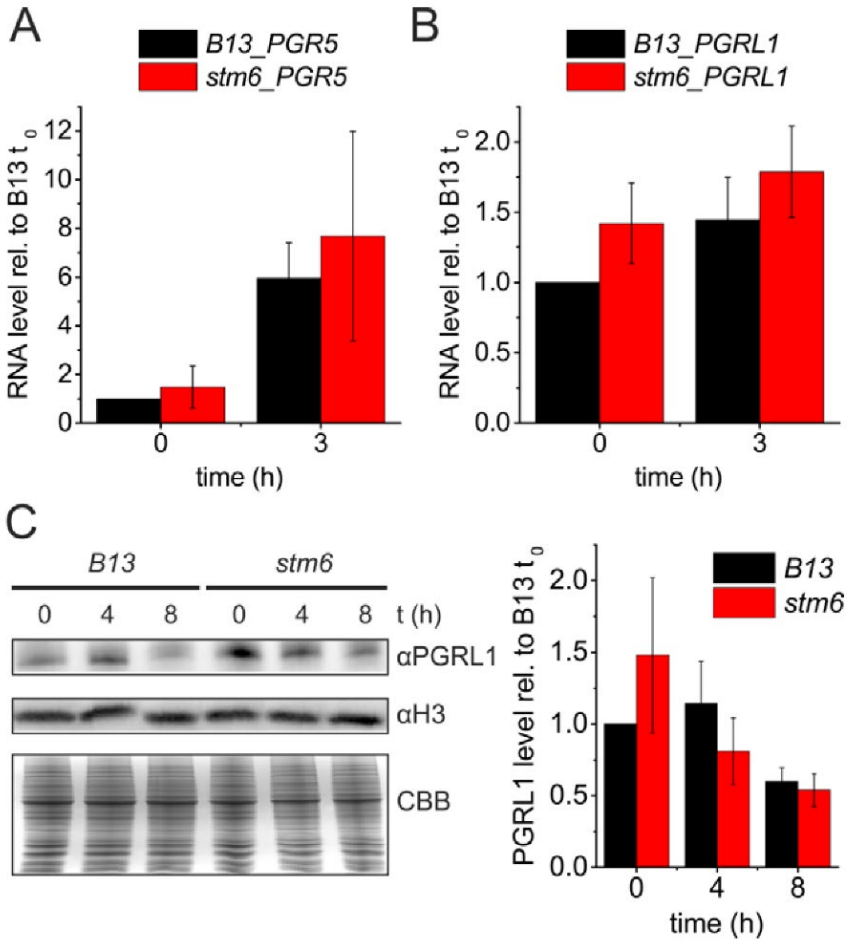

Chapter 2

Chlorella genus

Section A:

Molecular basis of autotrophic *vs* mixotrophic growth in *Chlorella sorokiniana*

Section B:

Chlorella vulgaris genome assembly and annotation reveals the molecular basis for metabolic acclimation to high light conditions

Section C:

Effect of CO_2 concentration on photosynthetic and respiratory pathways in two green algal species of the *Chlorella* genus

Section A

Molecular basis of autotrophic *vs* mixotrophic growth in *Chlorella sorokiniana*

M. Cecchin, S. Benfatto, F. Griggio, A. Mori, S. Cazzaniga, N. Vitulo, M. Delledonne and M. Ballottari

Università degli Studi di Verona, Department of Biotechnology, 37134 Verona, Italy

This work was published in Scientific Reports in April 2018.

In this work, we investigated the molecular basis of autotrophic *vs.* mixotrophic growth of *Chlorella sorokiniana*, one of the most productive microalgae species with high potential to produce biofuels, food and high value compounds. To increase biomass accumulation, photosynthetic microalgae are commonly cultivated in mixotrophic conditions, adding reduced carbon sources to the growth media. In the case of *C. sorokiniana*, the presence of acetate enhanced biomass, proteins, lipids and starch productivity when compared to autotrophic conditions. Despite decreased chlorophyll content, photosynthetic properties were essentially unaffected while differential gene expression profile revealed transcriptional regulation of several genes mainly involved in control of carbon flux. Interestingly, acetate assimilation caused upregulation of phosphoenolpyruvate carboxylase enzyme, enabling potential recovery of carbon atoms lost by acetate oxidation. The obtained results allowed to associate the increased productivity observed in mixotrophy in *C. sorokiniana* with a different gene regulation leading to a fine regulation of cell metabolism.

INTRODUCTION

Photosynthetic conversion of light provides the energy necessary for biomass formation in living organisms. Among photosynthetic species, unicellular microalgae are of great interest due to their high potential for industrial cultivation as light energy converting systems for the production of biomass, food and biofuels, without being in competition with traditional agriculture (Hannon et al. 2010b; Lum, Kim, and Lei 2013). Photo-autotrophic growth of microalgae indeed requires light, CO_2, water and nutrients yielding lipids, proteins and sugars rich biomass. However, some microalgae species have also the peculiar capability to grow in mixotrophic mode, where the autotrophic metabolism is integrated with a heterotrophic metabolism, that oxidizes the reduced carbon source available in the medium. Mixotrophic cultivation of microalgae holds the potential to significantly improve biomass production, thus fostering the revenues of industrial cultivation: this is particularly important for biofuels production, where productivity and cultivation costs must be respectively maximized and minimized to be sustainable (Hannon *et al.*, 2010; Wan *et al.*, 2011). The main substrates used for mixotrophic growth of microalgae are glucose, ethanol or cheaper waste products of several industrial processes as acetate or glycerol. Extensive work on *Chlamydomonas reinhardtii*, the model organism for green algae, demonstrated increased biomass and lipid productivity in mixotrophy compared to autotrophy (Johnson and Alric 2012, 2013). Even in the case of non-model species as *Chlorella spp*. or *Scenedesmus*, mixotrophic growth is effective to increase the biomass and lipid productivity (Combres et al. 1994; T. Li et al. 2014; Wan et al. 2011). However, this is not a general feature of microalgae, since some species, as the marine algae *Nannochloropsis gaditana*, exhibited similar growth in autotrophy and in presence of different reduced carbon source, due to a reduced photosynthetic efficiency in mixotrophy (Sforza et al. 2012). In this work autotrophic growth of the thermotolerant high productive strain *Chlorella sorokiniana* was compared to its mixotrophic growth in the presence of acetate as reduced carbon source in the medium. Acetate was reported to be assimilated in *C. reinhardtii* as acetyl-CoA which enters the Krebs cycle upon condensation with oxaloacetate to produce citrate. Acetate assimilation in several algae species is strictly linked to the activity of isocitrate lyase enzyme which redirects isocitrate toward the glyoxylate cycle, thus preventing carbon loss as CO_2 upon completion of the Krebs cycle (Combres et al. 1994; Martínez-Rivas and Vega 1993; Plancke et al. 2014a; Sun, Chen, and Du 2016). Acetyl-CoA is mainly produced in photosynthetic organisms by oxidation of pyruvate mediated by the mitochondrial pyruvate dehydrogenase enzyme and fuelled by photosynthetic produced sugars. An alternative pathway for acetate assimilation is present in the chloroplast, where acetyl-CoA is used for *de novo* production of fatty acids (J. Li et al. 2014). The interaction between photosynthesis and acetate metabolism is further complicated by the reciprocal influence of mitochondria and chloroplasts redox state: for instance, in *C. reinhardtii* alteration of

mitochondrial reduction state of plastoquinones (Johnson and Alric 2012; Uhmeyer et al. 2017). To investigate the influence of mixotrophic growth in presence of acetate in *C. sorokiniana*, photosynthetic properties and differential gene expression of autotrophic *vs*. mixotrophic cultures were thus analysed in order to identify strategy to further foster the metabolism and improve biomass production for industrial applications.

RESULTS

Cultivation of *C. sorokiniana* in autotrophy *vs.* mixotrophy

C. sorokiniana cells were grown in airlift photobioreactors in presence or absence of acetate, inducing respectively mixotrophic or autotrophic metabolism. Cells grown in mixotrophy reached higher cell density compared to cells grown in autotrophy, with a 61% increase in the presence of acetate (Fig. 1A). Growth curves were fitted with sigmoidal functions with lower dx values in mixotrophy (0.61)

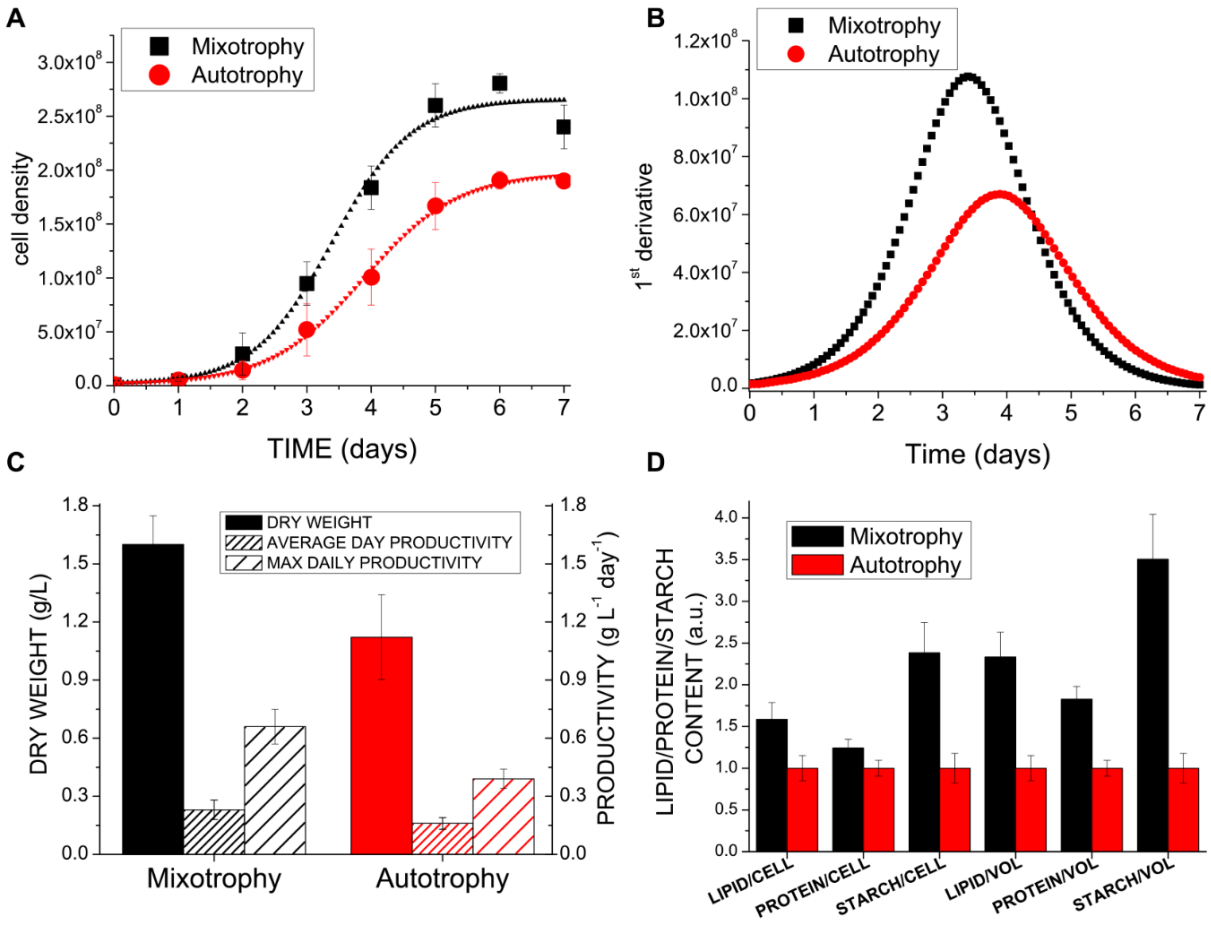

Figure 1. Growth curves, biomass productivity and accumulation of macromolecules in mixotrophy *vs.* autotrophy. Panel A: growth curves of *C. sorokiniana* growth in autotrophy *vs*. mixotrophy fitted with sigmoidal curves; Panel B: first derivate of growth curves reported in Panel A; Panel C: dry weight and average daily productivity; Panel D: relative protein, lipid and starch content per cell or volume of culture.

compared to autotrophy (0.73) indicating faster growth triggered by acetate. Moreover, mixotrophic growth was characterized by the highest daily maximum productivity estimated from the first derivate of the sigmoidal fitting functions (Fig. 1B). Mixotrophy determined 42% increase of total biomass production as compared to autotrophy, with an average and maximum daily productivity of 0.23 and 0.66 gr $L^{-1}day^{-1}$, respectively, in mixotrophy and 0.16 and 0.39 gr $L^{-1}day^{-1}$ in autotrophy (Fig. 1C). The productivity obtained in autotrophic conditions allowed to estimate a photosynthetic efficiency of ~2.36% on the basis of average daily productivity and ~5.86% considering the maximum daily productivity. In mixotrophy, 2 Kcal/L increase of energy stored as biomass was obtained as a consequence of the 3.48 Kcal/L added to the growth medium as acetate, indicating a metabolic energetic efficiency of acetate utilization of at least ~57%, close to the energetic yield of acetyl-CoA oxidized by the Krebs cycle previously reported in the case of *C. reinhardtii* (Johnson and Alric 2013). As expected, lipids, proteins and starch were all consistently increased in mixotrophy-grown cells when compared to autotrophic conditions, of 58%, 24% and 138% respectively on a cell basis. Considering the higher cell density reached in mixotrophy compared to autotrophy, the lipid, protein and starch productivity per volume of culture were increased in mixotrophy by ~133%, ~82% and ~250% respectively (Fig. 1D).

Photosynthetic properties of *C. sorokiniana* in autotrophy *vs.* mixotrophy

Photosynthetic properties of *C. sorokiniana* in autotrophy *vs*. mixotrophy were investigated to determine the influence of acetate assimilation on the autotrophic metabolism. *C. sorokiniana* cells was characterized by a ~50% reduction of chlorophyll content per cell in mixotrophy compared to autotrophy (Supplementary Table S1). Chl a/b and Chl/Car ratios however were similar in both conditions and the carotenoid composition was not significantly different when normalized to chlorophyll content. The fluorescence parameter F_v/F_m is generally used as an indicator of the wellness of the photosynthetic apparatus, being related to the photochemical efficiency of the PSII. As reported in Fig. 2A, cells grown either in autotrophic or mixotrophic conditions showed similar F_v/F_m values of ~0.6 through the entire cultivation period. Net oxygen evolution curves measured at different light intensities were similar on a chlorophyll basis for cells grown in autotrophy or mixotrophy (Fig. 2B) and the parameters Pmax and half saturation light intensities, calculated by hyperbolic fitting of the oxygen evolution curves, were not significantly different (Supplementary Table S2). However, dark respiration measured on mixotrophic cells was increased compared to autotrophic cells, either when normalized per chlorophyll content, or per cell concentration (Supplementary Table S2) indicating increase mitochondrial electron transport to oxygen as a consequence of increased NADH production in the presence of acetate. The photoprotective properties of *C. sorokiniana* cells were then investigated

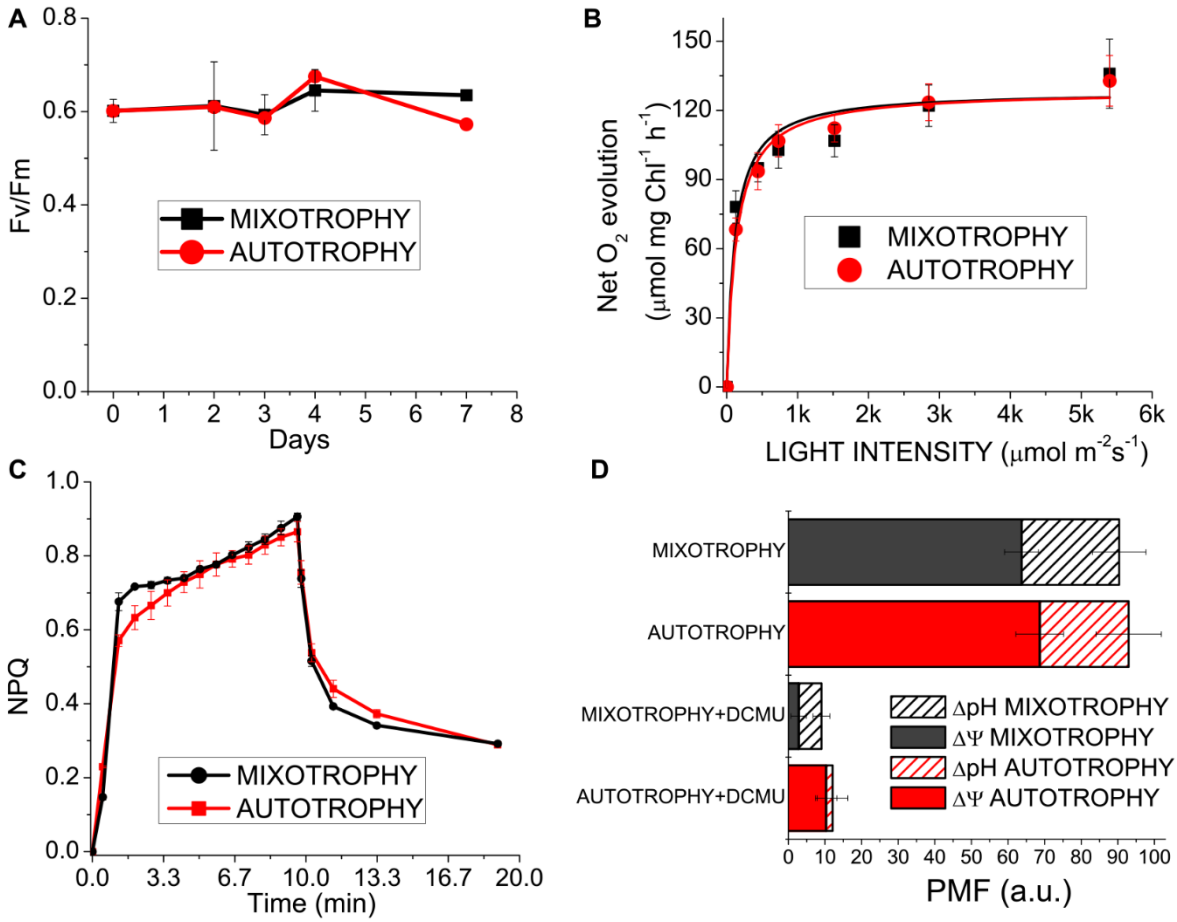

Figure 2. Photosynthetic properties of *C. sorokiniana* in autotrophy *vs.* mixotrophy. Panel A: PSII efficiency (F_v/F_m) variation during cultivation; Panel B: net oxygen evolution curves at different light intensities fitted with hyperbolic functions; Panel C: NPQ induction curves measured at 1500 µmol $m^{-2}s^{-1}$. Panel D: proton motive force (PMF) induced by 940 µmol $m^{-2}s^{-1}$ in autotrophic and mixotrophic cells. Chemical (ΔpH) and electric (ΔΨ) components of PMF are indicated.

measuring the Non-photochemical quenching (NPQ) induction curves: this process consists into thermal dissipation of a variable portion of the light absorbed by the photosynthetic apparatus and it is induced upon lumen acidification when light is absorbed in excess. As reported in Fig. 2C, NPQ curves were almost identical in autotrophic or mixotrophic cells, demonstrating that *C. sorokiniana* has similar photoprotective properties in the two conditions. NPQ induction is triggered by lumen acidification: total proton motive force (PMF) and its composition in chemical (ΔpH) and electric (ΔΨ) components were thus analyzed by pump-probe transient absorption at 520 nm, since carotenoids shift their absorption when electrochemical proton gradient across thylakoid membranes is established (Electro-Chromic Shift ECS) (Bailleul et al. 2010). PMF ΔpH and ΔΨ were not significantly different in mixotrophy compared to autotrophy (Fig. 2D). When linear photosynthetic electron transport was blocked adding the PSII inhibitor DCMU, a strong reduction in PMF was observed in both conditions, with a higher ΔpH formation in mixotrophy compared to autotrophy. This result indicates an increased PSII-independent

reduction of plastoquinones in the presence of acetate which oxidation causes release of protons, as reported in the case of *C. reinhardtii* (Plancke et al. 2014a; Uhmeyer et al. 2017).

De novo transcriptome assembly and gene expression analysis of *C. sorokiniana* in autotrophy vs. mixotrophy

To investigate the molecular basis of acetate assimilation, the transcriptome of *C. sorokiniana* was analyzed in autotrophy and mixotrophy conditions by the mean of RNA-sequencing. Transcriptome was assembled *de novo* identifying 123590 non-redundant contigs (Supplementary Dataset S1), ranging from 224 bp to 16 Kbp and with average length of 1.1 Kbp (Supplementary Figure S1). Transcriptome functional annotation was obtained for 70101 transcripts, of which 53435 were associated to Gene Ontology (GO) Terms (Fig. 3). N50 value of the assembled transcriptome was 1792 bp. To further evaluate the transcriptome quality and completeness, BUSCO analysis was run for a set of 303 universal single-copy genes putatively universally found in eukaryotes as single copies (Simão et al. 2015).

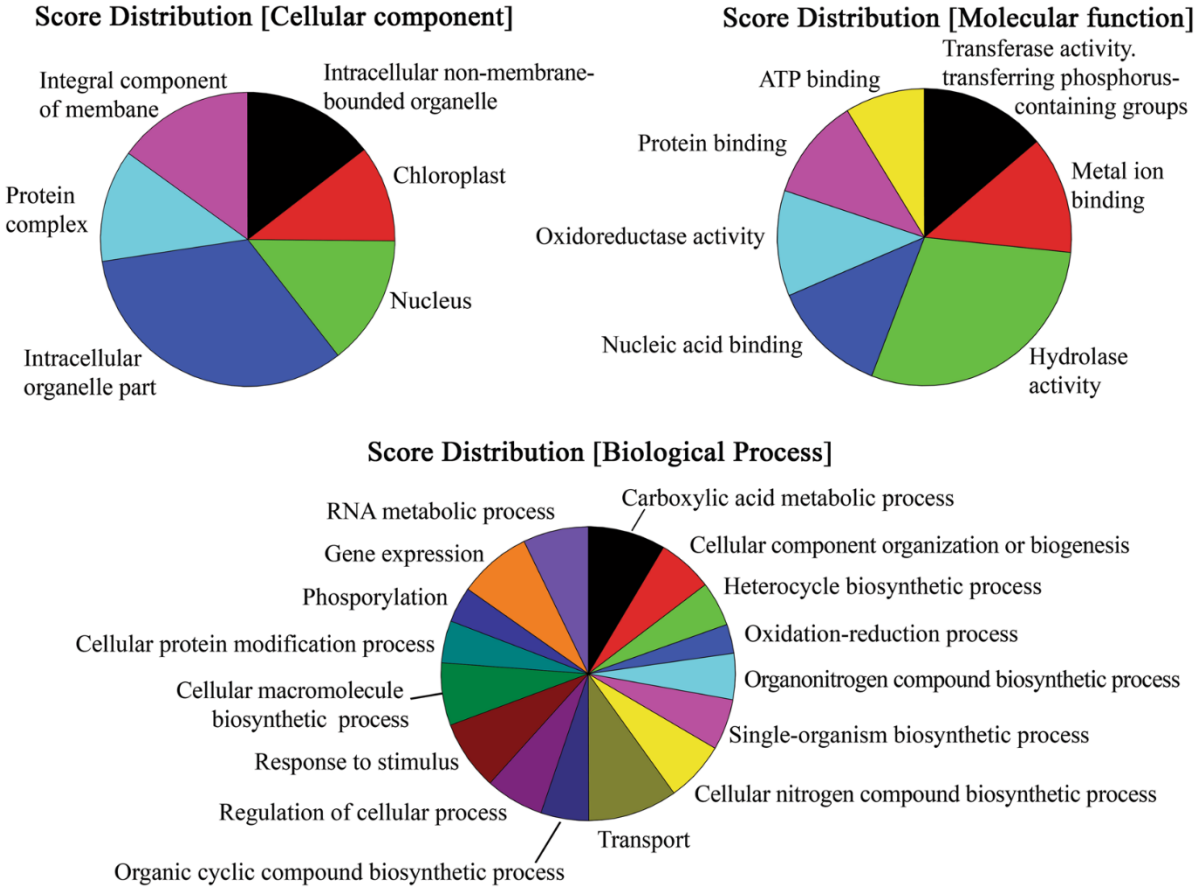

Figure 3. Annotation of *C. sorokoniana* transcriptome. *C. sorokiniana* transcripts annotated by blast2Go were functionally grouped on the basis of Gene Onthology (GO) terms "cellular component", "molecular function" and "biological processes". The distribution of the different groups is reported on the basis of the node score associated to each group considering GO term with node score higher than 1%.

This analysis identified complete information for 94.4% of orthologs and fragmented information for the 5.0%, only 0.6% are missing, demonstrating a high completeness of the *de novo* assembled transcriptome. Reconstructed 18 S rRNA (TR1035|c8_g4) matched the 18 S rRNA sequences available for *C. sorokiniana* UTEX 1230 deposited in NCBI with more than 97% of identity (Supplementary Table S3), confirming the identity of the strain analysed. Most annotations were obtained by alignment with the publicly available data of *Chlorella variabilis* (Supplementary Figure S2), due to the close evolutive origin of the two species (Mansfeldt et al. 2016; Rosenberg et al. 2014). In addition, 15496 annotated sequences were located in KEGG-derived metabolic pathways (Kanehisa et al. 2016, 2017; Kanehisa

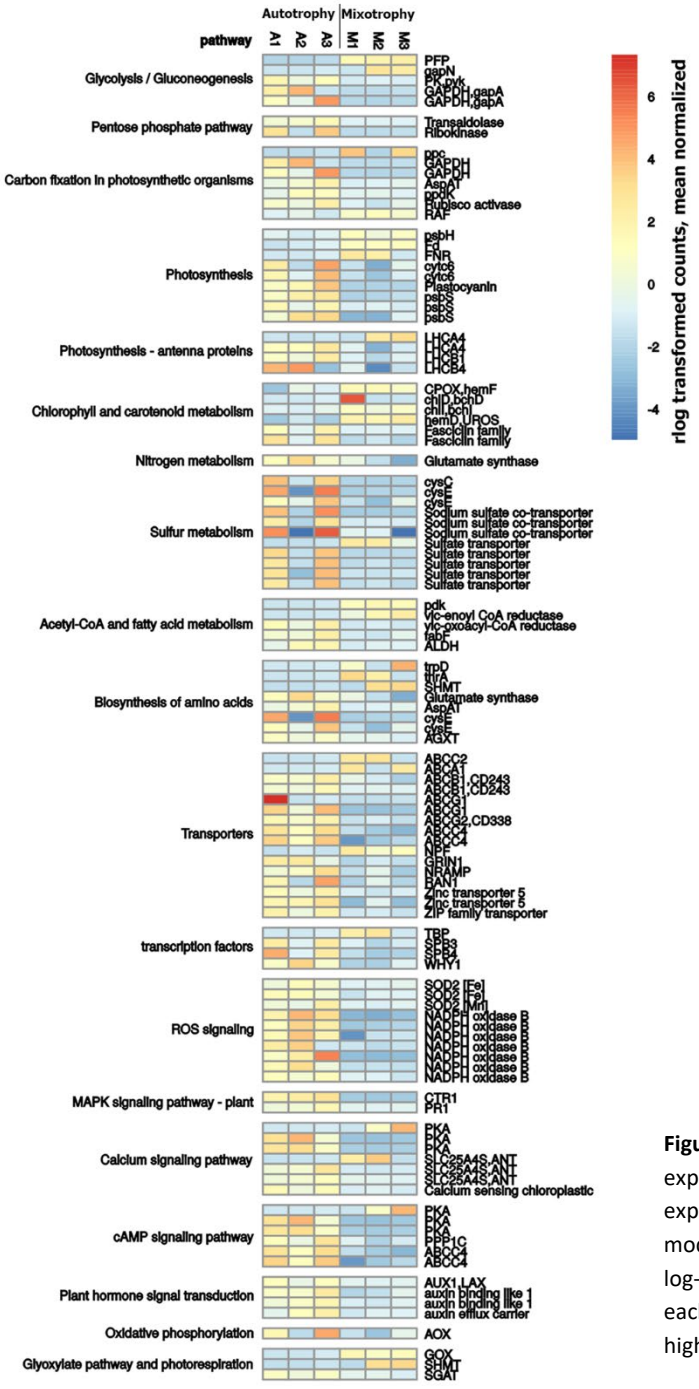

Figure 4. Heat map of selected genes differentially expressed in autotrophy *vs.* mixotrophy. The expression of genes involved in selected pathways modulated in autotrophy *vs.* mixotrophy is shown as log-transformed and mean normalized read counts for each sample analysed (blue, lower abundance; orange, higher abundance).

and Goto 2000) (Supplementary Figure S2) demonstrating that all the enzymes involved in glycolysis, gluconeogenesis, Krebs cycle, glyoxylate cycle, reductive and non-reductive pentose phosphate cycle and Calvin-Benson cycle were identified in the *de novo* assembled *C. sorokiniana* transcriptome. Differential expression analysis revealed that 285 transcripts encoding for 259 different proteins were upregulated in mixotrophy, while 721 transcripts corresponding to 620 proteins were downregulated as compared to autotrophic conditions (Supplementary Dataset S2).

Pathway annotation allowed to identify the differentially expressed transcripts involved in relevant biological processes crucial for the algae metabolism among which photosynthesis, chlorophyll and carotenoid metabolism, photorespiratory pathway, carbohydrates, acetyl-CoA, fatty acids and amino acids metabolism, sulphur, nitrogen, phosphate assimilation and transport processes across membrane (Fig. 4).

Photosynthesis. Transcripts coding for LHC subunits homologous to Lhcb4 and LHCII subunits were downregulated in mixotrophy compared to autotrophy, in agreement with the reduced chlorophyll content per cell in the presence of acetate. Similar downregulation of LHC genes has been reported in the case of *C. reinhardtii* grown in presence of acetate (Kindle 1987). However, any downregulation of PSI or PSII core subunits was not observed in mixotrophy, with translational and post-transduction regulative mechanisms likely involved in the overall accumulation of PSII and PSI subunits as previously suggested in the case of *A. thaliana* (Floris et al. 2013). The accumulation of PSI, PSII and LHCII subunits were thus investigated by immunoblotting (Fig. 5): when loaded with the same amount of chlorophylls, the PSII subunit CP43 and LHCII were detected in a similar amount in both autotrophic and mixotrophic conditions, while the PSI subunit PsaA was slightly increased in mixotrophy. The finding of almost double amount of the mitochondrial subunit COX2 in mixotrophy when SDS-PAGE were loaded at the same amount of chlorophylls nicely fit with the 50% reduction of chlorophyll content per cell in presence of acetate, indicating that in mixotrophy chlorophyll and chlorophyll binding proteins are generally reduced, with a slight increase on a chlorophyll basis of PSI. The increase in PSI content per cell in mixotrophy is likely related to the increased plastoquinone reduction in presence of acetate (Fig. 2D). Differential gene expression analysis indicated also the reduced expression of PSBS subunit in mixotrophy, which was confirmed by western blot analysis, where PSBS accumulation was detected only in autotrophy but not in mixotrophy (Fig. 5). PSBS is a protein subunit crucial for NPQ induction in higher plants, being the sensor of lumenal pH: occurrence of PSBS protein in microalgae has been recently reported for several species, being in *C. reinhardtii* transiently induced by high light or UV exposure, even if its functional role in photoprotection is still under debate (Allorent et al. 2016; Tibiletti et al. 2016). The similar NPQ traces observed in *C. sorokiniana* in presence (mixotrophy) or absence (autotrophy) of PSBS suggest that this protein has a minor role on NPQ induction in this

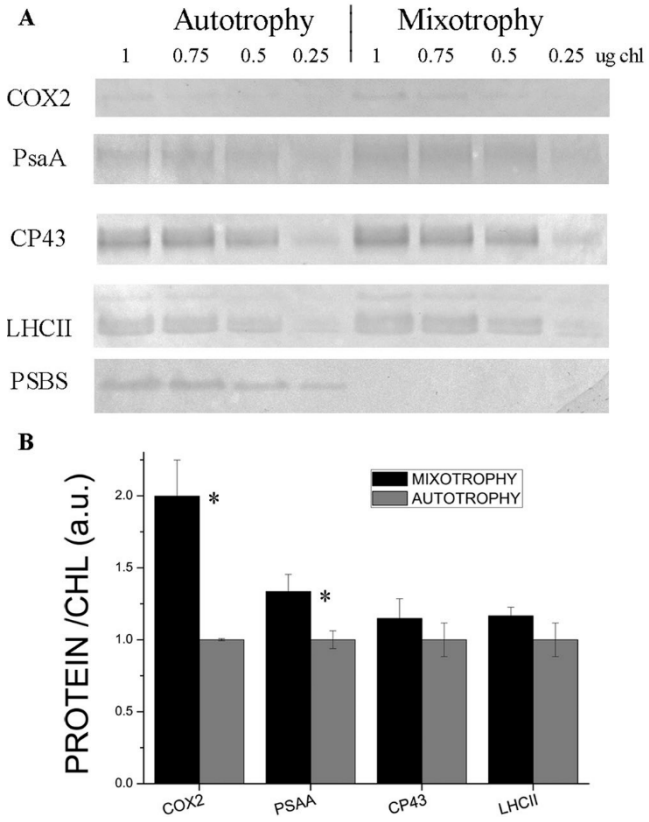

Figure 5. Western blot analysis of chlorophyll binding proteins. PSI, PSII, LHCII and PsbS accumulation in mixotrophy *vs*. autotrophy were investigated by immunoblot analysis. In the case of PSI and PSII their relative accumulation was investigated using antibody recognizing PsaA (subunit of PSI) and CP43 (subunit of PSII). Mitochondrial COX2 subunit was also quantified as a control. Samples were loaded on SDS-PAGE gels in different chlorophyll concentration reported in Panel A. Each immunoblotting analysis was performed loading samples from autotrophy and mixotrophy cultures on the same gel. PsaA, CP43 and LHCII immunoblotting were performed on the same filter cut between 30- and 40 KDa and between 50- and 60 KDa, while PSBS and COX2 immunoblotting analysis where performed on different filters. Quantification of resulting bands were performed by densitometry and normalized to the autotrophy case (Panel B). Significantly different data are indicated (n = 3; $P < 0.05$).

species but could be involved in other photoprotective mechanisms interacting with PSII or LHC subunits. Differently, *C. sorokiniana* transcripts homologous to LHCSR proteins, protein subunits involved in NPQ induction in *C. reinhardtii*, were not differentially expressed in presence or absence of acetate. Among protein subunits involved photosynthetic electron transport, plastocyanin and cytochrome c6 were downregulated in mixotrophy. It is interesting to note that in mixotrophy downregulation of a PGR5-like subunits was also detected: PGR5 has been reported to be involved in cyclic electron transport around PSI in higher plants and green algae, mediating plastoquinones reduction by Ferredoxin-NADP+ reductase (FNR) (Alric 2014). Differently, Ferredoxin and FNR subunits were upregulated in mixotrophy: in presence of acetate the increased reducing power derived from acetate consumption causes an overreduction of plastoquinones (Fig. 2), likely inhibiting plastoquinones reduction by cyclic electron transport around PSI but increasing demand of PSI electron acceptor as Ferredoxin and FNR, consistently with the increased PSI content on a chlorophyll basis detected in mixotrophic cells (Fig. 5, Supplementary Figure S3). Differential gene expression was observed in the case of enzymes involved in carbon fixation. Glyceraldehyde 3-phosphate dehydrogenase (phosphorylating) was downregulated in mixotrophy: this is the final enzyme producing glyceraldehyde 3-phosphate in the Calvin-Benson cycle, confirming the crucial role of photosynthates in autotrophy. It is interesting to note that *C. sorokiniana* transcriptome revealed the expression of enzymes involved also in a C4-like carbon fixation pathway like either the NAD- or NADP-

malic enzyme type or the phosphoenolpyruvate carboxykinase type C4 cycle (Supplementary Figure S4). The presence of a possible C4-like carbon fixation pathway in *C. sorokiniana* has been indeed already proposed in the case of the strain LS-211. Among these enzymes, the key subunit involved in carbon fixation is the cytoplasmic phosphoenolpyruvate carboxylase (PPC) was upregulated in mixotrophy, while all the other enzymes putatively involved in a C4-like carbon fixation pathway were similarly expressed in both autotrophy and mixotrophy. Upregulation of PPC in mixotrophy suggests that *C. sorokiniana* switches on C4-like carbon fixation in presence of acetate in order to recover CO_2 released by acetyl-CoA oxidation (Fig. 6). Upregulation of PPC in mixotrophy could also be involved in anaplerotic reaction for oxaloacetate production and CO_2 recovery in mixotrophic cells characterized by high mitochondrial respiration. Other enzymes putatively involved in C4-like fixation pathway as pyruvate-orthophosphate dikinase (PPDK) and aspartate aminotransferase (AspAT) are instead downregulated in mixotrophy; these enzymes allow respectively for production of phosphoenol-pyruvate (PEP) and oxaloacetate from pyruvate and aspartate. PEP and oxaloacetate are intermediates for both C4-like carbon fixation but also for gluconeogenesis and these enzymes could be involved in autotrophy to accumulate PEP and oxaloacetate to be used for glycolysis, gluconeogenesis or other metabolic pathways. Consistently with the increased CO_2 content in mixotrophy, carbonic anhydrase enzyme resulted to be downregulated. It is interesting to note that in mixotrophy RUBISCO activase was downregulated, while a RUBISCO accumulation factor (RAF) was upregulated: in autotrophy, the relative low CO_2 content compared to mixotrophy is likely responsible for the needing for increased rubisco activase expression, since this enzyme catalyses the carbamylation of RUBISCO required for its activation (Pollock et al. 2003), while in mixotrophy RAF upregulation contributes to the assembly of RUBISCO complex to improve carbon fixation. Consistently, increased activity of RUBISCO has been reported in *C. sorokiniana* cells grown in mixotrophy in presence of glucose (Li et al. 2016).

Carbohydrate metabolism. Among the glycolytic enzymes, fructokinase, glyceraldehyde 3-phosphate dehydrogenase, phosphoglycerate mutase and pyruvate kinase were downregulated in mixotrophy, indicating the crucial role of this metabolic process in absence of acetate, where sugars produced by the dark phase of photosynthesis are used to produce ATP and reducing power. Differently in mixotrophy diphosphate-fructose-6 -phosphate-1-phosphotransferase (PFP) and a NADP+ dependent glyceraldehyde-3-phosphate dehydrogenase (GapN) were upregulated. PFP, an enzyme found in plants and some bacteria, catalyses the formation of fructose 1,6-bisphosphate from fructose 6-phosphate using inorganic pyrophosphate as the phosphoryl donor, rather than ATP, as in the case of phosphofructokinase (PFK) enzyme: the use of inorganic pyrophosphate makes the reaction reversible, increasing the rate of gluconeogenesis (Alves et al. 2001), consistently with the increased starch

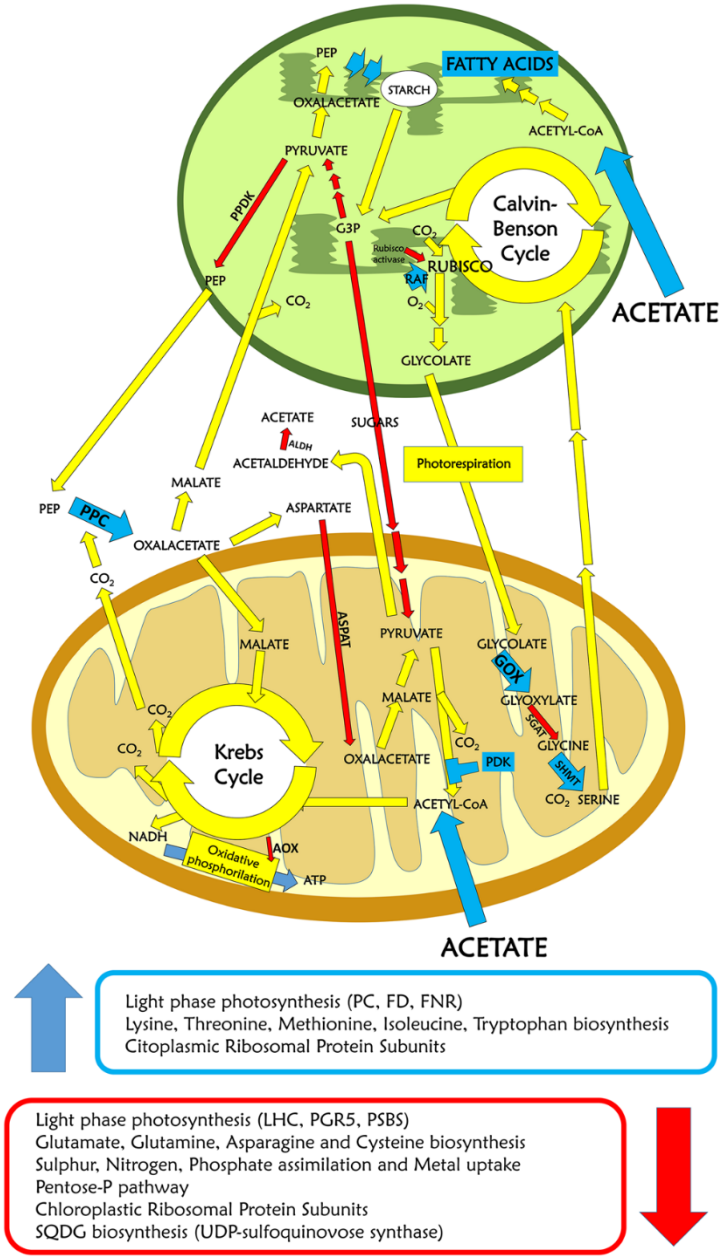

Figure 6. Model of metabolic pathways in autotrophy *vs*. mixotrophy in *C. sorokiniana*. Metabolic pathways are reported in yellow if not transcriptionally regulated, in red or blue if down or upregulated in mixotrophy respectively. PEP: phosphoenol-piruvate; RAF: RUBISCO accumulation factor; G3P: Glyceraldehyde 3-phosphate; PDK: pyruvate dehydrogenase kinase; PC: plastocyanin; Fd: ferredoxin; FNR: Ferredoxin-NADP+ reductase; PPC: phosphoenolpyruvate carboxylase; ALDH: aldehyde dehydrogenase; GOX: glycolate oxidase; SHMT: serine hydroxymethyltransferase; AOX: alternative oxidase; PPDK: pyruvate-orthophosphate dikinase; AspAT: aspartate aminotransferase.

accumulation observed in mixotrophy. GapN enzyme is a glycolytic enzyme which catalyses an alternative reaction to produce NADPH and glycerate 3-phosphate directly from glyceraldehyde-3-phosphate, without producing the intermediate glyceraldehyde-1,3-bisphosphate: this alternative reaction leads to only one ATP yield for each glyceraldehyde-3-phosphate, but produces NADPH rather than NADH (Ettema et al. 2008). Phylogenetic analyses and database searches indicated a preferred distribution of GapN in hyperthermophilic Archaea suggesting a role of GapN in metabolic thermoadaptation (Ettema et al. 2008), which could be related to the thermotolerance of *C. sorokiniana*. NADPH in autotrophy is rather produced by the light phase of photosynthesis and by the pentose phosphate pathway: downregulation of a transaldolase and a ribokinase involved in the pentose phosphate pathway were indeed detected in mixotrophy. It is worth to note that in

mixotrophy UDP-sulfoquinovose synthase enzyme was downregulated: this enzyme catalyzes the production of UDP-6-sulfoquinovose from UDP-glucose and sulphite, a precursor of sulfolipid sulfoquinovosyl diacylglycerol (SQDG), a key lipid in thylakoid membranes. Downregulation of UDP-sulfoquinovose synthase in mixotrophy could thus be related to the decreased thylakoid accumulation in mixotrophy, consistently with the reduced chlorophyll content observed in presence of acetate.

Acetyl-CoA and fatty acids metabolism. Regulative mitochondrial pyruvate dehydrogenase kinase (PDK) was found expressed only in mixotrophy: this serine/threonine kinase inactivates pyruvate dehydrogenase by phosphorylation, inhibiting acetyl-CoA accumulation from pyruvate (Roche et al. 2001), as expected in presence of acetate. In addition, an aldehyde dehydrogenase (ALDH) was found downregulated in mixotrophy. ALDH has been reported to be involved in the so called pyruvate dehydrogenase complex (PDHC) bypass pathway, by which pyruvate is converted into acetate which is then imported into chloroplast as acetyl-CoA for fatty acid accumulation (J. Li et al. 2014): in mixotrophy this enzyme is thus downregulated since acetate is already available in the medium. Only three enzymes involved in fatty acid metabolism were found differentially expressed: a plastid type II fatty acid synthase (FabF), catalysing the first step of fatty acid biosynthesis adding malonyl-ACP to a short fatty acid chain, was detected as downregulated in mixotrophy. This result is consistent with the main role of plastid in autotrophic metabolism and lipid biosynthesis. Interestingly both type I and type II fatty acid synthase enzymes were present in the assembled transcriptome of *C. sorokiniana*: type I fatty acid synthase as FAS1 has been reported to be active in the cytoplasm and not present in plants, where usually the plastid type II fatty acid synthase are present. However, the expression of FAS1 enzymes has been already reported in other microalgal species as *Nannochloropsis gaditana* (Alboresi et al. 2016). Other two enzymes involved in the elongation of very long (<16 C) fatty acids longer were found differentially expressed: a very-long-chain 3-oxoacyl-CoA and a very-long-chain enoyl-CoA reductase were downregulated and upregulated respectively in mixotrophy. These enzymes are components of the enzymatic system called elongase that adds two carbons to the chain of long- and very long-chain fatty acids (Millar and Kunst 1997). The different and opposite expression of elongase subunits indicates that the increase lipid content observed in mixotrophy is more influenced on the increased acetyl-CoA availability rather than on the different expression of biosynthetic enzymes.

Glyoxylate pathway and photorespiration. Differently from previous works in *C. reinhardtii*, isocitrate lyase, the key enzyme for the assimilation of acetate/acetyl-CoA in the glyoxylate pathway (Plancke et al. 2014a) was not upregulated in mixotrophy in *C. sorokiniana*. Since glyoxylate production by photorespiratory pathway has been recently proposed to participate to acetate assimilation in *C.*

sorokiniana, the different enzymes involved in photorespiration were considered, among which glycolate oxidase (GOX), serine hydroxymethyltransferase (SHMT) were upregulated while serine glyoxylate aminotransferase (SGAT) was downregulated. GOX produces glyoxylate from glycolate, which is then the substrate of SGAT which catalyses the interconversion of L-serine and glyoxylate to hydroxypyruvate and glycine (Fig. 6). SHMT catalyses the reversible, conversions of serine to glycine in the mitochondria. Downregulation of SGAT and upregulation of GOX can be related to increase glyoxylate production to be redirected toward the glyoxylate cycle to produce malate upon condensation with acetyl-CoA. The reduced activity of SGAT in mixotrophy would thus cause a reduction in the mitochondria of the substrate of SHMT, glycine, with consequent upregulation of SHMT to complete the photorespiratory cycle.

Oxidative phosphorylation. Any differential gene expression was not observed in the case of mitochondrial oxidative phosphorylation, with the exception of alternative oxidase (AOX) which was downregulated in mixotrophy. AOX indeed has been reported not to be involved in acetate metabolism in *C. reinhardtii*, and its downregulation in *C. sorokiniana* suggests the preferential activation of mitochondrial electron transport via the energy-conserving cytochrome c pathway to produce ATP consuming NADH produced by acetate assimilation.

Sulphur, nitrogen, phosphate assimilation and transport systems across membranes. A sodium sulphate co-transporter and adenylylsulphate kinase (CysC) enzyme, involved in sulphate conversion into sulphite, were detected as downregulated in mixotrophy, indicating downregulation of sulphur assimilation pathway in presence of acetate, likely related to the release of acetate caused by sulphur assimilation. Indeed, in plants sulphur assimilation proceeds mainly by cysteine biosynthesis: cysteine production starts from serine which is first acetylated to O-acetyl-serine and then de-acetylated reacting with sulphide to produce L-cysteine releasing acetate. Consistently, in presence of acetate the enzyme serine O-acetyltransferase (CysE) was found downregulated. Similarly, phosphate transporters and alkane phosphatases, involved in phosphate mobilization, were found downregulated in mixotrophy. In the case of nitrogen assimilation, the glutamate synthase resulted to be downregulated in mixotrophy, suggesting reduced nitrogen assimilation in this condition: nitrogen assimilation occurs indeed in the chloroplast where nitrate is reduced to nitrite and ammonium, which is then used for the production of glutamate and glutamine. Another enzyme linked to ammonium assimilation, asparagine synthase, was downregulated in mixotrophy. Considering the importance of nitrogen and glutamate for chlorophyll biosynthesis, this result indicates that downregulation of components of nitrogen assimilation is linked with the reduced chlorophyll content per cell observed in mixotrophy.

However it is worth to note that in mixotrophy a NRT1/PTR FAMILY (NPF) transporter was found upregulated: NPF is a nitrate or di/tri-peptide transporters which can also transport plant hormones auxin (indole-3-acetic acid), abscisic acid (ABA) and gibberellin (GA), as well as secondary metabolites (glucosinolates) (Chiba et al. 2015). NPF upregulation could thus be related to the activation of a different nitrate import system or be involved in signalling pathway in mixotrophy, as discussed below. Several ABC transporters resulted to be differentially expressed in autotrophy compared to mixotrophy: ABCB1, ABCC4, ABCG1, ABCG2 were downregulated while ABCA1 and ABCC2 were upregulated in mixotrophy. In mixotrophy, an ionotropic glutamate receptor (GRIN1) was found downregulated: these proteins are ligand gated channels which are involved in particular in Ca^{2+} influx, consistently with the peculiar role of Ca^{2+} in the regulation of cell function in autotrophy. Components involved in iron uptake were downregulated in mixotrophy as in particular the metal transporter NRAMP, the iron binding proteins ferritin and transferrin and multicopper ferroxidase for the oxidation of Fe^{2+} to Fe^{3+}. The reduced expression of components involved in iron uptake in mixotrophy is likely linked to the reduced chlorophyll per cell content in presence of acetate, since iron in photosynthetic organisms is mainly located in the thylakoid membranes (Glaesener, Merchant, and Blaby-Haas 2013). It is worth to note that also the copper transporter ATPase RAN1 kinase resulted to be downregulated in mixotrophy: this kinase is also a component of the ethylene signalling pathway (Iqbal et al. 2013). Moreover a zinc transporter and a ZIP family transporter (Rosakis and Köster 2004) were observed downregulated in mixotrophy, confirming the general reduced expression in mixotrophy of genes involved in nutrient assimilation and metal uptake.

Chlorophyll and carotenoid metabolism. Chlorophyll content per cell was reduced in presence of acetate (Supplementary Table S1). However, transcripts encoding for uroporphyrinogen-III synthase, coproporphyrinogen III oxidase and magnesium chelatase, which leads to production of the chlorophyll precursor Mg-protoporphyrin-IX from glycine were upregulated in mixotrophy. These results suggest that the regulation of nitrogen and iron uptake rather than differential expression of chlorophyll biosynthetic enzyme is at the base of the control of chlorophyll content per cell in *C. sorokiniana*. In the case of carotenoid biosynthetic pathway, a carotenoid oxygenase was downregulated in mixotrophy, even if the function of this enzyme remains unclear. Moreover, in mixotrophy two transcripts coding for astaxanthin binding fasciclin family proteins were detected as downregulated: these proteins were reported as water soluble protein that bind carotenoids and in particular astaxanthin, being involved in microalgae in the resistance to photo-oxidative stress (Kawasaki et al. 2013). Astaxanthin was not detected in *C. sorokiniana* in these conditions (Supplementary Table S1), even if the enzymes CrtO and CrtZ for its production were identified in the

annotated transcriptome. More stressful conditions could be required for astaxanthin significant production with a putative role of astaxanthin binding fasciclin family proteins for its accumulation (Raman and Mohamad 2012).

Amino acids metabolism. As discussed above, glutamate synthetase, asparagine synthase, serine O-acetyltransferase and aspartate aminotransferase enzymes involved respectively in glutamate/glutamine, asparagine and cysteine biosynthesis and aspartate de-amination to produce oxaloacetate were found downregulated in mixotrophy. In addition, transcripts encoding for a serine-glyoxylate transaminase were found downregulated in presence of acetate: this enzyme catalyses the production of glycine and 3-hydroxypyruvate from serine and glyoxylate and its downregulation is consistent with the increased requirement of glyoxylate in mixotrophy for acetate assimilation and with the reduced glycine demand, considering the use of glycine as the precursor for chlorophyll biosynthesis. Differently a chloroplastic-like bifunctional aspartokinase homoserine dehydrogenase (ThrA) was upregulated in presence of acetate: this enzyme was found in bacteria and plant chloroplasts, catalysing the first and third steps of the aspartate pathway, by which aspartate is used as a precursor for lysine, threonine, methionine and isoleucine. In addition, an anthranilate phosphoribosyltransferase (trpD) enzyme was upregulated in mixotrophy: this enzyme catalyses the accumulation of the precursors for tryptophan biosynthesis. Increased expression of enzymes involved in the biosynthesis of tryptophan, lysine, threonine, methionine and isoleucine could be the related to the increased protein content per cell observed in mixotrophy. Moreover, consistently with the increase protein accumulation observed in mixotrophy, several ribosomal protein subunits were upregulated in presence of acetate. Only in the case of ribosomal chloroplast subunit RP-S16 and RP-LE30 downregulation was observed in mixotrophy, consistently with the reduced chlorophyll content and reduced accumulation of chlorophyll binding subunits observed in presence of acetate.

Transcription factor and signalling. Three transcription factors were found differentially expressed in autotrophy compared to mixotrophy: a transcription initiation factor TFIID TATA-box-binding protein (TBP) were upregulated in mixotrophy, while two Squamosa promoter binding protein (SPB3 and SPB4) and a Whirly transcription factor were found downregulated in mixotrophy. TBP is a general transcription factor involved in the RNA polymerase II preinitiation complex (Lee and Young 2000), while SBP and a Whirly transcription factor are transcription factors commonly found in plants. SBP transcription factors play important roles among others in flower and fruit development, plant architecture and response to hormones (Chen et al. 2010), while Whirly transcription factors were reported to be involved in plant defence (Desveaux et al. 2004), chloroplast biogenesis (Prikryl et al. 2008) and plastid genome stability (Maréchal et al. 2009). Downregulation of SBP and Whirly

transcription factors in mixotrophy could be related to the reduced chlorophyll content photosynthetic proteins per cell and a reduced autotrophic metabolism observed in presence of acetate. Several transcripts involved in signalling were found differentially expressed in autotrophy compared to mixotrophy. The MAP kinases PKA, RAN1, CTR1 and PR1 were found downregulated in mixotrophy while a different transcript for PKA, CTR1 and LZK were upregulated in mixotrophy (Supplementary Table S3). It is interesting to note that PR1 kinase in *A*. *thaliana* has been reported to be involved in biotic stress defence being a component of the salicylic acid signalling (Ben Rejeb, Pastor, and Mauch-Mani 2014), while CTR1 and RAN1 are component of the ethylene signalling pathway in higher plants (Iqbal et al. 2013). In autotrophy, an increased expression of protein involved in auxin response as the auxin transporter AUX1, an auxin efflux carrier and an auxin binding protein were also detected suggesting a possible ethylene/auxin dependent modulation of gene expression in autotrophy. Interestingly a cyclin dependent kinase and G2/mitotic-specific cyclin-B were detected upregulated in mixotrophy, suggesting a possible role of cyclin in the increased cell density yielded in presence of acetate (Supplementary Table S4). Other serine/threonine kinase and phosphatase are upregulated or downregulated in mixotrophy, indicating specific signalling pathways and phosphorylation processes in these conditions (Supplementary Table S4). It is interesting to note the down-regulation of a chloroplast calcium sensing (CAS) protein and a calcium-dependent kinase in mixotrophy, consistently with the downregulation of putative calcium influx channel GRIN1 in presence of acetate as discussed above. CAS has been reported in *C*. *reinhardtii* to be involved in the regulation of photoacclimation and calcium dependent regulation of photosynthetic cyclic electron transport (Petroutsos et al. 2011; Terashima et al. 2012), which is indeed enhanced in autotrophy compared to mixotrophy. Interestingly a subunit of superoxide-generating NADPH oxidase was found downregulated in mixotrophy: this enzyme produces the reactive oxygen species superoxide and it has been reported to be involved in reactive oxygen species dependent signalling mechanisms (Jiménez-Quesada, Traverso, and Alché 2016). Similarly, two transcripts coding for superoxide dismutase, which catalyses superoxide scavenging was downregulated in the same mixotrophic conditions, indicating fine regulation of the superoxide concentration as a possible signal for acclimation to different growth conditions.

DISCUSSION

The study describes the impact of acetate availability on gene expression and photosynthetic properties of *C*. *sorokiniana*. The availability in the medium of a reduced carbon source as acetate increased biomass yield, cell density and daily productivity of *C*. *sorokiniana* cells compared to autotrophic growth. Increase in biomass yield and productivity in mixotrophy was related mainly to an increase of starch and lipid content per cell, even if total protein content was also increased.

Photosynthetic traits were not significantly affected in mixotrophy compared to autotrophy: however, upregulation of genes coding for electron acceptors downhill plastoquinones pool as plastocyanin, ferrodoxin and FNR, and downregulation of PGR5-like subunit suggests increased electron transport from plastoquinones to NADPH and reduced cyclic electron transport across PSI. Increased reduction of plastoquinone pool in presence of acetate is indeed related to increase transferring of reducing power from mitochondria to the chloroplast, as a consequence of increased NADH production during acetate assimilation. The reduced chlorophyll content per cell observed in mixotrophy was not controlled by differential gene expression of chlorophyll biosynthetic enzymes but rather by downregulation of protein subunits involved in nitrogen assimilation, glycine biosynthesis, iron uptake and accumulation of thylakoid lipid SQDG. Assimilation of acetate has been reported in several organisms to be linked to glyoxylate cycle (Martínez-Rivas and Vega 1993; Plancke et al. 2014b) and photorespiration (Xie et al. 2016), by which glyoxylate is produced. The advantage of glyoxylate cycle toward acetate assimilation is the production of NADH without decarboxylation of isocitrate occurring in the Krebs cycle with the loss of two CO_2 molecules. However, the presence of acetate did not induce in *C*. *sorokiniana* any upregulation of glyoxylate cycle enzymes but only caused an increased expression in mixotrophy of the enzymes GOX and serine hydroxymethyltransferase (SHMT), which are both involved in the photorespiratory pathway (Fig. 6) (Xie et al. 2016). Acetyl-CoA produces by acetate assimilation is thus likely consumed in the Krebs cycle or through the glyoxylate produced by a photorespiratory-like pathway: it is important to note that assimilation of acetate through these pathways is accompanied by CO_2 release by isocitrate decarboxylation or by the activity of the SHMT enzymes respectively, increasing the relative CO_2 concentration in mixotrophic cells. Increased CO_2 production in mixotrophic conditions is confirmed by the downregulation in presence of acetate of several genes commonly induced in *C*. *reinhardtii* by relative low CO_2 concentration as carbonic anhydrase, RUBISCO activase or components of carbon concentrating mechanism (Fig. 4) (Eriksson et al. 1998; Pollock et al. 2003). *De novo* transcriptomes reported in this or previous works (Sun et al. 2016), demonstrate in *C*. *sorokiniana* the presence and expression of genes involved in C4-like carbon fixation pathway: interestingly, the key CO_2 fixing enzyme PPC is upregulated in mixotrophy (Fig. 4). These findings suggest that, carbon loss due to acetate oxidation is reduced by the activation in mixotrophy of an alternative carbon fixation pathway by PPC. This strategy allows to maximize the energetic yield of acetate assimilation, reducing the loss of carbon atoms. C4-like carbon fixation pathway has been already reported in the case of diatoms (Reinfelder, Kraepiel, and Morel 2000), suggesting a peculiar properties of some unicellular microalgae to improve CO_2 assimilation using different pathway in parallel with the Calvin-Benson cycle.

In conclusion, a fine regulation of cellular metabolism is induced by the availability of acetate in the growth medium. The metabolism shift was characterized by the downregulation of glycolysis, pentose phosphate pathway and acetyl-CoA production from pyruvate, while glyoxylate production, biosynthesis of several amino acids and protein translation are increased. Acetate induces also an increase of lipid accumulation which however is not directly related to differential expression of biosynthetic genes. Three transcription factors were identified as differently expressed in autotrophy *vs*. mixotrophy with TBP upregulated in mixotrophy and the plant specific SBP and Whirly transcription factors downregulated in mixotrophy. These transcription factors are putatively responsible for the different gene expression herein reported, even if the activation/inhibition of other transcription factor cannot be excluded. Several kinases and phosphatases were indeed differently expressed in presence or absence of acetate, which could be involved in the regulation of gene expression. Components involved in ethylene, auxin, salicylic acid and calcium signalling were downregulated in mixotrophy, pointing for a complex network of regulation of gene expression and cell functions. Even if further work is necessary, these signalling components may have a role in the regulation of gene expression in *C. sorokiniana* under autotrophic condition and possibly in other unicellular microalgae, similar to what described in multicellular higher plants.

MATERIALS AND METHODS

Microalgae cultivation. *C. sorokiniana* UTEX 1230 cells were grown in 1 L airlift photobioreactors in BG11 medium at 450 µmol $m^{-2}s^{-1}$ with day/night cycles of 16/8 hours with CO_2 addition "on demand" on the base of the pH of the medium as described in Cazzaniga et al., 2014, with the addition of acetate (1 gr/L) in the case of mixotrophic cultivation. Daily cell counts and dry weight determination were performed as described in Cazzaniga et al., 2014.

Photosynthetic parameters. Fluorescence parameters (F_v/F_m, NPQ) were measured by WALZ PAM-100 fluorometer as described in Cazzaniga et al., 2014. Electrochromic shift (ECS) measurements at 520 nm were performed using a Joliot-type spectrophotometer JTS-10 (BioLogic) as described in Bailleul *et al.*, 2010. Oxygen evolution curves were measured as described in Cazzaniga *et al.*, 2014.

RNA extraction and RNA seq analysis. RNA was extracted from three independent biological replicates of each culture condition at exponential phase using a modified TRIzol SIGMA-ALDRICH protocol. Cells were disrupted by glass beads (Micro-organism lysing VKmix, Bertin Technologies). RNA samples were further purified with the SIGMA Spectrum Plant Total RNA kit including a DNAse treatment step. RNA quality and quantity were determined using a Nanodrop 2000 spectrophotometer (Thermo Scientific, Wilmington, DE) and a Bioanalyzer Chip RNA 7500 series II (Agilent, Santa Clara, CA). Directional RNA-seq library preparation was performed starting from 1 µg total RNA using the TruSeq RNA Sample Prep Kit v2 (Illumina Inc., San Diego, CA, USA) after capturing poly-adenylated transcripts. Library quality was assessed with a High Sensitivity DNA Kit on a 2200 Tape Station (Agilent, Wokingham, UK). Libraries were sequenced with an Illumina HiSeq. 1000 sequencer (Illumina Inc., San Diego, CA, USA) generating ~22 million 100-bp paired-end reads per sample. Low-quality reads (>50 bases with quality <7 or >10% undetermined bases) and putative PCR duplicate reads were removed and Illumina TruSeq adapter sequences were clipped. Low-quality bases at read ends were trimmed (minimum quality 16, minimum read length 50 bp) with cutadapt (http://code.google.com/p/cutadapt/).

Transcriptome de-novo assembly and differential expression analysis. *De novo* transcriptome assembly was carried out with the Trinity (v. 2.0.6) software using reads of all samples as input with the following parameters: -seqType fq, -max_memory 128 G, -CPU 20, -min_contig_length 200, jaccard_clip, -normalize_ reads -normalize_by_read_set, -SS_lib_type RF, and a default k-mer value of 25. Abundance of each transcript was calculated using the align_and_estimate_abundance.pl script from Trinity software 2.0.6. Default settings were used except for the options -est_method RSEM -aln_method bowtie -trinity_mode -prep_reference -SS_lib_type RFFR. RSEM version 1.2.2919 was used to estimate the abundance of each transcript. The row count matrix was at first filtered removing all the very low expressed genes showing a mean expression value below 10 reads count across all the samples. The identification of the differentially expressed genes was performed using the negative

binomial distribution-based method implemented in EdgeR (Robinson, McCarthy, and Smyth 2009). The counts were normalized to take into account the different sequencing depth using the TMM (Trimmed Mean of M-value) method implemented in EdgeR. Genes with a *p-value* lower or equal 0.05, after false discovery rate correction, were considered significantly differentially expressed. Differential expression analysis was performed using the negative binomial distribution-based method implemented in DESeq on the summed read counts per transcript (Anders and Huber 2010).

Transcriptome functional annotation. The transcriptome functional annotation was performed by means of a similarity search against the non-redundant protein database (NCBI) using Blastp and setting an e-value threshold of 1e-5. Further annotation were retrieved using InterProscan5 (Jones et al. 2014) against several different databases (PROSITE patterns, PRINTS, PFAM, PRODOM, SMART, TIGRFAM and PANTHER) for the identification of conserved protein domains and functional annotation. Gene Ontology annotations were assigned running Blast2GO 2.6.0 (Conesa et al. 2005) on the blast and InterProscan results. Sequences were also analysed by KAAS (KEGG Automatic Annotation Server) platform to obtain KO annotation (Kanehisa et al. 2016, 2017; Kanehisa and Goto 2000). Transcripts differently expressed with KO annotation were visualized by KEGG Mapper platform (http://www.kegg.jp/kegg/tool/map_pathway.html), while the remaining transcripts functionally annotated were manually inspected by retrieving the function of the closest homolog gene. List of transcripts identified in the *de novo C. sorokiniana* assembled transcriptome with functional annotation, where retrieved, are reported in Supplementary data, Data file S1. Trascriptome completeness was evaluated by BUSCO analysis using as a reference a dataset of 303 universal single-copy genes putatively universally found in eukaryotes as single copies (Simão et al. 2015).

Statistical analysis. Descriptive statistical analysis with mean and standard deviation were applied for all the data reported except for differential gene expression analysis. Differential gene expression was considered significant when the *p-value* associated to the comparison autotrophic *vs.* mixotrophic was lower or equal 0.05, after the false discovery rate correction implemented in the DESeq algorithm. The non-parametric Mann-Whitney was applied to compare the impact of autotrophic *vs.* mixotrophic conditions, unless otherwise stated. All the analyses were performed using OriginPro 8 software. Differences of $P < 0.05$ were considered significantly different.

Data availability. All the data generated during and/or analysed during the current study are available from the corresponding author on reasonable request. All next-generation sequencing data and contigs assembled from Illumina reads are available in the NCBI Bioproject PRJNA416862. In the Supplementary Dataset S3 the sequences of all transcripts identified in this work are reported.

ACKNOWLEDGEMENTS

The research was supported by the ERC Starting Grant SOLENALGAE (679814) and by the Italian Ministry of Education, University and Research through PRIN ("Progetti di Ricerca di Interesse Nazionale") project 2012XSAWYM to M.B.

AUTHOR CONTRIBUTIONS

M.B. conceived the study, designed and supervised the experiments. M.D. coordinated and supervised the transcriptomic analysis. M.C. prepared all the samples herein analysed and performed or contributed to all the experiments herein reported. S.B., F.G. and A.M. performed the transcriptomic experiments and analysed the sequencing data. S.C. contributed to growth experiments and biomass analysis. N.V. contributed to bioinformatic analysis. All the authors contributed to writing the manuscript. All the authors discussed the results and commented on the manuscript.

REFERENCES

Alboresi, Alessandro, Giorgio Perin, Nicola Vitulo, Gianfranco Diretto, Maryse Block, Juliette Jouhet, Andrea Meneghesso, Giorgio Valle, Giovanni Giuliano, Eric Maréchal, and Tomas Morosinotto. 2016. "Light Remodels Lipid Biosynthesis in *Nannochloropsis gaditana* by Modulating Carbon Partitioning between Organelles." Plant Physiology.

Allorent, Guillaume, Linnka Lefebvre-Legendre, Richard Chappuis, Marcel Kuntz, Thuy B. Truong, Krishna K. Niyogi, Roman Ulm, and Michel Goldschmidt-Clermont. 2016. "UV-B Photoreceptor-Mediated Protection of the Photosynthetic Machinery in *Chlamydomonas reinhardtii*." Proceedings of the National Academy of Sciences of the United States of America.

Alric, Jean. 2014. "Redox and ATP Control of Photosynthetic Cyclic Electron Flow in *Chlamydomonas reinhardtii*: (II) Involvement of the PGR5-PGRL1 Pathway under Anaerobic Conditions." Biochimica et Biophysica Acta - Bioenergetics.

Alves, A. M. C. R., G. J. W. Euverink, H. Santos, and L. Dijkhuizen. 2001. "Different Physiological Roles of ATP- and PPi-Dependent Phosphofructokinase Isoenzymes in the Methylotrophic Actinomycete *Amycolatopsis methanolica*." Journal of Bacteriology.

Anders, Simon and Wolfgang Huber. 2010. "Differential Expression Analysis for Sequence Count Data." Genome Biology.

Bailleul, B., P. Cardol, C. Breyton, and G. Finazzi. 2010. "Electrochromism: A Useful Probe to Study Algal Photosynthesis." Photosynth.Res. 106(1573-5079 (Electronic)):179–89.

Cazzaniga, Stefano, Luca Dall'Osto, Joanna Szaub, Luca Scibilia, Matteo Ballottari, Saul Purton, and Roberto Bassi. 2014. "Domestication of the Green Alga *Chlorella sorokiniana*: Reduction of Antenna Size Improves Light-Use Efficiency in a Photobioreactor." Biotechnology for Biofuels.

Chen, Xiaobo, Zenglin Zhang, Danmei Liu, Kai Zhang, Aili Li, and Long Mao. 2010. "SQUAMOSA Promoter-Binding Protein-like Transcription Factors: Star Players for Plant Growth and Development." Journal of Integrative Plant Biology.

Chiba, Yasutaka, Takafumi Shimizu, Shinya Miyakawa, Yuri Kanno, Tomokazu Koshiba, Yuji Kamiya, and Mitsunori Seo. 2015. "Identification of *Arabidopsis thaliana* NRT1/PTR FAMILY (NPF) Proteins Capable of Transporting Plant Hormones." Journal of Plant Research 128(4):679–86.

Combres, C., G. Laliberté, J. Sevrin Reyssac, and J. de la Noüe. 1994. "Effect of Acetate on Growth and Ammonium Uptake in the Microalga *Scenedesmus obliquus*." Physiologia Plantarum.

Conesa, Ana, Stefan Götz, Juan Miguel García-Gómez, Javier Terol, Manuel Talón, and Montserrat Robles. 2005. "Blast2GO: A Universal Tool for Annotation, Visualization and Analysis in Functional Genomics Research." Bioinformatics.

Desveaux, Darrell, Rajagopal Subramaniam, Charles Després, Jean Nicholas Mess, Caroline Lévesque, Pierre R. Fobert, Jeffery L. Dangl, and Normand Brisson. 2004. "A 'Whirly' Transcription Factor Is Required for Salicylic Acid-Dependent Disease Resistance in *Arabidopsis*." Developmental Cell.

Eriksson, Mats, Per Villand, Per Gardeström, and Göran Samuelsson. 1998. "Induction and Regulation of Expression of a Low-CO_2-Induced Mitochondrial Carbonic Anhydrase in *Chlamydomonas reinhardtii*." Plant Physiology.

Ettema, Thijs J. G., Hatim Ahmed, Ans C. M. Geerling, John Van Der Oost, and Bettina Siebers. 2008. "The Non-Phosphorylating Glyceraldehyde-3-Phosphate Dehydrogenase (GAPN) of Sulfolobus Solfataricus: A Key-Enzyme of the Semi-Phosphorylative Branch of the Entner-Doudoroff Pathway." Extremophiles.

Floris, Maïna, Roberto Bassi, Christophe Robaglia, Alessandro Alboresi, and Elodie Lanet. 2013. "Post-Transcriptional Control of Light-Harvesting Genes Expression under Light Stress." Plant Molecular Biology 82(1–2):147–54.

Glaesener, Anne G., Sabeeha S. Merchant, and Crysten E. Blaby-Haas. 2013. "Iron Economy in *Chlamydomonas reinhardtii*." Frontiers in Plant Science.

Hannon, Michael, Javier Gimpel, Miller Tran, Beth Rasala, and Stephen Mayfield. 2010a. "Biofuels from Algae: Challenges and Potential." Biofuels 1(5):763–84.

Iqbal, Noushina, Alice Trivellini, Asim Masood, Antonio Ferrante, and Nafees A. Khan. 2013. "Current Understanding on Ethylene Signaling in Plants: The Influence of Nutrient Availability." Plant Physiology and Biochemistry.

Jiménez-Quesada, María J., José Traverso, and Juan de Dios Alché. 2016. "NADPH Oxidase-Dependent Superoxide Production in Plant Reproductive Tissues." Frontiers in Plant Science.

Johnson, Xenie and Jean Alric. 2012. "Interaction between Starch Breakdown, Acetate Assimilation, and Photosynthetic Cyclic

Electron Flow in *Chlamydomonas reinhardtii*." Journal of Biological Chemistry.

Johnson, Xenie and Jean Alric. 2013. "Central Carbon Metabolism and Electron Transport in *Chlamydomonas reinhardtii*: Metabolic Constraints for Carbon Partitioning between Oil and Starch." Eukaryotic Cell.

Jones, Philip, David Binns, Hsin Yu Chang, Matthew Fraser, Weizhong Li, Craig McAnulla, Hamish McWilliam, John Maslen, Alex Mitchell, Gift Nuka, Sebastien Pesseat, Antony F. Quinn, Amaia Sangrador-Vegas, Maxim Scheremetjew, Siew Yit Yong, Rodrigo Lopez, and Sarah Hunter. 2014. "InterProScan 5: Genome-Scale Protein Function Classification." Bioinformatics.

Kanehisa, Minoru, Miho Furumichi, Mao Tanabe, Yoko Sato, and Kanae Morishima. 2017. "KEGG: New Perspectives on Genomes, Pathways, Diseases and Drugs." Nucleic Acids Research.

Kanehisa, Minoru and Susumu Goto. 2000. "KEGG: Kyoto Encyclopedia of Genes and Genomes." Nucleic Acids Research 28:27–30.

Kanehisa, Minoru, Yoko Sato, Masayuki Kawashima, Miho Furumichi, and Mao Tanabe. 2016. "KEGG as a Reference Resource for Gene and Protein Annotation." Nucleic Acids Research.

Kawasaki, Shinji, Keisuke Mizuguchi, Masaru Sato, Tetsuya Kono, and Hirofumi Shimizu. 2013. "A Novel Astaxanthin-Binding Photooxidative Stress-Inducible Aqueous Carotenoprotein from a Eukaryotic Microalga Isolated from Asphalt in Midsummer." Plant and Cell Physiology.

Kindle, K. L. 1987. "Expression of a Gene for a Light-Harvesting Chlorophyll a/b- Binding Protein in *Chlamydomonas reinhardtii*: Effect of Light and Acetate." Plant Mol.Biol. 9:547–63.

Lee, Tong Ihn and Richard A. Young. 2000. "Transcription of Eukaryotic Protein-Coding Genes." Annual Review of Genetics.

Li, Jing, Danxiang Han, Dongmei Wang, Kang Ning, Jing Jia, Li Wei, Xiaoyan Jing, Shi Huang, Jie Chen, Yantao Li, Qiang Hu, and Jian Xu. 2014. "Choreography of Transcriptomes and Lipidomes of *Nannochloropsis* Reveals the Mechanisms of Oil Synthesis in Microalgae." Plant Cell.

Li, Tingting, Helmut Kirchhoff, Mahmoud Gargouri, Jie Feng, Asaph B. Cousins, Philip T. Pienkos, David R. Gang, and Shulin Chen. 2016. "Assessment of Photosynthesis Regulation in Mixotrophically Cultured Microalga *Chlorella sorokiniana*." Algal Research.

Li, Tingting, Yubin Zheng, Liang Yu, and Shulin Chen. 2014. "Mixotrophic Cultivation of a *Chlorella sorokiniana* Strain for Enhanced Biomass and Lipid Production." Biomass and Bioenergy.

Lum, Krystal K., Jonggun Kim, and Xin G. Lei. 2013. "Dual Potential of Microalgae as a Sustainable Biofuel Feedstock and Animal Feed." Journal of Animal Science and Biotechnology.

Mansfeldt, Cresten B., Lubna V. Richter, Beth A. Ahner, William P. Cochlan, and Ruth E. Richardson. 2016. "Use of de Novo Transcriptome Libraries to Characterize a Novel Oleaginous Marine *Chlorella* Species during the Accumulation of Triacylglycerols." PLoS ONE.

Maréchal, Alexandre, Jean Sébastien Parent, Félix Véronneau-Lafortune, Alexandre Joyeux, B. Franz Lang, and Normand Brisson. 2009. "Whirly Proteins Maintain Plastid Genome Stability in *Arabidopsis*." Proceedings of the National Academy of Sciences of the United States of America.

Martínez-Rivas, José M. and José M. Vega. 1993. "Effect of Culture Conditions on the Isocitrate Dehydrogenase and Isocitrate Lyase Activities in *Chlamydomonas reinhardtii*." Physiologia Plantarum.

Millar, Anthony A. and Ljerka Kunst. 1997. "Very-Long-Chain Fatty Acid Biosynthesis Is Controlled through the Expression and Specificity of the Condensing Enzyme." Plant Journal.

Petroutsos, Dimitris, Andreas Busch, Ingrid Janßen, Kerstin Trompelt, Sonja Verena Bergner, Stefan Weinl, Michael Holtkamp, Uwe Karst, Jörg Kudla, and Michael Hippler. 2011. "The Chloroplast Calcium Sensor CAS Is Required for Photoacclimation in *Chlamydomonas reinhardtii*." Plant Cell.

Plancke, Charlotte, Helene Vigeolas, Ricarda Höhner, Stephane Roberty, Barbara Emonds-Alt, Véronique Larosa, Remi Willamme, Franceline Duby, David Onga Dhali, Philippe Thonart, Serge Hiligsmann, Fabrice Franck, Gauthier Eppe, Pierre Cardol, Michael Hippler, and Claire Remacle. 2014a. "Lack of Isocitrate Lyase in *Chlamydomonas* Leads to Changes in Carbon Metabolism and in the Response to Oxidative Stress under Mixotrophic Growth." Plant Journal 77(3):404–17.

Plancke, Charlotte, Helene Vigeolas, Ricarda Höhner, Stephane Roberty, Barbara Emonds-Alt, Véronique Larosa, Remi Willamme, Franceline Duby, David Onga Dhali, Philippe Thonart, Serge Hiligsmann, Fabrice Franck, Gauthier Eppe,

Pierre Cardol, Michael Hippler, and Claire Remacle. 2014b. “Lack of Isocitrate Lyase in *Chlamydomonas* Leads to Changes in Carbon Metabolism and in the Response to Oxidative Stress under Mixotrophic Growth.” Plant Journal.

Pollock, Steve V., Sergio L. Colombo, Davey L. Prout, Ashley C. Godfrey, and James V. Moroney. 2003. “Rubisco Activase Is Required for Optimal Photosynthesis in the Green Alga *Chlamydomonas reinhardtii* in a Low-CO_2 Atmosphere.” Plant Physiology.

Prikryl, Jana, Kenneth P. Watkins, Giulia Friso, Klaas J. van Wijk, and Alice Barkan. 2008. “A Member of the Whirly Family Is a Multifunctional RNA- and DNA-Binding Protein That Is Essential for Chloroplast Biogenesis.” Nucleic Acids Research.

Raman, Rinugah and Shaza Eva Mohamad. 2012. “Astaxanthin Production by Freshwater Microalgae *Chlorella sorokiniana* and Marine Microalgae *Tetraselmis sp*.” Pakistan Journal of Biological Sciences.

Reinfelder, John R., Anne M. L. Kraepiel, and François M. M. Morel. 2000. “Unicellular C4 Photosynthesis in a Marine Diatom.” Nature.

Ben Rejeb, Ines, Victoria Pastor, and Brigitte Mauch-Mani. 2014. “Plant Responses to Simultaneous Biotic and Abiotic Stress: Molecular Mechanisms.” Plants.

Robinson, Mark D., Davis J. McCarthy, and Gordon K. Smyth. 2009. “EdgeR: A Bioconductor Package for Differential Expression Analysis of Digital Gene Expression Data.” Bioinformatics.

Roche, Thomas E., Jason C. Baker, Xiaohua Yan, Yasuaki Hiromasa, Xiaoming Gong, Tao Peng, Jianchun Dong, Ali Turkan, and Shane A. Kasten. 2001. “Distinct Regulatory Properties of Pyruvate Dehydrogenase Kinase and Phosphatase Isoforms.” Progress in Nucleic Acid Research and Molecular Biology.

Rosakis, Alexandra and Wolfgang Köster. 2004. “Transition Metal Transport in the Green Microalga C*hlamydomonas reinhardtii* - Genomic Sequence Analysis.” Research in Microbiology.

Rosenberg, Julian N., Naoko Kobayashi, Austin Barnes, Eric A. Noel, Michael J. Betenbaugh, and George A. Oyler. 2014. “Comparative Analyses of Three *Chlorella* Species in Response to Light and Sugar Reveal Distinctive Lipid Accumulation Patterns in the Microalga *C. sorokiniana*.” PLoS ONE.

Sforza, Eleonora, Renato Cipriani, Tomas Morosinotto, Alberto Bertucco, and Giorgio M. Giacometti. 2012. “Excess CO_2 Supply Inhibits Mixotrophic Growth of *Chlorella protothecoides* and *Nannochloropsis salina*.” Bioresource Technology.

Simão, Felipe A., Robert M. Waterhouse, Panagiotis Ioannidis, Evgenia V. Kriventseva, and Evgeny M. Zdobnov. 2015. “BUSCO: Assessing Genome Assembly and Annotation Completeness with Single-Copy Orthologs.” Bioinformatics.

Sun, Zhilan, Yi Feng Chen, and Jianchang Du. 2016. “Elevated CO_2 Improves Lipid Accumulation by Increasing Carbon Metabolism in *Chlorella sorokiniana*.” Plant Biotechnology Journal.

Terashima, Mia, Dimitris Petroutsos, Meike Hüdig, Irina Tolstygina, Kerstin Trompelt, Philipp Gäbelein, Christian Fufezan, Jörg Kudla, Stefan Weinl, Giovanni Finazzi, and Michael Hippler. 2012. “Calcium-Dependent Regulation of Cyclic Photosynthetic Electron Transfer by a CAS, ANR1, and PGRL1 Complex.” Proceedings of the National Academy of Sciences of the United States of America.

Tibiletti, Tania, Pascaline Auroy, Gilles Peltier, and Stefano Caffarri. 2016. “*Chlamydomonas reinhardtii* PsbS Protein Is Functional and Accumulates Rapidly and Transiently under High Light.” Plant Physiology.

Uhmeyer, Andreas, Michela Cecchin, Matteo Ballottari, and Lutz Wobbe. 2017. “Impaired Mitochondrial Transcription Termination Disrupts the Stromal Redox Poise in *Chlamydomonas*.” Plant Physiology.

Wan, Minxi, Peng Liu, Jinlan Xia, Julian N. Rosenberg, George A. Oyler, Michael J. Betenbaugh, Zhenyuan Nie, and Guanzhou Qiu. 2011. “The Effect of Mixotrophy on Microalgal Growth, Lipid Content, and Expression Levels of Three Pathway Genes in *Chlorella sorokiniana*.” Applied Microbiology and Biotechnology.

Xie, Xiujun, Aiyou Huang, Wenhui Gu, Zhengrong Zang, Guanghua Pan, Shan Gao, Linwen He, Baoyu Zhang, Jianfeng Niu, Apeng Lin, and Guangce Wang. 2016. “Photorespiration Participates in the Assimilation of Acetate in *Chlorella sorokiniana* under High Light.” New Phytologist.

SUPPLEMENTARY INFORMATION

Supplemental Tables

Table S1. Pigment analysis of *C. sorokiniana* cells in autotrophy *vs.* mixotrophy. Chlorophyll content per cell is reported as pg of chlorophyll. Pigment data are reported normalized to 100 chlorophylls. Chl a/b: chlorophyll a/b; Car: carotenoid; Nx: neoxanthin; Vx: violaxanthin; Ax: anteraxanthin; Lut: Lutein; β-Car: β-carotene. Standard deviation (*s.d.*) are reported (n = 6).

	Chl/cell	**Chl a/b**	**chl/car**	**Chl *a***	**Chl *b***	**Nx**	**Vx**	**Ax**	**Lut**	**β-Car**
Mixotrophy	1.10E-07	2.71	3.50	73.04	26.96	5.24	1.76	0.53	18.13	2.88
s.d.	*1.43E-08*	*0.17*	*0.01*	2.58	1.43	*0.26*	*0.03*	*0.13*	*0.61*	*0.14*
Autotrophy	2.03E-07	3.01	3.53	75.08	24.92	5.24	1.87	0.47	18.00	2.79
s.d.	*3.19E-08*	*0.50*	*0.16*	6.86	3.42	*0.11*	*0.13*	*0.05*	*1.03*	*0.02*

Table S2. Photosynthesis and respiration rates. O_2 evolution/consumption were measured with a Clark-type oxygen electrode. Standard deviation is reported (n = 4).

	AUTOTROPHY	***s.d.***	**MIXOTROPHY**	***s.d.***
Pmax (μmol O_2 h^{-1} mg Chl^{-1})	128.60	*3.67*	128.36	*8.26*
Half-saturation intensity (μmol m^{-2} s^{-1})	135.17	*22.93*	115.22	*27.11*
Respiration (μmol O_2 h^{-1} $cells^{-1}$)	4.82E-09	1.43E-09	6.20E-09	9.84E-10
Respiration (μmol O_2 h^{-1} mg Chl^{-1})	23.75	8.55	53.61	11.28

Table S3. Identification of 18S transcripts in *C. sorokiniana de novo* assembled transcriptome using *C. sorokiniana* UTEX1230 18S sequences available at NCBI.

C. sorokiniana UTEX 1230 sequence	First sequence aligned in *de novo C. sorokiniana* transcriptome	e-value	Identities	Gaps
KR904895.1	TR1035|c8_g4_i1	0	1110/1140 (97%)	10/1140 (1%)
KJ676112.1		0	1404/1436 (98%)	11/1436 (1%)
KP645225.1		0	737/739 (99%)	1/739 (0%)

Table S4. Putative regulative phosphatases and kinases differently regulated in mixotrophy compared to autotrophy in *C. sorokiniana.*

	Transcript	logFC	Description
DOWNREGULATED IN MIXOTROPHY			
PHOSPHATASES	TR7705|c0_g1_i2	-4.34233	Phytochrome-associated serine threonine-phosphatase
	TR7716|c0_g8_i1	-1.85008	phosphatase 1
	TR7716|c0_g8_i3	-3.9312	phosphatase 1
	TR51265|c0_g1_i12	-1.62184	ser thr phosphatase family
	TR51284|c0_g1_i3	-7.73373	probable serine threonine phosphatase 2A regulatory subunit B delta isoform X2
	TR13958|c1_g2_i1	7.875484	phosphoinositide phosphatase SAC9
KINASES	TR9072|c0_g1_i2	-11.4016	Serine threonine- kinase CTR1
	TR1026|c3_g5_i8	-9.20802	Serine threonine- kinase CTR1
	TR1066|c3_g2_i16	-10.2851	cyclic nucleotide dependent kinase
	TR1066|c3_g2_i17	-9.15322	cyclic nucleotide dependent kinase
	TR43814|c1_g2_i4	-10.8645	Serine threonine- kinase CTR1
	TR43853|c0_g2_i1	-2.46651	probable receptor kinase At5g39020
	TR44339|c0_g1_i1	-7.78603	Serine threonine- kinase CTR1
	TR45584|c0_g4_i9	-3.22761	Serine threonine- kinase
	TR50242|c0_g1_i3	-3.82414	serine threonine- kinase
	TR50242|c0_g1_i4	-2.33285	serine threonine- kinase
	TR53297|c1_g1_i17	-9.12487	Calcium-dependent kinase 29
	TR9072|c0_g1_i2	-11.4016	Serine threonine- kinase CTR1

UPREGULATED IN MIXOTROPHY			
PHOSPHATASES	TR11354|c0_g1_i1	7.287051	phosphatase 1 regulatory subunit 7
	TR13958|c1_g2_i1	7.875484	phosphoinositide phosphatase SAC9
	TR24888|c0_g1_i2	7.714205	phosphoinositide phosphatase SAC6-like
KINASES	TR17426|c0_g2_i3	2.274882	Serine threonine- kinase CTR1
	TR2167|c0_g1_i1	8.781701	Serine Threonine kinase
	TR2977|c0_g1_i1	4.872873	cyclin dependent kinase
	TR4032|c0_g5_i10	7.556271	serine threonine- kinase receptor R831
	TR43839|c0_g1_i5	8.889553	serine threonine- kinase ATR
	TR45177|c0_g1_i20	3.200082	serine threonine- kinase
	TR45177|c0_g1_i32	8.550787	serine threonine- kinase
	TR45657|c5_g6_i5	7.554033	serine threonine- kinase receptor R831
	TR51340|c1_g3_i12	7.626945	probable serine threonine- kinase At1g09600
	TR981|c0_g1_i4	9.336607	Serine threonine- kinase CTR1

Supplemental Figures

Figure S1. *De novo* assembly of *C. sorokiniana* transcriptome, distribution of transcript lengths among the different sequences.

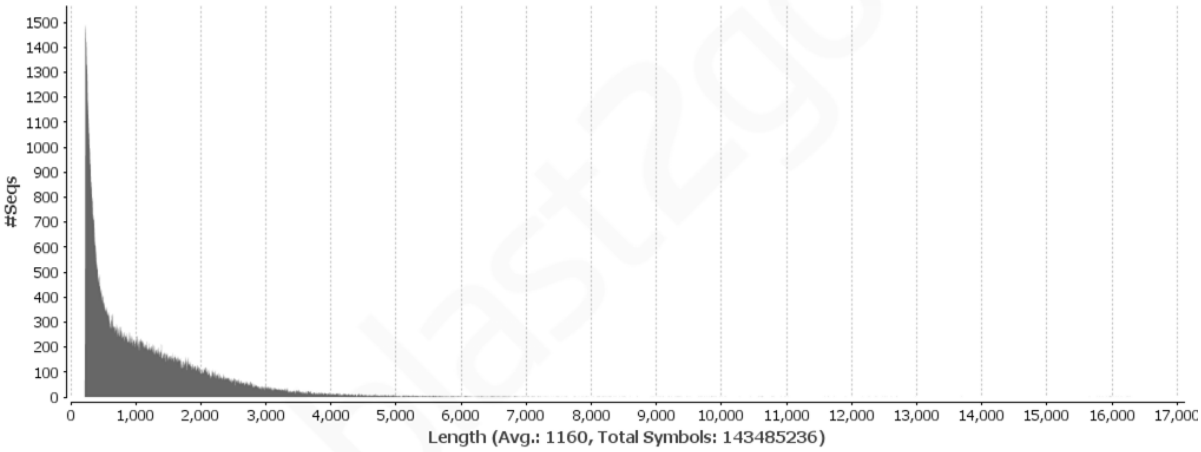

Figure S2. Functional annotation of *C. sorokiniana* transcriptome. Panel A. data distribution among total transcripts with Gene Ontology (GO) and KEGG Orthology (KO) annotation. Panel B: number of sequences with a number of GO terms reported on the X-axis. Panel C: Distribution of annotated sequences among different species.

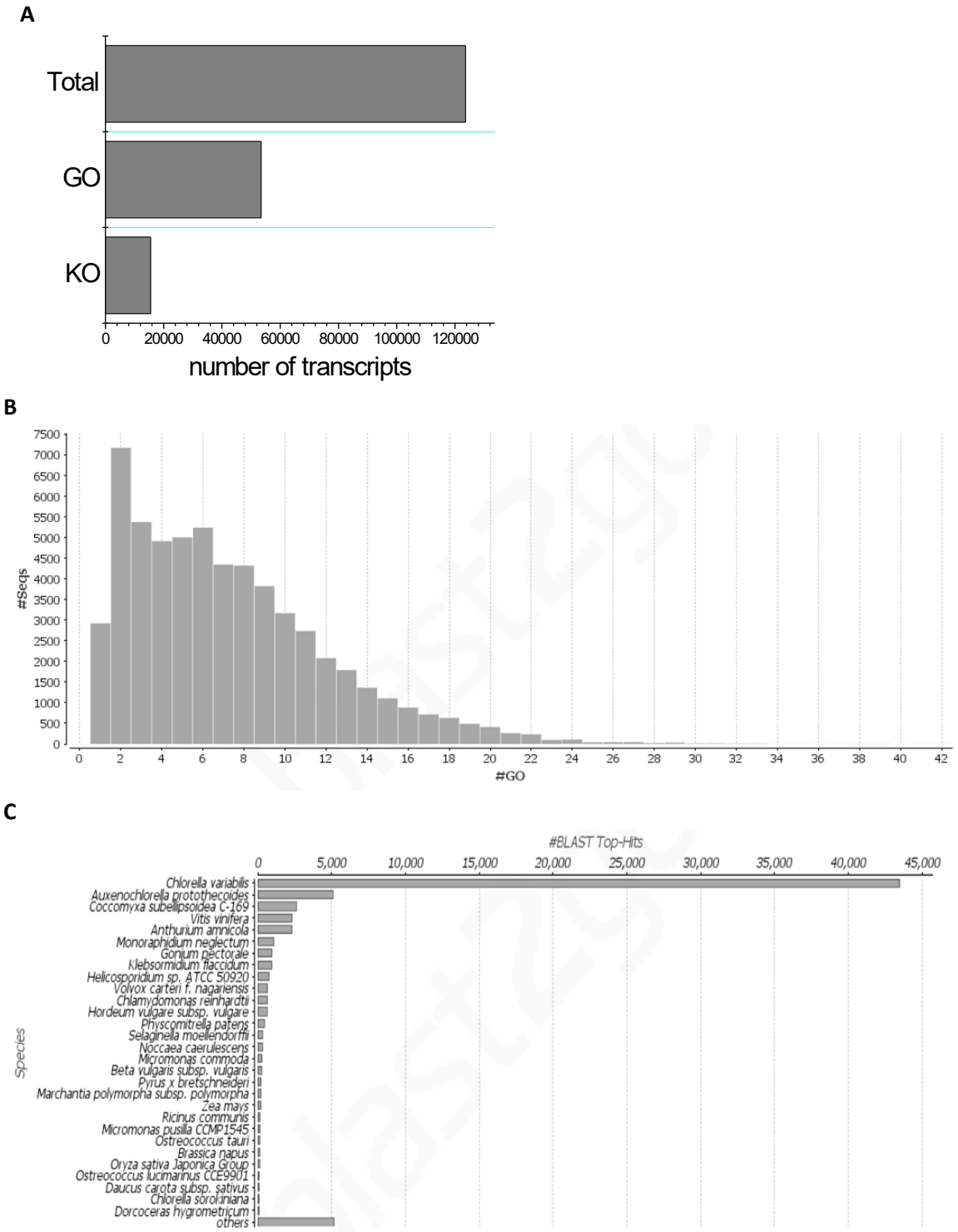

Figure S3. Western blot analysis on photosynthetic subunits. SDS-PAGE gels were transferred on nitrocellulose filters which were cut between 30 and 40 KDa and between 50 and 60 KDa according to the migration of prestained molecular marker (NIPPON Genetics Europe, PINK Prestained Protein Ladder). Immunoblotting analysis using LHCII, PSBS and COX2 specific antibodies were performed on the filters with protein at lower apparent MW, CP43 on the filters with proteins at intermediate (50-40 KDa) apparent MW, and PsaA on the filters with proteins at higher apparent MW.

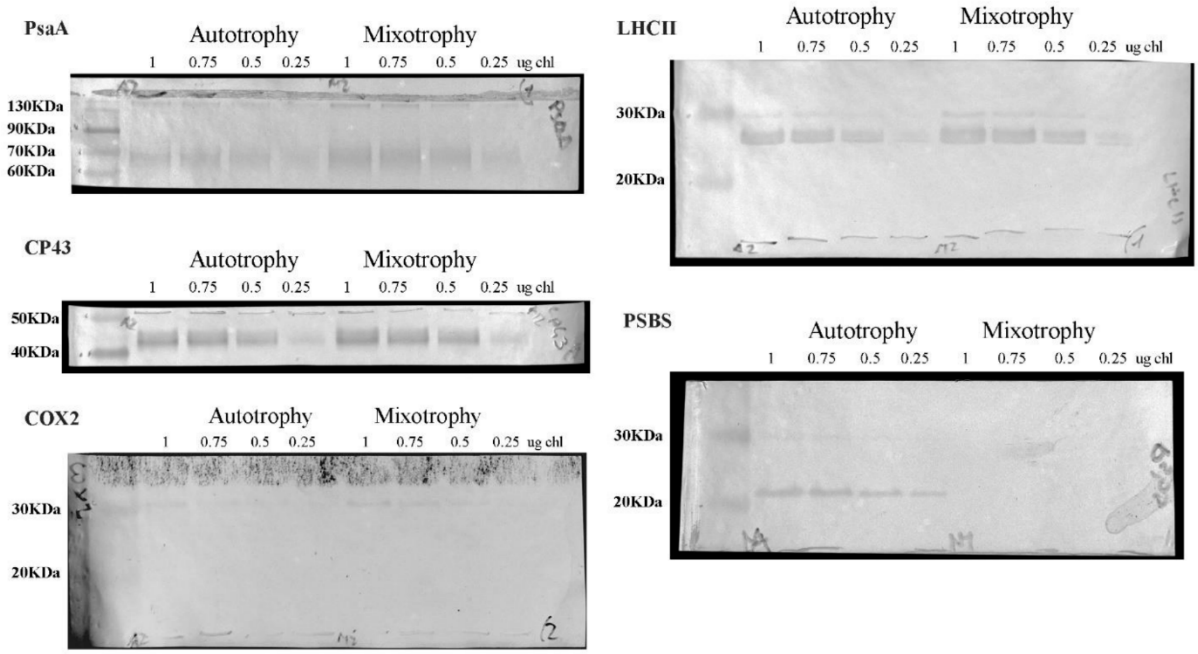

Figure S4. Carbon fixation pathways in *C. sorokiniana*. Carbon fixation pathways visualized on the base of KEGG Map Pathway (http://www.kegg.jp/kegg/tool/map_pathway.html) (Kanehisa et al. 2016, 2017; Kanehisa and Goto 2000). Metabolic reactions for which catalysing enzymes were detected in the *C. sorokiniana* transcriptome are indicated in yellow in the case of enzymes not differentially expressed, blue and red in case of enzymes respectively upregulated and downregulated in mixotrophy. PPC: phosphoenolpyruvate carboxylase; PPDK: pyruvate-orthophosphate dikinase; AspAT: aspartate aminotransferase; GAPDH: Glyceraldehyde 3-phosphate dehydrogenase (phosphorylating)

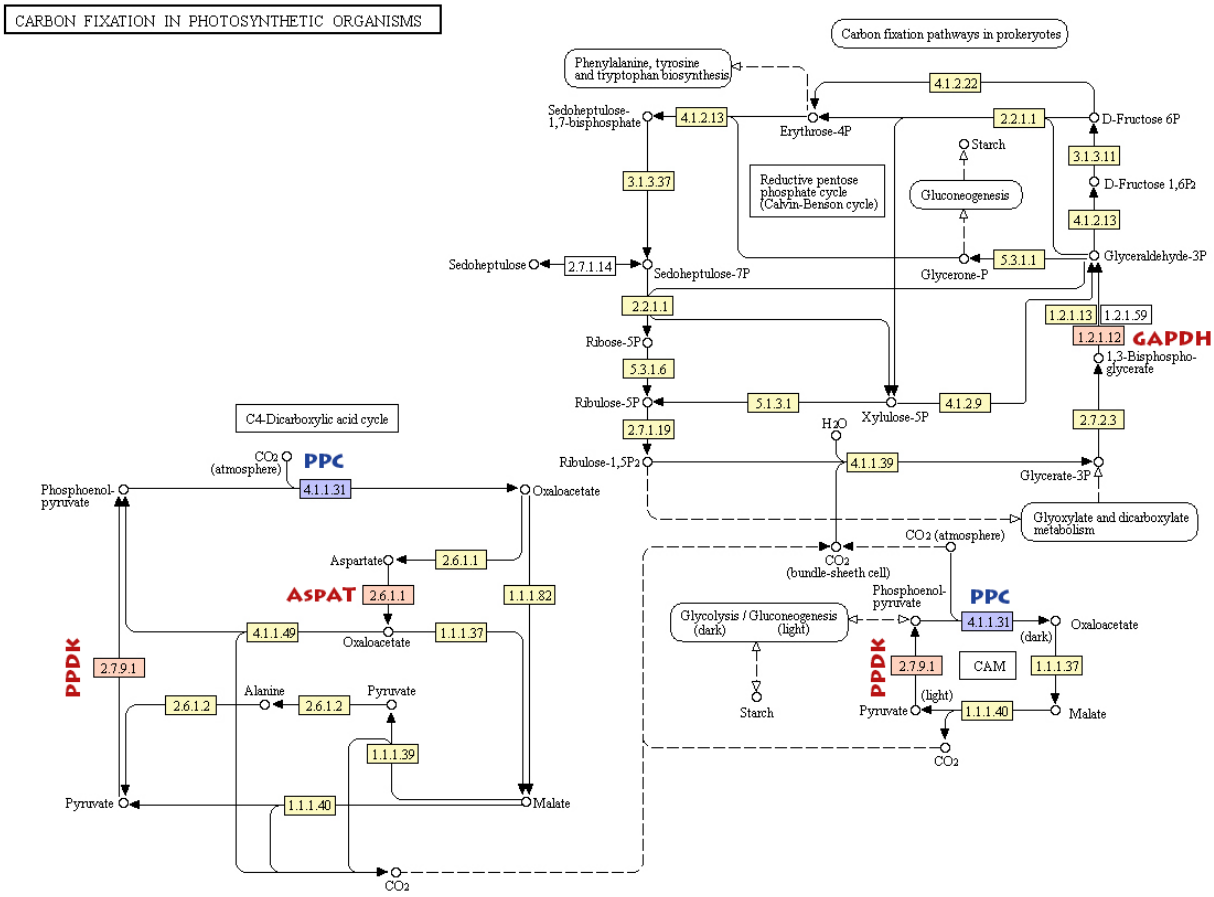

Supplemental Datasets

Dataset S1. List of *C. sorokiniana* transcripts identified in the *de novo* assembled transcriptome with functional annotation retrieved by blast2go. Available at https://doi.org/10.1038/s41598-018-24979-8.

Dataset S2. List of *C. sorokiniana* transcripts differently regulated in mixotrophy compared to autotrophy. Available at https://doi.org/10.1038/s41598-018-24979-8.

Dataset S3. FASTA sequences of all transcripts identified in this work in *C. sorokiniana* cells grown in autotrophy or mixotrophy. Available at https://doi.org/10.1038/s41598-018-24979-8.

REFERENCES

Kanehisa, Minoru, Miho Furumichi, Mao Tanabe, Yoko Sato, and Kanae Morishima. 2017. "KEGG: New Perspectives on Genomes, Pathways, Diseases and Drugs." Nucleic Acids Research.

Kanehisa, Minoru and Susumu Goto. 2000. "KEGG: Kyoto Encyclopedia of Genes and Genomes." Nucleic Acids Research 28:27–30.

Kanehisa, Minoru, Yoko Sato, Masayuki Kawashima, Miho Furumichi, and Mao Tanabe. 2016. "KEGG as a Reference Resource for Gene and Protein Annotation." Nucleic Acids Research.

Section B

Chlorella vulgaris genome assembly and annotation reveals the molecular basis for metabolic acclimation to high light conditions

M. Cecchin[1], L. Marcolungo[1], M. Rossato[1], L. Girolomoni[1], E. Cosentino[1], S. Cuine[2], Y. Li-Beisson[2], M. Delledonne[1] and M. Ballottari[1]

[1]Department of Biotechnology, Università degli studi di Verona, 37134 Verona, Italy

[2]Institute of Biosciences and Biotechnologies of Aix-Marseille, Aix-Marseille University, CEA, CNRS, CEA Cadarache, Saint-Paul-lez Durance F-13108, France

This work was published in The Plant Journal in August 2019.

In this section genetic basis of the highly productive phenotype of *C. vulgaris* was examined. *Chlorella vulgaris* is a fast-growing fresh-water microalga cultivated on the industrial scale for applications ranging from food to biofuel production. To advance our understanding of its biology and to establish genetics tools for biotechnological manipulation, we sequenced the nuclear and organelle genomes of *Chlorella vulgaris* 211/11P by combining next generation sequencing and optical mapping of isolated DNA molecules. This hybrid approach allowed us to assemble the nuclear genome in 14 pseudo-molecules with an N50 of 2.8 Mb and 98.9% of scaffolded genome. The integration of RNA-seq data obtained at two different irradiances of growth (high light, HL versus low light, LL) enabled us to identify 10 724 nuclear genes, coding for 11 082 transcripts. Moreover, 121 and 48 genes, respectively, were found in the chloroplast and mitochondrial genome. Functional annotation and expression analysis of nuclear, chloroplast and mitochondrial genome sequences revealed particular features of *Chlorella vulgaris*. Evidence of horizontal gene transfers from chloroplast to mitochondrial genome was observed. Furthermore, comparative transcriptomic analyses of LL versus HL provided insights into the molecular basis for metabolic rearrangement under HL versus LL conditions leading to

enhanced *de novo* fatty acid biosynthesis and triacylglycerol accumulation. The occurrence of a cytosolic fatty acid biosynthetic pathway could be predicted and its upregulation upon HL exposure was observed, consistent with the increased lipid amount under HL conditions. These data provide a rich genetic resource for future genome editing studies, and potential targets for biotechnological manipulation of *Chlorella vulgaris* or other microalgae species to improve biomass and lipid productivity.

INTRODUCTION

Photosynthetic conversion of light into chemical energy for CO_2 fixation is the primary process for biomass production on our planet. The improvement of photosynthetic biomass production is thus critical to satisfy the world demand for food and energy (Ort et al., 2015), which requires fundamentally improving photosynthetic efficiency (Ort et al., 2015; Kromdijk et al., 2016; Kirst et al., 2017). Among the organisms with the highest photosynthetic efficiency observed in real cultivation cases, microalgae scored efficiencies of 1-3%, although this is still significantly lower compared with their maximum potential (9-11%) (Walker, 2009), highlighting the potential for further improvement. In addition, unicellular microalgae are promising platforms for biomass, food or biofuel production: they can be cultivated in none-arable land in open ponds or in closed photobioreactors potentially employing waste products and wastewater-derived effluents as nutrients (Lum et al., 2013). However, biotechnological manipulation of microalgae to further boost biomass and metabolite productivity require the availability of high-quality genomes and transcriptomes (Merchant et al., 2007; Radakovits et al., 2012; Vieler et al., 2012; Ajjawi et al., 2017; Roth et al., 2017). High-quality genomes are especially critical considering the newly developed technology of genome editing methods (Naduthodi et al., 2018).

Among the many candidates of algal strains for biotechnological applications, a genus of considerable interest is *Chlorella* (Blanc et al., 2010; Juneja et al., 2016; Zuniga et al., 2016; Sarayloo et al., 2017; Arriola et al., 2018). Several species of *Chlorella* have been proposed or have already been used commercially over the past 40 years as a food and feed supplement because of their fast growth and their high resistance to biotic and abiotic stresses (Lum et al., 2013). *Chlorella vulgaris* is one of the most cultivated species at the industrial scale because of the high biomass yield and the possibility to grow either in autotrophic or mixotrophic conditions, in the latter case with the addition of reduced carbon source to further improve the biomass yield (Lv et al., 2010; Zuniga et al., 2016).

Lipid metabolism is among the most investigated topics for microalgae industrial application with the aim to produce biofuels or biomass with high nutrition content. *De novo* fatty acid biosynthesis occurs in plant cells mainly in the chloroplast catalyzed by fatty acid synthase type II (FAS2) multisubunit complex, while animals and fungi possess FAS type I complexes (FAS1) located in the cytosol which appear as large multi-enzyme complexes composed by one or two large polypeptide chains (Alboresi et al., 2016). In type I system, the constituent catalytic components are covalently linked in multifunctional megasynthases, whereas in type II system, the catalytic components are independent monofunctional polypeptides (Smith and Tsai, 2007). The occurrence of FAS1-like complexes in algal cell have already been suggested in the oleaginous species *Nannochloropsis oceanica* and *Nannochloropsis gaditana* (Vieler et al., 2012; Alboresi et al., 2016), but not yet in the green lineage,

where, however, the genome resources available for green algae are limited. For *Chlorella* genus, only a few species for which high-quality or draft genomes are available (Blanc et al., 2010, 2012; Gao et al., 2014; Roth et al., 2017; Arriola et al., 2018; Guarnieri et al., 2018; Hovde et al., 2018). In the specific case of *C. vulgaris*, a fragmented genome of 113 scaffolds has been recently reported (Guarnieri et al., 2018), and the high-number of scaffolds jeopardizes an effective implementation of genome editing methods. Indeed, the reported *C. vulgaris* genome has been obtained only based on short-reads produced with Illumina (San Diego, CA, USA) sequencing, whose assembly is challenging and error-prone (Yoshinaga et al., 2018). Moreover, several questions remained unsolved, such as the presence of genes involved in sexual reproduction (Merchant et al., 2007; Blanc et al., 2010; Roth et al., 2017) or the molecular basis for fatty acid biosynthesis (Vieler et al., 2012; Alboresi et al., 2016). In this work, in order to unravel the genetic information underlying *C. vulgaris* features, a combination of different sequencing technologies and optical mapping led to the reconstruction at near-chromosome level of the nuclear, chloroplast and mitochondrial genomes of *C. vulgaris* 211/11P strain. Moreover, we provide functional annotation of the genomes with the help of comparative RNA-seq analyses of strains grown under two most encountered conditions, that is, low light (LL) versus high light (HL).

RESULTS

Chlorella vulgaris biomass productivity and composition

Chlorella vulgaris 211/11P was grown photoautotrophically under LL (70 µmol m^{-2} s^{-1}) or HL (1000 µmol m^{-2} s^{-1}) to evaluate its biomass productivity and composition. Cultivation in HL conditions caused a strong decrease in chlorophyll and an increase in carotenoids/chlorophyll ratio (Figure 1 A and B). This is consistent with previous report for other green algae species as a mechanism to improve photoprotection and decrease the risk of photodamage (Bonente et al., 2012). Growth in HL was faster compared with the LL conditions (Figure 1C). Accordingly, the dry weight harvested when cell density reached the stationary phase was higher for cells grown in HL compared with cells grown in LL (Figure 1D). Cell diameter nevertheless remained similar in LL versus HL conditions (Figure 1E): the two-fold increase in biomass accumulation observed in HL was thus related to a combined effect of increased cell density and, more relevant, of increased weight of individual cell, likely due to different biomass composition. As reported in Figure 1F, starch and protein content per cell were not significantly different in LL compared with HL. Strikingly, HL-grown cells showed a strong increase in lipid accumulation. In particular, the triacylglycerol (TAG) fraction of the total lipid in the cell was increased from 12% in LL to 79% in HL. The increase in TAG content was accompanied by strong decrease in monogalactosyldiacylglycerol (MGDG), digalactosyldiacylglycerol (DGDG) and the phospholipid phosphatidylglycerol (PG) (Figure 2A). This result is consistent with the reduced chlorophyll content

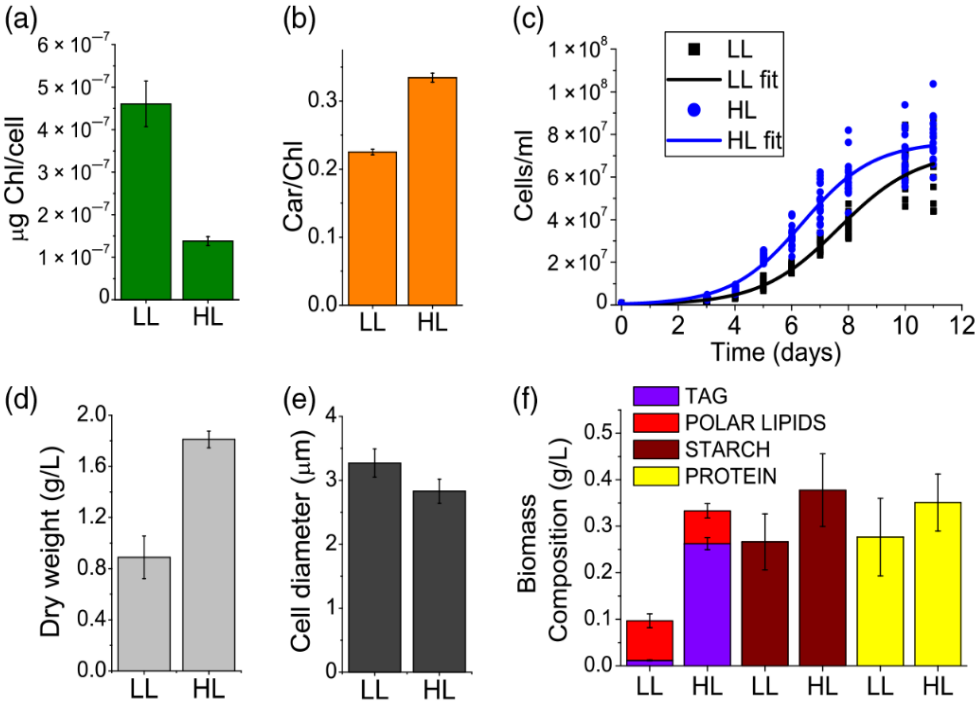

Figure 1. Growth curves, productivity and biomass composition of *Chlorella vulgaris* 211/11P in low light (LL) compared with high light (HL). (a, b) Chlorophyll (Chl) content per cell (a) and carotenoid to chlorophyll ratio (b) in LL and HL. (c) Growth curves of cells grown in LL and HL fitted by sigmoidal function (Hill function). (d) Dry weight of total biomass harvested at the end of the growth curves reported in (a). (e) Average cell diameter at the end of the growth curves reported in (c). (f) Biomass composition analysis in terms of lipids, proteins and starch. Lipid content are indicated either as triacylglycerol (TAG) or as polar lipids (PL, the sum of major membrane lipids). Error bars are reported in terms of standard deviation (n = 3 for data reported in a, b, e, f; n = 10 for data reported in (c) and (d)).

per cell observed in HL, being MGDG, DGDG, sulfoquinovosyldiacylglycerol (SQDG, not detectable in *C. vulgaris* 211/11P) and PG the main lipids present in the thylakoid membranes where chlorophyll binding proteins are embedded (Kobayashi, 2016). The fatty acid profile of cells grown in LL versus HL condition is reported in Figure 2B: HL-grown cells present a strong increase in palmitic acid (16:0), oleic acid (18:1), linoleic acid (18:2) and α-linolenic acid (18:3) with oleic acid as the most abundant fatty acid in HL-grown cells (Figure 2B).

Development of a high-quality reference genome sequence of *Chlorella vulgaris*

In order to investigate the genetic basis underlying the highly productive phenotype of *C. vulgaris* 211/11P, we have sequenced, assembled and functionally annotated its nuclear genome. Genome assembly was obtained by integrating different genomic approaches displaying complementary features, i.e., PacBio producing long-reads, Illumina for accurate short-reads and Bionano optical mapping providing high scaffolding power. Genome sequencing analysis was conducted initially predicting a potential genome size of ~50 Mb, as for other *Chlorella* spp. (Blanc et al., 2010; Arriola et al., 2018; Guarnieri et al., 2018). High coverage (~128x) raw PacBio reads (Table S1) were assembled

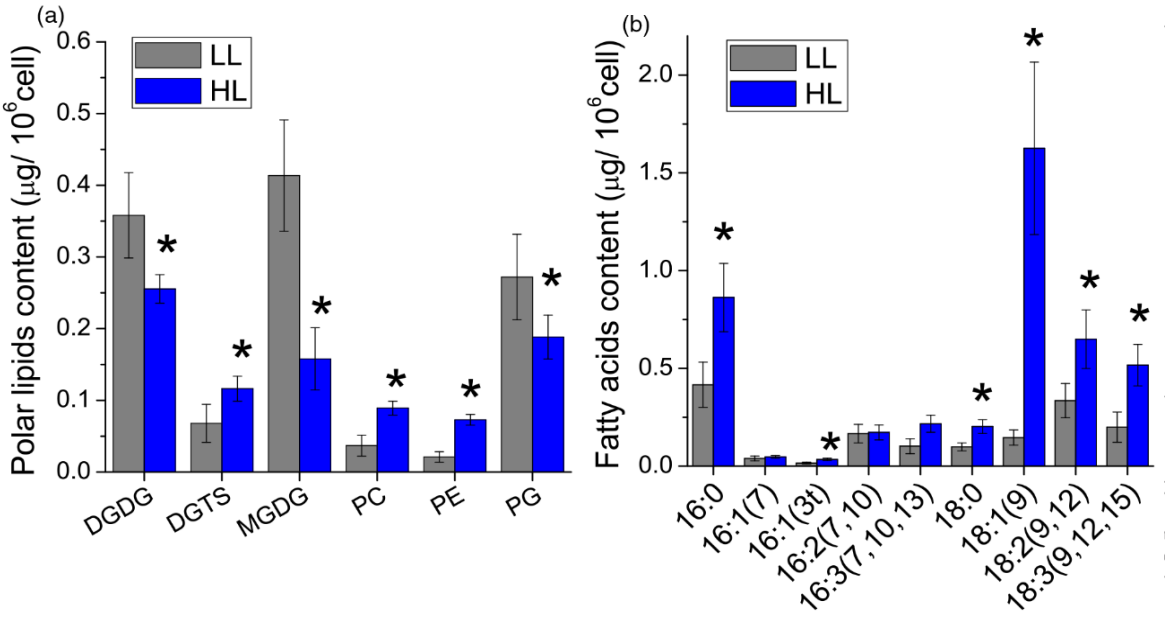

Figure 2. Polar lipid and fatty acid composition in *Chlorella vulgaris* 211/ 11P cells grown in LL versus HL conditions. (a) A given amount of lipid extracts, harvested from LL- or HL-grown conditions, was subjected to thin layer chromatography to investigate polar lipid profile. (b) Fatty acid profiles obtained by gas chromatography techniques as detailed in Materials and methods. Data are means of three biological replicates with standard deviation shown. Significantly different values in HL versus LL are indicated by * ($P < 0.05$). MGDG, monogalactosyldiacylglycerol; DGDG, digalactosyldiacylglycerol; PG, phosphatidylglycerol; PE, phosphatidylethanolamine; PC, phosphatidylcholine; DGTS, diacylglycerol *N,N,N*-trimethylhomoserine.

into a draft genome assembly of 39.8 Mb (Table S2), consisting of 641 Kb and N50 of 1.8 Mb. To improve the quality of the assembled genome, Illumina paired-end reads (~50x, Table S1), as well as raw PacBio reads, were aligned to the PacBio-based assembly to correct sequencing errors: 3076 single-nucleotide variants (SNVs) and 32821 small insertions and deletions (InDel) were corrected, whereas the remaining 81 SNV and 190 InDel account only for the 0.0007% of the reconstructed genome (Table S3). The resulting polished PacBio-based contigs were anchored into a nearly chromosome-scale assembly by integrating optical mapping data (~1400x) obtained using the Bionano Genomics (San Diego, CA, USA) technology (Figure S1 and Table S1). As reported in Table S1, the integration of Bionano data resulted into a genome assembly where 26 of the contigs obtained from PacBio data were anchored into 14 scaffolds (Figure 3) with an N50 value of 2.8 Mb and the longest scaffold of 5.4 Mb. Eight unplaced contigs were identified by subsequent manual analysis as part of the chloroplast and the mitochondrial genomes, and they were therefore removed from the nuclear genome assembly, remaining 29 unplaced contigs that counted only for <1.1%. The 14 scaffolds of the nuclear genome contained 98.9% of the assembled *C. vulgaris* 211/11P genome, i.e. the highest percentage when compared with other algal genomes available (Table 1). The generated assembly represents a greater than 100-fold improvement in contiguity compared with the previously published assembly of *C. vulgaris* UTEX395 (Table S4) and it has the highest N50 among other algal genomes of

similar size as *Chromochloris zofingiensis* (Roth et al., 2017) and *Chlorella variabilis* (Blanc et al., 2010) (Table 1).

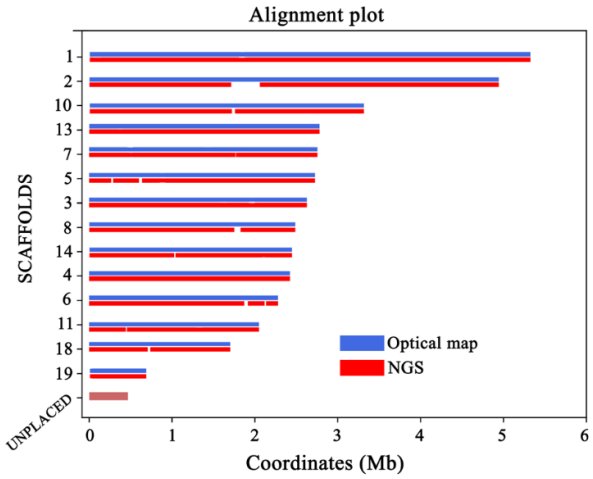

Figure 3. Assembled *Chlorella vulgaris* 211/11P nuclear genome. *Chlorella vulgaris* 211/11P genome was assembled in 14 pseudo-molecules based on integration of next generation sequencing (NGS) and optical maps as described in the main text. The resulting gaps in the assembled genome are reported as white spaces in the NGS data. Unplaced contigs are reported representing <1.1% of the *Chlorella vulgaris* 211/11P genome.

Chlorella vulgaris nuclear genome annotation and phylogenetic analysis

Identification of genes present in the assembled *C. vulgaris* 211/11P genome was performed by integration of directional RNA-seq data obtained from *C. vulgaris* 211/11P cells cultivated in LL and HL into the gene annotation pipeline. Genome annotation identified 10724 genes, coding for 11082 transcripts with an average length of 3062 bp and 8.12 exons per gene on average (Table 1). The gene models predicted for *C. vulgaris* 211/11P were used to determine codon usage (Table S5), which is found similar to the codon usage of *C. reinhardtii* (Merchant et al., 2007). The number of protein-coding genes is significantly higher compared with the previous genome presented for *C. vulgaris* UTEX395 where only 7100 transcripts were predicted (Guarnieri et al., 2018). Consistently, more than 20% of the genes identified in *C. vulgaris* 211/11P was not found in the draft genome of *C. vulgaris* UTEX395 by local BLAST (Figure S2). To further evaluate the transcriptome quality and completeness, Benchmarking Universal Single-Copy Orthologs (BUSCO) analysis was performed on a benchmark of 303 genes putatively found in all eukaryotes in single copy: this analysis identified complete information for 289 (95.4%) of orthologs and fragmented information for 3 (1%), while only 11 genes (3.6%) were missing, demonstrating a high completeness of the *de novo* assembled genome. Furthermore, when the mRNA-seq libraries were aligned to the genome assembly, 85.58 ± 0.32% of reads aligned uniquely (mean ± SD, n = 6) and an additional 11.81 ± 0.37% aligned to multiple locations, indicating that the genome assembly covered nearly all coding genes.

Functional genome annotation performed by BLAST2GO analysis reported 5642 associated to Gene Ontology (GO) terms (Figure 4). As reported in Figure S3, considering the top-hit species distribution, most of the *C. vulgaris* 211/11P genes (~71% of the total genes) were annotated with genes from *Chlorella variabilis*, followed by *Auxenochlorella protothecoides* and *Coccomyxa subellipsoidea*.

	Chlorella vulgaris *211/11P* (this work)	*Chromochloris zofingiensis* (Roth *et al.*, 2017)	*Chlamydomonas reinhardtii* (v5.5) (Merchant *et al.*, 2007; Blaby *et al.*, 2014)	*Chlorella variabilis* NC64A (Blanc *et al.*, 2010)	*Nannochloropsis gaditana* B-31 (Corteggiani Carpinelli *et al.*, 2014)	*Chlorella sorokiniana* *1230* (Hovde *et al.*, 2018)
Sequenced genome size	40 Mbp	57 Mbp	107 Mbp	46.2 Mbp	26.3 Mbp	58.5 Mbp
Genome technologies	PacBio + BioNano + Illumina	PacBio + OpGen + Illumina	Sanger + 454 + BAC + genetic map	Sanger WGS	454 + SOLiD + BAC	PacBio + Illumina
No of scaffold	14	19	17 chromosomes	30	21	20
% scaffolded genome	98.9%	95.4%	98.2%	89%	92.2%	100%
Scaffold N50	2.8 Mbp	3.72 Mbp	7 Mbp	1.5 Mbp	1 Mbp	3.82 Mbp
% G+C	61%	51%	64%	67%	54.2%	63.8%
No of genes	10 724	15 274	17 741	9791	10 646	12 871
Exon average length (bp)	194	291	261	170	449	152
Intron average Length (bp)	207	267	269	209	178	215
Ave Exons Per transcript	8.12	5	8.5	7.3	2.71	10.9

Table 1. Comparison of *Chlorella vulgaris* 211/11P genome with other known microalgae genomes.

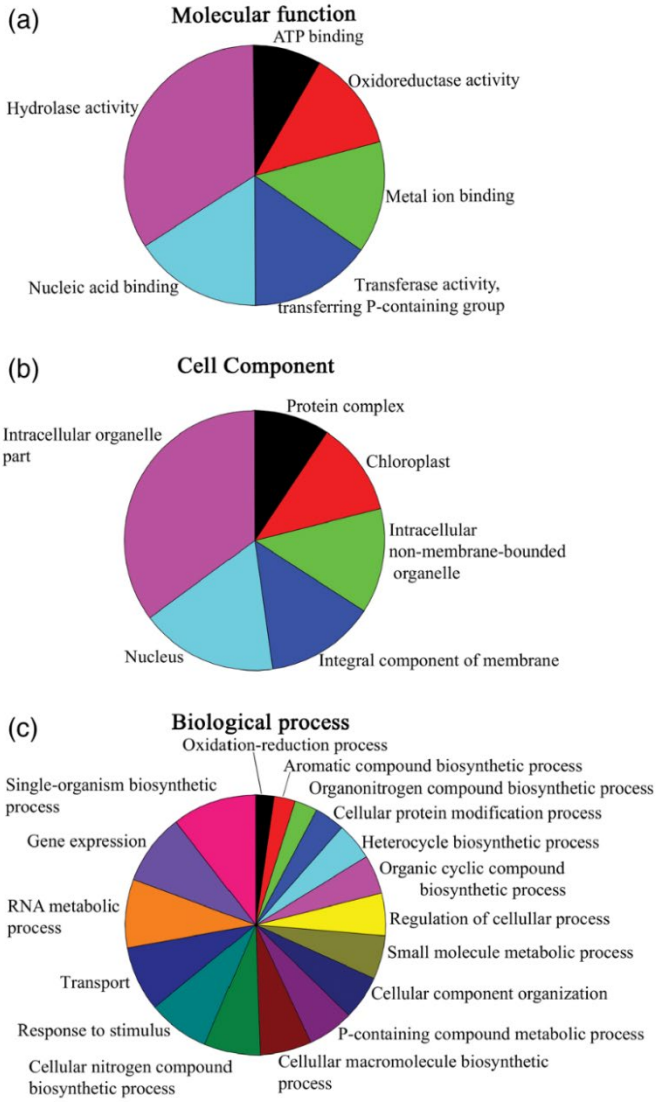

Figure 4. Gene Ontology (GO) classification of annotated *Chlorella vulgaris* 211/11P genes. *Chlorella vulgaris* transcripts annotated using the blast2Go program were functionally grouped based on the GO terms 'molecular function' (a), 'cellular component' (b) and 'biological process' (c). The distribution of the different groups is reported based on the node score associated to each group considering GO term with node score higher than 1%.

Functional annotation of the *C. vulgaris* 211/11P genome was then exploited for the analysis of the phylogenies of the 211/11P strain. In particular, 111 single-copy genes shared with other species with an available genome were used for protein alignment and phylogenetic tree construction. As reported in Figure S4, *C. vulgaris* 211/11P is closely related to *C. vulgaris* UTEX395 strain and to other species from the *Chlorella* genus as *C. variabilis* and *A. protothecoides*.

Chloroplast and mitochondrial genomes

Complete (circular) chloroplast genome of *C. vulgaris* 211/11P was reconstructed with no gaps or ambiguous nucleotides and is 165504 bp in length with 121 genes encoded (Figure 5 and Table 2). The overall GC content of the chloroplast genome is 32%, increased to 35% in coding sequence. Among the genes found in the chloroplast genome six genes encode for rRNA, 18 for ribosomal proteins, 46 genes encode for tRNA, seven genes are component of RNA polymerase and two genes encode for a

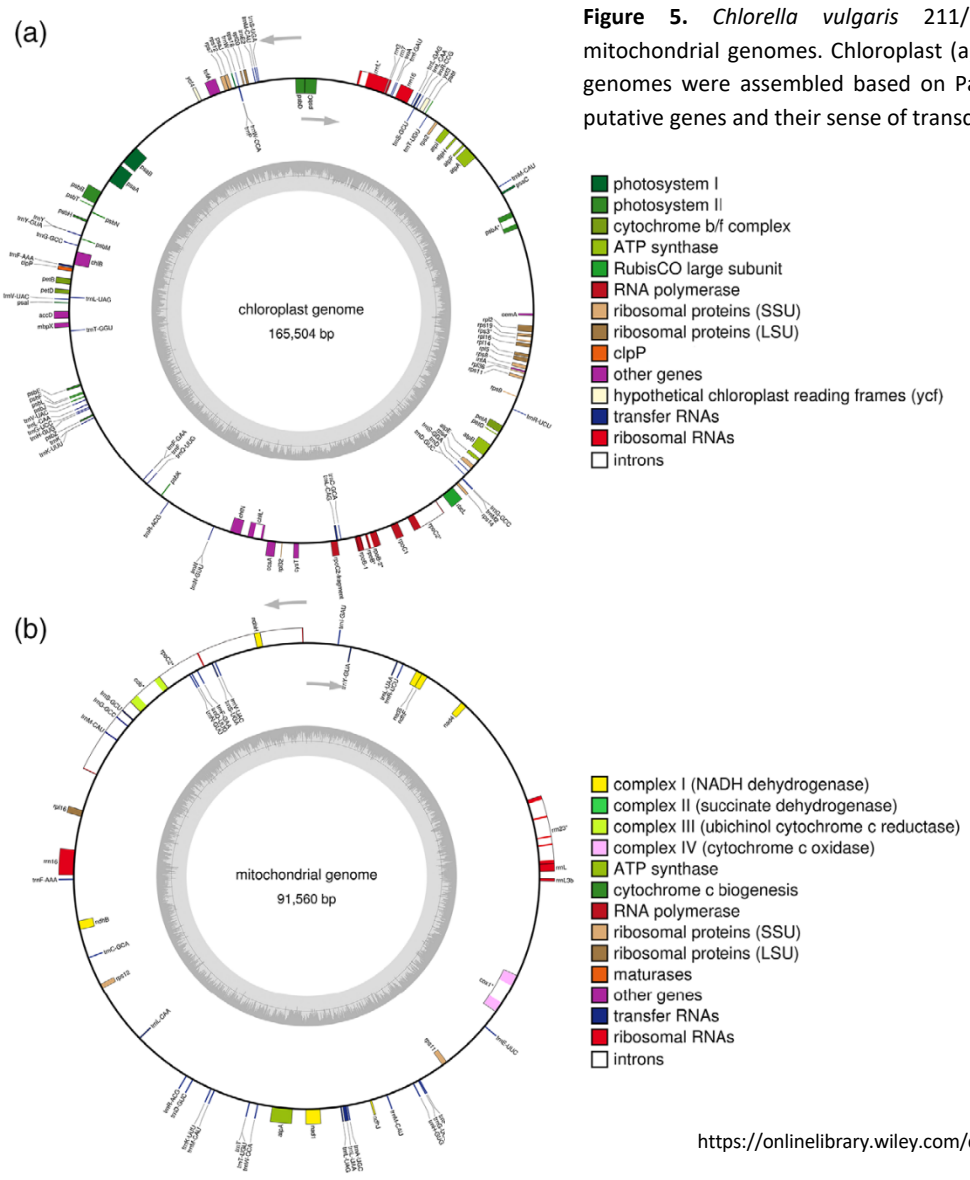

Figure 5. *Chlorella vulgaris* 211/11P chloroplast and mitochondrial genomes. Chloroplast (a) and mitochondrial (b) genomes were assembled based on PacBio data. Location of putative genes and their sense of transcription are indicated.

High resolution image:
https://onlinelibrary.wiley.com/doi/full/10.1111/tpj.14508

translation initiation factor (*infA*) and a protein elongation factor Tu (*tufA*). In total, 31 genes were identified encoding for subunits of the complexes involved in the light phase of photosynthesis (PSI, PSII, cytochrome b_6f and ATP synthase) and a gene for the large subunit of RUBISCO was also identified. Among the other genes present in the *C. vulgaris* 211/11P chloroplast genome, *ycf1-ycf4* were identified with the *ycf3* and ycf4 involved in PSI assembly (Boudreau et al., 1997). Genes involved in plastid division as *minD* and *minE* were also found in the chloroplast genome, as previously reported for other *Chlorella* spp. (Wakasugi et al., 1997). Notably, three introns were identified in genes *psbA*, *rpoC2* and *rrnL* as previously reported for *C. reinhardtii* (Maul et al., 2002). *RpoB*, *chlL* and *rps3* genes were also found to contain introns.

C. vulgaris 211/11P mitochondrial genome was entirely reconstructed as having a 91 560 bp size with 48 genes encoded, for a total of 16% of the coding region (Figure 5, Table 2). The large size of *C. vulgaris* 211/11P mitochondrial DNA is consistent with the mitochondrial genomes of other green algae as *C. zofingiensis* or higher plants, but significantly larger than the mitochondrial genome of some other green algae such as *Chlamydomonas eugametos* or *C. reinhardtii* (Denovan-Wright et al., 1998; Roth et al., 2017). The increased size of *C. vulgaris* 211/11P mitochondrial genome is largely due to the occurrence of high level of non-coding sequences (84%). Among the genes in the mitochondrial genome, four genes encode for rRNA and 30 for tRNA, while three genes encode for ribosomal proteins. Seven genes encoding for subunits of complex I, and two genes for complexes III and IV subunits (*cob* and *cox1* respectively) were also identified together with a gene for alpha subunit of mitochondrial ATP synthase. Notably, a pseudogene *rpoC2* was found also in the mitochondrial genome, even if with a low expression profile (*rpoC2*). *rpoC2* was usually found in the chloroplast genome coding for a RNA polymerase beta subunit (Shimada et al., 1990) but traces of *rpoC2* plastid

Chloroplast genome	*Chlorella vulgaris* 211/11P (this work)	*Chromochloris zofingiensis* (Roth *et al.*, 2017)	*Chlamydomonas reinhardtii* (v5.5) (Merchant *et al.*, 2007; Blaby *et al.*, 2014)	*Chlorella variabilis* NC64A (Blanc *et al.*, 2010)	*Nannochloropsis gaditana* B-31 (Corteggiani Carpinelli *et al.*, 2014)
Sequenced genome size	165 kbp	181 kbp	204 kbp	125 kbp	115 kbp
Annotated protein-coding genes	71	71	67 + 1 (tscA)	79	93
Annotated rRNAs	4	6	10	3	6
Annotated tRNAs	46	31	29	31	28
% G+C	31.7%	31%	34%	34%	54.2%

Mitochondrial genome	*Chlorella vulgaris* 211/11P (this work)	*Chromochloris zofingiensis* (Roth *et al.*, 2017)	*Chlamydomonas reinhardtii* (v5.5) (Merchant *et al.*, 2007; Blaby *et al.*, 2014)	*Chlorella variabilis* NC64A (Blanc *et al.*, 2010)	*Nannochloropsis gaditana* B-31 (Corteggiani Carpinelli *et al.*, 2014)
Sequenced genome size	92 kbp	42 kbp	16 kbp	78 kbp	42 kbp
Annotated protein-coding genes	14	22	8	32	5
Annotated rRNAs	4	6	14	3	2
Annotated tRNAs	30	24	3	27	26
% G+C	29.8%	36%	45%	28%	54.2%

Table 2. Comparison of *Chlorella vulgaris* 211/11P chloroplast and mitochondrial genome with other known microalgae genomes.

gene in the mitochondrial genome have been already reported occasionally in mitochondrial genome of land plants (Goremykin et al., 2009; Straub et al., 2013). This result suggests an uncommon horizontal gene transfer from chloroplast to mitochondrial genome in *Chlorophyta* which was previously reported only upon land colonization (Wang et al., 2007; Gandini and Sanchez-Puerta, 2017).

Differential gene expression in high light versus low light conditions

RNA-seq data allowed us to identify the genes which were differently expressed in LL versus HL. In particular, 684 genes were upregulated in LL, while 816 genes were upregulated in HL. GO classification of differentially expressed genes is reported in Figure S5. Putative transcription factors upregulated in LL or HL are reported in Table S6 with 23 genes and 16 genes, respectively, being identified. The genes showing the highest differential transcription (highest log2FC) in LL or in HL are reported in Table S7: genes encoding for chlorophyll binding proteins, nitrate transporter, ferric reductase, protein involved in the cell cycle and a subunit involved in mRNA stability were identified among the genes upregulated in LL. These findings agree with the higher content of chlorophyll per cells in LL, and with the involvement of nitrogen and iron metabolism involved in the biosynthesis of these pigments. In HL the genes showing the strongest upregulation were those encoding proteins for lipoylation, acetyl-CoA synthetase, early light-inducible chloroplastic-like proteins, H (+) hexose cotransporter and a cryptochrome subunits. Genome annotation and analysis of differentially expressed genes were then used to elucidate the different metabolic pathways and their changes in LL versus HL. Some of these pathways are detailed in the following sections.

Identification of genes involved in key metabolic pathways

The functional annotation of the *C. vulgaris* 211/11P genome allowed the identification of genes coding for the key enzymes involved in the different metabolic pathways of the cell, such as glycolysis, gluconeogenesis, the tricarboxylic acid (TCA) and glyoxylate cycles, photosynthesis, lipid and pigment metabolism (Table S8–S10). Genes involved in some critical metabolic pathways and cellular functions are described in detail here.

Photosynthesis. All genes, except for the *psbX* gene, encoding subunits of the membrane complexes or soluble electron carriers involved in the light phase of photosynthesis, are encoded either by nuclear or chloroplast genomes of *C. vulgaris* 211/11P (Table S8). Genes encoding for PSII core subunits were identified in the chloroplast and nuclear genome, in agreement with previous data reported for *A. thaliana* and *C. reinhardtii* (Daniell et al., 2016). No homologous gene could be found in the *C. vulgaris*

211/11P genome only in the case of the *psbX* gene. PSBX is a low molecular mass subunit of Photosystem II, which has been reported previously in higher plants and in some algae (Shi et al., 1999; Shi and Schröder, 2004). Antisense genotypes on this subunit in *A. thaliana* or knockout mutants in cyanobacteria were characterized by a 30–40% reduction of PSII accumulation, but no apparent growth phenotype was observed, suggesting this subunit is not essential for the photosynthetic process (Shi et al., 2012).

For the PSI complex, all core subunits were identified with the exception of PsaM and PsaX: PsaM has been previously reported in cyanobacteria, in some green algae, mosses and gymnosperms but not angiosperms, whereas PsaX has only been found in cyanobacteria (Scheller et al., 2001). Different genes were identified in *C. vulgaris* 211/ 11P genome encoding for Light Harvesting Complexes (LHC), the pigment-binding antenna proteins bound to the periphery of photosystems devoted to light harvesting and photoprotection.

While both LHCII and LHCI type complexes could be identified, being bound to PSII and PSI respectively, no gene coding for a LHCB6 (CP24) protein was found, supporting that this PSII antenna proteins appeared only in land plant, in agreement with previous finding (Kouřil et al., 2016). Interestingly a homolog for the LHCB4 (CP29) subunit could not be found in the *C. vulgaris* UTEX395 genome (Table S8). Most of the genes encoding for LHC complexes were heavily downregulated in HL, in agreement with the reduced chlorophyll content per cell observed in this condition (Figure 1).

Notably both the LHC-like subunits PSBS and LHCSR were found in *C. vulgaris* 211/11P encoded by single genes: these subunits are involved in the photoprotective mechanism known as non-photochemical quenching (NPQ), where a significant portion of the excitation energy absorbed by photosystems is thermally dissipated (Li et al., 2000; Peers et al., 2009). Distinct from *C. reinhardtii*, where LHCSR subunits are strongly overexpressed in HL (Peers et al., 2009), *lhcsr* gene in *C. vulgaris* 211/11P is constitutively expressed either in LL- or HL-grown cells (Table S8). Also, for *psbs*, *C. vulgaris* 211/11P behaves differently compared with *C. reinhardtii*: in the latter *psbs* is only transiently expressed under UV or HL conditions (Allorent et al., 2016; Correa-Galvis et al., 2016; Tibiletti et al., 2016), whereas in *C. vulgaris* 211/11P the *psbs* gene is always expressed but upregulated in HL (Table S8), as in the case of *A. thaliana* (Ballottari et al., 2007). These results suggested a different regulation of NPQ in *C. vulgaris* 211/11P compared with *C. reinhardtii*, even if the potential role of LHCSR and PSBS in NPQ induction in the former require additional confirmatory experiments.

Genes encoding for protein subunits reported in *C. reinhardtii* and involved in alternative chloroplast electron transport pathways are present in the *C. vulgaris* 211/11P genome, but not differently expressed in LL or in HL (Table S8), such as PGRL1 (Petroutsos et al., 2009), PGR5 (Johnson et al., 2014) and a type II calcium-dependent NADH dehydrogenase (NDA2) (Desplats et al., 2009; Saroussi et al.,

2016), involved in cyclic electron flow or PTOX involved in chlororespiration (Rumeau et al., 2007; Houille- Vernes et al., 2011).

For the dark phase of photosynthesis and carbon fixation, all subunits previously reported to be involved in this pathway have been identified (Table S8) but generally not differently expressed in LL versus HL. Only phosphoglycerate kinase and ribose 5-phosphate isomerase showed upregulation in LL: these enzymes are also involved in the oxidative pentose phosphate pathway, which might be more relevant in LL than in HL.

Notably, based on the KEGG Mapper tool, all enzymes required for a C4-like carbon fixation pathway are present in the *C. vulgaris* 211/11P genome (Figure S6), with the key enzyme involved in carbon fixation in C4 compound phosphoenolpyruvate carboxylase (PPC), encoded by two genes g3928 and g4635, predicted in the cytosol and in the mitochondria, respectively. These two isoforms of PPC might have a role in oxaloacetate formation in the anaplerotic reactions, or for gluconeogenesis or as alternative carbon fixation to RUBISCO, as previously suggested for *C. sorokiniana* (Cecchin et al., 2018).

Carotenoid biosynthesis. Carotenoid biosynthetic genes were identified in the *C. vulgaris* 211/11P genome (Table S8). Each of the genes involved in carotene and xanthophyll biosynthesis was found in single copy with some particular genes such as prolycopene isomerase, ζ-carotene desaturase and ζ-carotene isomerase being identified in the *C. vulgaris* 211/11P but not in the *C. vulgaris* UTEX395 genome. Notably, a gene coding for neoxanthin synthase could be identified in *C. vulgaris* 211/11P (Figure S7), catalyzing the synthesis of neoxanthin from violaxanthin (Dall'Osto et al., 2007), even if further experimental evidences are required to support the enzymatic activity of the putative neoxanthin synthase herein identified. Most of the genes encoding for enzymes involved in carotenoid biosynthesis were present in higher levels in HL (Table S8), in agreement with the increased carotenoid content per cell identified in this condition (Figure 1). In the *C. vulgaris* 211/11P genome no gene coding for a beta-carotene ketolase (BKT) was identified. This is the key enzyme together with a hydroxylase (CRTZ) for astaxanthin biosynthesis from beta-carotene or zeaxanthin in different algal species known to accumulate astaxanthin as *Haematococcus lacustris* (formerly known as *Haematococcus pluvialis*) or *C. zofingiensis* (Zhong et al., 2011). Whereas CTRZ is present in *C. vulgaris* 211/11P and upregulated in HL (gene g8453), the absence of BKT explains the absence of astaxanthin in this organism and suggests the possibility of biotechnological manipulation to induce the accumulation of this carotenoid that would have increased value to the market for *C. vulgaris*.

Glycolysis, gluconeogenesis and oxidative pentose phosphate pathway. Complete set of genes encoding for glycolysis and gluconeogenesis were retrieved in the *Chlorella vulgaris* 211/11P genome. Most of these genes were not differently expressed in LL versus HL except for genes coding a chloroplastic phosphoglycerate kinase and a cytoplasmic fructose-bisphosphate aldolase, and fructose- 1,6-bisphosphatase I, which were all downregulated in HL. While fructose-bisphosphate aldolase might be involved in both glycolysis and gluconeogenesis, fructose-1,6-bisphosphatase I is specifically involved in gluconeogenesis, leading to the accumulation of fructose-6P (Rufty and Huber, 1983). Considering the cytoplasmic predicted localization of both enzymes fructose-bisphosphate aldolase and fructose-1,6-bisphosphatase I upregulated in LL, a possible downregulation of cytosolic gluconeogenesis in HL can be proposed as a consequence of redirection of carbon flow towards lipid accumulation (Figure 1). The upregulation of chloroplastic phosphoglycerate kinase in LL is consistent with upregulation of the gene encoding ribose 5-phosphate isomerase (Table S8). These enzymes are involved in both carbon fixation and the oxidative pentose phosphate pathway and their upregulation in LL might be related to reduced photosynthetic NADPH formation at low irradiance, therefore with increased requirement for NADPH formation by oxidative pentose phosphate pathway. Further experimental evidence is required to support this hypothesis.

TCA cycle and glyoxylate cycle. Genes encoding for enzymes involved in the TCA cycle and the glyoxylate cycle were identified in *C. vulgaris* 211/11P. Among these genes, differential expression in LL versus HL was observed only for two genes encoding citrate synthase and malate synthase, both upregulated in HL. Interestingly both enzymes catalyze reactions in which acetyl-CoA is a substrate (Figure 6): citrate synthase catalyzes acetyl-CoA binding to oxaloacetate, forming citrate as the initial step in the TCA cycle or in the glyoxylate cycle. Malate synthase is involved in the glyoxylate cycle, catalyzing malate formation from acetyl-CoA and glyoxylate (Boyle and Morgan, 2009; Plancke et al., 2014). Glyoxylate cycle has been reported to be in ancestral peroxisomes in *C. reinhardtii* (Kong et al., 2017) but its localization should be further investigated in *C. vulgaris*. HL acclimation therefore stimulated upregulation of genes encoding for enzymes involved in acetyl-CoA consumption, which is likely to be more abundant at high irradiance due to increased carbon fixation and increased sugar production.

Lipid biosynthesis. Genes encoding key proteins of lipid metabolism were identified in *C. vulgaris* 211/11P genome, most of which showed alterations in transcription upon HL exposure (Table S9). Consistent with increased TAG accumulation under HL (Figure 1F), the genes encoding enzymes involved in earlier steps of *de novo* fatty acid synthesis, the formation of glycerol-3-phosphate (G3P)

and TAG packaging proteins were upregulated (Table S9). Intriguingly, no change in the expression of genes involved in polar membrane lipid synthesis nor TAG assembly enzymes was observed. Among the highly upregulated genes was a gene coding for acetyl-CoA synthetase (ACS). ACS is involved in the pyruvate dehydrogenase bypass pathway, by which acetyl-CoA is produced by glycolytic pyruvate through the intermediates acetaldehyde and acetate (Lin and Oliver, 2008). The importance of ACS enzymes in lipid biosynthesis in plant cells has been demonstrated in *A. thaliana*, in which mutations in *acs* genes caused a strong reduction in plant fitness (Lin and Oliver, 2008). Two genes coding for ACS enzymes were identified in *C. vulgaris* 211/11P, g2176 and g2145, the former being predicted in the cytosol, while the latter in the chloroplast: only the gene encoding the cytosolic ACS was upregulated in HL, suggesting a possible cytoplasmic biosynthesis of fatty acids triggered by HL exposure (Figure 6). However, fatty acid biosynthesis in *Chlorophyta* was generally considered to occur in the chloroplast catalyzed by fatty acid synthase (FAS) type II complex, while cytosolic fatty acid biosynthesis occurs in fungal/animal cells catalyzed by FAS type I complex (Schweizer and Hofmann, 2004). In HL conditions, several genes encoding for FAS type II subunits were downregulated (Figure 6 and Table S9), with the only exception being the chloroplastic malonyl-CoA: ACP transacylase. Intriguingly, in addition to genes coding for FAS type II subunits, a single large gene encoding for polyketide synthase (PKS)/FAS type I multisubunit complex was also identified (g276). The occurrence of PKS/FAS1-like complexes in algal cells has already been reported in the oleaginous species *Nannochloropsis oceanica* and *Nannochloropsis gaditana*, and suggested to be involved in cytosolic biosynthesis of fatty acids (Vieler et al., 2012; Poliner et al., 2015; Alboresi et al., 2016). For *Chlorophyta*, several PKS multisubunit complexes have been reported (Poliner et al., 2015; Heimerl et al., 2018), even if their function is still under debate. For *C. reinhardtii*, a PKS complex has been reported to be expressed only during zygote formation and to be involved in zygote maturation (Heimerl et al., 2018). The putative PKS/FAS type I gene identified in *C. vulgaris* 211/11P is 55 kbp and contains all the protein domains required for fatty acid biosynthesis containing 11 β-ketoacyl synthetase domains, nine ketoreductase domains, nine dehydroreductase domains and six enoylreductase domains (Smith and Tsai, 2007; Schweizer and Hofmann, 2004) (Figure S8). The absence of an acyltransferase domain can be compensated by the cytoplasmic isoform of malonyl-CoA: ACP transacylase enzyme (Figure S9), which catalyzes the acyltransferase reaction required for fatty acid biosynthesis by the PKS/FAS type I multisubunit complex identified. Consistent with the increase in several polyunsaturated fatty acids (Figure 2), upregulation under HL of *FAD4* (Zäuner et al., 2012) and *FAD7* (Nguyen et al., 2013) encoding genes was found.

In addition to *de novo* fatty acid biosynthesis, enzymes involved in the supply of glycerol backbones and TAG packaging were upregulated in HL. Two G3P dehydrogenase (GPD) enzymes were indeed

identified in the *C. vulgaris* 211/11P genome, but only the non-chloroplastic GPD2 was upregulated in HL: this enzyme has been reported in *C. reinhardtii* to be involved in supplying G3P for TAG synthesis and accumulation in nutrient starvation (Driver et al., 2017).

HL acclimation led to an increased accumulation of several plastid (PLAP/fibrillin) lipid-associated proteins: these subunits have been reported to be involved in the formation of lipid droplets (LDs) observed in cells accumulating neutral lipids or carotenoids (Youssef et al., 2010), which are both strongly increased under HL in *C. vulgaris* 211/ 11P (Figure 1). Surprisingly, no genes encoding oleosin or major lipid droplet protein (MLDP) were identified in *C. vulgaris*; these proteins are the main LD-associated proteins reported in higher plants (Murphy, 2012) and green algae (Moellering and Benning, 2010), respectively. Two genes were identified encoding for caleosin, a calcium binding protein that can be found in multicellular plants and green algae, and frequently described as an LD-associated protein (Lin et al., 2012; Charuchinda et al., 2015). Among the two caleosin genes identified in *C. vulgaris* 211/11P, none was upregulated in HL, but rather the g8244 gene was downregulated under these conditions. This result suggested that LD formation under HL involved not only *de novo* synthesis of fatty acids and TAG accumulation but also synchronization with LD packaging proteins.

Identification of genes involved in meiosis and motility. C. vulgaris strains have been usually described as nonmotile and asexual (Yamamoto et al., 2004). Genes previously reported to be associated with meiosis and motility were searched for in the *C. vulgaris* 211/11P genome. Previously DMC1 and Rad51 DNA recombinase homologs were reported in the *C. vulgaris* genome (Guarnieri et al., 2018). In addition to DMC1 and Rad51 DNA recombinase homologs, the main genes involved in meiosis (Malik et al., 2007) were present and transcribed in the *C. vulgaris* 211/11P genome (Table S8) and this situation is similar to that previously reported for other green algae such as *C. zofingiensis* (Roth et al., 2017) or *C. variabilis* NC64A (Blanc et al., 2010) in which sexual reproduction is cryptic and not well defined. This result suggested a possible sexual reproductive stage also in *C. vulgaris* 211/11P with gamete formation. In agreement with this finding, a gene in the *C. vulgaris* 211/11P genome encoding gametolysin was found (g3347), together with a gene encoding a protein containing a domain with a putative CGS1/HAP2 function and that is essential for cell fusion (Blanc et al., 2010; Wong and Johnson, 2010) (Figure S10). The genes involved in motility were then investigated by comparison with the genes listed in CiliaCut, a group of genes identified in *C. reinhardtii* involved in the formation of sensory or motility cilia and flagella (Merchant et al., 2007). Among the 195 genes in CiliaCut, 114 genes were identified in *C. vulgaris* 211/11P (58.4%). In particular, 78.2% of the genes in CiliaCut that were present in the diatom *Thalassiosira pseudonana* were present also in *C. vulgaris* 211/11P (Table S10): 84.2% of the *T. pseudonana* genes in MotileCut (genes in CiliaCut involved in motile flagella functions) were

present also in *C. vulgaris* 211/11P. This result suggested that *C. vulgaris* 211/11P might be able to form gametes with motile flagella as previously observed for *T. pseudonana* during gametogenesis (Moore et al., 2017).

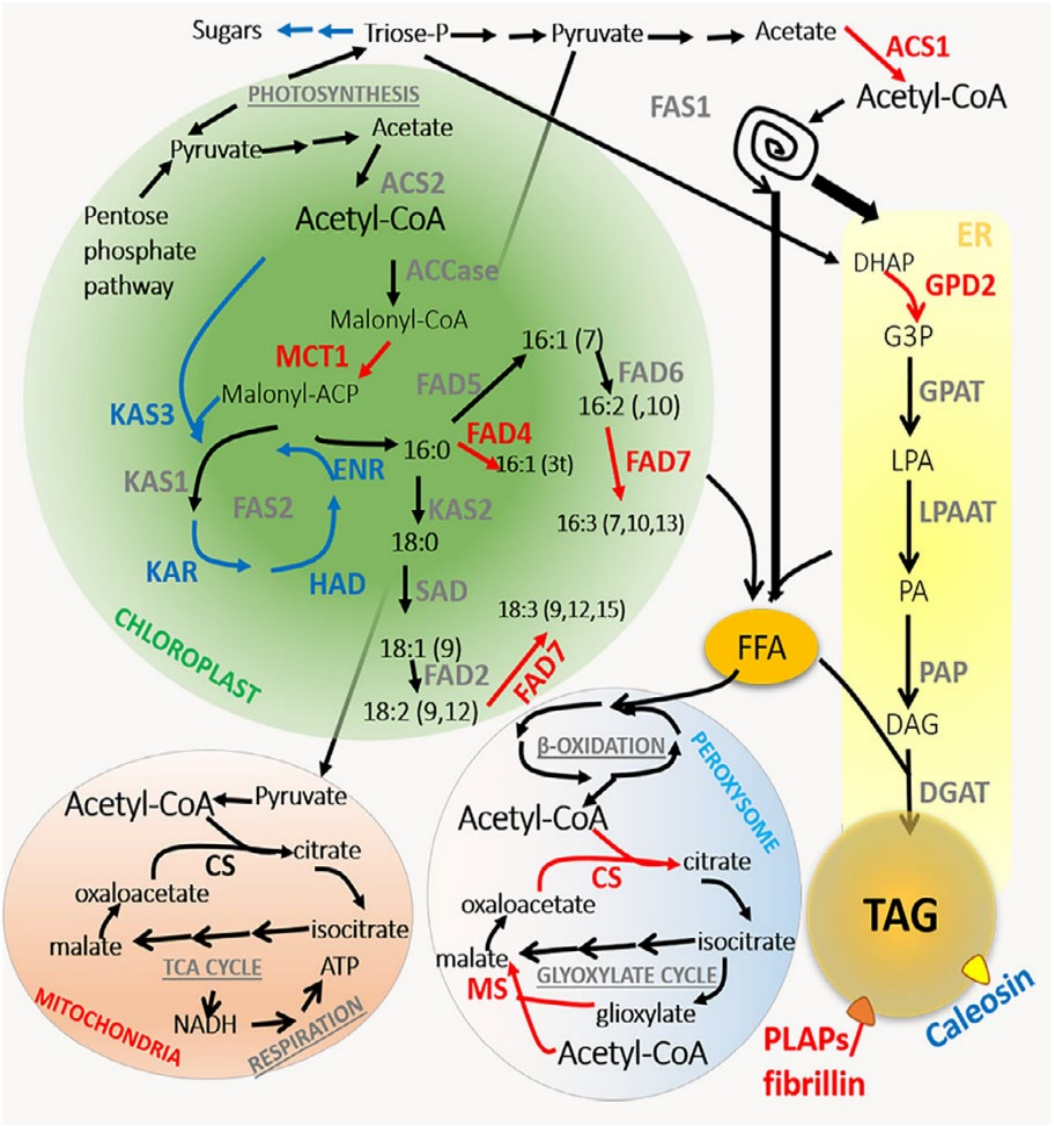

Figure 6. A schematic model of lipid biosynthesis in *Chlorella vulgaris* 211/11P. Proteins encoded by differently expressed genes are indicated in red (upregulated in HL) or in blue (downregulated in HL). Similar color code is used for chemical reactions catalyzed by differently expressed enzymes. ACCase, acetyl-CoA carboxylase; MCT, malonyl-CoA: ACP transacylase; KAS, 3-ketoacyl- synthase; KAR, 3-oxoacy-ACP reductase; HAD, 3-hydroxyacyl-ACP dehydratase; ENR, enoyl- ACP reductase; FAS1/2, fatty acid synthase type 1/2; SAD, stearate desaturase; FAD2, ω-6 fatty acid desaturase, Δ12; FAD4, Δ3 palmitate desaturase; FAD5, palmitate Δ7 desaturase; FAD6, ω6 fatty acid desaturase; FAD7, chloroplast glycerolipid ω3 fatty acid desaturase; FFA, free fatty acids; CS, citrate synthase; MS, malate synthase ACS, acetyl-CoA synthase; DHAP, dihydroxyacetone phosphate; GPD, glycerol-3-phosphate dehydrogenase; G3P, glycerol-3-phosphate; GPAT, Glycerol-3-phosphate *O*-acyltransferase; LPA, lysophosphatidic acid; LPAAT, lysophosphatidic acid acyltransferase; PA, phosphatidic acid; PAP, phosphatidate phosphatase; DAG, diacylglycerol; DGAT, diacylglycerol acyltransferase; PLAPs/fibrillin, Plastid-lipid-associated protein PAP/fibrillin family protein; ER, endoplasmic reticulum; TAG, triacyclglycerols.

DISCUSSION

Integration of highly accurate Illumina sequencing with long-reads (PacBio) and optical mapping (Bionano Genomics) allowed us to obtain the assembled genome of *C. vulgaris* 211/11P in 14 scaffolds with a relatively good N50 of 2.8 Mb. This is a >100-fold improvement compared with the recently released *C. vulgaris* genome (Guarnieri et al., 2018) (Table S4). We can speculate that the 14 pseudo-molecules reconstructed may represent the chromosomes of *C. vulgaris* 211/11P, with 98.9% of scaffolded genome, a much higher percentage compared with most other available genomes of green algae (Table 1). The *C. vulgaris* 211/11P genome size of 40 Mbp was close to that of other members of the *Chlorella* genus or closely related species (Table 2). The GC content of the *C. vulgaris* 211/11P genome was similar compared with *C. variabilis* or *C. reinhardtii*, but higher compared with *C. zofingiensis*. The integration of RNA-seq data allowed us to obtain a detailed functional annotation of the assembled *C. vulgaris* 211/11P genome with a number of transcripts and proteins consistent with the data reported for *C. variabilis*, but almost halved compared with *C. reinhardtii* or *C. zofingiensis*, revealing a strong variability in the green lineage. For comparison, for the microalga *Nannochloropsis gaditana* (Heterokonta) with a much smaller genome (23 Mbp) a similar protein number compared with *C. vulgaris* 211/11P was observed. Notably, exon and intron average length and the number of exons per transcript were similar when compared with another member of the *Chlorella* genus, *Chlorella variabilis* NC64A, but shorter compared with *C. reinhardtii* or *C. zofingiensis* (Table 1). It is worth noting that the improved quality of genome and functional annotation of *C. vulgaris* 221/11P strain allowed us to identify 2285 genes that were not previously predicted in *C. vulgaris* UTEX395 strain (Guarnieri et al., 2018), among which were genes highly differently expressed in LL versus HL conditions, transcription factors putatively involved in HL or LL acclimation, enzymes involved in carotenoid biosynthesis and genes involved in motility (Tables S6–S10). The absence of these and other genes in the previously reported genome of *C. vulgaris* UTEX395 strain could be related to the fact that *C. vulgaris* 211/11P and UTEX395 strains are different (Figure S5) or to the low quality of the reported *C. vulgaris* UTEX395 genome (Table S4).

The results obtained by genome assembly and functional annotation revealed the presence of some peculiar features in *C. vulgaris* 211/11P in common with higher plants, but different from the model organism for green algae, *C. reinhardtii*. Evidence for horizontal transfer from the chloroplast to the mitochondria could be found in *C. vulgaris* 211/11P, as for fragments of plastid *rpoC2* gene found as a pseudogene in the mitochondrial genome. Chloroplast gene or gene fragments were indeed previously observed only in mitochondria of higher plants, attributed to the earlier event of plastid to mitochondria horizontal gene transfer to the common ancestor of extant angiosperms and gymnosperms: the analysis of *C. vulgaris* 211/11P genome demonstrated that this horizontal gene

transfer can be found also in some *Chlorophyta*, but not in the model organism for green algae *C. reinhardtii* (Wang et al., 2007). The possible functions of plastid genes in mitochondrial genome is still not clear, being usually not expressed (Wang et al., 2007). For *C. vulgaris* 211/11P, the plastid gene *rpoC2* was found in the mitochondrial genome as a fragment with a low expression profile: further experiments are required to investigate its possible role in mitochondrial gene expression.

Another plant-like feature found in *C. vulgaris* 211/P is the mitochondrial genome size (91.5 kbp), which is larger than the mitochondrial genome of *C. reinhardtii* (15.7 kbp) and more similar to the mitochondrial genome found for higher plants (Blaby et al., 2014).

A mixed situation compared with higher plants and other green algae was found in *C. vulgaris* 211/11P considering the genes involved in photoprotection. LHCSR subunits have been reported to be critical for tuning photosynthetic efficiency and photoprotection in microalgae (Peers et al., 2009; Berteotti et al., 2016) while PSBS has a similar function in higher plants (Li et al., 2000). In *C. reinhardtii* LHCSR subunits are upregulated in HL (Peers et al., 2009) while PSBS is only transiently expressed in HL or upon UV exposure (Allorent et al., 2016; Correa-Galvis et al., 2016; Tibiletti et al., 2016). In *C. vulgaris* 211/11P both LHCSR and PSBS genes are expressed in LL and HL, with only PSBS being upregulated in HL (Table S8), adding further evidence of the strongly debated role of PSBS protein also in green algae and not only in higher plants. LHCSR and PSBS accumulation and functioning should be further investigated in detail in *C. vulgaris* to determine their role in photoprotection and HL acclimation.

In other cases, genes found in higher plants and in *C. reinhardtii* were not identified in *C. vulgaris*, as for oleosins: these proteins are the major lipid droplet-associated proteins found in higher plants, but their conservation was reported also for some green algae as *C. reinhardtii* and *Volvox carterii* (Huang et al., 2013). *C. vulgaris* 211/11P was also characterized by the absence of genes encoding MLDP proteins, the major proteins involved in LD formation in green algae (Moellering and Benning, 2010) as for the other green alga species *Auxenochlorella protothecoides* (Lin et al., 2012). Rather, caleosins and PLAP/ fibrillin proteins were the main proteins involved in LD formation in *C. vulgaris* 211/11P with a strong upregulation of the latter under HL conditions in which TAGs are mainly accumulated (Figure 1). These finding suggested a divergent evolution among green algae, leading to specialized molecular mechanisms at the base of the phenotypes observed with an evolutive pressure driven by interaction with the environment. Caleosins have been reported to be present both in higher plants and in green algae with a peroxidase activity associated that was proposed to be involved in oxylipin production (Charuchinda et al., 2015): oxylipins are molecules produced by enzymatic or non-enzymatic fatty acid oxidation that trigger the cell response to oxidative stress. In LL-adapted *C. vulgaris* 211/11P cells, caleosin genes were upregulated (Table S9), suggesting their main role in LD formation in LL with the possibility to produce oxylipin upon oxidative stress. In contrast, when cells were acclimated to HL

conditions, these gene were downregulated, this was likely to be due to the previous activation of cell mechanisms allowing HL acclimation and prevention of oxidative stress. Further experiments are required to validate the role of caleosins and PLAP/fibrillin proteins in TAGs accumulation and HL acclimation.

HL acclimation led to a strong increase in TAG and a decrease in the main lipids found in thylakoid membranes, such as galactolipids MGDG, DGDG and the phospholipid PG. Reduction of thylakoid lipids in HL is indeed consistent with a decrease in the chlorophyll content per cell and downregulation of the main chlorophyll binding proteins, the LHC (Table S8) in these conditions, as a consequence of increased irradiation and the reduced need for light harvesting. The observed TAG accumulation suggested that increased carbon fixation redirects carbon flow towards fatty acid biosynthesis with strong increase in the HL of palmitic acid (16:0), oleic acid (18:1), linoleic acid (18:2) and α-linolenic acid (18:3) (Figure 2). These fatty acids are then assembled into TAGs and stored in LDs.

The genomic and transcriptomic data described here allowed us to draw a model based on this phenotype, as discussed (Figure 6), taking into consideration that further events in translation or posttranslational levels could also take place, affecting the highlighted metabolic pathways. Potential dual sites for fatty acid biosynthesis in *C. vulgaris* 211/11P can be proposed based on identification of cytosolic ACS involved in the pyruvate dehydrogenase bypass pathway (Lin and Oliver, 2008), a PKS/FAS type I and a cytosolic malonyl-CoA: ACP transacylase. Cytosolic lipid production by PKS/FAS type I is a common metabolic pathway in animal and fungal cells but it was recently suggested to be present also in some microalgae species (Vieler et al., 2012; Alboresi et al., 2016); further experimental evidence is required to support this finding in *C. vulgaris*. The similar starch content per cell observed in HL further suggested that the increased carbon fixation caused increased triose-P to be used to produce acetyl-CoA in the plastid and, in the cytosol, to produce precursors for fatty acid biosynthesis. Accordingly, enzymes involved in cytosolic gluconeogenesis were downregulated in HL, suggesting a preferential use of chloroplast-derived triose-P to produce pyruvate and acetyl-CoA. Increased lipid accumulation in *C. vulgaris* 211/11P in HL can therefore be related to increased acetyl-CoA production in the chloroplast and in the cytosol by ACSs leading to upregulation of enzymes involved in TAG assembly, as the GDP2 enzyme and LD stabilization, as PLAP/fibrillin subunits (Figure 6). Further experiments are required to validate the metabolic model proposed in Figure 6 that, at the present stage, is based only on genomic and transcriptomic data. The different enzymes involved in lipid accumulation (Table S9) and the transcription factor identified as differently expressed in HL versus LL (Table S6) could be potential targets for biotechnological manipulation of *C. vulgaris* to increase lipid production and biomass productivity.

Interestingly, genes involved in sexual reproduction and motility were also identified in *C. vulgaris* 211/11P (Table S10) even if further research activity is required to induce gamete formation and mating under laboratory conditions. Understanding sexual reproduction in this species would be critical for accumulating in the same strain genetic traits for increased productivity.

In conclusion, the assembly and functional annotation of the *C. vulgaris* 211/11P genome potentially enabled the application of genome-editing technologies in this species and allowed the identification of potential targets for biotechnological manipulation of this organism, for its exploitation for biomass and high value products or for transferring specific *C. vulgaris* 211/11P properties to other species.

MATERIALS AND METHODS

***Chlorella vulgaris* cultivation.** The *C. vulgaris* 211/11P strain was obtained from the Culture Collection of Algae at Goettingen University (CCAP 211/11P strain). Cells were grown photoautotrophically in BG-11 medium at 25°C in flasks in low (70 µmol photons m^{-2} s^{-1}) or high (1000 µmol photons m^{-2} s^{-1}) white light irradiation with a 16 h light : 8 h dark photoperiod (Allen and Stanier, 1968).

Lipid, protein and starch analysis. Due to its strong cell wall, *C. vulgaris* 211/11P cells were first sonicated three times in a solution containing 1 ml EDTA 1 mM and acetic acid 0.15 M. Total lipid was extracted from sonicated cells following the method of Bligh and Dyer (1959). Lipid extracts were separated by thin layer chromatography and quantified for neutral or polar lipids based on densitometry and comparison with known amounts of lipid standards (Siaut et al., 2011). For fatty acid composition analysis, one given fraction of the lipid extracts was converted to their fatty acid methyl esters (FAMEs) and then analyzed using gas chromatography–flame ionization detection (GC-FID) as detailed in Siaut et al. (2011). Proteins and starch content of the harvested biomass were analyzed as reported previously in Cecchin et al. (2018).

DNA extraction and quality control. DNA was extracted from 500 ml *C. vulgaris* 211/11P liquid cultures with a cell density of 5 x 10^7 cell per ml using the cetyltrimethyl ammonium bromide (CTAB) extraction buffer. Extracted DNA was treated with 200 µg ml^{-1} RNase A at 37°C for 20 min and subsequently purified using 1.8x Agencourt AMPure XP beads (Beckman Coulter s.r.l., Milan, Italy). DNA purity and integrity were assessed using a NanoDrop 1000 spectrophotometer (Thermo Scientific, Wilmington, DE, USA) and by capillary electrophoresis on a 2200 TapeStation (Agilent Technologies, Santa Clara, CA, USA), respectively. DNA quantification was performed using the Qubit dsDNA HS Assay kit (Life Technologies, Monza, Italy).

Illumina sequencing. DNA (500 ng) was fragmented through sonication using a Covaris S220 instrument (Covaris, Woburn, MA, USA) and DNA-seq libraries were generated using the TruSeq DNA kit according to the manufacturer's instructions (Illumina, San Diego, CA, USA). Library length was assessed by capillary electrophoresis on a 2200 TapeStation (Agilent Technologies) and quantified by qPCR using primers annealing to the adapter sequences. DNA-seq libraries were sequenced on an Illumina HiSeq1000 platform and generating 100-bp paired-end reads for a total of 2.5 Gb.

PacBio sequencing. Genomic DNA (16 µg) was used for the preparation of two independent single-molecule real-time (SMRT) bell libraries according to the manufacturer's protocol (Pacific Biosciences; 20-kb template preparation using BluePippin, SageScience, Beverly, MA, USA size selection system with a 15-kb cut-off). Sequencing was performed on a PacBio RS-II platform (Pacific Biosciences, CA, USA) generating 6.4 Gb of SMRT data using PacBio P6-C4 chemistry.

BioNano genome mapping. High-molecular-weight DNA was extracted from the pellet of 2 L of cell culture with optical density $(OD)_{750}$ = 5.3, corresponding approximately to a total of 3 g. The cell wall was destroyed by grinding in liquid nitrogen. Ground cells were resuspended in IrysPrep Plant Homogenization Buffer (Bionano Genomics) supplemented with 0.2% beta-mercaptoethanol and 1 mM spermine-spermidine (HB+) and filtered through a 40-µm cell strainer. Nuclei were collected by centrifugation at 4500 *g* for 20 min at 4°C. A centrifugation at 60 *g* for 2 min at 4°C was used to remove debris, whereas nuclei were collected from the supernatant (3500 *g* for 20 min at 4°C). Nuclei were further purified by centrifugation over an IrysPrep Density Gradient (Bionano Genomics, San Diego, CA, USA) at 4500 *g* for 40 min at 4°C. The nuclei band (white layer) was collected from the gradient interphase and washed two times in HB+ and collected by centrifugation at 2500 g for 20 min. Only the nuclei pellet (white band) was collected with a wide bore tip and transferred for washing after each centrifugation step. Nuclei were embedded in agarose plugs and high-molecular-weight DNA was extracted as previously described (Staňková et al., 2016). The mega-base size of extracted DNA was verified by pulsed-field electrophoresis (PFGE). DNA (300 ng) was labelled and stained using the Nt. BspQI nicking endonuclease in combination with the NLRS DNA labelling kit (Bionano Genomics). The nicked and labelled DNA was then loaded onto an IrysChip for imaging on the Irys system (BioNano Genomics) for three runs of 30 cycles in one flow cell. Molecules of <150 kb in length, label SNR <2.75, label intensity >0.6 and having less than 20 labels were removed. Bionano data were assembled into consensus genome maps using the BioNano Solve pipeline (v5678.6119rel) with RefAligner (v.6119).

Genome assembly. The *C. vulgaris* 211/11P genome was assembled using FALCON (Chin et al., 2016) v1.8.7. A second assembly run was performed using the 12% of PacBio subreads that did not align on the first assembly, applying more relaxed parameters. The two assemblies were merged. PacBio subreads were aligned to the assembly using pbalign (v0.2.0.138342) and then the GenomicConsensus package (v0.9.2) with the Quiver algorithm was used to remove errors present in the consensus sequences. To further improve the genome quality, a second polishing iteration was performed using Illumina data: reads were aligned using BWA-MEM software (0.7.15-r1140) and the Pilon (v1.22) tool was used to correct errors. A hybrid assembly combining the polished PacBio assembly with the optical map was performed with the Bionano Solve Pipeline (v5678.6119rel), RefAligner (v.6119) using a merging-step *P-value* of 10^{-11} and a 'Min alignment length and Max endoutlier' parameter of 80.

Organelle genome assembly. The organelle genomes were assembled using the Organelle_PBA pipeline (Soorni et al., 2017). The sequences were then polished following the same approach used for the nuclear genome. The alignment between the FALCON assembly and the organelle genomes was performed using Blastn (v2.6.0). Those PacBio contigs aligning to the organelle genome with a similarity of at least of 99% were manually removed.

RNA extraction and RNA-seq analysis. RNA was extracted from 500 ml of *C. vulgaris* 211/11P in liquid cultures with a cell density of 7 x 10^7 cell per ml. RNA quality and quantity were determined using a NanoDrop 2000 spectrophotometer (Thermo Scientific) and a Bioanalyzer Chip RNA 7500 series II (Agilent, Santa Clara, CA, USA), respectively. Directional RNA-seq library preparation was performed starting from 1 µg total RNA using the TruSeq RNA Sample Prep Kit v2 (Illumina Inc.) after capturing poly-adenylated transcripts. Library quality was assessed using a High Sensitivity DNA Kit on a 2200 Tape Station (Agilent, Wokingham, UK) and quantification of libraries was performed by qPCR using primers annealing to the adapter sequences. Libraries were sequenced with an Illumina Next-Seq500 sequencer (Illumina Inc.) generating ~22 million 75-bp paired-end reads per sample.

Gene annotation. Gene annotation of the nuclear genome was performed using the unsupervised RNA-seq-based BRAKER1 pipeline, which takes advantage of two gene predictors: GeneMark-ET 4.32 and AUGUSTUS 3.0.3 (Specht et al., 2011). Briefly, both RNA-seq data from the two different growth conditions, LL and HL, were used for the annotation. Quality of reads obtained from each sample was assessed using FastQC software (http://www.bioinformatics.babraham.ac.uk/projects/fastqc/) and reads with more than 10% of undetermined bases or more than 50 bases with a quality score <7 were discarded. Reads were then clipped from the adapter sequences using Scythe software version 0.980 (https://github. com/vsbuffalo/scythe), and low-quality ends (Q score <20 on a 10-nt window) were trimmed with Sickle version 0.940 (https:// github.com/vsbuffalo/sickle). The two RNA-seq data were merged and alignment of reads to the assembled genome was performed using HISAT2 (https://ccb.jhu.edu/software/hisat2/index.shtml) v2.0.1. Finally, the aligned RNA-seq reads were used as input for the BRAKER1 pipeline. The quality and completeness of the transcriptome were evaluated using BUSCO (http://busco.ezlab.org/) (Simão et al., 2015). The web application GeSeq was used to annotate the organelle genomes with default parameters plus the tRNAscan-SE activated and selecting *C. reinhardtii* in the NCBI RefSeq database (Tillich et al., 2017). Some genes were also manually curated based on RNA-seq mapped reads. Organelle genome maps were then generated using the OGDRAW tool (Lohse et al., 2013).

Differential expression analysis. RNA-seq data were filtered as described in the previous section and aligned to the assembled reference genome with HISAT2 (v2.0.1) (Kim et al., 2015). Differential expression analysis between the two growth conditions was conducted with DESeq2 (v1.16.1) (Love et al., 2014) using the gene annotations generated.

Transcriptome functional annotation. Transcriptome functional annotation was performed by the Blast2Go platform based on NCBI's RefSeq database (Conesa et al., 2005). Annotated sequences were analyzed using the KAAS (KEGG Automatic Annotation Server) platform to obtain KO annotation (Kanehisa and Goto, 2000; Kanehisa et al., 2016, 2017). Transcripts differently expressed with KO

annotations were visualized using the KEGG Mapper platform, while the remaining transcripts functionally annotated were manually inspected by retrieving the function of the closest homolog gene.

Phylogenetic analysis. Phylogenetic analysis was performed by BUSCO analysis as previously reported (Waterhouse et al., 2017). In particular, 111 single copy genes shared with other species with an available genome were used for protein alignment and phylogenetic tree construction. BUSCO 3.0.2 software with the eukaryota_odb9 database and the genome of each species *Chlorella vulgaris*, *Chlorella protothecoides sp0710*, *Chlorella variabilis NC64A*, *Coccomyxa subellipsoidae*, *Chlamydomonas reinhardtii*, *Volvox carteri*, *Chromochloris zofingiensis*, *Arabidopsis thaliana*, *Micromonas pusilla CCMP1545* and *Ostreococcus tauri* were used to identify the single-copy orthologous genes. Of these, only those shared between the 10 species were selected. For each protein a multiple alignment was performed among the species using MUSCLE 3.8.31 (Edgar, 2004), and then the alignments were concatenated. The tree was built using the web application Phylogeny.fr running PhyMl and TreeDyn for construction and visualization, respectively (Dereeper et al., 2008).

Subcellular localization prediction. Subcellular localization prediction was performed using the PredAlgo tool, as previously described (Tardif et al., 2012).

ACCESSION NUMBERS

This Whole Genome Shotgun project was deposited in the DDBJ/ENA/GenBank database under the accession number SIDB00000000. The version described in this paper is version SIDB01000000. Accession numbers for the raw PacBio and Illumina reads are SRR8083355_SRR8083370.

ACKNOWLEDGEMENTS

The research was supported by the ERC Starting Grant SOLENALGAE (679814) to MB. We also acknowledge the European Union Regional Developing Fund (ERDF), the Region Provence Alpes Côte d'Azur, the French Ministry of Research and the CEA for funding the HelioBiotec platform. We thank the Centro Piattaforme Tecnologiche for providing access to the core facilities of the University of Verona, Italy.

AUTHOR CONTRIBUTIONS

MB conceived the study, designed and supervised the experiments. MD designed, coordinated and supervised the *C. vulgaris* genome assembly and annotation. MC prepared all the samples herein analyzed and performed or contributed to all the experiments herein reported. LM and MR performed genome assembly, genome annotation and performed transcriptome and differential gene expression

analysis. EC and MR contributed to sample preparation for next generation sequencing and optical mapping. LG contributed to growth experiments and biomass analysis. YL coordinated lipid analysis and contributed to experiment design. SC performed lipid analysis. MB, MD, MR and YL wrote the manuscript. All the authors discussed the results, contributed to data interpretation and commented on the manuscript.

REFERENCES

Ajjawi, I., Verruto, J., Aqui, M. et al. (2017) Lipid production in *Nannochloropsis gaditana* is doubled by decreasing expression of a single transcriptional regulator. Nat. Biotechnol. 35, 647.

Alboresi, A., Perin, G., Vitulo, N. et al. (2016) Light remodels lipid biosynthesis in *Nannochloropsis gaditana* by modulating carbon partitioning between organelles. Plant Physiol. 171, 2468–2482.

Allen, M.M. and Stanier, R.Y. (1968) Growth and division of some unicellular blue-green algae. J. Gen. Microbiol. 51, 199–202.

Allorent, G., Lefebvre-Legendre, L., Chappuis, R., Kuntz, M., Truong, T.B., Niyogi, K.K., Ulm, R. and Goldschmidt-Clermont, M. (2016) UV-B photoreceptor-mediated protection of the photosynthetic machinery in *Chlamydomonas reinhardtii*. Proc Natl Acad Sci USA, 113, 14864–14869.

Arriola, M., Velmurugan, N., Zhang, Y., Plunkett, M., Hondzo, H. and Barney, B. (2018) Genome sequences of *Chlorella sorokiniana* UTEX 1602 and *Micractinium conductrix* SAG 241.80: implications to maltose excretion by a green alga. Plant J. 93, 566–586.

Ballottari, M., Dall'Osto, L., Morosinotto, T. and Bassi, R. (2007) Contrasting behavior of higher plant photosystem I and II antenna systems during acclimation. J. Biol. Chem. 282, 8947–8958.

Berteotti, S., Ballottari, M. and Bassi, R. (2016) Increased biomass productivity in green algae by tuning non-photochemical quenching. Sci. Rep. 6, 21339.

Blaby, I.K., Blaby-Haas, C.E., Tourasse, N. et al. (2014) The *Chlamydomonas* genome project: a decade on. Trends Plant Sci. 19, 672–680.

Blanc, G., Duncan, G., Agarkova, I. et al. (2010) The *Chlorella variabilis* NC64A genome reveals adaptation to photosymbiosis, coevolution with viruses, and cryptic sex. Plant Cell, 22, 2943–2955.

Blanc, G., Agarkova, I., Grimwood, J. et al. (2012) The genome of the polar eukaryotic microalga *Coccomyxa subellipsoidea* reveals traits of cold adaptation. Genome Biol. 13, R39.

Bligh, E.G. and Dyer, W.J. (1959) A rapid method of total lipid extraction and purification. Can. J. Biochem. Physiol. 37, 911–917.

Bonente, G., Pippa, S., Castellano, S., Bassi, R. and Ballottari, M. (2012) Acclimation of *Chlamydomonas reinhardtii* to different growth irradiances. J. Biol. Chem. 287, 5833–5847.

Boudreau, E., Takahashi, Y., Lemieux, C., Turmel, M. and Rochaix, J.D. (1997) The chloroplast ycf3 and ycf4 open reading frames of *Chlamydomonas reinhardtii* are required for the accumulation of the photosystem I complex. EMBO J. 16, 6095–6104.

Boyle, N. and Morgan, J. (2009) Flux balance analysis of primary metabolism in *Chlamydomonas reinhardtii*. BMC Syst. Biol. 3, 4.

Cecchin, M., Benfatto, S., Griggio, F., Mori, A., Cazzaniga, S., Vitulo, N., Delledonne, M. and Ballottari, M. (2018) Molecular basis of autotrophic versus mixotrophic growth in *Chlorella sorokiniana*. Sci. Rep. 8, 6465.

Charuchinda, P., Waditee-Sirisattha, R., Kageyama, H., Yamada, D., Sirisattha, S., Tanaka, Y., Mahakhant, A. and Takabe, T. (2015) Caleosin from *Chlorella vulgaris* TISTR 8580 is salt-induced and heme-containing protein. Biosci. Biotechnol. Biochem. 79, 1119–1124.

Chin, C.S., Peluso, P., Sedlazeck, F.J. et al. (2016) Phased diploid genome assembly with single-molecule real-time sequencing. Nat. Methods, 13, 1050–1054.

Conesa, A., Gotz, S., Garcia-Gomez, J., Terol, J., Talon, M. and Robles, M. (2005) Blast2GO: a universal tool for annotation, visualization and analysis in functional genomics research. Bioinformatics, 21, 3674–3676.

Correa-Galvis, V., Redekop, P., Guan, K., Griess, A., Truong, T.B., Wakao, S., Niyogi, K.K. and Jahns, P. (2016) Photosystem II subunit PsbS Is involved in the induction of LHCSR protein-dependent energy dissipation in *Chlamydomonas reinhardtii*. J. Biol. Chem. 291, 17478–17487.

Corteggiani Carpinelli, E., Telatin, A., Vitulo, N., Forcato, C., D'Angelo, M., Schiavon, R., Vezzi, A., Giacometti, G.M., Morosinotto, T. and Valle, G. (2014) Chromosome scale genome assembly and transcriptome profiling of *Nannochloropsis gaditana* in nitrogen depletion. Mol. Plant, 7, 323–335.

Dall'Osto, L., Cazzaniga, S., North, H., Marion-Poll, A. and Bassi, R. (2007) The *Arabidopsis* aba4-1 mutant reveals a specific function for neoxanthin in protection against photooxidative stress. Plant Cell, 19, 1048–1064.

Daniell, H., Lin, C.S., Yu, M. and Chang, W.J. (2016) Chloroplast genomes: diversity, evolution, and applications in genetic engineering. Genome Biol. 17, 134.

Denovan-Wright, E.M., Nedelcu, A.M. and Lee, R.W. (1998) Complete sequence of the mitochondrial DNA of *Chlamydomonas eugametos*. Plant Mol. Biol. 36, 285–295.

Dereeper, A., Guignon, V., Blanc, G. et al. (2008) Phylogeny.fr: robust phylogenetic analysis for the non-specialist. Nucleic Acids Res. 36, W465–W469.

Desplats, C., Mus, F., Cuiné, S., Billon, E., Cournac, L. and Peltier, G. (2009) Characterization of Nda2, a plastoquinone-reducing type II NAD(P)H dehydrogenase in *Chlamydomonas* chloroplasts. J. Biol. Chem. 284, 4148–4157.

Driver, T., Trivedi, D.K., McIntosh, O.A., Dean, A.P., Goodacre, R. and Pittman, J.K. (2017) Two Glycerol-3-Phosphate Dehydrogenases from *Chlamydomonas* have distinct roles in lipid metabolism. Plant Physiol. 174, 2083–2097.

Edgar, R.C. (2004) MUSCLE: a multiple sequence alignment method with reduced time and space complexity. BMC Bioinformatics, 5, 113.

Gandini, C.L. and Sanchez-Puerta, M.V. (2017) Foreign plastid sequences in plant mitochondria are frequently acquired via mitochondrion-to-mitochondrion horizontal transfer. Sci. Rep. 7, 43402.

Gao, C., Wang, Y., Shen, Y., Yan, D., He, X., Dai, J. and Wu, Q. (2014) Oil accumulation mechanisms of the oleaginous microalga *Chlorella protothecoides* revealed through its genome, transcriptomes, and proteomes. BMC Genom. 15, 582.

Goremykin, V.V., Salamini, F., Velasco, R. and Viola, R. (2009) Mitochondrial DNA of *Vitis vinifera* and the issue of rampant horizontal gene transfer. Mol. Biol. Evol. 26, 99–110.

Guarnieri, M.T., Levering, J., Henard, C.A., Boore, J.L., Betenbaugh, M.J., Zengler, K. and Knoshaug, E.P. (2018) Genome sequence of the Oleaginous Green Alga, *Chlorella vulgaris* UTEX 395. Front. Bioeng. Biotechnol. 6, 37.

Heimerl, N., Hommel, E., Westermann, M., Meichsner, D., Lohr, M., Hertweck, C., Grossman, A.R., Mittag, M. and Sasso, S. (2018) A giant type I polyketide synthase participates in zygospore maturation in *Chlamydomonas reinhardtii*. Plant J. 95, 268–281.

Houille-Vernes, L., Rappaport, F., Wollman, F.A., Alric, J. and Johnson, X. (2011) Plastid terminal oxidase 2 (PTOX2) is the major oxidase involved in chlororespiration in *Chlamydomonas*. Proc. Natl. Acad. Sci. USA, 108, 20820–20825.

Hovde, B., Hanschen, E., Tyler, C. et al. (2018) Genomic characterization reveals significant divergence within *Chlorella sorokiniana* (Chlorellales, Trebouxiophyceae). Algal Res. 35, 449–461.

Huang, N.L., Huang, M.D., Chen, T.L. and Huang, A.H. (2013) Oleosin of subcellular lipid droplets evolved in green algae. Plant Physiol. 161, 1862–1874.

Johnson, X., Steinbeck, J., Dent, R.M. et al. (2014) Proton gradient regulation 5-mediated cyclic electron flow under ATP- or redox-limited conditions: a study of DATPase pgr5 and DrbcL pgr5 mutants in the green alga *Chlamydomonas reinhardtii*. Plant Physiol. 165, 438–452.

Juneja, A., Chaplen, F. and Murthy, G. (2016) Genome scale metabolic reconstruction of *Chlorella variabilis* for exploring its metabolic potential for biofuels. Biores. Technol. 213, 103–110.

Kanehisa, M. and Goto, S. (2000) KEGG: Kyoto encyclopedia of genes and genomes. Nucleic Acids Res. 28, 27–30.

Kanehisa, M., Sato, Y., Kawashima, M., Furumichi, M. and Tanabe, M. (2016) KEGG as a reference resource for gene and protein annotation. Nucleic Acids Res. 44, D457–D462.

Kanehisa, M., Furumichi, M., Tanabe, M., Sato, Y. and Morishima, K. (2017) KEGG: new perspectives on genomes, pathways, diseases and drugs. Nucleic Acids Res. 45, D353–D361.

Kim, D., Langmead, B. and Salzberg, S.L. (2015) HISAT: a fast spliced aligner with low memory requirements. Nat. Methods, 12, 357–360.

Kirst, H., Gabilly, S.T., Niyogi, K.K., Lemaux, P.G. and Melis, A. (2017) Photosynthetic antenna engineering to improve crop yields. Planta, 245, 1009–1020.

Kobayashi, K. (2016) Role of membrane glycerolipids in photosynthesis, thylakoid biogenesis and chloroplast development. J. Plant. Res. 129, 565–580.

Kong, F., Liang, Y., L_egeret, B., Beyly-Adriano, A., Blangy, S., Haslam, R.P., Napier, J.A., Beisson, F., Peltier, G. and Li-Beisson,

Y. (2017) *Chlamydomonas* carries out fatty acid β-oxidation in ancestral peroxisomes using a bona fide acyl-CoA oxidase. Plant J. 90, 358–371.

Kouřil, R., Nosek, L., Bartoš, J., Boekema, E.J., Ilík, P. (2016) Evolutionary loss of light-harvesting proteins Lhcb6 and Lhcb3 in major land plant groups–break-up of current dogma. New Phytol. 210, 808–814.

Kromdijk, J., Głowacka, K., Leonelli, L., Gabilly, S.T., Iwai, M., Niyogi, K.K. and Long, S.P. (2016) Improving photosynthesis and crop productivity by accelerating recovery from photoprotection. Science, 354, 857– 861.

Li, X.P., Bj€orkman, O., Shih, C., Grossman, A.R., Rosenquist, M., Jansson, S. and Niyogi, K.K. (2000) A pigment-binding protein essential for regulation of photosynthetic light harvesting. Nature, 403, 391–395.

Lin, M. and Oliver, D.J. (2008) The role of acetyl-coenzyme a synthetase in *Arabidopsis*. Plant Physiol. 147, 1822–1829.

Lin, I.P., Jiang, P.L., Chen, C.S. and Tzen, J.T. (2012) A unique caleosin serving as the major integral protein in oil bodies isolated from *Chlorella* sp. cells cultured with limited nitrogen. Plant Physiol. Biochem. 61, 80–87.

Lohse, M., Drechsel, O., Kahlau, S. and Bock, R. (2013) OrganellarGenomeDRAW– a suite of tools for generating physical maps of plastid and mitochondrial genomes and visualizing expression data sets. Nucleic Acids Res. 41, W575–W581.

Love, M.I., Huber, W. and Anders, S. (2014) Moderated estimation of fold change and dispersion for RNA-seq data with DESeq2. Genome Biol. 15, 550.

Lum, K.K., Kim, J. and Lei, X.G. (2013) Dual potential of microalgae as a sustainable biofuel feedstock and animal feed. J. Anim. Sci. Biotechnol. 4, 53.

Lv, J.M., Cheng, L.H., Xu, X.H., Zhang, L. and Chen, H.L. (2010) Enhanced lipid production of *Chlorella vulgaris* by adjustment of cultivation conditions. Bioresour. Technol. 101, 6797–6804.

Malik, S.B., Pightling, A.W., Stefaniak, L.M., Schurko, A.M. and Logsdon, J.M. (2007) An expanded inventory of conserved meiotic genes provides evidence for sex in *Trichomonas vaginalis*. PLoS ONE, 3, e2879.

Maul, J.E., Lilly, J.W., Cui, L., dePamphilis, C.W., Miller, W., Harris, E.H. and Stern, D.B. (2002) The *Chlamydomonas reinhardtii* plastid chromosome: islands of genes in a sea of repeats. Plant Cell, 14, 2659–2679.

Merchant, S.S., Prochnik, S.E., Vallon, O. et al. (2007) The *Chlamydomonas* genome reveals the evolution of key animal and plant functions. Science, 318, 245–250.

Moellering, E.R. and Benning, C. (2010) RNA interference silencing of a major lipid droplet protein affects lipid droplet size in *Chlamydomonas reinhardtii*. Eukaryot. Cell, 9, 97–106.

Moore, E.R., Bullington, B.S., Weisberg, A.J., Jiang, Y., Chang, J. and Halsey, K.H. (2017) Morphological and transcriptomic evidence for ammonium induction of sexual reproduction in *Thalassiosira pseudonana* and other centric diatoms. PLoS ONE, 12, e0181098.

Murphy, D.J. (2012) The dynamic roles of intracellular lipid droplets: from archaea to mammals. Protoplasma, 249, 541–585.

Naduthodi, M.I.S., Barbosa, M.J. and van der Oost, J. (2018) Progress of CRISPR-Cas based genome editing in photosynthetic microbes. Biotechnol. J. 13, e1700591.

Nguyen, H.M., Cuin_e, S., Beyly-Adriano, A., L_egeret, B., Billon, E., Auroy, P., Beisson, F., Peltier, G. and Li-Beisson, Y. (2013) The green microalga *Chlamydomonas reinhardtii* has a single ω-3 fatty acid desaturase that localizes to the chloroplast and impacts both plastidic and extraplastidic membrane lipids. Plant Physiol. 163, 914–928.

Ort, D.R., Merchant, S.S., Alric, J. et al. (2015) Redesigning photosynthesis to sustainably meet global food and bioenergy demand. Proc. Natl. Acad. Sci. USA, 112, 8529–8536.

Peers, G., Truong, T.B., Ostendorf, E., Busch, A., Elrad, D., Grossman, A.R., Hippler, M. and Niyogi, K.K. (2009) An ancient light-harvesting protein is critical for the regulation of algal photosynthesis. Nature, 462, 518–521.

Petroutsos, D., Terauchi, A.M., Busch, A., Hirschmann, I., Merchant, S.S., Finazzi, G. and Hippler, M. (2009) PGRL1 participates in iron-induced remodeling of the photosynthetic apparatus and in energy metabolism in *Chlamydomonas reinhardtii*. J. Biol. Chem. 284, 32770–32781.

Plancke, C., Vigeolas, H., Höhner, R. et al. (2014) Lack of isocitrate lyase in *Chlamydomonas* leads to changes in carbon metabolism and in the response to oxidative stress under mixotrophic growth. Plant J. 77, 404–417.

Poliner, E., Panchy, N., Newton, L., Wu, G., Lapinsky, A., Bullard, B., Zienkiewicz, A., Benning, C., Shiu, S.H. and Farré, E.M. (2015) Transcriptional coordination of physiological responses in *Nannochloropsis oceanica* CCMP1779 under light/dark cycles. Plant J. 83, 1097–1113.

Radakovits, R., Jinkerson, R.E., Fuerstenberg, S.I., Tae, H., Settlage, R.E., Boore, J.L. and Posewitz, M.C. (2012) Draft genome sequence and genetic transformation of the oleaginous alga *Nannochloropis gaditana*. Nat. Commun. 3, 686.

Roth, M.S., Cokus, S.J., Gallaher, S.D. et al. (2017) Chromosome-level genome assembly and transcriptome of the green alga *Chromochloris zofingiensis* illuminates astaxanthin production. Proc. Natl. Acad. Sci. USA, 114, E4296–E4305.

Rufty, T.W. and Huber, S.C. (1983) Changes in starch formation and activities of sucrose phosphate synthase and cytoplasmic fructose-1,6-bisphosphatase in response to source-sink alterations. Plant Physiol. 72, 474–480.

Rumeau, D., Peltier, G. and Cournac, L. (2007) Chlororespiration and cyclic electron flow around PSI during photosynthesis and plant stress response. Plant Cell Environ. 30, 1041–1051.

Sarayloo, E., Tardu, M., Unlu, Y., Simsek, S., Cevahir, G., Erkey, C. and Kavakli, I. (2017) Understanding lipid metabolism in high-lipid-producing *Chlorella vulgaris* mutants at the genome-wide level. Algal Res. 28, 244–252.

Saroussi, S.I., Wittkopp, T.M. and Grossman, A.R. (2016) The type II NADPH dehydrogenase facilitates cyclic electron flow, energy-dependent quenching, and chlororespiratory metabolism during acclimation of *Chlamydomonas reinhardtii* to nitrogen deprivation. Plant Physiol. 170, 1975–1988.

Scheller, H.V., Jensen, P.E., Haldrup, A., Lunde, C. and Knoetzel, J. (2001) Role of subunits in eukaryotic Photosystem I. Biochim. Biophys. Acta, 1507, 41–60.

Schweizer, E. and Hofmann, J. (2004) Microbial type I fatty acid synthases (FAS): major players in a network of cellular FAS systems. Microbiol. Mol. Biol. Rev. 68, 501–517. table of contents.

Shi, L.X. and Schröder, W.P. (2004) The low molecular mass subunits of the photosynthetic supracomplex, photosystem II. Biochim. Biophys. Acta, 1608, 75–96.

Shi, L.X., Kim, S.J., Marchant, A., Robinson, C. and Schröder, W.P. (1999) Characterisation of the PsbX protein from Photosystem II and light regulation of its gene expression in higher plants. Plant Mol. Biol. 40, 737–744.

Shi, L.X., Hall, M., Funk, C. and Schröder, W.P. (2012) Photosystem II, a growing complex: updates on newly discovered components and low molecular mass proteins. Biochim. Biophys. Acta, 1817, 13–25.

Shimada, H., Fukuta, M., Ishikawa, M. and Sugiura, M. (1990) Rice chloroplast RNA polymerase genes: the absence of an intron in rpoC1 and the presence of an extra sequence in rpoC2. Mol. Gen. Genet. 221, 395–402.

Siaut, M., Cuiné, S., Cagnon, C. et al. (2011) Oil accumulation in the model green alga *Chlamydomonas reinhardtii*: characterization, variability between common laboratory strains and relationship with starch reserves. BMC Biotechnol. 11, 7.

Simão, F.A., Waterhouse, R.M., Ioannidis, P., Kriventseva, E.V. and Zdobnov, E.M. (2015) BUSCO: assessing genome assembly and annotation completeness with single-copy orthologs. Bioinformatics, 31, 3210–3212.

Smith, S. and Tsai, S.C. (2007) The type I fatty acid and polyketide synthases: a tale of two megasynthases. Nat. Prod. Rep. 24, 1041–1072.

Soorni, A., Haak, D., Zaitlin, D. and Bombarely, A. (2017) Organelle_PBA, a pipeline for assembling chloroplast and mitochondrial genomes from PacBio DNA sequencing data. BMC Genom. 18, 49.

Specht, M., Stanke, M., Terashima, M., Naumann-Busch, B., Janssen, I., Höhner, R., Hom, E.F., Liang, C. and Hippler, M. (2011) Concerted action of the new Genomic Peptide Finder and AUGUSTUS allows for automated proteogenomic annotation of the *Chlamydomonas reinhardtii* genome. Proteomics, 11, 1814–1823.

Staňková, H., Hastie, A.R., Chan, S. et al. (2016) BioNano genome mapping of individual chromosomes supports physical mapping and sequence assembly in complex plant genomes. Plant Biotechnol. J. 14, 1523–1531.

Straub, S., Cronn, R., Edwards, C., Fishbein, M. and Liston, A. (2013) Horizontal transfer of DNA from the mitochondrial to the plastid genome and its subsequent evolution in milkweeds (Apocynaceae). Genome Biol. Evol. 5, 1872–1885.

Tardif, M., Atteia, A., Specht, M. et al. (2012) PredAlgo: a new subcellular localization prediction tool dedicated to green algae. Mol. Biol. Evol. 29, 3625–3639.

Tibiletti, T., Auroy, P., Peltier, G. and Caffarri, S. (2016) *Chlamydomonas reinhardtii* PsbS protein is functional and accumulates rapidly and transiently under high light. Plant Physiol. 171, 2717–2730.

Tillich, M., Lehwark, P., Pellizzer, T., Ulbricht-Jones, E.S., Fischer, A., Bock, R. and Greiner, S. (2017) GeSeq - versatile and accurate annotation of organelle genomes. Nucleic Acids Res. 45, W6–W11.

Vieler, A., Wu, G., Tsai, C.H. et al. (2012) Genome, functional gene annotation, and nuclear transformation of the heterokont

oleaginous alga *Nannochloropsis oceanica* CCMP1779. PLoS Genet. 8, e1003064.

Wakasugi, T., Nagai, T., Kapoor, M. et al. (1997) Complete nucleotide sequence of the chloroplast genome from the green alga *Chlorella vulgaris*: the existence of genes possibly involved in chloroplast division. Proc. Natl Acad. Sci. USA, 94, 5967–5972. Walker, D. (2009) Biofuels, facts, fantasy, and feasibility. J. Appl. Phycol. 21, 509–517.

Wang, D., Wu, Y.W., Shih, A.C., Wu, C.S., Wang, Y.N. and Chaw, S.M. (2007) Transfer of chloroplast genomic DNA to mitochondrial genome occurred at least 300 MYA. Mol. Biol. Evol. 24, 2040–2048.

Waterhouse, R.M., Seppey, M., Simão, F.A., Manni, M., Ioannidis, P., Klioutchnikov, G., Kriventseva, E.V. and Zdobnov, E.M. (2017) BUSCO applications from quality assessments to gene prediction and phylogenomics.

Mol. Biol. Evol. 35, 543–548. Wong, J.L. and Johnson, M.A. (2010) Is HAP2-GCS1 an ancestral gamete fusogen? Trends Cell Biol. 20, 134–141.

Yamamoto, M., Fujishita, M., Hirata, A. and Kawano, S. (2004) Regeneration and maturation of daughter cell walls in the autospore-forming green alga *Chlorella vulgaris* (Chlorophyta, Trebouxiophyceae). J. Plant. Res. 117, 257–264.

Yoshinaga, Y., Daum, C., He, G. and O'Malley, R. (2018) Genome sequencing. Methods Mol. Biol. 1775, 37–52.

Youssef, A., Laizet, Y., Block, M.A., Mar_echal, E., Alcaraz, J.P., Larson, T.R., Pontier, D., Gaff_e, J. and Kuntz, M. (2010) Plant lipid-associated fibrillin proteins condition jasmonate production under photosynthetic stress. Plant J. 61, 436–445.

Z€auner, S., Jochum, W., Bigorowski, T. and Benning, C. (2012) A cytochrome b5-containing plastid-located fatty acid desaturase from *Chlamydomonas reinhardtii*. Eukaryot. Cell, 11, 856–863.

Zhong, Y.J., Huang, J.C., Liu, J., Li, Y., Jiang, Y., Xu, Z.F., Sandmann, G. and Chen, F. (2011) Functional characterization of various algal carotenoid ketolases reveals that ketolating zeaxanthin efficiently is essential for high production of astaxanthin in transgenic *Arabidopsis*. J. Exp. Bot. 62, 3659–3669.

Zuniga, C., Li, C., Huelsman, T. et al. (2016) Genome-scale metabolic model for the green alga *Chlorella vulgaris* UTEX 395 accurately predicts phenotypes under autotrophic, heterotrophic, and mixotrophic growth conditions. Plant Physiol. 172, 589–602.

SUPPLEMENTARY INFORMATION

Supplemental Figures

Figure S1. Example of optical mapping-based scaffolding of *Chlorella vulgaris* 211/11P genome. PacBio contigs and Bionano consensus map are colored in blue, while hybrid assembly in green; vertical lines represent the recognition sites of the enzyme Nt.BspQI used for the insertion of the fluorescent probes in the isolated DNA molecules for the generation of the optical maps.

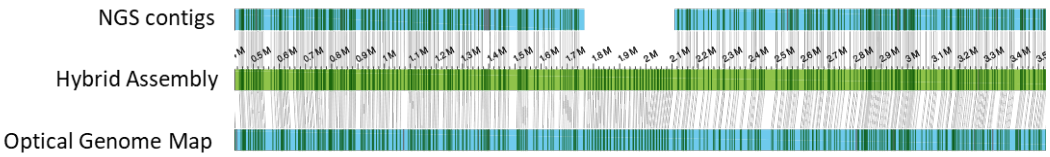

Figure S2. Number of transcripts identified in *Chlorella vulgaris* 211/11P based on BLAST results using *Chlorella vulgaris* UTEX 395 as a reference genome. Selected threshold value for e-value was set to $1x10^{-3}$.

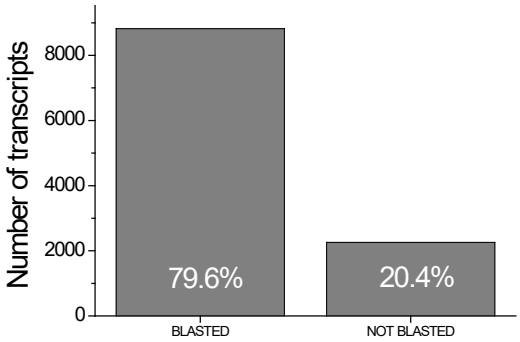

Figure S3. Distribution of *Chlorella vulgaris* 211/11P gene annotation results. The top-Hit species distribution obtained by functional annotation of *C. vulgaris* genome by BLAST2GO software is reported.

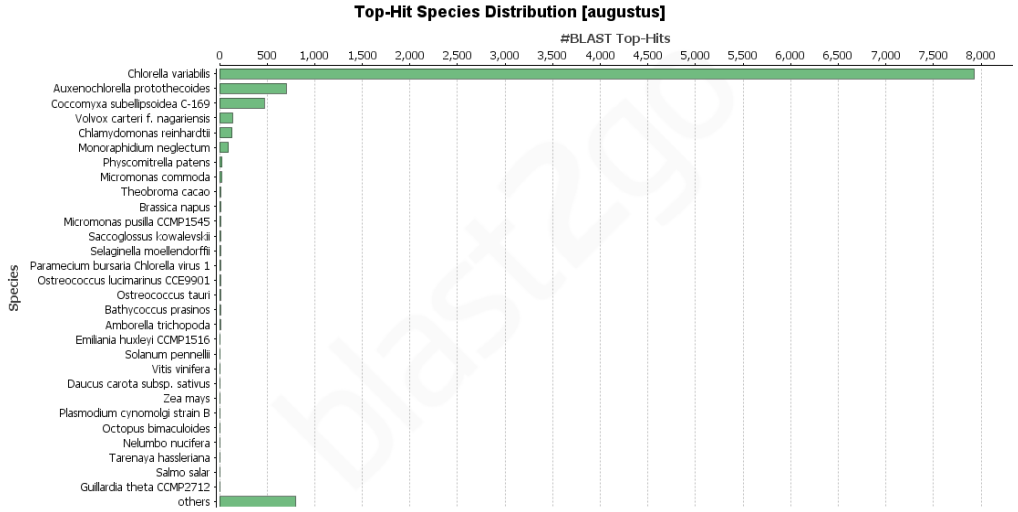

Figure S4. Phylogenetic analysis of *Chlorella vulgaris* 211/11P strain.

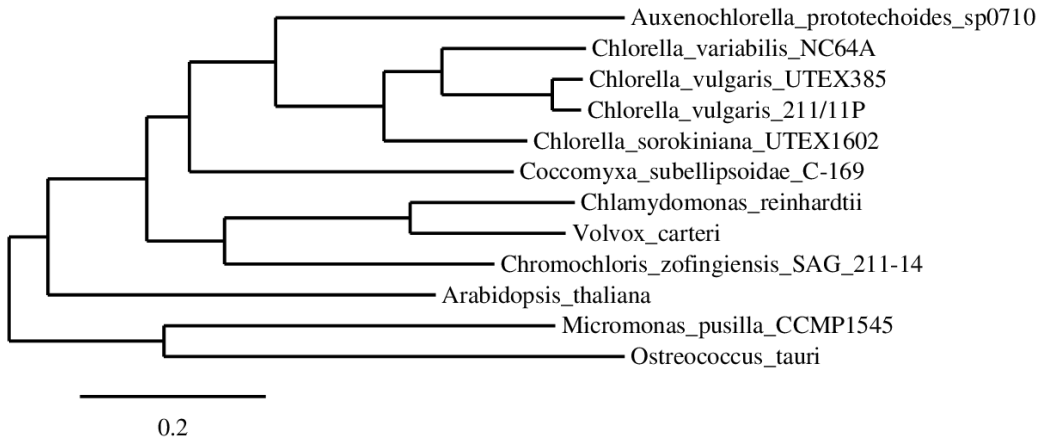

Figure S5. Gene Ontology (GO) classification of *Chlorella vulgaris* 211/11P differently expressed genes in LL *vs.* HL conditions. Differentially expressed genes up-regulated in low light (LL) (a, b, c) or high light (HL) (d, e, f) were functionally grouped on the basis of GO terms cellular component (a, d), molecular function (b, e) and biological processes (c, f). The distribution of the different groups is reported based on the node score associated to each group considering GO term with node score higher than 1%.

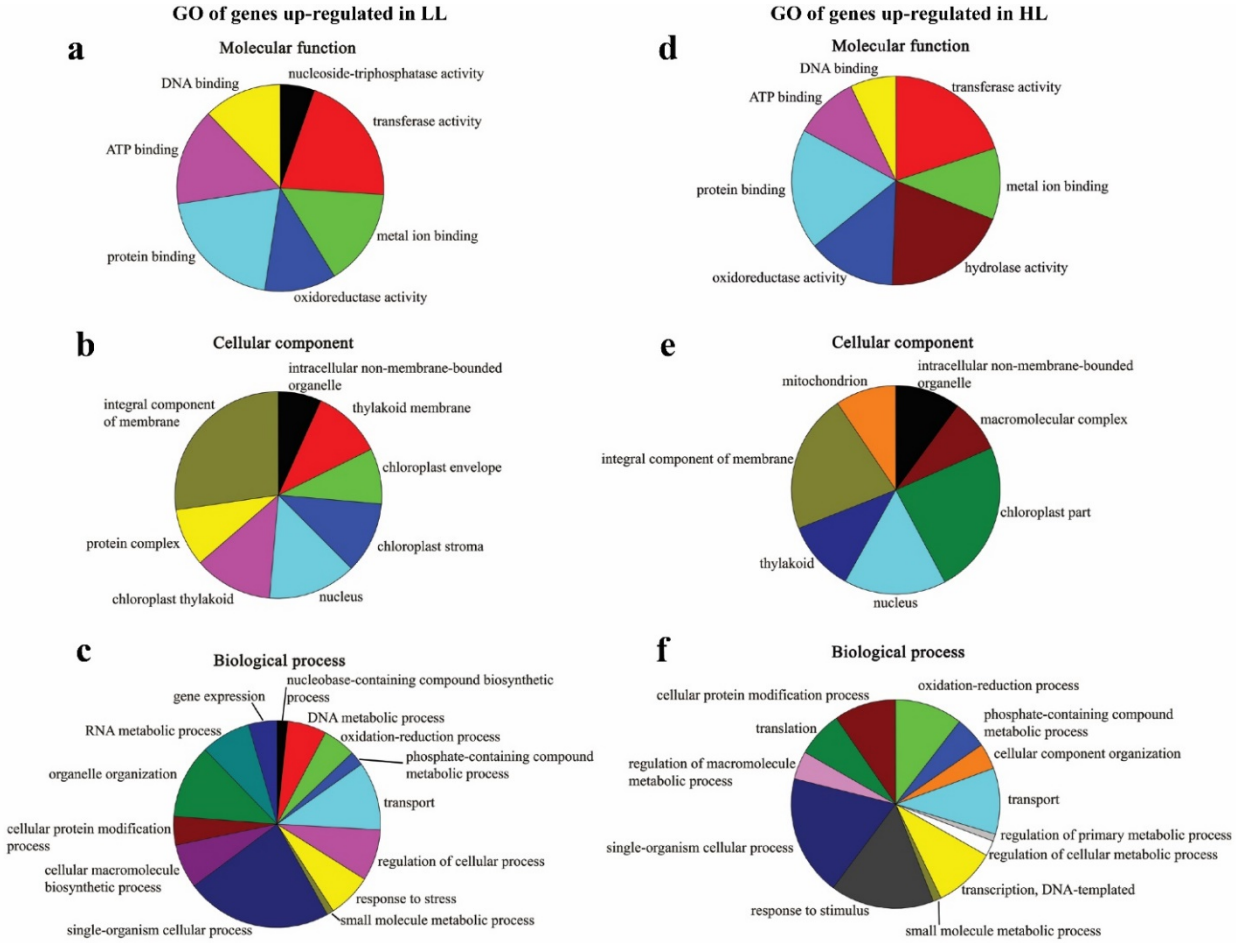

Figure S6. Carbon fixation pathway in *Chlorella vulgaris* 211/11P identified by KEGG Mapper. Carbon fixation map by KEGG Mapper (map00710) is reported. The enzymes identified in *C. vulgaris* genome are reported in green.

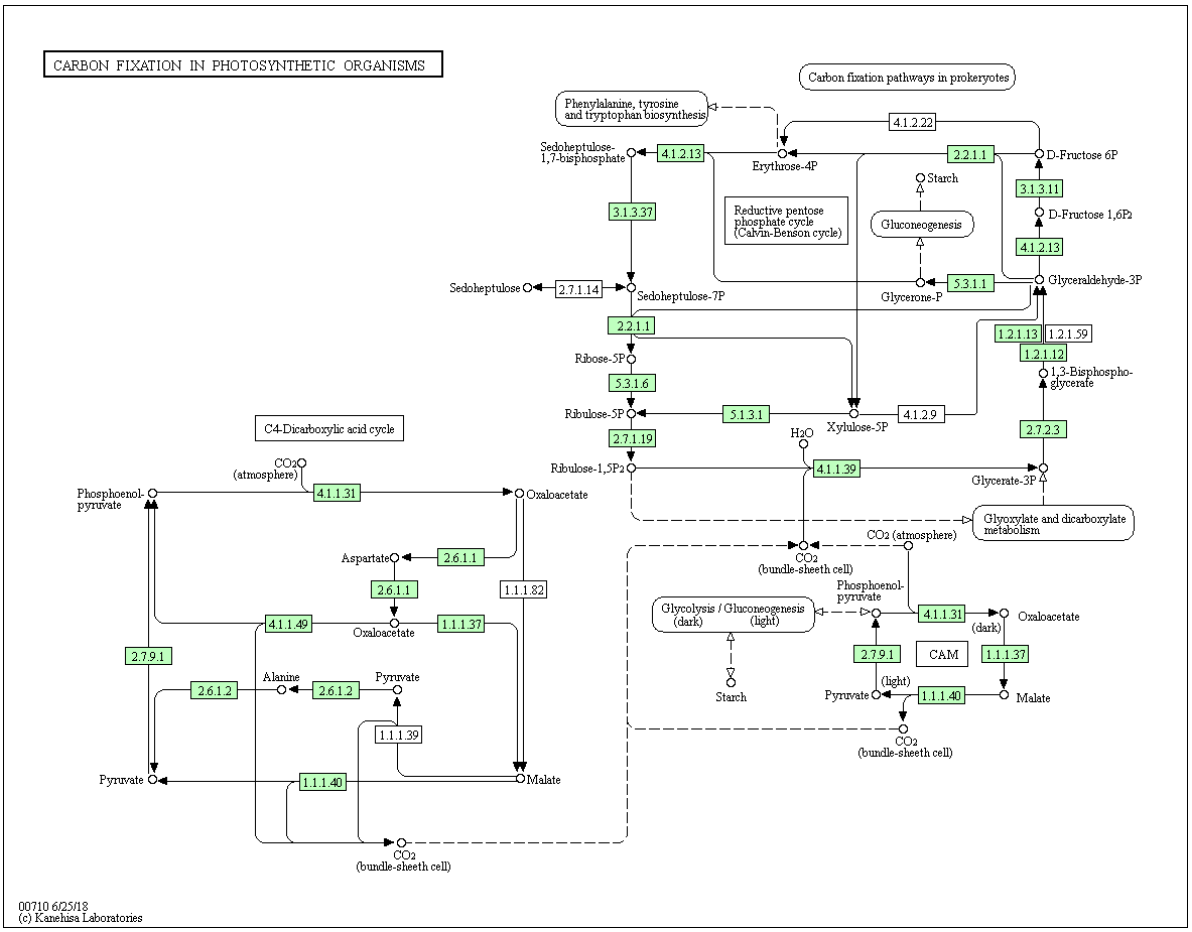

Figure S7. Identification of a neoxanthin synthase enzyme in *Chlorella vulgaris* 211/11P. Panel A: Clustal Omega protein alignment of the protein sequence encoded by *Chlorella vulgaris* 211/11P gene g5367 and the protein sequence identified in *Arabidopsis thaliana* as neoxanthin synthase. Panel B: representation of the domain identified in the putative neoxanthin synthase of *C. vulgaris* and the identified neoxanthin synthase encoded in the *A. thaliana* genome.

Figure S8. Polyketide synthase/fatty acid synthase Type I enzyme in *C. vulgaris* 211/11P. Panel A: phylogenetic tree of putative PKS/FAS type I enzyme found in *C. vulgaris* 211/11P (g276.t1), highlighted in yellow). Panel B: protein domains identified by INTERPROSCAN in g276 gene product.

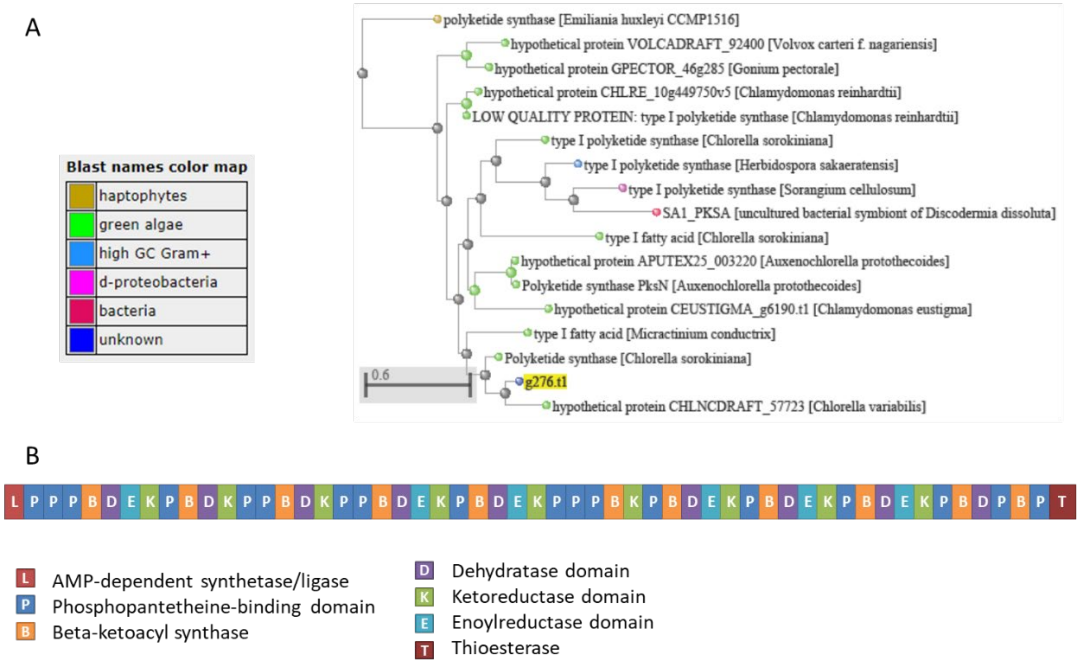

Figure S9. Protein alignment of two Malonyl-CoA: ACP transacylase enzymes identified in *C. vulgaris* 211/11P. In the case of g6284.t1 transit peptide for chloroplast import is indicated as predicted by PREDALGO software.

```
CLUSTAL O(1.2.4) multiple sequence alignment


g6284.t1        ------------------------------------------------------------      0
g8816.t1        MPRDMTATGRFPPSPCYLPINFYSAVRMGDPEQLAKIMETDPYFITQDNGAGAPIHFATT      60


g6284.t1        ------------------------------------------------------------      0
g8816.t1        YRQLDMIHHLLNNGAEINQRDDKGFTALHRAAYLAHYDGYLEIYEYLLSRGADPTLRTEN      120


g6284.t1        ------------------------------------------------------------      0
g8816.t1        YDPYLNPGKKLPIEIALDDEEGLTRAKLLELEKRYADVPRAKRAHPDTGCWWALYDYGLE      180

                           PREDICTED SIGNAL PEPTIDE
g6284.t1        -----------MQAAAIQSAVRGFAVRQ--GAGRHGRRQV-----AVKASSDAKFADYKP      42
g8816.t1        RIKTWAPDYVHPYPEVLKRARDEAELKKAKEERRKARAAADVAATTAPAATPARAKVQET      240
                             .:: *     :::     *:.*  .     :. *:: *:    :

g6284.t1        KVAFFFPGQGAQTVGMGKEVAESVPAAKQLFERASDILGYDLLAVCGEGPKERLDSTAVS      102
g8816.t1        PIAFLFPGQGSQAVGMLKESQ-ELPAVKKMLATAQAMLGYDLLALCLEGPKEKLDDTVYS      299
                 :**:*****:*:*** **   .:**.*:::  *. :*******:* *****:**.*. *

g6284.t1        QPAIYVASLAALEKLKAEQGPEAADAADVCCGLSLGEYTALTHAGALSFDDGVRLVKIRG      162
g8816.t1        QPALFVAGLAAVERLRS-QSPATVDGCSACAGLSLGEYAALVFAGAMSFEDGLKVVKVRA      358
                ***::**.***:*:*:: *.* :.*....*.*******:**..***:**:**:::**:*.

g6284.t1        ESMQAAAD-AQPSGMVSVIGLSADKVAELCEAASKEVPEGQGVRIANYLCNGNYAVSGGI      221
g8816.t1        ESMAAAAKLGKGHGMLSVVGLGDADLEAICASVRASRP-GDICQLANFLFPQGRVVSGHK      417
                *** ***. .:  **:**:**.  .:  :* :.  . * *:  ::**:*   . .***

g6284.t1        AGCEALEGMAKSFKARMTVRLAVAGAFHTDFMAPAREKLQEALAGTTIREPRIPVVSNVD      281
g8816.t1        DALEEVQRQATAKGALKAVPLAVSGAFHTPLMQPARDALTQVLASVTISEPRIPIYSNVT      477
                 . * ::  *.:  *  :* ***:***** :* ***: * :.**..** *****: ***

g6284.t1        AAPHSDPDVIKSILAQQLTAPVQWETSIRTLLDRGLERSYEIGPNKVIAGIMKRIDKTHP      341
g8816.t1        GEPFKDAADIQALLPRQLVEPVQWEGTVRKLVAAGKNQMHELGPGMQIKAMVKRIDNTAW      537
                . *..*   *:::* :**. ***** ::*.*:  * :: :*:**.  * .::****:*

g6284.t1        LENITV--  347
g8816.t1        AAFKNLAA  545
                    .:
```

Figure S10. Alignment of *Chlorella vulgaris* 211/11P g3658 gene product with HAP2 from *Chlamydomonas reinhardtii.*

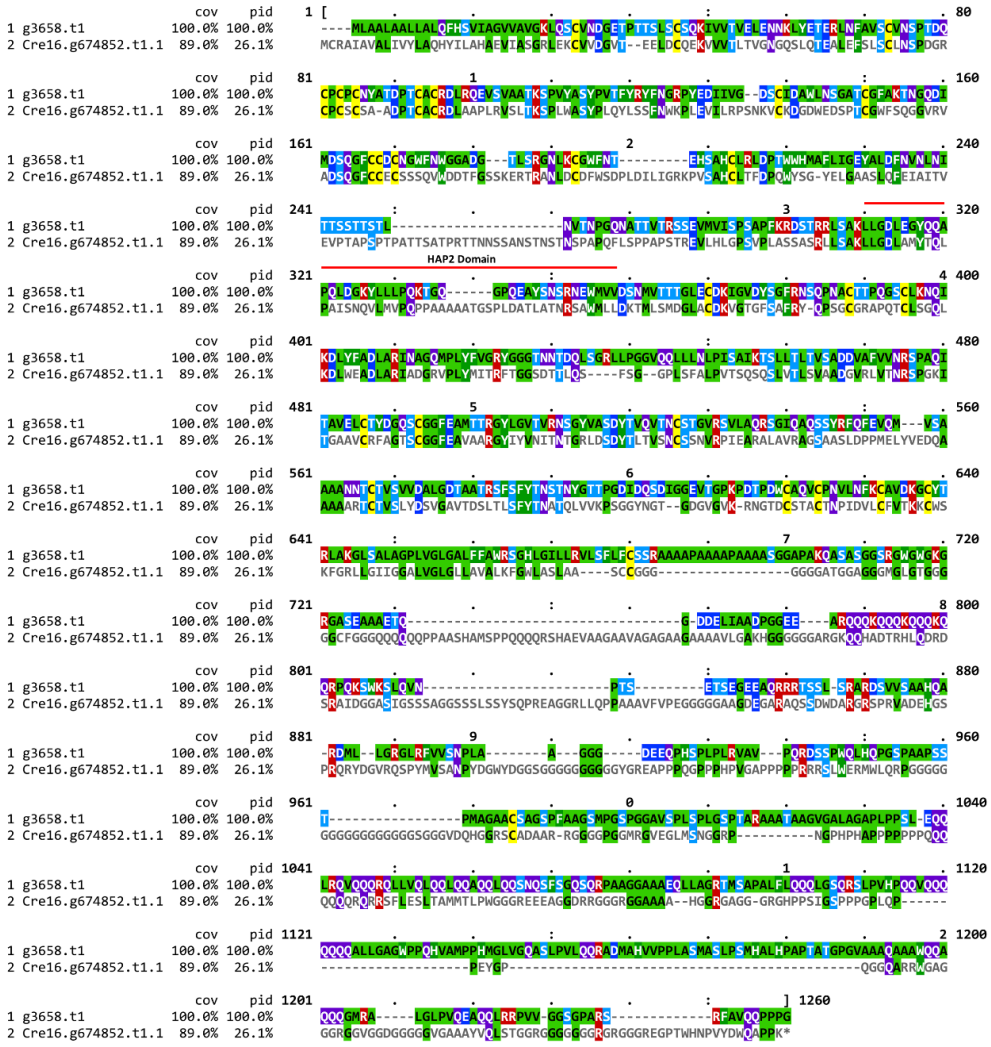

Supplemental Tables

Table S1. Summary of raw PacBio and Illumina sequencing data and Bionano mapping data.

	PacBio	Illumina	Bionano
Number of bases (Gb)	6.4	2.5	69.0
Number of reads	1,113,721	25,428,036	566,536
Genome coverage	128X	50X	1380X
Mean read length (bp)	5,784	100	121,810
N50 (in bp)	8,757	100	191,600

Table S2. *Chlorella vulgaris* 211/11P genome assembly statistics. *Two round assembly merged, not polished

	Falcon assembly*	Bionano consensus genome Map	Hybrid assembly	Unplaced	Chloroplast	Mitochondrion	Hybrid assembly + Unplaced without organelle contamination
Total assembly length (bp)	39,785,701	171,505	39,740,717	440,075	165,504	91,583	40,180,792
Number of sequences	62	255	14	29	1	1	43
Sequence average length (bp)	641,704	673,000	2,838,622	15,175	165,504	91,583	934,437
Sequence N50 (bp)	1,800,706	1,049,000	2,825,136	29,425	165,504	91,583	2,825,136
Sequence L50	8	54	6	4	1	1	6
Sequence N90 (bp)	795,186	346,446	2,150,204	6,908	165,504	91,583	2,150,204
Sequence L90	19	160	12	16	1	1	12
Largest sequence (bp)	5,417,522	5,015,440	5,422,624	128,459	165,504	91,583	5,422,624
Smallest sequence (bp)	416	50,112	795,975	416	165,504	91,583	416
% GC content	61.6	//	60.2	59.4	31.7	29.8	60.0
Number of gap	0	//	12	0	0	0	12
Total gap length (bp)	0	//	634,943	0	0	0	634,943

Table S3. Single nucleotide variants (SNV) and insertion-deletion (InDel) in the *Chlorella vulgaris* 211/11P assembled genome before and after correction with Illumina and PacBio data.

	PacBio	PacBio+Illumina
SNV	3076	81
InDel	32821	190
TOTAL	35897	271
% GENOME	0.09%	0.0007%

Table S4. Comparison of *Chlorella vulgaris* genomes reported for strain UTEX 395 and 211/11P.

	Chlorella vulgaris UTEX 395 (Guarnieri et al 2018)	*Chlorella vulgaris* 211/11P (this work)
Total sequence length	37,342,230	40,437,856
Total assembly gap length	40,625	634,943
Gaps between scaffolds	0	0
Number of scaffolds	3,600	14
Scaffold N50	27,824	2,825,136
Scaffold L50	358	6
Number of contigs	4,754	45
Contig N50	20,333	1,802,178
Contig L50	501	8
Number of component sequences (WGS or clone)	3,600	43

Table S5. Codon usage in *Chlorella vulgaris* 211/11P. The codon usage table gives for each codon: i. Sequence of the codon. ii. The encoded amino acid. iii. The proportion of usage of the codon among its redundant set, i.e. the set of codons which code for this codon's amino acid. iv. The expected number of codons, given the input sequence(s), per 1000 bases. v. The observed number of codons in the input sequences.

#Codon	AA	Fraction	Frequency	Number
GCA	A	0.253	37.206	219120
GCC	A	0.299	44.031	259312
GCG	A	0.257	37.744	222285
GCT	A	0.191	28.126	165643
TGC	C	0.807	13.076	77007
TGT	C	0.193	3.132	18448
GAC	D	0.673	30.175	177711
GAT	D	0.327	14.646	86253
GAA	E	0.174	9.821	57841
GAG	E	0.826	46.536	274064
TTC	F	0.574	15.009	88392
TTT	F	0.426	11.137	65592
GGA	G	0.101	8.659	50998
GGC	G	0.579	49.753	293009
GGG	G	0.194	16.684	98255
GGT	G	0.126	10.870	64018
CAC	H	0.757	17.008	100166
CAT	H	0.243	5.454	32123
ATA	I	0.120	3.013	17743
ATC	I	0.610	15.291	90055
ATT	I	0.270	6.762	39822
AAA	K	0.144	4.609	27143
AAG	K	0.856	27.343	161029
CTA	L	0.030	3.019	17777
CTC	L	0.149	14.949	88040
CTG	L	0.636	63.856	376067
CTT	L	0.072	7.198	42392
TTA	L	0.008	0.852	5017
TTG	L	0.104	10.452	61556
ATG	M	1.000	19.628	115598
AAC	N	0.784	16.095	94787
AAT	N	0.216	4.424	26056
CCA	P	0.210	13.228	77906
CCC	P	0.322	20.337	119770
CCG	P	0.265	16.701	98356
CCT	P	0.204	12.849	75669
CAA	Q	0.149	9.126	53746
CAG	Q	0.851	51.994	306208
AGA	R	0.036	2.264	13336
AGG	R	0.133	8.447	49746
CGA	R	0.096	6.071	35754
CGC	R	0.383	24.222	142651
CGG	R	0.260	16.441	96828
CGT	R	0.092	5.836	34368
AGC	S	0.431	31.268	184148
AGT	S	0.068	4.947	29137
TCA	S	0.105	7.604	44785
TCC	S	0.169	12.228	72014
TCG	S	0.127	9.212	54252
TCT	S	0.101	7.292	42943
ACA	T	0.220	10.108	59529
ACC	T	0.392	18.005	106035
ACG	T	0.232	10.661	62786
ACT	T	0.156	7.150	42107
GTA	V	0.052	3.318	19543
GTC	V	0.201	12.871	75804
GTG	V	0.635	40.676	239551
GTT	V	0.112	7.183	42301
TGG	W	1.000	13.320	78445
TAC	Y	0.754	13.708	80730
TAT	Y	0.246	4.481	26391
TAA	*	0.086	0.164	964
TAG	*	0.210	0.398	2346
TGA	*	0.703	1.331	7840

These supplementary are available online:

https://onlinelibrary.wiley.com/doi/full/10.1111/tpj.14508

Table S6. Identification of *Chlorella vulgaris* 211/11P transcription factor differently expressed in low light (LL) *vs.* high light (HL) conditions.

Table S7. Identification of *Chlorella vulgaris* 211/11P most differently expressed genes in low light *vs.* high light.

Table S8. Identification of key genes involved in different metabolic pathway in *Chlorella vulgaris* 211/11P.

Table S9. Identification of key genes involved in lipid biosynthesis and degradation in *Chlorella vulgaris* 211/11P.

Table S10. Identification of genes involved in flagella and cilia formation in *Chlorella vulgaris* 211/11P according to the CiliaCut list.

Section C

Effect of CO_2 concentration on photosynthetic and respiratory pathways in two green algal species of the *Chlorella* genus

M. Cecchin[1], M. Paloschi[1], G. Busnardo[1], S. Cuine[2], Y. Li-Beisson[2], L. Wobbe[3] and M. Ballottari[1]

[1]Università degli Studi di Verona, Department of Biotechnology, 37134 Verona, Italy

[2]Institute of Biosciences and Biotechnologies of Aix-Marseille, Aix-Marseille University, CEA, CNRS, CEA Cadarache, Saint-Paul-lez Durance F-13108, France

[3]Bielefeld University, Faculty of Biology, Center for Biotechnology (CeBiTec), 33615, Bielefeld, Germany.

In this section we evaluated the metabolic adaptation to high CO_2 level of the two *Chlorella* species previously analysed. Indeed, microalgae, unicellular photosynthetic organisms, represent potential solutions to efficiently fix CO_2 through the light driven photosynthetic process. In order to boost CO_2 fixation in microalgae it is essential to elucidate the physiologic and metabolic responses at the base of CO_2 assimilation and carbon flow. In this work two different Trebouxiophyceae species, *Chlorella sorokiniana* and *Chlorella vulgaris*, were investigated for their metabolic responses to different CO_2 availability. High CO_2 flux caused a common increase in biomass accumulation but a different response of plastid and mitochondrial metabolisms. In *C. sorokiniana* we observed a higher carbon fixation in high CO_2 condition, a balance of the NADPH redox state and a similar total respiration in the two conditions analysed. Moreover, in this species were observed several rearrangements of the photosynthetic machinery. In *C. vulgaris* we reported a higher carbon fixation in high CO_2 condition and a higher NADPH consumption suggesting that the chloroplast subtract reducing power from the mitochondrion that indeed showed a lower total dark respiration. These findings highlight different metabolic response to high/low CO_2 availability among green algae and suggest possible biotechnological manipulation in order to boost CO_2 fixation.

INTRODUCTION

Microalgae produce half of the oxygen present in the atmosphere and contribute to half of the total carbon worldwide (Li-Beisson et al. 2019; Salomé and Merchant 2019). Indeed, thanks to the photosynthetic process algae exploit light to fix CO_2 in organic compound. Carbon dioxide is one of the most important greenhouse gasses responsible of the global warning. CO_2 level in the Earth's surface is constantly increasing reaching 407.4 ± 0.1 ppm for 2018, an increase of 2.4 ± 0.1 ppm from 2017 (Dlugokencky et al., 2019). Finding a way to reduce the global impact of CO_2 emissions is fundamental to reduce the effects of human activity in the worldwide poise.

Microalgae are emerging as possible solution to their ability to growth with high level of CO_2 producing biomass that can be exploited for several aims: as food or feed supplement, biofuels or to produce high value products. Moreover, these photosynthetic organisms do not require arable land, have a fast life cycle and can growth employing waste products and wastewater-derived effluent (Lum, Kim, and Lei 2013).

Light is harvested in the algae chloroplast by pigment binding protein complexes called Photosystem I (PSI) and II (PSII). These complexes are composed by a core complex, where photochemical reactions occur, and an external antenna system which increases light harvesting efficiency and is involved in photoprotection (Gao et al. 2018; Pan et al. 2019). PSI and PSII work in series in order to strip electrons from water and transfer them to $NADP^+$ producing NADPH. During this linear electron transport protons are pumped from stroma to the lumen generating an electrochemical gradient used by ATPase to synthetize ATP. ATP and NADPH are then used by the Calvin Benson cycle to fix CO_2 into sugars. In parallel in the mitochondria another electron transport chain takes place, consuming oxygen and NADH and releasing NAD^+ and ATP. A constantly balance between chloroplast and mitochondrion activity is fundamental for the survival of the cells and to overcome the ever-changing environmental conditions.

It is important to point out that CO_2 diffusion in the water environments, where microalgae live, is strongly reduced compared to CO_2 diffusion in air: for this reason microalgae evolved an efficient system for CO_2 accumulation in the cell called Carbon Concentrating Mechanism (CCM), a complex mechanism by which inorganic carbon is actively transported close to the enzyme responsible for its fixation, the RUBISCO enzyme, which is co-localized with the carbonic anhydrase necessary for dehydration of bicarbonate. CCM mechanism is induced at low CO_2 concentration due to the fact that CO_2-limitation reduces the consumption of ATP and NADPH by the Calvin Benson cycle leading to an over-reduced photosynthetic electron transport chain (Wang, Stessman, and Spalding 2015). CO_2 availability is thus a critical issue for photosynthetic efficiency and biomass accumulation in microalgae cultures: in the case of model organism *Chlamydomonas reinhardtii* CO_2 has been reported to act as a

molecular switch inducing a complex network of cell adaptation, among which a fine control of accumulation of PSII antenna complexes at the translation level. In particular, in condition of low CO_2 concentration, the accumulation of cytosolic RNA-binding protein NAB1 is triggered: this subunits down-regulates the translation of transcripts encoding light-harvesting antenna proteins acting as a translational repressor (Berger et al. 2014; Mussgnug et al. 2005). The reduction of PSII antenna proteins reduces the excitation pressure on the photosynthetic apparatus as a response of reduced CO_2 availability (Berger et al. 2014).

Among several microalgae species discovered nowadays Trebouxiophyceae represent an evolutionary defined class of green algae (Chlorophyta) comprising the green freshwater algae of the *Chlorella* genus, one of the first microalgae to be cultured on a large scale due to their easy cultivation and high resistance to stresses (Borowitzka et al. 2018; Yang et al. 2016). Species belonging to the Trebouxiophyceae class are evolutionarily divided from the model species of green algae, *C. reinhardtii*, belonging to the Chlorophyceae class. *Chlorella* species are interesting for industrial cultivation of microalgae, being reported rapidly accumulating biomass containing high lipids, proteins, carotenoids and vitamins content (Lum et al. 2013). However, the lack of genetic resources and the low efficiency of transformation methods has limited the development of genetic engineering in these species (Lin et al. 2019).

In this work two *Chlorella* species, *Chlorella sorokiniana* and *Chlorella vulgaris*, were investigated for their physiologic and metabolic responses to different CO_2 availability highlighting different metabolic response to high/low CO_2 availability among green algae. Indeed, to boost carbon use efficiency is necessary elucidate in fine details the metabolic rearrangements at the base of CO_2 assimilation and carbon flow.

RESULTS

Biomass productivity and composition

C. sorokiniana and *C. vulgaris* cells were grown in 80 ml batch airlift photobioreactors bubbled with air (atmospheric level of CO_2 concentration of ~0.04%, defined as AIR condition throughout the manuscript) or air enriched with 3% of CO_2 (defined as CO_2 condition throughout the manuscript). *Chlorella* strains were cultivated at 300 µmol photons m^{-2} s^{-1} until the saturation phase was reached. Growth kinetics were followed by measuring the optical density at 720nm and fitted with sigmoidal function as showed in Figure 1A and 1D, for *C. sorokiniana* and *C. vulgaris* respectively. In both species the supplement of CO_2 enhanced the growth with a steeper growth rate as highlight by first derivate of the growth curves (Figure 1B-1E). Total biomass production showed an increase by 153% and 169%, respectively in *C. sorokiniana* and *C. vulgaris*, in CO_2 compared to AIR condition (Figure 1C-1F). Moreover, the maximum daily productivity was increased of more than 4 times in both species in CO_2

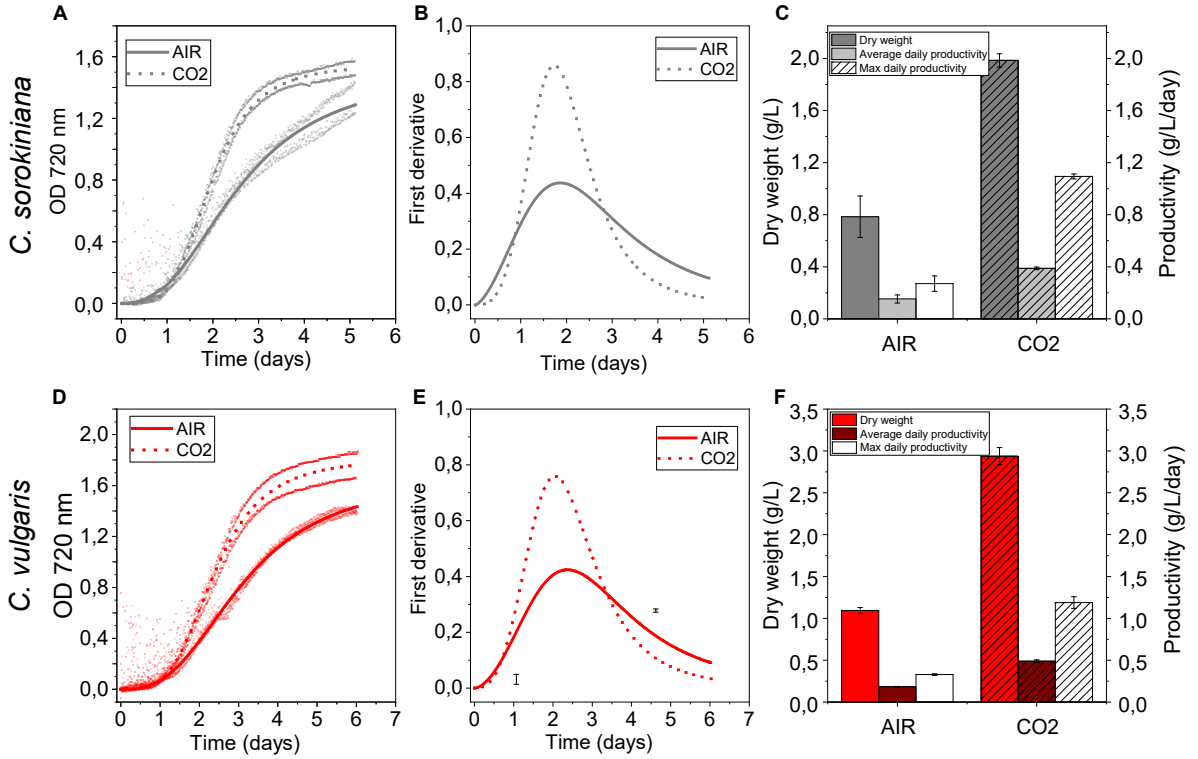

Figure 1. Growth curve and biomass productivity in *C. sorokiniana* (panel A-C) and *C. vulgaris* (panel D-F) in AIR condition (~0.04% CO_2, solid line or full colour) compared to CO_2 condition (3% CO_2, dash line or colour). (A, D): growth curve obtained measuring OD at 720nm fitted with sigmoidal function. (B, E): first derivate of growth curves reported in panels A and D. (C, F) Dry weight (g/L), average and maximum daily productivity (g L^{-1} day^{-1}) obtained harvesting the biomass at the end of the growth curve. Error bars are indicated as standard deviation (n=3).

condition (Figure 1C-1F). These data confirmed that in the cultivation conditions adopted the photosynthetic process was limited by the CO_2 availability in AIR condition.

Biomass composition at the end of the growth curve was evaluated underling a significant increase of lipids in both species, while different effects were observed in the case of proteins and starch content per dry weight (Figure 2). Indeed, CO_2 condition triggered an accumulation of proteins only in the case of *C. sorokiniana*, while a decrease of starch content was observed in *C. vulgaris* grown in CO_2. This suggests a different behaviour of the two species characterized by diverse metabolic rearrangement leading to different storage strategies in presence of the surplus of carbon dioxide.

Lipid analysis was then performed showing in both species a decrease of the fraction of phospholipids in CO_2 condition with an increase of galactolipids in *C. sorokiniana* and of triacylglycerols (TAG) in *C. vulgaris* (Figure 3A-3D). Lipid fraction was further investigated by GC analysis (Figure 3B-3E) and by thin layer chromatography (Figure 3C-3F). Interestingly a strong increased of monogalactosyldiacylglycerol (MGDG) and digalactosyldiacylglycerol (DGDG) were observed in *C. sorokiniana* in CO_2 (Figure 3C). These classes of lipids constitute the major component of the chloroplast

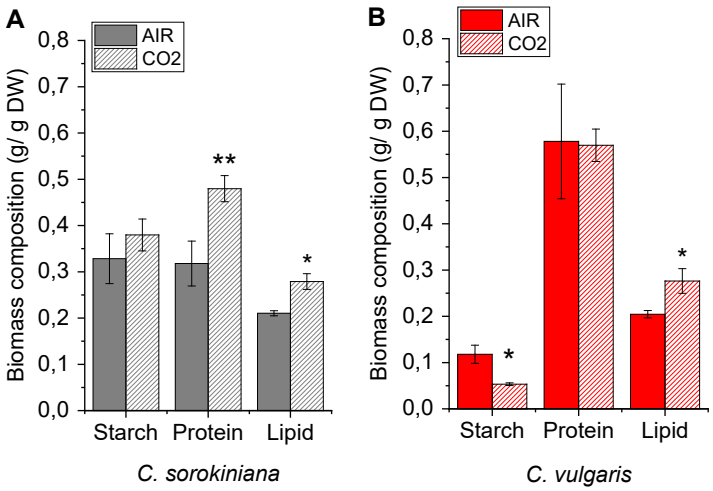

Figure 2. Relative starch, protein and lipid content per dry weight in *C.sorokiniana* (Panel A) and *C. vulgaris* (Panel B) in AIR (full colour) *vs.* CO_2 condition (dash colour). Data are means of three biological replicates with standard deviation shown (n=3). Significantly different values in CO_2 versus AIR are indicated by * if $p < 0.05$ and ** if $p < 0.01$, as determined by student *t*-test.

membrane suggesting possible rearrangements at level of the chloroplast organization.

TAG can derivate by recycling of preexisting membrane polar glycerolipids as well as from *de novo* biosynthesis of fatty acids (Simionato et al. 2013), in *C. vulgaris* most of the polar lipids classes were decreased in CO_2 condition (Figure 3F), likely due to the redirection of the metabolism in the TAG biosynthesis. Thus, at high CO_2 concentration *C. vulgaris* redirect the metabolism from the storage of starch to the storage of TAG, a more energetic biomass sink, while *C. sorokiniana* increased the fraction of lipids involved in thylakoids assembly.

Interesting DGTS content was increased in both species (Figure 3C-3F). DGTS are non-phosphorous betaine lipids that were found involved in the phosphate starvation response in fungi and recently found also in *Nannochloropsis oceanica* (Murakami et al. 2018; Riekhof et al. 2014). This might suggest that DGTS was accumulated in both species grown in CO_2 conditions due to nutrient deficiency at the end of the growth curve related to the fast growth rate.

The fatty acid profile resulting in *C. vulgaris* and *C. sorokiniana* grown in AIR and CO_2 is reported in Figure 3B-3E: in *C. vulgaris* cells grown in 3% CO_2 a strong increase in palmitic acid (16:0), hexadecadienoic acid (16:2), stearic acid (18:0) and oleic acid (18:1) was observed, together with a decreased of 3-hexadecenoic acid (16:1 (3t)). In *C. sorokiniana* in CO_2 condition an increase of palmitoleic acid (16:1 (9)), hexadecadienoic acid (16:2), hexadecatrienoic acid (16:3), linoleic acid (18:2) and α-Linolenic acid (18:3) and a decrease of oleic acid (18:1) was reported. The strong increase in palmitic and oleic acid observed in *C. vulgaris* is in line with the increased TAG accumulation observed in this species, being C16:0 and C18:1 fatty acids the main constituent of TAG in oil bodies in microalgae (Siaut et al. 2011).

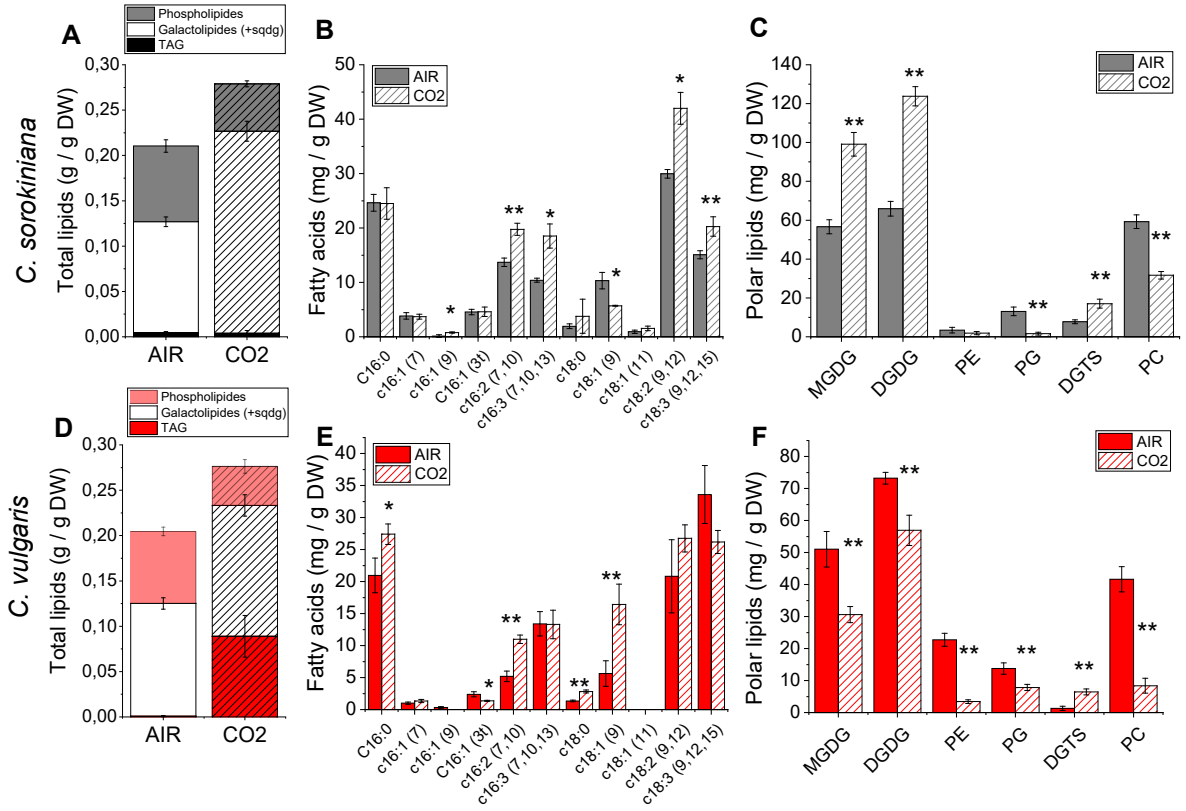

Figure 3. Lipid composition of biomass in *C. sorokiniana* (panel A-C) and *C. vulgaris* (panel D-F). Panel A and D: lipid composition in AIR (full colour) *vs.* CO_2 (dash colour) condition in terms of phospholipids, galactolipids and triacylglycerol (TAG). Panel B and E: Fatty acids profile obtained by gas chromatography. Panel C and F: Polar lipid profile obtained by thin layer chromatography. Data are means of three biological replicates with standard deviation shown. Significantly different values in CO_2 versus AIR are indicated by * if $p < 0.05$ and ** if $p < 0.01$, as determined by student *t*-test. MGDG, monogalactosyldiacylglycerol; DGDG, digalactosyldiacylglycerol; PG, phosphatidylglycerol; PE, phosphatidylethanolamine; PC, phosphatidylcholine; DGTS, diacylglycerol N,N,N-trimethylhomoserine.

High CO_2 level altered chlorophylls content and photosystems organization only in *C. sorokiniana*

The fluorescence parameter of F_v/F_m define the PSII maximum quantum yield and thus can be used as indicator of the wellness of the culture. As reported in Figure 4C similar F_v/F_m values were reported in both conditions. Interesting we observed a strong decreased chlorophylls per cells ratio in *C. sorokiniana* grown in CO_2 condition, but any difference was detected in *C. vulgaris* (Figure 4A). Cells of *C. sorokiniana* grown with 3% CO_2 showed a 40% less Chl/cell ratio compared to cell grown in AIR condition, suggesting a rearrangement of the photosynthetic machinery, not observed in the case of *C. vulgaris* but previously reported for the model algae *C. reinhardtii* (Polukhina et al. 2016).

Interestingly in the case of *C. sorokiniana* an increased Chl a/b ratio was evident in CO_2 condition (Figure 4B): Chl *b* is bound only to the Light Harvesting Complexes (LHC) subunits, the external antenna proteins of photosystems, while Chl *a* is bound to both antennae and core complex. A variation of the Chl a/b ratio suggests a change in the antenna/core complex stoichiometry.

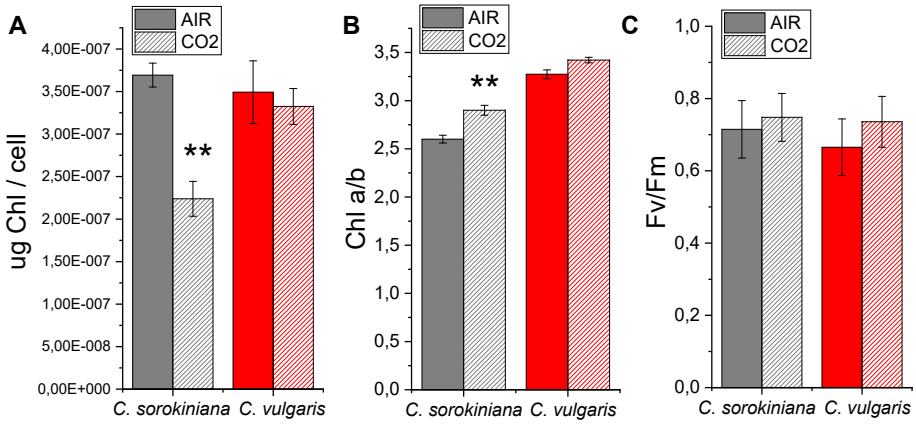

Figure 4. (A) Chlorophylls content per cell, (B) chlorophylls a/b ratio and (C) PSII maximum quantum yield expressed as F_v/F_m ($(F_m-F_0)/F_m$) in *C. sorokiniana* (grey colour) and *C. vulgaris* (red colour) in AIR (full colour) or CO_2 (dash colour) condition. Data are means of three biological replicates with standard deviation shown. Significantly different values in CO_2 versus AIR are indicated by ** ($p < 0.01$), as determined by student *t*-test.

To better investigated remodelling of the component of electron transport chain PSI/PSII ratio and LHCII/PSII ratio were evaluated (Figure 5). Immunoblot analysis confirmed rearrangements of the photosynthetic apparatus in *C. sorokiniana* but not in *C. vulgaris*: in *C. sorokiniana* both PSI/PSII and LHCII/PSII ratio were decreased in CO_2 condition indicating a reduction of the light harvesting complexes of PSII and a reduced content of PSI on chlorophylls basis in CO_2 enriched condition. The reduced LHCII/PSII ratio observed in *C. sorokiniana* fits well with the reduced Chl/cell and increased Chl a/b ratio.

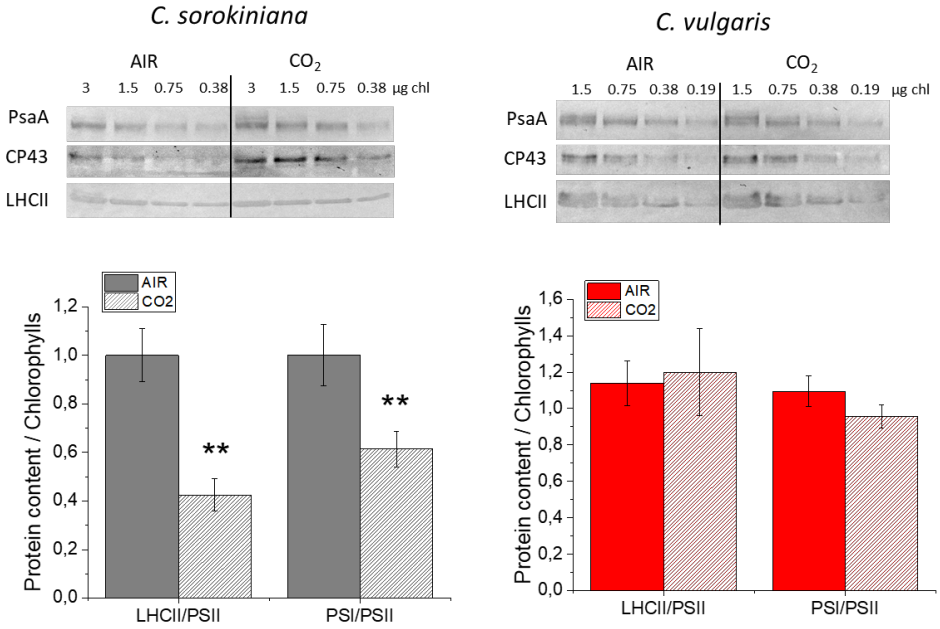

Figure 5. Immunoblot analysis of the PSI (PsaA antibody), PSII (CP43 antibody) and LHCII (LHCII antibody) and ratio PSI/PSII and LHCII/PSII calculated by lane quantification for *C. sorokiniana* (left panel, grey colour) and *C. vulgaris* (right panel, red colour) in AIR (full colour) or CO_2 (dash colour) condition. Data are means of three biological replicates with standard deviation shown. Significantly different values in CO_2 versus AIR are indicated by ** ($p < 0.01$), as determined by student *t*-test.

In *C. reinhardtii* was reported that the higher CO_2 availability increased the functional PSII antenna size (Berger et al. 2014), thus we investigated PSII antenna size in the *Chlorella* species herein analysed. Fast Chl *a* fluorescence emission in presence of DCMU was measured for both *C. vulgaris* and *C. sorokiniana* grown in AIR and CO_2 condition: functional antenna size of PSII was indeed reported to be inversely proportional to the time require to reach 2/3 of the maximum fluorescence emission (Shmuel Malkin et al. 1981). As reported in Supplemental Figure S2 no difference in PSII functional antenna size was measured neither in *C. sorokiniana* nor in *C. vulgaris* depending on CO_2 availability. This result indicates that the reduction of LHCII/PSII ratio measured in the case of *C. sorokiniana* was not affecting the PSII light harvesting capacity.

LHC complexes are also involved in the process called state transitions, where a fraction of the antenna complexes bound to PSII moves to PSI in order to maintain the excitation balance between the two photosystems. This process is triggered in *C. reinhardtii* by LHC phosphorylation catalysed by a kinase enzyme called STT7 (Depege, Bellafiore, and Rochaix 2003). As reported in Figure 6, upon induction both *C. vulgaris* and *C. sorokiniana* were able to undergo state transitions in both AIR and CO_2 conditions. However, in the case of *C. vulgaris*, cells grown in 3% CO_2 exhibited an increased capacity for state transitions compared to cells grown in AIR.

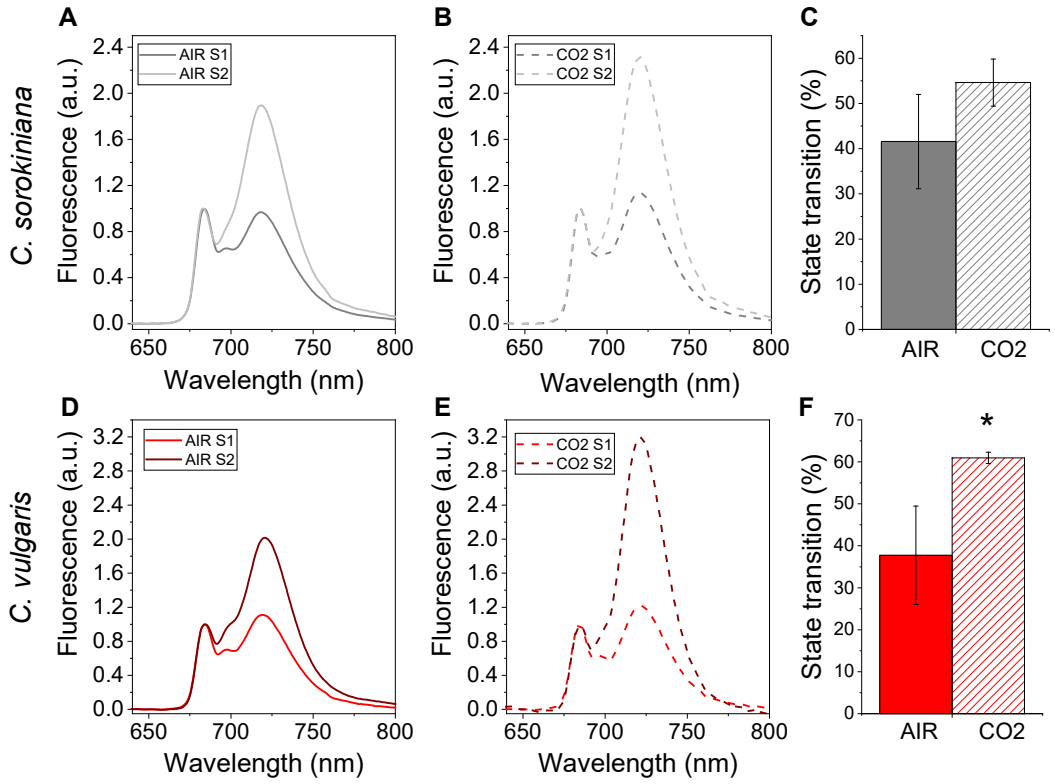

Figure 6. State transitions analysis by 77K fluorescence emission spectra in state 1 (S1) or state 2 (S2) conditions in *C. sorokiniana* (grey colour, upper part) and *C. vulgaris* (red colour, bottom part) in AIR (full colour or solid line) or CO_2 (dash colour or line). Data in C e F are means of biological replicates with standard deviation shown (n=4 per *C. vulgaris*, n=3 per *C. sorokiniana*). Significantly different values in CO_2 versus AIR are indicated by * ($p < 0.05$), as determined by student *t*-test.

The lower level of PSI on chlorophylls basis in *C. sorokiniana* in CO_2 condition was confirmed by *in vivo* measurement of P700 photochemical activity, being P700 the reaction center of PSI (Figure 7). PSI activity was followed measuring the formation of oxidized P700 by transient absorption measurements at 830 nm: increased P700 oxidation was measured during a saturating pulse of light in the presence of DCMU, which inhibits linear electron transport, and ascorbate and methyl viologen as electron donor and acceptor, respectively. In the case of *C. sorokiniana* a reduction of the maximum PSI activity was observed in CO_2 condition, confirming the western blot analysis.

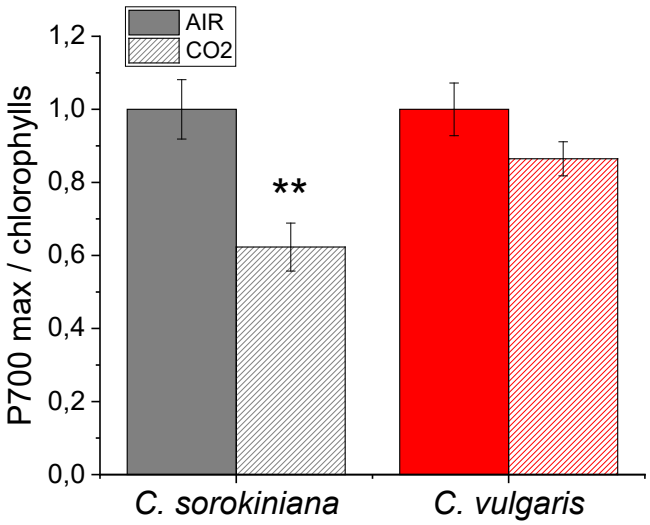

Figure 7. Maximal P700 oxidation on a chlorophyll basis in *C. sorokiniana* (left, grey colour) and *C. vulgaris* (right, red colour) in AIR (full colour) or CO_2 (dash colour) normalized to AIR condition. Data are means of three biological replicates with standard deviation shown. Significantly different values in CO_2 versus AIR are indicated by ** ($p < 0.01$), as determined by student *t*-test.

High CO_2 concentration altered ATP and NADPH balance

Photosynthetic electron transport is coupled with the formation of a proton gradient across the thylakoid membrane, exploited by ATPase as proton motif force to produce ATP. ATPase content on chlorophylls basis and proton-motive force (*pmf*) upon exposure to different light intensity were evaluated (Figure 8). Proton motive force (*pmf)* can be quantified measuring the light dependent-electrochromic shift of carotenoid absorption (Bailleul et al. 2010). In this case the behavior of the two *Chlorella* species was similar: an increase of the ATPase content in CO_2 condition combined with a reduced *pmf*. Likely the higher level of ATPase pumped faster the proton in the stroma resulting in a higher ATP production in CO_2 sample reducing the accumulation of the *pmf* across the membrane. Furthermore, we investigated the influence of cyclic electron flow (CEF) around PSI measuring ECS in presence of DCMU to inhibit linear electron flow (Figure 8B-8D, darker lines). Only a 2-7% of residual *pmf* was detected, indicating a low level of CEF not correlated with CO_2 concentration level.

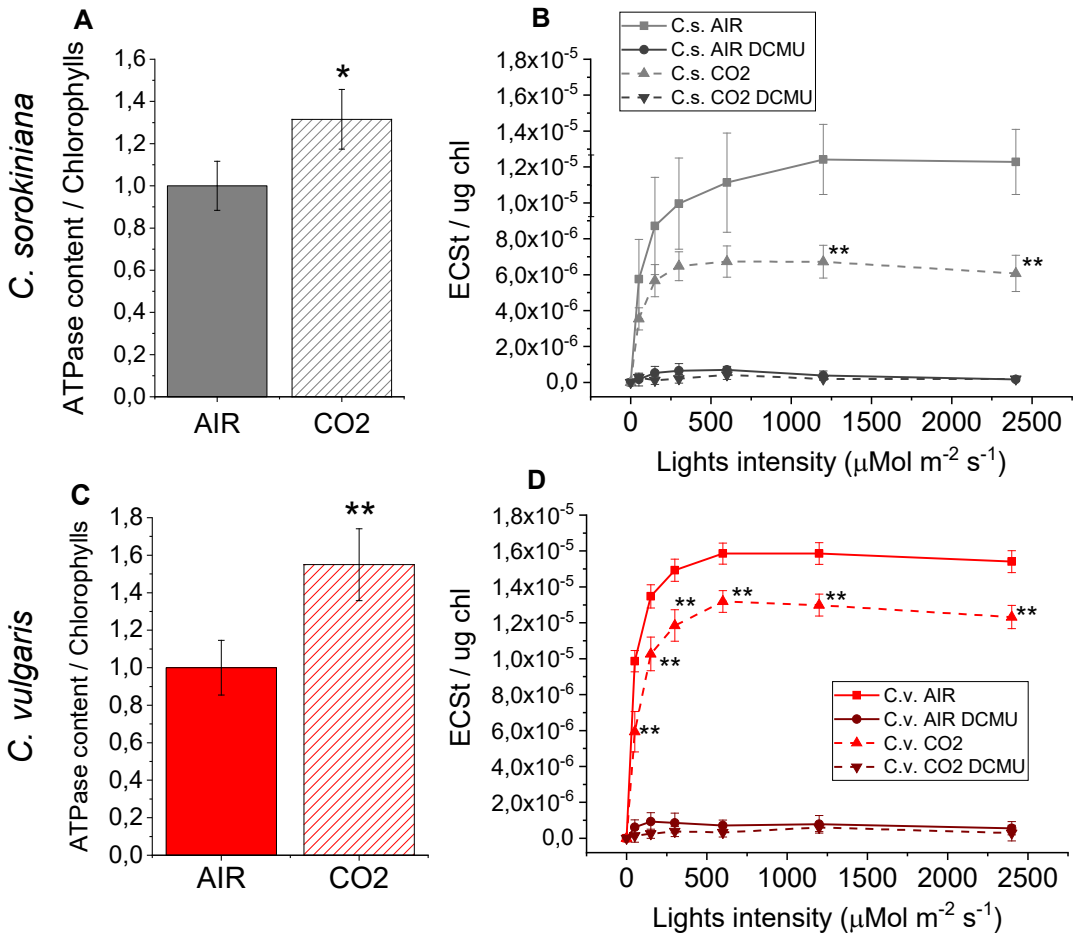

Figure 8. Immunoblot analysis of ATPase content (atpC subunit antibodies) and ECS measurements in *C. sorokiniana* (grey colour) and *C. vulgaris* (red colour) in AIR (full colour or solid line) or CO_2 (dash colour or line) condition. Data are means of three biological replicates with standard deviation shown. Significantly different values in CO_2 versus AIR are indicated by * if $p < 0.05$ and ** if $p < 0.01$, as determined by student *t*-test.

PSI is a plastocyanin-ferredoxin oxidoreductase that reduces $NADP^+$ to NADPH by a ferredoxin–$NADP^+$ reductase (FNR) enzyme. In parallel in the mitochondrion the respiratory electron transport chain oxidase NADH releasing NAD^+. Chloroplasts and mitochondria communicate to balance the NAD^+/NADH pool (Johnson and Alric 2013; Uhmeyer et al. 2017). We evaluated the NADPH formation rate by following NADPH fluorescence changes upon exposure to actinic light of 300 µmol photons m^{-2} s^{-1} for 120s. In both species either in AIR and CO_2 condition the rates of NADPH fluorescence during actinic light exposure were negative, indicating that the NADPH consumption was higher than the production (Figure 9). It's interesting to observe that in *C. sorokiniana* the same balance between NADPH formation and consumption was maintained comparing AIR *vs.* CO_2 condition, while in *C. vulgaris* a higher rate of NADPH consumption was observed in CO_2 condition.

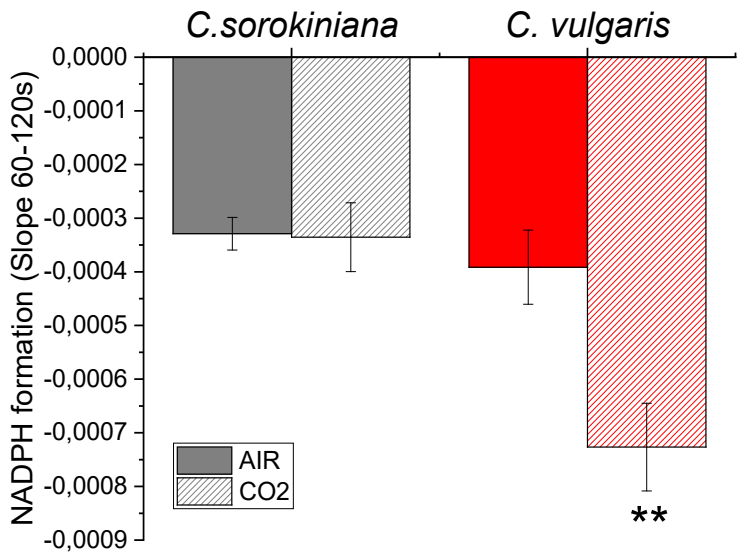

Figure 9. Rate of NADPH formation upon exposure to 300 µmol photons $m^{-2}s^{-1}$ of light for 120s in *C. sorokiniana* (grey colour) and *C. vulgaris* (red colour) in AIR (full colour) or CO_2 (dash colour) condition. Data are means of three biological replicates with standard deviation shown. Significantly different values in CO_2 versus AIR are indicated by ** ($p < 0.01$), as determined by student *t*-test.

Effects of CO_2 on the mitochondrial respiration

Mitochondrial respiration is a fundamental process that allows to produce ATP releasing NAD^+ that can return to the chloroplast where is reduced by FNR enzyme. The mitochondrial electron transport chain, also called cytochrome pathway, includes an ATP synthase complex, called also complex V, and four oxidoreductase complexes that oxidase the reducing power and produce ATP thank to the electrochemical gradient that is formed across the membrane. In addition, an alternative oxidase (AOX) might operate directly coupling the oxidation of ubiquinol with the reduction of O_2 to H_2O introducing a branch in the electron transport chain dramatically reducing the energy yield (ATP). AOX have a role in the protection mechanism for the respiratory chain (Boekema and Braun 2007; Vanlerberghe 2013).

The contribution of cytochrome and alternative pathways (Figure 10) was investigated measuring the dark respiration in the presence of two specific inhibitor: SHAM (salicylhydroxamic acid) that inhibits the alternative oxidase and so the alternative pathway, and myxothiazol that locks the complex III blocking the cytochrome pathway (Dang et al. 2014). We observed that the total dark respiration on cells basis is essentially unaffected in *C. sorokiniana*, instead a strong reduction was reported for *C. vulgaris* in CO_2 condition. In both species a reduction of the fraction of dark respiration operating through AOX was evident, leading to an increased efficiency of ATP production by NADH oxidation through the cytochrome pathway.

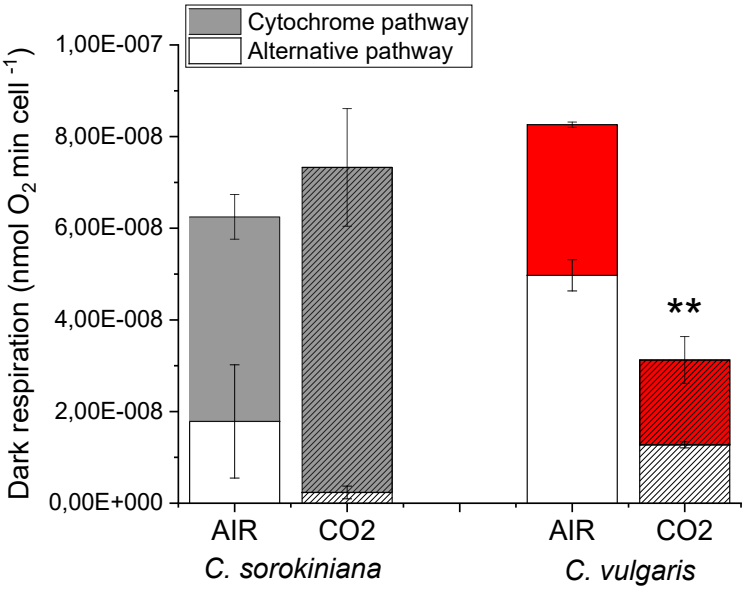

Figure 10. Dark respiration in *C. sorokiniana* and *C. vulgaris* in AIR and CO_2 conditions normalized to cells content. The relative contribution of cytochrome (full colour) and alternative respiration (blank colour) was reported. Data are means of three biological replicates with standard deviation shown. Significantly different values in CO_2 versus AIR are indicated by ** ($p < 0.01$), as determined by student *t*-test.

DISCUSSION

Atmospheric CO_2 concentration has significantly increased over the last 100 years. This has strongly contributed to climate change and global warming leading to a potential severe environmental crisis. Microalgae are promising platforms to capture CO_2, possibly integrating microalgae cultivation with CO_2 recovery from flue gasses, thus reducing industry derived CO_2 emission. For this reason, understanding the metabolic pathways involved in the CO_2 metabolism is crucial to develop new strategies for improving the ability of microalgae to acquire and accumulate carbon. In this work we focus our attention in two *Chlorella* species widely use at industrial level, *C. sorokiniana* and *C. vulgaris,* growing them bubbled with atmospheric level of CO_2 (~0.04% CO_2, AIR condition) or 3% CO_2 (CO_2 condition). In CO_2 condition a ~160% increased of biomass yield was observed in both species, but the biomass composition was different in the two species (Figure 1 and 2). In *C. vulgaris* a decrease of starch accumulation and an increase of lipid accumulation, in particular of TAG, were detected. This suggests a redirection of the energy reserves from starch to TAG accumulation, a class of macromolecules with a higher energy content per gram, indicating an improved light energy conversion. In *C. sorokiniana* not only lipids, but also proteins content increased, being the latter the major sink for the extra-carbon fixation occurring in cells grown at high CO_2 concentration. Differently from *C. vulgaris*, in *C. sorokiniana* the increase in the lipid fraction of total dry biomass was mainly related to an increase in polar lipid DGDG and MGDG, the major lipids of photosynthetic membranes

(Li-Beisson et al. 2019) (Figure 3). This increased content of DGDG and MGDG, however, was not correlated with the chlorophyll content per cell: the strong increase in protein content observed in *C. sorokiniana* grown in 3% CO_2 was indeed more evident than the increase in DGDG and MGDG, likely causing a preferential accumulation of macromolecules not related with the thylakoidal membranes or with a general re-organization of the thylakoid membranes. The observed reduction of Chl content per cell in *C. sorokiniana* grown in CO_2 condition compared to AIR was in line with the results obtained previously in *C. reinhardtii* (Polukhina et al. 2016), while this was not the case of *C. vulgaris*, where a similar Chl content was detected independently from CO_2 availability (Figure 4A). Again, similarly to the *C. reinhardtii* case, *C. sorokiniana* grown in CO_2 condition was characterized by reduction of LHCII/PSII content and a reduction of PSI/PSII ratio, while these adaptations were not observed in the case of *C. vulgaris* (Figure 5). The reduced LHCII/PSII content observed in the case of *C. sorokiniana* grown in CO_2 condition was not affecting the functional antenna size of PSII: differently from previous observation in *C. reinhardtii*, functional antenna size of PSII was not influenced by CO_2 availability in both *Chlorella* species herein investigated (Figure S2). In *C. reinhardtii* it was indeed reported that high CO_2 availability caused an increase of the functional antenna size of PSII, by translational control of antenna proteins by NAB1, repressor of translation of specific LHC subunit, inhibited at high CO_2 concentration (Berger et al. 2014). A following paper was instead reporting a general reduction of LHCII/PSII content in *C. reinhardtii* grown in high CO_2, in parallel with a decrease of PSI/PSII ratio (Polukhina et al. 2016). Considering the possibility of LHCII proteins to function as PSI antenna, it was not excluded by Polukhina and coworkers that the decrease of LHCII content per PSII observed at high CO_2 might be mainly related to the amount of LHCII proteins acting as PSI antenna. Here we report a similar acclimation mechanism only in the case of *C. sorokiniana*, with the difference that PSII antenna size was not modulated by CO_2 availability. In general it si possible to hypothisize that the increased capacity of Calvin Benson cycle to regenerate NAD^+ and ADP, thanks to the increased CO_2 availability, trigger the light phase of photosynthesis in order to keep the NADPH/NAD^+ ratio similar to the AIR case, as reported in Figure 9: this occurs by increasing the total amount of PSII compared to PSI and relatively redistributing the excitation pressure among PSI and PSII reducing the excitation pressure at the level of the former reducing the LHCII content bound. This acclimation process would explain the reduced LHCII/PSII content despite the similar PSII antenna size observed. The absence of such acclimation mechanisms in the case of *C. vulgaris* could be at the base of the strong reduction of NADPH/NAD^+ ratio observed at high CO_2 concentration, as a consequence of increased NADPH consumption by the Calvin Benson cycle.

Interestingly, the amount of RUBISCO was similar in both species in the two conditions analysed on a cell basis (Supplemental Figure S1), suggesting an enhanced RUBISCO activity due to the higher

availability of substrate rather than an upregulation of the enzyme.

In both species in CO_2 condition a decrease of *pmf* was reported together with an increased ATPase content (Figure 8), likely the higher level of ATPase prevent the accumulation of the electrochemical gradient, suggesting a higher ATP production in CO_2 condition. Interestingly, the total dark respiration is differentially regulated in the two *Chlorella* species (Figure 10): in *C. sorokiniana* total dark respiration was similar in AIR compared to CO_2 condition, with an increased NADH oxidation through the cytochrome pathway and reduced AOX activity. Differently, in *C. vulgaris* a strong reduction of dark respiration in CO_2 condition was evident, despite an increase of cytochrome/alternative pathway ratio. Additionally, in *C. vulgaris* there was a higher NADPH consumption in CO_2 suggesting that chloroplast acts as a sink of reducing power subtracting them from the mitochondrion. Moreover, the reduction of starch accumulation and the increase of TAG suggested a redirection of photosynthate. As already reported for *P. tricornutum* an increase of acetyl-coA, likely produced by glycolic pathway in our *Chlorella*, and reducing power is at the base of the increased TAG accumulation (Li-Beisson et al. 2019). In *C. sorokiniana* we observed the same balance of the NADPH redox state and a similar dark respiration in the two conditions analysed. The rearrangements of the photosynthetic machinery in CO_2 condition improved the pool of NADPH and ATP, likely matching the increased substrate (CO_2) availability for sugar production by the Calvin Benson cycle.

Increased photosynthates production in both *C. vulgaris* and *C. sorokiniana* is at the base of the observed increased biomass yield in CO_2 condition: sugars produced in the chloroplast are indeed redirected to the biosynthesis mainly of lipids (TAG) in *C. vulgaris*, and proteins in *C. sorokiniana*,

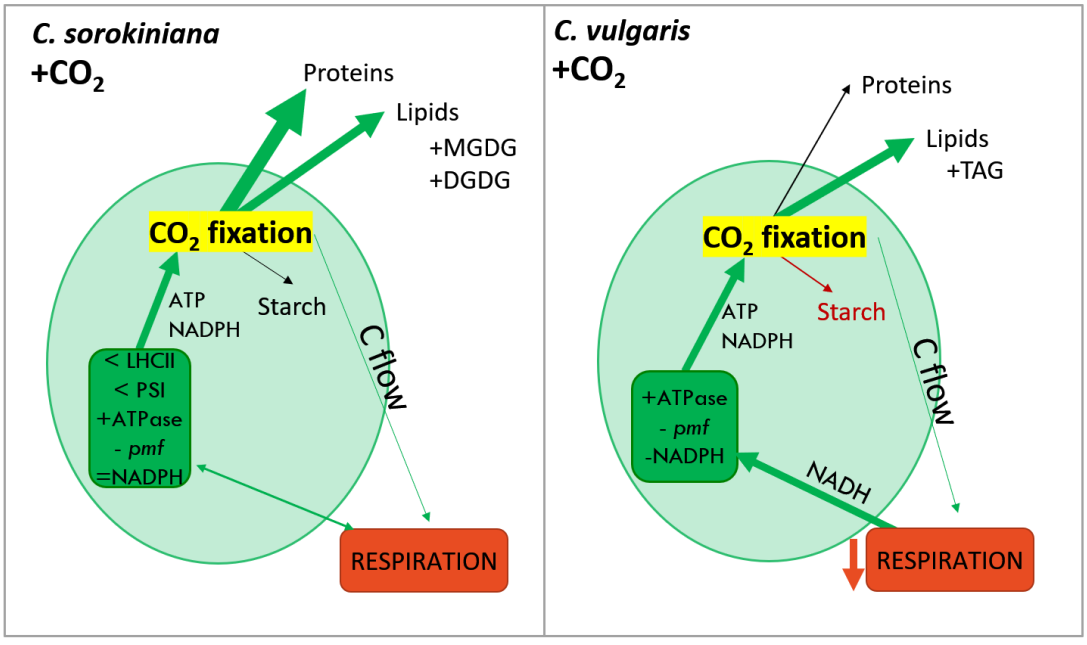

Figure 11. Model of the main metabolic rearrangements of *C. sorokiniana* and *C. vulgaris* cells grown with 3% CO_2.

indicating a general enhanced metabolism leading to a faster cell divisions and a steeper exponential growth phase in CO_2 condition. A summary of the adaptation to CO_2 condition is shown in Figure 11. Elucidation of the molecular rearrangements in enriched CO_2 condition could be useful in order to develop strategies to improve in these species and in other microalgae of industrial interest their sustainability, biomass yield and utilization for bioremediation.

MATERIAL AND METHODS

Microalgae cultivation. *C. sorokiniana* UTEX 1230 and *C. vulgaris* 211/11P strain (Culture Collection of Algae at Goettingen University CCAP 211/11P strain) cells were grown in the Multi-Cultivator MC 1000 tubes aerated with air or with 3% CO_2-enriched air obtained by a gas mixing system. Cells were grown in BG11 medium starting from $1*10^6$ cell/ml at 300 µmol photons $m^{-2}s^{-1}$ (Allen and Stanier 1968). Cell number was determined Countless®II FL automated cell counter (Thermo Fisher). The cell density was automatically monitored every ten minutes by measuring the absorption at 720 nm. For physiological measurements, cultures were harvested during the exponential growth phase. At the end of the growth curve the dry weight determination was performed: cell culture was harvested by centrifugation at 4500g for 5 min at 20°C then drying in a lyophilizer for 48h and then net dry weight was calculated.

Biomass composition analysis. Lipid, starch and protein content of the biomass harvested at the end of the exponential phase were analyzed as previously reported in Cecchin et al. 2019.

Photosynthetic parameters and pigments extraction. The pigments were extracted with 100% DMSO at 60°C in dark conditions and measured with Jasco V-550 UV/VIS spectrophotometer. Proton motive force upon exposure to different light intensities was measured by Electrochromic shift (ECS) with MultispeQ v2.0 (PhotosynQ) according to Kuhlgert et al. 2016 and normalized to the chlorophylls content of the sample. PSII activity was analyzed by fluorescence measurements on whole cells using a Dual-PAM 100 instrument (WALZ). 77K fluorescence emission spectra were acquired with a charge-coupled device spectrophotometer (JBeamBio) as previously described (Allorent et al. 2013). State transitions were measured on whole cells induced to state 1 or state 2 as described in Fleischmann et al. 1999. PSII functional antenna size was measured from fast chlorophyll induction kinetics induced with a red light of 11 µmol photons m^{-2} s^{-1} on dark-adapted cells incubated with 50 µM DCMU (S Malkin et al. 1981). The reciprocal of time corresponding to two-thirds of the fluorescence rise ($\tau_{2/3}$) was taken as a measure of the PSII functional antenna size (Shmuel Malkin et al. 1981). P700 activity was measured with the DUAL-PAM-100 (Heinz-Walz) following the transient absorption at 830 nm upon exposure to actinic light. Maximum P700 activity was measured after a pulse of saturating light. Whole cells were treated with DCMU (3-(3,4-dichlorophenyl)-1,1-dimethylurea), ascorbate, and methyl-viologen, as described in Bonente et al. 2012. The formation rate of NADPH was determined with the NADPH/9-AA module of the Dual-PAM 101 (Schreiber and Klughammer 2009). Cells were harvested and resuspended in BG11 medium with 10% of Ficol to reduce cells precipitation. Measurement was performed as described in Schreiber and Klughammer 2009 at the same light intensity of growth (300 µmol photons $m^{-2}s^{-1}$). The slope during the light phase, between 60-120s, was used to determine the rate of NADPH formation.

SDS-PAGE and immunoblotting. SDS-PAGE and immunoblotting were performed as described in Bonente et al. 2011. Antibodies used were obtained from Agrisera company (https://www.agrisera.com/). Protein content was quantified by image analysis software (Imagelab, Biorad) and normalized on the basis of chl or cell content of the loaded sample.

Mitochondrial respiration. Samples in the exponential phase were subjected to respiratory rate measurements in the dark using a Clark-type O_2 electrode (Oxygraph Plus; Hansatech Instruments; Clark, 1956). Respiratory rates were normalized to cells number obtained by Countless®II FL automated cell counter (Thermo Fisher). To discriminate between the individual contributions of the alternative and the cytochrome pathway dark respiration measurements were conducted as follows: cell samples ($5*10^7$ cell/ml) were transferred to the measurement chamber of the Clark electrode, respiration rates were recorded for 3 min prior to the addition of the first inhibitor, then respiration rates were recorded for 3 additional min finally the second inhibitor was added and measurements were continued for another 3 min. Alternative respiration was inhibited by adding 2 mM SHAM (Salicylhydroxamic acid), while the cytochrome pathway (complex III) was inhibited by adding 5µM myxothiazol. To assess the relative contribution of the cytochrome pathway, respiration was first measured in the absence of inhibitors (total dark respiration) before alternative respiration was inhibited by adding SHAM. Cytochrome dependent respiration was then inhibited using myxothiazol and the residual respiration determined in relation to the uninhibited state. The contribution of alternative respiration was determined by reversing the order of inhibitor addition (myxothiazol followed by SHAM) (Bailleul et al. 2015).

REFERENCES

Allen, M. M. and R. Y. Stanier. 1968. "Growth and Division of Some Unicellular Blue-Green Algae." *Journal of General Microbiology*.

Allorent, Guillaume, Ryutaro Tokutsu, Thomas Roach, Graham Peers, Pierre Cardol, Jacqueline Girard-Bascou, Daphné Seigneurin-Berny, Dimitris Petroutsos, Marcel Kuntz, Cécile Breyton, Fabrice Franck, Francis André Wollman, Krishna K. Niyogi, Anja Krieger-Liszkay, Jun Minagawa, and Giovanni Finazzi. 2013. "Dual Strategy to Cope with High Light in *Chlamydomonas reinhardtii*." *Plant Cell*.

Bailleul, B., P. Cardol, C. Breyton, and G. Finazzi. 2010. "Electrochromism: A Useful Probe to Study Algal Photosynthesis." *Photosynth.Res.* 106(1573-5079 (Electronic)):179–89.

Bailleul, Benjamin, Nicolas Berne, Omer Murik, Dimitris Petroutsos, Judit Prihoda, Atsuko Tanaka, Valeria Villanova, Richard Bligny, Serena Flori, Denis Falconet, Anja Krieger-Liszkay, Stefano Santabarbara, Fabrice Rappaport, Pierre Joliot, Leila Tirichine, Paul G. Falkowski, Pierre Cardol, Chris Bowler, and Giovanni Finazzi. 2015. "Energetic Coupling between Plastids and Mitochondria Drives CO_2 Assimilation in Diatoms." *Nature*.

Berger, Hanna, Olga Blifernez-Klassen, Matteo Ballottari, Roberto Bassi, Lutz Wobbe, and Olaf Kruse. 2014. "Integration of Carbon Assimilation Modes with Photosynthetic Light Capture in the Green Alga *Chlamydomonas reinhardtii*." *Molecular Plant*.

Boekema, Egbert J. and Hans Peter Braun. 2007. "Supramolecular Structure of the Mitochondrial Oxidative Phosphorylation System." *Journal of Biological Chemistry* 282(1):1–4.

Bonente, G., M. Ballottari, T. B. Truong, T. Morosinotto, T. K. Ahn, G. R. Fleming, K. K. Niyogi, and R. Bassi. 2011. "Analysis of LhcSR3, a Protein Essential for Feedback de-Excitation in the Green Alga *Chlamydomonas reinhardtii*." *PLoS.Biol.* 9(1545-7885 (Electronic)):e1000577.

Bonente, Giulia, Sara Pippa, Stefania Castellano, Roberto Bassi, and Matteo Ballottari. 2012. "Acclimation of *Chlamydomonas reinhardtii* to Different Growth Irradiances." *Journal of Biological Chemistry*.

Borowitzka M.A., Microalgae in Medicine and Human Health: A Historical Perspective, Chapter 9 in Microalgae in Health and Disease Prevention Ira A. Levine, Joël Fleurence Academic Press, 2018, Pages 195-210.

Cecchin, Michela, Luca Marcolungo, Marzia Rossato, Laura Girolomoni, Emanuela Cosentino, Stephan Cuine, Yonghua Li-Beisson, Massimo Delledonne, and Matteo Ballottari. 2019. "*Chlorella Vulgaris* Genome Assembly and Annotation Reveals the Molecular Basis for Metabolic Acclimation to High Light Conditions." *Plant Journal* 1–17.

Dang, Kieu-Van, Julie Plet, Dimitri Tolleter, Martina Jokel, Stéphan Cuiné, Patrick Carrier, Pascaline Auroy, Pierre Richaud, Xenie Johnson, Jean Alric, Yagut Allahverdiyeva, and Gilles Peltier. 2014. " Combined Increases in Mitochondrial Cooperation and Oxygen Photoreduction Compensate for Deficiency in Cyclic Electron Flow in *Chlamydomonas reinhardtii* ." *The Plant Cell* 26(7):3036–50.

Depege, N., S. Bellafiore, and J. D. Rochaix. 2003. "Role of Chloroplast Protein Kinase Stt7 in LHCII Phosphorylation and State Transition in *Chlamydomonas*." *Science* 299(1095–9203):1572–75.

Dlugokencky, E.J., Hall, B.D., Montzka, S.A., Dutton, G., Mühle, J., Elkins, J.W. (2019). Atmospheric composition [in State of the Climate in 2018, Chapter 2: Global Climate]. Bulletin of the American Meteorological Society, 100(9), S48–S50.

Fleischmann, M. M., S. Ravanel, R. Delosme, J. Olive, F. Zito, F. A. Wollman, and J. D. Rochaix. 1999. "Isolation and Characterization of Photoautotrophic Mutants of *Chlamydomonas reinhardtii* Deficient in State Transition." *J.Biol.Chem.* 274(0021–9258):30987–94.

Gao, Jinlan, Hao Wang, Qipeng Yuan, and Yue Feng. 2018. "Structure and Function of the Photosystem Supercomplexes." *Frontiers in Plant Science* 9(March):1–7.

Johnson, Xenie and Jean Alric. 2013. "Central Carbon Metabolism and Electron Transport in *Chlamydomonas reinhardtii*: Metabolic Constraints for Carbon Partitioning between Oil and Starch." *Eukaryotic Cell* 12(6):776–93.

Kuhlgert, Sebastian, Greg Austic, Robert Zegarac, Isaac Osei-Bonsu, Donghee Hoh, Martin I. Chilvers, Mitchell G. Roth, Kevin Bi, Dan TerAvest, Prabode Weebadde, and David M. Kramer. 2016. "MultispeQ Beta: A Tool for Large-Scale Plant Phenotyping Connected to the Open PhotosynQ Network." *Royal Society Open Science*.

Li-Beisson, Yonghua, Jay J. Thelen, Eric Fedosejevs, and John L. Harwood. 2019. "The Lipid Biochemistry of Eukaryotic Algae."

Progress in Lipid Research 74(January):31–68.

Lin, Way-Rong, Shih-I. Tan, Chuan-Chieh Hsiang, Po-Kuei Sung, and I. Son Ng. 2019. "Challenges and Opportunity of Recent Genome Editing and Multi-Omics in Cyanobacteria and Microalgae for Biorefinery." *Bioresource Technology* 291(June):121932.

Lum, Krystal K., Jonggun Kim, and Xin G. Lei. 2013. "Dual Potential of Microalgae as a Sustainable Biofuel Feedstock and Animal Feed." *Journal of Animal Science and Biotechnology* 4(1):1–7.

Malkin, S, P. A. Armond, H. A. Mooney, and D. C. Fork. 1981. "Photosystem II Photosynthetic Unit Sizes from Fluorescence Induction in Leaves. Correlation to Photosynthetic Capacity." *Plant Physiol.* 67:570–79.

Malkin, Shmuel, Paul A. Armond, Harold A. Mooney, and David C. Fork. 1981. "Photosystem II Photosynthetic Unit Sizes from Fluorescence Induction in Leaves." *Plant Physiology*.

Murakami, Hiroki, Takashi Nobusawa, Koichi Hori, Mie Shimojima, and Hiroyuki Ohta. 2018. "Betaine Lipid Is Crucial for Adapting to Low Temperature and Phosphate Deficiency in *Nannochloropsis*." *Plant Physiology*.

Mussgnug, Jan H., Lutz Wobbe, Ingolf Elles, Christina Claus, Mary Hamilton, Andreas Fink, Uwe Kahmann, Aliki Kapazoglou, Conrad W. Mullineaux, Michael Hippler, Jörg Nickelsen, Peter J. Nixon, and Olaf Kruse. 2005. "NAB1 Is an RNA Binding Protein Involved in the Light-Regulated Differential Expression of the Light-Harvesting Antenna of *Chlamydomonas reinhardtii*." *Plant Cell*.

Pan, Xiaowei, Peng Cao, Xiaodong Su, Zhenfeng Liu, and Mei Li. 2019. "Structural Analysis and Comparison of Light-Harvesting Complexes I and II." *Biochimica et Biophysica Acta (BBA) - Bioenergetics* (June):0–1.

Polukhina, Iryna, Rikard Fristedt, Emine Dinc, Pierre Cardol, and Roberta Croce. 2016. "Carbon Supply and Photoacclimation Cross Talk in the Green Alga *Chlamydomonas reinhardtii*." *Plant Physiology*.

Riekhof, Wayne R., Surabhi Naik, Helmut Bertrand, Christoph Benning, and Dennis R. Voelker. 2014. "Phosphate Starvation in Fungi Induces the Replacement of Phosphatidylcholine with the Phosphorus-Free Betaine Lipid Diacylglyceryl-N,N,N-Trimethylhomoserine." *Eukaryotic Cell*.

Salomé, Patrice A. and Sabeeha S. Merchant. 2019. "A Series of Fortunate Events: Introducing *Chlamydomonas* as a Reference Organism." *The Plant Cell* 31(8):1682–1707.

Schreiber, Ulrich and Christof Klughammer. 2009. "New NADPH / 9-AA Module for the DUAL-PAM-100 : Description , Operation and Examples of Application ." *PAM Application Notes*.

Siaut, Magali, Stéphan Cuiné, Caroline Cagnon, Boris Fessler, Mai Nguyen, Patrick Carrier, Audrey Beyly, Fred Beisson, Christian Triantaphylidès, Yonghua Li-Beisson, and Gilles Peltier. 2011. "Oil Accumulation in the Model Green Alga *Chlamydomonas reinhardtii*: Characterization, Variability between Common Laboratory Strains and Relationship with Starch Reserves." *BMC Biotechnology*.

Simionato, Diana, Maryse A. Block, Nicoletta La Rocca, Juliette Jouhet, Eric Maréchal, Giovanni Finazzi, and Tomas Morosinotto. 2013. "The Response of *Nannochloropsis gaditana* to Nitrogen Starvation Includes de Novo Biosynthesis of Triacylglycerols, a Decrease of Chloroplast Galactolipids, and Reorganization of the Photosynthetic Apparatus." *Eukaryotic Cell*.

Uhmeyer, Andreas, Michela Cecchin, Matteo Ballottari, and Lutz Wobbe. 2017. "Impaired Mitochondrial Transcription Termination Disrupts the Stromal Redox Poise in *Chlamydomonas*." *Plant Physiology*.

Vanlerberghe, Greg C. 2013. "Alternative Oxidase: A Mitochondrial Respiratory Pathway to Maintain Metabolic and Signaling Homeostasis during Abiotic and Biotic Stress in Plants." *International Journal of Molecular Sciences* 14(4):6805–47.

Wang, Yingjun, Dan J. Stessman, and Martin H. Spalding. 2015. "The CO_2 Concentrating Mechanism and Photosynthetic Carbon Assimilation in Limiting CO_2: How *Chlamydomonas* Works against the Gradient." *Plant Journal*.

Yang, Bo, Jin Liu, Yue Jiang, and Feng Chen. 2016. "*Chlorella* Species as Hosts for Genetic Engineering and Expression of Heterologous Proteins: Progress, Challenge and Perspective." *Biotechnology Journal* 11(10):1244–61.

SUPPLEMENTARY INFORMATION

Figure S1. RUBISCO content determined by western blot. Content of RUBISCO normalized to cell number in *C. sorokiniana* (grey colour) and *C. vulgaris* (red colour) in AIR (full colour) or CO_2 (dash colour) condition determined by western blot analysis (RbcL subunit antibody). Data are means of three biological replicates with standard deviation shown. No statistical differences were determined by *t*-student test.

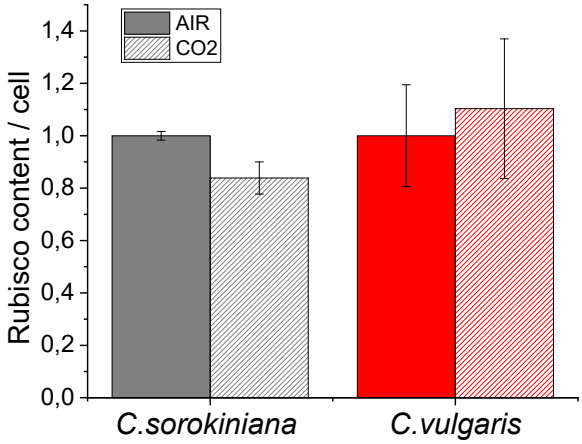

Figure S2. Functional antenna size of the photosystem II. Functional antenna size of the photosystem II ($1/\tau_{2/3}$) normalized to AIR condition in *C. sorokiniana* (grey colour) and *C. vulgaris* (red colour) in AIR (full colour) or CO_2 (dash colour) condition. Data are means of three biological replicates with standard deviation shown. No statistical differences were determined by *t*-student test.

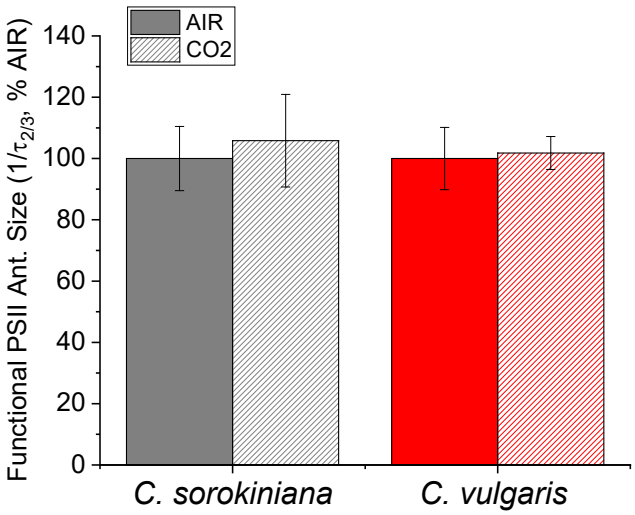

Chapter 3

Marine microalgae

Section A:

Improved lipid productivity in *Nannochloropsis gaditana* in nitrogen replete conditions by selection of pale green mutants

Section B:

Incorporating a molecular antenna in diatom microalgae cells enhances photosynthesis

Section A

Improved lipid productivity in *Nannochloropsis gaditana* in nitrogen replete conditions by selection of pale green mutants

M. Cecchin[1], S. Berteotti[1], S. Paltrinieri[1], I. Vigliante[2], B. Iadarola[1], B. Giovannone[1], M.E. Maffei[2], M. Delledonne[1] and M. Ballottari[1]

[1]Dipartimento di Biotecnologie, Università degli Studi di Verona, Verona, Italy

[2]Dipartimento di Scienze della Vita e Biologia dei Sistemi, Unità di Fisiologia Vegetale, Università di Torino, Torino, Italy.

This work was published in Biotechnology for Biofuels in April 2020.

Nannochloropsis gaditana is a photosynthetic unicellular microalga considered one of the most interesting marine algae to produce biofuels and food additive due to its rapid growth rate and high lipids accumulation. Although microalgae are attractive platforms for solar energy bioconversion, the overall efficiency of photosynthesis is reduced due to the steep light gradient in photobioreactors. Moreover, accumulation of lipids in microalgae for biofuels production is usually induced in a two-phase cultivation process by nutrient starvation, with additional time and costs associated. In this work a biotechnological approach was directed for the isolation of strains with improved light penetration in photobioreactor combined with increased lipids productivity. Mutants of *Nannochloropsis gaditana* were obtained by chemical mutagenesis and screened for having both a reduced chlorophyll content per cell and increased affinity for Nile Red, a fluorescent dye which binds to cellular lipid fraction. Accordingly, one mutant, called *e8*, was selected and characterized for having a 30% reduction of chlorophyll content per cell and an almost 80% increase of lipid productivity compared to WT in nutrient replete conditions, with C16:0 and C18:0 fatty acids being more than doubled in the mutant. Whole genome sequencing revealed mutations in 234 genes in *e8* mutant among which a non-conservative mutation in *dgd1* synthase gene. This gene encodes for an enzyme being involved in the biosynthesis of DGDG, one of the major lipids found in the thylakoid membrane and it thus involved in

chloroplast biogenesis. Lipid biosynthesis is strongly influenced by light availability in several microalgae species, including *Nannochloropsis gaditana*: reduced chlorophyll content per cell and more homogenous irradiance in photobioreactor is at the base for the increased lipid productivity observed in the *e8* mutant. The results herein obtained presents a promising strategy to produce algal biomass enriched in lipid fraction to be used for biofuel and biodiesel production in a single cultivation process, without the additional complexity of the nutrient starvation phase. Genome sequencing and identification of the mutations introduced in *e8* mutant suggests possible genes responsible for the observed phenotypes, identifying putative target for future complementation and biotechnological application.

INTRODUCTION

Microalgae are photoautotrophic organisms that can be cultivated to exploit light energy to fix CO_2 into organic biomass. Microalgae derived biomass can then be used for several applications, among which the production of food, high value products and/or biofuels (Akbari, Eskandani, and Khosroushahi 2014; Bernaerts et al. 2019; Camacho, Macedo, and Malcata 2019; Rösch, Roßmann, and Weickert 2019). Some microalgal species indeed can accumulate high amounts of lipids, the biomass constituents with the highest energy associated (Rodolfi et al. 2009). Fatty acids are mainly synthesized in the chloroplast and then used as building blocks for triacylglycerols (TAGs), which are deposited in densely packed lipids bodies located in the cytoplasm of the algal cell (Siaut et al. 2011). In oleaginous algae the lipid content varies between 20 to 70% and can reach values up to 90% of algal total dry weight under certain conditions, such as nitrogen deprivation (Chen and Jiang 2017). Nutritional stress is a common strategy adopted by the microalgae research community to boost TAGs accumulation which can be converted to biodiesel by a transesterification reaction (Wijffels and Barbosa 2010). Two-phase cultivation for inducing lipid biosynthesis in microalgae is however a costly process, requiring modification of the growth medium and additional time required before biomass harvest. Species belonging to the genus *Nannochloropsis* are marine unicellular microalgae (HIBBERD 1981) considered among the most promising strains for cultivation in large scale systems, as open ponds or closed photobioreactors, for biodiesel production due to their fast growth rate, lipids accumulation (up to 65-70% of total dry weight) and ability to adapt to different irradiation (Hodgson et al. 1991; Ma et al. 2014; Rodolfi et al. 2009). In addition, 30% of fatty acids accumulated in *Nannochloropsis* are polyunsaturated fatty acids among which Eicosapentaenoic acid (EPA, 20:5ω3), one of the major omega-3 fatty acid reported to have positive effect in human health (Gill and Valivety 1997). This yellow green alga belongs to the class the pico-plankton *Eustigmatophyceae*, composed by species mainly living on the coasts. The cells of *Nannochloropsis* have reduced size (3-5 µm) (HIBBERD 1981), with a single chloroplast occupying most of the cell volume (Andersen et al. 1998; Lubián 1982). It shows a peculiar pigments content, presenting only chlorophyll (Chl) *a* and lacking other accessory chlorophylls such as Chl *b* or *c* while violaxanthin and vaucheriaxanthin are the most represented carotenoids (Basso et al. 2014). The *N. gaditana* genome is available and its assembly includes nuclear (~29 Mbp) and organellar genomes, containing ~10.000 gene models (Corteggiani Carpinelli et al. 2014; Radakovits et al. 2012). The availability of a genome sequence and transformation methods allow genetic engineering strategies to further improve this naturally productive species (Simionato et al. 2013; Verruto et al. 2018).

Although microalgae are attractive biomass, bioproducts and biofuel producers, their photosynthetic efficiency is much lower compared to their theoretical potential (Formighieri, Franck, and Bassi 2012). Light use efficiency of microalgae in photobioreactors is indeed limited by the steep light gradient due

to the strong optical density of the near-molar concentration of chlorophylls in cells (Melis 2009). This non-homogeneous light penetration results in a low productivity of the system, being the inner layers almost in the dark (Melis 2009). Mutant strains with reduced pigment content per cell resulting either from a truncated antenna size or a lower overall density of photosynthetic units per cell were reported for different species, as *C. reinhardtii, C. vulgaris, C. sorokiniana* and *N. gaditana*, being characterized by an increased productivity (Cazzaniga et al. 2014; Jeong et al. 2017; Kirst, Garcia-Cerdan, et al. 2012; Perin et al. 2015). In addition, up to 80% of the light absorbed by the external layers is dissipated as heat by the activation of photoprotective processes, with consequent loss of light use efficiency and biomass productivity (Erickson, Wakao, and Niyogi 2015). The photoprotective mechanism involved in the energy dissipation as heat, is known as non-photochemical quenching (NPQ), a short-time response to energy absorbed in excess, triggered by lumen acidification when the photosynthetic apparatus is saturated (Ballottari et al. 2016; Liguori et al. 2013).

These photosynthetic limitation influences both biomass yield and lipid accumulation. Indeed, the key challenge for the oleaginous algae is to maximize lipid production maintaining high biomass yields (Janssen, Wijffels, and Barbosa 2019; Rodolfi et al. 2009). The main strategies at industrial level to trigger lipids accumulation in microalgae is to induce nutrients starvation, especially nitrogen starvation: in these conditions cells redirect carbon metabolism into nitrogen-free lipid molecules (Rodolfi et al. 2009). However, this approach strongly reduces cells growth rate, affecting overall biomass and lipid productivities. Some positive results were obtained by overexpression or downregulation of transcriptional factor increasing the lipid production with moderate or even positive effects for the growth (Ajjawi et al. 2017; Kang et al. 2019). However, the possibility to use genetic modified organisms (GMOs) at industrial scale is still limited by the different acceptance and legislation in the different countries, hampering the application of the promising results obtained.

In this work we report a biotechnological approach by chemical mutagenesis to isolate *N. gaditana* strains with increased lipid productivity in absence of nutrient starvation. The strategy adopted was the selection of strains with both a reduction in cell pigmentation, to allow a better light distribution in photobioreactor, and an increased Nile Red staining, as a probe for lipid accumulation.

RESULTS

Mutagenesis and selection of mutant strains

N. gaditana mutants were obtained by chemical mutagenesis, using the alkylating agent Ethyl-Methane-Sulfonate (EMS) that inserts random single-point mutations (SNP) in the genome. Surviving colonies with a visible “pale green” phenotype in solid medium were initially selected, transfer to liquid medium and screened by measuring absorption of chlorophyll *a* (at 680nm) and cell scattering (at 730nm).

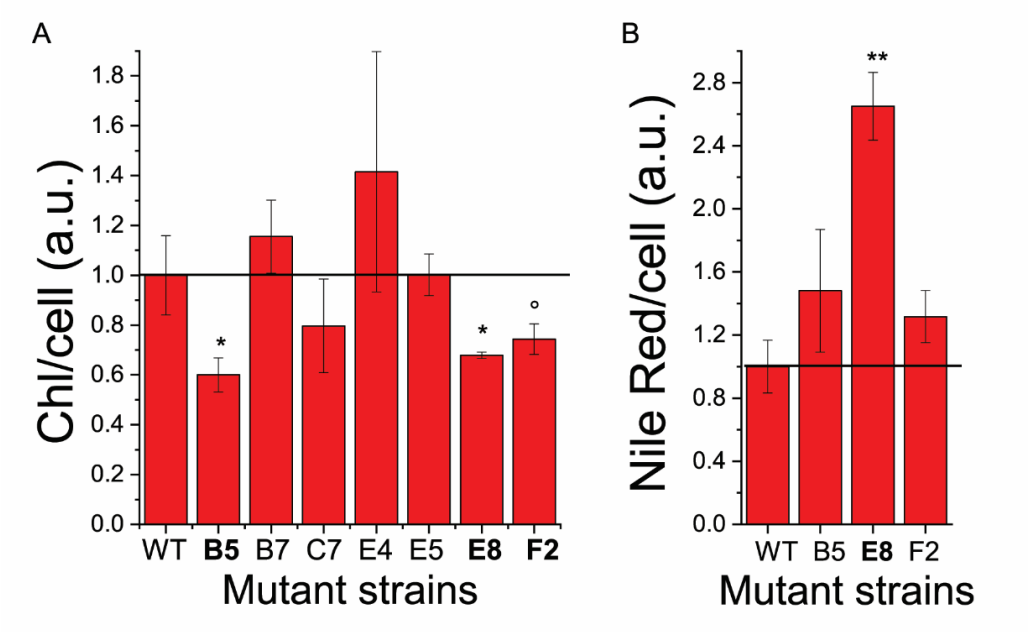

Figure 1. Chlorophylls per cell and Nile Red staining of mutated strains. Chlorophyll content per cell (A) and Nile Red fluorescence per cell (B) were normalized to the WT case. Errors are reported as standard deviation (n=3), significantly different values are marked with * if $p < 0.05$ and ** if $p < 0.01$, as determined by unpaired two sample *t*-test (n=3). In the case of sample marked with ° p-value of 0.0597 was obtained.

The resulting 680/730 nm absorption ratio provides a relative indication of the chlorophyll content per cell. Seven strains were selected having a 680/730 nm absorption at least 25% decreased compared to the WT case (Supplementary Figure S1). These strains were then evaluated for their chlorophyll content per cell by extracting pigments, quantifying them and counting the cells: only 3 mutants showed a decreased Chl/cell ratio (Figure 1A). These mutants were then further analysed for their lipid content by Nile Red staining: as reported in Figure 1B, only in the case of mutant *e8*, an increased Nile Red fluorescence was measured per cell. The selected mutant *e8* was thus characterized by a 30% reduction of chlorophyll content per cell and ~180% increase in Nile Red staining, suggesting an increased lipid content.

Photosynthetic characterization of *e8* mutant

Pigment composition of *e8* strain was analyzed by HPLC and compared to the WT case. As reported in Table 1, the accumulation of the different carotenoid species was similar in the *e8* mutant strain compared to WT. Chl/cell reduction observed in *e8* mutant was related to the total cell content of chlorophylls but the pigments composition on a chlorophylls basis was essentially unaffected. Only in the case of zeaxanthin a significant increase was observed in the *e8* mutant compared to WT, with a ~180% increase on a chlorophyll basis.

In order to evaluate if the reduced Chl/cell ratio observed in *e8* mutant was related to a truncated antenna phenotype (Kirst, Garcia-Cerdan, et al. 2012; Kirst, Formighieri, and Melis 2014), the

	Chl/cell (%)	Chl *a*	Chl/ Car	Vio	Vau	Anthera	Cantha	Zea	β-car	(Vio+Vau)/ β-car
WT	100 ± 15.9	100 ± 5.04	2.31 ± 0.17	20.51 ± 1.11	12.17 ± 0.71	3.56 ± 0.48	0.67 ± 0.53	3.21 ± 0.6	3.27 ± 0.31	10.49 ± 1.06
e8	67.9 ± 1.2*	100 ± 9.16	2.17 ± 0.18	19.14 ± 0.94	13.37 ± 0.73	3.64 ± 0.5	1.03 ± 0.34	5.90 ± 1.32*	2.97 ± 0.38	9.92 ± 0.8

Table 1. Pigment analysis of WT and *e8* mutant strain. Chlorophyll content per cell (Chl/cell) was set to 100% in the case of WT. The concentration of pigments in pmol was determined by HPLC and normalized to 100 pmol of chlorophyll *a* (Chl). Violaxanthin: vio, vaucheriaxanthin: vau, β-carotene: β-Car, antheraxanthin: anthera, zeaxanthin: zea, canthaxanthin: cantha. Standard deviations are reported for the different values (n=5 for Chl/cell values, n=3 for the other values). Significantly different values are marked with * if $p < 0.05$, as determined by unpaired two sample *t*-test (n=3).

functional antenna size of Photosystem II (PSII) was estimated measuring the kinetics of fluorescence induction in cells treated with the PSII inhibitor 3- (3,4-dichlorophenyl)-1,1-dimethylurea (DCMU) (Malkin et al. 1981). The inhibitor DCMU blocks the electron transport from PSII to plastoquinone pool, inducing PSII to re-emit as fluorescence the excitation energy absorbed: upon DCMU treatment, in limiting light, the capacity of light harvesting and energy transfer to reaction center of PSII is inversely proportional to the fluorescence emission kinetics (Figure 2A) (Malkin et al. 1981). The differences in antenna size were thus quantified as the reciprocal of the time required to reach 2/3 of the maximum fluorescence ($1/\tau_{2/3}$, Figure 2B). As reported in Figure 2A *e8* mutant strain showed fluorescence induction kinetics similar to the WT case. Thus, the reduced Chl/cell ratio was not related to a reduced

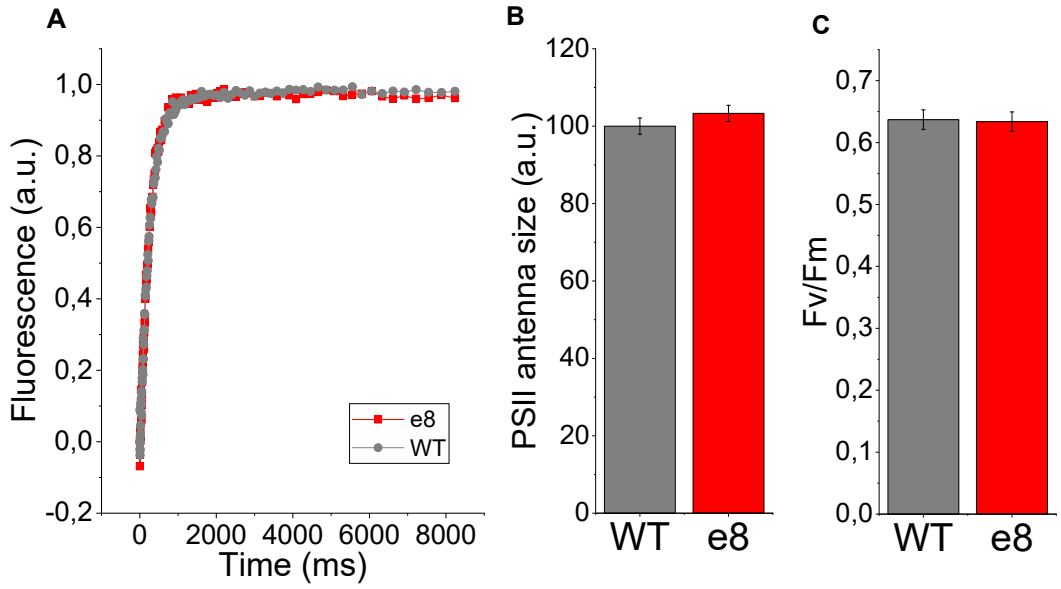

Figure 2. PSII functional antenna size and PSII maximum quantum yield. (A) Fluorescence induction kinetics of PSII antenna size of wild type and selected mutant. (B) PSII functional antenna size expressed as the reciprocal of the time required to reach 2/3 of the maximum fluorescence emission, $\tau_{2/3}^{-1}$(%). (C) PSII maximum quantum yield calculated as $(F_M-F_0) / F_M$ from basal chlorophyll fluorescence in the dark (F_0) and maximum chlorophyll fluorescence induced by a saturating pulse (F_M). The statistical analysis of the results obtained was performed by unpaired two sample *t*-test (n=4, no statistically significant difference being p-value=0.09 for PSII functional antenna size and p=0.78 for F_v/F_m values).

antenna/core complex ratio and reduced light harvesting capacity of PSII. PSII maximum quantum yield was then measured by pulse amplitude modulated fluorescence as F_v/F_m (Figure 2C). F_v/F_m was not significantly different in *e8* mutant compared to WT, suggesting that the mutations introduced in *e8* were not deleterious to photosynthesis.

Photosynthetic performances of *e8* was then evaluated measuring the light dependent oxygen evolution. Net oxygen evolution rates at different light intensities are reported in Figure 3A normalized to the chlorophyll content and fitted with hyperbolic functions, showing no major differences between WT and *e8* mutant. Similarly, dark respiration rate of WT and *e8* was not significantly different, suggesting that mitochondrial respiration was not affected by the mutation introduced in the mutant (Figure 3B).

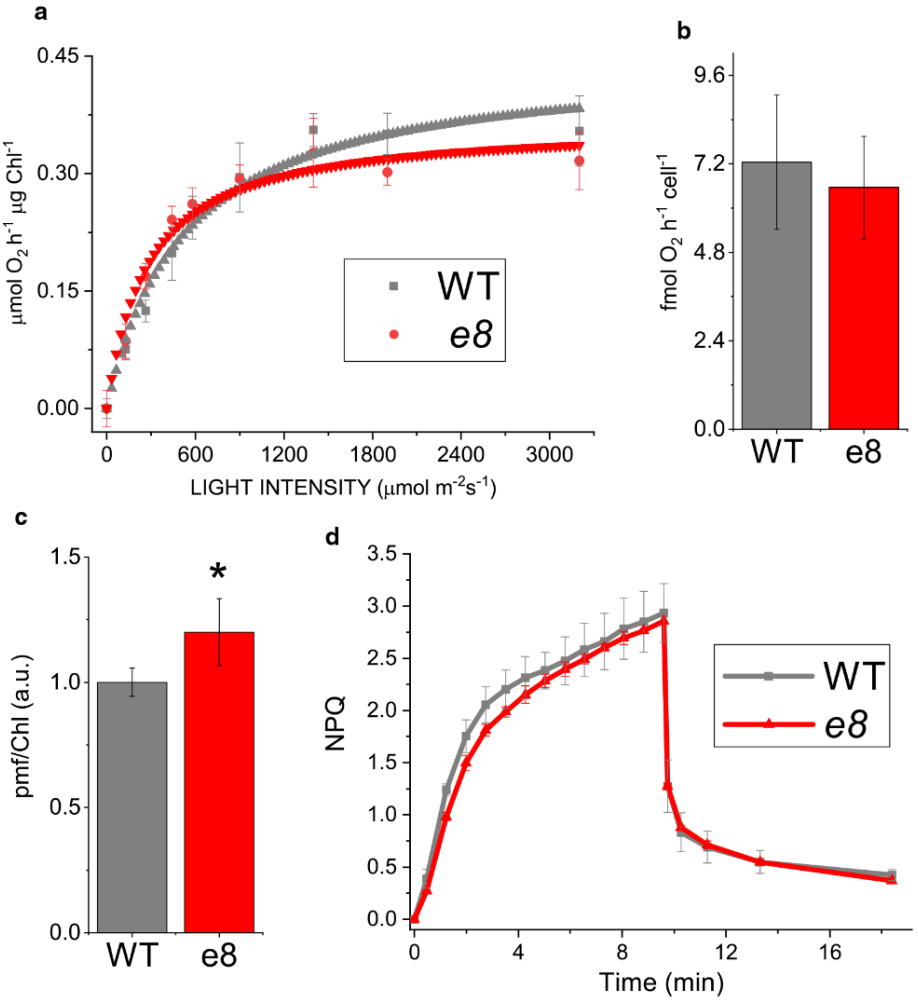

Figure 3. Photosynthetic parameters of *e8* mutant compared to WT. (A) Net oxygen production of wild type and *e8* mutant strain normalized to chlorophyll content, measured at different actinic light intensities. Experimental data were fitted with hyperbolic function. (B) Dark respiration rate normalized to cell content. (C) Non-Photochemical Quenching (NPQ) formation and relaxation in wild type and *e8* mutated strain, actinic light 1500 µmol photons m^{-2} s^{-1}. (D) Proton-motive force (*pmf*) for wild type (WT) and *e8* obtained by electrochromic shift measurement (ECS) at 1000 µmol photons m^{-2} s^{-1} and normalized to the chlorophyll content. Errors are reported as standard deviation, the statistical significance of differences between WT and *e8* is indicated as * ($p < 0.05$), as determined by unpaired two sample t-test (n=4).

Light dependent electron transport in photosynthetic organisms is coupled to proton transport across the thylakoid membrane into the lumen, which are then used by ATPase to produce ATP. Light dependent proton motive force (*pmf)* can be estimated measuring the light dependent-electrochromic shift (ECS) of carotenoid absorption. Carotenoid absorption spectra are indeed sensitive to the membrane potential (Bailleul et al. 2010). As reported in Figure 3C a significant increase in *pmf* was evident in *e8* mutant when exposed to actinic light, indicating an increased proton transport across thylakoid membranes. This result suggests that the reduction of Chl content per cell observed in *e8* mutant did not negatively influenced trans-thylakoid proton transport but rather increased the light dependent *pmf*, because of possible adaptation of the photosynthetic apparatus to the *e8* mutant phenotype.

Considering the increased *pmf* observed in *e8* mutant, the activation of photoprotective mechanisms triggered by lumenal ΔpH was then investigated as xanthophyll cycle activation and NPQ induction. Light dependent zeaxanthin accumulation was measured in WT and *e8* mutant upon exposure to strong light (2500 µmol photons m^{-2} s^{-1}) for one hour in order to induce violaxanthin de-epoxidation (Supplementary Figure S2): *e8* mutant strain showed a higher de-epoxidation index only in the first minutes of illumination, due to the higher accumulation of zeaxanthin at time zero compared to the WT, but on a longer time scale the zeaxanthin content was similar in the two strains. Considering the role of this xanthophyll in the photoprotective mechanisms adopted by *N. gaditana* (Cao et al. 2013; Chukhutsina et al. 2017) we measured the NPQ induction kinetics in *e8* mutant compared to WT. As reported in Figure 3D the NPQ kinetics were similar in *e8* mutant compared to the WT case. NPQ induction was indeed reported to be only partially related to the xanthophyll cycle activation in *N. gaditana* (Chukhutsina et al. 2017): the zeaxanthin content in *e8* mutant and WT, even if different in the first minutes of illumination, was likely sufficient to saturate the zeaxanthin dependent NPQ component in both strains at the actinic light used.

In order to investigate possible different photosensitivity of the *e8* mutant compared to WT, chlorophyll bleaching kinetics were measured upon exposure to strong light (2500 µmol photons m^{-2} s^{-1}). As reported in Supplementary Figure S3, the exposure to strong light causes in both WT and *e8* strain a similar decrease in chlorophyll absorption, with a ~30% chlorophyll loss after 14 hours of illumination. This result demonstrates that the *e8* strain is not impaired in photoprotective mechanisms.

Biomass and lipid productivity

Biomass productivity, defined as biomass dry weight obtained on a daily basis, in WT and *e8* mutant strain were analyzed in 80 ml batch airlift photobioreactors illuminated with continuous white light at different irradiances, from 60 to 1500 µmol photons m^{-2} s^{-1}. As reported in Figure 4 and Supplementary

Figure S4A increased biomass productivity was measured at 60 and 200 µmol photons m^{-2} s^{-1}, but not at higher irradiances. Lipid accumulation at these growth conditions was thus evaluated by Nile Red staining (Chen et al. 2009). As reported in Supplementary Figure S4B an increased lipid accumulation on a dry weight basis was evident in *e8* mutant at all the different irradiances of growth, with the exception of the highest one, 1500 µmol photons m^{-2} s^{-1}. Lipid content per volume of culture was thus increased in *e8* mutant grown at 60, 200 and 400 µmol photons m^{-2} s^{-1} compared to the WT case

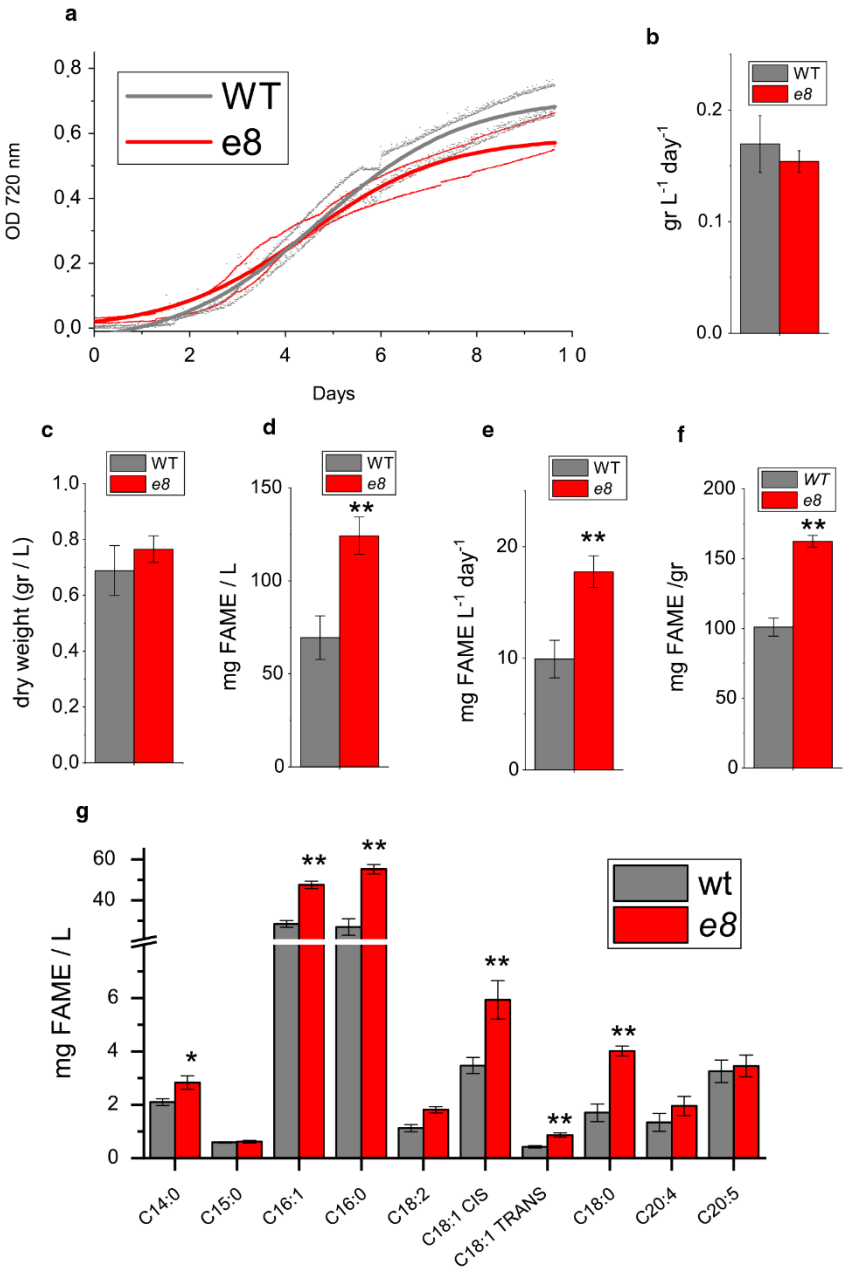

Figure 4. Biomass and lipid productivity of wild type and *e8* mutant growth at 400 µmol photons m^{-2} s^{-1}. (A) Growth curves of WT and *e8* mutant obtained measuring the optical density at 720 nm fitted with sigmoidal function. (B) Maximum daily productivity in terms of gr L^{-1} day^{-1}. (C) Dry weight at the end of the growth curve (g/L). (D, E) Lipid content in terms of mg of lipids per liters of culture (D) or mg of lipids per gram of dry weight (E). (F) Lipid productivity in terms of mg of lipids per liters of culture per day. (G) Acyl chain composition of lipid fraction from WT and *e8* mutant. Errors are reported as standard deviation, significantly different values are marked with * if $p < 0.05$ and ** if $p < 0.01$, as determined by unpaired two sample t-test (n=3).

(Supplementary Figure S4C). As reported in Supplementary Figure S4D a 295%, 100% and 34% increase in Nile Red staining was measured respectively at 60, 200 and 400 µmol photons m^{-2} s^{-1} compared to WT. The increased lipid accumulation phenotype of *e8* mutant was thus more evident at lower irradiances, suggesting a role of light availability on the lipid accumulation phenotype observed. Interestingly, on a volume basis *e8* mutant grown at 400 µmol photons m^{-2} s^{-1} was accumulating a similar level of lipid compared to the WT case grown at 1500µmol photons m^{-2} s^{-1} (Supplementary Figure S4C).

Fatty acid accumulation and productivity were then analyzed at 400 µmol photons m^{-2} s^{-1}, being this light intensity sufficient to essentially reach the maximum Nile red staining on a volume basis in *e8* mutant. In particular, lipid fraction of WT and *e8* mutant strain were explored by GC analysis of the total acyl lipid as Fatty acid methyl esters (FAME). As reported in Figure 4, *e8* mutant was characterized by a ~80% increase of FAME accumulation and daily productivity compared to WT on a volume basis. Accordingly, FAME fraction on total biomass was increased by ~60% in *e8* mutant compared to the WT case (Figure 4E), while on a cell basis the FAME accumulation of *e8* mutant was increased by 115%. As reported in Figure 4G, palmitic acid (C16:0) and palmitoleic acid (C16:1) were the major fatty acids accumulated in both WT and *e8* mutant, with a strong increase being observed in the latter. Moreover, myristic acid (C14:0), stearic acid (C18:0), oleic acid (cis C18:1), elaidic acid (trans C18:1) and linoleic acid (C18:2) were also strongly increased in *e8* mutant compared to WT on a volume basis. Interestingly, the strongest increase was observed in the case of the saturated stearic acid (C18:0) and palmitic acid (C16:0) with a more than two-fold increase in *e8* compared to WT.

Lipids production in *N. gaditana* is triggered upon nitrogen deficiency, where metabolism is switched accumulating nitrogen-free lipids (Hodgson et al. 1991; Rodolfi et al. 2009; Simionato et al. 2011). The influence of nitrogen starvation on the FAME accumulation properties of *e8* mutant compared to WT were thus investigated: reduced nitrogen source (nitrate) were thus removed at the end of the growth curve reported in Figure 4A, in order to boost lipid biosynthesis (Hodgson et al. 1991; Rodolfi et al. 2009; Simionato et al. 2011). A slight reduction of total biomass yield was evident in nitrogen deplete condition (-N) in *e8* mutant compared to WT (Supplementary Figure S5A), while a more evident difference was measured in the case of lipid fraction (Supplementary Figure S5B). In -N condition the WT strain induced a strong accumulation of fatty acids as previously reported (Alboresi et al. 2016; Simionato et al. 2013), especially palmitic acid (C16:0), palmitoleic acid (C16:1), stearic acid (C18:0), linoleic acid (C18:2) and oleic acid (C18:1 CIS), while no significant increase of total FAME was evident in *e8* mutant in -N compared to nitrogen replete (+N) condition (Supplementary Figure S6). *e8* mutant is thus more productive in terms of lipid accumulation in nitrogen replete conditions, but it is not able to further increase its lipid fraction in nitrogen deficiency.

Light distribution is improved in *e8* mutant

The results obtained demonstrate that the reduced Chl/cell ratio and the improved light distribution observed yielded an increased lipid productivity in +N condition. Light distribution in the photobioreactors herein adopted were thus estimated considering the chlorophyll concentration measured in photobioreactors at exponential phase, the absorption spectra of whole cells in the 400 – 700 nm region, the irradiance arriving to the surface of photobioreactor (400 µmol photons m^{-2} s^{-1}) and its diameter (3 cm). As reported in Figure 5A and in Supplementary Figure S7, the transmittance at 675 nm and 450 nm, the main peaks of chlorophyll *a* absorption, were higher in the *e8* mutant compared to WT: being the transmittance the ratio between the light not being absorbed or reflected by the sample and the incident light, it was possible to calculate the irradiance arriving at the center of photobioreactor (1.5 cm) considering an incident irradiance of 400 µmol photons $m^{-2}s^{-1}$. As reported in Figure 5B *e8* mutant was exposed to a 6-fold higher irradiance at the center of the photobioreactor compared to the WT case.

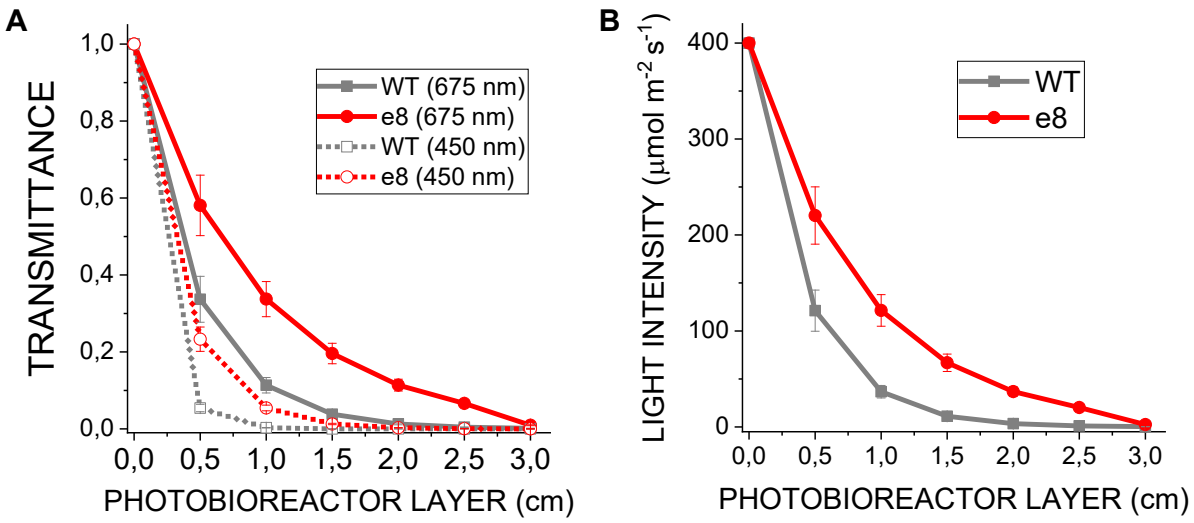

Figure 5. Transmittance and light penetration in photobioreactors. Transmittance (A) and irradiances (B) at different layer of photobioreactors were calculated considering the absorption spectra of whole cells, the incident light intensity (400 µmol photons m^{-2} s^{-1}) and the concentration of chlorophyll at exponential phase in photobioreactors. Error bars are reported as standard deviation (n=3).

Genetic characterization of the mutant strain

e8 mutant strain was investigated at genetic level to identify those mutations putatively responsible for the phenotypic traits observed. Whole genome Illumina sequencing was performed for WT and *e8*, using the reference genome available for *N. gaditana* for reads alignment and genome assembly (Corteggiani Carpinelli et al. 2014). As reported in Supplementary Table S1, a 20X coverage was obtained for at least 95% of the genome of both WT and mutant strain. The comparison between WT and *e8* allowed to identify the single nucleotide polymorphisms (SNP) induced in mutant strain by EMS

Total SNPs	Predicted effect			OTHERs
	LOW	MODERATE	HIGH	
240	36	80	1	123 SNPs

Table 2. Statistics of the mutations found in *e8* mutant strain. Total number of SNPs found is reported in the first column. The predicted effect of mutations are reported according to SNPeff software: HIGH is for mutation probably causing protein truncation, loss of function or triggering nonsense mediated decay, MODERATE are non-disruptive variants that might change protein effectiveness and LOW are mutations harmless or unlikely to change protein behavior. SNPs with predicted non-coding variants or variants affecting non-coding genes, where predictions are difficult or there is no evidence of impact were not considered: the number of remaining SNPs are reported in the last column (OTHER).

treatment. In particular, *e8* resulted to be mutated in 234 genes, among which 113 genes with not-silent mutations (Table 2 and Supplementary Dataset S1). The high number of mutations identified complicates the association of the phenotypes observed with the genetic traits of the *e8* mutant. Mutated genes were grouped according to their Gene Ontology (GO) terms and clustered using GO slim terms of plant: as reported in Supplementary Figure S8 several biological processes, molecular functions and cellular component were potentially affected by mutations.

Among the different mutations, genes encoding for chloroplast located proteins were investigated in order to find possible mutations at the base of the reduced chlorophyll content phenotype: chloroplast transit peptides were predicted using HECTAR software (Gschloessl, Guermeur, and Cock 2008) identifying only 4 mutated genes for putative plastid located proteins (Supplementary Table S2). In particular, a plastid chaperone protein with a DnaJ domain (Naga_100340g1) was mutated: protein subunits with DnaJ domains have been previously reported to be involved in plastids in several processes ranging from biogenesis of thylakoid membranes, translation, to mRNA stability (Chiu et al. 2013). Other mutations on chloroplast targeted proteins were on genes encoding for NHL-repeat protein (Naga_100040g45), for a dehydrogenase reductase SDR (Short-chain dehydrogenase/reductase) -family protein (Naga_100641g4) and a protein of unknown function (Naga_100008g127). Homologous proteins in the case for NHL-repeat protein (Naga_100040g45) and dehydrogenase reductase SDR-family protein were reported to be respectively involved in biotic and abiotic stresses (Hemsley et al. 2013) and in the secondary metabolism (Moummou et al. 2012) but their possible correlation with the phenotype observed in *e8* mutant is not obvious.

Among the SNPs identified in gene upstream regions, possibly affecting gene expression, a mutation was identified in a Photosystem II s4 domain protein (Naga_100303g8). Photosystem II s4 domain protein in the cyanobacterium *Synechocystis sp. PCC 6803* has been reported to be involved in balancing photosynthetic electron transport (Inoue-Kashino et al. 2011). However, the similar PSII

quantum yield (F_v/F_m) observed in WT and *e8* mutant suggest that impact of the mutation in this Photosystem II s4 domain protein is minor.

Other mutated genes found in *e8* mutant possibly linked with the reduced chlorophyll content per cell observed include genes involved in regulation of gene expression, as a CCT (CONSTANS, CO-like and TOC1) domain containing protein (Naga_100027g10). This gene in higher plants is involved in control of flowering and heading (Li and Xu 2017; ZHANG et al. 2017) and could thus be putatively involved in the regulation of chlorophyll biosynthesis and/or plastid morphology. Other mutations identified on a transcription elongation factor (Naga_100012g30), a regulator of chromosome condensation (Naga_100664g1) and a ribosomal RNA small subunit methyltransferase B (Naga_100044g6) could generally lead to altered gene expression and protein synthesis.

Since the selected mutant showed an increased lipid content per cell, mutations affecting lipid metabolism were also investigated: mutations in a beta-ketoacyl synthase (Naga_100086g24), 24-dehydrocholesterol reductase (Naga_100012g52) and digalactosyldiacylglycerol synthase 1 (*dgd1*, Naga_100010g107) were identified. The beta-ketoacyl synthase (Naga_100086g24) and 2,4-dehydrocholesterol reductase are involved in lipid biosynthesis (Alboresi et al. 2016; Lu et al. 2014), and the correlation between mutations in these genes and the observed phenotypes in *e8* is not obvious. More interesting is the case of the gene encoding for the digalactosyldiacylglycerol synthase 1 (*dgd1*, Naga_100010g107): this gene is mutated in the CDS region, leading to the substitution of a proline residue with a serine. Thus, the mutation introduced caused the substitution of an aliphatic residue with a polar one, potentially affecting the enzymatic activity of the protein. A *dgd1* mutant of *Arabidopsis* was previously isolated showing a reduction of 90% of DGDG content and strong reduction in chlorophyll content per leaf area (Klaus et al. 2002). Consistently with a reduced activity of DGD1 enzyme, a strong reduction of C20:5 fatty acid (EPA) on total lipid fraction was evident in *e8* mutant either in +N or -N conditions (Supplementary Information Figure S6B). C20:5 has been indeed previously reported in *N. gaditana* to be the major constituents of MGDG and DGDG being found almost essentially in these lipids in +N conditions (Simionato et al. 2013). For these reasons, in the specific case of *N. gaditana*, the quantification of C20:5 fatty acid can be used as a proxy of MGDG and DGDG accumulation, demonstrating a reduced content of the main thylakoidal lipids in *e8* mutant compared to the WT case.

DISCUSSION

In this work mutants with reduced chlorophyll content per cell and increased lipid productivity were screened upon random chemical mutagenesis in *N. gaditana*. The strategy to improve productivity reducing the chlorophyll content per cell has been reported for several microalgae as *N. gaditana* (Perin et al. 2015), *Chlamydomonas reinhardtii* (Jeong et al. 2017; Kirst, García-Cerdán, et al. 2012;

Polle, Kanakagiri, and Melis 2003), *Chlorella sorokiniana* (Cazzaniga et al. 2014), *Chlorella vulgaris* (Dall'Osto et al. 2019) and cyanobacteria (Kirst et al. 2014) among others. Generation of mutants by chemical mutagenesis presents the advantage to produce strains not considered as GMO (genetically modified organism, and thus more easily cultivatable in outdoor systems without the restrictive authorizations required for GMO strains in several countries (Beacham, Sweet, and Allen 2017).

Functional PSII antenna size and light dependent oxygen evolution were not altered in pale green mutant *e8*, indicating a more general reorganization of plastid assembly in this mutant leading to a similar functioning of the photosynthetic apparatus on a chlorophyll basis, despite the reduction in total chlorophyll per cell. In line with this finding *e8* mutant did not present any mutations on light harvesting subunits. Unaltered photosynthetic efficiency in pale green mutant has been previously reported in several microalgae species (Cazzaniga et al. 2014; Dall'Osto et al. 2019; Jeong et al. 2017; Kirst, García-Cerdán, et al. 2012; Kirst et al. 2014; Perin et al. 2015; Polle et al. 2003), being chlorophyll content per cell not necessarily influencing the functionality of the photosynthetic apparatus, but rather being possibly linked to chloroplast biogenesis. Consistently *e8* mutant was characterized by a strong reduction in C20:5 fatty acid accumulation, being this lipid the main constituent of thylakoid glycerolipids MGDG, DGDG and SQDG in *N. gaditana* (Simionato et al. 2013).

e8 mutant was characterized by an increased biomass productivity compared to the WT case at low-medium light, while at saturating irradiances an increased lipid accumulation was rather observed (Figure 4, Supplementary Figure S4). Since lipids are a class of macromolecules with the highest energy density, an increased lipid accumulation implies an improved light energy conversion efficiency. Considering the irradiance dependent phenotype and the similar photosynthetic properties compared to the WT case (Figure 3, Figure 5, Supplementary Figure S4), the improved photosynthetic efficiency at the base of the increased lipid content in *e8* mutant is thus related to the improved light penetration in the photobioreactor and more homogenous light availability due to the reduced chlorophyll content per cell observed in the mutant (Table 1, Figure 5). Accordingly, the zeaxanthin content measured in *e8* mutant was increased compared to WT (Table 1): zeaxanthin accumulation is indeed triggered in high light, providing other evidences for the increased penetration of light in photobioreactors in the case of *e8* mutant cultivation. In *N. gaditana* lipids production is triggered by high light (Alboresi et al. 2016): the improved light distribution in *e8* mutant could thus be the major reason for the increased lipid productivity observed in the *e8* mutant.

In order to elucidate the genetic base of the reduced chlorophyll content per cell phenotype and to investigate other possible genetic traits associated to the increased lipid content phenotype whole genome sequencing was performed and mutations on 234 genes were identified, among which 113 in coding regions. Interestingly, *e8* mutant present a non-conservative mutation of *dgd1* gene, encoding for a key enzyme involved in DGDG biosynthesis. DGDG and MGDG are the major lipids of

photosynthetic membranes. *dgd1* mutant of *Arabidopsis* showed an impaired DGDG synthesis with a rearrangements in all pigment-protein complexes (Klaus et al. 2002). In plants and in algae DGDG is synthetized in at least two parallel pathways, the 'prokaryotic pathway', restricted to plastid, and the 'eukaryotic pathway' which involves both plastid and endoplasmic reticulum (Klaus et al. 2002; Liang, Wen, and Liu 2019). The *dgd1* gene mutated in the *e8* mutant encodes for an enzyme involved in the 'eukaryotic pathway'. Mutation in *dgd1* gene in *A. thaliana* caused a reduction in DGDG biosynthesis for thylakoid assembly and pale green leaves (Dormann et al. 1995). Thus, we suggest that mutation in in *dgd1* gene in *e8* mutant is responsible for the reduction in chlorophyll content per cell. The increased lipid accumulation in *e8* mutant could be a consequence of an improved light availability experienced by the mutant strain compared to WT (Figure 5), because of the reduced cells pigmentation. This consideration is consistent with previous observations about increased lipid accumulation in *N. gaditana* upon exposure to high irradiances (Alboresi et al. 2016; Meneghesso et al. 2016; Simionato et al. 2011). Similar effects of high irradiances on lipid biosynthesis were reported also in the case of *Nannochloropsis oceanica* and *Phaeodactylum tricornutum* (Huete-Ortega et al. 2018). Alternatively, the high lipid accumulation observed in the case of *e8* could be a consequence of a re-direction of fatty acid metabolism due to altered glycerolipids accumulation: this is however unlikely, considering similar lipid accumulation in the *dgd1* mutant of *A. thaliana* (Klaus et al. 2002).

However, the mutations introduced in *e8* mutant have a side effect in nitrogen starvation: in -N condition, the increased lipid production trait was lost in *e8*. In *N. gaditana* nitrogen starvation induces a lipid accumulation through the degradation of existing membrane lipids (MGDG and DGDG mainly) and in part by the *de novo* synthesis of TAG (Simionato et al. 2013). In *e8* mutant, due to the mutation in *dgd1* gene, membrane glycerolipids are likely kept to a minimum level sufficient to avoid impairment of photosynthetic membrane integrity, allowing for a sustainable photoautotrophic growth, but the reduced pool of thylakoid membrane lipids impairs the lipid boost observed in nitrogen starvation.

Whole genomic sequencing of the mutant revealed that it was characterized by several SNPs: this is a disadvantage in using chemical mutagenesis to produce strains with phenotypic traits of interest, making the correlation between genotype and phenotype extremely difficult and increasing the possibility of unexpected phenotypes in some peculiar conditions. RNA-seq analysis could also provide additional information in order to interpret the phenotypic traits observed in *e8* mutant.

Mutant complementation or specific mutagenesis with homologous recombination or genome editing will allow to prove the correlation between specific mutations and the observed phenotypes. The mutations introduced leading to reduced pigmentation and improved lipid productivity could then be considered to possibly extend these phenotypic traits in other microalgal species.

CONCLUSIONS

The characterization of the biomass and lipid production of *N. gaditana e8* mutant demonstrate that reduced chlorophyll content per cell could be a convenient trait to be selected for improving lipid production in nitrogen replete conditions. Indeed, the selected mutant exhibited an increased lipid productivity in +N condition of ~80% compared to WT on a volumetric base. This trait is interesting considering the strong increased in C16:0, C16:1, C18:0 and C18:1 without the energetic and economic costs of inducing nutrient starvation, and their possible use for biodiesel production (Dianursanti, Sistiafi, and Putri 2018; Hoffmann et al. 2010). Improved photosynthetic efficiency by manipulating chlorophyll per cell content is thus a suitable strategy to increase lipid productivity in *N. gaditana.* Reduced chlorophyll per cell phenotype can be obtained by chemical mutagenesis, as reported in this work, or by specific genetic manipulation by homologous recombination (Kilian et al. 2011) or genome editing (Ajjawi et al. 2017; Naduthodi et al. 2019). Direct genetic engineering would have also allow reducing the risk of introducing additional mutations with possible negative side effects.

MATERIAL AND METHODS

Culture conditions, mutagenesis and mutant selection. *N. gaditana* WT (CCAP849/5) and mutants were cultivated in sterile filtered f/2 medium (Guillard and Ryther 1962) modified as described in Alboresi et al. 2016. Cells were grown at temperature of 24 ± 1°C, in a 16h light/8h dark photoperiod with a fluorescent light of about 70 µmol photons m^{-2} s^{-1} (low light = LL). Cells number were monitored with a Bürker Counting Chamber (HBG, Germany) under light microscope. Chemical mutagenesis was induced using the mutagenic agent ethyl-methane-sulfonate (EMS) as described in the following: EMS was added to 10^8 cell/ml at concentrations of 0.75%, 1.5%, 2% and 2.5%. Samples were incubated for 2h in dark and then diluted in 10% sodium thiosulfate solution inactivating the EMS activity. Cells were then centrifuged, washed twice with 1M NaCl, dissolved in 500µl of f/2 medium and kept overnight under low light. Cells were then plated on f/2 solid medium and kept under control light for at least 2 weeks. The cells treated with EMS concentration inducing a 95% of mortality was used for the following screening procedure. Pale green mutants were selected on the base of visible phenotype. Selected colonies were cultured in liquid f/2 medium and the chlorophyll content per cell was estimated by measuring absorption of whole cells at 680 nm and at 730 nm: strains with at least a 25% reduced 680/730 absorption ratio were selected. Further screening was performed measuring the chlorophyll content per cell and nile red staining as described below and in the Results section.

Nile red staining. Lipid content by Nile Red staining was evaluated as previously reported (Chen et al. 2009)**.**

Measurement of photosynthetic parameters. *In vivo* chlorophyll fluorescence was measured with Dual PAM-100 fluorometer (Walz, Effeltrich, Germany) at room temperature (RT) using a saturating light at 6000 µmol photons m^{-2} s^{-1} and actinic light of 1500 µmol photons m^{-2} s^{-1}. The NPQ parameter were calculated form the maximum fluorescence induced by a saturating pulse in the dark (F_M) or after actinic light exposure (F_M') as (F_M – F_M')/F_M'. Proton motive force upon exposure to different light intensities was measured by Electrochromic shift (ECS) with MultispeQ v2.0 (PhotosynQ) according to (Kuhlgert et al. 2016). PSII functional antenna size was measured following kinetic of PSII fluorescence emission in cells treated with 1 x 10^{-5} M 3-(3,4-dichlorophenyl)-1,1-dimethylurea (DCMU). PSII antenna size is inversely proportional to the time required for reaching 2/3 of the maximum fluorescence emission (Malkin et al. 1981). Oxygen evolution curves were performed as described (Perozeni, Stella, and Ballottari 2018). Net oxygen production was calculated subtracting the oxygen consumption in the dark after each measurement at the different actinic lights. Experimental data were fitted with hyperbolic functions in order to retrieve the Pmax (maximum photosynthetic activity) and half saturation light intensity values (light intensity at which the oxygen evolved is half of Pmax).

Pigment extraction and analysis. The chlorophyll *a* and total carotenoids were extracted from *N. gaditana* with 100% DMSO at 60°C for 24 h in dark conditions and analyzed by HPLC as described in

(Lagarde, Beuf, and Vermaas 2000). De-epoxidation index was calculated as (zea + anthera/2) /(antera+viola+zea).

Biomass and lipid productivity. Biomass productivity of WT and *e8* mutant were evaluated in small photobioreactors (80 ml) in Multi-Cultivator MC1000 system (Photon System Instrument, Cech republic) at 24°C under continuous light at 60, 200, 400 or 1500 µmol m^{-2} s^{-1} as described in the Results section. Biomass accumulation were evaluated considering the dry weight per volume (gr/L) obtained at the end of the growth curve. Maximum daily productivity (gr $L^{-1}day^{-1}$) were determined at the exponential phase of growth curve. Fatty acid methyl esters (FAME) were measured at the end of the exponential phase as reported in (Dall'Osto et al. 2019). Lipid and fatty acids accumulation were expressed on a volume base (mg/L) or as a fraction of biomass dry weight (mg/gr). Daily lipid productivity was calculated from lipid content and the time (days) at which the lipid analysis was performed.

Sequencing and computational analysis. Sequencing of mutant and WT strain was carried out on an Illumina NextSeq and an Illumina HiSeq1000 respectively. The raw reads resulting from sequencing were processed using Scythe (Anon n.d.) and Sickle (Joshi and Fass 2011) to remove Illumina adapters and low-quality reads. All sequences were mapped to the *N.gaditana* B-31 assembly (Corteggiani Carpinelli et al. 2014) using the Burrows- Wheeler Aligner (BWA)(Li and Durbin 2010). Deduplication and indel realignment were performed with PicardTools(Anon n.d.). Variants were identified were identified using three software: GATK (Depristo et al. 2011), Freebayes v1.3.1(Garrison and Marth 2012) and breseq v0.35.1 (Deatherage and Barrick 2014). Variants were quality filtered (DP>5 and QUAL>30) and for each sample only mutations identified by three out of three variant callers were selected. Variants found in both samples were then discarded. Prediction of SNPs effect was performed using SNPeff software (Cingolani et al. 2012). The dataset of SNPs identified are reported in Supplementary Dataset S1. Only SNPs not predicted with MODIFIER effect, thus only SNPs located elsewhere than upstream or downstream of a gene, 5' or 3' UTR regions or intergenic regions were considered for the following analysis. Targeting prediction was performed using HECTAR (Gschloessl et al. 2008). GO analyses were performed on Blast2go (Conesa et al. 2005), using Blast2go GO term grouped using plant slim subset and eventually visualized with REVIGO (Supek et al. 2011) in base of the number of gene for each GO term.

ACKNOWLEDGEMENTS

We thank the Centro Piattaforme Tecnologiche for providing access to the core facilities of University of Verona.

AUTHOR CONTRIBUTIONS

M.B. conceived the work. M.B., M.E.M and M.D. supervised experiments. M.C. performed or contributed to all the experiments herein reported. S.B. and S.P. contributed to the selection and preliminary characterization of *e8* mutant. M.E.M. and I.V. performed lipid analysis. B. I., B. G. and M. D. performed the whole genome sequencing and bioinformatics analysis for the identification of SNPs. M.B., M.C. and S.B. wrote the manuscript with contributions from all the authors. All the authors discussed the results, contributed to data interpretation and commented on the manuscript.

REFERENCES

Ajjawi, Imad, John Verruto, Moena Aqui, Leah B. Soriaga, Jennifer Coppersmith, Kathleen Kwok, Luke Peach, Elizabeth Orchard, Ryan Kalb, Weidong Xu, Tom J. Carlson, Kristie Francis, Katie Konigsfeld, Judit Bartalis, Andrew Schultz, William Lambert, Ariel S. Schwartz, Robert Brown, and Eric R. Moellering. 2017. "Lipid Production in *Nannochloropsis gaditana* Is Doubled by Decreasing Expression of a Single Transcriptional Regulator." *Nature Biotechnology*.

Akbari, Fariba, Morteza Eskandani, and Ahmad Yari Khosroushahi. 2014. "The Potential of Transgenic Green Microalgae; a Robust Photobioreactor to Produce Recombinant Therapeutic Proteins." *World Journal of Microbiology and Biotechnology*.

Alboresi, Alessandro, Giorgio Perin, Nicola Vitulo, Gianfranco Diretto, Maryse Block, Juliette Jouhet, Andrea Meneghesso, Giorgio Valle, Giovanni Giuliano, Eric Maréchal, and Tomas Morosinotto. 2016. "Light Remodels Lipid Biosynthesis in *Nannochloropsis gaditana* by Modulating Carbon Partitioning between Organelles." *Plant Physiology*.

Andersen, Robert A., Robyn W. Brett, Daniel Potter, and Julianne P. Sexton. 1998. "Phylogeny of the Eustigmatophyceae Based upon 18s RDNA, with Emphasis on Nannochloropsis." *Protist*.

Anon. n.d. "Picard Tools. Broad Institute." Retrieved (http://broadinstitute.github.io/picard).

Anon. n.d. "Scythe - A Bayesian Adapter Trimmer (Version 0.994 BETA)." Retrieved (https://github.com/vsbuffalo/scythe).

Bailleul, B., P. Cardol, C. Breyton, and G. Finazzi. 2010. "Electrochromism: A Useful Probe to Study Algal Photosynthesis." *Photosynth.Res.* 106(1573-5079 (Electronic)):179–89.

Ballottari, Matteo, Thuy B. Truong, Eleonora Re De, Erika Erickson, Giulio R. Stella, Graham R. Fleming, Roberto Bassi, and Krishna K. Niyogi. 2016. "Identification of Ph-Sensing Sites in the Light Harvesting Complex Stress-Related 3 Protein Essential for Triggering Non-Photochemical Quenching in *Chlamydomonas reinhardtii*." *Journal of Biological Chemistry*.

Basso, Stefania, Diana Simionato, Caterina Gerotto, Anna Segalla, Giorgio M. Giacometti, and Tomas Morosinotto. 2014. "Characterization of the Photosynthetic Apparatus of the Eustigmatophycean *Nannochloropsis gaditana*: Evidence of Convergent Evolution in the Supramolecular Organization of Photosystem I." *Biochimica et Biophysica Acta - Bioenergetics*.

Beacham, Tracey A., Jeremy B. Sweet, and Michael J. Allen. 2017. "Large Scale Cultivation of Genetically Modified Microalgae: A New Era for Environmental Risk Assessment." *Algal Research*.

Bernaerts, Tom M. M., Lore Gheysen, Imogen Foubert, Marc E. Hendrickx, and Ann M. Van Loey. 2019. "The Potential of Microalgae and Their Biopolymers as Structuring Ingredients in Food: A Review." *Biotechnology Advances*.

Camacho, Franciele, Angela Macedo, and Francisco Malcata. 2019. "Potential Industrial Applications and Commercialization of Microalgae in the Functional Food and Feed Industries: A Short Review." *Marine Drugs* 17(6).

Cao, Shaona, Xiaowen Zhang, Dong Xu, Xiao Fan, Shanli Mou, Yitao Wang, Naihao Ye, and Wenqi Wang. 2013. "A Transthylakoid Proton Gradient and Inhibitors Induce a Non-Photochemical Fluorescence Quenching in Unicellular Algae *Nannochloropsis sp*." *FEBS Letters*.

Cazzaniga, Stefano, Luca Dall'Osto, Joanna Szaub, Luca Scibilia, Matteo Ballottari, Saul Purton, and Roberto Bassi. 2014. "Domestication of the Green Alga *Chlorella sorokiniana*: Reduction of Antenna Size Improves Light-Use Efficiency in a Photobioreactor." *Biotechnology for Biofuels*.

Chen, Hao Hong and Jian Guo Jiang. 2017. "Lipid Accumulation Mechanisms in Auto- and Heterotrophic Microalgae." *Journal of Agricultural and Food Chemistry* 65(37):8099–8110.

Chen, Wei, Chengwu Zhang, Lirong Song, Milton Sommerfeld, and Qiang Hu. 2009. "A High Throughput Nile Red Method for Quantitative Measurement of Neutral Lipids in Microalgae." *Journal of Microbiological Methods*.

Chiu, Chi Chou, Lih Jen Chen, Pai Hsiang Su, and Hsou min Li. 2013. "Evolution of Chloroplast J Proteins." *PLoS ONE*.

Chukhutsina, Volha U., Rikard Fristedt, Tomas Morosinotto, and Roberta Croce. 2017. "Photoprotection Strategies of the Alga *Nannochloropsis gaditana*." *Biochimica et Biophysica Acta - Bioenergetics*.

Cingolani, Pablo, Adrian Platts, Le Lily Wang, Melissa Coon, Tung Nguyen, Luan Wang, Susan J. Land, Xiangyi Lu, and Douglas M. Ruden. 2012. "A Program for Annotating and Predicting the Effects of Single Nucleotide Polymorphisms, SnpEff: SNPs in the Genome of *Drosophila melanogaster* Strain W1118; Iso-2; Iso-3." *Fly*.

Conesa, Ana, Stefan Götz, Juan Miguel García-Gómez, Javier Terol, Manuel Talón, and Montserrat Robles. 2005. "Blast2GO: A Universal Tool for Annotation, Visualization and Analysis in Functional Genomics Research." *Bioinformatics*.

Corteggiani Carpinelli, Elisa, Andrea Telatin, Nicola Vitulo, Claudio Forcato, Michela D'Angelo, Riccardo Schiavon, Alessandro Vezzi, Giorgio Mario Giacometti, Tomas Morosinotto, and Giorgio Valle. 2014. "Chromosome Scale Genome Assembly and Transcriptome Profiling of *Nannochloropsis gaditana* in Nitrogen Depletion." *Molecular Plant* 7(2):323–35.

Dall'Osto, Luca, Stefano Cazzaniga, Zeno Guardini, Simone Barera, Manuel Benedetti, Giuseppe Mannino, Massimo E. Maffei, and Roberto Bassi. 2019. "Combined Resistance to Oxidative Stress and Reduced Antenna Size Enhance Light-to-Biomass Conversion Efficiency in *Chlorella vulgaris* Cultures." *Biotechnology for Biofuels* 12(1):1–17.

Deatherage, Daniel E. and Jeffrey E. Barrick. 2014. "Identification of Mutations in Laboratory-Evolved Microbes from next-Generation Sequencing Data Using Breseq." *Methods in Molecular Biology*.

Depristo, Mark A., Eric Banks, Ryan Poplin, Kiran V. Garimella, Jared R. Maguire, Christopher Hartl, Anthony A. Philippakis, Guillermo Del Angel, Manuel A. Rivas, Matt Hanna, Aaron McKenna, Tim J. Fennell, Andrew M. Kernytsky, Andrey Y. Sivachenko, Kristian Cibulskis, Stacey B. Gabriel, David Altshuler, and Mark J. Daly. 2011. "A Framework for Variation Discovery and Genotyping Using Next-Generation DNA Sequencing Data." *Nature Genetics*.

Dianursanti, A. G. Sistiafi, and D. N. Putri. 2018. "Biodiesel Synthesis from *Nannochloropsis oculata* and *Chlorella vulgaris* through Transesterification Process Using NaOH/Zeolite Heterogeneous Catalyst." in *IOP Conference Series: Earth and Environmental Science*.

Dormann, P., S. Hoffmann-Benning, I. Balbo, and C. Benning. 1995. "Isolation and Characterization of an *Arabidopsis* Mutant Deficient in the Thylakoid Lipid Digalactosyl Diacylglycerol." *Plant Cell*.

Erickson, Erika, Setsuko Wakao, and Krishna K. Niyogi. 2015. "Light Stress and Photoprotection in *Chlamydomonas reinhardtii*." *Plant Journal* 82(3):449–65.

Formighieri, Cinzia, Fabrice Franck, and Roberto Bassi. 2012. "Regulation of the Pigment Optical Density of an Algal Cell: Filling the Gap between Photosynthetic Productivity in the Laboratory and in Mass Culture." *Journal of Biotechnology*.

Garrison, Erik and Gabor Marth. 2012. "Haplotype-Based Variant Detection from Short-Read Sequencing -- Free Bayes -- Variant Calling -- Longranger." *ArXiv Preprint ArXiv:1207.3907*.

Gill, Iqbal and Rao Valivety. 1997. "Polyunsaturated Fatty Acids, Part 1: Occurrence, Biological Activities and Applications." *Trends in Biotechnology*.

Gschloessl, Bernhard, Yann Guermeur, and J. Mark Cock. 2008. "HECTAR: A Method to Predict Subcellular Targeting in Heterokonts." *BMC Bioinformatics*.

Guillard, Robert R. L. and John H. Ryther. 1962. "Studies of Marine Planktonic Diatoms, I, *Cyclotella Nanna* (Hustedt) and *Detonula Convervacea* (Cleve)." *Canadian Journal of Microbiology*.

Hemsley, Piers A., Thilo Weimar, Kathryn Lilley, Paul Dupree, and Claire Grierson. 2013. "Palmitoylation in Plants." *Plant Signaling & Behavior*.

HIBBERD, D. J. 1981. "Notes on the Taxonomy and Nomenclature of the Algal Classes Eustigmatophyceae and Tribophyceae (Synonym Xanthophyceae)." *Botanical Journal of the Linnean Society*.

Hodgson, Paul A., R. James Henderson, John R. Sargent, and John W. Leftley. 1991. "Patterns of Variation in the Lipid Class and Fatty Acid Composition of *Nannochloropsis oculata* (Eustigmatophyceae) during Batch Culture - I. The Growth Cycle." *Journal of Applied Phycology*.

Hoffmann, Maren, Kai Marxen, Rüdiger Schulz, and Klaus Heinrich Vanselow. 2010. "TFA and EPA Productivities of *Nannochloropsis salina* Influenced by Temperature and Nitrate Stimuli in Turbidostatic Controlled Experiments." *Marine Drugs*.

Huete-Ortega, María, Katarzyna Okurowska, Rahul Vijay Kapoore, Matthew P. Johnson, D. James Gilmour, and Seetharaman Vaidyanathan. 2018. "Effect of Ammonium and High Light Intensity on the Accumulation of Lipids in *Nannochloropsis oceanica* (CCAP 849/10) and *Phaeodactylum tricornutum* (CCAP 1055/1)." *Biotechnology for Biofuels*.

Inoue-Kashino, Natsuko, Yasuhiro Kashino, Hidefumi Orii, Kazuhiko Satoh, Ichiro Terashima, and Himadri B. Pakrasi. 2011. "S4 Protein Sll1252 Is Necessary for Energy Balancing in Photosynthetic Electron Transport in *Synechocystis sp.* PCC 6803." *Biochemistry*.

Janssen, Jorijn H., René H. Wijffels, and Maria J. Barbosa. 2019. "Lipid Production in *Nannochloropsis gaditana* during Nitrogen Starvation." *Biology*.

Jeong, Jooyeon, Kwangryul Baek, Henning Kirst, Anastasios Melis, and Eon Seon Jin. 2017. "Loss of CpSRP54 Function Leads to a Truncated Light-Harvesting Antenna Size in *Chlamydomonas reinhardtii*." *Biochimica et Biophysica Acta - Bioenergetics*.

Joshi, N. and J. Fass. 2011. "Sickle: A Sliding-Window, Adaptive, Quality-Based Trimming Tool for FastQ Files (Version 1.33) [Software]." *Available at Https://Github.Com/Najoshi/Sickle.*

Kang, Nam Kyu, Eun Kyung Kim, Min Gyu Sung, Young Uk Kim, Byeong ryool Jeong, and Yong Keun Chang. 2019. "Increased Biomass and Lipid Production by Continuous Cultivation of *Nannochloropsis salina* Transformant Overexpressing a BHLH Transcription Factor." *Biotechnology and Bioengineering*.

Kilian, Oliver, Christina S. E. Benemann, Krishna K. Niyogi, and Bertrand Vick. 2011. "High-Efficiency Homologous Recombination in the Oil-Producing Alga *Nannochloropsis sp.*" *Proceedings of the National Academy of Sciences of the United States of America*.

Kirst, Henning, Cinzia Formighieri, and Anastasios Melis. 2014. "Maximizing Photosynthetic Efficiency and Culture Productivity in Cyanobacteria upon Minimizing the Phycobilisome Light-Harvesting Antenna Size." *Biochimica et Biophysica Acta - Bioenergetics*.

Kirst, Henning, Jose Gines García-Cerdán, Andreas Zurbriggen, and Anastasios Melis. 2012. "Assembly of the Light-Harvesting Chlorophyll Antenna in the Green Alga *Chlamydomonas reinhardtii* Requires Expression of the TLA2-CpFTSY Gene." *Plant Physiology*.

Kirst, Henning, Jose Gines Garcia-Cerdan, Andreas Zurbriggen, Thilo Ruehle, and Anastasios Melis. 2012. "Truncated Photosystem Chlorophyll Antenna Size in the Green Microalga *Chlamydomonas reinhardtii* upon Deletion of the TLA3-CpSRP43 Gene." *Plant Physiology*.

Klaus, Dörte, Heiko Härtel, Lynda M. Fitzpatrick, John E. Froehlich, Jamie Hubert, Christoph Benning, and Peter Dörmann. 2002. "Digalactosyldiacylglycerol Synthesis in Chloroplasts of the *Arabidopsis* Dgd1 Mutant." *Plant Physiology*.

Kuhlgert, Sebastian, Greg Austic, Robert Zegarac, Isaac Osei-Bonsu, Donghee Hoh, Martin I. Chilvers, Mitchell G. Roth, Kevin Bi, Dan TerAvest, Prabode Weebadde, and David M. Kramer. 2016. "MultispeQ Beta: A Tool for Large-Scale Plant Phenotyping Connected to the Open PhotosynQ Network." *Royal Society Open Science*.

Lagarde, Delphine, Laurent Beuf, and Wim Vermaas. 2000. "Increased Production of Zeaxanthin and Other Pigments by Application of Genetic Engineering Techniques to *Synechocystis sp.* Strain PCC 6803." *Applied and Environmental Microbiology*.

Li, Heng and Richard Durbin. 2010. "Fast and Accurate Long-Read Alignment with Burrows-Wheeler Transform." *Bioinformatics*.

Li, Yipu and Mingliang Xu. 2017. "CCT Family Genes in Cereal Crops: A Current Overview." *Crop Journal*.

Liang, Jibei, Fang Wen, and Jianhua Liu. 2019. "Transcriptomic and Lipidomic Analysis of an EPA-Containing *Nannochloropsis*

sp. PJ12 in Response to Nitrogen Deprivation." *Scientific Reports*.

Liguori, Nicoletta, Laura M. Roy, Milena Opacic, Grégory Durand, and Roberta Croce. 2013. "Regulation of Light Harvesting in the Green Alga *Chlamydomonas reinhardtii*: The c-Terminus of Lhcsr Is the Knob of a Dimmer Switch." *Journal of the American Chemical Society*.

Lu, Yandu, Wenxu Zhou, Li Wei, Jing Li, Jing Jia, Fei Li, Steven M. Smith, and Jian Xu. 2014. "Regulation of the Cholesterol Biosynthetic Pathway and Its Integration with Fatty Acid Biosynthesis in the Oleaginous Microalga *Nannochloropsis oceanica*." *Biotechnology for Biofuels*.

Lubián, Luis. 1982. " *Nannochloropsis gaditana sp.* Nov., Una Nueva Eustigmatophyceae Marina." *Lazaroa*.

Ma, Yubin, Zhiyao Wang, Changjiang Yu, Yehu Yin, and Gongke Zhou. 2014. "Evaluation of the Potential of 9 *Nannochloropsis* Strains for Biodiesel Production." *Bioresource Technology*.

Malkin, Shmuel, Paul A. Armond, Harold A. Mooney, and David C. Fork. 1981. "Photosystem II Photosynthetic Unit Sizes from Fluorescence Induction in Leaves." *Plant Physiology*.

Melis, Anastasios. 2009. "Solar Energy Conversion Efficiencies in Photosynthesis: Minimizing the Chlorophyll Antennae to Maximize Efficiency." *Plant Science*.

Meneghesso, Andrea, Diana Simionato, Caterina Gerotto, Nicoletta La Rocca, Giovanni Finazzi, and Tomas Morosinotto. 2016. "Photoacclimation of Photosynthesis in the Eustigmatophycean *Nannochloropsis gaditana*." *Photosynthesis Research*.

Moummou, Hanane, Yvonne Kallberg, Libert Brice Tonfack, Bengt Persson, and Benoît van der Rest. 2012. "The Plant Short-Chain Dehydrogenase (SDR) Superfamily: Genome-Wide Inventory and Diversification Patterns." *BMC Plant Biology*.

Naduthodi, Mihris Ibnu Saleem, Prarthana Mohanraju, Christian Südfeld, Sarah D'Adamo, Maria J. Barbosa, and John Van Der Oost. 2019. "CRISPR-Cas Ribonucleoprotein Mediated Homology-Directed Repair for Efficient Targeted Genome Editing in Microalgae *Nannochloropsis oceanica* IMET1." *Biotechnology for Biofuels*.

Perin, Giorgio, Alessandra Bellan, Anna Segalla, Andrea Meneghesso, Alessandro Alboresi, and Tomas Morosinotto. 2015. "Generation of Random Mutants to Improve Light-Use Efficiency of *Nannochloropsis gaditana* Cultures for Biofuel Production." *Biotechnology for Biofuels* 8(1):1–13.

Perozeni, Federico, Giulio Rocco Stella, and Matteo Ballottari. 2018. "LHCSR Expression under HSP70/RBCS2 Promoter as a Strategy to Increase Productivity in Microalgae." *International Journal of Molecular Sciences*.

Polle, Juergen E. W., Sarada Devi Kanakagiri, and Anastasios Melis. 2003. "Tla1, a DNA Insertional Transformant of the Green Alga *Chlamydomonas reinhardtii* with a Truncated Light-Harvesting Chlorophyll Antenna Size." *Planta*.

Radakovits, Randor, Robert E. Jinkerson, Susan I. Fuerstenberg, Hongseok Tae, Robert E. Settlage, Jeffrey L. Boore, and Matthew C. Posewitz. 2012. "Draft Genome Sequence and Genetic Transformation of the Oleaginous Alga *Nannochloropis gaditana*." *Nature Communications*.

Rodolfi, Liliana, Graziella Chini Zittelli, Niccolo Bassi, Giulia Padovani, Natascia Biondi, Gimena Bonini, and Mario R. Tredici. 2009. "Microalgae for Oil: Strain Selection, Induction of Lipid Synthesis and Outdoor Mass Cultivation in a Low-Cost Photobioreactor." *Biotechnology and Bioengineering*.

Rösch, Christine, Max Roßmann, and Sebastian Weickert. 2019. "Microalgae for Integrated Food and Fuel Production." *GCB Bioenergy*.

Siaut, Magali, Stéphan Cuiné, Caroline Cagnon, Boris Fessler, Mai Nguyen, Patrick Carrier, Audrey Beyly, Fred Beisson, Christian Triantaphylidès, Yonghua Li-Beisson, and Gilles Peltier. 2011. "Oil Accumulation in the Model Green Alga *Chlamydomonas reinhardtii*: Characterization, Variability between Common Laboratory Strains and Relationship with Starch Reserves." *BMC Biotechnology*.

Simionato, Diana, Maryse A. Block, Nicoletta La Rocca, Juliette Jouhet, Eric Maréchal, Giovanni Finazzi, and Tomas Morosinotto. 2013. "The Response of *Nannochloropsis gaditana* to Nitrogen Starvation Includes de Novo Biosynthesis of Triacylglycerols, a Decrease of Chloroplast Galactolipids, and Reorganization of the Photosynthetic Apparatus."

Eukaryotic Cell.

Simionato, Diana, Eleonora Sforza, Elisa Corteggiani Carpinelli, Alberto Bertucco, Giorgio Mario Giacometti, and Tomas Morosinotto. 2011. "Acclimation of *Nannochloropsis gaditana* to Different Illumination Regimes: Effects on Lipids Accumulation." *Bioresource Technology*.

Supek, Fran, Matko Bošnjak, Nives Škunca, and Tomislav Šmuc. 2011. "Revigo Summarizes and Visualizes Long Lists of Gene Ontology Terms." *PLoS ONE*.

Verruto, John, Kristie Francis, Yingjun Wang, Melisa C. Low, Jessica Greiner, Sarah Tacke, Fedor Kuzminov, William Lambert, Jay McCarren, Imad Ajjawi, Nicholas Bauman, Ryan Kalb, Gregory Hannum, and Eric R. Moellering. 2018. "Unrestrained Markerless Trait Stacking in *Nannochloropsis gaditana* through Combined Genome Editing and Marker Recycling Technologies." *Proceedings of the National Academy of Sciences of the United States of America*.

Wijffels, René H. and Maria J. Barbosa. 2010. "An Outlook on Microalgal Biofuels." *Science*.

ZHANG, Jia, Yong HU, Li he XU, Qin HE, Xiao wei FAN, and Yong zhong XING. 2017. "The CCT Domain-Containing Gene Family Has Large Impacts on Heading Date, Regional Adaptation, and Grain Yield in Rice." *Journal of Integrative Agriculture*.

SUPPLEMENTARY INFORMATION

Sequenced data discussed in this work have been submitted to the Sequence Read Archive (SRA) repository of the NCBI database and are available under Bioproject accession number PRJNA623339.

Supplemental dataset

Supplemental dataset S1. List of the 240 SNPs identified in *e8* and their effect predicted by SNPeff software.

The dataset is available online:

https://biotechnologyforbiofuels.biomedcentral.com/articles/10.1186/s13068-020-01718-8

Supplemental Tables

Table S1. Coverage obtained by Illumina sequencing for WT and *e8* mutant strain.

	WT	***e8***
mean coverage	115.02	72.42
% 1X cov	98.79	98.81
% 5X cov	98.47	98.63
% 10X cov	98.01	98.10
% 20X cov	96.92	95.77

Table S2. Mutation identified on gene coding for proteins putatively located in the chloroplast. Prediction of chloroplast transit peptide was performed with Hectar software.

Mutant	Gene	Mutation	Annotation
e8	Naga_100008g127	3_prime_UTR_variant	Protein of unknown function DUF1118
e8	Naga_100040g45	missense_variant	nhl repeat containing protein 2
e8	Naga_100340g1	missense_variant	chaperone protein
e8	Naga_100641g4	missense_variant	dehydrogenase reductase sdr family member 9

Supplemental Figures

Supplementary Figure S1. Mutants screening by 680/730 nm absorption ratio. Absorption ratio 680/730 nm was used to assay the chlorophylls per cell content. Only colonies with a reduction of at least 25% was selected for further analyses. Error bars are reported as standard deviation (n=3).

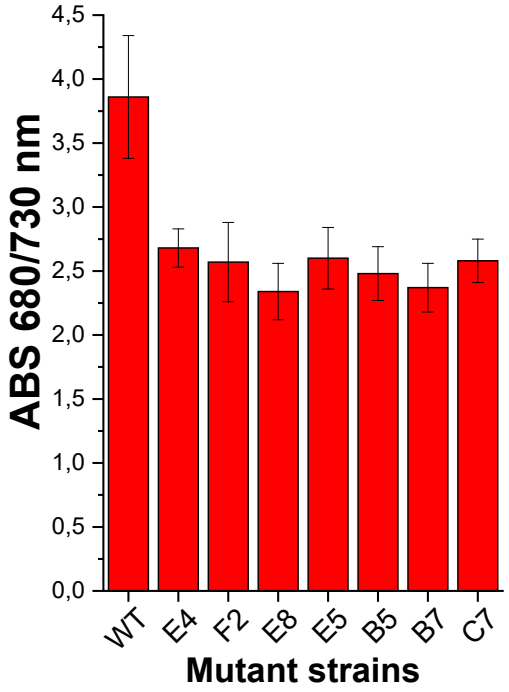

Supplementary Figure S2. Light dependent zeaxanthin accumulation in WT and *e8*. Samples were illuminated for 1 h with a strong light (2500 µmol photons m^{-2} s^{-1}). Pigments composition was evaluated at different time points by DMSO extraction and HPLC analysis. (A) Depoxidation index calculated as (zea + anthera/2) /(antera+viola+zea). (B) Zeaxanthin per carotenoid content. (C) Zeaxanthin per chlorophyll content. Errors are reported as standard deviation, significantly different values are marked with * if $p < 0.05$ and ** if $p < 0.01$, as determined by unpaired two-sample t-test (n=3).

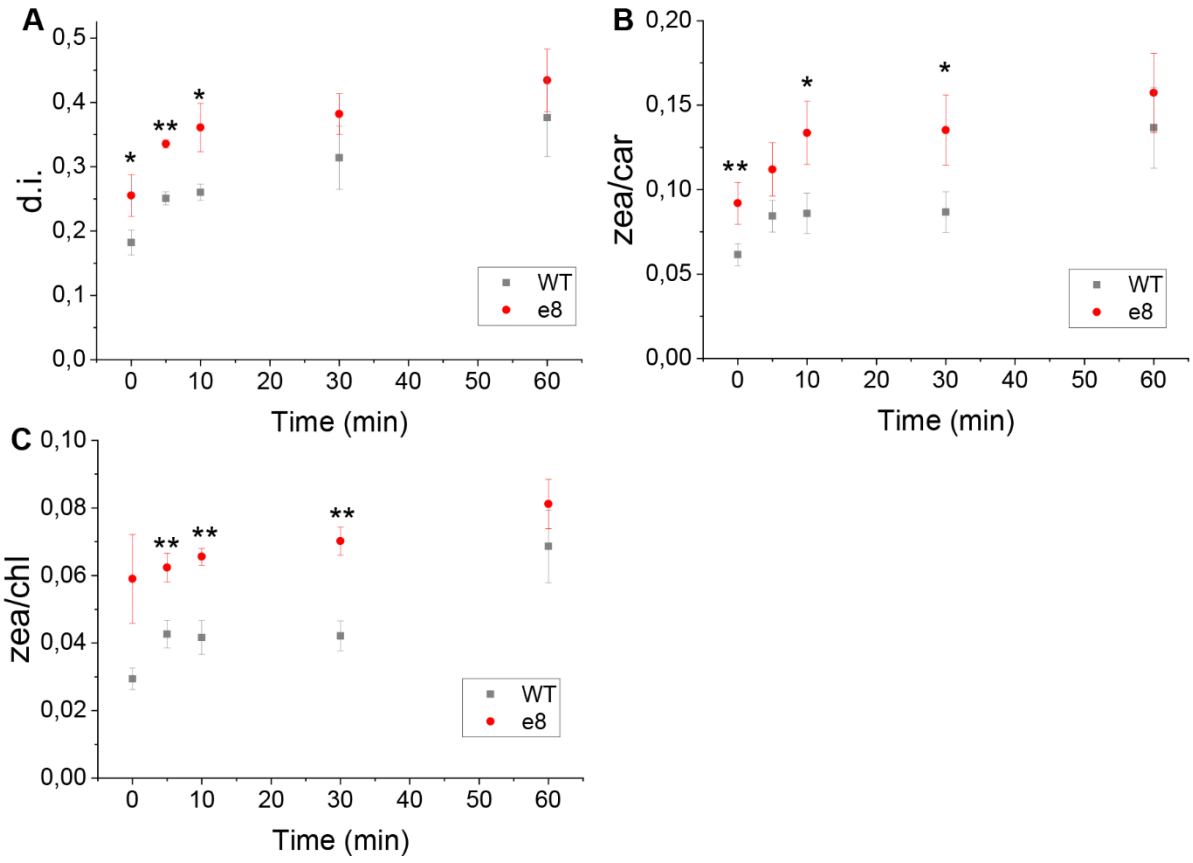

Supplementary Figure S3. Chlorophyll bleaching in wild type and *e8* mutant strain exposed to strong light. Chlorophyll bleaching kinetics of WT and *e8* mutant strains were determined measuring the decrease of chlorophyll absorption upon exposure to 2500 µmol photons m^{-2} s^{-1}. Errors are reported as standard deviation (n=3). The statistical analysis of the results obtained was performed by unpaired two sample t-test revealing no statistically significant difference being p-values > 0.1 at the different time points.

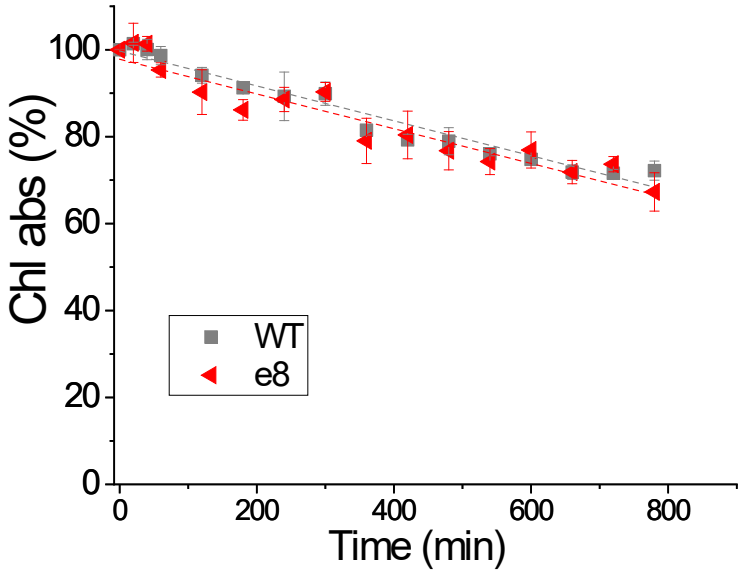

Supplementary Figure S4. Biomass and lipid productivity of WT and *e8* mutant at different irradiances. (A) Maximum daily productivity in terms of gr L^{-1} day^{-1}. (B, C) Nile Red fluorescence of WT and *e8* mutant normalized to dry weight (B) or to the culture volume (C). (D) Fold change of Nile Red fluorescence and biomass dry weight on a volumetric base in *e8* mutant compared to WT. Errors are reported as standard deviation, significantly different values are marked with * if $p < 0.05$ and ** if $p < 0.01$, as determined by unpaired two sample *t*-test (n=3).

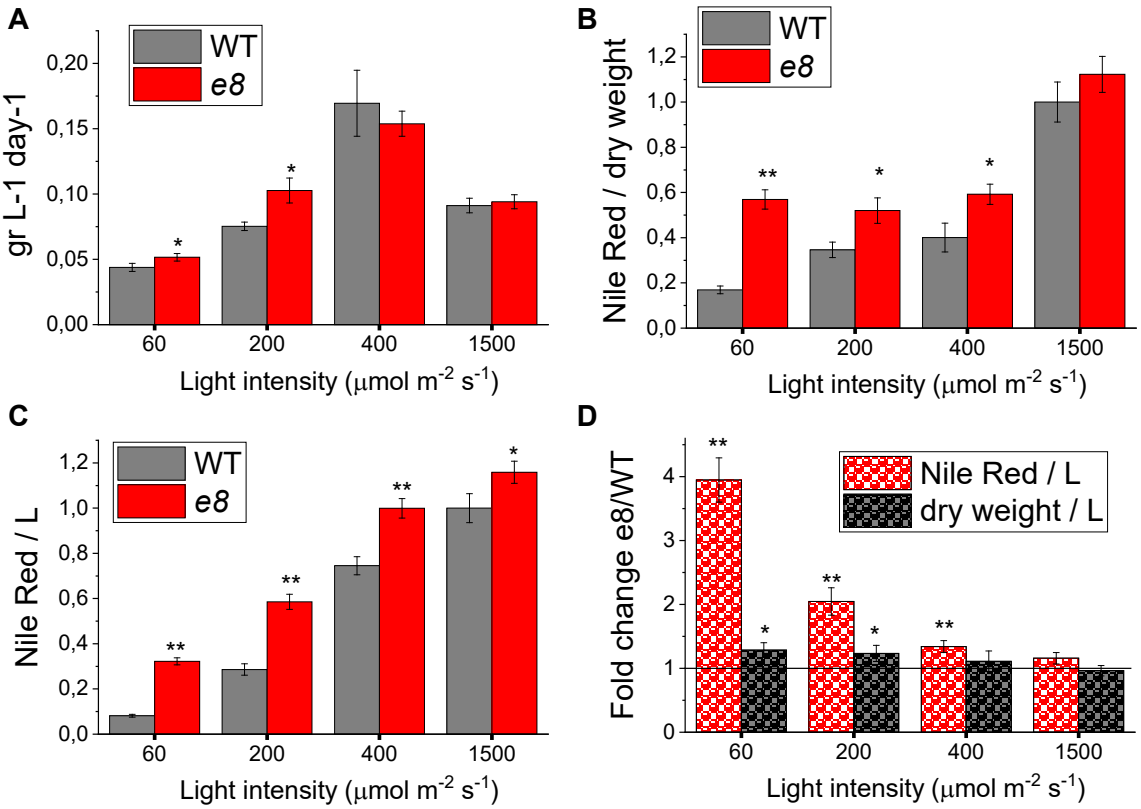

Supplementary Figure S5. Dry weight and FAME content in WT and *e8* mutant in nitrogen starvation. Dry weight (A) and FAME content (B) in cells grown in nitrogen deplete medium for WT and *e8* mutant strain. Errors are reported as standard deviation, the statistical significance of differences between WT and *e8* is indicated as ** ($p < 0.01$), as determined by unpaired two-sample *t*-test (n=3).

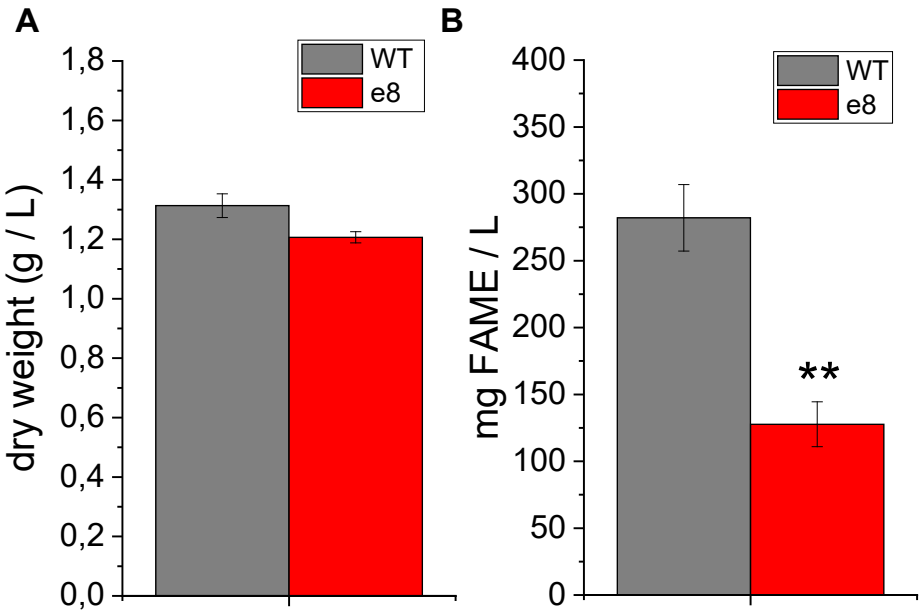

Supplementary Figure S6. Acyl chain composition of lipid fraction from WT and *e8* mutant in nitrogen replete conditions (+N) or after nitrogen starvation (-N). (A) fatty acid content per liter of culture. (B) Fold change of fatty acid fraction on total fatty acids content in *e8* normalized to the WT case. Errors are reported as standard deviation, statistically significantly different values between WT and *e8* in (A) and values statistically significantly different than 1 in (B) are marked with * if $p < 0.05$ and ** if $p < 0.01$, as determined by unpaired two sample t-test (n=3).

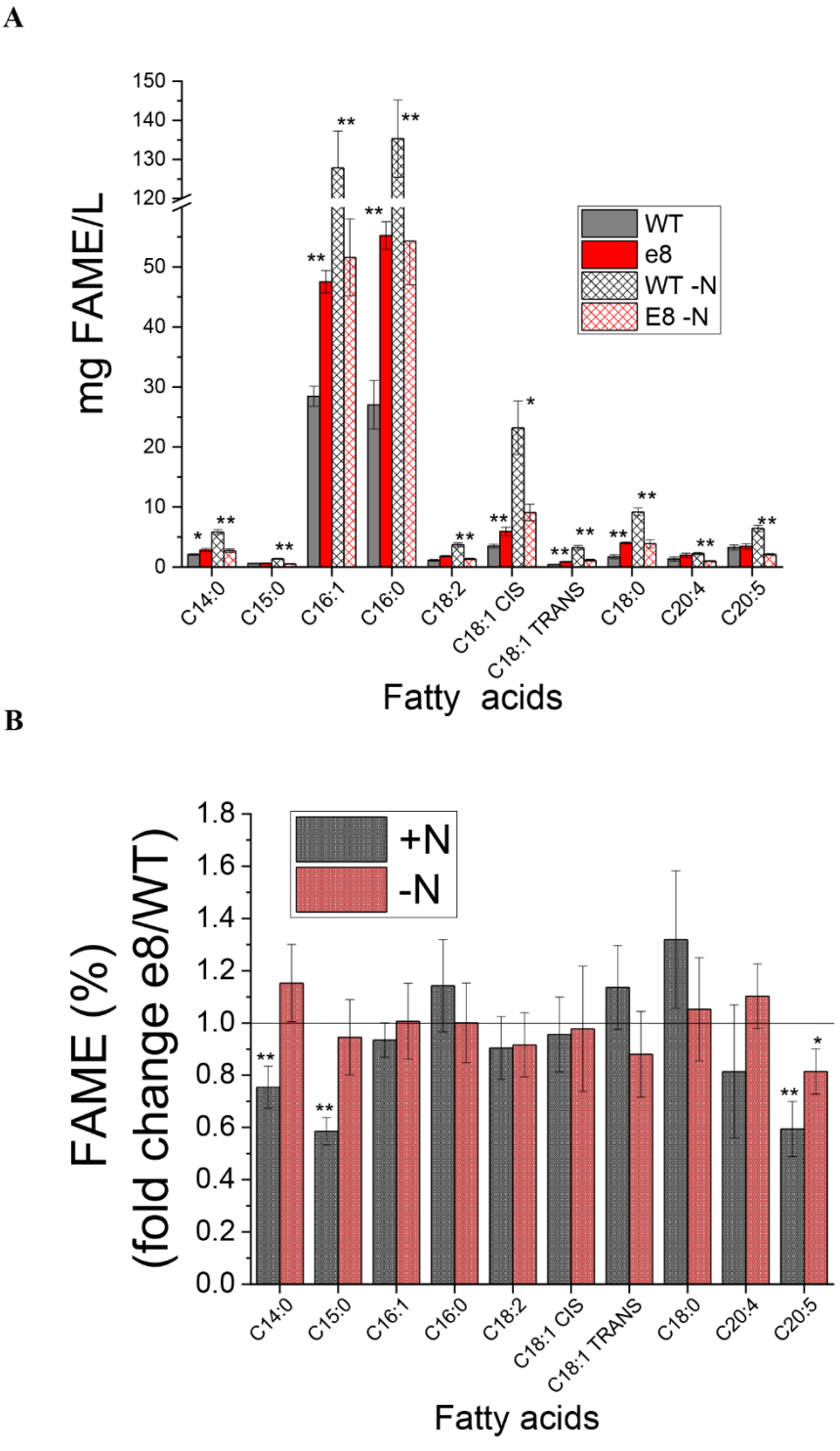

Supplementary Figure S7. Visible light transmittance in photobioreactors at different layers for WT and *e8* mutant cultures.

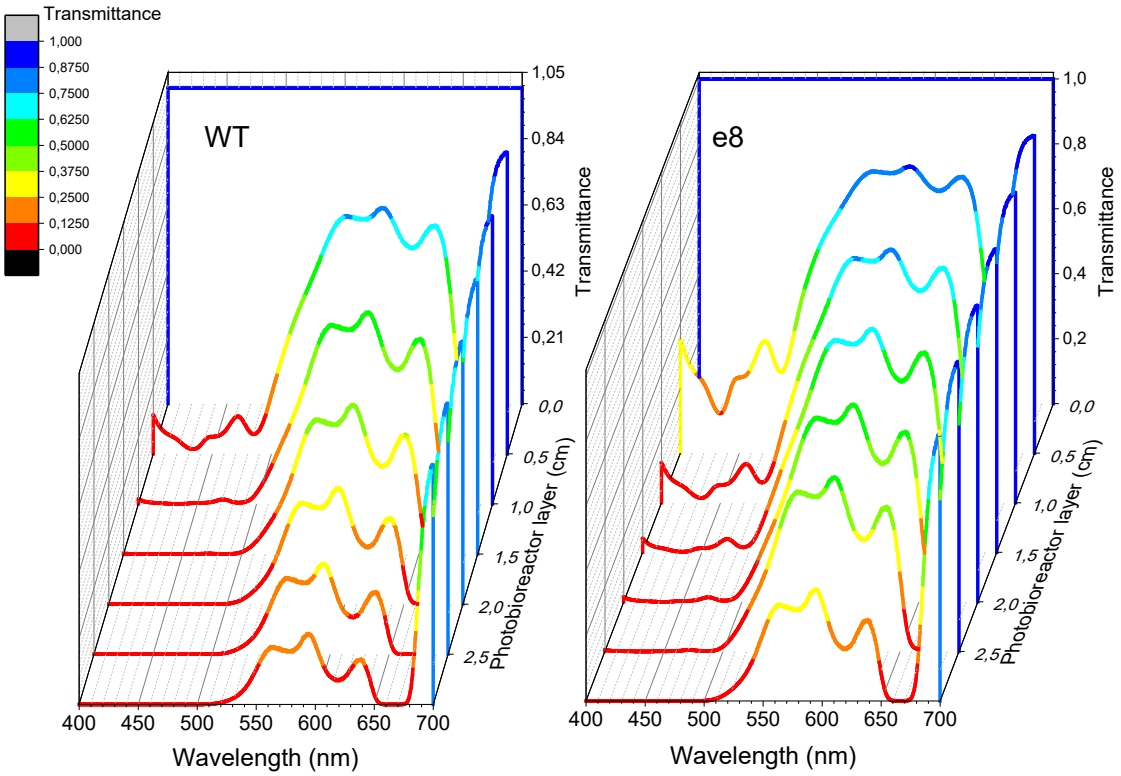

Supplementary Figure S8. GO slim terms of mutated genes of *e8*. The GO terms were restricted to GO slim terms of plant for an easier visualization. Each dot is proportional with the number of genes related to a specific category of GO terms (max 30 genes, min 1 genes).

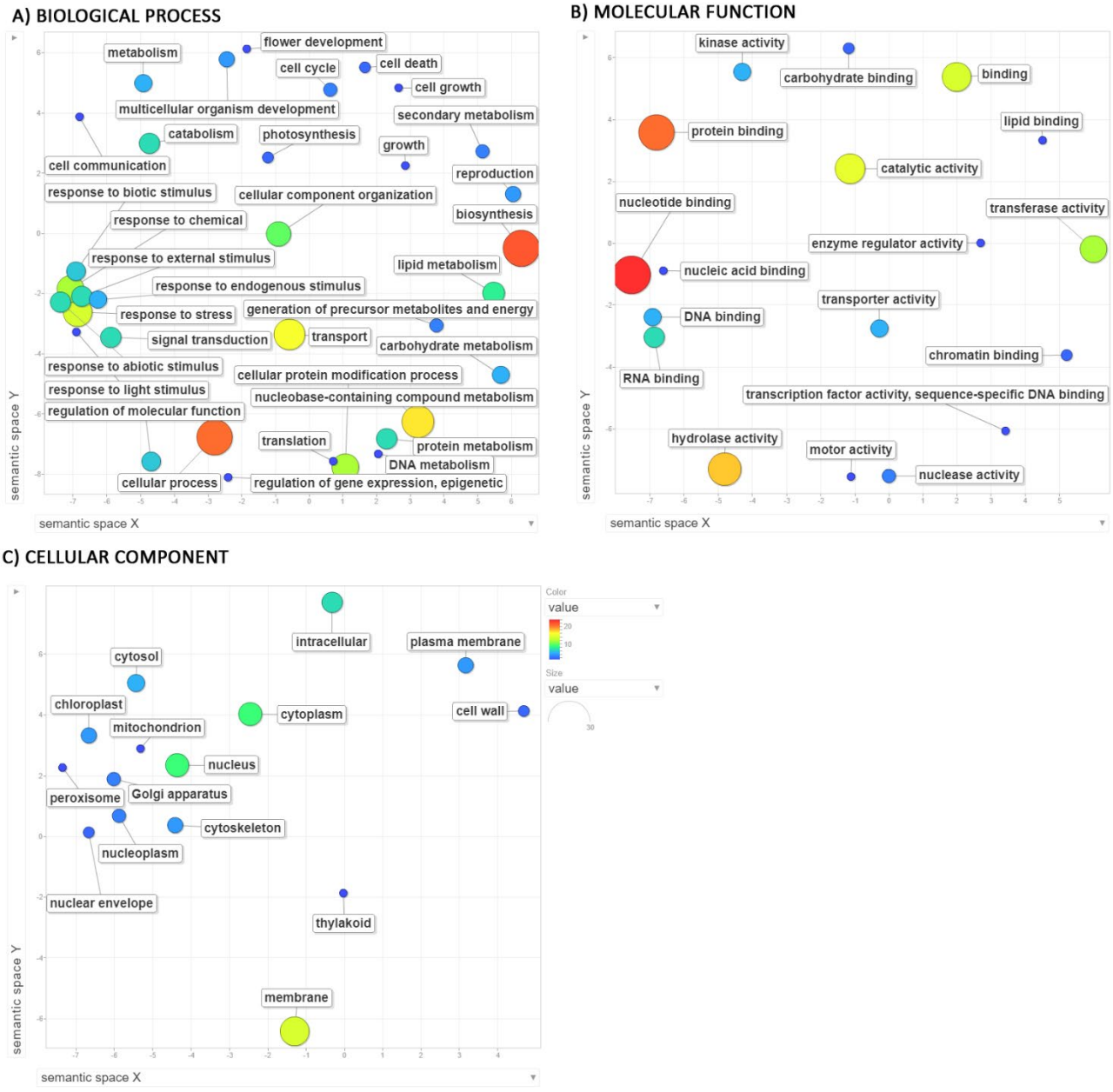

Section B

Incorporating a molecular antenna in diatom microalgae cells enhances photosynthesis

G. Leone[a,b], G. De la Cruz Valbuena[c], S.R. Cicco[d], D. Vona[a], E. Altamura[a], R. Ragni[a], E. Molotokaite[c], **M. Cecchin**[e], S. Cazzaniga[e], M. Ballottari[e], C. D'Andrea[c], G. Lanzani[b,c*] and G.M. Farinola[a*]

[a]Dipartimento di Chimica, Università degli Studi di Bari "Aldo Moro", 70126 Bari (Italy).

[b]Istituto Italiano di Tecnologia, Center for Nano Science and Technology, 20133 Milano (Italy).

[c]Dipartimento di Fisica, Politecnico di Milano, 20133 Milano (Italy).

[d]CNR-ICCOM, Dipartimento di Chimica, Università degli Studi di Bari "Aldo Moro", 70126 Bari (Italy).

[e]Dipartimento di Biotecnologie, Università degli studi di Verona, 37134 Verona (Italy)

*Corresponding author

This work was submitted to PNAS.

Diatom microalgae have great industrial potential as next-generation sources of biomaterials and biofuels. Effective scale-up of their production can be pursued by enhancing the efficiency of their photosynthetic process in a way that increases the solar-to-biomass conversion yield. A proof-of-concept demonstration is given of the possibility of enhancing the light absorption of algae and increasing their efficiency in photosynthesis by *in vivo* incorporation of an organic dye which acts as an antenna and enhances cell growth and biomass without resorting to genetic modification. A molecular dye (Cy5) is incorporated in *Thalassiosira weissflogii* diatom cells by simply adding it to the culture medium and thus filling the orange gap that limits their absorption of sunlight. Cy5 enhances diatoms' photosynthetic efficiency and cell density by 49% and 40%, respectively. Time-resolved spectroscopy reveals Förster Resonance Energy Transfer (FRET) from Cy5 to algal chlorophyll. Our approach lays the basis for non-genetic tailoring of diatoms' spectral response to light harvesting, opening up new ways for their industrial valorisation.

INTRODUCTION

Drastic changes in climate and reduction in the availability of raw chemical materials are drawing academic and industrial research, as a matter of considerable urgency, towards photosynthetic organisms as living factories for the large-scale production of fuels and active chemical products. Phytoplankton have great industrial potential in this context, which includes diatoms, the major group of microalgae responsible for ocean pH, worldwide carbon recycling and atmospheric CO_2 regulation (Priyadarshani and Rath 2012). Diatoms are envisioned as a valuable energy and food source for the nearfuture, potentially producing more biomass per unit of land area than terrestrial organisms (Sayre 2010). These unicellular eukaryotic microalgae (Lavaud, Rousseau, and Etienne 2004) ensure the oxygen content in marine ecosystems (Field et al. 1998; Yang, Lopez, and Rosengarten 2011) and control the Earth's carbon cycle, as they are responsible for ~40% of total organic carbon produced yearly in seawater (Falkowski et al. 2004; Rabosky and Sorhannus 2009). Their excellent lipid-accumulation properties make diatoms promising candidates for large-scale production of biofuels (Hildebrand et al. 2012). Further scientific interest in diatoms focuses on their suitability for application in biomedicine (Cicco et al. 2015; Leone et al. 2017; Ragni, Cicco, et al. 2018; Vona et al. 2016) and photonics (Irimia-Vladu et al. 2017; Ragni et al. 2017; Ragni, Scotognella, et al. 2018) given their mesoporous silica cell walls (frustules), whose hierarchically organized nanostructure has functions linked to cell protection from predators and harmful solar wavelengths. Despite the variety of applications, the high costs of large-scale cultivation have so far restricted diatoms' suitability for industrial production (Trentacoste et al. 2013). A possible way of circumventing this problem is to enhance their growth-improving photosynthetic efficiency that increases biomass and CO_2 fixation (Kirschbaum 2011). In principle, photosynthesis can be enhanced by modifying external parameters such as CO_2 concentration, light intensity (Terry 1986) or algal excitation wavelengths (Mann and Myers 1968; Schofield, Bidigare, and Prézelin 1990) but these procedures face several limitations including cost of artificial illumination, change of the natural light availability, possible photoinhibition phenomena occurring at high irradiances and CO_2 trapping in the liquid phase (Stephenson et al. 2011). Photosynthetic efficiency can also be enhanced by genetic modification of microalgae, for example by inhibiting their photoprotective mechanisms that limit light absorption (Melis 2009; de Mooij et al. 2015). Genetic modification can overcome microalgal non-photochemical quenching (NPQ) by inhibition of genes that normally reduce photosynthetic efficiency under high light intensities. In the last ten years, an alternative approach to the photosynthetic enhancement has been explored, based on the enlargement of sunlight absorption capability (la Gatta et al. 2019; Hassan Omar et al. 2016; Milano et al. 2012; Sissa et al. 2019) by endowing microalgae cells with chromophores capable of absorbing light in solar spectral regions where algal absorption is otherwise limited, and transferring

the collected light energy to the pigment-protein complexes of the photosystem units, thus favoring photochemical reactions. Following this approach, Fu *et al.* genetically expressed the enhanced green fluorescent protein (eGFP) in *Phaeodactylum tricornutum* diatoms, outperforming the wild-type parental strain in biomass production rate under outdoor simulated sunlight conditions (Fu et al. 2017). However, genetic tools are expensive and still limited to a few genetically fully-sequenced species of diatoms (Banerjee et al. 2018; Jeon et al. 2017; Ng et al. 2017), which prevents general industrial applications. Tailored organic dyes can, in principle, constitute an alternative photosynthesis-enhancing tool in living algal cells, promoting light harvesting without the need for genetic modification. Proof of the possibility of enhancing photosynthesis by organic dyes in green microalgae such as *Chlorella sorokiniana* (Prokop et al. 1984), *Dunaliella salina* (Burak, Dunbar, and Gilmour 2019) and *Nannochloropsis gaditana* (Sung et al. 2018) was demonstrated using solutions of spectral shifting dyes located in external cavities surrounding the photo-bioreactors used for the cell growth. This protocol ensures transfer of the energy harvested by the dyes to algal cells without altering their viability. However, it requires expensive equipment to avoid direct contact of dyes with cell cultures and is thus incompatible with large scale applications. Alternative photosynthesis-enhancing strategies, which in principle are more profitable in terms of scalability, resort to the incorporation of spectral shifting dyes into living algal cells. The dyes used must fulfill certain requirements: (*i*) irrelevant toxicity for the target living organisms, (*ii*) light absorption and emission properties suitable for energy transfer to algal photosystems, and (*iii*) amphiphilic chemical structures that are both dispersible in water and easily incorporated into cells. Current literature gives a few examples of studies relating to the effects on photosynthesis of the *in vivo* incorporation of organic dyes in living diatoms cells. In particular, rhodamines have shown considerable efficiency in penetrating diatom cells and staining both their cell wall and their cytoplasm (Li, Chu, and Lee 1989). However, they were found to be toxic for various species such as *Coscinodiscus granii* and *wailesii* (Kucki and Fuhrmann-Lieker 2012). Their toxicity was also demonstrated for plants and fungal cells (Strugger 1938; Weber 1937), and the suitability of rhodamines was thus restricted to enhancing the efficiency of photosynthetic complexes extracted from photosynthetic organisms (Gundlach et al. 2009). Recently, *in vivo* incorporation of a BODIPY (dipyrromethene borondifluoride) dye into diatom microalgae has been shown to increase diatoms' biomass rapidly in short-term cultivation but a decrease in cell population was observed 24 hours after adding the dye, revealing overall harmful effects on diatom cultures rather than the expected beneficial cell proliferation (Fu et al. 2017). These studies thus confirm that in principle enhancement of algal photosynthesis can be pursued by the *in vivo* incorporation of dyes selected to extend algal absorption cross-sections, but that the biocompatibility of incorporated dyes is an issue that must be overcome. Here we demonstrate that the *in vivo* incorporation of a cyanine dye (Cy5, Figure 1) in

Thalassiosira weissflogii diatom cells simply by adding it to the culture medium is not detrimental for cells and increases light-dependent cell growth, oxygen and biomass production, by improving diatoms' spectral response to light harvesting with no need for genetic engineering. Time-resolved spectroscopy indicates that energy transfer compatible with a FRET mechanism occurs between Cy5 and the chlorophyll *a* of living diatoms. This proof-of-concept paves the way for the development of light harvesting dyes that, upon incorporation into living algae cells, enhance photosynthesis and favor large scale biomass production.

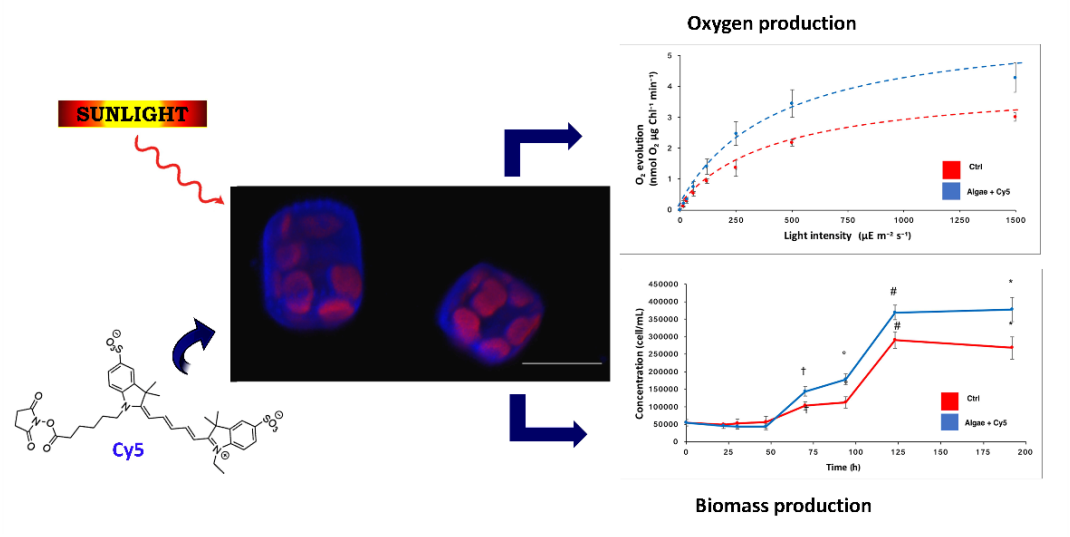

Figure 1. Effects of *in vivo* incorporation of the Cy5 antenna dye in *Thalassiosira weissflogii* diatoms. Scale bar of the confocal diatoms micrograph: 10 µm.

RESULTS

The antenna dye

Cy5 is a cyanine dye selected as a model molecular antenna due to its (*i*) commercial availability, (*ii*) recognized suitability as an imaging tool for biomolecular systems, (*iii*) amphiphilic chemical structure (Figure 1) favoring both molecular dispersion in aqueous media in the presence of biocompatible content of dimethylsulphoxide and molecular permeation through cell membranes. Moreover, (*iv*) light absorption and emission properties of Cy5 are suitable for light harvesting and energy transfer to chlorophylls of *Thalassiosira weissflogii* diatoms since Cy5 absorbs light in the range 570 - 650 nm and emits light at wavelengths (λ_{max}: 660 nm) where the chlorophyll *a* absorption in diatoms cells is maximum (Figure 2). In fact, the UV-vis absorption spectrum (red line in Figure 2) of photosynthetic pigments extracted from *Thalassiosira weissflogii*, shows the major Chl *a* absorption peaks at 430 and 662 nm and less intense peaks due to xanthophylls (480 nm) and Chl *c* (580, 620 nm) (Mantoura and Llewellyn 1983; Yacobi 2012). The major Chl *c* absorption peak at 450 nm is weakly visible, being hidden by xanthophylls and Chl *a* absorption.

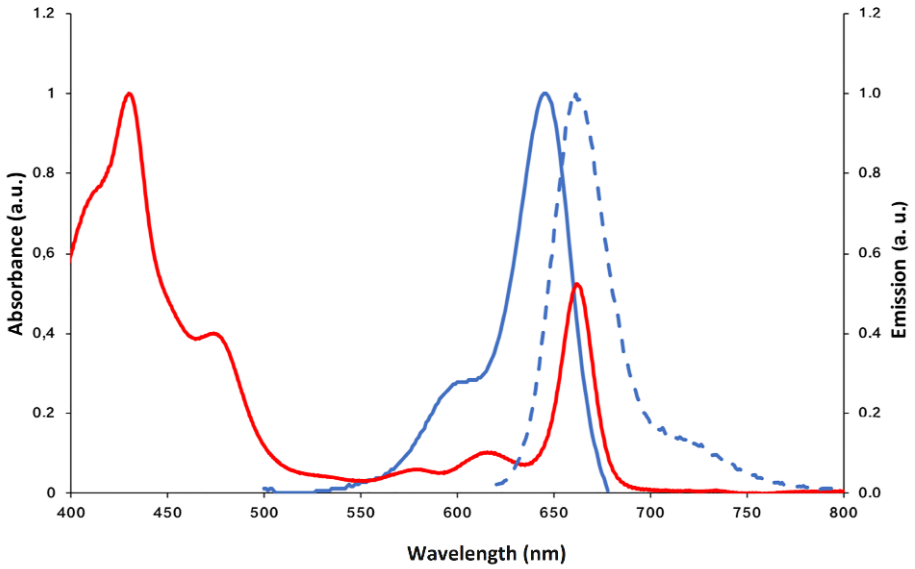

Figure 2. Absorption spectra of Cy5 (blue continuous line) and pigments (red line) extracted from *Thalassiosira weissflogii* diatoms and emission spectrum of Cy5 (dashed blue line) in seawater.

Diatoms' growth kinetics

Diatoms' growth in culture medium enriched with Cy5 (1 µM final concentration) was monitored under normal lighting conditions (light:dark 16h:8h, light intensity 70 µmol m^{-2} s^{-1}) and compared to a reference sample of diatoms grown in the absence of the dye (Figure 3A): in both cases, exponential growth started after 48h, reaching a plateau at the 5th day. In particular, the concentration curve of Cy5-treated diatoms was steeper than in the control in the exponential growth period 48-70h. After 8 days, the cell concentration of the sample treated with Cy5 exceeded the value observed for the control sample by 40%. The growth rate, calculated in the exponential phase between 48h and 70h, was 0.9 ± 0.2 for algae grown with Cy5 and 0.4 ± 0.3 for the control. We also observed a 23% increase in biomass dry weight (Figure 3B) for algae grown for 8 days, under normal lighting conditions, in the presence of Cy5 versus the control. To check that the increase of algal growth and biomass is effectively related to photosynthetic enhancement (Kirschbaum 2011), we performed the same experiments in the absence of light, inhibiting photosynthesis (Figure 3C). In this case, the growth curve of algae incubated with Cy5 did not differ from the control growth curve. This result confirms that the effect of Cy5 on cell growth and biomass are dependent on dye photoexcitation and rules out any possible effects of Cy5 in non-photosynthetic related metabolic pathways. As an additional control experiment, diatoms were grown in the presence of Cy5 and the culture excited with blue light (410 – 450 nm), which allowed algal photosynthesis to occur but excluded the contribution of Cy5, which is not excited at that wavelength (Figure 3D). In this case, too, Cy5 did not affect algal growth with respect to the control.

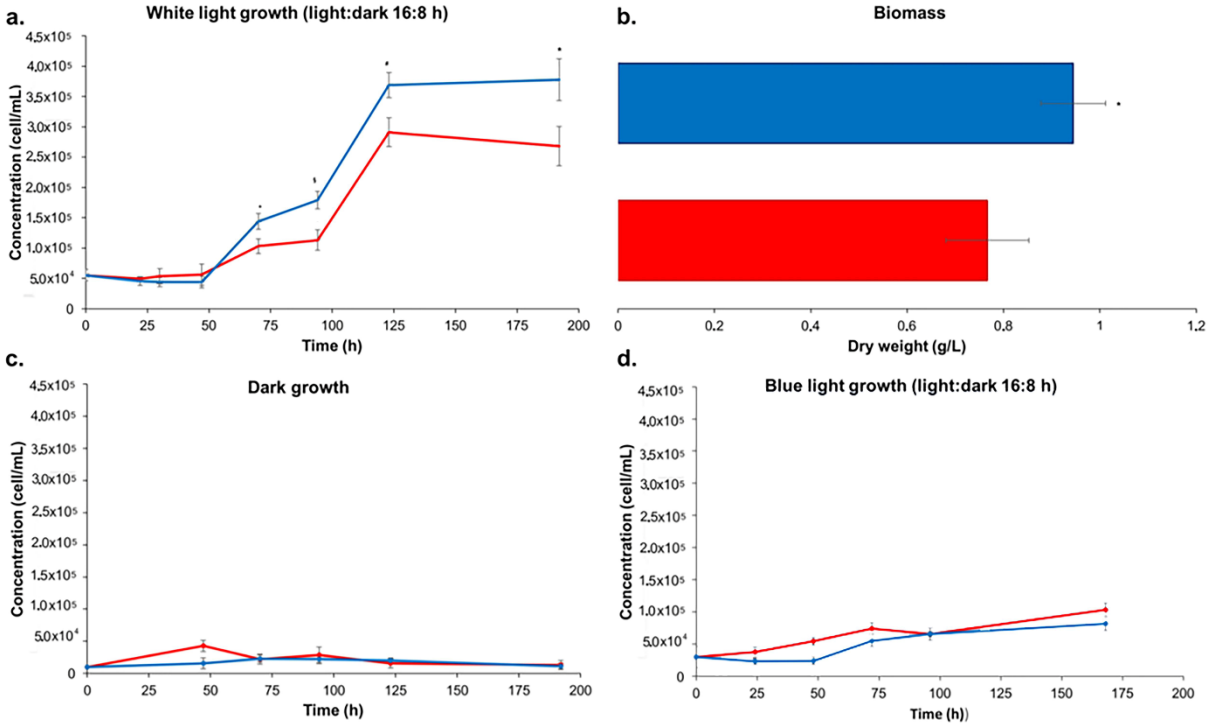

Figure 3. (A) Curves for diatom growth and (B) biomass recorded under normal lighting conditions, in the presence (blue line) and absence (red line) of Cy5. Curves for diatom growth recorded under (C) darkness and (D) under blue light excitation.

Photosynthetic activity

Cy5's ability to enhance diatom photosynthesis was also investigated by measuring the photosynthetic activity as light-dependent evolution of oxygen by cells, in an early exponential phase, grown in the presence and absence of Cy5 (Figure 4A). The presence of Cy5 increases the maximum photosynthetic activity (Pmax) by 49% versus the control sample (Figure 4B). This result, together with the light-dependent effect of Cy5, supports the hypothesis that the dye generates photosynthetic enhancement. In fact, oxygen production is related to the water splitting photosynthetic mechanism that fuels electron transport chains; hence, the improved O_2 production in the presence of Cy5 can be regarded as plausible proof of photosynthetic enhancement. Moreover, oxygen consumption in the dark was similar in the presence and absence of Cy5, suggesting that there are no major effects of Cy5 on mitochondrial oxidative pathways (Figure 4C). Increased photosynthetic activity was consistent with the increased growth rate.

Location of the dye in the cells

Once the light-dependent effect of Cy5 on diatom growth had been assessed, confocal analysis was performed on bare and Cy5 treated diatoms to investigate the location of the dye in cell structures.

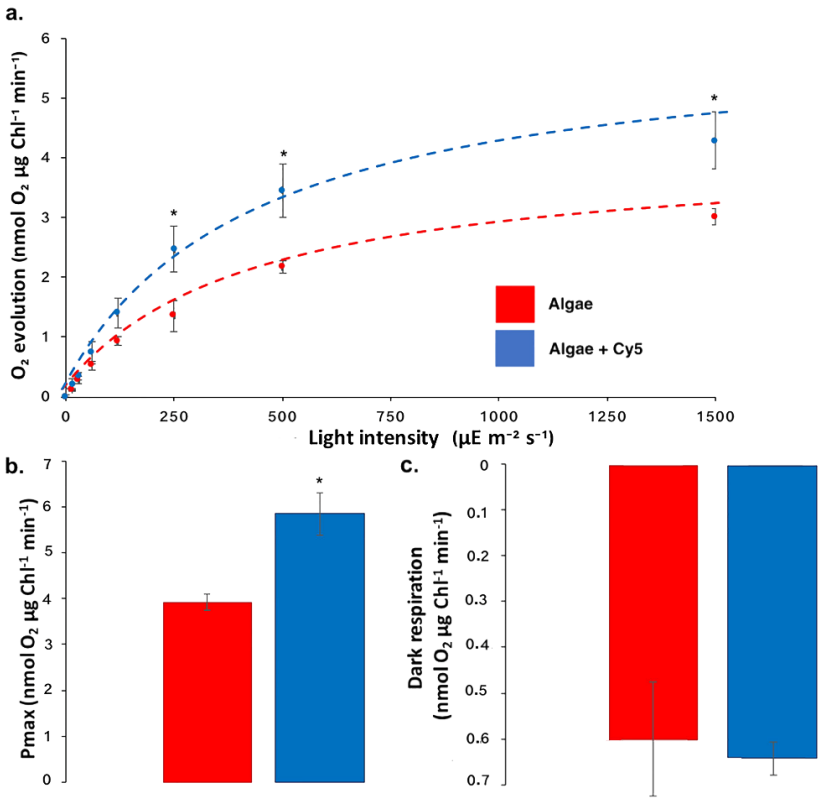

Figure 4. Light response curves. (A) Algae oxygen evolution rates at different actinic lights in the presence (blue line) and absence (red line) of Cy5. Experimental data were fitted with hyperbolic function y= Pmax * x/(K_I + x), obtaining Pmax values (B); (C) Oxygen consumption by dark respiration.

Samples were obtained using diatoms incubated with Cy5 in the earlier stage (45 minutes) and in the growth plateau stage (8 days), to evaluate both the incorporation of Cy5 and cell morphology related to their viability. Emission colours were arbitrarily assessed as red and blue for chloroplasts and Cy5, respectively, to distinguish their photoluminescence. Confocal microscopy images detected 45 min after incubation unequivocally showed the presence of Cy5 in diatom frustules (Figure 5A: ii. Row 2) where chloroplasts appeared sticker (Figure 5A: i. Row 2). Interference from the fluorescence of photosynthetic organelles in the Cy5 channel, also observed in the control sample (Figure 5A: ii. Rows 1-4) did not allow the location of Cy5 in chloroplasts to be unambiguously assessed. The dye's incorporation in cells was also confirmed observing Cy5 emission in the mitotic septum, as shown in Figure 5A (ii. and iii. Row 2) and in the 3D reconstruction of Figure 5B (Desclés et al. 2008). Confocal analysis was also performed after 8 days' incubation with Cy5, *i.e.* in proximity of the growth plateau (Figure 5: row 3 and 4). A weak photoluminescence of Cy5 was still observed in the cell walls (Figure 5A: ii. and iii. Row 4), moreover diatoms' morphology, as well as the location and intensity of chloroplasts' luminescence (Figure 5A: ii. and iii. Row 4) confirmed the viability of Cy5 treated microalgae versus the control (Figure 5A: Rows 1 and 3). General morphological assessment using bright

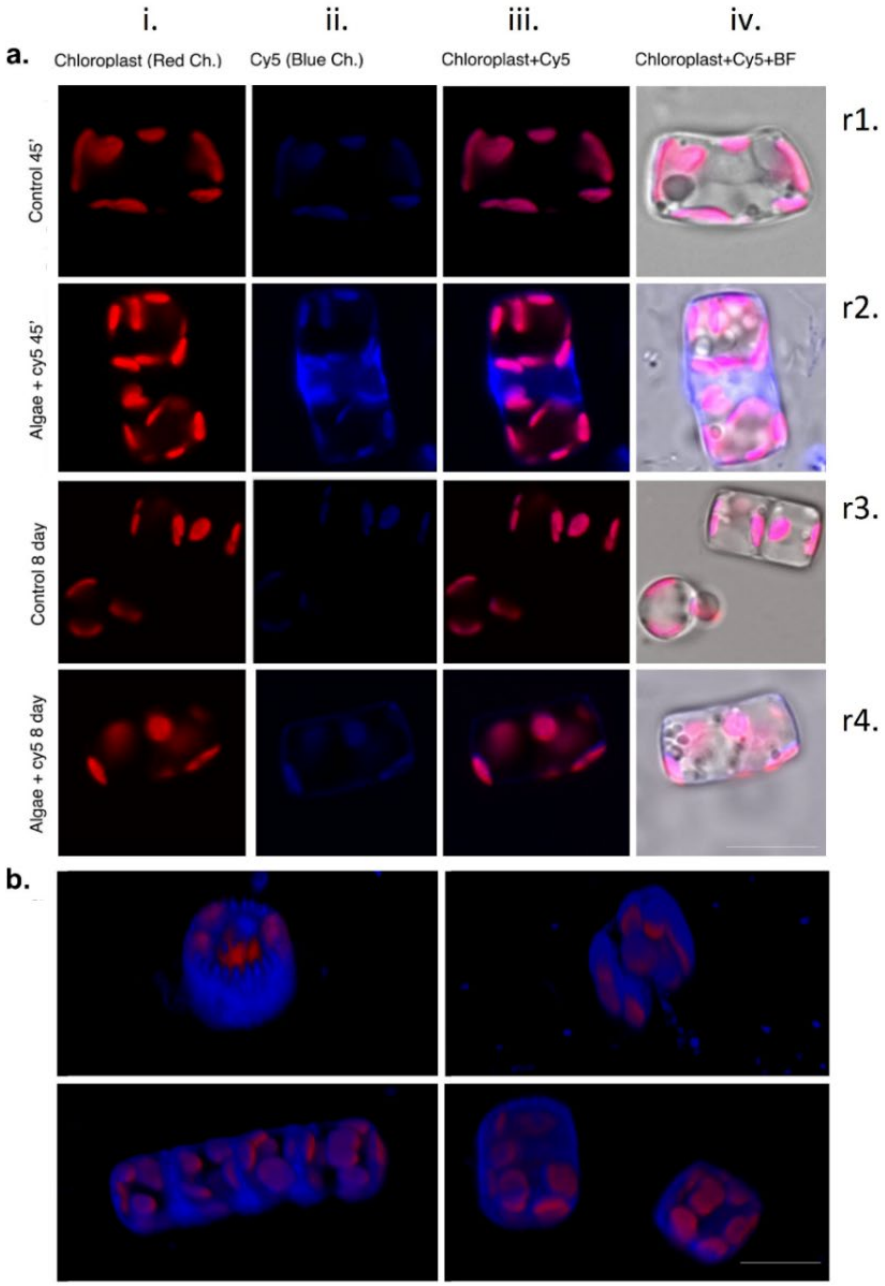

Figure 5. (A) Confocal microscopy images of diatom control, and diatoms grown with Cy5 1 µM after 45 minutes and 8 days' incubation in normal lighting conditions (light: dark 16:8 h). Red and blue colors were arbitrarily assigned for chloroplast and Cy5 emission, respectively (Size bar 10 µm). (B) 3D reconstruction of diatom incubated with Cy5 after 45 minutes (Size bar 10 µm).

field microscopies showed that all diatoms, examined at 45 min and 8 days (Figure 5A: iv. Rows 1-4) were able to produce similar box-like silica structures both in the presence and absence of Cy5. Confocal microscopy images were also recorded for bare and Cy5 treated cells under darkness, in order to inhibit photosynthesis (Figure S1). The presence of Cy5 was still evident after 8 days but with a weaker signal and, after 8 days, diatoms and chloroplasts changed morphology due to the negative effects of prolonged darkness that inhibited photosynthesis.

Time resolved fluorescence spectroscopy

Interaction between Cy5 and the photosynthetic apparatus was investigated by time-resolved fluorescence spectroscopy measurements using a streak camera, as described in the Materials and Methods section. Figures 6A and Supplementary Figure S2 showed the temporal decays from Cy5 incorporated in the diatoms at different times after incubation, obtained by integrating the fluorescence signal over the 625-775 nm spectral range. Temporal decay of the molecular Cy5 dye was also recorded. Figure 6B showed the fluorescence lifetime obtained fitting, with a monoexponential decay function, the temporal profiles as a function of the incubation time of diatoms with Cy5.

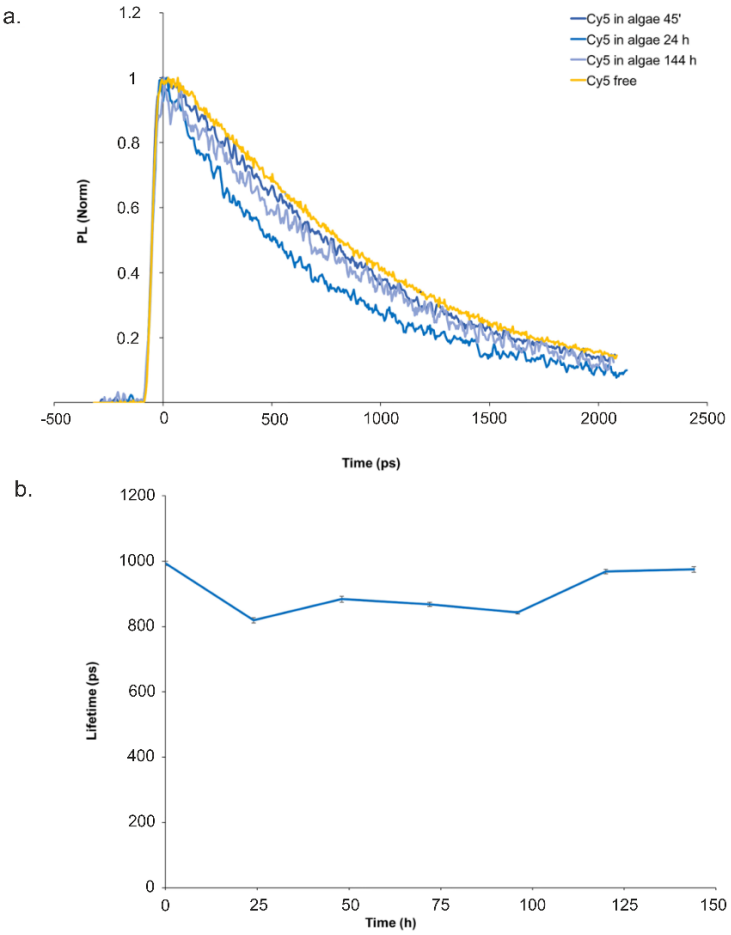

Figure 6. (A) Temporal evolution of Cy5 alone and inside diatoms at different incubation times. (B) Evolution of the fluorescence lifetime decay of Cy5 incorporated into diatoms after different incubation times.

A decrease of Cy5 fluorescence lifetime after 24 h incubation was observed and kept almost constant up to 96 hours (Figure 6B). Over longer time periods, a recovery of the fluorescence lifetime was detected but even at 144 h, the fluorescence decay was still faster versus the measurements carried out after 45 minutes (Figure 6A). Lifetime decrease of Cy5 is consistent with the FRET process between Cy5 (donor) and Chl *a* (acceptor). Förster radius (R_0), the distance at which energy transfer rate is 50%, for this donor acceptor pair is 5.1 nm (Yacobi 2012). By comparing the Cy5 fluorescence lifetime in the

presence and absence of the Chl acceptor from our diatoms we evaluated a FRET yield of energy transfer between donor and acceptor of about 20% and 5% at 24 h and 144 h, respectively.

Immunoblotting quantification of photosynthetic subunits

Immunoblotting analysis was performed with specific antibodies recognizing subunits of PSI (PsaA), PSII (CP43), chloroplast ATPase (ATPase C subunit) and RUBISCO (RbcL) (Figure 7), in order to evaluate whether the increased photosynthetic efficiency observed in the presence of Cy5 could be related to an effect of Cy5 on the stoichiometry of the photosynthetic apparatus. As reported in the Supplementary material (Figure S3), no major changes were observed for PSI, PSII and RUBISCO content on a chlorophyll basis in the presence or absence of Cy5. Cy5 caused a ~30% increase only for chloroplast ATPase protein. These results indicate that the increased light harvesting properties of the photosynthetic apparatus in the presence of Cy5 did not change the PSI/PSII or the RUBISCO/chlorophylls ratios but caused a relative increase in ATPase content per chlorophyll, allowing more efficient proton transport from the lumen back to the stroma for the production of ATP.

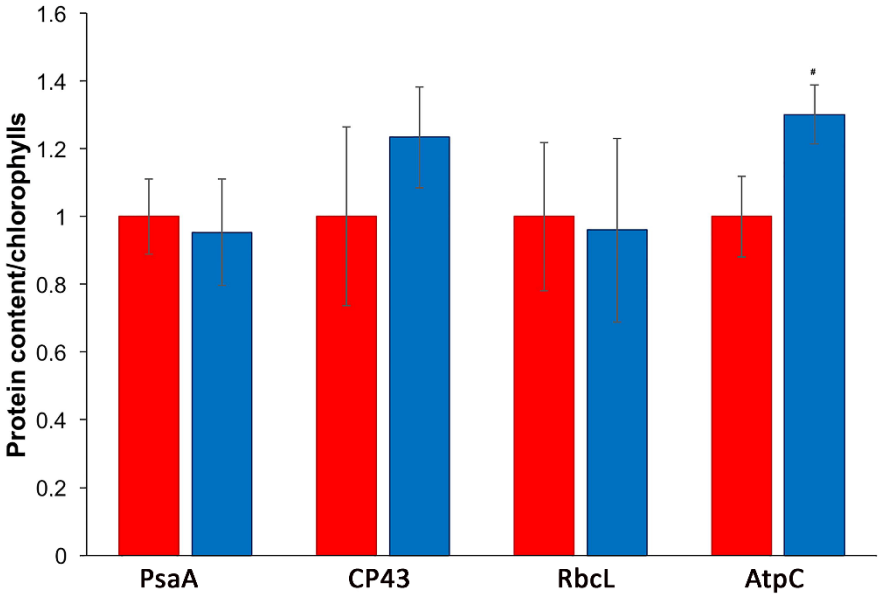

Figure 7. Immunoblotting quantification of photosynthetic subunits. The bands appearing upon western blot analysis were quantified by densitometry and normalized to the control case (blue line) to determine the protein content in the Cy5 treated sample (red line).

DISCUSSION

Effective ways of increasing the productivity and growth rate of diatoms have an important impact on their use as a source of biomaterials and biofuels (Lavaud et al. 2004). The large-scale production of microalgae and related biocomponents can be facilitated by enhancing photosynthesis. The use of light-absorbing molecules to increase light collection in spectroscopic regions not covered by

photosynthetic pigments of the microalgae represents a suitable and scalable approach which would rule out the need to use technologies based on genetic modification. A limited number of spectral shifting systems and dyes (Prokop et al. 1984; Wondraczek et al. 2013) converting unabsorbed wavelength regions from white light sources into absorbable light have been reported in the literature. However, due to their toxicity, these dyes had to be maintained physically separate from the algal culture, acting, that is, just as spectral shifting solutions. This introduces complexity into the structure of bioreactors and reduces the industrial applicability of this approach (Weber 1937).

Here we have described a simple amphiphilic cyanine molecule Cy5 (Figure 1) functioning as an artificial antenna. The dye can fill the diatom pigment absorbance gap in the orange spectral region, is non-toxic and leads to increased growth and biomass production (Figure 2 and 3). The introduction of Cy5 in *Thalassiosira weissflogii* diatoms occurs simply by adding the dye in the culture medium exploiting its water solubility and amphiphilic properties for crossing cell membranes. In normal white lighting conditions (70 µmol m^{-2} s^{-1}), the addition of Cy5 leads to a ~23% increase in diatom biomass production (Figure 3B) with a 40% increase in cell density (Figure 3A) in a week. The enhanced cell density mediated by Cy5 was achieved using 1 µM dye concentration, which is significantly lower than that previously used for dyes spatially confined from cultures (Prokop et al. 1984). The involvement of Cy5 in the photosynthetic pathway was demonstrated in a preliminary way by evaluating the consistent Cy5 light dependent effect on diatoms' growth in different lighting conditions (Figure 3). In fact, the growth of Cy5 treated diatoms was increased under a white light source that excites the Cy5 antenna (Figure 3A). On the contrary, no effect was observed when diatom cells treated with Cy5 were grown in dark conditions (Figure 3C) or on illumination with blue light (410-450 nm) which is not absorbed by Cy5 (Figure 3D).

Oxygen production measurements provided further evidence of increased photosynthetic activity by Cy5 (Figure 4). The Pmax parameter (Figure 4B), indicating the maximum oxygen produced by the photosystem, was 49% higher on Cy5 stained diatoms, while no Cy5 effect was observed in dark respiratory conditions (Figure 4C). Cy5's effect on O_2 production occurs both at low and high light irradiance: as reported in the literature, this result may be due to a photosynthetic apparatus rearrangement in order to manage the increased metabolic activity (Bonente et al. 2012).

Confocal microscopy images demonstrated the dye's incorporation (Figure 5). The presence of the dye in cells, in close proximity to chloroplasts, is significant when attempting to bring about Cy5-Chl energy transfer. Time-resolved fluorescence spectroscopy (Figure 6 and Supplementary Figure S2) revealed a decrease in Cy5 excited state lifetime over a period of days with a maximum after 24h of incubation, suggesting that a FRET mechanism from Cy5 to Chl *a* pigments potentiating light harvesting is a plausible explanation for the increase observed in photosynthetic efficiency. After 24h, the observed

quenching of the incorporated Cy5 emission gradually decreases but never reaches the start value, suggesting that energy transfer occurs over days. Slow Cy5 degradation over a period of days and consequent absorbance-emission decay can be held responsible for FRET rate fading over time, since reducing the donor concentration determines a consequent increase in donor-acceptor average distance.

In keeping with the hypothesis that energy transfer from the Cy5 antenna to the chlorophyll *a* determines enhanced photosynthetic efficiency, increased chloroplast ATPase enzyme was detected in cells treated with Cy5, allowing more efficient proton transport from the lumen to the stroma producing the ATP. Hence, improved light harvesting by Cy5 causes increased electron transport across the photosynthetic apparatus, as witnessed by increased light-dependent oxygen evolution compared to the control. We evaluated the expression of protein relating to photosynthesis after the incorporation of Cy5 in normal lighting conditions. Photosynthetic electron transport is coupled with proton transport from lumen to stroma to establish the electrochemical proton gradient used by the ATPase to produce ATP: accordingly, in the presence of Cy5 a ~30% increase in the chloroplast ATPase complex was detected enabling Cy5 stained cells to properly manage the increased proton transport into the lumen, likely preventing lumen over-acidification (Figure 7 and Supplementary Figure S3). RUBISCO is a key enzyme for photosynthesis, whose activity is strongly controlled by the organism in order to manage metabolic activity. The RUBISCO content was similar in both the presence and absence of Cy5, suggesting that the increased photosynthetic efficiency of Cy5 treated cells is due to increased production of ATP and NADPH during the photosynthetic light phase, which are then used by the Calvin- Benson cycle to fix CO_2 in the biomass.

In summary, we achieved enhanced photosynthesis in *Thalassiosira weissflogii* diatoms by simple addition of the Cy5 dye to the algal growing medium. The dye acts as a FRET donor to diatom Chlorophyll *a*, increasing growth and biomass.

CONCLUSION

Microalgae are highly attractive for industry as feedstock for food and pharmaceutics and as a source of lipids for biofuel production. However, the costs of achieving a high rate of growth, the difficulties in genetically modifying non model microalgal species for increasing growth, and the resistance of public opinion toward genetically modified organisms, limit their industrial use. In this work, we demonstrated enhanced photosynthesis in diatom microalgae that increases biomass and growth without resorting to genetic modification. We stained living *Thalassiosira weissflogii* diatoms with a cyanine Cy5 dye, which fills the orange absorption gap of the photosynthetic pigments and increases light harvesting. Besides the enhanced growth and biomass, Cy5 increases diatom oxygen production.

The most credited role for Cy5, demonstrated by spectroscopic measurements, is that it acts as an energy transfer donor for chlorophyll. Moreover, the energy transfer occurs on Chl *a*, which is a pigment present in most photosynthetic organisms. This approach may thus be in principle extended to other classes of photosynthetic organisms and can sustain diatoms and, in general, microalgae industrial valorization. The enhanced light response may boost algal growth by increasing the photoactive range in large incubators. In addition, the potential tuning of the spectral response makes it possible to envision the use of algae with any desired light spectrum, whether natural or artificial.

MATERIALS AND METHODS

Algal culture conditions. The algal strain of *Thalassiosira weissflogii* diatoms (CCAP 1085/10, Scottish marine Institute, Scotland UK) was used. Diatoms were grown in F/2 Guillard-enriched seawater medium (Vona et al. 2018) with 1:3000 of the stock sodium metasilicate, under sterile conditions in polystyrene 250 mL flasks. Before producing F/2 Guillard, seawater was sterilized in an autoclave and filtered twice (4- 7µm ø). Flasks were maintained in a photobioreactor under continuous fluorescent light (18 ± 2°C, 65% ± 5% humidity, light : dark cycle 16 : 8h, Pump Photon Flux: 70 µmol $m^{-2}s^{-1}$).

Pigments extraction and spectrophotometric analysis. In keeping with the literature (Calvano et al. 2015), 1mL of washed algae was added in pigment extraction solution containing 8mL of pure acetone, 1820µL of distilled water and 180µl of ammonium hydroxide 19%. The mixture was then centrifuged (5000rpm for 15') and 2mL of pure hexane were added. The absorbance spectrum of pigments in hexane was evaluated by UV-visible spectrophotometer (Shimadzu UV-2401 PC).

Diatom incubation with Cy5 and evaluation of cells' growth and biomass. *Thalassiosira weissflogii* diatoms were added in polystyrene 50mL flasks containing freshly prepared F/2 Guillard enriched seawater medium (final diatom density of $5*10^4$ cell/mL; final flask volume 50mL). Diatoms in flasks were incubated with Cy5 by adding 1µL of Amersham Pharmacia Cyanine 5 NHS ester (concentration of the stock of 0.0019M in pure DMSO, λ_{exc} = 640nm, λ_{em} = 670nm) in the 50mL flask. Diatom samples treated with the dye (Cy5) and used as bare cells in the control (Ctrl) were produced in triplicates. Algae were grown for 8 days in the photobioreactor, (18 ± 2°C, 65% ± 5% humidity, light : dark cycle 16 : 8h), maintained at different light regimes. Growth in white light was achieved using 70 µmol m^{-2} s^{-1} neon source conditions. Blue light (440 - 480nm) was used at the same intensity and lighting cycle conditions used for white light. Diatom growth was evaluated daily by Thoma Chamber in contrast phase microscopy. Diatom density of each sample was calculated in triplicates and monitored for a week. According to literature, diatom growth rate was evaluated from 48h to 70h of incubation, in the exponential growth phase. Biomass accumulation at the end of the growth curve was determined as dry weight per liter, as reported in the literature (Perozeni et al. 2018).

Confocal microscopy. Diatom samples were washed in Milli-Q water. Diatoms were then pelleted and characterized by confocal laser scanning microscopy (LSM-510 confocal microscope, Zeiss). Microscopy configuration used was: UV/Diode laser (λ_{exc} = 405nm for chlorophyll, λ_{exc} = 640nm for Cy5) and HC PL APO CS2 63x/1.40 Oil objective. Emission spectra were recorded in the visible spectral range ($\Delta\lambda_{em}$ = 670 - 750nm for chlorophyll, $\Delta\lambda_{exc}$ = 650 - 670nm for Cy5). Colors were arbitrarily assessed as blue for Cy5 and red for chloroplasts.

Time resolved fluorescence spectroscopy. Time-resolved fluorescence measurements were carried out using a Ti:sapphire laser (Chameleon Ultra II, Coherent) with a repetition rate of 80 MHz and pulses

with a temporal full width half maximum (FWHM) of ∼140fs. The output was sent to an optical parametric oscillator (OPO) providing pulses in the NIR (1000 - 1400nm). The signal was, then, doubled by beta barium borate crystal (BBO) to reach the final excitation light at 620nm. A streak camera system (C5680, Hamamatsu), coupled to a spectrometer, was selected as the detection system giving spectro-temporal matrices with spectral and temporal resolutions of ∼1nm and ∼20ps, respectively. The fluorescence signal was separated from excitation light by a proper set of high pass filters.

Oxygen evolution curves. Oxygen evolution curves were performed as described in the literature (Perozeni et al. 2018). Net oxygen production was calculated subtracting oxygen consumption in the dark after each measurement at different actinic lights. Experimental data were fitted with hyperbolic functions in order to retrieve the Pmax (maximum photosynthetic activity).

SDS-PAGE and immunoblotting. SDS-PAGE and immunoblotting were performed as described in the literature (Bonente et al. 2011). Antibodies used were obtained from the Agrisera company (https://www.agrisera.com/).

Statistics. A one-way ANOVA test was performed to evaluate the significance in difference between samples. Data were considered statistically significant for $p < 0.05$.

ACKNOWLEDGMENTS

We gratefully acknowledge Prof. Angela Falciatore (CNRS-Sorbonne Université Institut de Biologie Paris Seine) for valuable discussion and suggestions on algal culture conditions under blue light and gene expression measurements. This work was financially supported by the European Commission through EU project 800926-HyPhOE (Hybrid Electronics based on Photosynthetic Organisms) and H2020-MSCA-ITN-2019 project 860125 - BEEP (Bio-inspired and bionic materials for enhanced photosynthesis).

AUTHOR CONTRIBUTIONS

G. Leone and D. Vona performed algal cultures and in vivo incorporation experiments of the dye under different lighting conditions. R. Ragni and S.R. Cicco contributed to the elaboration of data and to the manuscript production. E. Altamura performed confocal microscopy. G. De La Cruz Valbuena, C. D'Andrea and E. Molotokaite performed and elaborated data on time resolved spectroscopy. M. Cecchin, S. Cazzaniga and M. Ballottari carried out measurements of oxygen production, biomass detection and protein expression. G.M. Farinola and G. Lanzani provided conceptual guidance of the project.

REFERENCES

Banerjee, Avik, Chiranjib Banerjee, Sangeeta Negi, Jo Shu Chang, and Pratyoosh Shukla. 2018. "Improvements in Algal Lipid Production: A Systems Biology and Gene Editing Approach." Critical Reviews in Biotechnology.

Bonente, G., M. Ballottari, T. B. Truong, T. Morosinotto, T. K. Ahn, G. R. Fleming, K. K. Niyogi, and R. Bassi. 2011. "Analysis of LhcSR3, a Protein Essential for Feedback de-Excitation in the Green Alga *Chlamydomonas reinhardtii*." PLoS.Biol. 9(1545-7885 (Electronic)):e1000577.

Bonente, Giulia, Sara Pippa, Stefania Castellano, Roberto Bassi, and Matteo Ballottari. 2012. "Acclimation of *Chlamydomonas reinhardtii* to Different Growth Irradiances." Journal of Biological Chemistry.

Burak, Hatice, Alan Dunbar, and D. James Gilmour. 2019. "Enhancement of Dunaliella Salina Growth by Using Wavelength Shifting Dyes." Journal of Applied Phycology.

Calvano, Cosima Damiana, Giovanni Ventura, Tommaso R. I. Cataldi, and Francesco Palmisano. 2015. "Improvement of Chlorophyll Identification in Foodstuffs by MALDI ToF/ToF Mass Spectrometry Using 1,5-Diaminonaphthalene Electron Transfer Secondary Reaction Matrix." Analytical and Bioanalytical Chemistry.

Cicco, Stefania R., Danilo Vona, Elvira De Giglio, Stefania Cometa, Monica Mattioli-Belmonte, Fabio Palumbo, Roberta Ragni, and Gianluca M. Farinola. 2015. "Chemically Modified Diatoms Biosilica for Bone Cell Growth with Combined Drug-Delivery and Antioxidant Properties." ChemPlusChem.

Desclés, Julien, Mathieu Vartanian, Abdeslam El Harrak, Michelle Quinet, Nicolas Bremond, Guillaume Sapriel, Jérome Bibette, and Pascal J. Lopez. 2008. "New Tools for Labeling Silica in Living Diatoms." New Phytologist.

Falkowski, Paul G., Miriam E. Katz, Andrew H. Knoll, Antonietta Quigg, John A. Raven, Oscar Schofield, and F. J. R. Taylor. 2004. "The Evolution of Modern Eukaryotic Phytoplankton." Science.

Field, Christopher B., Michael J. Behrenfeld, James T. Randerson, and Paul Falkowski. 1998. "Primary Production of the Biosphere: Integrating Terrestrial and Oceanic Components." Science.

Fu, Weiqi, Amphun Chaiboonchoe, Basel Khraiwesh, Mehar Sultana, Ashish Jaiswal, Kenan Jijakli, David R. Nelson, Ala'a Al-Hrout, Badriya Baig, Amr Amin, and Kourosh Salehi-Ashtiani. 2017. "Intracellular Spectral Recompositioning of Light Enhances Algal Photosynthetic Efficiency." Science Advances 3(9):1–12.

la Gatta, Simona, Francesco Milano, Gianluca M. Farinola, Angela Agostiano, Mariangela Di Donato, Andrea Lapini, Paolo Foggi, Massimo Trotta, and Roberta Ragni. 2019. "A Highly Efficient Heptamethine Cyanine Antenna for Photosynthetic Reaction Center: From Chemical Design to Ultrafast Energy Transfer Investigation of the Hybrid System." Biochimica et Biophysica Acta - Bioenergetics.

Gundlach, Kristina, Mara Werwie, Sabine Wiegand, and Harald Paulsen. 2009. "Filling the 'Green Gap' of the Major Light-Harvesting Chlorophyll a/b Complex by Covalent Attachment of Rhodamine Red." Biochimica et Biophysica Acta - Bioenergetics.

Hassan Omar, Omar, Simona La Gatta, Rocco Roberto Tangorra, Francesco Milano, Roberta Ragni, Alessandra Operamolla, Roberto Argazzi, Claudio Chiorboli, Angela Agostiano, Massimo Trotta, and Gianluca M. Farinola. 2016. "Synthetic Antenna Functioning As Light Harvester in the Whole Visible Region for Enhanced Hybrid Photosynthetic Reaction Centers." Bioconjugate Chemistry.

Hildebrand, Mark, Aubrey K. Davis, Sarah R. Smith, Jesse C. Traller, and Raffaela Abbriano. 2012. "The Place of Diatoms in the Biofuels Industry." Biofuels.

Irimia-Vladu, Mihai, Eric D. Glowacki, Niyazi S. Sariciftci, Siegfried Bauer, Roberta Ragni, Stefania R. Cicco, Danilo Vona, and Gianluca M. Farinola. 2017. "Nanostructured Silica from Diatoms Microalgae: Smart Materials for Photonics and Electronics." in Green Materials for Electronics.

Jeon, Seungjib, Jong Min Lim, Hyung Gwan Lee, Sung Eun Shin, Nam Kyu Kang, Youn Il Park, Hee Mock Oh, Won Joong Jeong, Byeong Ryool Jeong, and Yong Keun Chang. 2017. "Current Status and Perspectives of Genome Editing Technology for Microalgae." Biotechnology for Biofuels.

Kirschbaum, Miko U. F. 2011. "Does Enhanced Photosynthesis Enhance Growth? Lessons Learned from CO_2 Enrichment Studies." Plant Physiology.

Kucki, Melanie and Thomas Fuhrmann-Lieker. 2012. “Staining Diatoms with Rhodamine Dyes: Control of Emission Colour in Photonic Biocomposites.” Journal of the Royal Society Interface.

Lavaud, Johann, Bernard Rousseau, and Anne Lise Etienne. 2004. “General Features of Photoprotection by Energy Dissipation in Planktonic Diatoms (Bacillariophyceae).” Journal of Phycology.

Leone, G., D. Vona, M. Lo Presti, L. Urbano, S. Cicco, R. Gristina, F. Palumbo, R. Ragni, and G. M. Farinola. 2017. “Ca2+-in Vivo Doped Biosilica from Living *Thalassiosira weissflogii* Diatoms: Investigation on Saos-2 Biocompatibility.” in MRS Advances.

Li, C. W., S. Chu, and M. Lee. 1989. “Characterizing the Silica Deposition Vesicle of Diatoms.” Protoplasma.

Mann, James E. and Jack Myers. 1968. “ Photosynthetic Enhancement in the Diatom *Phaeodactylum tricornutum* .” Plant Physiology.

Mantoura, R. F. C. and C. A. Llewellyn. 1983. “The Rapid Determination of Algal Chlorophyll and Carotenoid Pigments and Their Breakdown Products in Natural Waters by Reverse-Phase High-Performance Liquid Chromatography.” Analytica Chimica Acta.

Melis, Anastasios. 2009. “Solar Energy Conversion Efficiencies in Photosynthesis: Minimizing the Chlorophyll Antennae to Maximize Efficiency.” Plant Science.

Milano, Francesco, Rocco Roberto Tangorra, Omar Hassan Omar, Roberta Ragni, Alessandra Operamolla, Angela Agostiano, Gianluca M. Farinola, and Massimo Trotta. 2012. “Enhancing the Light Harvesting Capability of a Photosynthetic Reaction Center by a Tailored Molecular Fluorophore.” Angewandte Chemie - International Edition.

de Mooij, Tim, Marcel Janssen, Oscar Cerezo-Chinarro, Jan H. Mussgnug, Olaf Kruse, Matteo Ballottari, Roberto Bassi, Sandrine Bujaldon, Francis André Wollman, and René H. Wijffels. 2015. “Antenna Size Reduction as a Strategy to Increase Biomass Productivity: A Great Potential Not yet Realized.” Journal of Applied Phycology.

Ng, I. Son, Shih I. Tan, Pei Hsun Kao, Yu Kaung Chang, and Jo Shu Chang. 2017. “Recent Developments on Genetic Engineering of Microalgae for Biofuels and Bio-Based Chemicals.” Biotechnology Journal.

Perozeni, Federico, Giulio Rocco Stella, and Matteo Ballottari. 2018. “LHCSR Expression under HSP70/RBCS2 Promoter as a Strategy to Increase Productivity in Microalgae.” International Journal of Molecular Sciences.

Priyadarshani, Indira and Biswajit Rath. 2012. “Commercial and Industrial Applications of Micro Algae – A Review.” 3(4):89–100.

Prokop, A., M. F. Quinn, M. Fekri, M. Murad, and S. A. Ahmed. 1984. “Spectral Shifting by Dyes to Enhance Algae Growth.” Biotechnology and Bioengineering.

Rabosky, Daniel L. and Ulf Sorhannus. 2009. “Diversity Dynamics of Marine Planktonic Diatoms across the Cenozoic.” Nature.

Ragni, Roberta, Stefania R. Cicco, Danilo Vona, and Gianluca M. Farinola. 2018. “Multiple Routes to Smart Nanostructured Materials from Diatom Microalgae: A Chemical Perspective.” Advanced Materials.

Ragni, Roberta, Stefania Cicco, Danilo Vona, Gabriella Leone, and Gianluca M. Farinola. 2017. “Biosilica from Diatoms Microalgae: Smart Materials from Bio-Medicine to Photonics.” Journal of Materials Research.

Ragni, Roberta, Francesco Scotognella, Danilo Vona, Luca Moretti, Emiliano Altamura, Giacomo Ceccone, Dora Mehn, Stefania R. Cicco, Fabio Palumbo, Guglielmo Lanzani, and Gianluca M. Farinola. 2018. “Hybrid Photonic Nanostructures by In Vivo Incorporation of an Organic Fluorophore into Diatom Algae.” Advanced Functional Materials.

Sayre, Richard. 2010. “Microalgae: The Potential for Carbon Capture.” BioScience.

Schofield, O., RR Bidigare, and BB Prézelin. 1990. “Spectral Photosynthesis, Quantum Yield and Blue-Green Light Enhancement of Productivity Rates in the Diatom Chaetoceros Gracile and the Prymnesiophyte *Emiliania huxleyi*.” Marine Ecology Progress Series.

Sissa, Cristina, Anna Painelli, Francesca Terenziani, Massimo Trotta, and Roberta Ragni. 2019. “About the Origin of the Large Stokes Shift in Aminoalkyl Substituted Heptamethine Cyanine Dyes.” Physical Chemistry Chemical Physics.

Stephenson, Patrick G., C. Mark Moore, Matthew J. Terry, Mikhail V. Zubkov, and Thomas S. Bibby. 2011. “Improving Photosynthesis for Algal Biofuels: Toward a Green Revolution.” Trends in Biotechnology.

Strugger, S. 1938. “Die Vitalfärbung Des Protoplasmas Mit Rhodamin B Und 6 G.” Protoplasma.

Sung, Min Gyu, Jong In Han, Bongsoo Lee, and Yong Keun Chang. 2018. “Wavelength Shift Strategy to Enhance Lipid Productivity of *Nannochloropsis gaditana*.” Biotechnology for Biofuels.

Terry, Kenneth L. 1986. “Photosynthesis in Modulated Light: Quantitative Dependence of Photosynthetic Enhancement on Flashing Rate.” Biotechnology and Bioengineering.

Trentacoste, Emily M., Roshan P. Shrestha, Sarah R. Smith, Corine Glé, Aaron C. Hartmann, Mark Hildebrand, and William H. Gerwick. 2013. “Metabolic Engineering of Lipid Catabolism Increases Microalgal Lipid Accumulation without Compromising Growth.” Proceedings of the National Academy of Sciences of the United States of America.

Vona, Danilo, Stefania Roberta Cicco, Roberta Ragni, Gabriella Leone, Marco Lo Presti, and Gianluca Maria Farinola. 2018. “Biosilica/Polydopamine/Silver Nanoparticles Composites: New Hybrid Multifunctional Heterostructures Obtained by Chemical Modification of *Thalassiosira weissflogii* Silica Shells.” MRS Communications.

Vona, Danilo, Gabriella Leone, Roberta Ragni, Fabio Palumbo, Antonio Evidente, Maurizio Vurro, Gianluca M. Farinola, and Stefania R. Cicco. 2016. “Diatoms Biosilica as Efficient Drug-Delivery System.” in MRS Advances.

Weber, Friedl. 1937. “Assimilationsfähigkeit Und Doppelbrechung Der Chloroplasten.” Protoplasma.

Wondraczek, Lothar, Miroslaw Batentschuk, Markus A. Schmidt, Rudolf Borchardt, Simon Scheiner, Benjamin Seemann, Peter Schweizer, and Christoph J. Brabec. 2013. “Solar Spectral Conversion for Improving the Photosynthetic Activity in Algae Reactors.” Nature Communications.

Yacobi, Yosef Z. 2012. “From Tswett to Identified Flying Objects: A Concise History of Chlorophyll a Use for Quantification of Phytoplankton.” Israel Journal of Plant Sciences.

Yang, Wenrong, Pascal J. Lopez, and Gary Rosengarten. 2011. “Diatoms: Self Assembled Silica Nanostructures, and Templates for Bio/Chemical Sensors and Biomimetic Membranes.” Analyst.

SUPPLEMENTARY INFORMATION

Supplementary Figure S1. Confocal microscopy of diatoms incubated with Cy5 under dark. Confocal microscopy of diatom control and diatoms grown with Cy5 1 µM after 45 minutes and 8 days of incubation in darkness, avoiding photosynthesis (Size bar 10 µm). Samples were produced as described in the main text. Under normal lighting conditions, the presence of Cy5 was still evident after 8 days but with a weaker signal due to the degradation of the dye. After 8 days, diatoms and chloroplasts changed morphology due to the negative effects of prolonged darkness on *Thalassiosira weissflogii* cultures.

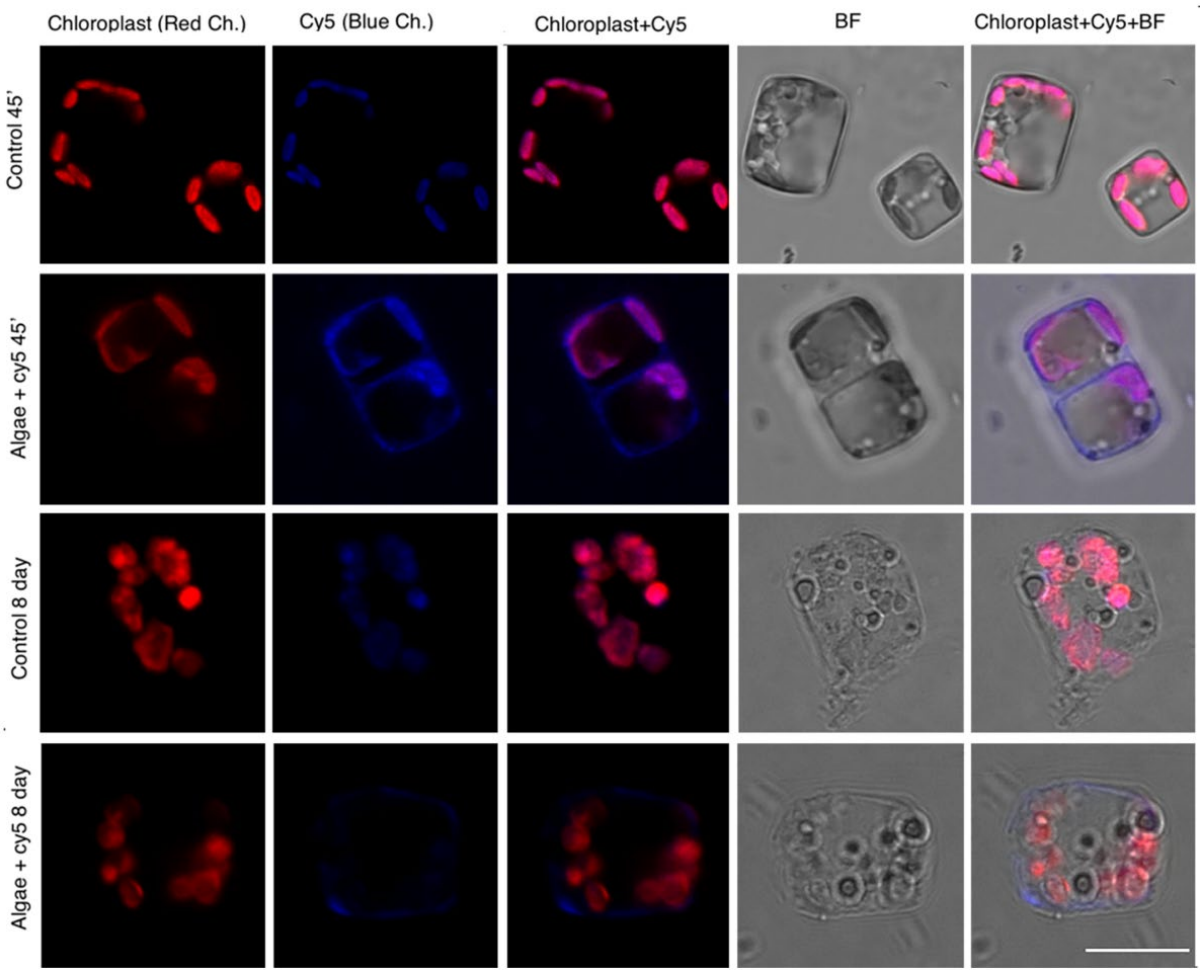

Supplementary Figure S2. Time-resolved fluorescence spectroscopy of Cy5 treated diatoms. Time-resolved fluorescence spectroscopy measurements were performed every day over a week on living pigmented diatoms grown with Cy5 and the temporal decay was compared to the one of Cy5 free in solution. The maximum quenching occurs after 24 hours of incubation and it is preserved until 96 hours. For longer times an increase of the fluorescence lifetime was observed. These evidences support the hypothesis of energy transfer among Cy5 and Chlorophyll *a*.

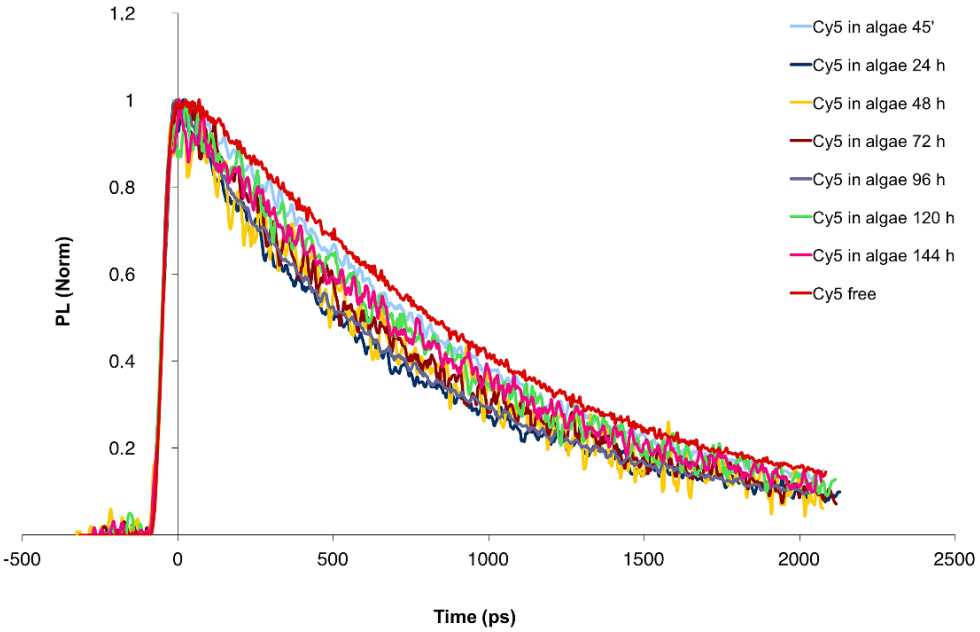

Supplementary Figure S3. Protein expression. Photosynthetic protein expression of bare and Cy5 treated diatoms was monitored by immunoblotting analysis. Specific antibodies recognizing the large subunits of RUBISCO (RbcL), CP43, PsaA and the C subunit of chloroplastic ATPase (AtpC) were used to perform immunoblotting reactions. Samples were loaded with the same amount of chlorophylls (0.7 µg) in the descriptive figure. Similar results were obtained with different loading. As mentioned in the main text, no difference of PsaA, CP43 and RUBISCO (RbcL) amounts was observed between the control and the Cy5 treated sample. Conversely, the ATPase C subunit was more present in diatoms grown in the presence of the dye.

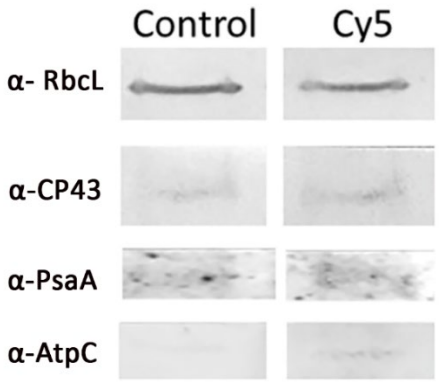

Conclusion

The aim of this thesis is the study of molecular mechanisms in order to improve the carbon use efficiency in several species of microalgae. This work contributes to the knowledge of the microalgae world, with a molecular approach in order to developed new biotechnologically intervention fundamental nowadays to increased yield in terms of biomass, lipid or production of high value products, reducing costs of the industrial application.

In the chapter 2 we contribute to lack of genetic and metabolic information of two species of the *Chlorella* genus. *Chlorella* genus includes several species widely used at industrial level for their fast growth and high resistance to biotic and abiotic stresses. However, the lack of efficient and reproducible transformation protocols and the limited genetic information restrict the biotechnological approach in these species. In the section A the transcriptome of *C. sorokiniana* was *de novo* assembled and annotated, while in the section B the genome and also transcriptome of *C. vulgaris* were *de novo* assembled. The collected data allow to define the metabolic pathway present in these microalgae, identifying peculiar genes and regulation. Finally, in the section C a direct comparison at metabolic level of the two species was performed underling several differences beside they belong to the same green algae family.

Interestingly in both species a type I and type II fatty acid synthase enzymes can be found at genomic and transcriptomic level. In plant cells *de novo* fatty acid biosynthesis occurs mainly in the chloroplast catalysed by FAS2 multisubunit complex, while in animals and fungi FAS1 large multi-enzyme complexes located in the cytosol appear. The occurrence of a FAS1-like complexes in microalgae has already been suggested in the oleaginous alga *Nannochloropsis spp*. but not in the green lineage. *C. vulgaris* and *C. sorokiniana* genetic data suggested the presence of both FAS1 and FAS2 complexes, pointing out a different lipid metabolism compared to the model green algae *C. reinhardtii*. Further experiments are necessary to confirm these data and the role of these proteins. The inducted conditions in *C. vulgaris* (HL *vs.* LL) and *C. sorokiniana* (mixotrophy *vs.* autotrophy) affected the lipid content with an increased in particular of triacylglycerols. In both cases, the higher availably of reducing power, due to the excess of light in the former and the assimilation of acetate in the latter, enriched the acetyl-CoA pool that is the precursor for fatty acids biosynthesis. In *C. sorokiniana* any genes directly related to lipid pathway was differential expressed suggesting that the increased lipid content is more influenced on the increased acetyl-coA availability. In *C. vulgaris* an upregulation of the cytosolic acetyl-coA synthetase (ACS) gene was observed: this enzyme is responsible for the synthesis of acetyl-CoA by glycolytic pyruvate. In addition, enzymes involve in the supply of glycerol backbones (GDP2 enzyme) and TAG packaging (PLAP/fibrillin subunits) were upregulated. The increased lipid accumulation in high light could be related to increased acetyl-CoA production in the

chloroplast and in the cytosol (by ACS) leading to upregulation of enzyme involved in TAG assembly and lipid droplets stabilization.

Another common characteristic of the *Chlorella* species herein analysed is the presence of genes encoding for C4-like carbon fixation pathway. In *C. sorokiniana* in mixotrophy the upregulation of the phosphoenolpyruvate carboxylase enzyme enabled potential recovery of carbon atoms lost by acetate oxidation.

Finally, both Trebouxiophyceae species showed an uncommon regulation of genes involved in the photoprotective mechanisms of nonphotochemical quenching (NPQ), a mechanism that dissipate as heat the excess of absorbed light. In higher plant PSBS protein controls non-photochemical induction, as well as, LHCsr protein done in the case of *C. reinhardtii*, where only a transient expression of PSBS gene under UV or HL condition was reported. In the model algae LHCsr transcription is induced in high light condition, instead in both *C. vulgaris* and *C. sorokiniana* any significant differential expression was observed (in HL and mixotrophy conditions respectively). Moreover, in mixotrophic conditions in *C. sorokiniana* PSBS gene was downregulated leading to a lower protein accumulation but unaffecting the NPQ level. In HL conditions in *C. vulgaris* PSBS protein is induced although NPQ induction was not evaluated. Despite further experiment are necessary to confirm the role of LHCsr and PSBS protein in *Chlorella* species a behaviour different from *C. reinhardtii* is predictable.

In the section C the two *Chlorella* species previously analysed were compared for their adaptation to 3% CO_2. Despite the similarities found by genetic analysis, the comparison of the metabolic rearrangements induced by high CO_2 level showed considerable differences. The two species showed opposite behaviour, altering mainly the photosynthetic apparatus in *C. sorokiniana* and mainly the mitochondrial metabolism in *C. vulgaris*. Indeed, *C. sorokiniana* showed rearrangements of chloroplast light-dependent machinery similar to that was previously reported for *C. reinhardtii* grown in high CO_2 condition. The modifications of the photosynthetic apparatus led to the optimization of the light usage, improving carbon fixation rate. The major sink for the extra-carbon fixation was mainly proteins, but also polar lipids. Instead, in *C. vulgaris* was detected a decrease of starch content and an increase of lipid accumulation, in particular of TAG. This suggests a redirection of the energy reserves from starch to TAG accumulation, a class of macromolecules with a higher energy content per gram, indicating an improved light energy conversion. In *C. vulgaris* the photosynthetic apparatus was essentially unaffected, while the mitochondrial respiration was strongly downregulated, the opposite behaviour of *C. sorokiniana*. The different metabolic responses to CO_2 availability highlight different adaptation response among green algae, underling the needs to elucidate metabolic pathways and their regulation in fine detail in each species for rational metabolic engineering.

Also in *C. reinhardtii* we studied the behaviour of chloroplast and mitochondrion and in particular their crosstalk, studying a knockout mutant for a mitochondrial transcription termination factor (Chapter 1B). MOC1 mutant was identified in a forward genetic screen aimed at the identification of nuclear genes involved in light acclimation processes. Interestingly a mitochondrial factor was identified, remarking the importance of the communication between several compartments of the cell. The mutant had an excess uptake of reducing power in the mitochondrion preventing the high light acclimation of the cells. In wild type cells lumen acidification triggered photoprotective mechanisms as NPQ and chlororespiration, instead in the mutant the increased mitochondrial energy-dissipating pathway (AOX pathway) decreased the reducing power in the stroma damaging the feedback photoprotective mechanisms. The incorrect perception of the stromal redox state, over-oxidize by the excessive uptake of reducing power, explains the high-light sensitive phenotype of the mutant. This study underlines the importance of a more integrated vision of all the cell metabolisms instead to focus our attention only in the analysis of one specific metabolism/process.

Regarding *C. reinhardtii*, in the Chapter 1A a CRISPR-cas9 knock-out mutant was studied determining the role of LPA2 protein for PSII assembly and for its proper function. Our results suggested that LPA2 is likely involved in CP43 cooperation during PSII repair, as well as, in *de novo* biogenesis of PSII. CP43 acts as an inner PSII antenna and it is also essential for oxygen evolution in PSII. The lack of the LPA2 protein resulted in a drastic reduction in CP43 and thus in the inability of the *lpa2* mutant to grow in autotrophic condition. The CP43 transcript remained unaffected in the mutant indicating that LPA2 protein is involved in the post-translational regulation or integration of CP43 in the thylakoid membranes. Interestingly, the abundance of PSI core subunits and PSI activity were not reduced and CEF was increased, suggesting that *lpa2* mutant overcomes lack of PSII operating PSI-mediated electron transport flow to supplement photosynthetic energy production, but those increases were insufficient to support photoautotrophic growth. We conclude that LPA2 protein is a critical factor for PSII assembly, both *de novo* biogenesis and repair, in *C. reinhardtii*.

The knowledge of basic mechanisms of photosystems assembly and their regulation is important in order to develop new molecular approaches to improve yields. Such as, several mutants of proteins involved in the chloroplast signal recognition particle (CpSRP) pathway were generated. This pathway correctly assembles LHC proteins and some PSII-core and PSI-core proteins: knock-out of SRP proteins generate pale green mutants with a higher oxygen saturation curve and thus with an improved growth rate (Kirst and Melis 2014). The reduction of the chlorophylls content is a well-known strategy to increased biomass yield already utilized for several species as *Chlamydomonas reinhardtii* (Jeong et al. 2017; Polle, Kanakagiri, and Melis 2003), *Chlorella sorokiniana* (Cazzaniga et al. 2014)*, Chlorella vulgaris* (Dall'Osto et al. 2019) and cyanobacteria (Kirst, Formighieri, and Melis 2014) among others. In

this thesis a pale green mutant was generated by chemical mutagenesis for *N. gaditana* (Chapter 3A). The mutant showed a reduced chlorophyll content per cell combined with an increased lipid accumulation. Indeed, differently from other reported pale green mutants, in *e8* mutant the higher light availability, due to the better light distribution, is converted in a higher lipid accumulation rather than an increased biomass yield. Since lipids are a class of macromolecules with the highest energy density, an increased lipid accumulation indicates an improved light energy conversion efficiency. The reduced chlorophyll content per cell and consequently a more homogeneous irradiation in the photobioreactor were suggested to be at the basis of the increased lipid productivity observed in the *e8* mutant. Whole genomic sequencing of the mutant revealed several SNPs: this is a disadvantage in using chemical mutagenesis, because it makes genotype-phenotype correlation extremely difficult and it increases the possibility of unexpected phenotypes in some peculiar conditions. *dgd1* gene was proposed as main responsible of the phenotype: it encode for a key enzyme involved in DGDG biosynthesis, one of the major lipids of photosynthetic membranes and it thus involved in chloroplast biogenesis. However, only mutant complementation or specific mutagenesis with homologous recombination or genome editing will allow to confirm the correlation between specific mutations and the observed phenotypes.

The presence of several mutations is the main disadvantage of the chemical mutagenesis approach, on the other hand, the fact that they are non-GMO organisms is a strong advantage. Indeed, this ensures a more easily cultivatable in outdoor systems without the restrictive authorizations required for GMO strains in several countries.

A no-GMO strategy was applied also for the diatom *Thalassiosira weissflogii* for which the light absorption spectra was extended, better exploiting the light available and thus improving biomass yield and growth (Chapter 3B). In this work we demonstrated the ability to increase biomass production extending the absorbance range of the photosynthetic apparatus, thanks to the addition of an amphiphilic cyanine molecule, Cy5, that exploits light energy in the orange spectral region. Our data suggested a FRET mechanism that transfer energy from Cy5 to Chl *a* pigment. Diatoms showed an increased maximum oxygen production that outcomes in an increase biomass production and cells growth. However, a decreased Cy5 excited state lifetime was observed over day, making this dye not ideal for a prolonged use. The strategy based on the enlargement of sunlight absorption capability were already applied for *Dunaliella salina* (Burak, Dunbar, and Gilmour 2019) and *Nannochloropsis gaditana* (Sung et al. 2018), where dyes were located in an external space between light and the growing cells, and for *P. tricornutum*, for which was generated a mutant expressing eGFP protein (Fu et al. 2017). The advantages of our work lie in the ease of application: transformation protocol was not needed neither generation of GMO organisms nor specific structures to keep the dye separated from cells. We

achieved enhanced photosynthesis in the diatom *Thalassiosira weissflogii* by simple addition of the Cy5 dye to the algae growth medium.

Future perspective

Despite the variety of applications, the high costs of large-scale cultivation of microalgae have so far limited their use for industrial production. For this reason, it is necessary to enhance their photosynthetic efficiency, improving their growth, biomass yield and CO_2 fixation. The work presented in this thesis proposed different mode of action in order to improve future researches given by the high quantities of genetic information and experimental material provide.

In particular in the Chapter 1 two mutants of *Chlamydomonas* were studied. MOC1 is a mTERF factor which knock-out causes an impaired HL acclimation of the strain; instead LPA2 is a protein fundamental for the proper assembly and function of the PSII and thus to sustain the phototrophic growth. Tuning photoprotection to increased biomass yield it's a well-known strategy. Indeed, plants and algae dissipate an excess of light in stress conditions that could be used to photochemical reactions. For example, Kromdijk et al. 2016 increased photosynthetic efficiency of *Nicotiana tabacum* plants through acceleration of NPQ relaxation. MOC1 factor doesn't act directly as photoprotective mechanism but its fundamental for the HL acclimation of the strain. For this reason, accelerate the HL-stress perception could favour a faster cell response, reducing ROS generation and better exploiting the available energy for photochemistry. Thus, if we overexpressed MOC1 under a HL-induced promoter, maybe we could reduce HL-stress condition of the cell optimizing light use efficiency. Moreover, also LPA2 protein could be overexpressed. Indeed, increase the expression of LPA2 could accelerate the D1 repair in stressful condition, allowing a faster recovery to stress and a better functionality of PSII. Understanding the molecular basis of cells acclimation and its regulation is fundamental to study new approaches to improve yields. A deeper knowledge of the microalgae biology and in particular in our case of the photosynthetic apparatus, is a key tool in order to design new strategies to improve the growth phenotype.

Then in the Chapter 2, we focused our effort on *Chlorella* genus. In the last section we focused on photosynthetic and mitochondrial rearrangements that occur under high CO_2 availability. Further investigations are necessary to elucidate the response of the Calvin-Benson cycle, being it the first and mainly site of CO_2 organication. The key regulatory enzymes of the cycle could be differently express and regulate in order to manage the higher availability of CO_2. Their activity influences the redox state of the cell, due to their consumption of NADPH and ATP, thus study these enzymes is important to better understand the redox balance of the cell.

Chlorella is a genus of huge interest for industrial application, however biotechnological approaches are restricted by the limited genetic information available and the lack of efficient and reproducible transformation protocols. This prevent not only to generate insertional mutants, but also to confirm role of genes identified by genetic analysis. This thesis reduced the lack of genetic information by making available the complete transcriptome of two *Chlorella* species and the high-resolution genome of one of them. The genomic data of *C. vulgaris* makes accessible the species-specific codon usage and the possibility to identify promoter and regulatory elements to optimize transformation vectors. Furthermore, thanks to our data, we identified new potential targets to improve growth and biomass yield in the *Chlorella* genus and peculiar metabolic pathways not present in the model algae. However, the availability of reliable transformation protocols is necessary to verify role of genes identified by genomic/transcriptomic analysis: studies with knock-out or overexpression mutants will allow to confirm genes function, actually only predicted *in silico*. In particular the new pathways identified, such as C4-like pathway and FAS genes, require further investigation, as well as, the regulation of the photoprotection mechanisms involving LHCsr and PSBS proteins. Among the putative targets to improve growth, the overexpression of the phosphoenolpyruvate carboxylase enzyme could be an interesting possibility. Indeed, in *Chlorella sorokiniana* under mixotrophic condition this gene was overexpressed in order to recovery of carbon atoms lost by acetate oxidation.

Generation of mutants are necessary also in the case of mutant of *Nannochloropsis gaditana*. We generated a pale green chemical mutant that showed an increased lipid accumulation in nitrogen replete medium without affecting cells growth. The mutation responsible for the observed phenotype was not completely assay, indeed several mutations were identified from the SNPs study. For these reason generation of knock-out mutants is necessary to confirm the phenotype-genotype correlation. Moreover, further studies could be addressed to large-scale cultivation of the mutant strain in order to evaluate if the higher lipid accumulation and growth phenotype will be confirmed in not-controlled laboratory conditions and if the strain is suitable for industrial applications.

Another interesting approach to improved growth for industrial application is the addition of a dye that enlarges the light absorption capacity of the cultivated strain. The strategy reported in this thesis is based on the utilization of an amphiphilic dye, Cy5, added directly to the growth medium. In particular, the energy transfer occurs from Cy5 to Chl *a*, which is a pigment present in most photosynthetic organisms. Therefore, this approach can be in principle extended to other diatoms species, but also in general to other microalgae, paying particular attention in the algae pigment composition with respect to the spectrum of absorption/emission of dye. However, the dye utilized in our work, Cy5, have still some limitations, indeed it's partially degraded over the days. Further studies

are necessary to improved Cy5 lifetime and/or to find other dyes with higher stability over long periods. Moreover, it is necessary take into account the costs that should not be prohibitive with respect to benefits, in order to boost the revenues for an industrial application.

Taken together, the data discussed in this thesis represent a rich genetic resource for future genome editing studies, and potential targets for biotechnological manipulation to improve biomass and lipid productivity of several microalgae species of industrial interest.

REFERENCES

Burak, Hatice, Alan Dunbar, and D. James Gilmour. 2019. “Enhancement of Dunaliella Salina Growth by Using Wavelength Shifting Dyes.” *Journal of Applied Phycology*.

Cazzaniga, Stefano, Luca Dall’Osto, Joanna Szaub, Luca Scibilia, Matteo Ballottari, Saul Purton, and Roberto Bassi. 2014. “Domestication of the Green Alga Chlorella Sorokiniana: Reduction of Antenna Size Improves Light-Use Efficiency in a Photobioreactor.” *Biotechnology for Biofuels*.

Dall’Osto, Luca, Stefano Cazzaniga, Zeno Guardini, Simone Barera, Manuel Benedetti, Giuseppe Mannino, Massimo E. Maffei, and Roberto Bassi. 2019. “Combined Resistance to Oxidative Stress and Reduced Antenna Size Enhance Light-to-Biomass Conversion Efficiency in Chlorella Vulgaris Cultures.” *Biotechnology for Biofuels* 12(1):1–17.

Fu, Weiqi, Amphun Chaiboonchoe, Basel Khraiwesh, Mehar Sultana, Ashish Jaiswal, Kenan Jijakli, David R. Nelson, Ala’a Al-Hrout, Badriya Baig, Amr Amin, and Kourosh Salehi-Ashtiani. 2017. “Intracellular Spectral Recompositioning of Light Enhances Algal Photosynthetic Efficiency.” *Science Advances* 3(9):1–12.

Jeong, Jooyeon, Kwangryul Baek, Henning Kirst, Anastasios Melis, and Eon Seon Jin. 2017. “Loss of CpSRP54 Function Leads to a Truncated Light-Harvesting Antenna Size in Chlamydomonas Reinhardtii.” *Biochimica et Biophysica Acta - Bioenergetics*.

Kirst, Henning, Cinzia Formighieri, and Anastasios Melis. 2014. “Maximizing Photosynthetic Efficiency and Culture Productivity in Cyanobacteria upon Minimizing the Phycobilisome Light-Harvesting Antenna Size.” *Biochimica et Biophysica Acta - Bioenergetics*.

Kirst, Henning, Jose Gines García-Cerdán, Andreas Zurbriggen, and Anastasios Melis. 2012. “Assembly of the Light-Harvesting Chlorophyll Antenna in the Green Alga Chlamydomonas Reinhardtii Requires Expression of the TLA2-CpFTSY Gene.” *Plant Physiology*.

Kirst, Henning and Anastasios Melis. 2014. “The Chloroplast Signal Recognition Particle (CpSRP) Pathway as a Tool to Minimize Chlorophyll Antenna Size and Maximize Photosynthetic Productivity.” *Biotechnology Advances*.

Kromdijk, Johannes, Katarzyna Głowacka, Lauriebeth Leonelli, Stéphane T. Gabilly, Masakazu Iwai, Krishna K. Niyogi, and Stephen P. Long. 2016. “Improving Photosynthesis and Crop Productivity by Accelerating Recovery from Photoprotection.” *Science*.

Polle, Juergen E. W., Sarada Devi Kanakagiri, and Anastasios Melis. 2003. “Tla1, a DNA Insertional Transformant of the Green Alga Chlamydomonas Reinhardtii with a Truncated Light-Harvesting Chlorophyll Antenna Size.” *Planta*.

Sung, Min Gyu, Jong In Han, Bongsoo Lee, and Yong Keun Chang. 2018. “Wavelength Shift Strategy to Enhance Lipid Productivity of Nannochloropsis Gaditana.” *Biotechnology for Biofuels*.